# Semi-synthesis and Biological Evaluations of Tunicamycin Lipid Analogues and Investigation of the Tunicamycin Biosynthetic Pathway

*A thesis submitted in partial fulfilment for the degree of Doctor of Philosophy at the University of Oxford*

by **Hua Wang**

Department of Chemistry, University of Oxford

Trinity Term 2014

ORIEL
COLLEGE

*The Doctor*: It all just disappears, doesn't it? Everything you are, gone in a moment, like breath on a mirror. Any moment now, he's a coming.

*Clara*: Who's coming?

*The Doctor*: The Doctor.

*Clara*: You... you are the Doctor.

*The Doctor*: Yep. And I always will be. But times change, and so must I.

…

*The Doctor*: We all change when you think about it. We're all different people all through our lives. And that's okay, that's good. You've gotta keep moving. As long as you remember all the people that you used to be. I will not forget one line of this, not one day. I swear. I will always remember when the Doctor was me.

*- The Doctor (The Eleventh Doctor, portrayed by Matt Smith)*
*and Clara Oswald (portrayed by Jenna Coleman)*
*Doctor Who, The Time of the Doctor, 800th Episode*
*Written by Steven Moffat and Directed by Jamie Payne*

I declare the work presented in this thesis was carried out at the Chemistry Research Laboratory and Inorganic Chemistry Laboratory, University of Oxford, UK. All the work is my own, except where otherwise stated, and has not been submitted for any other degree at this or any other university.

The *M. tuberculosis* studies presented in *Chapter Three* were done by Drs Helena Boshoff and Andaleeb Sajid at the National Institute of Health (NIH), Maryland, USA.

The PCR-targeting work in *Chapter Four* was carried out with Dr Juan Pablo Gomez-Escribano at the John Innes Centre, Norwich, UK.

**Semi-synthesis and Biological Evaluations of Tunicamycin Lipid Analogues and Investigation of the Tunicamycin Biosynthetic Pathway**

Hua Wang
Oriel College
University of Oxford, Department of Chemistry
Submitted towards the degree of D.Phil. in Trinity Term 2014

Tunicamycins are potent antimicrobial agents but are also toxic to mammalian cells, which render them clinically impractical to use to treat infectious diseases. Instead, they have been used extensively as biochemical tools to study the *N*-linked glycosylation of proteins. However, despite such a routine application, their inhibitory mechanisms are still not clear. The central objective of this thesis was to develop novel tunicamycin analogues that are non-toxic to eukaryotic cells that could serve as potential antimicrobial drug candidates. We hypothesised that if we retain the lipid character of tunicamycin structure and modify the GlcNAc moiety then the antimicrobial activity would be retained but the tunicamycins inhibitory action towards GPT would be abolished, thus diminishing tunicamycins cytotoxicity towards mammalian cells.

**I - Semi-synthesis of the Tunicamycin Core Scaffolds and Lipid Analogues**

Semi-synthetic strategies were devised for isolating tunicamycin core scaffolds and for the selective addition of lipid chains at the 10'-*N* and 2"-*N* positions of tunicamycin, yielding the first library of novel tunicamycin lipid analogues.

**II - Biological Evaluations of the Tunicamycin Core Scaffolds and Lipid Analogues**

For the first time, the antibacterial activity of tunicamycins was shown to be dependent on the presence of a lipid chain. The tunicamycin core scaffolds were shown to lack antibacterial activity and cytotoxicity. More importantly, the library of tunicamycin lipid analogues with lipid chain length from seven to twelve carbons showed titrated antibacterial activity profile. Furthermore, the tunicamycin lipid analogues were not only found to have potent antibacterial and anti-*M. tuberculosis* activities but were non-cytotoxic compared to tunicamycins. The relative therapeutic index calculated for the tunicamycin lipid analogues was up to several thousand folds more than tunicamycins.

**III - Investigation of the *tunB* and *tunF* Knockout in the *tun* Gene Cluster**

The *tunB* and *tunF* single knockout mutations were made in the *tun* gene cluster by PCR-targeting and then heterologously expressed in *S. coelicolor*. The *tunB* knockout successfully abolished tunicamycin biosynthesis and showed evidence by MS the first existence of exo-glycal intermediates in sugar biology, further supporting the discovery of TunA as a novel NDP-sugar 5,6-dehydrogenase.

**IV - Investigation of the TunD and TunE Enzymatic Activities in Tunicamycin Biosynthetic Pathway**

The recapitulation of TunD glycosyltransferase and TunE deacetylase activities *in vitro* were attempted. Recombinant TunD was refolded from insoluble TunD inclusion bodies, while TunE was isolated in small quantities. However, no TunD and TunE activities were found using proposed intermediates. The co-translation of the *tun* gene cluster and the formation of multi-protein complex are proposed to be involved in the tunicamycin biosynthesis.

This thesis is dedicated to my teachers, family and friends.

A special thank you to the teachers that helped me from the start, Mrs Cicciline (née Miss Caproni), Mrs Higgins, Mrs Mack, and many others! I thank them for their dedication in teaching with fairness, perseverance, patience, and kindness. They went beyond the duty of their job and they saw potential in every student. They are a true inspiration.

I want to thank Prof. Benjamin G. Davis for giving me the opportunity to work on the tunicamycins project. Many thanks for the BGD group members, past and present. Special thanks to Fil, Seung, Bala, Albu, Macarena, Conor, Feng, Filippo, Sara, Sylvain, Rodolfo, M@, Shirley, Smita, Therese, Regis, Guillaume, Sonia, Leanne, Lukas, Pieter, Jenny, Amy, Erika, Yiqun, and Mark.

Thank you to Smita, Chris, Wei-min, Sylvain, Lingbing, Ned, and Manasi, for proofreading of this thesis and also for providing helpful comments and questions.

I would like to thank Oriel College for their support, including travel grants, during my DPhil.

Thank you Merv, JuanPa and David for making the work at John Innes Centre enjoyable and exciting.

Shout-outs to Mahima (thesis writing partner), the Hermes Club members, the entering class of 2010 members (Mahima, Bhaskar, Lukas ‘LuLu’, Inga, Phin, and Matt) who have been an amazing company throughout this journey and provided many helpful discussions in and out of the laboratory, the Adventures of Hannah and Ho, Leanne with FACS, Esther, Mathias ‘Franco’, Birte, Matias, and of course, my running partners ;)

We worked hard and we played hard. #2010to2011

Special thanks to Kevin, Erin, and Ned, and their families.

Last, but not least, thank you to my viva examiners Profs Christopher Schofield (Oxford) and Timothy Bugg (Warwick) for making my viva enjoyable and insightful.

## Publication

Filip J. Wyszynski, Seung Seo Lee, Tomoaki Yake, Hua Wang, Juan Pablo Gomez-Escribano, Mervyn J. Bibb, Soo Jae Lee, Gideon J. Davies and Benjamin G. Davis **Biosynthesis of the Tunicamycin Antibiotics Proceeds via Unique Exo-Glycal Intermediates** *Nature Chemistry* **2012**, *4,* 539-546.

Wang, H.; Wyszynski, F. J.; Royer, S. F.; Widdick, D. A.; Boshoff, H. I.; Barry 3rd, C. E.; Bibb, M. J.; Davis, B. G. Lipid-Altered Tunicamycin Analogues are Non-toxic but Retain Antibacterial Activity. *Manuscript in preparation.*

## Poster

'Tunicamycin Analogues and Investigation of their Biosynthetic Pathway' Wang, H.; Wyszynski, F. J.; Lee, S. S.; Gomez-Escribano, J. P.; Bibb, M. J.; Davis, B. G. Poster, Pfizer Neusentis Mini-Symposium 2012, University of Oxford, Department of Chemistry, Oxford, UK. (October 2012)

## Presentation

Wang, H. 'Synthesis and biological evaluation of tunicamycin analogues.' AstraZeneca, Final Year D.Phil. Talks, University of Oxford, Department of Chemistry, Oxford, UK. (October 2013)

**Carbohydrate structure numbering convention:** the structural numbering on carbohydrates in this thesis is in accordance to the standard carbohydrate convention:

*Exempli gratia,*

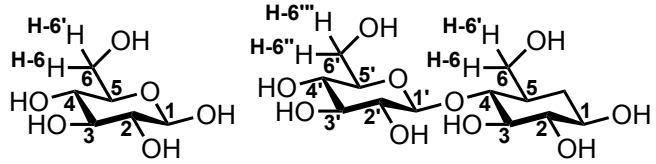


**Tunicamycin structure numbering system:**

*Exempli gratia***,**

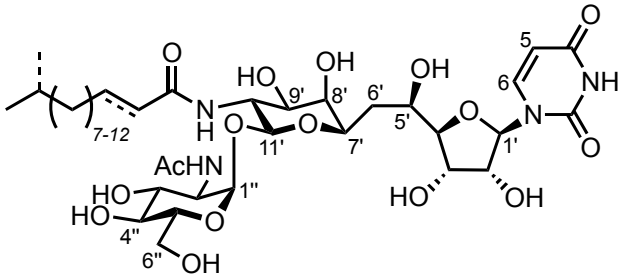


**Molecular weight for tunicamycin homologues and its derivatives:** an average molecular weight is conventionally used for the tunicamycins, or its derivatives, when referring to the mixture of homologues. An average molecular weight of 838 g $mol^{-1}$, or equivalent of the derivative, is used in this thesis based on common homologue carbon chain lengths of $n$ = 8, 9, 10, 11, or unless specified.

# Table of Contents

# *Chapter One*

## *An Introduction to Tunicamycins and the Bacterial Cell Wall*

## Preface

Tunicamycins were first isolated from the bacterial strain *Streptomyces lysosuperificus* by Takatsuki *et al*. in 1971 while screening for new antivirals and antibiotics produced by 4,000 *Actinomycetes* in soil samples.[1] Since then, tunicamycins have also been isolated from *Streptomyces chartreusis*,[2,3] *Streptomyces griseus*,[4] *Streptomyces clavuligerus*,[5] *Bacillus cereus,*[6] *Clavibacter toxicus,* and *Clavibacter michiganensis* subsp. *michiganensis.*[7]

Tunicamycins are unique among nucleoside antibiotics (**Fig. 1.1a**). Structurally, they contain an unusual eleven-carbon aminodialdose sugar (C-1' to C-11') and an α,β-(1"-11')-glycosidic linkage. Tunicamycins do not exist as a single compound but rather multiple homologues due to variations in the lipid chain. These homologues can be elegantly revealed by mass spectrometric analysis (**Fig. 1.1b**). Biologically, tunicamycins are potent antibiotics that target MraY translocase, an essential bacterial enzyme involved in peptidoglycan biosynthesis. However, they are also toxic to eukaryotic cells, rendering them unsuitable for human use. The central objective of this thesis is to build upon these intriguing discoveries: to develop novel tunicamycin analogues as potential antimicrobial drug candidates that are non-toxic to eukaryotic cells.

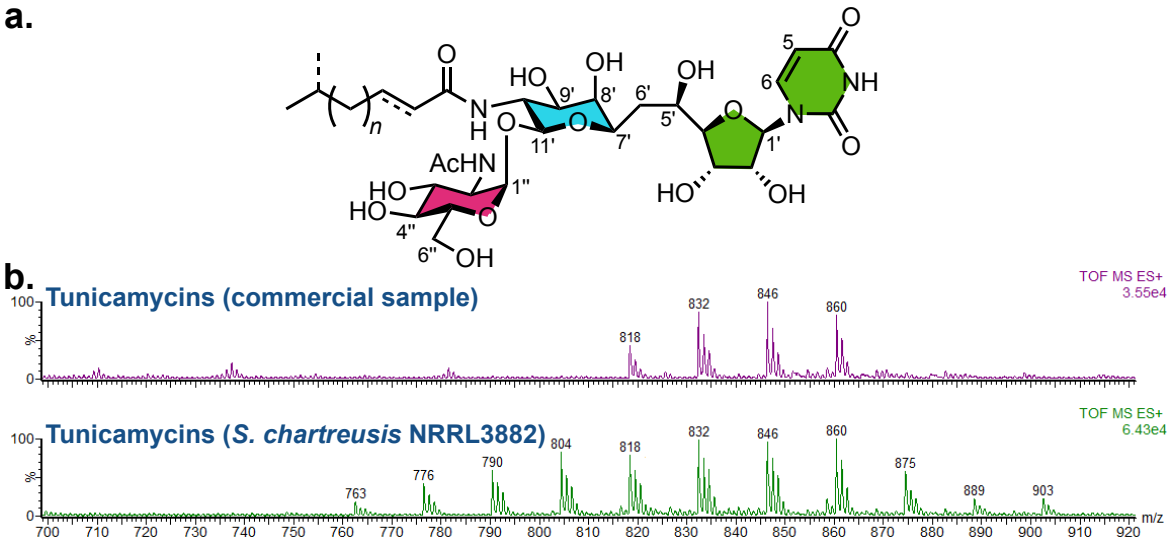


**Figure 1.1 | Tunicamycins. (a)** The chemical structure of tunicamycins consists of a uridine (green), galactose (blue), GlcNAc (magenta), and an amide-linked lipid chain at the 10' position. The *n* denotes the number of carbon atoms in the lipid chain, whereas *n* has been found to be between 7-12. The dashed lines on the lipid chain represent the existence of regioisomers. **(b)** TOF MS ES$^+$ analysis of tunicamycins is a classic way to show the homologues due to the difference in the mass of ±14 by the $CH_2$. Top: commercial tunicamycins ≥99% purity (TLC). Bottom: tunicamycins extracted from *S. chartreusis* NRRL3882, with 12 possible tunicamycin homologues.

## 1.1 Tunicamycins

Tunicamycins[i] were first observed as antiviral antibiotics that inhibited the replication of the Newcastle disease virus in chick embryo fibroblasts, but were quickly shown to be wide spectrum antibiotics.[1,8,9] They have now been reported not only to have antiviral properties, but also antibacterial, antifungal, and antitumour characteristics.[10] Not surprisingly, the interest in tunicamycins and tunicamycin-related antibiotics grew as a result of these findings. As such, due to the inhibitory properties of tunicamycins in eukaryotes, tunicamycins have found use as biological tools, for studying the unfolded protein response (UPR) in eukaryotic cells, rather than as antimicrobial agents. To this day, tunicamycin's mode of action is still not completely understood.

[i] The name 'Tunicamycin' is derived from the latin word *tunica* for coat, envelope, or surface. This was based of the fundamental understanding that tunicamycin inhibits the biosynthesis of some components present in the viral envelope or cell surface.

### 1.1.1 Physical Properties of Tunicamycins

Tunicamycins are soluble in alkaline solutions, pyridine, methanol, dimethyl-sulfoxide, and dimethylformamide, and are slightly soluble in ethanol and butanol. They are insoluble in acetone, ethyl acetate, chloroform, benzene, and acidic solutions. When using tunicamycins in biological experiments, they can be dissolved in basic solutions and diluted into the appropriate buffer as needed. Precipitation occurs when the pH falls below 6. However, tunicamycins may be used in biological experiments at acidic pH values and be maximally active *in vivo* if diluted in acidic buffers in the range of 0.1-10 μg $mL^{-1}$.[1,11,12] Tunicamycins degrade when heated in strong acid, *e*.g., HCl, or when exposed to strong oxidants such as periodate, but there is no loss of activity following treatment with 2 N KOH at 105 °C.[1]

In the ultraviolet absorption spectra, tunicamycins exhibit two absorption maxima: 205 nm and 260 nm, in methanol solution resulting from the presence of the uracil moiety, with an extinction coefficient ($E^{1\%}_{1cm}$) range of 76-110.[11] In infrared absorption spectrum, -OH and/or -NH (3400 and 3300 $cm^{-1}$) and secondary amide (1690, 1550 and 1280 $cm^{-1}$) can be distinctly observed.[1] By reversed-phase HPLC and MS analysis, tunicamycins are resolved into a series of structurally related compounds, or homologues.[11]

### 1.1.2 Chemical Structure of Tunicamycins

The chemical structure of tunicamycins were first solved through chemical degradation using hydrochloric acid and analysis of the degraded components, revealing the presence of glucosamine and galactosamine.[1,13] Further analysis by HPLC, NMR, IR and MS, indicated the presence of uracil and lipid chains.[13,14] These analyses helped to

determine the chemical structures of tunicamycins as having a unique eleven-carbon aminodialdose sugar (C-1' to C-11'), or also called tunicamine, and possessing an α,β-1-1-glycosidic bond. The lipid chains resulting from the degradation revealed tunicamycins to not be a single compound, but rather as a mixture of homologues.[13] Structural assignment was further thoroughly reported by Xu *et al.* to support the galactosamine configuration of tunicamine and the α,β-(1"-11')-glycosidic linkage in tunicamycins.[15] A summary of these structural analyses and the common names assigned to the core scaffolds are illustrated in **Fig. 1.2**.

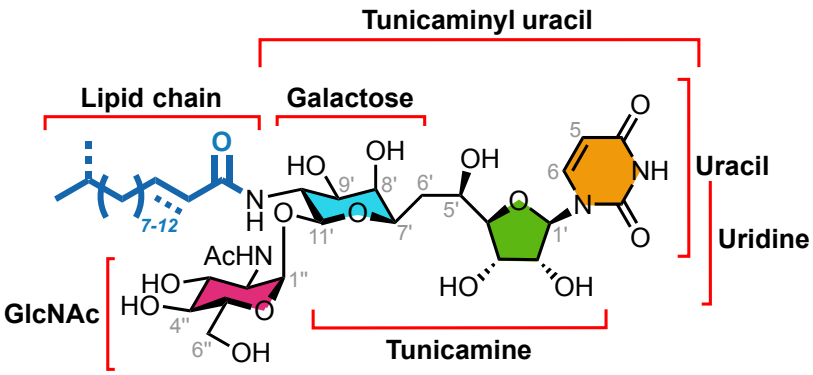


**Figure 1.2 | Chemical structure of tunicamycins.** Tunicamycins can be broken down into the core structural units, tunicamine for the eleven-carbon aminodialdose sugar and tunicaminyl uracil when including the uracil moiety.

Tunicamycins isolated from *Streptomyces* strains can be resolved into a series of homologues using reversed-phase HPLC (**Fig. 1.3**) and MS analysis (**Fig. 1.1b**). Commercial tunicamycins are typically a mixture of the homologues isolated from *S. lysosuperificus* (**Fig. 1.1b**).

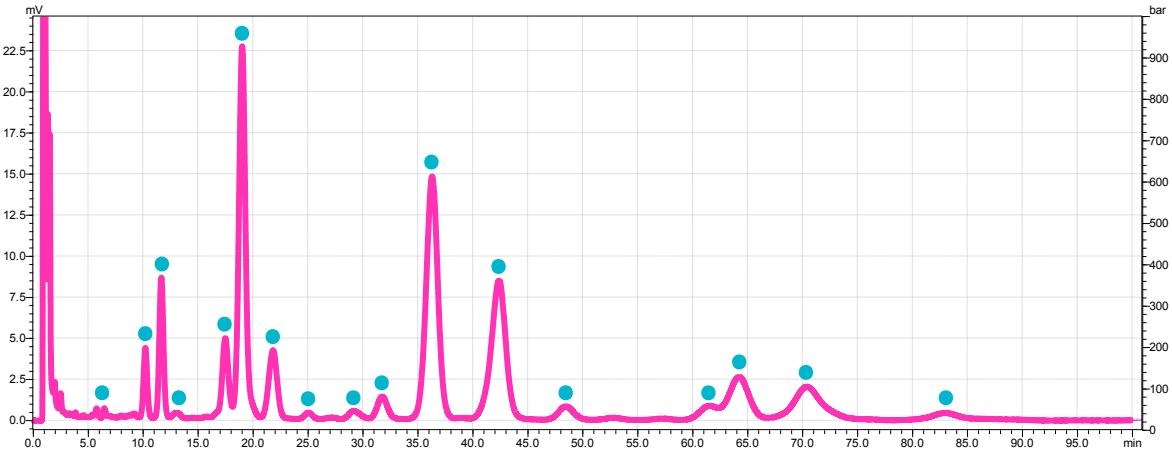


**Figure 1.3 | Reversed-phase HPLC chromatogram of tunicamycins.** Tunicamycins sample from *S. chartreusis* NRRL3882. Tunicamycins have a signature reversed-phase HPLC chromatogram due to the tunicamycin homologues (see **Fig. 1.4**). The blue dots on top of the peaks indicate the homologues, and the distribution of the peaks from left to right is resulted from the time of elution.

Ten tunicamycin homologues have been characterised (**Fig. 1.4**) of the 18 homologues that are thought to exist.[16] Interestingly, the lipid chain of the homologues differ not only in the length of the chain but also the terminal branching and the degree of unsaturation. Fascinatingly, the lipid chain appears to strongly influence the unique biological activities of each homologues.[6,17-22]

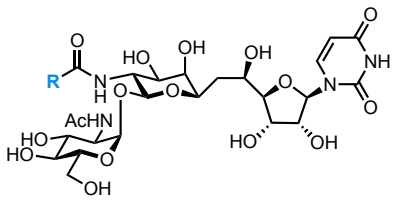

| Previous Notations | TunX:$Y_z$ | R = | M.W. (u) |
|---|---|---|---|
| I, $A_0$ | Tun13:1 | | 802.86 |
| II, $A_1$ | Tun14:1$_A$ | | 816.89 |
| III, $A_2$ | Tun14:1$_B$ | | 816.89 |
| IV, $B_1$ | Tun15:1$_A$ | | 830.92 |
| V, $B_2$ | Tun15:1$_B$ | | 830.92 |
| VI, $B_3$ | Tun15:0 | | 832.93 |
| VII, $C_1$ | Tun16:1$_A$ | | 844.94 |
| VIII, $C_2$ | Tun16:1$_B$ | | 844.94 |
| IX, $D_1$ | Tun17:1$_A$ | | 858.97 |
| X, $D_2$ | Tun17:1$_B$ | | 858.97 |

**Figure 1.4 | Naming conventions proposed for the tunicamycin homologues.** The first nomenclature for tunicamycin homologues used roman numerals, which depended in the order they eluted out from reversed-phase chromatography.[11] This was changed to alphabetics to reflect the regioisomers and using the subscript to denote the order of elution.[23] More recently, another naming convention was proposed to include the degree of saturation, using the convention in the form of TunX:$Y_z$.[16] In the latter convention, the X represents the number of carbon in the lipid chain including the carbon of the amide, the Y represents the degree of saturation, and the subscript Z represents the order of elution in the specific X:Y group.

### 1.1.3 Nucleoside Antibiotics

Tunicamycins belong to a distinct class of nucleoside antibiotics.[24,25] Nucleoside antibiotics are found in various microorganisms, and may differ in their biosynthetic origins, but they all share at least one nucleoside unit in their chemical structure. There exists an assorted mix of nucleoside antibiotics with notable chemical structure hybrids featuring nucleosides, higher monosaccharides, disaccharides, peptides, and/or lipids (**Fig. 1.5**). They exhibit a wide-range of biological properties that include antifungal, anthelmintic, herbicidal, insecticidal, antiviral, and antitumor characteristics.[25-28] A notable property of some nucleoside antibiotics is their ability to inhibit cell wall biogenesis, *i.e.*, bacterial peptidoglycan biosynthesis and fungal chitin biosynthesis.[25,29] These are important targets because they are absent in mammalian cells, and thus selectively inhibit bacteria and fungus growth *via* unique modes of action.

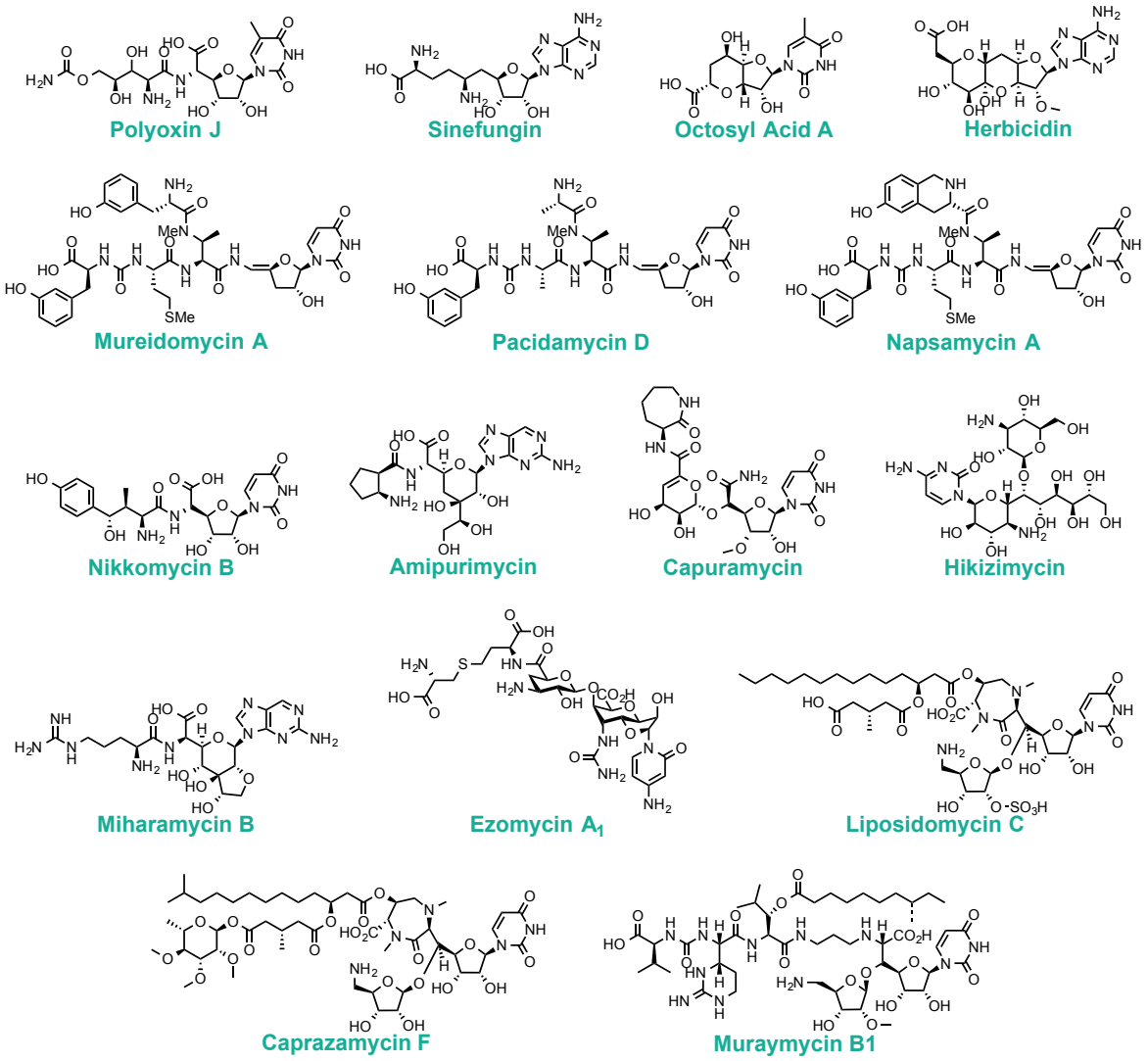


**Figure 1.5 | Examples of nucleoside antibiotics.**[25,28]

### 1.1.3.1 Other Members of the Tunicamycin Family of Nucleoside Antibiotics

Tunicamycins make up a unique subclass of nucleoside antibiotics, and are sometimes referred to as the 'tunicamycins family of nucleoside antibiotics' due to the similarity in their physiochemical properties. Others in the subclass include streptovirudins,[30] corynetoxins,[31] MM-19290,[5] Antibiotic 24010,[32] and mycospocidin.[24,33] Although MM-19290, Antibiotic 24010, and mycospocidin have not been studied in detail and their structures remain undetermined, antibiotic 24010 and mycospocidin, like tunicamycins, have been shown to inhibit the *N*-glycosylation of proteins.[34-36] Other nucleoside

antibiotics that have similar biological properties to tunicamycins but are not included in the subclass are mureidomycins, pacidomycins, liposidomycins, caprazamycins, and muraymycins.[25,37] Section **1.2** provides a summary detailing the proposed mode of action of tunicamycins and other relevant antibiotics.

Streptovirudins (**Fig. 1.6**) were first isolated from *Streptomyces griseoflavus* in 1975.[30] Ten streptovirudin homologues have been characterised, with structures almost identical to tunicamycin. Indeed, two of the homologues, streptovirudin $B_{2a}$ and $C_2$, are the same as tunicamycin homologues, Tun13:1 and Tun14:$1_A$. The streptovirudins have similar lipid chain variations but are shorter, α,β-unsaturated, and present as *iso*- or *anteiso*-mono-methyl regioisomers. One major difference is the presence of a dihydrouracil in place of the uracil moiety in five of the ten homologues. Not surprisingly, streptovirudins were found to have similar inhibitory activities to tunicamycins and these were also influenced by the lipid chain.[24,30,38,39]

Corynetoxins (**Fig. 1.6**) were first reported as a causative agent of annual ryegrass (*Loliurn rigidurn*) cytotoxicity to grazing animals. More specifically, corynetoxins were found to be produced by the bacterium *Corynebacteriurn rathayi* that infests galled seed-heads, along with the nematode *Anguina agrostis*.[40] Interestingly, although corynetoxins and tunicamycins occur as secondary metabolites from two different taxonomic groups, they share a very similar chemical structure.[24] There are fourteen corynetoxin homologues, with homologues U16i and U17i the same as tunicamycin homologues Tun16:$1_A$ and Tun17:$1_B$. The only difference between corynetoxins and tunicamycins is the lipid chain. Corynetoxins lipid chains are typically longer and more varied; they can be either

saturated or α,β-unsaturated, with *iso*- or *anteiso*-mono-methyl regioisomers, or may possess a β-hydroxyl group. Again, it is not a surprise that corynetoxins, like streptovirudins and tunicamycins, were also found to have the same inhibitory activities and are influenced by the lipid chain.[24,31,40-42]

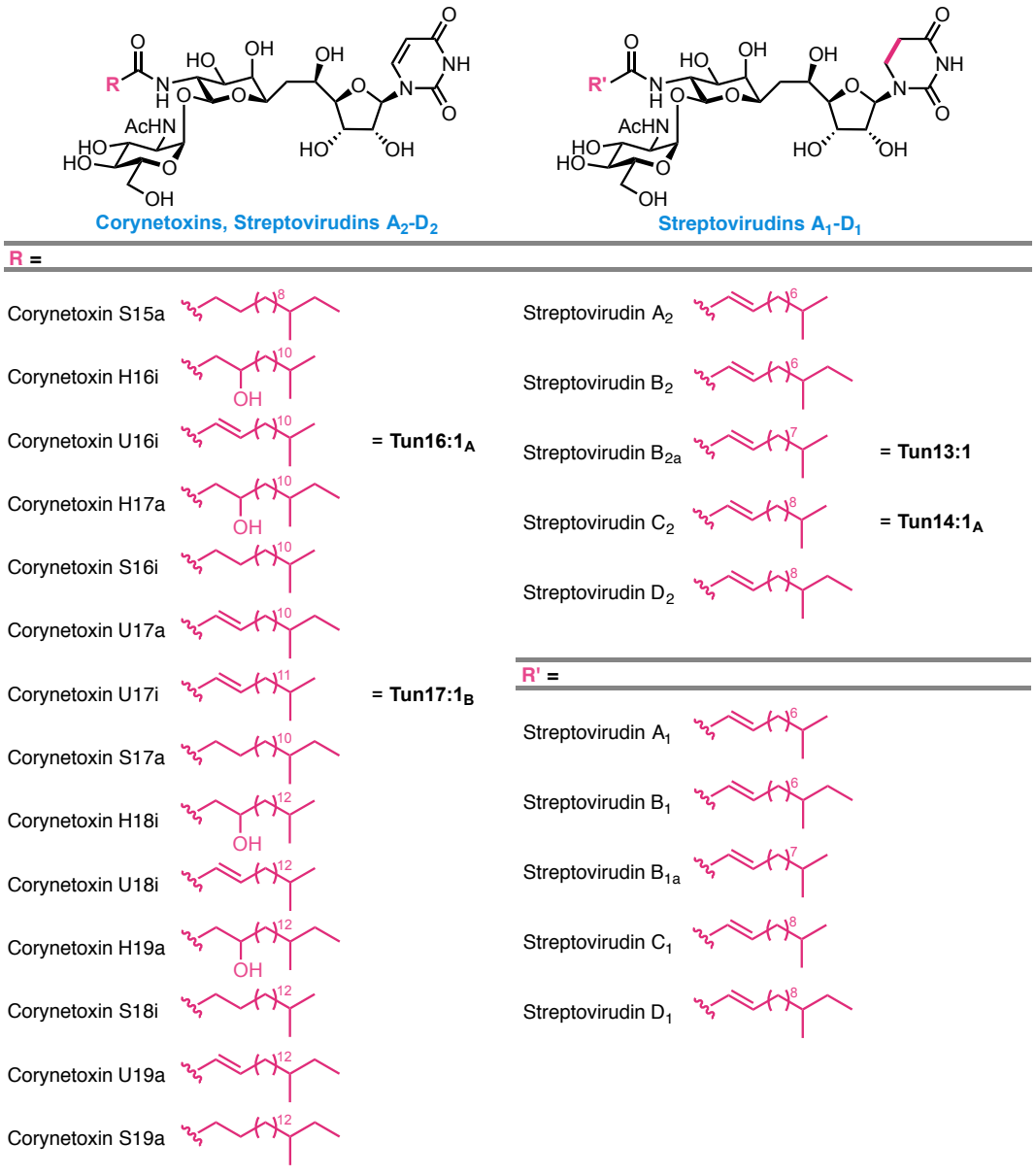


**Figure 1.6 | Streptovirudin and Corynetoxin homologues.** The nomenclature for both streptovirudins and corynetoxins is defined by the structure of the lipid chain. Streptovirudins nomenclature uses the alphabet based on the order of elution of the homologues from chromatography and the subscript number refers to series I (with dihydroxyluracil) and II (with uracil moiety).[38,43] Corynetoxins nomenclature uses number 15-19 to refer to the number of carbon

of the lipid chain, (S) for saturated, (U) for αβ-unsaturated, (H) for β-hydroxylated, and (n), (i), or (a), for normal, *iso*- or *anteiso*-termination, respectively.[40,42]

## 1.2 Biological Properties of Tunicamycins

A comprehensive review covering the first decade of work on tunicamycins can be found in G. Tamura's 1982 monograph titled 'Tunicamycin'.[44] Tunicamycins were first discovered based on the criteria set for an antiviral antibiotic to show little cytotoxicity on a confluent monolayer of chick embryo fibroblast cells culture and to specifically inhibit the plaque formation caused by viruses.[1,8] Tunicamycins were found not only to inhibit the multiplication of a wide range of enveloped RNA and DNA viruses[ii], but also the *Bacillus* peptidoglycan biosynthesis, protein palmitoylation,[45] ganglioside biosynthesis,[46,47] proteoglycan biosynthesis,[48] and also to interfere with 3-hydroxyl-3-methylglutaryl coenzyme-A (HMG-CoA) activity[49] and glycoprotein biosynthesis.[44,50-53] During peptidoglycan biosynthesis, tunicamycins block the transfer of the UDP-MurNAc-pentapeptide to undecaprenol phosphate to form undecaprenol-*N*-acetyl-muramyl-pentapeptidyl-pyrophosphate (also known as lipid I), making tunicamycins the first known antibiotics to selectively inhibit lipid I formation in bacteria.[53]

In addition to these inhibitory activities, tunicamycins were found to retard cell growth and induce morphological changes in microorganisms such as Gram-positive bacteria, yeasts, and fungi.[54-57] These suggested that tunicamycins influenced some component in the cell surface synthesis of eukaryotic cells. Following a series of investigations, *i.e.,* targeting DNA, RNA, and protein synthesis, and the stages of the virus

[ii] Newcastle disease virus, vesicular stomatitis virus, Semliki forest virus, fowl plague virus, Sindbis virus, measles virus, influenza virus, Rous sarcoma virus, Rauscher murine sarcoma virus, herpes complex virus.

cell cycle, specific inhibition of glycoprotein biosynthesis was deduced when hemagglutinin and neuraminidase, which are both glycoprotein components of the viral envelope, were found unglycosylated.[44,58-60] Due to glycoprotein biosynthesis that typically first requires the sugar to be transferred from a nucleotide *via* an isopolyprenol, *e.g.,* dolichol-phosphate, it was speculated that tunicamycins inhibit a *N*-acetylglucosamine transferase as supported by sugar incorporation experiments.[52,61] The enzymes responsible for the lipid I formation and the *N*-acetylglucosamine transfer, which tunicamycins target, were later found to be MraY translocase and *N*-acetylglucosamine-1-phosphate transferase (GlcNAc-1-P transferase, or GPT), in prokaryotic and eukaryotic cells, respectively.[62-65]

It is important to keep in mind that tunicamycins exist as multiple homologues. The separation of these homologues is a difficult and tedious process. Early studies showed that longer chain homologues are generally more biologically active in prokaryotes, whereas shorter chain homologues are generally more active in eukaryotes.[6,17-22] The differences in activity were speculated as a result from the lipid chain of homologues affecting how tunicamycins penetrate the cell membrane.[6,17-22,61] However, despite potential variations in biological activity between individual homologues, almost all studies in the literature have used tunicamycins as a mixture.

The following subsections discuss the origin and pathways targeted by tunicamycins and their proposed mode of action.

### 1.2.1 Bacterial Cell Wall and The Peptidoglycan

Bacteria are generally categorised as either Gram-positive or Gram-negative. This is the result of Gram staining, a technique invented by the Danish bacteriologist, Hans Christian Gram, in 1882.[66] The technique relies on the retention of Crystal Violet[iii]-iodine (CVI) complex by a bacterium in accordance to its cell wall composition (**Fig. 1.7**), more specifically due to the peptidoglycan. However, this Gram staining technique does not always yield a clear and unambiguous result, and sometimes even leads to misinterpretation of a result.[67,68] This is due to that fact that bacteria are unique and diverse, it is not possible for Gram staining to account for the influences by the age of the bacterial cell culture, changes in cell wall composition during stages of a cell division,[69] absence of peptidoglycan[iv] *e.g.,* mycoplasma and *Wolbachia*,[70-72] differences in chemical composition and spatial structure of peptidoglycan, or influences from other components in the cell membrane.[67,73-75]

Peptidoglycan can account for 5-90% of the bacterial cell wall mass.[74] Gram-positive bacteria have a much higher peptidoglycan content in their cell wall, which helps to retain the CVI complex resulting in a purple colour stain, whereas Gram-negative bacteria have a lower peptidoglycan content, allowing the CVI complex to leak out and resulting in a pink colour stain. Gram-negative bacteria also have an outer membrane that is absent in Gram-positive bacteria.[76,77]

[iii] Also known as Basic Violet 3, Gentian Violet, Hexamethylpararosaniline chloride, or Methyl Violet 10B.

[iv] Both, *Wolbachia* and Chlamydiales, have genes for peptidoglycan synthesis. Chlamydiales were also thought to be an exception of having no peptidoglycan but a recent work by Liechti *et al.* detected the presence of peptidoglycan.

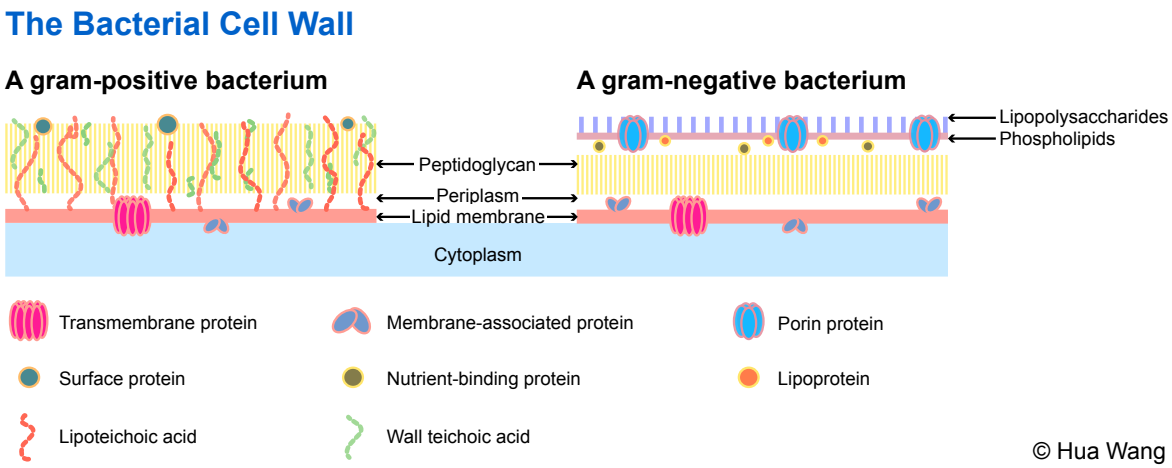


**Figure 1.7 | The Gram-positive and Gram-negative bacterial cell wall.**[74,78-80] The major difference between Gram-positive and Gram-negative is the composition of the cell wall membrane. In Gram-positive bacteria, the cell wall has a thick peptidoglycan layer that also contain proteins and anionic polymers (lipoteichoic acids and wall teichoic acids) important for host adherence and pathogenicity. Lipoteichoic acids are anchored to the cell membrane, while the wall teichoic acids are covalently attached to the MurNAc of the peptidoglycan. In Gram-negative bacteria, despite having a thin layer of peptidoglycan, they have an asymmetrical outer membrane composed of phospholipids and lipopolysaccharides. The lipopolysaccharides protect the bacterial cell from hydrophilic molecules, and also play a role in adherence to host cells and evasion of immune response. This outer membrane makes it difficult for foreign molecules to pass into the bacterial cell periplasm and cytosol, which is why most antibiotics are not effective against Gram-negative bacteria. To compensate for the limited permeability of the outer membrane barrier, Gram-negative bacteria have porins that allow certain molecules to enter. It is not shown, but in some Gram-positive and Gram-negative, there is also polysaccharides called the capsule that cover the bacterial the cell wall resulting in poor antigenic and antiphagocytic properties.

Peptidoglycan[v] is unique to bacteria, and is an essential component of the bacterial cell wall that can be found in almost all bacteria. It is a macromolecule composed of repeating units of disaccharide *N*-acetylglucosamine (GlcNAc) and *N*-acetylmuramic acid (MurNAc), linked by β-(1⟶4) bonds, and further cross-linked by short peptide chains substituted at the D-lactyl group of each MurNAc residues (**Fig. 1.8**).[81] The nature of the peptide chain varies between bacteria (**Table 1.1**), but is often composed of L-Ala-γ-D-Glu-

[v] Also known as murein (derived from the Latin word for wall, *murus*), and more rarely as mucopeptide, glycopeptide, or basal structure.

*meso*-$A_2$pm (or L-Lys)-D-Ala-D-Ala. The last D-Ala is lost in the maturation of the macromolecule.[81] Peptidoglycan wraps around the cytoplasmic membrane and helps with the mechanical stability of bacteria from fluctuations in osmotic pressure in the environment, maintains cell shape, and acts as an anchoring platform for proteins and other macromolecules and as a transport barrier by preventing the leakage of membrane particles and large molecules between the internal and external environment of the cell. To emphasise the importance of the peptidoglycan layer, a Gram-negative bacterial cell wall with a thin layer of peptidoglycan can resist pressures of up to 5 atm, whereas a Gram-positive bacterial cell wall with a thick layer of peptidoglycan can resist pressures up to 50 atm.[74]

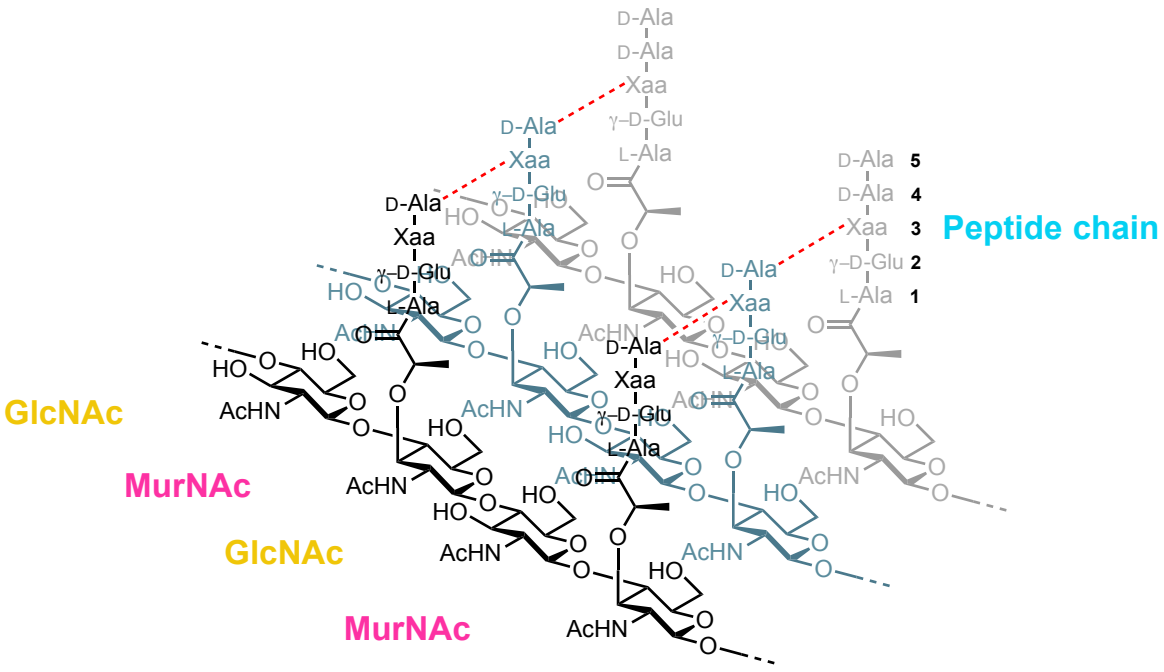


**Figure 1.8 | The typical chemical structure of peptidoglycan.** The last D-Ala, the fifth amino acid, is lost during the maturation process. Amino acid, Xaa, is typically a *meso*-$A_2$pm in Gram-negative bacteria, *e.g.*, *Escherichia coli*, or L-Lys in Gram-positive bacteria, *e.g.*, *Staphylococcus aureus*. The red dotted line shows the interpeptide bond that can be found in the *E. coli* peptidoglycan. In the *S. aureus* peptidoglycan, there is an interpeptide bridge made up of five glycine residues called the pentaglycine bridge.[81]

**Table 1.1 | Amino acid variations in the peptide subunits of the peptidoglycan.**[81]

| Position | Amino acid residue | Examples |
|---|---|---|
| **1** | L-Ala | Most species |
| | Gly | *Mycobacterium leprae*, *Brevibacterium imperiale* |
| | L-Ser | *Butyribacterium rettgeri* |
| **2** | D-Isoglutamate | Most Gram-negative species |
| | D-Isoglutamine* | Most Gram-positive species, Mycobacteria |
| | *threo*-3-Hydroxyglutamate* | *Microbacterium lacticum* |
| **3** | *meso*-$A_2$pm | Most Gram-negative species, Bacilli, Mycobacteria |
| | L-Lys | Most Gram-positive species |
| | L-Orn | Spirochetes, *Thermus thermophilus* |
| | L-Lys/L-Orn | *Bifidobacterium globosum* |
| | L-Lys/D-Lys | *Thermotoga maritima* |
| | LL-$A_2$pm | *Streptomyces albus*, *Propionibacterium petersonii* |
| | *meso*-Lanthionine | *Fusobacterium nucleatum* |
| | L-2,4-Diaminobutyrate | *Corynebacterium aquaticum* |
| | L-Homoserine | *Corynebacterium poinsettiae* |
| | L-Ala | *Erysipelothrix rhusiopathiae* |
| | L-Glu | *Arthrobacter* J. 39 |
| | Amidated *meso*-$A_2$pm* | *Bacillus subtilis* |
| | 2,6-Diamino-3-hydroxypimelate† | *Ampuraliella regularis* |
| | L-5-Hydroxylysine† | *Streptococcus pyogenes*‡ |
| | $N^{\gamma}$-Acetyl-L-2,4-diaminobutyrate* | *Corynebacterium insidiosum* |
| **4** | D-Ala | All bacteria |
| **5** | D-Ala | Most bacteria |
| | D-Ser | *Enterococcus gallinarum* |
| | D-Lac | *Lactobacillus casei*, Enterococci§ |

*Residue result from Mur ligases reactions
†Residue formation is unclear
‡Found as 10:1 ratio of lysine:hydroxylysine
§Acquired the residue through resistance to vancomycin

### 1.2.1.1 Peptidoglycan Biosynthetic Pathway

Despite the generality of peptidoglycan in microbial cells, it has a construction that is widespread across bacteria, as described above. It is worthy to note the extensive work covering the peptidoglycan pathway since the 1950s.[82,83] Yet, a complete picture is still not available. There remain more enzymes to discover and information about the pathway to understand, *e.g.*, flippases, $C_{55}$-P recycling enzymes, role and regulation in peptidoglycan biosynthesis during cell division, elongation, cell wall maturation, the types of peptidoglycan cross-links in relation to the spatial structure and cell shape and thickness, and behaviour in response to environmental stress and antibiotics.

The entire peptidoglycan biosynthetic pathway takes place in three locations, as three distinguishable stages, in a bacterium (**Fig. 1.9**). All three stages are potential drug targets for antibiotics. The first stage is the biosynthesis of UDP-*N*-acetylmuramyl pentapeptide (UDP-MurNAc-pp) in the cytoplasm. The second stage is the construction of the disaccharide pentapeptide building block *via* a lipid carrier, undecaprenyl-phosphate, in the cytoplasmic membrane. The third, and final stage, is the integration of the building block to the pre-existing peptidoglycan lattice in the periplasm. The following subsections elucidate the generic peptidoglycan biosynthetic pathway in *Staphylococcus aureus* or *Escherichia coli*, unless specified.

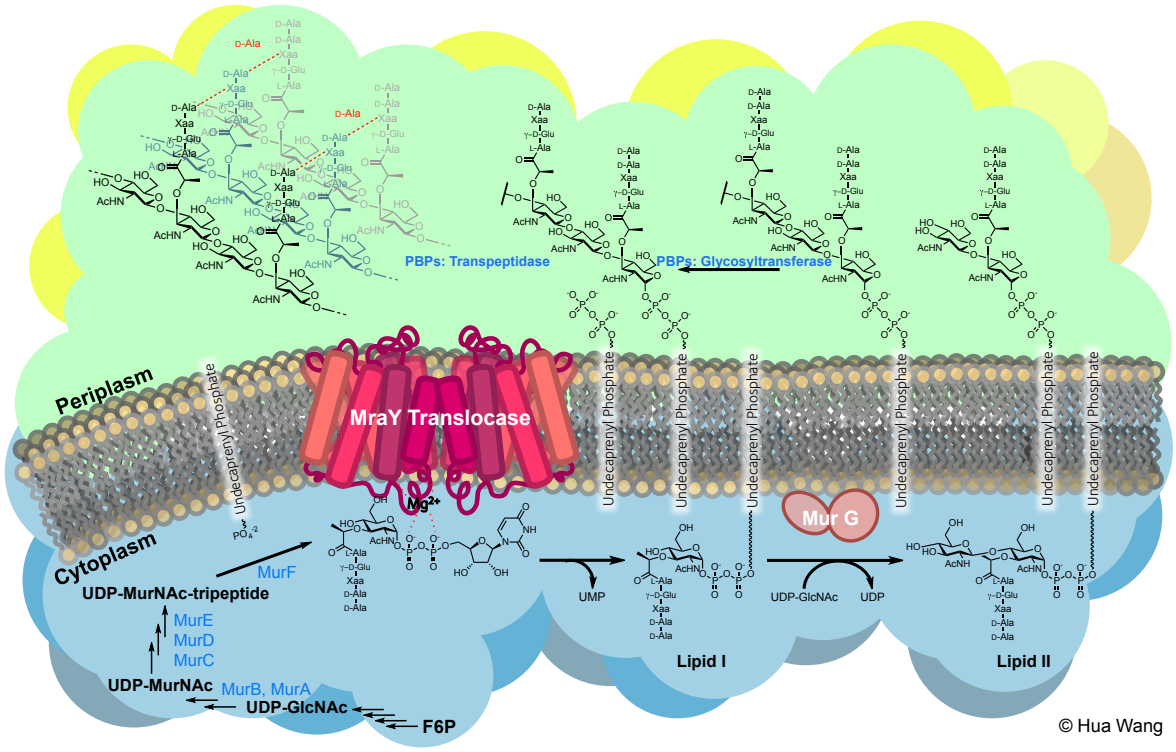


**Figure 1.9 | A schematic diagram of the peptidoglycan biosynthesis pathway highlighting the MraY translocase.** In the three stages of the peptidoglycan biosynthesis, *i.e.,* cytoplasmic, membrane and periplasmic stages, MraY translocase is the first enzyme involve in the membrane step. Amino acid, Xaa, is typically $A_2pm$ in Gram-negative bacteria, or L-Lys in Gram-positive bacteria. The figure is more representative of the peptidoglycan biosynthesis found in *E. coli*. In the *S. aureus* peptidoglycan biosynthetic pathway, lipid II in the membrane stage would be further

modified with a pentaglycine by an enzyme called FemABX.[84,85] In either case, the hydrophilic unit of lipid II has to translocate through the lipid membrane. There is an enzyme coined the 'Flippase', not shown, that carries out the translocation of the hydrophilic unit from the cytoplasm through the lipid membrane to the periplasm.[86,87] This mechanism is not well understood.

#### 1.2.1.1.1 Biosynthesis of UDP-*N*-acetylmuramyl Pentapeptide

Intracellular biosynthesis of the peptidoglycan starts from the biosynthesis of UDP-*N*-acetylmuramyl pentapeptide (UDP-MurNAc-pp) and UDP-*N*-acetylglucosamine (UDP-GlcNAc). This begins with the primary metabolite D-fructose-6-phosphate (Fru-6-P) resulting from the glycolytic pathway and the pentose phosphate pathway (PP pathway).[88] Fru-6-P is first converted into glucosamine-6-phosphate (GlcN-6-P) by a dimeric enzyme called glucosamine-6-phosphate synthase (GlmS), which follows an ordered bi-bi mechanism, using L-glutamine as the nitrogen source. The GlmS monomer has two distinct functional domains. In the N-domain, it hydrolyses glutamine into glutamate and ammonia (**Fig. 1.10a**), then the C-domain uses the ammonia to convert Fru-6-P into GlcN-6-P (**Fig. 1.10b**).[89,90] GlcN-6-P is then interconverted by GlmM, upon activation by phosphorylation, to form GlcN-1-P isomer *via* a ping-pong bi-bi mechanism (**Fig. 1.10c**).[91,92] This is followed by the action of GlmU, a bifunctional enzyme that catalyses the acetyltransfer and uridyltransfer to GlcN-1-P to form UDP-GlcNAc (**Fig. 1.10d**).[93,94]

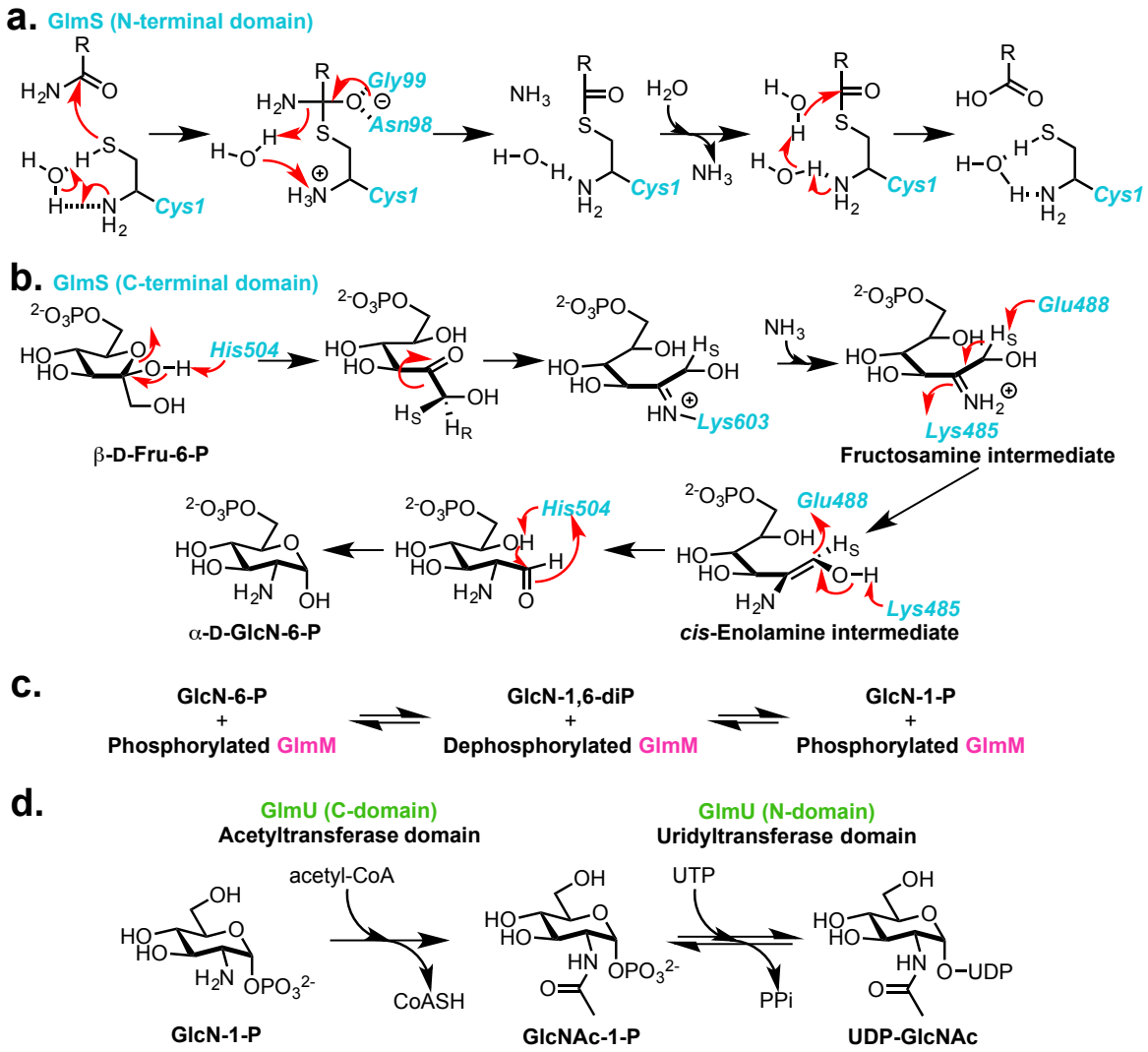


**Figure 1.10 | Biosynthesis of UDP-*N*-acetylglucosamine *via* GlmS, GlmM, and GlmU.**[90-92,94] A general representation in the prokaryotic system. **(a)** Proposed mechanism for the hydrolysis of glutamine at the GlmS N-terminal domain performed by a cysteine thiol. **(b)** The rate of spontaneous ring opening of Fru-6-P is about 20 $s^{-1}$, which is comparable to the catalytic rate of GlmS. In the GlmS C-terminal domain, it is proposed that His504 carries out the ring opening and catalyses the reaction *via* stereospecific abstraction of the C-1 $H_R$ hydrogen from Fru-6-P to form a *cis*-enolamine intermediate. **(c)** Currently, there is no crystal structure available for GlmM. The GlmM site of phosphorylation has been shown to be Ser102. GlcN-1,6-diphosphate appears as an intermediate but acts as both the first product and the second substrate. GlmM is inactive in its dephosphorylated form. However, it has been shown to undergo autophosphorylation when incubated with ATP. **(d)** GlmU is a bifunctional enzyme that first catalyses the acetyltransfer reaction in the C-terminal domain and then the uridyltransfer reaction in presence of $Mg^{2+}$ in the N-terminal domain.

Following the formation of UDP-GlcNAc, it is converted into UDP-MurNAc-pp by a series of Mur enzymes, the first of which is MurA. MurA carries out a rare biochemical process involving *enol*pyruvyl transfer from phospho*enol*pyruvate (PEP) to a hydroxyl group with the release of phosphate ($P_i$). The only other known enzyme that does the same biochemical process is AroA in the shikimic acid pathway. MurA then catalyses the formation of UDP-GlcNAc-*enol*pyruvate with UDP-GlcNAc following an addition-elimination reaction (**Fig. 11a**).[92,95] Next, a flavoenzyme, MurB, converts UDP-GlcNAc-*enol*pyruvate to UDP-MurNAc at the expense of a reduced nicotinamide adenine dinucleotide phosphate (NADPH) *via* a ping-pong bi-bi mechanism (**Fig. 11b**).[96] UDP-MurNAc is then decorated with the pentapeptide by Mur ligases (MurC, MurD, MurE, and MurF). Mur ligases exist as 'closed' or 'open' conformation, where the 'closed' conformation is thought to be provoked by ligand binding. They share the same reaction mechanism and three-dimensional structure. The N-terminal domain is involved in the binding of UDP-MurNAc, the central domain is involved in the binding of adenosine triphosphate (ATP), and the C-terminal domain is involved with the binding of the amino acid. Interestingly, the N-terminal domain between the ligases shows some topological differences that are related to the growing polypeptide tail of the UDP-MurNAc precursors. The amino acids are added in sequential order, and variation of the amino acid sequence is dependent on the bacterial species as mentioned previously (**Table 1.1**, **Fig. 1.11c**).[92,97] The formation of UDP-MurNAc-pp is then followed by the membrane-associated steps of the peptidoglycan biosynthesis.

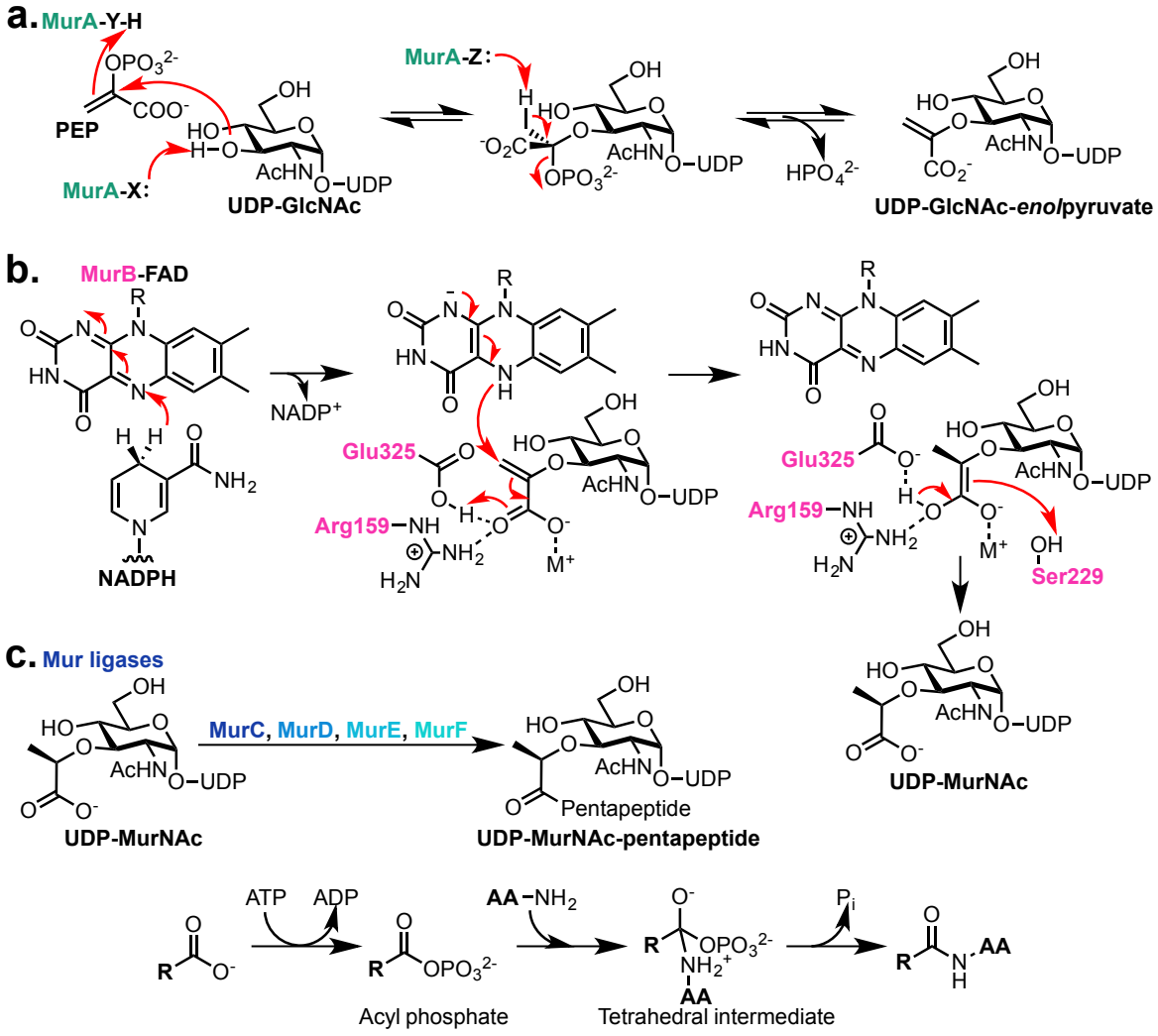


**Figure 1.11 | Biosynthesis of UDP-*N*-acetylmuramyl pentapeptide *via* MurA-F.**[92,95-99] A general representation in the prokaryotic system. **(a)** The X, Y, and Z represent the side chains involved, but the amino acid residues involved are unclear. Cys115 has been proposed to act as the acid-base catalyst in the addition-elimination reaction, but Asp305 has also been considered to participate in the proton abstraction of the hydroxyl group and the final proton abstraction to form the product. PEP is protonated by MurA-Y-H forming a PEP oxocarbenium ion, while the OH is deprotonated by MurA-X. The nucleophilic attack from the deprotonated OH group to PEP oxocarbenium ion forms an adduct in tetrahedral configuration. The proton from the methyl group is then abstracted by MurA-Z to form the vinyl ether product, UDP-GlcNAc-*enol*pyruvate. **(b)** MurB is maximally activated in the presence of $K^+$, $NH_4^+$ and $Rb^+$. In the first half-reaction, flavin adenine dinucleotide (FAD) non-covalently binds to MurB, serving as a cofactor by mediating hydride transfer between NADPH and UDP-GlcNAc-*enol*pyruvate. FAD is first reduced to $FADH_2$ by NADPH, upon the transfer of the 4-pro-S hydrogen and release of $NADP^+$. In the second half-reaction, UDP-GlcNAc-*enol*pyruvate is reduced by the hydride transfer from the reduced MurB-$FADH_2$, generating a carbanionic intermediate that is stabilised by Arg159 and Glu325. Quenching of the carbanion is proposed to be mediated by Ser229 to yield the D-configuration lactyl ether

product, UDP-MurNAc. **(c)** Mur ligases share the same reaction mechanism to form the amide or the peptide bond. The reaction is dependent on a divalent cation, $Mg^{2+}$ or $Mn^{2+}$. They first activate the carboxyl group of UDP-MurNAc ($R\text{-}COO^-$) by ATP to generate the acyl phosphate intermediate and adenosine diphosphate. Then the UDP-precursor undergoes a nucleophilic attack by the amino group of the amino acid ($AA\text{-}NH_2$) forming a high-energy tetrahedral intermediate that breaks down into the amide product and phosphate ($P_i$). MurF adds the dipeptide D-Ala-D-Ala. The D-Ala-D-Ala is synthesised from two molecules of L-Ala, first through alanine racemase to form D-Ala and then D-Ala-D-Ala ligase to form the dipeptide product. As mentioned in **Fig. 9**, in *S. aureus*, the lysine at the third peptide position of UDP-MurNAc-pp at this stage would be further modified by three enzymes. FemX adds the first glycine *via* a tRNA-Gly, and then FemA and FemB add the four glycines *via* four of tRNA-Gly.[84,100]

#### 1.2.1.1.2 Biosynthesis of Disaccharide Pentapeptide Building Block Lipid II

In the membrane stage of the peptidoglycan biosynthesis, the UDP-MurNAc-pp is transformed into lipid precursors by MraY translocase and MurG *via* the lipid carrier undecaprenyl-phosphate ($C_{55}$-P) (**Fig. 1.12a**).

$C_{55}$-P[vi] is an important lipid carrier in prokaryotes that assists not only in the biosynthesis of the peptidoglycan, but also O-antigen, enterobacterial common antigen, lipoteichoic acids, and other bacterial carbohydrate polymers.[101,102] $C_{55}$-P starts from eight isoprenoids, isopentenyl diphosphate (IPP), that are used in consecutive condensation reactions by *cis*-prenyltransferase undecaprenyl-diphosphate synthase (UppS) to elongate a farnesyl diphosphate ($C_{15}$-PP) to form the undecaprenyl-diphosphate ($C_{55}$-PP) precursor (**Fig. 1.12b**). Most organisms either inherited the mevalonate pathway or the metherythritol phosphate pathway that produce the universal five-carbon isoprenoids, isopentenyl diphosphate (IPP) and its isomer dimethylallyl diphosphate (DMAPP). It is suggested that UppS, because it is a soluble cytoplasmic protein, is in close proximity to

[vi] There are also decaprenyl phosphate ($C_{50}$-P) and nonaprenyl phosphate ($C_{45}$-P) that exist in mycobacterial species and *Paracoccus denitrificans*, respectively.

the membrane which allows for rapid release of the lipid precursor product and integration into the phospholipid bilayer. $C_{55}$-PP is then dephosphorylated by a putative pyrophosphate phosphatase, UppP[vii], into its active form and used by MraY translocase in the membrane step of the peptidoglycan biosynthetic pathway.[101-104]

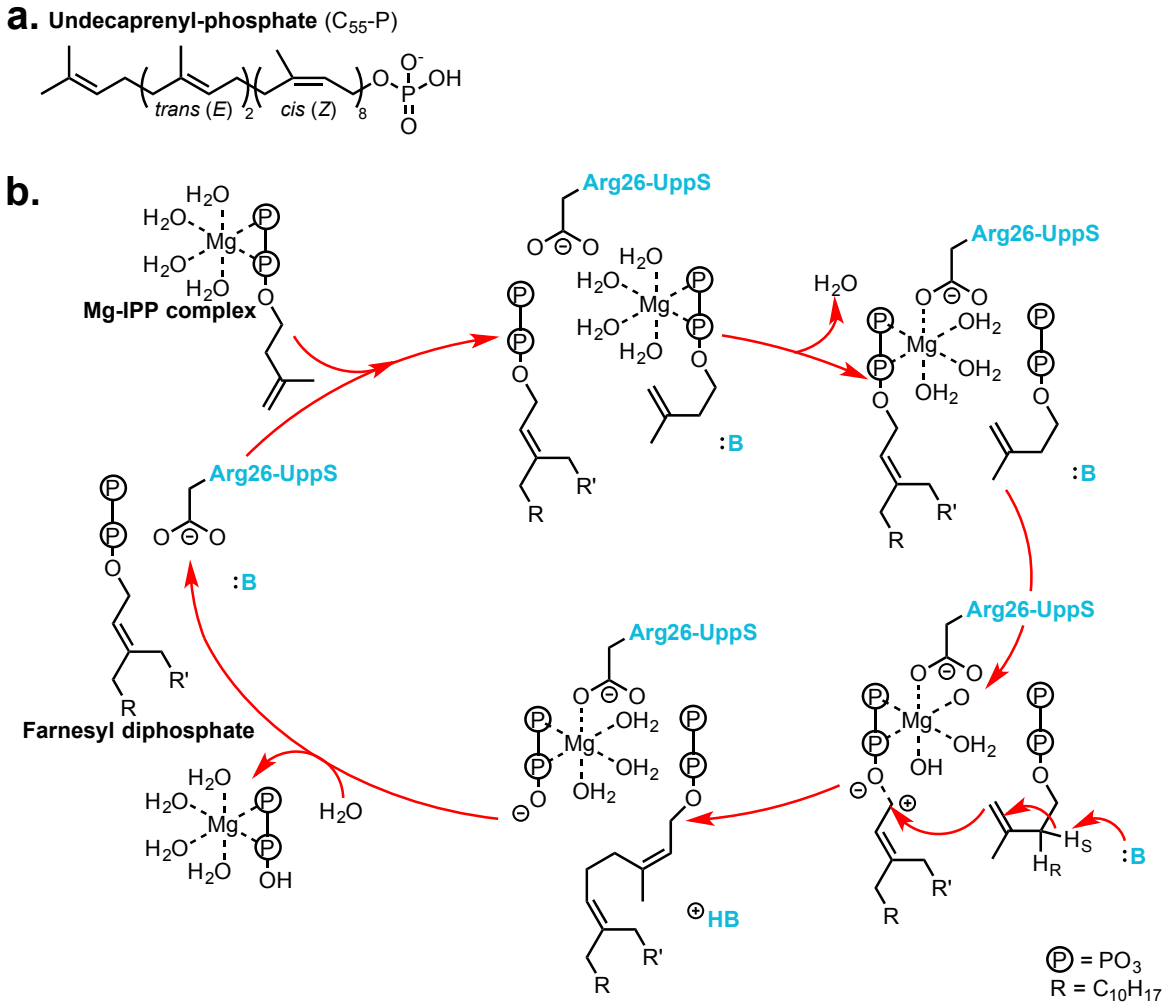


**Figure 1.12 | Biosynthesis of undecaprenyl-diphosphate.**[102,105,106] A general representation in the prokaryotic system. **(a)** Chemical structure of the undecaprenyl-phosphate, $C_{55}$-P. **(b)** The proposed UppS catalytic mechanism. UppS has been shown to be dependent on $Mg^{2+}$ for $C_5$-PP binding and for catalysis, but not for $C_{15}$-PP binding. $C_{15}$-PP first binds to UppS, where the diphosphate is stabilised by Asn28, Gly29, Arg39, and His43, and the $C_{15}$-prenyl tail is stabilised by the hydrophobic amino acids. The His43 may serve as a proton donor, based on mutation studies. This first interaction changes the UppS from open to the closed conformation. Then the Mg-IPP

[vii] Also known as BacA.

complex binds to another region of the active site, where the carboxyl group of Arg26 assists in the migration of $Mg^{2+}$ from IPP to $C_{15}$-PP. Possible candidates for the stereospecific abstraction of the C-2 $H_S$ hydrogen are Asn74 or Ser71. The cycle is repeated seven more times to form the $C_{55}$-PP, where the length is controlled *via* a molecular ruler mechanism. The product would then be pushed away from the active site due to the length of the lipid chain, and then enzyme relaxes to the open conformation. The R is switched to R' after the first cycle to account for the *cis*-configuration of the new double bond.

MraY translocase is involved in the first committed membrane step of peptidoglycan biosynthesis, where the catalytic process can be inhibited by tunicamycins. The MraY structure and reaction mechanism in relation to tunicamycins are further discussed in detail in subsection **1.2.2.1**. MraY is suggested to require a divalent metal ion, most commonly $Mg^{2+}$, to catalyse the translocation of the cytoplasmic precursor UDP-MurNAc-pp to a membrane-associated $C_{55}$-P to form undecaprenyl-diphosphate-*N*-acetylmuramyl-pentapeptide ($C_{55}$-MurNAc-pp, lipid I[viii]) with the release of uridine monophosphate (UMP).[65,107,108] The reaction mechanism for MraY has been proposed to be either a one-step or two-step process (**Fig. 1.13a**). Following the formation of lipid I, MurG (translocase II) catalyses the second membrane-associated step. MurG is a peripheral membrane glycosyltransferase that transfers GlcNAc from UDP-GlcNAc to lipid I, *via* a β-glycosidic bond, to yield the disaccharide undecaprenyl-diphosphate-*N*-acetylmuramyl-*N*-acetylglucosamine-pentapeptide ($C_{55}$-PP-MurNAc-GlcNAc, lipid II) and the release of uridine diphosphate (UDP) (**Fig. 1.13b**).[108,109] The formation of lipid II is followed by a translocation process, carried out by a 'Flippase' *via* a mechanism that is not currently understood, to the periplasmic layer of a bacterial cell where the disaccharide building block is integrated into the pre-existing peptidoglycan matrix of the bacteria by penicillin-binding proteins.

[viii] Also known as Park's nucleotide.

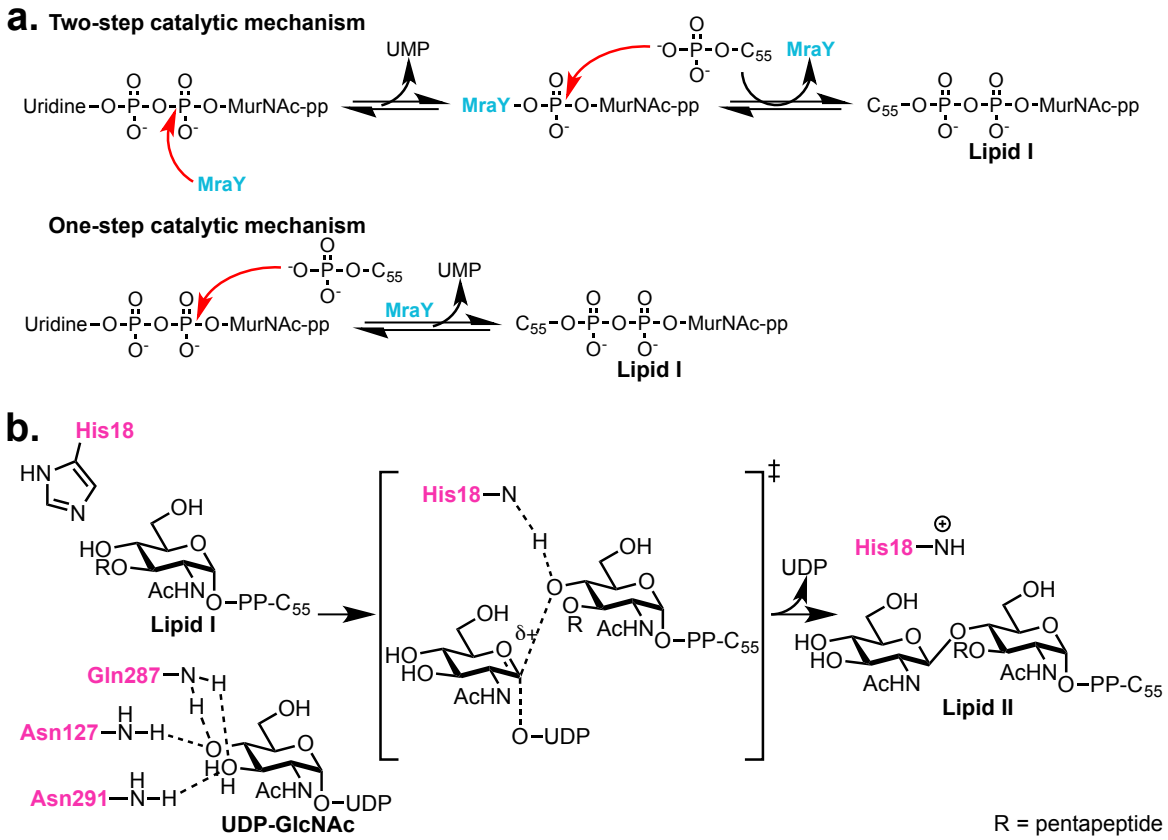


**Figure 1.13 | Biosynthesis of lipid I and lipid II.**[107,108,110-120] A general representation in the prokaryotic system. **(a)** Two catalytic mechanisms have been proposed for MraY translocase. The one-step mechanism is based on the hypothesised *B. subtilis* Asp98, deprotonating and activating the C55-P hydroxyl for the nucleophilic attack phosphate atom. Asp98 is Asp115 in *E. coli* and Asp117 in *Aquifex aeolicus*. There are literature reports that indicate MraY is capable of carrying out the exchange of radiolabelled UMP of UDP-MurNAc-pp in presence or absence of $C_{55}$-P. Additionally, in the presence of dodecylamine, the exchange reaction was inhibited with the release of phospho-MurNAc-pentapeptide. The exchange reaction results have been challenged due to the use of unpurified MraY. Although the mechanism still remains unclear, recent mutational studies on the highly conserved *E. coli* Asp115, Asp116, and Asp267 residues, and the first crystal structure of MraY from *A. aeolicus* have shown more compelling evidence for the two-step mechanism. It has been proposed that the amino acid Asp115 and Asp116 are involved in magnesium ion chelation with the diphosphate bridge of the UDP, and Asp267 is involved in the hydrolysis of the nucleotide diphosphate. The catalytic mechanism of MraY is generally depicted as a two-step mechanism. **(b)** The proposed catalytic mechanism for MurG. MurG is a member of the GT-B glycosyltransferase and is metal-independent. It follows an ordered bi-bi mechanism, *via* an oxocarbenium-ion-like transition state. The UDP-GlcNAc first binds to the active site followed by nucleophilic attack at C1 by the oxyanion of MurNac to form the β-(1⟶4) glycosidic bond. The UDP is released and lipid II is generated.

#### 1.2.1.1.3 Integration of Disaccharide Pentapeptide in Peptidoglycan

In the last stage of the peptidoglycan biosynthesis the disaccharide head of lipid II faces the periplasm, polymerises as linear glycans, and cross-links into the pre-existing peptidoglycan. The polymerisation alternates between MurNAc and GlcNAc, and the cross-linking occurs to peptides *via* transglycosylation and transpeptidation by peptidoglycan glycosyltransferases (PGTs), or transglycosylases, and penicillin-binding proteins (PBPs), respectively. PBPs are probably the most widely known and scrutinised enzymes in the peptidoglycan biosynthetic pathway due to their highly successful targeting by β-lactam antibiotics. PBPs are an unique, large family of membrane-associated enzymes that are classed as A, B, or C, depending on their structure and catalytic activity of the N-terminal domain.[121] PBPs in class A and B have high molecular mass. Class A has both the glycosyltransferase and transpeptidase activities. Generally, the name PGTs is used for the glycosyltransferase region and PBPs is used for the transpeptidase region of the enzyme. Class B has only transpeptidase activity. Both classes possess transpeptidase activity on the C-terminal domain.[122] Class C is the PBPs of class A and B but with low molecular mass.[121] Bacteria can have multiple types of PBPs present. Some bacteria also have monofunctional PGTs that are similar to the N-terminal glycosyltransferase domain of PBPs, or PGTs. Their exact role is currently not known but is speculated that they participate in the cell elongation and division processes.[123-125] Additionally, some PBPs can carry out reverse reactions, hydrolysing the last D-alanine of stem pentapeptides (DD-carboxypeptidation) or the peptide bond connecting two glycan strands (endopeptidation). Furthermore, PBPs are not only involved in the construction of the peptidoglycan, but also play a role in cell division, cell elongation, and peptidoglycan maturation or recycling.[121,124,126,127]

The general catalytic mechanisms for PGTs and PBPs are shown in **Fig. 1.14**. In the last step of the periplasmic stage of the peptidoglycan biosynthesis, the disaccharide building block is integrated into the pre-existing peptidoglycan and $C_{55}$-PP is regenerated. However, this time, the diphosphate head is facing the periplasm. It has been proposed that there is a dephosphorylation step, similar to UppP as mentioned earlier, where $C_{55}$-PP is recycled back to $C_{55}$-P, flipped to the cytosol, and then reused by the bacteria. The mechanism for this $C_{55}$-P regeneration step still remains unclear.[101,102]

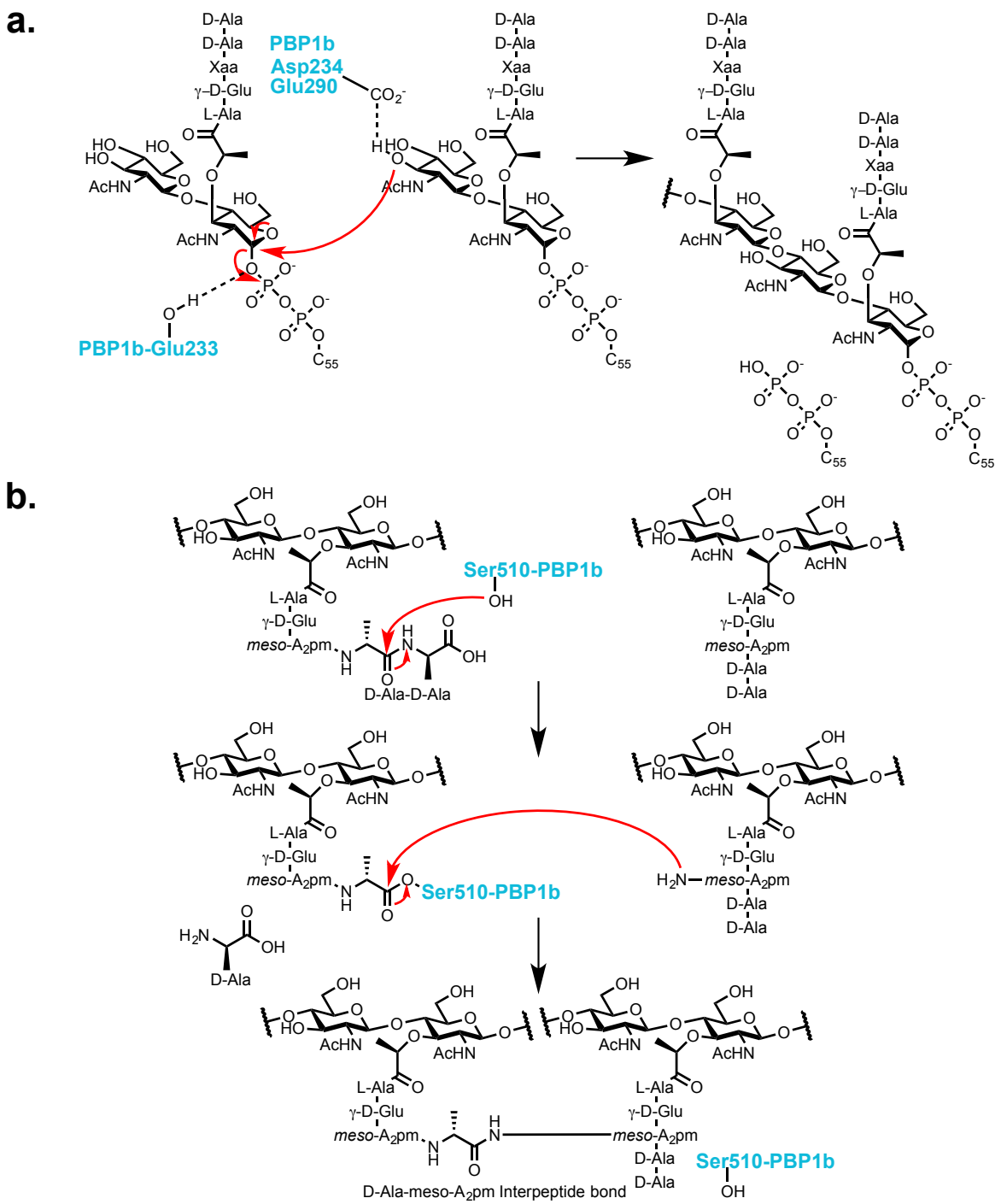


**Figure 1.14 | Transglycosylation and transpeptidation in the peptidoglycan biosynthesis.** [121,125,127-131] A general representation of the prokaryotic system, based on the *E. coli* PBP1b. Transglycosylation and transpeptidation are performed by PBPs. PBPs exist as an individual enzyme that carries out one of the two processes, or as a bifunctional enzyme that carries out both of the processes, or even the recycling process. Different PGTs have been found to produce different glycan polymer lengths. A growing chain is incorporated into the pre-existing peptidoglycan after endopeptidation by PBPs with endopeptidase functionality. **(a)** The proposed mechanism for the glycosylation of lipid II. Monofunctional PGTs perform a similar transglycosylation. Either Asp234 or Glu290 is responsible for the activation of the C4 hydroxyl

group. The reaction follows an $S_N2$ displacement that leads to the inversion at C1 of lipid II from α-configuration to β-configuration. The elongation process can occur either to a growing chain or by transferring of the lipid II to C4 of GlcNAc at the non-reducing end. **(b)** The proposed mechanism for the transpeptidation of lipid II. The serine residue is highly conserved in the transpeptidase domain and is the main target of β-lactam antibiotics.

### 1.2.1.2 Inhibitors of the Peptidoglycan Biosynthetic Pathway

The introduction of antibiotics has revolutionised the practice of modern medicine and treatment of infectious diseases, and has hugely improved human health. The peptidoglycan being uniquely present in bacteria and absent in mammalian cells, makes its biosynthesis amongst the most attractive antibiotic drug targets. Inhibitors of the peptidoglycan biosynthetic pathway have been highly sought after since the discovery of penicillin by Alexander Fleming in 1928.[132] However, due to the short shelf life of antibiotics from short-term use and antibacterial resistance, the pharmaceutical industry has steered away from antibiotic development and ventured into more profitable long-term use drugs for chronic diseases. This resulted in a fifty year antibiotic innovation gap since the 1960s.[133] Only three new antibiotics were approved by the US Food and Drug Administration between 2005 and 2009, compared to twenty between 1980 and 1984. More recently, due to the emerging rise of antimicrobial resistance bacteria and the shortage of antimicrobial drugs in drug pipeline, many governments and pharmaceuticals have now refocused on antibiotic regulations, research and development, and finding alternatives to antibiotics.[134-136]

Undoubtedly, peptidoglycan biosynthesis has been the most valuable target for modern day antibiotic development. In theory, every step in the pathway has the potential for drug target development. Unfortunately in practice, only few steps in the pathway are

targeted by clinical antibiotics largely due to many natural products also being toxic to humans or displaying poor absorption and pharmacokinetic properties. The β-lactam class of antibiotics, including penicillin, remains the most widely used antibiotics for the treatment of bacterial infections. **Table 1.2** lists some of the peptidoglycan biosynthesis and cell wall inhibitors known to date.

**Table 1.2 | Inhibitors of Peptidoglycan Biosynthesis and Cell Wall.**[25,85,92,127,137-152]

| Inhibitors | Target and Mode of Action |
|---|---|
| Fosfomycin▽ | Blockade of UDP-GlcNAc-*eno*lpyruvate biosynthesis by inactivating MurA |
| Fosmidomycin▽ | Blockade of isoprenoid biosynthesis in the non-mevalonate pathway |
| D-Cycloserine▼ | Blockade of UDP-MurNAc-pp biosynthesis by mimicking D-Ala used in Alanine racemase and D-Ala-D-Ala ligase reactions |
| Liposidomycins*<br>Tunicamycins*<br>Strepoviridins*<br>Corynetoxins*<br>Caprazamycins*<br>Muraymycins*<br>Capuramycin*<br>Mureidomycins†<br>Pacidomycins†<br>Napsamycins† | Blockade of lipid I biosynthesis by preventing MraY translocase reaction |
| Vancomycin‡<br>Teicoplanin‡¶ | Blockade of peptidoglycan biosynthesis by preventing penicillin binding proteins transpeptidase and glycosyltransferase reactions *via* non-covalent interaction with D-Ala-D-Ala tail of UDP-MurNAc-pp |
| Moenomycins☆ | Blockade of peptidoglycan biosynthesis by mimicking lipid II used in peptidoglycan glycosyltransferases reactions |
| Nisin§<br>Epidermin§ | Disruption of bacterial cell membrane integrity by first interacting with lipid II and then forming a pore in the membrane |
| Mersacidin#<br>Actagardine# | Blockade of peptidoglycan biosynthesis by binding to lipid II and then preventing penicillin binding proteins transpeptidase and glycosyltransferase reactions |
| Daptomycin¶ | Disruption of Gram-positive bacterial cell membrane potential by forming a pore complex with calcium ions |
| Ramoplanin⊹<br>Mannopeptomycins‡<br>Katanosin✦<br>Plectasin✳ | Blockade of peptidoglycan biosynthesis by binding to lipid II |
| Amphomycin¶<br>Friulimicin¶ | Blockade of undecaprenyl-phosphate biosynthesis by forming a calcium ion complex with $C_{55}$-P |
| Bacitracin✧ | Blockade of undecaprenyl-diphosphate recycling in the periplasm by forming a zinc-dependent complex with $C_{55}$-PP |

| | |
|---|---|
| Penicillins★<br>Cephalosporins★<br>Monobactams★<br>Carbapenems★<br>Doripenem★<br>Ceftobiprole★<br>Meticillin★ | Blockade of peptidoglycan biosynthesis by inactivating penicillin binding proteins transpeptidases |
| Polymyxin✧ | Disruption of Gram-negative bacterial outer membrane integrity by binding to lipid A |

▽Phosphonic acid antibiotic; ▼Analogue of D-Ala; *Nucleoside antibiotic; †Uridylpeptide antibiotic: a polypeptide with core structure of a 3'-deoxyuridine nucleoside attached *via* a 4',5'-enamide linkage to an *N*-methyl 2,3-diaminobutyric acid residue; ‡Glycopeptides: glycosylated cyclic or polycyclic non-ribosomally peptides and comprises some non-proteinogenic amino acids; ¶Lipopeptide antibiotic: a peptide consists of a lipid chain; ☆Phosphoglycolipid antibiotic; §Type A lantibiotic: post-translationally modified, ribosomal-synthesised peptides that are flexible, elongated, amphipathic molecules; #Type B lantibiotic: post-translationally modified, ribosomal-synthesised peptides that are rigid and globular in shape; ✣Glycolipodepsipeptide: a glycopsylated and lipid containing peptide with ester group in place of the amide group; ✦Cyclic depsipeptide: a peptide with ester group in place of the amide group; ✳Defensin: a cysteine-rich cationic protein; ✧Polypeptide antibiotics; ⋆β-lactam: a molecules with a core structure of a four-membered ring with nitrogen attached to the β-carbon of a carbonyl group.

#### 1.2.1.2.1 Bacterial Resistance Mechanisms to Antibiotics

Bacteria are sophisticated and diverse microorganisms that can adapt to changing and hostile environments, including threats like antibiotics. That is to say, not surprisingly, bacteria have adapted ways to combat antibiotics and become resistant. The rise in antibiotic resistance bacteria is a global catastrophe, which mainly the result of poor surveillance and misuse of antibiotics. According to the Centers for Disease Control and Prevention, there were 400% more deaths partly due to intestinal infections caused by resistant *Clostridium difficile* strains in 2007 than in 2000 in the United States.[153] Furthermore, the World Health Organisation reported close to a 650% increase of multi-drug resistant tuberculosis in Africa with 18,146 cases in 2012 compared to 2,445 cases in 2005.[154]

Bacteria manifest resistance, or multi-resistance, to antibiotics by inheriting resistance genes coding for enzymes which destroy or modify antibiotics. Alternatively, bacteria can respond by modifying their cell wall to prevent antibiotics from entering the

cell, mutating their enzymes to prevent antibiotics from binding, or pumping the antibiotics out of the cell.[155,156] Moreover, antibiotics that target one peptidoglycan biosynthetic pathway may not work in all bacteria due to differences in the bacterial cell structure and internal biological processes. While much is already known about the process of peptidoglycan biosynthesis, there remains more to explore and understand about bacteria and thus there is still the potential for antibiotic drug development *via* new strategies for tackling bacterial virulence. **Table 1.3** summarises the known mechanisms of resistance that bacteria have developed and the antibiotics that are affected, and **Fig. 1.15** highlights a few of the common modes of action by the current clinical antibiotics and their resistance mechanisms by bacteria.

A point that is often overlooked is that bacterial resistance has been a known phenomenon since the use of penicillin.[157] In recent reports, speculations point toward the innate resistance by the majority of bacteria, *i.e.,* microorganisms have constant competitive/survival mechanisms with each other and there are pre-existing resistance genes.[158] Considering that the majority of antibiotics originated as secondary metabolites from microorganisms, and there remains many unknowns regarding their actual role in nature and the symbiotic relationship that exists between humans and bacteria. It questions whether ‘anti’-bacterial approaches are the best method in tackling bacterial virulence.[159] Surprisingly, despite our overuse of antibiotics, the relationship between antibiotics and bacteria in the natural environment remains poorly understood.

**Table 1.3 | Bacterial resistance mechanisms.***[155,156,160-162]

| Strategy | Mechanism of Resistance | Antibiotics affected |
|---|---|---|
| Hydrolysis | Inactivating the antibiotic by degrading the chemical structure (β-lactamases, C-O lyases, epoxide hydroxylase) | Penicillins, cephalosporins, penems, monobactams, erythromycin, azithromycin, synercid, fosfomycin |
| Group transfer | Inactivating antibiotics by:<br>Phosphorylation<br>Acetylation<br>Nucleotidylation<br>ADP-ribosylation<br>Monooxygenation<br>Glycosylation<br>Glutathione/thiol transfer | Gentamicin, streptomycin, spectinomycin, erythromycin, azithromycin, clindamycin, synercid, chloramphenicol, ciprofloxacin, rifampin, rifamycin, fosfomycin, tunicamycin |
| Efflux | Up-regulation or presence of protein pumps capable of expelling antibiotics from the cell | Penicillins, cephalosporins, penems, monobactams, gentamicin, streptomycin, spectinomycin, erythromycin, azithromicin, clindamycin, synercid, linezolid, chloramphenicol, ciprofloxacin, trimethoprim, sulfamethoxazole, rifampin, colistin, fluoroquinolones, bacitracin |
| Target alteration | Mutation/modification of target site preventing interaction with the antibiotic, up- or down-regulation of target/affected protein to dilute the damage of the antibiotics, or producing pathways to avoid interaction | Penicillins, cephalosporins, penems, monobactams, gentamicin, streptomycin, spectinomycin, erythromycin, azithromicin, clindamycin, synercid, linezolid, chloramphenicol, ciprofloxacin, trimethoprim, sulfamethoxazole, rifampin, daptomycin, colistin, vancomycin, tunicamycin |
| Peptidoglycan response | Reprogramming the peptidoglycan, *e.g.*, increase in thickness of the cell wall | Vancomycin, teicoplanin |

*The antibiotics listed target RNA and DNA replications, cellular metabolism, protein synthesis, peptidoglycan or cell membrane. Bacteria can acquire and pass on plasmids that encode proteins to combat threats like antibiotics, or respond in stressful situations by initiating cellular stress response or induce mutation under extended exposure to antibiotics. Plasmids can encode for proteins to carry out hydrolysis, group transfer, or efflux resistance mechanisms. The exchange of plasmid can occur through transformation, conjugation, or transduction.

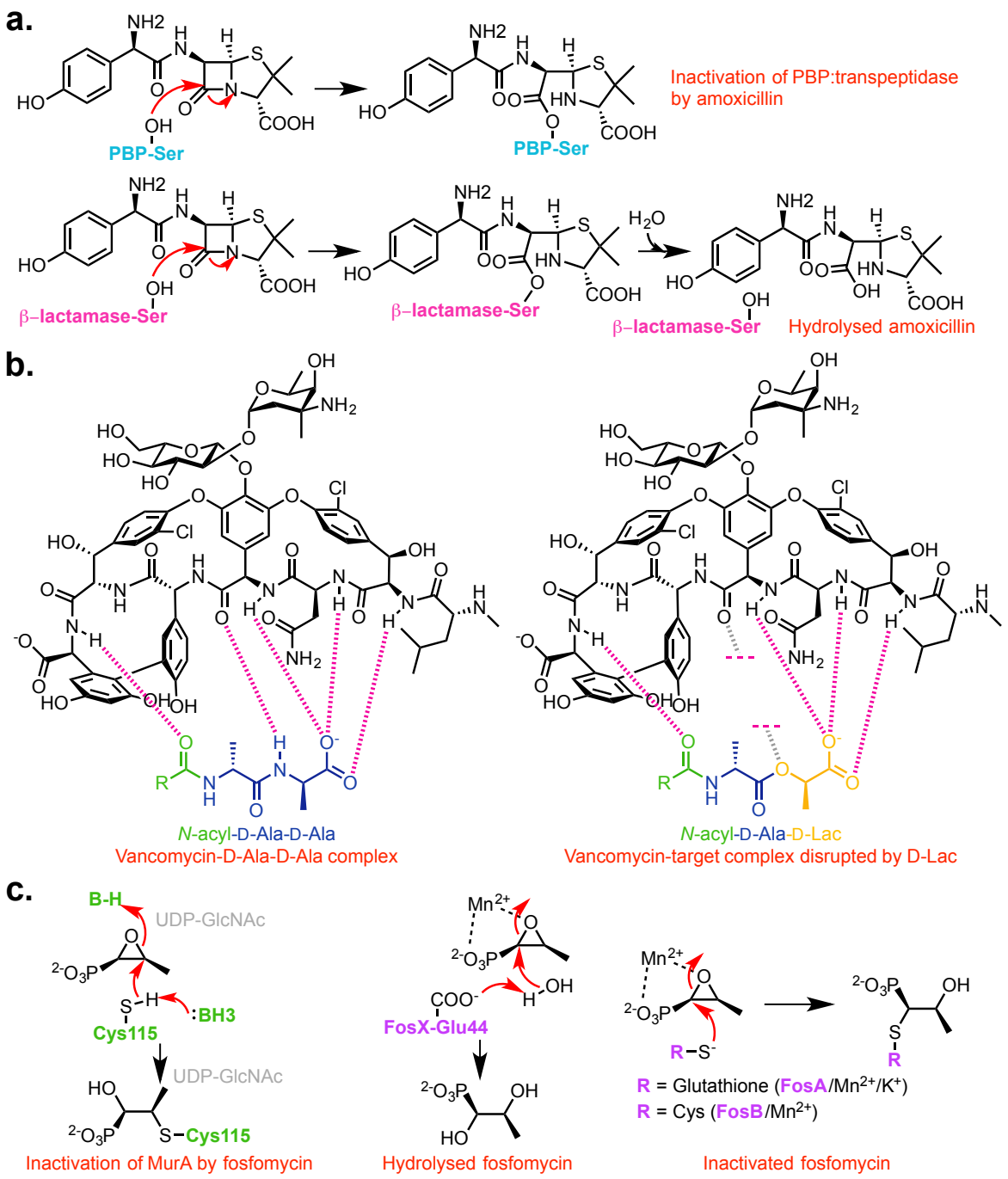


**Figure 1.15 | Examples of antibiotic actions and resistance mechanism by bacteria.** [99,140,141,155,160,161,163-167] **(a)** Inhibition of PBP:transpeptidase by a β-lactam antibiotic, amoxicillin, *via* formation of a slow hydrolysing acyl-enzyme intermediate. PBP:transpeptidase configuration limits its access to water, leading to a near dead-end complex. β-lactamase has a different three-dimensional structure that allows ready access of water and therefore inactivates the amoxicillin and regenerates the β-lactamase. **(b)** Inhibition of transpeptidation and transglycosylation on the bacterial cell wall by vancomycin. Vancomycin forms a complex with the termini peptide on the bacterial cell wall surface. Vancomycin-resistant bacteria acquires vancomycin-resistant enzymes that carry out the synthesis of the amino acid and modification of the termini peptide chain. The

modification of the termini peptide chain to D-Ala-D-Lac has been shown to disrupt the hydrogen bond of the vancomycin-target complex, which decreases the binding affinity by >1000-fold. Other vancomycin resistance mechanisms include cell wall stress response that induces thickening of the cell wall peptidoglycan to prevent vancomycin reaching its target. **(c)** Inhibition of MurA by fosfomycin. It has been proposed that fosfomycin inactivates MurA in a stoichiometric manner with natural substrates UDP-GlcNAc and PEP. PEP and fosfomycin compete with the same cysteine115 in the active site. UDP-GlcNAc facilitates in the inactivation of MurA by promoting the change of the active site conformation. Fosfomycin is inactivated by fosfomycin-resistant enzymes FosX (hydrolysis by a conserved Glu44), FosA (glutathione-transfer), and FosB (L-Cys transfer).

### 1.2.2 Polyprenol-phosphate *N*-acetylhexosamine-1-phosphate Transferases

Polyprenyl-phosphate *N*-acetylhexosamine-1-phosphate transferases (PNPTs) are an important superfamily of transmembrane enzymes responsible for the synthesis of cell envelope polymers in prokaryotes to *N*-linked glycosylation of protein in eukaryotes. MraY translocase, responsible for the biosynthesis of lipid I as previously mentioned in subsection **1.2.1.1**, is a member of this PNPTs superfamily. Others in the PNPTs family include TagO/TarO, Llm, WecA, WecP, WbpL, WbcO, RgpG, Alg7, PglF, and GPT (**Table 1.4**). They all have a common mechanistic function of carrying out the transfer of a sugar from a sugar nucleotide utilising a polyisoprenyl phosphate. However, despite their similarity in enzymatic process, they seem to be substrate selective and differ in their susceptibility to inhibitors. The reason behind the substrate discrimination is largely unknown and elusive due to difficulties in studying the PNPTs as transmembrane proteins that are notoriously fragile and problematic to express and isolate for crystallisation. However, recent gene sequence and topological analysis of the PNPTs and the exciting first crystal structure in the PNPTs family, MraY translocase from *Aquifex aeolicus*, has begun to provide some insights for their discriminative behaviour.[117,120]

PNPTs have six conserved sequences that can be found in the hydrophilic and hydrophobic domains. These suggest their possible involvement in the substrate bindings of the hydrophilic sugar nucleotide donor and hydrophobic polyprenol acceptor.[168] Correspondingly, the conserved C-terminal domain code for nucleophilic aspartic acid residues, thus implying the region as the diphosphate bond formation region. This creates five PNPTs subgroups in bacteria, based on their substrate preferences as listed in **Table 1.4**, MraY, WecA/TagO/TarO, WecP, WbcO/WbpL, and RgpG.[117,168,169] There are eukaryotic homologues Alg7 and GPT in yeast and mammalian cells, respectively, that carry out *N*-linked protein glycosylation in cells.[170,171]

The following subsections aim to describe the specific inhibitory properties of tunicamycins in relation to MraY translocase and GPT for the purpose of background information and to explain the rational behind designing the non-cytotoxic tunicamycin analogues. Additionally, a summary on TagO/TarO and WecA is also provided to broaden the scope and applications of the analogues.

**Table 1.4 | PNPTs superfamily of enzymes.**[117,168,169,171-177]

| Enzyme | Pathway | Reaction |
|---|---|---|
| MraY | Peptidoglycan biosynthesis | UDP-MurNAc-pentapeptide + undecaprenyl-phosphate ⇌ undecaprenyl-diphosphate-MurNAc-pentapeptide + UMP |
| TagO* | Polyglycerol-phosphate wall teichoic acid biosynthesis | UDP-GlcNAc + undecaprenyl-phosphate ⇌ undecaprenyl-diphosphate-GlcNAc + UMP |
| TarO† | Polyribitol-phosphate wall teichoic acid biosynthesis | UDP-GlcNAc + undecaprenyl-phosphate ⇌ undecaprenyl-diphosphate-GlcNAc + UMP |
| WecA | Enterobacterial common antigen and O-antigen biosynthesis | UDP-GlcNAc + undecaprenyl-phosphate ⇌ undecaprenyl-diphosphate GlcNAc + UMP |
| WecP | O34-antigen lipopolysaccharide biosynthesis | UDP-GalNAc + undecaprenyl-phosphate ⇌ undecaprenyl-diphosphate-GalNAc + UMP |
| WbpL‡ | O-antigen lipopolysaccharide biosynthesis | UDP-FucNAc + undecaprenyl-phosphate ⇌ undecaprenyl-diphosphate-FucNAc + UMP<br>UDP-QuiNAc + undecaprenyl-phosphate ⇌ undecaprenyl-diphosphate-QuiNAc + UMP<br>UDP-GlcNAc + undecaprenyl-phosphate ⇌ undecaprenyl-diphosphate-GlcNAc + UMP |
| WbcO‡ | O-antigen lipopolysaccharide biosynthesis | UDP-FucNAc + undecaprenyl-phosphate ⇌ undecaprenyl-diphosphate-FucNAc + UMP |
| RgpG‡ | Rhamnose-glucose polysaccharide biosynthesis | UDP-GlcNAc + undecaprenyl-phosphate ⇌ undecaprenyl-diphosphate-GlcNAc + UMP<br>UDP-FucNAc + undecaprenyl-phosphate ⇌ undecaprenyl-diphosphate-FucNAc + UMP |
| Alg7§ | N-linked glycosylation | UDP-GlcNAc + dolichol-phosphate ⇌ dolichol-diphosphate-GlcNAc + UMP |
| GPT☆ | N-linked glycosylation | UDP-GlcNAc + dolichol-phosphate ⇌ dolichol-diphosphate-GlcNAc + UMP |

**Bacillus subtilis*
†*Staphylococcus aureus*
‡Molecular basis for substrate specificity is unclear. The sugar nucleotide is based on their end product, lipopolysaccharide. In *Pseudomonas aeruginosa,* WbpL is reported as a bifunctional enzyme catalysing the FucNAc-1-P and GlcNAc-1-P transfer for A-band and B-band lipopolysaccharide biosynthesis, respectively. RgpG is reported as a WecA-Wbc hybrid.
§*Saccharomyces cerevisiae*
✢*Campylobacter jejuni*
☆Mammalian cells

### 1.2.2.1 MraY Translocase

MraY translocase[ix] is a ubiquitous bacterial protein that catalyses the synthesis of lipid I using UDP-MurNAc-pentapeptide and $C_{55}$-P, as previously mentioned in subsection **1.2.1.1.2**. The *mraY* gene can be found in all bacteria genomes sequenced to date, but not archaebacteria or eukaryotic organisms that lack peptidoglycan.[108] Interestingly, *mraY* gene orthologues can also be found in some plants.[178-180] Since MraY is responsible for the first committed membrane step in synthesising lipid I during peptidoglycan biosynthesis, any disruption of this protein or enzyme activity has been reported to cause cell stress and cell death.[181] This makes MraY an attractive antibiotic drug target since peptidoglycan is present in the majority of bacteria.[118]

MraY is a transmembrane protein with ten transmembrane α-helices. A topological model of MraY typically illustrates ten transmembrane α-helices with five cytoplasmic loops and four periplasmic loops (**Fig. 1.16**).[182] Both the N-terminal and the C-terminal ends face the periplasm.

[ix] Also known as MraY transferase or translocase I.

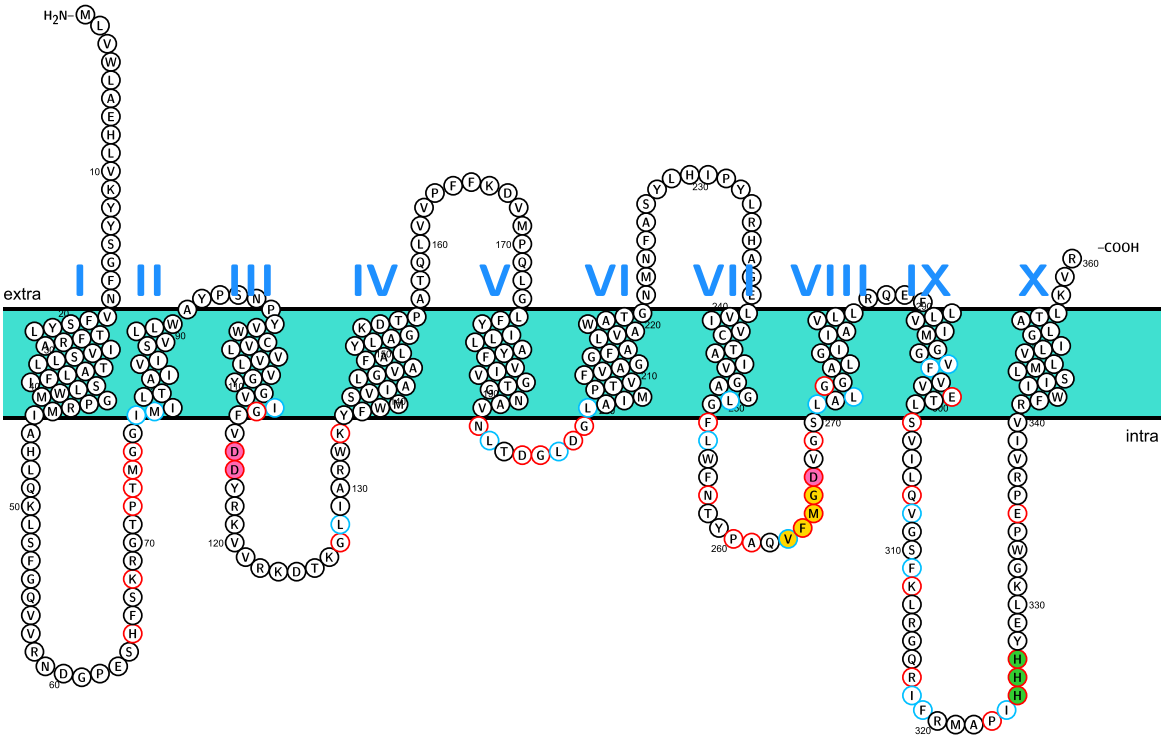


**Figure 1.16 | A common two-dimensional topological model of MraY.**[108,182,183] Topology model of MraY, predicted by Protter, based on *E. coli* K12 $MraY_{EC}$ amino acid sequence. Sequence alignment of MraY from various sources have identified conserved sequences in the cytoplasmic loops. The cytoplasmic loops II, III, and IV are proposed to be involved with the substrate binding, and cytoplasmic loops I and V are involved in the sugar nucleoside recognition. Red circle: conserved residue by identity. Blue circle: conserved residue by similarity. Pink: aspartic residues 115, 116, 267. Yellow: VFMGD sequence. Green: HHH motif.

The enzymatic activity for MraY was first demonstrated in 1965. It is reported to be dependent on the presence of both mono- and divalent metal ions such as $K^+$, $Na^+$, $Rb^+$, $Cs^+$, $Mg^{2+}$, and $Mn^{2+}$.[108] However, the molecular basis for the enzymatic mechanism and substrate interactions are still not well understood.[184,185] Mutagenic studies and functional characterisation of *E. coli* MraY have found that Asp115, Asp116, and Asp267 located in the cytoplasmic loop are vital catalytic residues in the enzymatic process.[116,117,182] Asp115 and Asp116 are proposed to be involved in $Mg^{2+}$ chelation, while the Asp267 is proposed to be the nucleophilic residue in the active site. As shown in **Fig. 1.13**, MraY is more likely to follow a two-step mechanism than an one-step mechanism based on the exchange of

radiolabelled UMP of UDP-MurNAc-pp and the release of the intermediate phospho-MurNAc-pentapeptide upon inhibition by dodecylamine.[107,108,110-114,116-120] Furthermore, MraY has been shown to be specific for the MurNAc moiety of UDP-MurNAc-penta-peptide but with low tolerance in the variability of the pentapeptide.[108,117,168] This reflects the variation of the peptide units that exists in the peptidoglycan between bacteria, as shown in **Table 1.1**. *In vitro*, MraY has also been shown to accept shorter polyprenyl phosphates, despite $C_{55}$-P being the natural substrate in bacteria. However optimal activity is observed for polyprenyl phosphates bigger than $C_{35}$.[108] This may be due to the possible interaction of the polyprenyl phosphate with the lipid membrane and with MraY. A molecular basis for the enzymatic reaction has been proposed and is shown in **Fig. 1.17**.

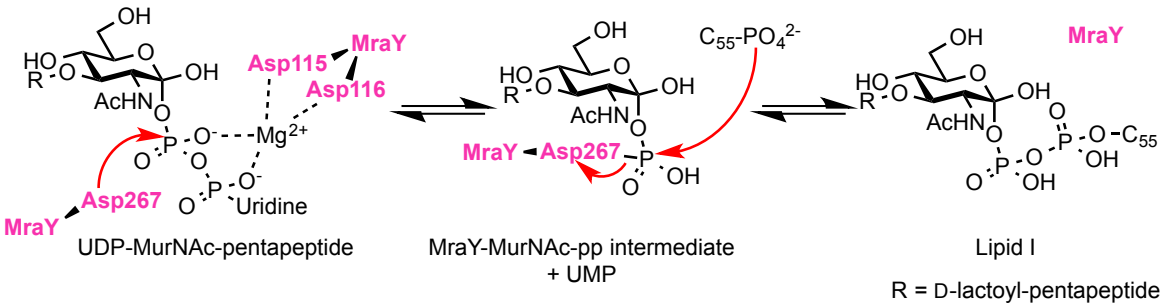


**Figure 1.17 | The proposed two-step catalytic mechanism by MraY.**[116,117,186] In *E. coli*, the first step involves Asp115 and Asp116 chelated to a cationic divalent $Mg^{2+}$ with the negatively charged diphosphate of UDP-MurNAc-pp. This promotes the nucleophilic attack of the phosphate by Asp267 followed by the liberation of UMP, and the formation of a the MraY-phospho-MurNAc-pp intermediate. In the second step, the hydroxyl group of the undecaprenyl phosphate attacks the phosphate regenerating the enzyme. The resulting product is lipid I.

Due to the nature of MraY as a transmembrane protein, active MraY sample has mainly been extracted from the bacterial cell membranes of micrococci, *S. aureus,* or *E. coli* using detergents such as Triton X-100 or CHAPS. The detergent-solubilised MraY is found to require the addition of phospholipids such as phosphatidyl choline, dioleoyl-

phosphatidyl choline, or phosphatidylglycerol for enzyme activity.[108] However, having to use partially purified protein can lead to ambiguity in results from unknown contaminants. The first time MraY was purified to homogeneity was by Bouhss *et al*. in 2004.[107] Subsequently a cell-free expression system was devised by Yi *et al*. in 2011.[187] An array of assays have been developed to study MraY enzyme and inhibition activity, including fluorescent or radiolabelled substrates, thin-layer chromatography, and HPLC. However, there are some differences in observed enzymatic activity between the assays and also in using either partially purified MraY from membrane extract or purified MraY.[108,188-192]

More recently, the first crystal structure of a MraY from *Aquifex aeolicus* ($MraY_{AA}$) **(Fig. 1.18)** was solved by Chung *et al*.[120] It is also the first crystal structure solved in the PNPTs superfamily. This has finally allowed the overlapping of previous mutagenic and functional characterisations to a three-dimensional plane. It was shown that $MraY_{AA}$ forms a dimer in detergent micelles and the membrane, which was also indicated in a two-hybrid study in *Caulobacter crescentus* reported by White *et al*., and has a topology consistent with previous predictions.[182,193] For functional studies, Chung *et al*. mutated the conserved Asp117, Asp118 and Asp265 residues, and His324, His325 and His326 residues that did not appear to influence the structure of the active site. Consistent with previous findings, mutation of the three Asp residues nearly abolished enzyme activity. Interestingly, mutation of His324 had a similar effect. This demonstrated that Asp117, Asp118, Asp265 and His324 residues in $MraY_{AA}$ are important for catalysis. Furthermore, they investigated the $Mg^{2+}$ chelation site by anomalous scattering studies. The $Mg^{2+}$ chelation site has been predicted as the Asp115 and Asp116, in *E. coli*, but it has also been questioned as other mutational studies shown it not to be the case.[116,119] In

anomalous scattering studies with $Mn^{2+}$ co-crystallised crystals, surprisingly, $Mn^{2+}$ was revealed to interact with Asp265 and not Asp117 and Asp118. But given that native crystal data had unassigned density peaks at the active site, the metal chelation site is still uncertain. Moreover, the nucleotide sugar binding site predicted from conserved sequences in the PNPTs superfamily in the cytoplasmic loop V was investigated. The cytoplasmic loop V, or cytoplasmic loop E, contains a highly conserved triple histidine, HHH motif, and anomalous scattering studies found two $Ni^{2+}$ ions present (**Fig. 1.18k**). One $Ni^{2+}$ coordinated to His324 and His325, while the other coordinated to His326 and Glu328. Full activity of MraY was observed in the presence of both $Mg^{2+}$ and $Ni^{2+}$, suggesting the importance of metal coordination at the nucleotide sugar binding site. The $MraY_{AA}$ crystal structure supports the proposed Asp117[x] involvement in the deprotonation of the hydroxyl moiety of $C_{55}$-P, based on the residues, Lys121, Lys133, and Asp265, and $Mg^{2+}$ around the active site.[119] In addition, the most revealing aspect from the $MraY_{AA}$ crystal structure is the physical presence of an inverted-U-shaped groove at the active site that may serve as a binding pocket for the $C_{55}$-P.[120] These structural insights provide invaluable information to understand the MraY enzymatic process and allow for improved design of inhibitors.

[x] Asp115 in *E. coli* and Asp98 in *B. subtilis*.

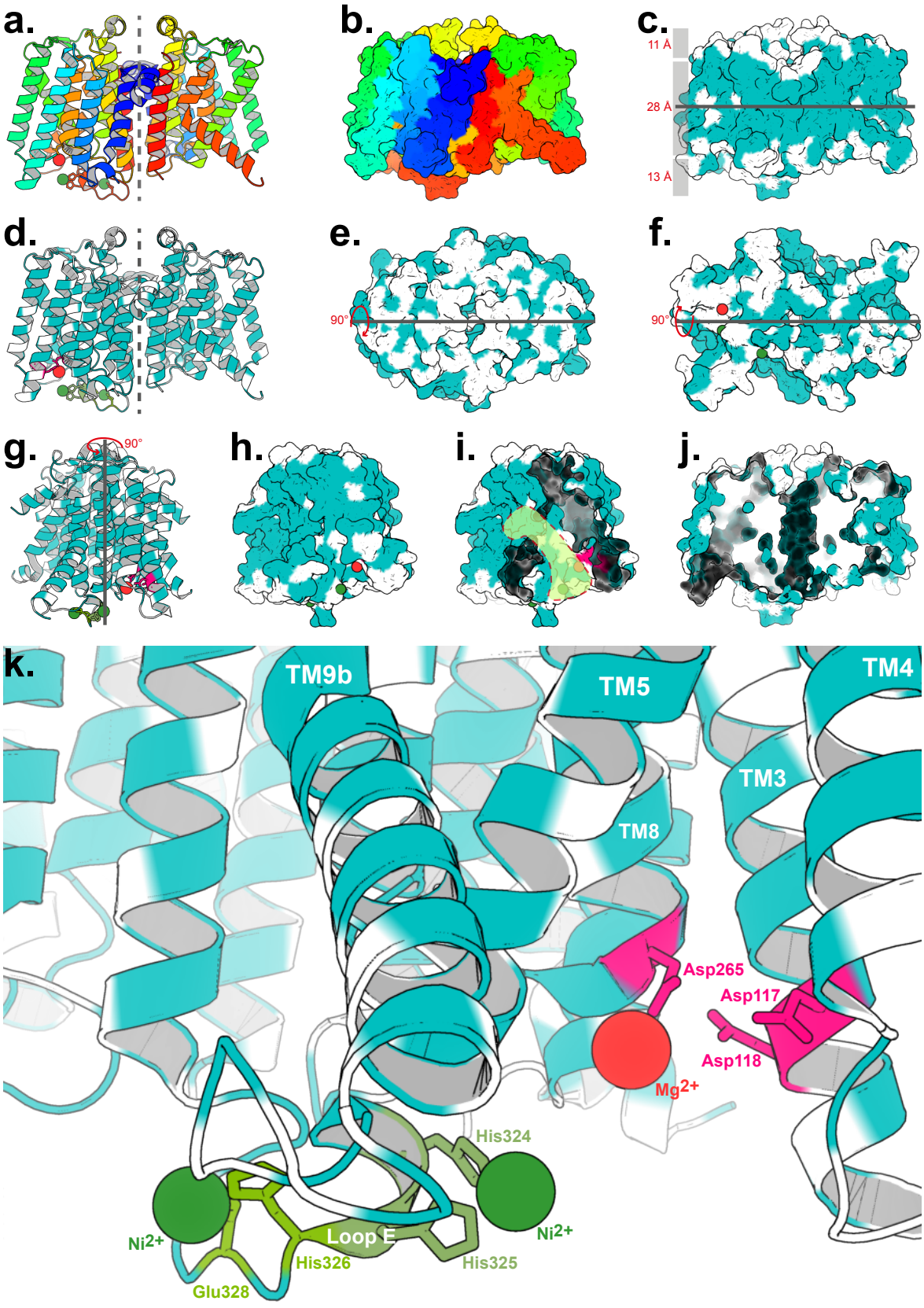


**Figure 1.18 | Crystal structures of *Aquifex aeolicus* MraY$_{AA}$.**[120] PyMOL renderings of MraY$_{AA}$. **(a)** The ribbon structure rendering of MraY$_{AA}$ dimer. The dotted line splits the dimer to show the two monomers and the transmembrane helices coloured to show each transmembrane helices in the monomer. **(b)** The surface structure rendering of MraY$_{AA}$ dimer, with each transmembrane helices

coloured. **(c)** The surface structure rendering of $MraY_{AA}$ dimer highlighting the hydrophobic amino acid residues highlighted in blue (Ala, Gly, Val, Ile, Phe, Met, Pro, Trp). **(d)** The ribbon structure rendering of $MraY_{AA}$ dimer highlighting the hydrophobic amino acid residues. **(e)** The top view of $MraY_{AA}$ surface structure. **(f)** The bottom view of $MraY_{AA}$ surface structure. **(g)** The side view of $MraY_{AA}$ ribbon structure. **(h)** The side view of $MraY_{AA}$ surface structure. **(i)** The side sliced view of $MraY_{AA}$ surface structure revealing the putative hydrophobic groove. **(j)** The sliced view of $MraY_{AA}$ surface structure revealing the oval-tunnel in the dimer that is proposed to accommodate lipids. **(k)** The $MraY_{AA}$ active site showing the divalent metals, the putative catalytic residues on TM3 and TM8 (Asp117, 118, and 265), and the HHH motif (His324, 325, and 326). $Mg^{2+}$ is found to interact with Asp265 on TM8 and two $Ni^{2+}$ are found to interact with His324, 325, 326, and Glu328 on LoopE.

#### 1.2.2.1.1 Tunicamycins Inhibit MraY Translocase *via* Substrate Mimicry

Tunicamycins were the first discovered antibiotics to inhibit the MraY.[53,194,195] Tunicamycins are reversible inhibitors, with a $K_i$ = 0.55 μM and $IC_{50}$ = 0.5 - 22 μM (0.4 - 18 μg $mL^{-1}$)[xi].[107,143,187,190] They compete with the UDP-MurNAc-pentapeptide and not with $C_{55}$-P.[143] The molecular basis for inhibition is proposed to involve the 5'- and 8'-hydroxy groups and the oxygen of the pseudo-galactopyranosyl ring that mimic the diphosphate of UDP-MurNAc-pentapeptide, and thus compete for the active site (**Fig. 1.19**).[15] The mechanism is unclear but it has been proposed that the lipid chain plays a role in cell membrane penetration, phospholipid interaction, or even possibly MraY interaction.[6,52,61,196]

[xi] A range of $IC_{50}$ value is presented but it is dependent on sample source and assay method. It is also worth to note that the reported values are based on using a mixture of the tunicamycin homologues, as mentioned in **1.2 Biological Properties of Tunicamycins**. Thus, some discrepancies may exist and possibly due to the difference in the potency of the individual homologues in different biological systems.

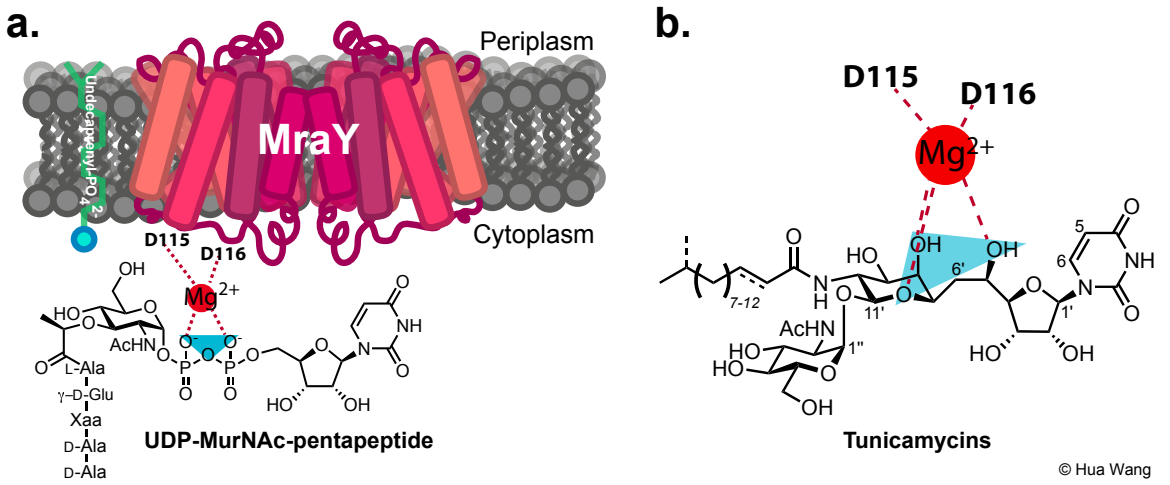


**Figure 1.19 | An illustration of the proposed UDP-MurNAc-pentapeptide and tunicamycins chelation with $Mg^{2+}$ and MraY residues Asp115 and Asp116.** In the *E. coli* system. **(a)** A cartoon illustration of the MraY dimer with Asp115 and Asp116 chelating with $Mg^{2+}$ and UDP-MurNAc-pentapeptide. **(b)** The 5'- and 8'-hydroxyl and oxygen of the pseudo-galactopyranosyl ring of tunicamycins mimic the diphosphate of UDP-MurNAc-pentapeptide, and thus compete with the metal chelation in the MraY active site.

Other known inhibitors of MraY are mainly uridylpeptide antibiotics and nucleoside antibiotics. These include strepoviridins, corynetoxins, caprazamycins, pacidomycins, napsamycins, muraymycins ($IC_{50}$ = 0.027 mg $\mu l^{-1}$), capuramycin ($IC_{50}$ = 0.017 mg $\mu l^{-1}$), liposidomycin B ($K_i$ is not determined, $K_i$* = 80 nM, $IC_{50}$ = 0.03 $\mu g$ $\mu l^{-1}$), mureidomycin A ($K_i$ = 36 nM, $K_i$* = 2.2 nM, $IC_{50}$ = 0.5 $\mu g$ $\mu l^{-1}$), A-94964, and A-102395.[108,143,197-199]. The chemical structures of the inhibitors mentioned, except for A-94964 and A-102395, are shown in **Fig. 1.5** and **Fig. 1.6**. The inhibitors are proposed to work in a similar fashion as tunicamycins, based on substrate mimicry and chelation with $Mg^{2+}$. Mureidomycin A has been found to be slow binding and competitive against both substrates, UDP-MurNAc-pentapeptide and $C_{55}$-P. Liposidomycin B is also found to be slow binding but is only competitive against $C_{55}$-P.[143] Interestingly, unlike tunicamycins that are toxic in bacteria and mammalians cells, these other inhibitors are specific inhibitors of MraY and appear to be non-toxic to mammalian cells.

Moreover, there is a unique inhibitor of MraY that has been isolated from bacteriophage ΦX174 called the bacteriolytic E protein. The E protein is a 91-amino acid protein with a transmembrane domain located at the N-terminus.[200,201] E protein is a non-competitive inhibitor and seems to require a host protein peptidyl-prolyl isomerase, SlyD, for the killing action. It has been proposed that the E protein disrupts MraY activity by forming a protein-protein interaction within the transmembrane region, possibly at helix 9, and not at the active site, preventing MraY from assembling with other membrane and membrane-associated proteins to form a highly-active protein complex during cell division.[192]

Lastly, there is another interesting protein called colicin M. Colicin M is a plasmid encoded toxin that *E. coli* synthesises and releases to kill susceptible *E. coli* and other related bacterial species. Colicin M does not act on MraY but instead enzymatically degrades undecaprenyl-phosphate linked peptidoglycan precursors such as the lipid I or lipid II products of MraY and MurG, respectively. The resulting outcome is the arrest of peptidoglycan biosynthesis and then cell lysis. This is the first example of such an inhibition mechanism of peptidoglycan biosynthesis.[202]

#### 1.2.2.2 GPT in the *N*-linked Glycosylation Pathway

*N*-Acetylglucosamine-1-phosphate transferase (GlcNAc-1-P transferase, or GPT) is an important protein encoded by the *DPAGT1* gene in mammalian cells.[172,203,204] GPT carries out the transfer of GlcNAc from UDP-GlcNAc to the lipid carrier dolichol-phosphate (Dol-P) upon the liberation of UDP to form GlcNAc-PP-Dol. This is the first committed membrane step in the *N*-linked protein glycosylation pathway on the endo-

plasmic reticulum (ER). GPT, like MraY, is a transmembrane protein with ten helices and with both the N-terminal and C-terminal ends facing the ER lumen (**Fig. 1.20**). Similar to $MraY_{AA}$, it has been proposed that GPT also exists as a dimer based on radiation, cross-linking, and mutation studies.[204-206] Unfortunately, there is no crystal structure available for GPT. Its enzymatic reaction follows the conventional PNPTs sugar nucleotide transfer to a polyprenol phosphate. Protein glycosylation is ubiquitous and a crucial biological process that affects the physiological role of proteins in eukaryotic cells. The process follows complex biological pathways in the ER and the Golgi apparatus, which have been extensively studied and comprehensively reviewed.[207-213] The following subsections highlight the biological relevance of the *N*-linked glycosylation pathway, the initial lipid-linked oligosaccharide precursor synthesis, and the proposed inhibitory mechanism of tunicamycins on GPT.

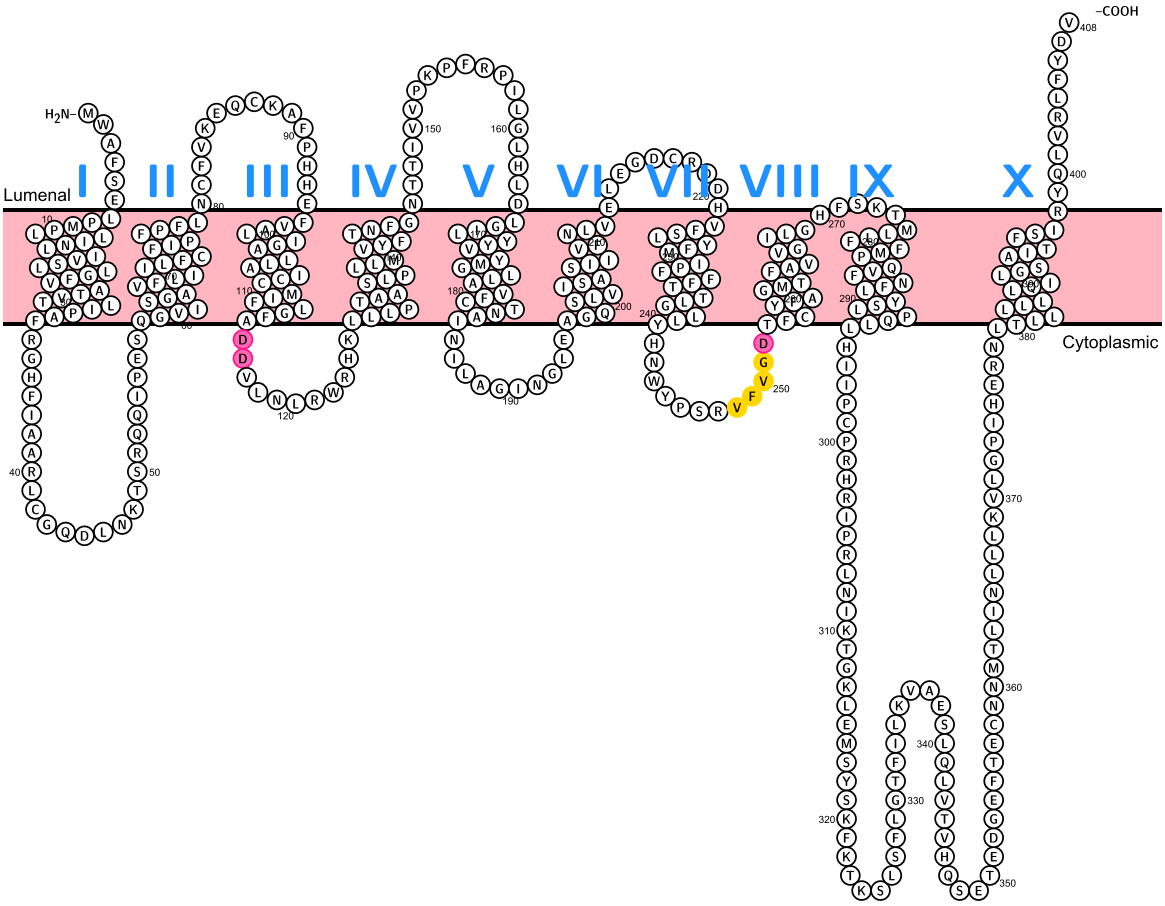


**Figure 1.20 | A two-dimensional topological model of GPT. A topology of GPT has never been published.**[183] Topology model of GPT predicted by Protter, based on *Homo sapiens* $GPT_{HS}$ amino acid sequence (UniPro: Q9H3H5, EC 2.7.8.15). Pink: putative catalytic aspartic acid residues. Yellow: the conserved VFVGD motif.

#### 1.2.2.2.1 *N*-linked Glycosylation of Proteins

Protein glycosylation adds complex glycans, or oligosaccharides, to cell surface or intracellular proteins. *N*-linked glycosylation is one of five distinct types of sugar-peptide bonds known to date that can be found in eukaryotes. Others include *O*-glycosylation, *C*-mannosylation, *P*-glycosylation, and glypiation.[207] All of these serve as a set of biological processes that impart additional information content on polypeptide structures, *i.e.*, post-translational modification. There are estimated to be >7,000 glycan structures that are assembled from ten monosaccharides: fucose (Fuc), galactose (Gal), glucose (Glc), *N*-acetylgalactosamine (GalNAc), *N*-acetylglucosamine (GlcNAc), glucuronic acid (GlcA),

iduronic acid (IdoA), mannose (Man), sialic acid (SA), and xylose (Xyl).[214] The glycans serve various roles in the biological system. Interestingly, the assembly of the glycan structure is dependent on many factors in a cell, such as enzyme abundance and localisation, the availability of glycoprotein substrates and sugar donors, and the cellular environment. Generally, glycans contribute to cellular regulation of cytosolic and nuclear functions, immune surveillance, inflammatory reactions, autoimmunity, hormone action, and tumour metastasis. The examples include function and signalling, dynamics of glycoprotein endocytosis and cell surface half-life, ligands for cell adhesion, macromolecule interaction, and pathogen invasion. The glycans on newly synthesised glycoproteins play an important and crucial role in protein secretion and mediation, protein folding, and quality control surveillance in the ER.[212,215,216] It has been postulated that *N*-linked glycans mimic molecular chaperons and promote conformational changes during protein folding, and increase protein solubility. However, this does not apply to every protein synthesis. The removal of *N*-linked glycans on some fully folded proteins does not diminish enzymatic activity, although they do become more susceptible to proteases and denaturing conditions.[64,215,217,218]

It is estimated that half of mammalian proteins are glycosylated at some point, with most being *N*-linked glycosylated.[219] *N*-linked glycosylation occurs through asparagine-linked modification of proteins *via* a specific GlcNAc-β-Asn linkage that is carried out by an ER membrane protein complex called the oligosaccharyltransferase (OST).[220] This starts from the lipid-linked oligosaccharide precursor biosynthesis of the conserved tetradecasaccharide $Glc_3Man_9GlcNAc_2$ on the cytoplasmic surface of the ER *via* the lipid carrier dolichol-phosphate (Dol-P), where the first step is carried out by GPT (**Fig. 1.21**).

The $Glc_3Man_9GlcNAc_2$-P-Dol ends up in the ER lumen. OST then transfers the $Glc_3Man_9GlcNAc_2$ glycan to the Asn-X-Ser/Thr[xii] motif on a nascent growing polypeptide chain *via* cotranslational addition.[212,218] The glycan then undergoes trimming and editing through a variety of glycosidases and glycosyltransferases on the ER and Golgi apparatus. The resulting protein-bound glycan varies in construct complexity, but are classified into three main groups: high-mannose, hybrid, and complex (**Fig. 1.22**).[211,212,218]

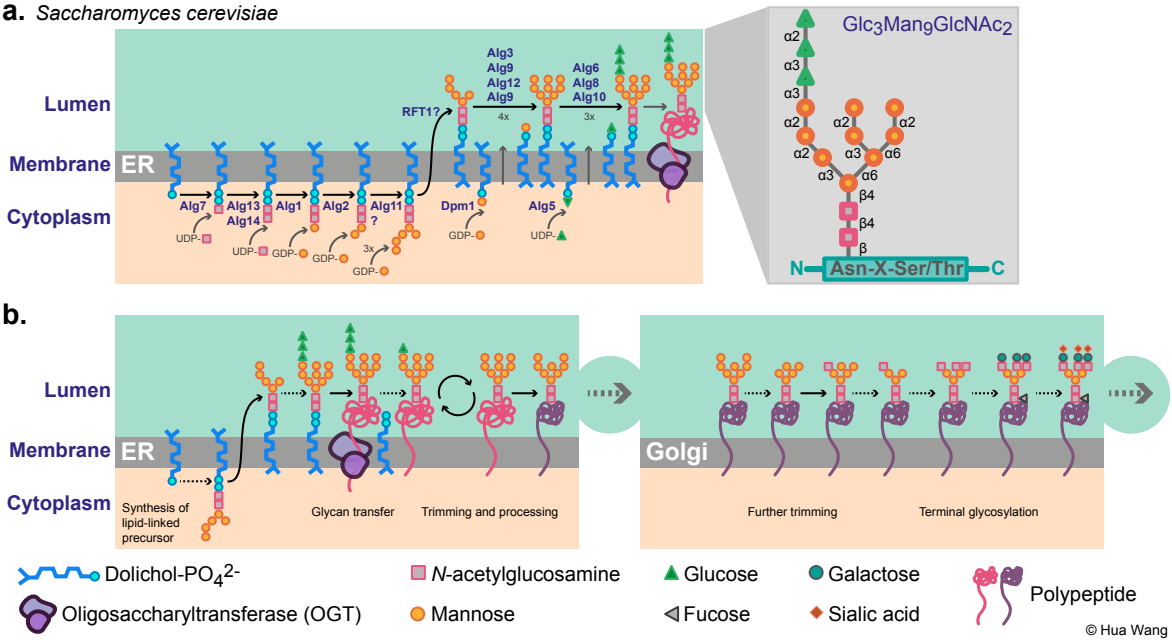


**Figure 1.21 | Lipid-linked oligosaccharide biosynthesis in the *N*-linked glycosylation pathway.**[212,218,220-222] **(a)** the lipid-linked oligosaccharide biosynthesis in *Saccharomyces cerevisiae*. The conserved $Glc_3Man_9GlcNAc_2$ scaffold biosynthesis first starts on the cytoplasmic side of the ER *via* a lipid carrier dolichol-phosphate (Dol-P). After the addition of two molecules of GlcNAc and five Man molecules on Dol-P, the heptasaccharide is flipped to the lumen of the ER where the biosynthesis towards the $Glc_3Man_9GlcNAc_2$ continues. **(b)** a example of many *N*-linked glycosylation pathway followed modification from the ER to the Golgi apparatus. The cycle in the pathway shown in the ER represents the calnexin-calreticulin cycle. The pink-coloured polypeptide represents the nascent polypeptide, and the purple-coloured polypeptide represents the folded polypeptide.

[xii] X is any amino acid except proline. Other recognition motif that is less common includes Asn-X-Cys, Asn-Gly, and Asn-X-Val.

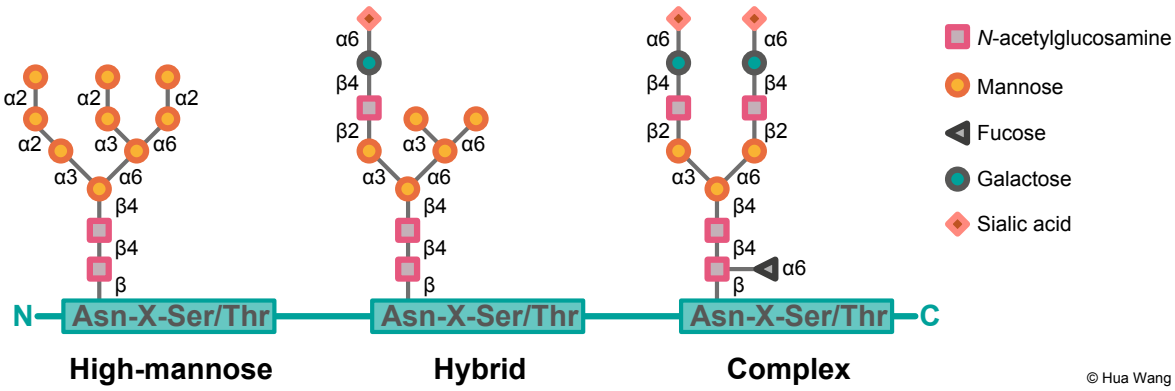


**Figure 1.22 | Structures of the three main *N*-glycans in eukaryotic cells.**[211,212,218] The pentasaccharide core, $Man_3GlcNAc_2$, is derived from $Glc_3Man_9GlcNAc_2$.

#### 1.2.2.2.2 Tunicamycins Inhibit GPT as Substrate-Product Transition-state Analogues, and Induce ER Stress Response

Naturally, due to the similarity of MraY and GPT, tunicamycins are also found to inhibit the enzymatic activity of GPT. Bioinformatic analyses show GPT to contain the conserved DDxxD $Mg^{2+}$-binding motif and the conserved VFVGD motif proposed to be part of the nucleophilic active site.[117,172,223] In fact, the binding affinity between tunicamycins and GPT is stronger compared to tunicamycins and MraY due to the substrate-product transition-state mimicry (**Fig. 1.23**). This inhibition resulting in non-glycosylation of nascent polypeptides in the cell, as mentioned previously, is the sole reason that tunicamycins are not suitable as clinical antibiotics.[15,63,224] Despite this setback, tunicamycins have been very useful as biochemical tools for studying the role of glycoproteins and the *N*-linked glycosylation pathway in biological systems.[64] In essence, tunicamycins allow the study of non-glycosylated proteins because they terminate *N*-linked glycosylation by inhibiting GPT.

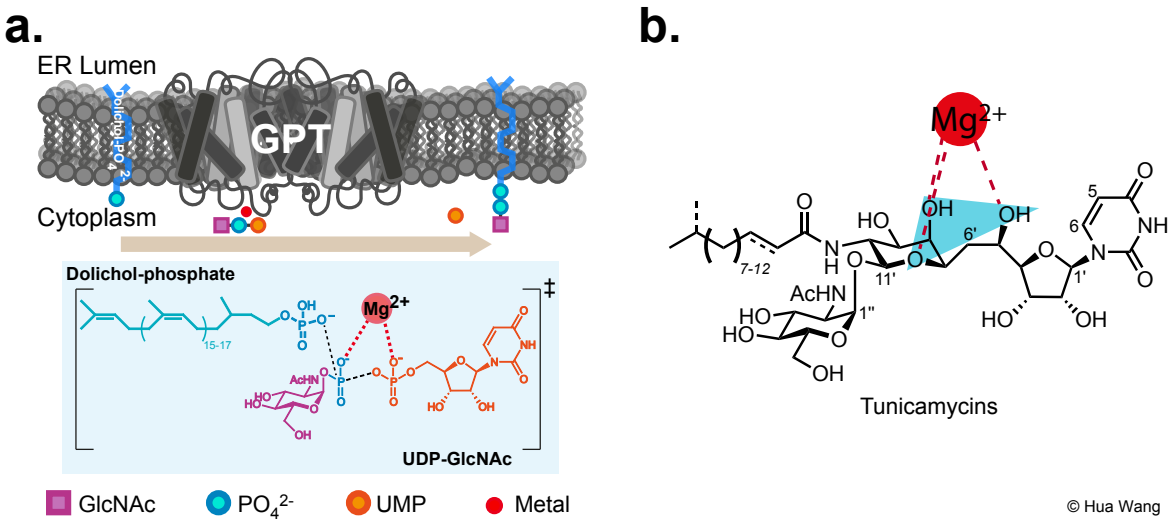


**Figure 1.23 | The proposed GPT reaction substrates in relation with tunicamycins.**[15,63,117,172] A crystal structure for GPT is not available. **(a)** the molecular basis for tunicamycin-mediated inhibition of GPT is limited due to the transmembrane nature of the protein. It is proposed to follow a double displacement mechanism involving the formation of the enzyme-substrate complex intermediate of the GPT-Asp-P-GlcNAc upon literation of UMP, followed by the displacement of GPT with dolichol phosphate. **(b)** molecular modelling and $^{1}H$ and $^{13}C$ NMR studies have shown the preferred conformation of tunicamycins where the 5'- and 8'-hydroxyl and oxygen of the pseudo-galactopyranosyl ring are proposed to mimic the diphosphate of UDP-GlcNAc.

Due to the nature of GPT as a transmembrane protein, like MraY, obtaining a pure sample has proven to be difficult. Thus, GPT is prepared as a partially purified or detergent solubilised protein from various sources, like soy bean, mung bean seedlings, yeast, pig aortas, or calf livers.[52,203,224,225] Tunicamycins are reported to act as irreversible and non-competitive inhibitors with respect to dolichol-phosphate (Dol-P) and UDP-GlcNAc. The enzymatic activity is reported to be enhanced by the addition of phospholipids like phosphatidylethanolamine, cardiolipin, or monogalactosyldiglyceride.[226] GPT activity assays use radiolabelled UDP-GlcNAc substrates to quantify the conversion into the product Dol-PP-GlcNAc. Tunicamycins inhibit GPT with an $IC_{50}$ range of 0.05 - 0.1 μg $ml^{-1}$ (0.6 - 100 nM), (the variation is due to differences in sample preparation and cell type response and

possibly the potency from each tunicamycin homologues).[64] In comparison to MraY (cf. 0.4 - 18 μg $mL^{-1}$, 0.5 - 22 μM), tunicamycins are better inhibitors of GPT. Since tunicamycins exist as homologues, each homologue has been observed to exhibit different levels of GPT inhibition in cell cultures. The mechanism is unclear but it has been proposed that the lipid chain plays a role in cell membrane penetration, phospholipid interactions, or even possibly, protein interactions.[17-19,21,52,61,64]

The inhibitors of the lipid-linked oligosaccharide biosynthesis, the ER stage of the *N*-linked glycosylation pathway, are indicated in **Fig. 1.24**. As previously mentioned, glycans on newly synthesised glycoproteins influence protein secretion and mediation, protein folding, and quality control surveillance in the ER. A halt in the *N*-glycosylation pathway can lead to a wide range of cellular regulatory responses. Furthermore, in addition to blocking the *N*-linked glycosylation, they have also been reported to induce apoptosis and inhibit protein synthesis.[227-229] The mechanism by which these occur is unclear, but may be the result of a cellular regulatory response that up-regulates apoptotic proteins or stops the production of non-glycosylated proteins. The result of non-glycosylated proteins and therefore misfolded proteins would then cause ER stress. This activates signal transduction pathways within the cell, which are cumulatively called the Unfolded Protein Response (UPR). The UPR is a mechanism that serves to maintain the homeostasis in the cell (**Fig. 1.25**).[230-233] The UPR is also associated with a wide range of diseases such as Parkinson's disease, Huntington's disease, diabetes, obsesity, ischaemia, prion-related disorder, retinal degeneration, retinas pigmentosa, glaucoma, amyotrophic lateral sclerosis, excitotoxicity, and cancer. It is uncertain, however, whether the UPR in cancer cells is pro- or anti-oncogenic.[234] In essence, tunicamycins can be extremely valuable biochemical

tools in disease research. Implications of such potential applications should be considered when designing tunicamycin analogues.

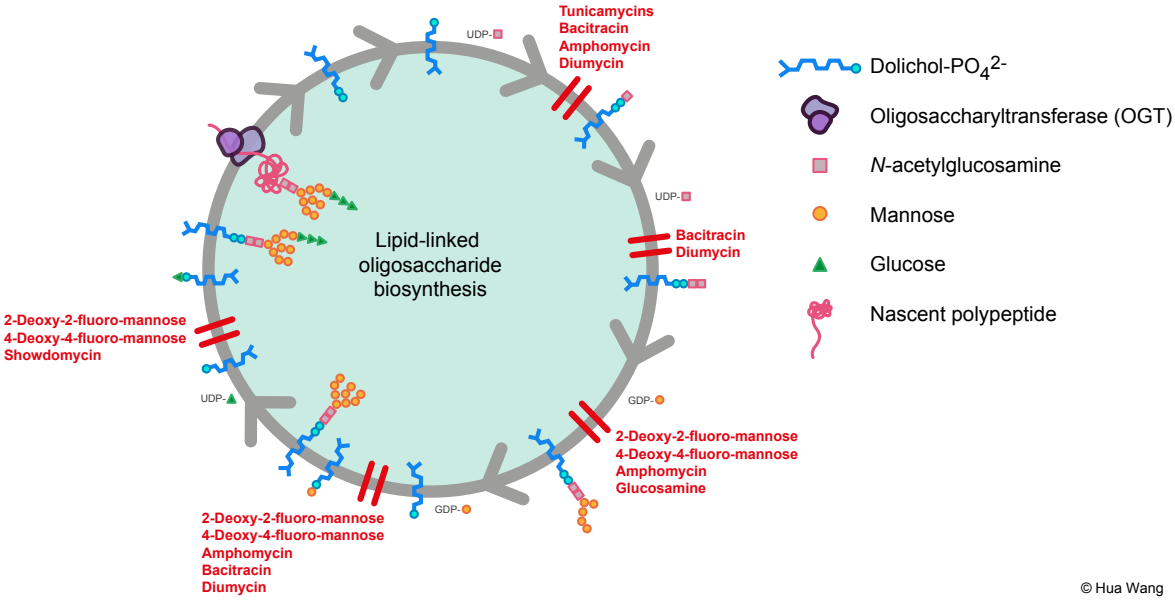


**Figure 1.24 | Inhibitors of the lipid-linked oligosaccharide biosynthesis.**[235] The inhibitors are shown in red.

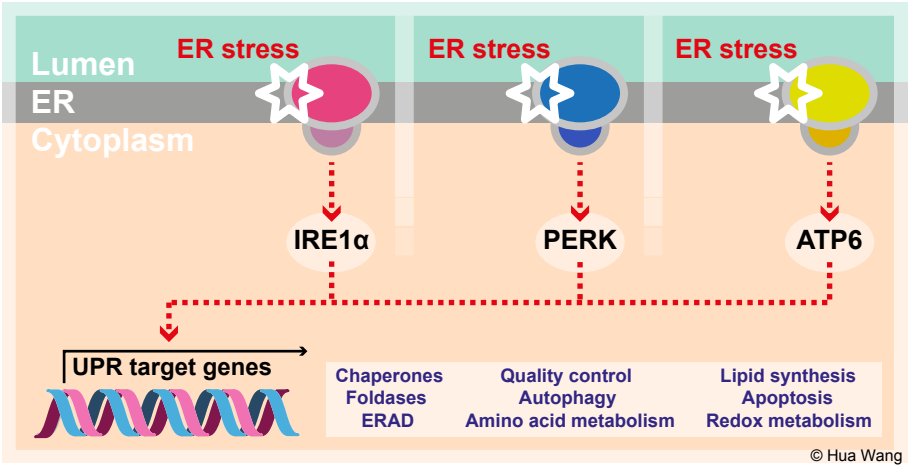


**Figure 1.25 | The unfolded protein responses.**[230,231] There are three distinct unfolded protein responses (UPR), and each pathway ultimately induces the transcription of one of several UPR target genes that intends to overcome the cellular stress.

### 1.2.2.3 Tunicamycins Inhibit TagO/TarO as Substrate-Product Transition-state Analogues

Tunicamycins have also been found to inhibit TagO/TarO, a member of the PNPTs superfamily, found in Gram-positive bacteria.[236,237] TagO/TarO is a transmembrane protein that catalyses the first membrane step in the wall teichoic acid (WTA) biosynthesis. It utilises UDP-GlcNAc and undecaprenyl-phosphate ($C_{55}$-P) in the presence of a divalent metal, $Mg^{2+}$, to form undecaprenyl-diphosphate-GlcNAc ($C_{55}$-PP-GlcNAc) upon the liberation of UMP.[238,239] Similarly to MraY, TagO in *B. subtilis* has been suggested to form a multi-enzyme complex with the peptidoglycan-synthesis machinery.[240,241] There is not a crystal structure available for TagO/TarO, but the molecular basis for the enzymatic reaction is proposed to follow a similar reaction mechanism to MraY. Tunicamycins have been found to inhibit TagO/TarO at lower concentrations than MraY.[236,242] This may be because tunicamycins have more resemblance to the natural substrate UDP-GlcNAc than UDP-MurNAc-pp due to the GlcNAc moiety.[238] The tunicamycins inhibition mechanism is proposed to be similar to the inhibition mechanism of the MraY translocase and GPT systems due to the similarity of their substrates.

Both the names, TagO and TarO, have been used in the literature to refer to the first membrane enzyme step in the Wall Teichoic Acid (WTA) biosynthesis in Gram-positive bacteria. This has caused some confusion. For clarification, there are two types of WTA (**Fig. 1.26a**). WTA is an anionic polysaccharide polymer of glycerol phosphate or ribitol phosphate that is covalently attached to the *N*-acetylmuramyl unit in the peptidoglycan. In most *B. subtilis*, WTA contains polyglycerol phosphate (poly-GroP). The name TagO is used in the *B. subtilis* WTA biosynthetic pathway. In most *S. aureus*, WTA contains poly-

ribitol phosphate (poly-RboP). The name TarO is used in the *S. aureus* WTA biosynthetic pathway (**Fig. 1.26b**).[176,177,238]

WTA is one of two essential polymers in Gram-positive bacteria, with the other being the well-characterised peptidoglycan. WTA contributes to the Gram-positive bacterial cell wall integrity, anchoring of surface proteins, biofilm development, autolysin regulation, cell adhesion, antibiotic resistance, and cell division.[243-245] Moreover, WTA is proposed to also act as a phosphate reservoir and in cation homeostasis. In *S. aureus*, WTA is implicated in virulence.[177,246] Due to the importance of WTA to Gram-positive bacteria physiology, it creates another avenue for antibiotic development. Currently, there is no clinical drug that targets WTA biosynthesis.[245] Thus designing tunicamycin analogues that can also target TagO/TarO broadens their applicability not just as antibiotics but also as chemical probes to study WTA biosynthesis and its role in Gram-positive bacteria.

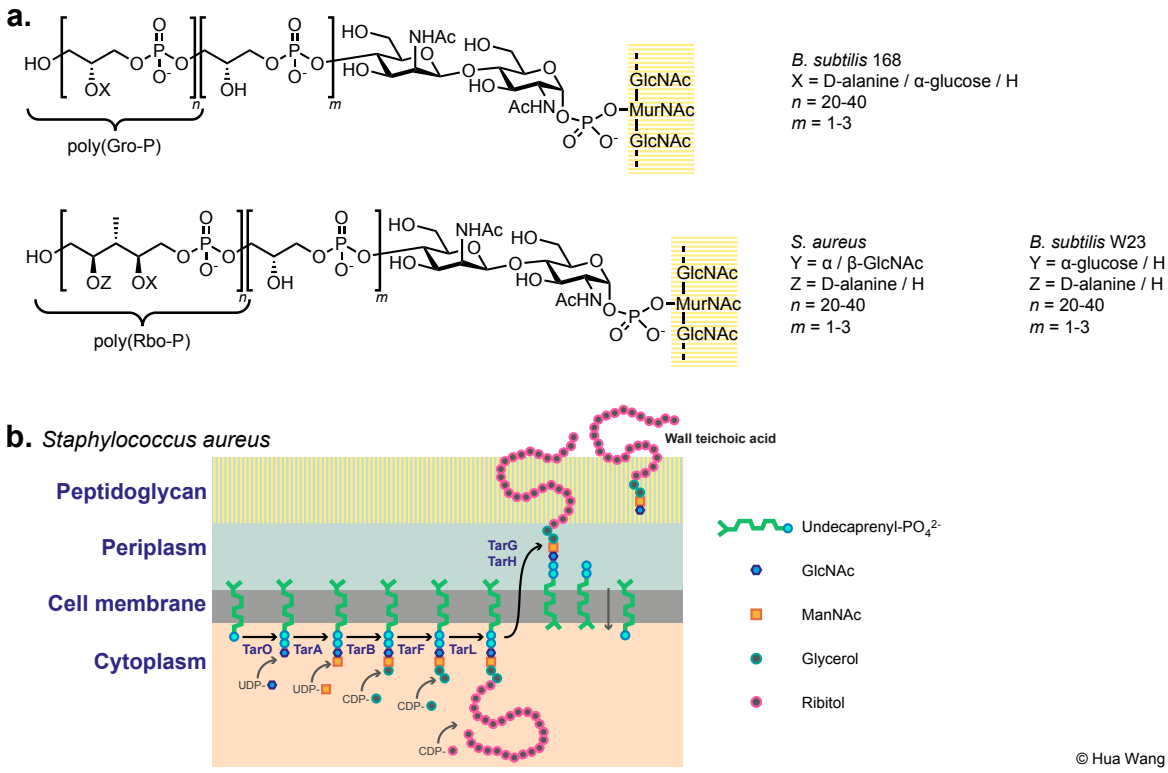


**Figure 1.26 | Wall teichoic acid.**[238] **(a)** chemical structures of polyglycerol phosphate (poly-GroP) and polyribitol phosphate (poly-RboP). **(b)** the membrane stages of the wall teichoic acid biosynthetic pathway in *S. aureus*.

### 1.2.2.4 Tunicamycins Inhibit WecA as Substrate-Product Transition-state Analogues

Tunicamycins are also found to target WecA, a member of the PNPTs superfamily, an enzyme found in Gram-negative bacteria. WecA is a transmembrane protein, having 11 transmembrane α-helices with the C-terminal end facing the cytoplasm (**Fig. 1.27**).[247] In *E. coli*, $WecA_{EC}$ catalyses the first membrane step of the synthesis of bacterial polymers such as O-antigen and enterobacterial common antigen in Gram-negative bacteria. WecA, like TagO/TarO, carries out the transfer of phospho-GlcNAc from UDP-GlcNAc *via* lipid carrier undecaprenyl-phosphate ($C_{55}$-P) in the presence of $Mg^{2+}$ or $Mn^{2+}$, to form undecaprenyl-diphopshate-GlcNAc ($C_{55}$-PP-GlcNAc) upon the liberation of UMP.[247] $C_{55}$-PP-GlcNAc is the precursor to O-antigen and enterobacterial common antigen. In *Mycobacterium*, the lipid carrier is decaprenyl-phosphate ($C_{50}$-P) ($WecA_{Myco}$ EC 2.7.8.33).[248]

There is not a crystal structure available for WecA, but the molecular basis for the enzymatic reaction is proposed to follow a similar reaction mechanism as with the PNPTs superfamily of enzymes. The tunicamycins inhibition mechanism is proposed to be similar to the inhibition mechanism of MraY translocase, GPT, and TagO/TarO systems, as previously described. In fact, tunicamycins are reported to be a better inhibitor of WecA, with $IC_{50}$ = 11 nM. This may be, like GPT and TagO/TarO, because tunicamycins have more resemblance to UDP-GlcNAc than UDP-MurNAc-pentapeptide.[223,247]

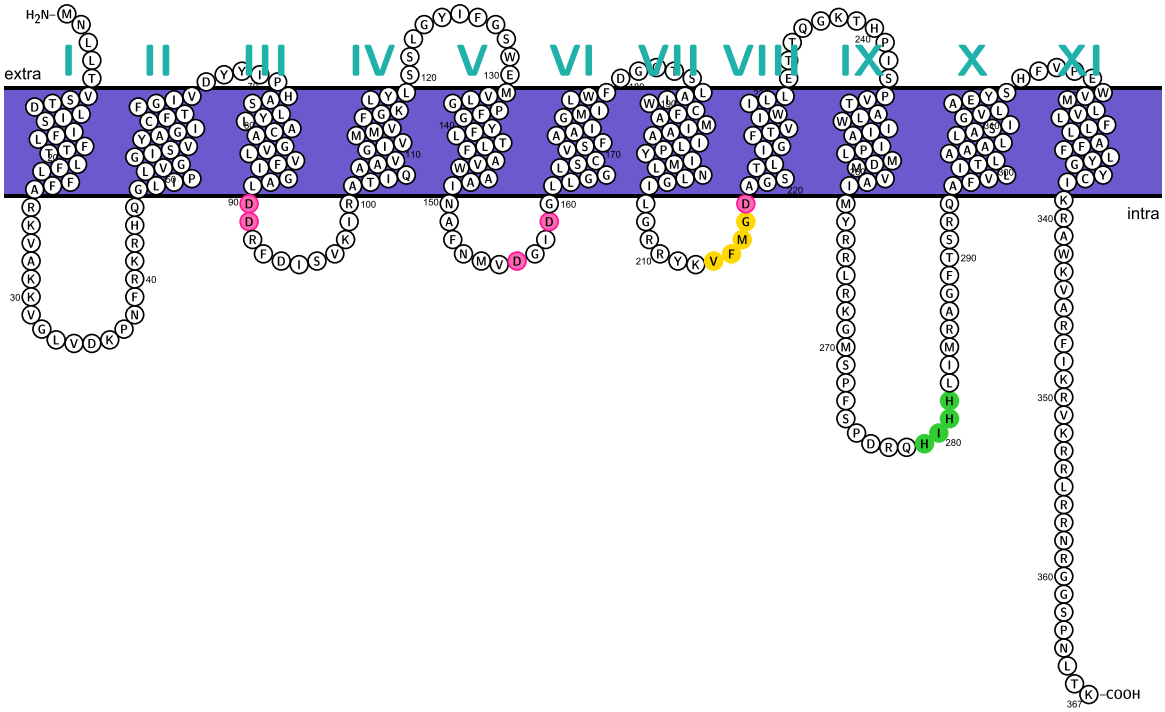


**Figure 1.27 | Topology model of WecA**[168,223,249] Topology model of WecA predicted by Protter, based on *E. coli* $WecA_{EC}$ amino acid sequence (UniPro: P0AC78, EC 2.7.8.33). For $WecA_{EC}$, the Asp217 at VFMGD may not be involved as a nucleophile in the catalysis, but instead the Asp156 and Asp159 residues. Pink: putative catalytic aspartic acid residues. Yellow: the conserved VFVGD motif. Green: HIHH motif.

*O*-antigen, or *O*-polysaccharide, is the oligosaccharide portion of lipopolysaccharide (LPS). LPS is a unique cell surface component of Gram-negative bacteria that

maintains the structural rigidity of the outer membrane, but consequently elicits an innate immune response. The *O*-antigen is important in pathogenicity/host colonisation, resistance to complement-mediated killing, and resistance to cationic antimicrobial peptides.[249]

Enterobacterial common antigen (ECA) is a glycolipid that is produced by all members of *Enterobacteriaceae*. It is a heteropolysaccharide comprised of trisaccharide repeating units consisting of →3)-α-D-Fuc*p*4NAc-(1→4)-β-D-Man*p*NAcA-(1→4)-α-D-Glc*p*NAc-(1→, with *O*-acetyl groups. The heterosaccharide chains are linked to the phosphatidic acids on the bacterial cell wall *via* phosphodiester linkage, and are also linked to LPS in some strains.[250] ECA exists in three forms, a cycle polysaccharide form ($ECA_{cyc}$), a linear phosphatidylglycerol-linked polysaccharide ($ECA_{PG}$), or as an endotoxin/lipopolysaccharide ($ECA_{LPS}$). The biological significance of ECA is not well understood, but it has been suggested that ECA has a role in cell membrane integrity, flagellum expression, and resistance to enteric bacteria, acetic acid, and bile salts.[250]

*Mycobacterium tuberculosis*, the causative agent of tuberculosis (TB), has a unique and complex cell membrane structure that is almost indestructible and impenetrable to majority of clinical antibiotics (**Fig. 1.28**). The World Health Organisation (WHO) estimated 8.7 million people developed TB in 2012 and 1.3 million death as a result of TB the same year.[154] WecA is present in *M. tuberculosis* where it carries out sugar transfer from UDP-GlcNAc to the lipid carrier decaprenyl-phosphate ($C_{50}$-P) during mycolylarabinogalactan biosynthesis. The mycolylarabinogalactan is one of many cell wall components present in *M. tuberculosis*.[248] This makes WecA a favourable target for anti-*M. tb* drug development. WecA is an underexploited target for antimicrobial drugs, considering

its important physiological roles of O-antigen and enterobacterial common antigen in Gram-negative bacteria and in *M. tuberculosis*. Currently, there is no clinical drug that targets WecA.[247] Tunicamycins are reported to inhibit WecA in *M. tuberculosis* but cytotoxicity has hindered their clinical potential.[248] Thus designing non-cytotoxic tunicamycin analogues that can target WecA as anti-*M. tb* drugs would be extremely valuable.

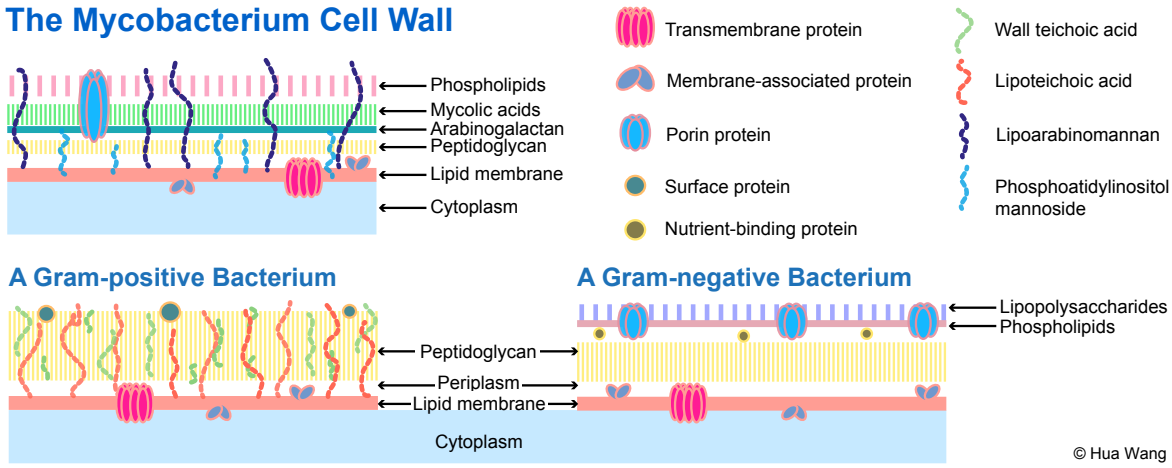


**Figure 1.28 | The mycobacterium cell wall compared to the Gram-positive and Gram-negative bacterial cell walls.**[74] In *Mycobacterium*, WecA is involved in the first membrane step in the GlcNAc transfer to decaprenyl-phosphate to make the building block for arabinogalactan and lipopolysaccharides.

### 1.2.3 Tunicamycins Inhibit Posttranslation Protein Palmitoylation *via* Substrate Mimicry

Palmitoylation is the lipid modification of a protein carried out by transmembrane proteins called protein acyltransferases (PATs). However, *in vitro*, cysteine-containing proteins and peptides are able to auto-acylate in the presence of palmitoyl-CoA. Therefore, it has been considered that acylation may also be a spontaneous process in the cell, depending on the presence of the acyl-CoA and the cellular environment.[251] Several PATs have been identified, which all share a conserved Asp-His-His-Cys (DHHC) motif located

within a cysteine-rich domain.[251,252] There is a lack of available information on substrate interactions, thus protein-substrate specificity is difficult to generalise. The substrates which interact with the DHHC have mainly been identified *via* coexpression.[253] There are two types of palmitoylation. *N*-palmitoylation is the *N*-linked covalent lipid modification of a protein *via* an amide bond. This happens when a palmitoylate is added to a cysteine at the N-terminus of a protein *via* a thioester intermediate.[251] The other is *S*-palmitoylation (thiosylation), which is palmitoylation at a cysteine residue of a protein *via* thioester linkage. *S*-palmitoylation is a reversible modification *via* thioesterases that lends itself to regulatory processes, where as *N*-palmitoylation is an irreversible modification.[254] Palmitoylation is one of several posttranslational lipid modifications of proteins in eukaryotic cells. There are other lipids that can be modified on proteins, these include myristate (myristoylation), cholesterol (cholesterol modification), glycosyl-phosphatidylinositols (GPO anchoring of proteins), geranylgeranyl and farnesyl (protein prenylation).[255] Each type of lipid moiety is transferred by a specific type of lipid transferase, and each modification confers a distinct outcome on a protein. Lipid modification of proteins commonly leads to an increase in membrane affinity.[254] Palmitoylation of proteins is associated with protein trafficking, protein stability, protein aggregation, organelle inheritance, and vesicle fusion.[251,254] As such, the associated functions have been linked to diseases such as Huntington's disease, cancer, and cardiovascular and T-cell mediated immune disorders.[252] Thus, the proteins associated with palmitoylation are interesting targets for drug developments.

Tunicamycins have been shown to inhibit *N*-palmitoylation.[45,256] The mechanism of action is unknown but it has been proposed as the result of palmitoyl-CoA mimicry, which

involves competing with the natural substrate for binding to PATs (**Fig. 1.29**). A tunicamycins inhibition study comparing palmitoylation and *N*-glycosyation was reported by Skene *et al*. The authors distinguished and noted the tunicamycins homologues, showing that the effect of protein palmitoylation is dependent on the chain length. This further adds to the long speculated importance of the lipid chain on tunicamycins. Furthermore, they noted the structural differences in natural substrates. Tunicamycins do not act as a substrate-product transition-state analogue but rather as a substrate mimic. This may have been reflected in the dose range of 1-25 μg $mL^{-1}$ needed in palmitoylation inhibition compared to only 0.05-0.5 μg $mL^{-1}$ reported for *N*-glycosylation inhibition.[256] Not surprisingly, the substrate mimicry modes of inhibition observed for MraY and PATs tend to require higher doses and have lower affinity than with the substrate-product transition-state mimicry mode of inhibition as observed from TagO/TarO and GPT.

PATs involve in palmitoylation have only begun to be studied due to the difficulty in the past to express, isolate, and study membrane proteins of eukaryotic origin. Thus, designing tunicamycin analogues to regulate palmitoylation would be very useful in treating palmitoylation-associated diseases, or tunicamycin chemical probes that would be able to assist in the understanding of the biological properties of PATs in eukaryotic cells.

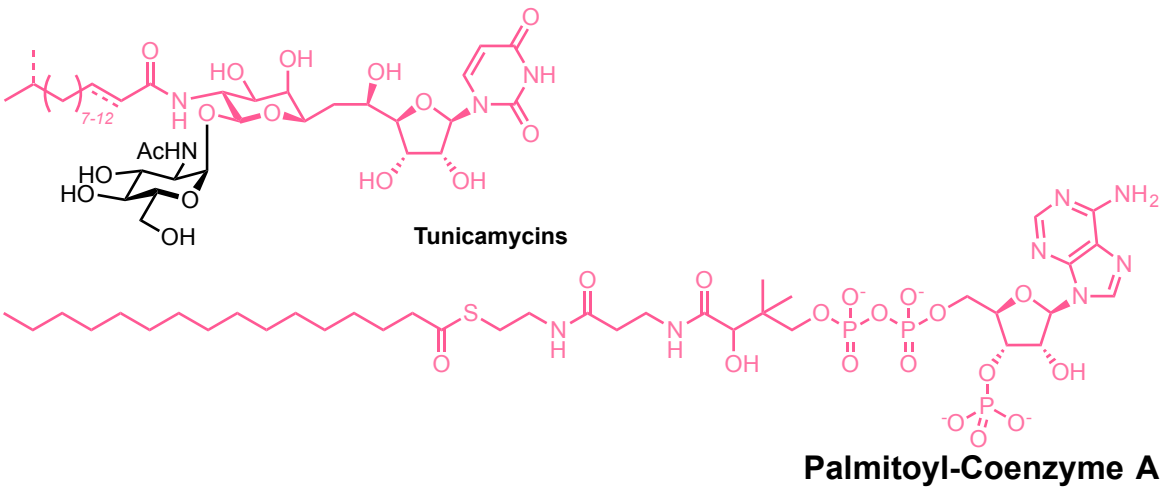


**Figure 1.29 | The chemical structure of palmitoyl-coenzme A.**[45,257] The structural resemblance is highlighted in pink for tunicamycins.

### 1.2.4 Mechanisms of Resistance Towards Tunicamycins

Bacterial resistance to antibiotics is inevitable. Understanding the mechanisms of resistance is crucial in drug design, and as well understanding the mode of action of the drug. This helps in the initial design stage that could help to extend the shelf-life of antibiotics by preventing or delaying the on-set of resistance in the early stage. This is done by creating a first-line of potent antimicrobial drug, or a second generation of anti-microbial drug. Tunicamycin-resistance has been reported in prokaryotic and eukaryotic cells through several of the mechanisms listed previously in **Table 1.3**, such as group transfer or target alteration. Below is a summary of the tunicamycin resistance mechanisms known to date.

Tunicamycin-resistant strains of *Bacillus subtilis* were first isolated in 1978, just seven years after tunicamycins were first reported.[1,258] The tunicamycin-resistance gene is identified as *tmrB*. It codes for the TmrB protein, an ATP-binding membrane associated protein.[259] Based on heterologous expression studies carried out by Noda *et al*., *tmrB*

cloned in *E. coli* resulted in TmrB protein that was cytoplasmic and membrane-bound. It is proposed that the C-terminal end of TmrB forms an amphiphilic α-helix, involved in membrane interactions and tunicamycin binding.[259,260] Although the exact function of TmrB is unknown, it is speculated that TmrB may act as a drug transporter or a permeability barrier in the bacterial cell membrane (**Fig. 1.30a**).

Another putative tunicamycin-resistance gene, DR_1419, was noted in 2001, from radiation-resistant bacterium *Deinococcus radiodurans,* predicted to code for a protein similar to TmrB.[261] The gene was later cloned and expressed, and coined as TmrD by Kapp *et al*. in 2008, for which they solved the crystal structure.[262] They suggested that TmrD is a phosphotransferase based on the structural similarity of TmrD to nucleoside monophosphate kinases and chloramphenicol phosphotransferase, even though the gene sequence analysis of DR_1419 showed the presence of the GxxxxGKT/S ATP-binding signature motif and similarity to *tmrB* as an ATP-binding membrane associated protein.[261,263] Thus, another mode of tunicamycin-resistance is proposed to involve inactivation of tunicamycins by phosphorylation of the hydroxyl groups at the 2', 3', and 5' positions (**Fig. 1.30b**).

Tunicamycin-resistant mechanisms have also been reported in the eukaryotic systems. Their resistance mechanisms involve the up-regulation of the targeted protein, *e.g.*, GPT, GPT-like proteins, or induction of aneuploidy. For instance, a tunicamycin-resistant soybean cell line showed a 40-fold increase in GPT activity, resulting in over-expression of GPT in the cell.[264] No drastic increase in other enzymes in the lipid-linked oligosaccharide biosynthesis were observed, although the oligosaccharide constructs were

found to be shorter and had a lower quantity of large constructs. Similar observations have also been reported in species of *Leishmania,*[265] plants cells,[266] mammalian cells,[267,268] and *Saccharomyces cerevisiae*.[269]

Recently, a major facilitator superfamily 2A (MFSD2A) was identified by Reiling *et al*.[270] The authors reported a mechanism by which tunicamycins enter the cell. They identified MFSD2A as a putative plasma tunicamycins transporter in mammalian cells. The MFSD2A-depleted cells were found to be resistant to tunicamycins, whereas MFSD2A-overexpressing cells had cellular accumulation of tunicamycins (**Fig. 28c**). This is a crucial find for understanding the mode of action of tunicamycins in mammalian cells that could provide valuable information for designing non-cytotoxic tunicamycin analogues.

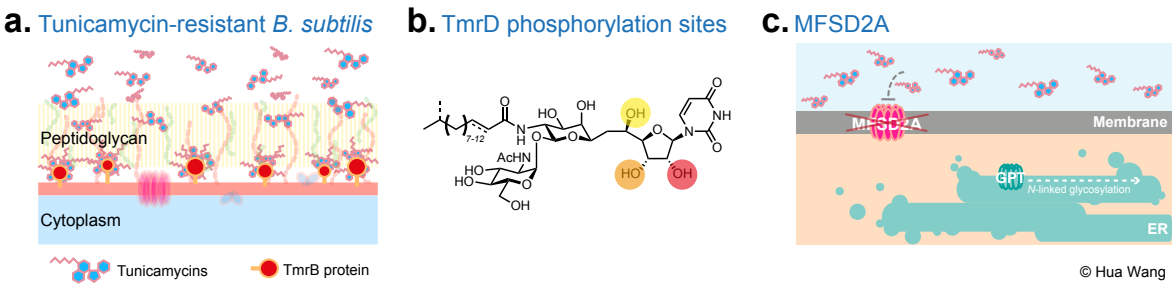


**Figure 1.30 | Tunicamycin resistant mechanisms.**[259,260,262,270] **(a)** The membrane-assosicated TmrB protein is proposed to bind to tunicamycins, preventing the accumulation of tunicamycins in the cytoplasm. **(b)** TmrD is proposed to inactivate tunicamycins *via* phosphorylation. The likelihood of tunicamycins prophorylation site deduced from TmrD crystal structure; the red highlighted hydroxyl group as most likely, and the yellow as least likely. **(c)** MFSD2A depleted cells are unable to uptake tunicamycins, thus *N*-linked glycosylation continues.

## 1.3 The Tunicamycin Biosynthetic Pathway

In practice, the majority of pharmaceutical drugs originate from microorganisms, or are derived from natural product scaffolds.[271] This is unsurprising as nature has evolved to produce a diverse range of bioactive molecules, like tunicamycins, that are otherwise difficult to synthesise in a laboratory. Nature is able to synthesise compounds more efficiently through complex biosynthetic pathways. Despite the first report of tunicamycins in 1971, there is still very little that is understood about the tunicamycin biosynthetic pathway. The genomes of three tunicamycin-producing *Streptomyces* strains were only recently reported in 2011.[7] Thus, by unlocking the pathway and understanding the enzymatic processes that formulate and construct the unusual tunicamycin scaffold, enzymes can be engineered to produce tunicamycins *in vitro* and in addition to unnatural analogues. Moreover, the enzymes in the pathway would add to the existing library of accessible enzymes to construct a diverse range of pharmaceutical drugs.

There are several groups that have proposed the tunicamycin biosynthetic pathway based on gene sequence analysis and mutational studies. The following subsections summarise the reported biosynthetic pathways that were known up to the start of the work presented in this thesis in October 2010.

### 1.3.1 Tunicamycin Biosynthetic Pathway Proposed by Tsvetanova *et al.* 2002

In 2002, Tsvetanova *et al*. reported the first attempt to elucidate the tunicamycin biosynthetic pathway.[272] The authors conducted metabolic radiolabelling experiments and stable isotope incorporations on tunicamycin-producing *S. chartreusis* NRRL3882 to understand the origin of the eleven-carbon aminodialdose sugar, tunicamine (**Fig. 1.31**). In

the metabolic radiolabelling experiments, [2-$^{14}$C]uridine was found to be incorporated into the tunicamycins, with D-[1-$^{14}$C]glucosamine being incorporated into the tunicamine and the GlcNAc moieties. This suggested that both uridine and glucosamine are biosynthetic precursors. In the stable isotope incorporation experiments, *S. chartreusis* were fed D-[1-$^{13}$C]glucose. Enrichment was analysed by HSQC $^{13}$C-$^{1}$H correlation NMR spectroscopy. Major enrichments were observed at C-11' and C-1", indicating that both are derived from the same metabolic pool of GlcNAc or UDP-GlcNAc. Moderate enrichments were observed at C-1', C-5', C-6', and C-6". Additionally, enrichment in the lipid chains were also observed at C-2" and C-4". These enrichments can be derived from the primary metabolism of D-[1-$^{13}$C]glucose *via* glycolysis and gluconeogensis that produce [3-$^{13}$C]-phosphoenolpyruvate (PEP), [2-$^{13}$C]acetyl-CoA, D-[6-$^{13}$C]glucose and UDP-[6-$^{13}$C]-glucose, and the pentose phosphate pathway that produces the [1',5'-$^{13}$C]uridine. Furthermore, the authors carried out D-[6,6'-$^{2}$H,$^{2}$H]glucose and deuterium incorporation experiments that were monitored by ESI-CDI-MS. The $^{2}$H atoms were found on tunicamycins at positions C-5', C-6', C-11', C-1", and C-6", which are similar to the incorporation sites to those observed in D-[1-$^{13}$C]glucose incorporation experiment. Presumably the metabolism of both D-[6,6'-$^{2}$H,$^{2}$H]glucose and D-[1-$^{13}$C]glucose follows the same metabolic pathway. Altogether, a tunicamycin biosynthetic pathway was proposed as shown in **Fig. 1.32**. The next step would be to identify the tunicamycin biosynthetic gene cluster.

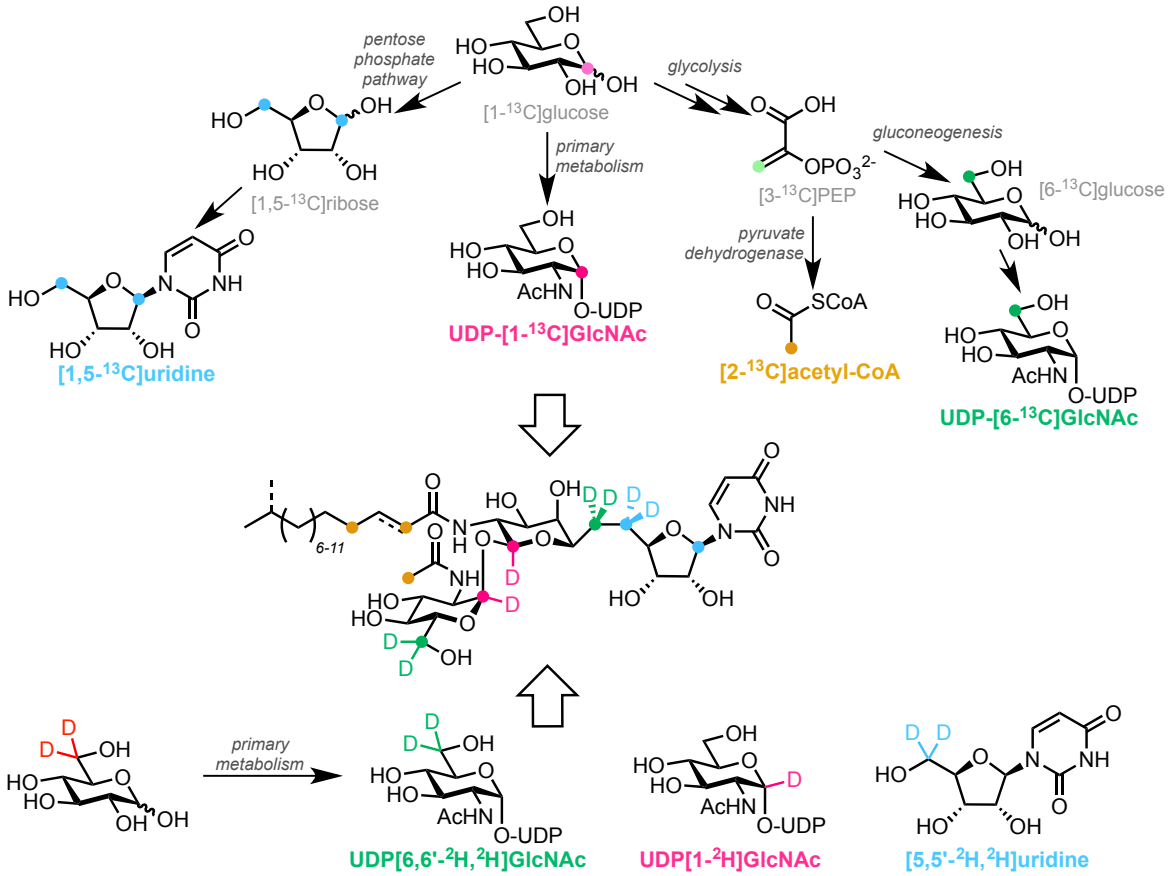


**Figure 1.31 | The summary of the isotope enrichment incorporation patterns found in tunicamycins.**[272]

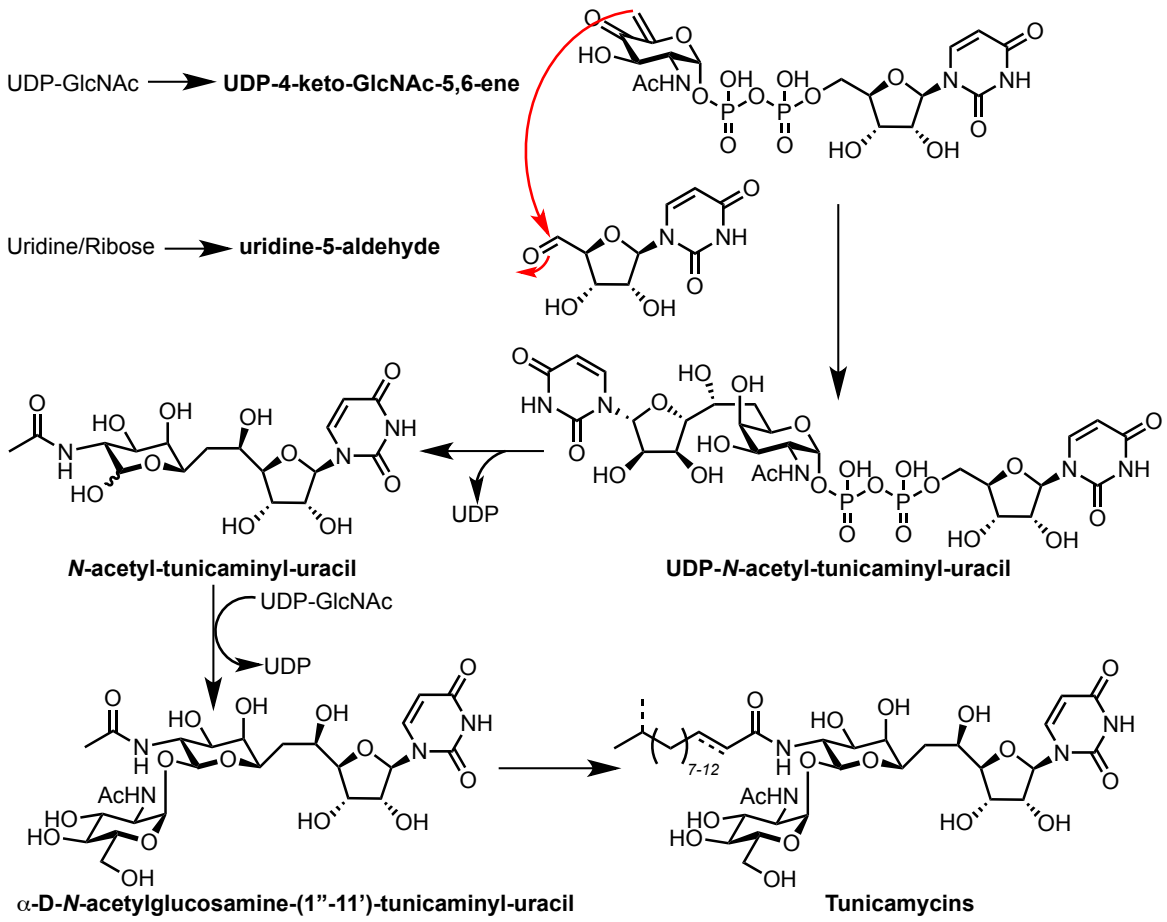


**Figure 1.32 | Tunicamycin biosynthetic pathway proposed by Tsvetanova *et al.*[272,273]**

### 1.3.2 Tunicamycin Biosynthetic Pathway Proposed by Wyszynski *et al.* 2010

In 2010, Wyszynski *et al.* identified the minimal tunicamycin biosynthetic gene cluster, *tun*, from *S. chartreusis* NRRL3882.[274] The *tun* gene cluster was heterologously cloned and expressed in *S. coelicolor* M1152. The authors selected a wide range of gene products that could perform biochemical processes similar to the putative tunicamycin biosynthetic gene cluster. These included glycosidic linkage by glycosyltransferases, *N*-acetyl-hexosamine *N*-deacetylases, lipid-processing enzymes, NDP-hexose epimerases and dehydratases. Their bioinformatic analysis showed *tun* consisted of a 12.0 kb stretch of DNA containing 14 ORFs that orient in the same direction and are translationally coupled to the preceding gene. Interestingly, the authors proposed the *tun* cluster was acquired

elsewhere due to the atypical G+C content (65%) in comparison to that that of *Streptomyces* genome (73%).[274,275] Fourteen putative enzymes were proposed to participate in the tunicamycin biosynthesis (**Table 1.4**). The authors proposed a tunicamycin biosynthetic pathway from the deduced *tun* gene products (**Fig. 1.33**). The next steps would be to isolate the enzymes and perform *in vitro* experiments to confirm their proposal of the tunicamycin biosynthetic pathway.

**Table 1.4 | The *S. chartreusis* NRRL3882 *tun* gene cluster products and their proposed functions.**[274]

| Gene (protein) | aa* | Proposed function in the tunicamycin biosynthetic biosynthesis |
|---|---|---|
| *tunA* (TunA) | 321 | UDP-GlcNAc epimerase/dehydratase |
| *tunB* (TunB) | 338 | Uridine oxidoreductase |
| *tunC* (TunC) | 318 | *N*-acyltransferase |
| *tunD* (TunD) | 474 | Glycosyltransferase |
| *tunE* (TunE) | 234 | *N*-deacetylase |
| *tunF* (TunF) | 327 | UDP-GlcNAc-4-epimerase |
| *tunG* (TunG) | 203 | UMP phosphatase |
| *tunH* (TunH) | 515 | UDP-tunicaminyl-uracil pyrophosphatase |
| *tunI* (TunI) | 304 | ABC transporter ATP-binding subunit |
| *tunJ* (TunJ) | 262 | ABC transporter permease subunit |
| *tunK* (TunK) | 81 | Acyl carrier protein |
| *tunL* (TunL) | 229 | Phospholipid phosphatase |
| *tunM* (TunM) | 216 | Radical SAM protein |
| *tunN* (TunNN | 152 | UTP pyrophosphatase |

*number of amino acids

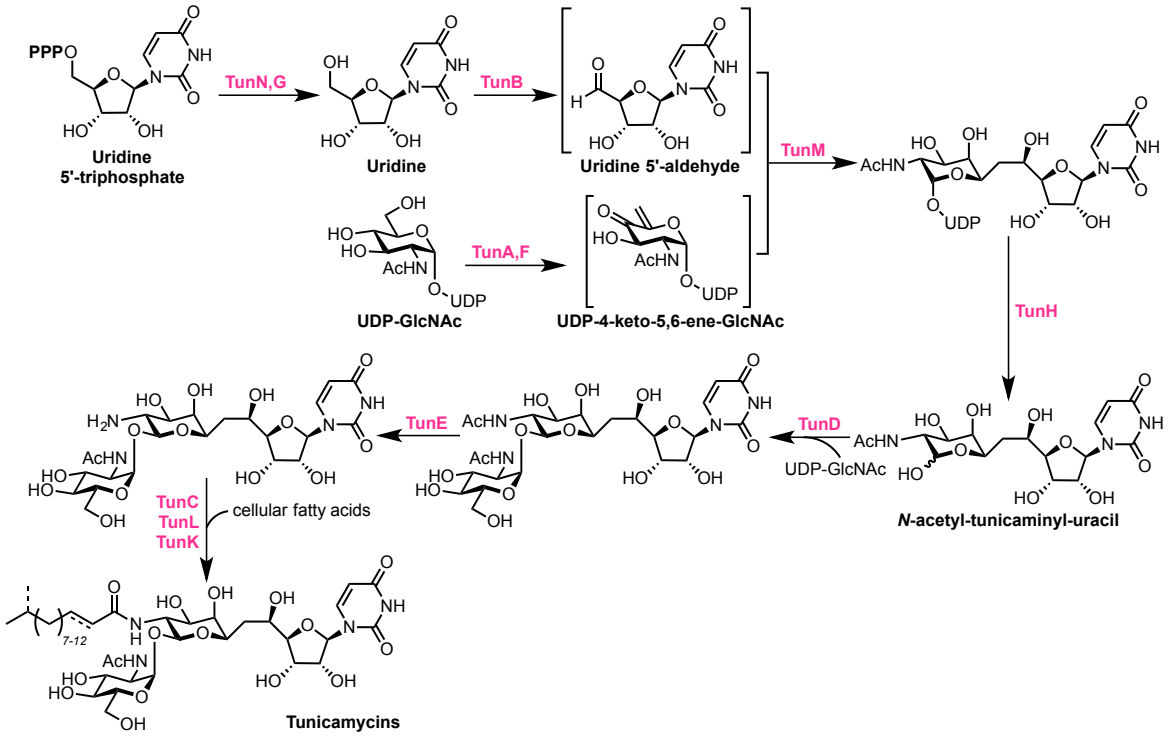


**Figure 1.33 | Tunicamycin biosynthetic pathway proposed by Wyszynski *et al.*[274]**

### 1.3.3 Tunicamycin Biosynthetic Pathway Proposed by Chen *et al.* 2010

Chen *et al*. reported the essential gene cluster for tunicamycin biosynthesis in *S. clavuligerus* ATCC27064, and additionally, they reported two additional gene clusters for the potential biosynthesis of tunicamycin-like antibiotics from *S. clavuligerus* ATCC27064 (Antibiotic MM19290) and *Actinosynnema mirums* DSM43827.[276] The tunicamycin biosynthetic gene cluster was heterologously expressed in *S. lividans* TK24. The authors listed twelve gene products, *tunA*-*tunL* (**Table 1.5**), that were deduced from gene disruption experiments and bioinformatic analysis, rather than the fourteen reported by Wyszynski *et al.* With their findings, they also proposed a tunicamycin biosynthetic pathway (**Fig. 1.34**). In the gene disruption experiments, the authors performed in-frame deletion of the gene *tunA*, a putative NAD-dependent epimerase/dehydratase. The *tunA* deletion resulted in the abolishment of the production of tunicamycins, hence identifying

*tunA* to be essential in tunicamycin biosynthesis. This is the first knockout experiment reported, and further gene knockout experiments would need to be conducted to confirm their proposal of the tunicamycin biosynthetic pathway.

**Table 1.5 | The *S. clavuligerus* ATCC 27064 *tun* gene cluster products and their proposed functions.**[276]

| Gene (protein) | aa* | Proposed function in the tunicamycin biosynthetic biosynthesis |
|---|---|---|
| *tunA* (A) | 321 | NAD-dependent epimerase/dehydratase |
| *tunB* (B) | 338 | Radical SAM protein |
| *tunC* (C) | 318 | GCN5-related *N*-acetyltransferase |
| *tunD* (D) | 472 | Glycosyltransferase |
| *tunE* (E) | 234 | *N*-deacetylase |
| *tunF* (F) | 327 | UDP-Glc-4-epimerase |
| *tunG* (G) | 203 | Phosphoglycerate mutase |
| *tunH* (H) | 515 | Pyrophosphatase |
| *tunI* (I) | 304 | ABC transporter |
| *tunJ* (J) | 262 | ABC-2 transporter |
| *tunK* (K) | 81 | Acyl carrier protein |
| *tunN* (L) | 229 | PA-phosphatase related protein |

*number of amino acids

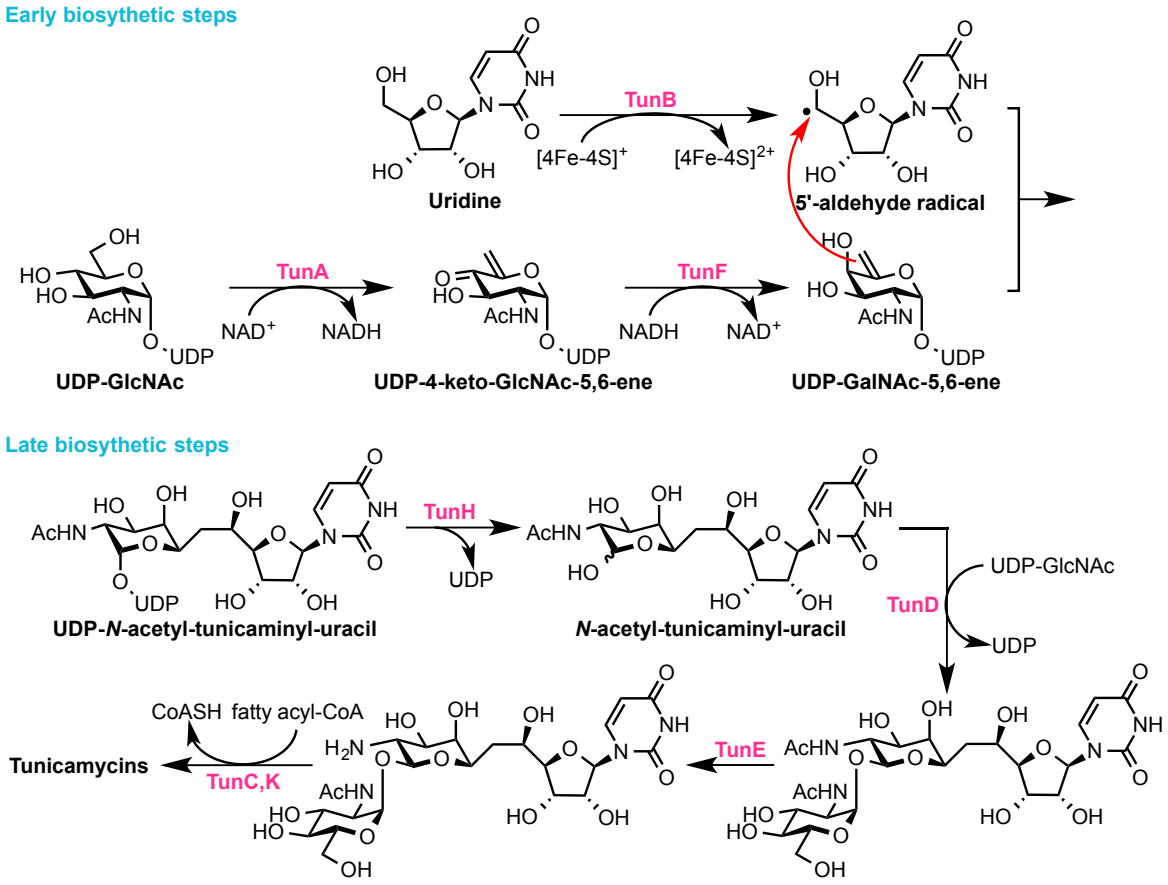


**Figure 1.34 | Tunicamycin biosynthetic pathway proposed by Chen *et al.* 2010.**[276]

### 1.3.4 Tunicamycin Biosynthetic Pathway Proposed by Karki *et al.* 2011

Karki *et al.* reported the genome mining of the tunicamycin biosynthetic gene cluster in *S. clavuligerus* ATCC27064.[277] The authors listed twelve gene products, *tun1-tun12* (**Table 1.6**), deduced from the gene cluster, rather than the fourteen as reported by Wyszynski *et al.*[274,277] With their findings, they proposed a biosynthetic pathway similar to the others mentioned above (**Fig. 1.35**). Additionally, to confirm the existence of the *tun* gene in *S. chartreusis*, $tun1_{Sch}$, the putative NDP-hexose 4,6-dehydratase was inactivated that resulted in the abolishment of tunicamycins production. The next steps would involve isolating the enzymes, carrying out *in vitro* activity test and performing further gene knockout experiments to confirm their proposal of the tunicamycin biosynthetic pathway.

**Table 1.6 | The *S. clavuligerus* ATCC 27064 *tun* gene cluster products and their proposed functions.**[277]

| Gene (protein) | aa* | Proposed function in the tunicamycin biosynthetic biosynthesis |
|---|---|---|
| *tun1* (Tun1) | 323 | NDP-hexose 4,6-dehydratase |
| *tun2* (Tun2) | 259 | Radical SAM domain protein |
| *tun3* (Tun3) | 322 | *N*-acetyltransferase |
| *tun4* (Tun4) | 461 | Glycosyltransferase |
| *tun5* (Tun5) | 236 | *N*-deacetylase |
| *tun6* (Tun6) | 327 | NDP-hexose 4-epimerase |
| *tun7* (Tun7) | 208 | Phosphatase |
| *tun8* (Tun8) | 518 | Phosphodiesterase |
| *tun9* (Tun9) | 302 | ABC transporter protein |
| *tun10* (Tun10) | 263 | ABC transporter protein |
| *tun11* (Tun11) | 81 | Acyl-carrier protein |
| *tun12* (Tun12) | 223 | Phosphatase |

*number of amino acids

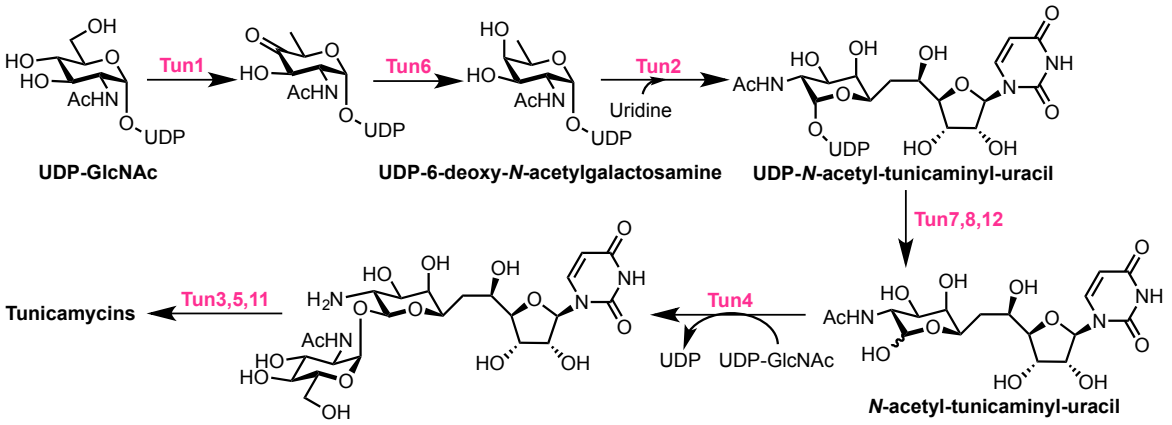


**Figure 1.35 | Tunicamycin biosynthetic pathway proposed by Karki *et al.* 2011.**[277]

## 1.4 Literature Reports on Tunicamycin Analogues

The first total synthesis of a natural product, urea, was reported by Friedrich Wöhler in 1828.[278] Since then, the importance of chemical synthesis of various natural products, such as tunicamycins, has benefited research across the disciplines of chemistry and biology, and more importantly pharmacology; this continues to challenge the capability of synthetic chemists to reproduce the chemistry that occurs in nature. These

valuable contributions of synthesising natural products have expanded the fundamental understanding of chemical theories and the repertoire of synthetic methodologies; they have allowed structural validation of natural products, as well as large scale production, and functionalisation for therapeutic drug analogues or biochemical tools.

The chemical syntheses of tunicamycins have been reported by several groups, [279-294] with four total syntheses of tunicamycins published.[295-299] The total synthesis of tunicamycins typically faces several challenges due to their spatial complexity and atypical construction, such as the R-configuration of the 5'-carbon, the α,β-glycosidic linkage, and the carbon-carbon linkage of the eleven-carbon tunicamine. The chemical routes published towards each of those products revolve around multi-step protection and deprotection strategies that are lengthy and consequently produced low yields. However, despite the range of synthetic routes toward tunicamycins, to the best of the author's knowledge, there are only two reports on the syntheses of tunicamycin analogues that had followed up with biological evaluations. The following subsections summarise these reports.

### 1.4.1 Minor Modification of Tunicamycins by Hashim *et al.* 1987

Three tunicamycin analogues were reported by Hashim *et al.,* which suggested the sensitivity and structural importance of tunicamycins pertaining to their mode of inhibition towards GPT in the *N*-linked glycosylation (**Fig. 1.36**).[300] This was concluded from several inhibitory experiments. The authors measured the *N*-linked glycosylation of immuno-globulins (Igs) IgM *via* tritiated mannose incorporation, established whether the tunica-mycins inhibit cellular transport of the Igs, investigated tunicamycins acting as substrate-

product transition-state analogues, and also the effect of tunicamycins on RNA, DNA, and protein syntheses.

The transport experiment measured the biosynthesis and secretion of radiolabelled IgM from rat hybridoma cells, upon treatment with 2 μg $mL^{-1}$ of unmodified tunicamycins and three modified tunicamycin analogues. By analysing both the cell lysate and the supernatant, the transport of Ig molecules was found to be affected by the absence of the glycan. Only unmodified tunicamycins were capable of inhibiting the *N*-glycosylation of IgM. Although Tunicamycins-3 did reduce the rate at which IgM was secreted from the cell, unmodified tunicamycins had a more drastic effect with very little IgM secreted over a six hour time frame in comparison (**Fig. 1.36**).

The experiment conducted to determine whether tunicamycins are substrate-product transition-state analogues showed that any minor modification on tunicamycins would abolish the inhibitory activity. Upon treatment with unmodified and modified tunicamycins, intracellular and extracellular IgG products were immunoprecipitated, digested with endoglycosidase H, and analysed by SDS-polyacrylamide gel electro-phoresis (SDS-PAGE). The high-mannose glycan product resulting from GPT activity are not susceptible to endoglycosidase H treatment. The authors successfully showed that the modified tunicamcyins either failed to inhibit GPT activity or had drastic reduced binding affinity to GPT.

Furthermore, inhibition of DNA, RNA, and protein syntheses were measured *via* $^{3}$H-thymidine, $^{3}$H-uridine, and $^{3}$H-leucine incorporations, respectively. The authors noted

that only natural tunicamycins had any inhibitory effect on DNA synthesis, whereas the tunicamycin analogues were slightly mitogenic on the cells. In protein synthesis, the greatest inhibitory effect was again observed by unmodified tunicamycins, with modified Tunicamycins-3 having minor effect, whereas Tunicamycins-1 and Tunicamycins-2 had no pronounced inhibitory effect on the dose tested. This suggested that the unmodified tunicamycins may have inhibitory effect on macromolecule synthesis.

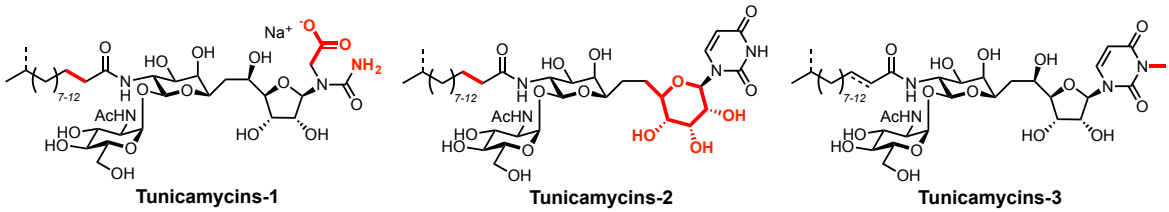


**Figure 1.36 | Minor modification of tunicamycins by Hashim *et al.*[300]** Tunicamycins-1 and Tunicamycins-2 resulted in the impairment of tunicamycins antibiotic activity. which may be due to non-specific or low-affinity interaction of the antibiotic with the target protein active site. This appears to be consistent with other studies in which binding of tunicamycins to yeast protoplasts may be inhibited in the presence of unsaturated phospholipids.[55,61] However, the difference between the ribose and the lipid modifications was not distinguished. Modification on the uracil ring generally eliminated the ability of tunicamycins to inhibit *N*-linked glycosylation. This is consistent with the substrate discrimination that distinguishes the enzymes in the PNPTs superfamily.

### 1.4.2 Synthesis of 2-Acetamido-2-deoxy-α-D-galactopyranosyl Analogue of Tunicamycin by Kominato *et al.* 1988

Kominato *et al*. synthesised the 2-acetamido-2-deoxy-α-D-galactopyranosyl, or *N*-acetyl-galactose (GalNAc) analogue of tunicamycin (**Fig. 1.37**).[301] Their synthesis followed similar steps as the reported total synthesis of tunicamycin V.[297] First, two precursors are synthesised from D-glucosamine and D-allose (**1-5**) and condensed in the presence of KF in acetonitrile to construct the tunicamine undecaose skeleton (**6**) in 51% yield.[295,302] This undecose skeleton (**6**) was then converted to the acetylated tunicamine (**7**) over five

steps. The condensation of **7** with bis(trimethylsilyl)uracil in presence of $SnCl_4$ followed by hydrogenation, acetylation and then chlorination afforded chlorinated tunicaminyl uracil (**8**). The protected GalNAc was added to **8** in DCM in the presence of silver carbonate and silver perchlorate to give the anomeric products (**9 α,β**). **9α** was O-de-acetylated and hydrogenolysed to afford the amine product (**10α**). The **10α** product was treated with tetradecanoic acid and DCC in DCM to give the GalNAc-tunicamycin precursor **11α** product in 72% yield, then finally O-deisopropylidenation with 70% aqueous acetic acid afforded the final GalNAc analogue of tunicamycin (**12α**).

The authors carried out a competitive assays using natural substrates UDP-GlcNAc and dolichol phosphate, which measured the transfer of the GlcNAc-P in the presence of either the GalNAc analogue or tunicamycins. The GalNAc tunicamycin analogue showed only 25% of the inhibitory activity of tunicamycins. This further supports previous findings and the proposed substrate-product transition-state analogue mode of inhibition of tunicamycins. Interestingly, the authors noted no antiviral or antimicrobial activity for the GalNAc tunicamycin analogues. The GalNAc analogue of tunicamycin that showed reduced inhibitory activity supports the findings by Hashim *et al.*[300] that minor modification of the tunicamycin scaffold could abolish the substrate-product transition-state mimicry mode of inhibition. However, no procedure or condition for the antimicrobial susceptibility tests was reported, thus it would be difficult to draw any conclusion from the inhibition studies.

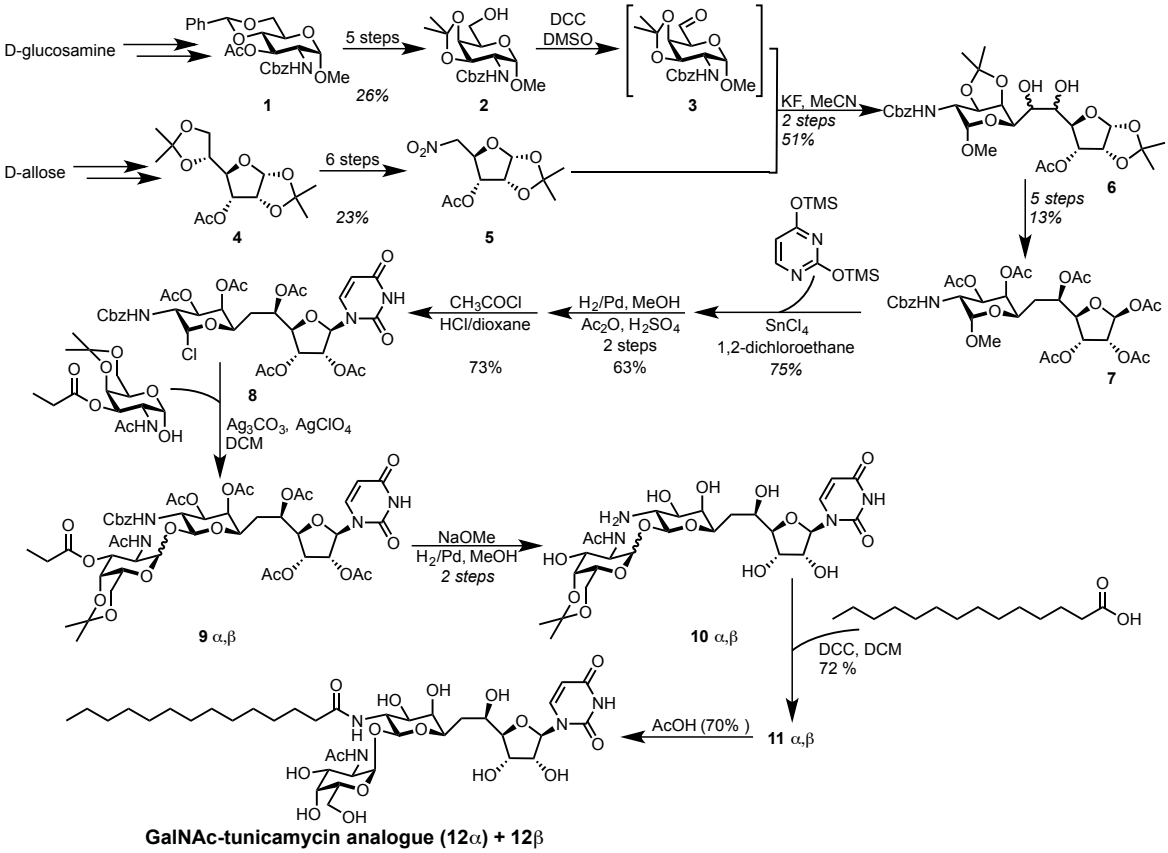


**Figure 1.37 | 2-acetamido-2-deoxy-α-D-galadopyranosyl analogue of tunicamycin Kominato *et al.*** [295,296,301,302] **1** to **3**: **1** was treated with warm aqueous acetic acid and followed by treatment with mesyl chloride. The mesyl group was then displaced by acetate ions *via* epimerisation, followed by deacetylation with methanolic ammonia after which acetonation and Pfitzner-Moffat oxidation give the requisite galactosamine aldehyde **3**. **4** to **5**: **4** was first hydrolysed in acetic acid which preferentially hydrolyses the 5,6-*O*-isopropylidene group, followed by periodic acid oxidation, $NaBH_4$ reduction, and tosylation. An $S_N2$ displacement of a subsequent 5-iodo intermediate with sodium nitrate resulted in **5**. **6** to **7**: **6** was first dehydrated with acetic anhydride, which was followed by hydrogenation with $NaBH_4$, oxidation with $KMnO_4$ in presence of sodium tert-butoxide, and then continued with successive hydrogenation with $NaBH_4$ and hydrolysis with NaOMe yielding two diastereomers where the desired α product was isolated after flash column purification. This was then followed by acetylation and then hydrolysis to afford the protected tunicamine product **7**. The protected-GalNAc building block: allyl 2-acetamido-2-deoxy-a-D-glucopyranoside was first acetylated, then followed by *O*-deisopropylidenation, mesylation, displacement of sulfonylxyl group with acetate ion, *O*-deacetylation, and then finally *O*-isopropylidenation to afford the protected-GalNAc building block. Finally, the condensation of the tunicamine and the galactose building block in DCM in presence of silver carbonate and silver perchlorate afforded two products: **9a** and **9b**. This was followed by O-deacetylation with NaOMe and then hydrogenolysed using Methanol-Pd black to afford **10α** and **10β**. this was treated with tetradecanoic acid and dicyclohexylcarbodiimide in DCM to afford **11α** and **11β** in 72% yield.

Then O-deisopropylidenation with 70% aqueous acetic acid afford the final tunicamycin galactose analogue **12α** and **12β**.

## 1.5 Hypothesis and Strategy

### 1.5.1 Hypothesis

The central objective of this thesis is to develop novel tunicamycin analogues that are non-toxic to eukaryotic cells as potential antimicrobial drug candidates. We hypothesise that by retaining the lipid character of tunicamycin structure and modifying the GlcNAc moiety then the antimicrobial activity would be retained but the tunicamycins inhibitory action towards GPT would be abolished, thus diminishing tunicamycins cytotoxicity towards mammalian cells.

As discussed earlier in subsection **1.1.2**, the lipid chain has long been speculated to play an important role in tunicamycins biological activities; the tunicaminyl uracil core and the GlcNAc are proposed to act as substrate mimics. Upon these considerations, as summarised in **Fig. 1.38**, several modifications for tunicamycin analogue designs are proposed. Of the four main modification sites suggested, modifications of lipid chain and the GlcNAc moieties would be the prime rational choices for the purpose of developing non-cytotoxic tunicamycin analogues. To the best of our knowledge, no tunicamycin analogues have been reported to show the retention of their antimicrobial properties with reduced cytotoxicity in eukaryotic cells. When we envisioned the tunicamycin analogue design, by taking into consideration of what is reported in the literature, we chose not to modify the uracil or the tunicamine moiety of tunicamycin as both are speculated to interact with MraY (as discussed in subsection **1.2.2.1.1**). Whilst the importance of the

tunicaminyl uracil scaffold in antimicrobial activity and the GlcNAc moiety in mammalian cytotoxicity are reported, the GlcNAc and/or aliphatic chain have never been directly shown to contribute to either. More so, we were particularly interested in modifying the GlcNAc moiety to reduce structural similarity of tunicamycin to UDP-GlcNAc but also to retain the carbon chain and its lipid character.

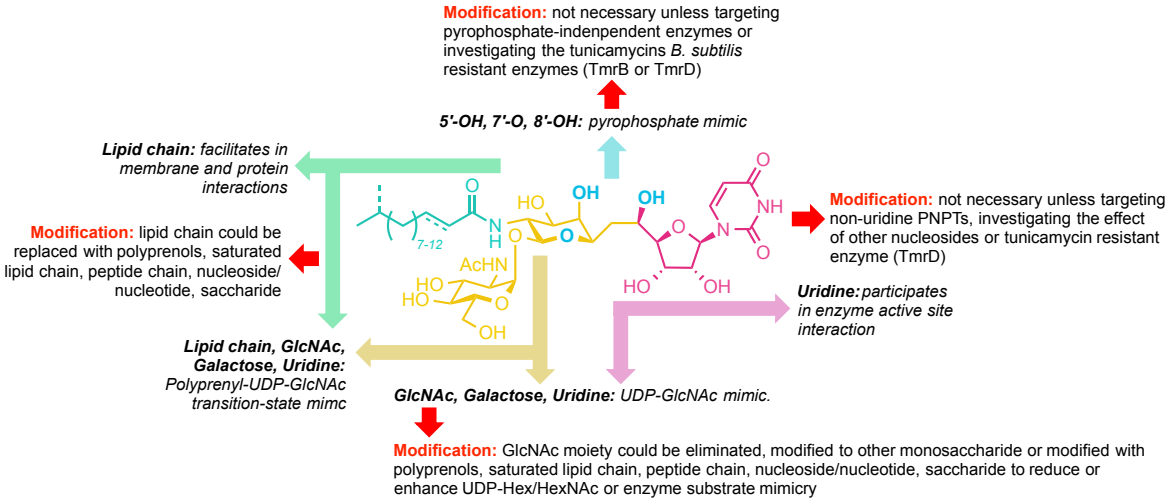


**Figure 1.38 | Structure of Tunicamycins dissected by their biological relevance for analogue designs.** Modification of the tunicamycins structure for analogue designs are highlighted in red.

The substrate mimicry mode of inhibition observed for MraY and PATs tend to require a higher dosage and have a lower affinity than the substrate-product transition-state mimicry mode of inhibition with a lower dosage and a higher affinity observed for TagO and GPT. This could suggest that analogues of tunicamycins resembling the substate-product transition-state of $C_{55}$-PP-MurNAc-pentapeptide could be more selective to MraY than GPT (**Fig. 1.39**). Furthermore, this may also imply that the tunicamycin core scaffold without a lipid chain would be the ideal template to use for designing analogues. This is further speculated from other natural inhibitors of MraY that appear to be non-toxic to mammalian cells that have the complex architecture resembling the substrate-product transition-state mimicry without the GlcNAc moiety. Of course, other avenues can be

explored for using tunicamycin as a template for potential inhibitors to use in biological applications to understand biological pathways and diseases, and therapeutics as anti-fungal, antiviral, antitumour, and anti-diabetics. These may involve making tunicamycin analogues as inhibitors for glycosyltransferases and *N*-linked glycosylation such as the DPM1[xiii] (as discussed in subsection **1.2.2.2.1**), investigating the UPR and the associated diseases (as discussed in subsection **1.2.2.2.2**), palmitoylation process and the associated diseases (as discussed in subsection **1.2.3**), PNPTs listed previously in **Table 1.4** that utilise UDP-GalNAc, UDP-FucNAc, or UDP-QuiNAc, the resistance mechanisms (as discussed in subsection **1.2.4**), and other enzymes such as WbbL[xiv] for TB drug development.[303] These and other possible applications from tunicamycin analogues, such as fluorescent probes to investigate cellular processes and imaging, and inhibitors for glycosyltransferases, kinases, pathways and crystallisation studies, are noted in **Fig. 1.39**.

[xiii] Dolichyl-phosphate β-D-mannosyltransferase. DPM1 is involved in the *N*-linked glycosylation.

[xiv] *N*-acetylglucosaminyl-diphospho-decaprenol L-rhamnosyltransferase. WbbL is involved in the early stages of the arabinogalactan biosynthesis in *Mycobacterium* cell wall.

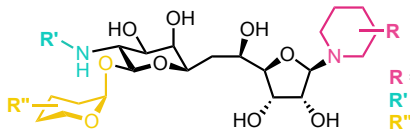

Tunicamycin template

R = adenine, guanine, thymine, uracil, cytosine
R' = lipid chains, peptides, nucleoside, saccharide, fluorophores
R'' = lipid chains, peptides, nucleoside, saccharide, fluorophores

| Proposed Function | Analogue |
|---|---|
| *MraY inhibitor* | 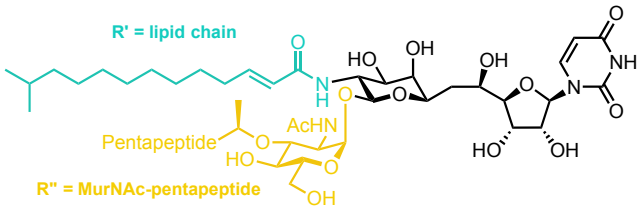 |
| *WbbL inhibitor* | 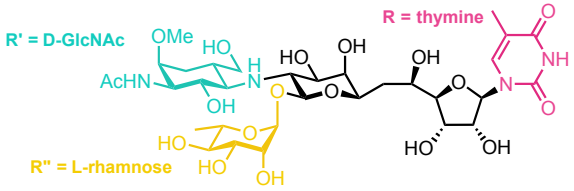 |
| *OGT inhibitor* | 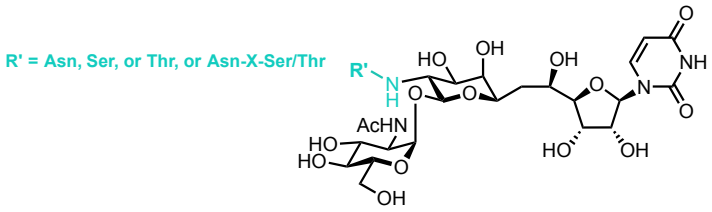 |
| *PATs inhibitor* | 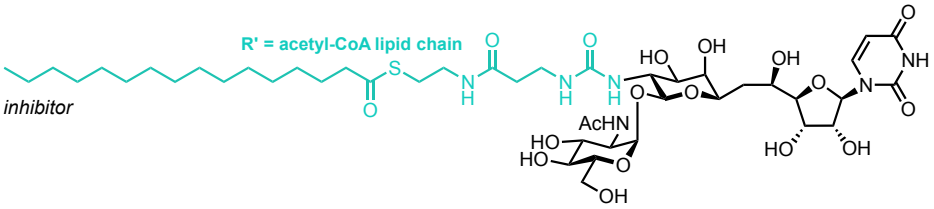 |
| *PNPTs inhibitor* | 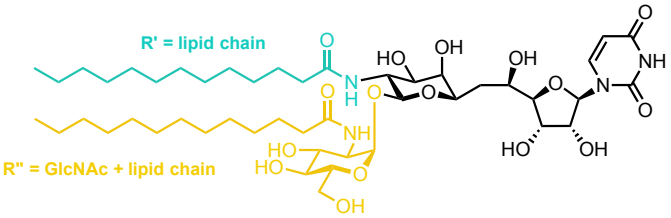 |

*Chitin synthase inhibitor*
R = uracil; R'/R'' = GlcNAc

*Glycosyltransferases inhibitors*
R = uracil, guanine, cytosine; R'/R'' = saccharide

*Kinases inhibitors*
R = adenine

*Fluorescent probes*
R'/R'' = dansyl chloride,
1-hydroxy-4-(1-phenyl-1H-tetrazol-5-yl-thio)-2-naptholic acid

*Inhibitors (based on the three scaffolds)*
R/R'/R'' = nucleoside, lipid chains, peptides, saccharide

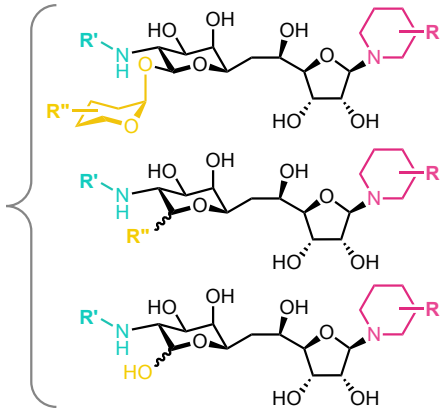

**Figure 1.39 | Proposed tunicamycin analogues.** MraY, WbbL, OGT, and PATs inhibitors can be designed based on the substrate-product transition-state mimicry. Chitin synthase, glycosyl-

transferases, kinases, and fluorescent probes can be designed from the three scaffolds shown. Our interest in the lipid chain analogues can be designed from the three scaffolds.

### 1.5.2 Strategy

There are several strategies that can be applied to access the tunicamycin core scaffolds and tunicamycin analogues. As we have previously discussed in subsections **1.3** on the identification of the tunicamycin biosynthetic gene clusters, the gene cluster can be bioengineered. Although this is an enticing approach to create a wide range of tunicamycin analogues, our understanding of the biosynthetic pathway is still in its infancy. Alternatively, as we have discussed in subsections **1.4** on the synthetic procedures published on the total syntheses and analogue syntheses of tunicamycins, synthetic strategies can be adopted. However, the low yields and numerous steps required as reported in the published procedures render them impractical for our purposes. We have therefore chosen a semi-synthetic approach to achieve our desired goals.

Firstly, we would isolate the tunicamycins from *S. chartreusis*, which would provide sufficient quantities for further experimentation when compared to chemical syntheses. Subsequently, we would chemically degrade the tunicamycins to isolate the core scaffolds and additionally use those scaffolds to synthesise the tunicamycin lipid analogues. We would continue to investigate the tunicamycin biosynthetic pathway by investigating the enzymes *in vivo* and *in vitro*. The investigation of the enzymes in the biosynthetic pathway could lead to the discovery of unique and novel enzymatic mechanisms for the construction of tunicamycin's eleven carbon tunicamine and the α,β-(1"-11')-glycosidic linkage. Moreover, the enzymes from the pathway would greatly complement the semi-synthetic strategies of the tunicamycin core scaffolds and analogues.

Furthermore, the scaffolds may be used as intermediate substrates for enzyme activity characterisation and then the characterised enzymes could be used as biochemical tools to generate analogues. Finally, we would also investigate the biological properties of the tunicamycin core scaffolds and the lipid analogues to fill the gap in the literature regarding the influence of the lipid chain. A summary of the strategy is shown in **Fig. 1.40**. Our results to this extent will be detailed in this thesis.

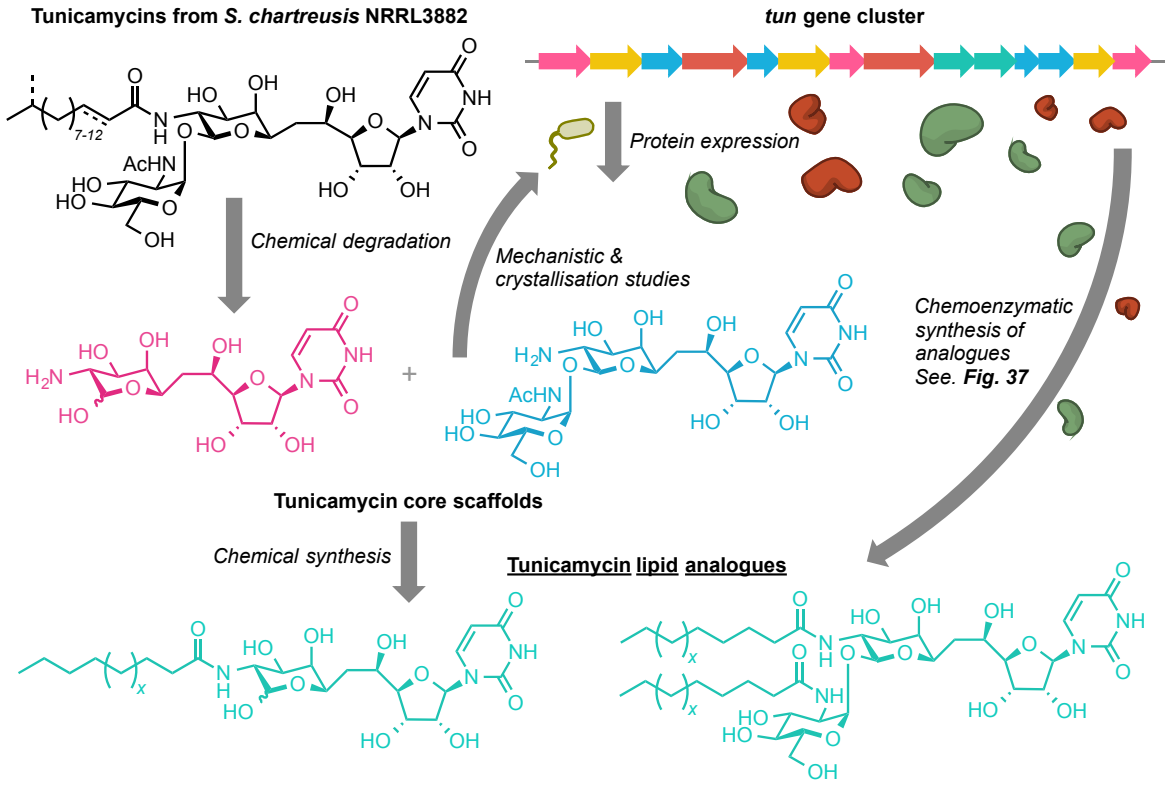


**Figure 1.40 | A summary of the semi-synthetic approach towards the tunicamycin core scaffolds and analogues.** The *x* represents the diversity of the lipid chain possible that can be placed on the 10' and 2" terminal end of tunicamycins to make a library of lipid analogues.

## 1.6 References


1 Takatsuki, A., Arima, K. & Tamura, G. Tunicamycin, A New Antibiotic. I: Isolation and Characterization of Tunicamycin. *The Journal of Antibiotics* **24**, 215-223 (1971).

2 Hamill, R. L. Process for preparing tunicamycin. United States patent 4237225 (1980).

3 Hamill, R. L., Hoehn, M. M. & Boeck, L. D. Process for preparing tunicamycin. United States patent 4336333 (1982).

4 Tejera, E., Currie, S. A., Flor, J. E. & Monaghan, R. L. Process for producing tunicamycin. United States patent 4330624 (1982).

5 Kenig, M. & Reading, C. Holomycin and an Antibiotic (MM 19290) Related to Tunicamycin, Metabolites of Streptomyces clavuligerus. *The Journal of Antibiotics* **32**, 549-554 (1979).

6 Kamogashira, T., Takegata, S. & Sugiura, K. Isolation of Tunicamycin Produced by Bacillus cereus K-279. *Agric. Biol. Chem.* **52**, 859-861 (1988).

7 Doroghazi, J. R. *et al.* Genome Sequences of Three Tunicamycin-Producing Streptomyces Strains, S. chartreusis NRRL 12338, S. chartreusis NRRL 3882, and S. lysosuperificus ATCC 31396. *J. Bacteriol.* **193**, 7021-7022 (2011).

8 Takatsuki, A. & Tamura, G. Tunicamycin, A New Antibiotic. II: Some Biological Properties of The Antiviral Activity of Tunicamycin. *The Journal of Antibiotics* **24**, 224-231 (1971).

9 Takatsuki, A. & Tamura, G. Tunicamycin, A New Antibiotic. III: Reversal of the Antiviral Activity of Tunicamycin by Aminosugars and their Derivatives. *The Journal of Antibiotics* **24**, 232-238 (1971).

10 Banerjee, A. *et al.* Unfolded Protein Response Is Required in nu/nu Mice Microvasculature for Treating Breast Tumor with Tunicamycin. *The Journal of biological chemistry* **286**, 29127-29138 (2011).

11 Ito, T., Takatsuki, A., Kawamura, K., Sato, K. & Tamura, G. Isolation and Structures of Components of Tunicamycin. *Agric. Biol. Chem.* **44**, 695-698 (1980).

12 Tkacz, J. S. in *Antibiotics VI: Modes and Mechanisms of Microbial Growth Inhibitors* Vol. 6 (ed Fred E. Hahn) 255-278 (Springer Berlin Heidelberg, 1983).

13 Takatsuki, A. *et al.* The Structure of Tunicamycin. *Agric. Biol. Chem.* **41** (1977).

14 Ito, T. *et al.* The Structure of Tunicaminyl Uracil, a Degradation Product of Tunicamycin. *Agric. Biol. Chem.* **41**, 2303-2305 (1977).

15 Xu, L., Appell, M., Kennedy, S., Momany, F. A. & Price, N. P. J. Conformational Analysis of Chirally Deuterated Tunicamycin as an Active Site Probe of UDP-N-Acetylhexosamine:Polyprenol-P N-Acetylhexosamne-1-P Translocases. *Biochemistry* **43**, 13248-13255 (2004).

16 Tsvetanova, B. C. & Price, N. P. J. Liquid Chromatography-Electrospray Mass Spectrometry of Tunicamycin-Type Antibiotics. *Analytical Biochemistry* **289**, 147-156 (2001).

17 Mahoney, W. C. & Duskin, D. Biological activities of the two major components of tunicamycin. *J. Biol. Chem.* **254**, 6572-6576 (1979).

18 Keenan, R. W., Hamill, R. L., Occolowitz, J. L. & Elbein, A. D. Biological Activities of Isolated Tunicamycin and Streptovirudin Fractions. *Biochemistry* **20**, 2968-2973 (1981).

19 Duksin, D. & Mahoney, W. C. Relationship of the Structure and Biological Activitoyf the Natural Homologues of Tunicamycin. *J. Biol. Chem.* **257**, 3105-3109 (1982).

20 Duskin, D., Seiberg, M. & Mahoney, W. C. Inhibition of Protein Glycosylation and Selective Cytotoxicity toward Virally Transformed Fibroblasts Caused by B3-Tunicamycin. *Eur. J. Biochem.* **129**, 77-80 (1982).

21 Seiberg, M. & Duksin, D. Selective Cytotoxicity of Purified Homologues of Tunicamycin on Transformed BALB/3T3 Fibroblasts. *Cancer Res.* **43**, 845-850 (1983).

22 Eren, R. & Duskin, D. Inhibition of the formation of lipid-linked intermediates in normal and transformed cells by a purified tunicamycin homologue. *Molecular and Cellular Biochemistry* **67**, 39-46 (1985).

23 Mahoney, W. C. & Duksin, D. Separation of tunicamycin homologues by reversed-phased high-performance liquid chromatography. *Journal of Chromatography* **198**, 506-510 (1980).

24 Eckardt, K. Tunicamycins, Streptovirudins, and Corynetoxins, a Special Subclass of Nucleoside Antibiotics. *J. Nat. Prod.* **46**, 544-550 (1983).

25 Winn, M., Goss, R. J. M., Kimura, K.-i. & Bugg, T. D. H. Antimicrobial Nucleoside Antibiotics Targeting Cell Wall Assembly: Recent Advances in Structure-Function Studies and Nucleoside Biosynthesis. *Natural Product Reports* **27**, 279-304 (2010).

26 Isono, K. Nucleoside Antibiotics: Structure, Biological Activity, and Biosynthesis. *The Journal of Antibiotics* **41** (1988).

27 Périgaud, C., Gosselin, G. & Imbach, J. L. Nucleoside Analogues as Chemotherapeutic Agents: A Review. *Nucleosides and Nucleotides* **11**, 903-945 (1992).

28 Knapp, S. Synthesis of Complex Nucleoside Antibiotics. *Chem. Rev.* **95**, 1859-1876 (1995).

29 Ichikawa, S. & Matsuda, A. Nucleoside Natural Products and Related Analogs with Potential Therapeutic Properties as Antibacterial and Antiviral Agents. *Expert Opinion on Therapeutic Patens* **17**, 487-498 (2007).

30 Thrum, H. *et al.* Streptovirudins, New Antibiotics with Antibacterial and Antiviral Activity. I. Culture Taxonomy, Fermentation and Production of Streptovirudin Complex. *The Journal of Antibiotics* **28**, 514-521 (1975).

31 Vogel, P. *et al.* Isolation of a Group of Glycolipid Toxins from Seedheads of Annual Ryegrass (Lolium rigidum Gaud.) Infected by Corynebacterium rathayi. *Aust. J. Exp. Biol. Med. Sci.* **59**, 455-467 (1981).

32 Mizuno, M., Shimojima, Y., Sugawara, T. & Takeda, I. An Antibiotic 24010. *The Journal of Antibiotics* **24**, 896-899 (1971).

33 Nakamura, S., Arai, M., Karasawa, K. & Yonehara, H. On an Antibiotic, Mycospocidin. *The Journal of Antibiotics* **10**, 248-253 (1957).

34 Tkacz, J. S. & Wong, A. Comparison of the Biological and Chemical Properties of Tunicamycin and Mycospocidin. *Fed. Proc.* **37**, 1766 (1978).

35 Yamamori, S., Murazumi, N., Araki, Y. & Ito, E. Formation and Function of N-acetyloglucosamine-linked Phosphoryl- and Pyrophosphorylundecaprenols in Membranes from Bacillus cereus. *J. Biol. Chem.* **253**, 6516-6522 (1978).

36 Elbein, A. D., Gafford, J. & Kang, M. S. Inhibition of Lipid-linked Saccharide Synthesis: Comparison of Tunicamycin, Streptovirudin, and Antibiotic 24010. *Archives of Biochemistry and Biophysics* **196**, 311-318 (1979).

37 McDonald, L. A. *et al.* Structures of the Muraymycins, Novel Peptidoglycan Biosynthesis Inhibitors. *J. Am. Chem. Soc.* **124**, 10260-10261 (2002).

38 Eckardt, K., Thrum, H., Bradler, G., Tonew, E. & Tonew, M. Streptovirudins, New Antibiotics with Antibacterial and Antiviral Activity. II. Isolation, Chemical Characterisation and Biological Activity of Streptovirudins A1, A2, B1, B2, C1, C2, D1, and D2. *The Journal of Antibiotics* **28**, 274-279 (1975).

39 Elbein, A. D., Occolowitz, J. L., Hamill, R. L. & Eckardt, K. Streptovirudins of Series I and II: Chemical and Biological Properties. *Biochemistry* **20**, 4210-4216 (1981).

40 Edgar, J. A. *et al.* Corynetoxins Causative Agents of Annual Ryegrass Toxicity; Their Identification as Tunicamycin Group Antibiotics. *J. Chem. Soc., Chem. Commun.*, 222-224 (1982).

41 Jago, M. V., Payne, A. L., Peterson, J. E. & Bagust, T. J. Inhibition of Glycosylation by Corynetoxin, the Causative Agent of Annual Ryegrass Toxicity: a Comparison with Tunicamycin. *Chem. Biol. Interact.* **45**, 223-234 (1983).

42 Cockrum, P. A. & Edgar, J. A. Corynetoxin: A Chromatographic Study. *Toxicon* **21**, 65-68 (1983).

43 Eckardt, K., Ihn, W., Tresselt, D. & Krebs, D. The Chemical Structures of Streptovirudins. *The Journal of Antibiotics* **34**, 1631-1632 (1981).

44 *Tunicamycin*. (Japan Scientific Societies Press, 1982).

45 Patterson, S. I. & Skene, J. H. P. Novel Inhibitory Action of Tunicamycin Homologues Suggests a Role for Dynamic Protein Fatty Acylation in Growth Cone-mediated Neurite Extension. *The Journal of cell biology* **124**, 521-536 (1994).

46 Yusuf, H. K. M., Pohlentz, G. & Sandhoff, K. Tunicamycin inhibits ganglioside biosynthesis in rat liver Golgi apparatus by blocking sugar nucleotide transport across the membrane vesicles. *Proc. Natl. Acad. Sci. USA* **80**, 7075-7079 (1983).

47 Guarnaccia, S. P., Shaper, J. H. & Schnaar, R. L. Tunicamycin inhibits ganglioside biosynthesis in neuronal cells. *Proc. Natl. Acad. Sci. USA* **80**, 1551-1555 (1983).

48 Yanagishita, M. Tunicamycin Inhibits Proteoglycan Synthesis in Rat Ovarian Granulosa Cells in Culture. *Archives of Biochemistry and Biophysics* **251**, 287-298 (1986).

49 Volpe, J. J. & Goldberg, R. I. Effect of Tunicamycin on 3-Hydroxy-3-methylglutaryl Coenzyme A Reductase in C-6 Glial Cells. *J. Biol. Chem.* **258**, 9220-9226 (1983).

50 Takatsuki, A. & Tamura, G. Effect of Tunicamycin on the Synthesis of Macromolecules in Cultures of Chick Embryo Fibroblasts Infected with Newcastle Disease Virus. *The Journal of Antibiotics* **24**, 785-794 (1971).

51 Bettinger, G. E. & Young, F. E. Tunicamycin, An Inhibitor of Bacillus Peptidoglycan Synthesis: A New Site of Inhibition. *Biochem Biophys Res. Commun.* **67**, 16-21 (1975).

52 Tkacz, J. S. & Lampen, J. O. Tunicamycin Inhibition of Polyisoprenyl N-Acetylglucosaminyl Pyrophosphate Formation in Calf-Liver Microsomes. *Biochem. Biophys. Res. Commun.* **65**, 248-257 (1975).

53 Tamura, G., Sasaki, T., Matsuhashi, M., Takatsuki, A. & Yamasaki, M. Tunicamycin Inhibits the Formation of Lipid Intermediate in Cell-free Peptidoglycan Synthesis of Bacteria. *Agric. Biol. Chem.* **40**, 447-449 (1976).

54 Takatsuki, A., Shimizu, K.-I. & Tamura, G. Effect of Tunicamycin on Microorganisms: Morphological Changes and Degradation of RNA and DNA Induced by Tunicamycin. *The Journal of Antibiotics* **25**, 75-85 (1972).

55 Kuo, S. C. & Lampen, J. O. Tunicamycin - An Inhibitor of Yeast Glycoprotein Synthesis. *Biochem. Biophys. Res. Commun.* **58**, 287-295 (1974).

56 Kohno, K., Hiragun, A., Mitsui, H., Takatsuki, A. & Tamura, G. Effect of Tunicamycin on Cell Growth and Morphology of Nontransformed and Transformed Cell Lines. *Agric. Biol. Chem.* **43**, 1553-1561 (1979).

57 Nedvidek, J., Antalikova, L. & Romanovsky, A. Cell surface morphology of the mophorgenetically active system of the embryo after treatment with Tunicamycin, a glycosylation blocking drug. *Histochemical Journal* **17**, 529-531 (1985).

58 Leavitt, R., Schlesinger, S. & Kornfeld, S. Impaired Intracellular Migration and Altered Solubility of Nonglycosylated Glycoproteins of Vesicular Stomatitis Virus and Sindbis Virus. *The Journal of biological chemistry* **252**, 9018-9023 (1977).

59 Leavitt, R., Schlesinger, S. & Kornfeld, S. Tunicamycin Inhibits Glycosylation and Multiplication of Sindbis and Vesicular Stomatitis Viruses. *Journal of virology* **21**, 375-385 (1977).

60 Morrison, T. G. & Simpson, D. Synthesis, Stability, and Cleavage of Newcastle Disease Virus Glycoproteins in the Absence of Glycosylation. *Journal of virology* **36**, 171-180 (1980).

61 Kuo, S. C. & Lampen, O. Tunicamycin Inhibition of [3H] Glucosamine Incorporation into Yeast Glycoprotein: Binding of Tunicamycin and Interaction with Phospholipids. *Archives of Biochemistry and Biophysics* **172**, 574-581 (1976).

62 Heifetz, A. & Elbein, A. D. Solubilization and Properties of Mannose and N-acetylglucosamine Transferases Involved in Formation of Polyprenyl-sugar Intermediates. *J. Biol. Chem.* **252**, 3057-3063 (1977).

63 Heifetz, A., Keenan, R. W. & Elbein, A. D. Mechanism of Action of Tunicamycin on UDP-GlcNAc:Dolichyl-Phosphate GlcNAc-1-Phosphate Transferase. *Biochemistry* **18**, 2186-2192 (1979).

64 Elbein, A. D. The Tunicamycins - Useful Tools for Studies of Glycoproteins. *Trends in Biochemical Sciences* **6**, 219-221 (1981).

65 Ikeda, M., Wachi, M., Jung, H. K., Ishino, F. & Matsuhashi, M. The Escherichia coli mraY Gene Encoding UDP-N-Acetylmuramoyl-Pentapeptide:Undecaprenyl-Phosphate Phospho-N-Acetylmuramoyl-Pentapeptide Transferase. *Journal of bacteriology* **173**, 1021-1026 (1991).

66 Gram, C. Ueber die isolirte Färbung der Schizomyceten in Schnitt-und Trockenpräparaten. *Fortschritte der Medcin* **2**, 185-189 (1884).

67 Visca, P. *et al.* Community-Acquired Acinetobacter radioresistens Bacteremia in an HIV-Positive Patient. *Emerging Infectious Diseases* **7**, 1033-1035 (2001).

68 Noviello, S. *et al.* Laboratory-acquired Brucellosis. *Emerging Infectious Diseases* **10**, 1848-1850 (2004).

69 Beveridge, T. J. Mechanism of Gram Variability in Select Bacteria. *Journal of bacteriology* **172**, 1609-1620 (1990).

70 Ghuysen, J.-M. & Goffin, C. Lack of Cell Wall Peptidoglycan versus Penicillin Sensitivity: New Insights into the Clamydial Anomaly. *Antimicrob. Agents Chemother.* **43**, 2339-2344 (1999).

71 Vollmer, J. *et al.* Requirement of Lipid II Biosynthesis for Cell Division in Cell Wall-less Wolbachia, Endobacteria of Arthropods and Filarial Nematodes. *International Journal of Medical Microbiology* **303**, 140-149 (2013).

72 Liechti, G. W. *et al.* A New Metabolic Cell-wall Labelling Method Reveals Peptidoglycan in Chlamydia trachomatis. *Nature* **506**, 507-510 (2014).

73 Sadhu, K. *et al.* Gardnerella vaginalis has a Gram-positive Cell-wall Ultrastructure and Lacks Classical Cell-wall Lipopolysaccharide. *J. Med. Microbiol.* **29** (1989).

74 Seltmann, G. & Holst, O. *The Bacterial Cell Wall*. (Springer-Verlag Berlin Heidelberg, 2002).

75 Saviola, B. & Bishai, W. in *The Prokarytoes* Vol. 3 (eds Martin Dworkin *et al.*) 919-933 (Springer New York, 2006).

76 Davies, J. A., Anderson, G. K., Beveridge, T. J. & Clark, H. C. Chemical Mechanism of the Gram Stain and Synthesis of a New Electron-Opaque Marker for Electron Microscopy which Replaces the Iodine Mordant of the Stain. *J. Bacteriol.* **156**, 837-845 (1983).

77 Beveridge, T. J. & Davies, J. A. Cellular Responses of Bacillus subtilis and Escherichia coli to the Gram Stain. *J. Bacteriol.* **1983**, 846-858 (1983).

78 Navarre, W. W. & Schneewind, O. Surface Proteins of Gram-Positive Bacteria and Mechanisms of Their Targeting to the Cell Wall Envelope. *Microbiology and Molecular Biology Reviews* **63**, 174-229 (1999).

79 Nikaido, H. Molecular Basis of Bacterial Outer Membrane Permeability Revisited. *Microbiology and Molecular Biology Reviews* **67**, 593-656 (2003).

80 Rosenthal, K. S. & Tan, M. J. *Rapid Review Microbiology and Immunology*. 3rd edn, (Elsevier, 2011).

81 Vollmer, W., Blanot, D. & Pedro, M. A. d. Peptidoglycan Structure and Architecture. *FEMS Microbiol. Rev.* **32**, 149-167 (2008).

82 Park, J. T. Uridine-5'-pyrophosphate Derivatives. I. Isolation from Staphylococcus aureus. *J. Biol. Chem.* **194**, 877-884 (1952).

83 Heijenoort, J. v. Recent Advances in the Formation of the Bacterial Peptidoglycan Monomer Unit. *Nat. Prod. Rep.* **18**, 503-519 (2001).

84 Hegde, S. S. & Shrader, T. E. FemABX Family Members Are Novel Nonribosomal Peptidyltransferases and Important Pathogen-specific Drug Targets. *J. Biol. Chem.* **276**, 6998-7003 (2001).

85 Schneider, T. & Sahl, H.-G. An Oldie but a Goodie - Cell Wall Biosynthesis as Antibiotic Target Pathway. *International Journal of Medical Microbiology* **300**, 161-169 (2010).

86 Ruiz, N. Bioinformatics Identification of MurJ (MviN) as the Peptidoglycan Lipid II Flippase in Escherichia Coli. *PNAS* **105**, 15553-15557 (2008).

87 Sanyal, S. & Menon, A. K. Flipping Lipids: Why an' What's the Reason For? *ACS Chem. Biol.* **4**, 895-909 (2009).

88 Komatsuzawa, H. *et al.* The Gate Controlling Cell Wall Synthesis in Staphylococcus aureus. *Mol. Microbiol.* **53**, 1221-1231 (2004).

89 Golinelli-Pimpaneau, B., Goffic, F. L. & Badet, B. Glucosamine-6-phosphate Synthase from Escherichia coli: Mechanism of the Reaction at the Fructose 6-Phosphate Binding Site. *J. Am. Chem. Soc.* **111**, 3029-3034 (1989).

90 Teplyakov, A., Leriche, C., Obmolova, G., Badet, B. & Badet-Denisot, M.-A. From Lobry de Bruyn to Enzyme-catalyzed Ammonia Channelling: Molecular Studies of D-glucosamine-6P Synthase. *Natural Product Reports* **19**, 60-69 (2002).

91 Jolly, L. *et al.* Reaction Mechanism of Phosphoglucosamine Mutase from Escherichia coli. *Eur. J. Biochem.* **262**, 202-210 (1999).

92 Barreteau, H. *et al.* Cytoplasmic Steps of Peptidoglycan Biosynthesis. *FEMS Microbiol. Rev.* **32**, 168-207 (2008).

93 Mengin-Lecreulx, D. & Heijenoort, J. v. Copurification of Glucosamine-1-phosphate Acetyltransferase and N-acetylglucosamine-1-phosphate Uridyltransferase Activities of Escherichia coli: Characterization of the glmU gene Product as a Bifunctional Enzyme Catalyzing Two Subsequent Steps in the Pathway for UDP-N-acetylglucosamine Synthesis. *J. Bacteriol.* **176**, 5788-5795 (1994).

94 Gehring, A. M., Lees, W. J., Mindiola, D. J., Walsh, C. T. & Brown, E. D. Acetyltransfer Precedes Uridylyltransfer in the Formation of UDP-N-acetylglucosamine in Separable Active Sites of the Bifunctional GlmU Protein of Escherichia coli. *Biochemistry* **35**, 579-585 (1996).

95 Eschenburg, S., Kabsch, W., Healy, M. L. & Schönbrunn, E. A New View of the Mechanisms of UDP-N -Acetylglucosamine Enolpyruvyl Transferase (MurA) and 5-Enolpyruvylshikimate-3-phosphate Synthase (AroA) Derived from X-ray Structures of Their Tetrahedral Reaction Intermediate States. *J. Biol. Chem.* **278**, 49215-49222 (2003).

96 Benson, T. E., Walsh, C. T. & Hogle, J. M. The Structure of the Substrate-free Form of MurB, an Essential Enzyme for the Synthesis of Bacterial Cell Walls. *Structure* **4**, 47-54 (1996).

97 Smith, C. A. Structure, Function and Dynamics in the mur Family of Bacterial Cell Wall Ligases. *Journal of molecular biology* **362**, 640-655 (2006).

98 Dhalla, A. M. *et al.* Steady-State Kinetic Mechanism of Escherichia coli UDP-N-Acetylenolpyruvylglucosamine Reductase. *Biochemistry* **34** (1995).

99 Eschenburg, S., Priestman, M. & Schönbrunn, E. Evidence that the Fosfomycin Target Cys115 in UDP-N-acetylglucosamine Enolpyruvyl Transferase (MurA) is Essential for Product Release. *J. Biol. Chem.* **280**, 3757-3763 (2005).

100 Rohrer, S. & Berger-Bächi, B. FemABX Peptidyl Transferases: a Link between Branched-Chain Cell Wall Peptide Formation and β-Lactam Resistance in Gram-Positive Cocci. *Antimicrob. Agents Chemother.* **47**, 837-846 (2003).

101 Tatar, L. D., Marolda, C. L., Polischuk, A. N., Leeuwen, D. v. & Valvano, M. A. An Escherichia coli Undecaprenyl-pyrophosphate Phosphatase Implicated in Undecaprenyl Phosphate Recycling. *Microbiology* **153**, 2518-2529 (2007).

102 Manat, G. *et al.* Deciphering the Metabolism of Undecaprenyl-Phosphate: The Bacterial Cell-Wall Unit Carrier at the Membrane Frontier. *Microbial Drug Resistance* **20**, 199-214 (2014).

103 Ghachi, M. E., Bouhss, A., Blanot, D. & Mengin-Lecreulx, D. The bacA Gene of Escherichia coli Encodes an Undecaprenyl Pyrophosphate Phosphatase Activity. *The Journal of biological chemistry* **279**, 30106-30113 (2004).

104 Lombard, J. & Moreira, D. Origins and Early Evolution of the Mevalonate Pathway of Isoprenoid Biosynthesis in the Three Domains of Life. *Mol. Biol. Evol.* **28**, 87-99 (2011).

105 Ko, T.-P. *et al.* Mechanism of Product Chain Length Determination and the Role of a Flexible Loop in Escherichia coli Undecaprenyl-pyrophosphate Synthase Catalysis. *J. Biol. Chem.* **276**, 47474-47482 (2001).

106 Guo, R.-T. *et al.* Crystal Structures of Undecaprenyl Pyrophosphate Synthase in Complex with Magnesium, Isopentenyl Pyrophosphate, and Farnesyl Thiopyrophosphate. *J. Biol. Chem.* **280** (2005).

107 Bouhss, A., Crouvoisier, M., Blanot, D. & Mengin-Lecreulx, D. Purification and Characterization of the Bacterial MraY Translocase Catalyzing the First Membrane Step of Peptidoglycan Biosynthesis. *J. Biol. Chem.* **279**, 29974-29980 (2004).

108 Bouhss, A., Trunkfield, A. E., Bugg, T. D. H. & Mengin-Lecreulx, D. The Biosynthesis of Peptidoglycan Lipid-linked Intermediates. *FEMS Microbiol. Rev.* **32**, 208-233 (2008).

109 Ha, S., Walker, D., Shi, Y. & Walker, S. The 1.9 Å Crystal Structure of Escherichia coli MurG, a Membrane-Associated Glycosyltransferase Involved in Peptidoglycan Biosynthesis. *Protein Science* **9**, 1045-1052 (2000).

110 Struve, W. G., Sinha, R. K. & Neuhaus, F. C. On the Initial Stage in Peptidoglycan Synthesis. Phospho-N-acetylmuramyl-pentapeptide Translocase. *Biochemistry* **5**, 82-93 (1966).

111 Stickgold, R. A. & Neuhaus, F. On the Initial Stage in Peptidoglycan Synthesis: Effect of 5-fluorouracil Substitution on Phospho-N-acetylmuramyl-pentapeptide Translocase (Uridine 5'-Phosphate). *J. Biol. Chem.* **242**, 1331-1337 (1967).

112 Menard G . Heydanek, J., Struve, W. G. & Neuhaus, F. C. On the Initial Stage in Peptidoglycan Synthesis. III. Kinetics and Uncoupling of Phospho-N-acetylmuramyl-pentapeptide Translocase (Uridine 5'-Phosphate). *Biochemistry* **8**, 1214-1221 (1969).

113 Menard G. Heydanek, J. & Neuhaus, F. C. The initial stage in peptidoglycan synthesis. IV. Solubilization of phospho-N-acetylmuramyl-pentapeptide translocase. *Biochemistry* **8**, 1474-1481 (1969).

114 Pless, D. D. & Neuhaus, F. C. Initial membrane reaction in peptidoglycan synthesis: lipid dependence of phospho-N-acetylmuramyl-pentapeptide translocase (exchange reaction). *J. Biol. Chem.* **248**, 1568-1576 (1973).

115 Chen, L. *et al.* Intrinsic Lipid Preferences and Kinetic Mechanism of Escherichia coli MurG. *Biochemistry* **41**, 6824–6833 (2002).

116 Lloyd, A. J., Brandish, P. E., Gilbey, A. M. & Bugg, T. D. H. Phospho-N-Acetyl-Muramyl-Pentapeptide Translocase from Escherichia coli: Catalytic Role of Conserved Aspartic Acid Residues. *J. Bacteriol.* **186**, 1747-1757 (2004).

117 Price, N. P. & Momany, F. A. Modeling bacterial UDP-HexNAc: polyprenol-P HexNAc-1-P transferases. *Glycobiology* **15**, 29R-42R, doi:10.1093/glycob/cwi065 (2005).

118 Bugg, T. D. H., Lloyd, A. J. & Roper, D. I. Phospho-MurNAc-Pentapeptide Translocase (MraY) as a Target for Antibacterial Agents and Antibacterial Proteins. *Infectious Disorders - Drug Targets* **6**, 85-106 (2006).

119 Al-Dabbagh, B. *et al.* Active Site Mapping of MraY, a Member of the Polyprenyl-phosphate N-Acetylhexosamine 1-Phosphate Transferase Superfamily, Catalyzing the First Membrane Step of Peptidoglycan Biosynthesis. *Biochemistry* **47**, 8919–8928 (2008).

120 Chung, B. C. *et al.* Crystal Structure of MraY, an Essential Membrane Enzyme for Bacterial Cell Wall Synthesis. *Science* **341**, 1012-1016 (2013).

121 Sauvage, E., Kerff, F., Terrak, M., Ayala, J. A. & Charlier, P. The Penicillin-binding Proteins: Structure and Role in Peptidoglycan Biosynthesis. *FEMS Microbiology Review* **32** (2008).

122 Goffin, C. & Ghuysen, J.-M. Multimodular Penicillin-Binding Proteins: An Enigmatic Family of Orthologs and Paralogs. *Microbiology and Molecular Biology Reviews* **62**, 1079-1093 (1998).

123 Spratt, B. G., Zhou, J., Taylor, M. & Merrick, M. J. Monofunction Biosynthetic Peptidoglycan Transglycosylases. *Molecular microbiology* **19**, 639-641 (1996).

124 Derouaux, A. *et al.* The Monofunctional Glycosyltransferase of Escherichia coli Localizes to the Cell Division Site and Interacts with Penicillin-Binding Protein 3, FtsW, and FtsN. *J. Bacteriol.* **190**, 1831-1834 (2007).

125 Barrett, D. *et al.* Analysis of Glycan Polymers Produced by Peptidoglycan Glycosyltransferases. *J. Biol. Chem.* **282** (2007).

126 Höltje, J.-V. Growth of the Stress-Bearing and Shape-Maintaining Murein Sacculus of Escherichia coli. *Microbiology and Molecular Biology Reviews* **62**, 181-203 (1998).

127 Macheboeuf, P., Contreras-Martel, C., Job, V., Dideberg, O. & Dessen, A. Penicillin Binding Proteins: Key Players in Bacterial Cell Cycle and Drug Resistance Processes. *FEMS Microbiology Review* **30**, 673-691 (2006).

128 Terrak, M. *et al.* The Catalytic, Glycosyl transferase and Acyl Transferase Modules of the Cell Wall Peptidoglycan-polymerizing Penicillin-binding Protein 1b of Escherichia coli. *Molecular microbiology* **34**, 350-364 (1999).

129 Heijenoort, J. v. Formation of the Glycan Chains in the Synthesis of Bacterial Peptidoglycan. *Glycobiology* **11**, 25R-36R (2001).

130 Lee, W. *et al.* A 1.2-Å snapshot of the Final Step of Bacterial Cell Wall Biosynthesis. *PNAS* **98**, 1427-1431 (2001).

131 Huang, C.-Y. *et al.* Crystal Structure of Staphylococcus aureus Transglycosylase in Complex with a Lipid II Analog and Elucidation of Peptidoglycan Synthesis Mechanism. *PNAS* **109**, 6496-6501 (2012).

132 Hare, R. New Light on the History of Penicillin. *Medical History* **26**, 1-24 (1982).

133 Walsh, C. Where Will New Antibiotics Come From? *Nature Reviews Microbiology* **1**, 65-70 (2003).

134 Butler, M. S., Blaskovich, M. A. & Cooper, M. A. Antibiotics in the Clinical Pipeline in 2013. *J. Antibiot.* **66**, 571-591 (2013).

135 May, M. Time for Teamwork. *Nature* **509**, S4-S5 (2014).

136 Reardon, S. Antibiotic Resistance Sweeping Developing World. *Nature* **509**, 141-142 (2014).

137 Stone, K. J. & Strominger, J. L. Mechanism of Action of Bacitracin: Complexation with Metal Ion and C55-Isoprenyl Pyrophosphate. *Proc. Natl. Acad. Sci. USA* **68**, 3223-3227 (1971).

138 Lambert, M. P. & Neuhaus, F. C. Mechanism of D-Cycloserine Action: Alanine Racemase from Escherichia coli W. *J. Bacteriol.* **110**, 978-987 (1972).

139 Kahan, F. M., Kahan, J. S., Cassidy, P. J. & Kropp, H. The Mechanism of Action of Fosfomycin (Phosphonomycin). *Ann. N. Y. Acad. Sci.* **235**, 264-386 (1974).

140 Sheldrick, G. M., Jones, P. G., Kennard, O., Williams, D. H. & Smith, G. A. Structure of Vancomycin and its Complex with acetyl-D-alanyl-D-alanine. *Nature* **271**, 223-225 (1978).

141 Reynolds, P. E. Structure, Biochemistry and Mechanism of Action of Glycopeptide Antibiotics. *Eur. J. Clin. Microbiol. Infect. Dis.* **8**, 943-950 (1989).

142 Shigi, Y. Inhibition of Bacterial Isoprenoid Synthesis by Fosmidomycin, a Phosphonic Acid-containing Antibiotic. *J. Antimicrob. Chemother.* **24**, 131-145 (1989).

143 Brandish, P. E. *et al.* Modes of Action of Tunicamycin, Liposidomycin B, and Mureidomycin A: Inhibition of Phospho-N-acetylmuramyl-pentapeptide Translocase from Escherichia coli. *Antimicrob. Agents Chemother.* **40**, 1640-1644 (1996).

144 Brötz, H. & Sahl, H.-G. New Insights into the Mechanism of Action of Lantibiotics —Diverse Biological Effects by Binding to the Same Molecular Target. *J. Antimicrob. Chemother.* **46**, 1-6 (2000).

145 Jung, D., Rozek, A., Okon, M. & Hancock, R. E. W. Structural Transitions as Determinants of the Action of the Calcium-Dependent Antibiotic Daptomycin. *Chemistry & Biology* **11** (2004).

146 Mygind, P. H. *et al.* Plectasin is a Peptide Antibiotic with Therapeutic Potential from a Saprophytic fungus. *Nature* **437**, 975-980 (2005).

147 Breukink, E. & Kruijff, B. d. Lipid II as a Target for Antibiotics. *Nature Reviews Drug Discovery* **5**, 321-332 (2006).

148 Schneider, T. *et al.* The Lipopeptide Antibiotic Friulimicin B Inhibits Cell Wall Biosynthesis through Complex Formation with Bactoprenol Phosphate. *Antimicrob. Agents Chemother.* **53**, 1610-1618 (2009).

149 Ostash, B. & Walker, S. Moenomycin Family Antibiotics: Chemical Synthesis, Biosynthesis, and Biological Activity. *Nat. Prod. Rep.* **27**, 1594-1617 (2010).

150 Velkov, T., Thompson, P. E., Nation, R. L. & Li, J. Structure−Activity Relationships of Polymyxin Antibiotics. *J. Med. Chem.* **53**, 1898-1916 (2010).

151 Bugg, T. D. H., Braddick, D., Dowson, C. G. & Roper, D. I. Bacterial Cell Wall Assembly: Still an Attractive Antibacterial Target. *Trends in Biotechnology* **29**, 167-173 (2011).

152 Lewis, K. Platforms for Antibiotic Discovery. *Nature Reviews Drug Discovery* **12**, 371-387 (2013).

153 Antibiotics Resistance Threats in the United States. (Centers for Disease Control and Prevention, 2013).

154 Global Tuberculosis Report. (World Health Organization, 2013).

155 Wright, G. D. Bacterial Resistance to Antibiotics: Enzymatic Degradation and Modification. *Advanced Drug Delivery Reviews* **57**, 1451-1470 (2005).

156 Davies, J. & Davies, D. Origins and Evolutions of Antibiotic Resistance. *Microbiology and Molecular Biology Reviews* **74**, 417-433 (2010).

157 Fleming, A. in *Nobel Lecture*, 83-93 (1945).

158 Allen, H. K. *et al.* Call of the Wild: Antibiotic Resistance Genes in Natural Environments. *Nature Reviews Microbiology* **8**, 251-259 (2010).

159 Davies, J. & Ryan, K. S. Introducing the Parvome: Bioactive Compounds in the Microbial World. *ACS Chem. Biol.* **7**, 252-259 (2012).

160 Walsh, C. Molecular Mechanisms that Confer Antibacterial Drug Resistance. *Nature* **406**, 775-781 (2000).

161 Rigsby, R. E., Fillgrove, K. L., Beihoffer, L. A. & Armstrong, R. N. Fosfomycin Resistance Proteins: A Nexus of Glutathione Transferases and Epoxide Hydrolases in a Metalloenzyme Superfamily. *Methods in Enzymology* **401**, 367-379 (2005).

162 Tenover, F. C. Mechanisms of Antimicrobial Resistance in Bacteria. *AJIC* **34**, S3-S10 (2006).

163 Bugg, T. D. H. *et al.* Molecular Basis for Vancomycin Resistance in Enterococcusfaecium BM4147: Biosynthesis of a Depsipeptide Peptidoglycan Precursor by Vancomycin Resistance Proteins VanH and VanA. *Biochemistry* **30**, 10408-10415 (1991).

164 Marquardt, J. L. *et al.* Kinetics, Stoichiometry, and Identification of the Reactive Thiolate in the Inactivation of UDP-GlcNAc Enolpyruvoyl Transferase by the Antibiotic Fosfomycin. *Biochemistry* **33**, 10646-10651 (1994).

165 Bernat, B. A., Laughlin, L. T. & Armstrong, R. N. Regiochemical and Stereochemical Course of the Reaction Catalyzed by the Fosfomycin Resistance Protein, FosA. *J. Org. Chem.* **63**, 3778-3780 (1998).

166 Cui, L. *et al.* Novel Mechanism of Antibiotic Resistance Originating in Vancomycin-Intermediate Staphylococcus aureus. *Antimicrob. Agents Chemother.* **50**, 428-438 (2006).

167 Fillgrove, K. L., Pakhomova, S., Schaab, M. R., Newcomer, M. E. & Armstrong, R. N. Structure and Mechanism of the Genomically Encoded Fosfomycin Resistance Protein, FosX, from Listeria monocytogenes. *Biochemistry* **46**, 8110-8120 (2007).

168 Anderson, M. S., Eveland, S. S. & Price, N. P. Conserved cytoplasmic motifs that distinguish sub-groups of the polyprenol phosphate:N-acetylhexosamine-1-phosphate transferase family. *FEMS microbiology letters* **191**, 169-175 (2000).

169 Merino, S. *et al.* A UDP-HexNAc:Polyprenol-P GalNAc-1-P Transferase (WecP) Representing a New Subgroup of the Enzyme Family. *J. Bacteriol.* **193**, 1943-1952 (2011).

170 Kukuruzinska, M. A. & Robbins, P. W. Protein glycosylation in yeast: Transcript heterogeneity of the ALG7 gene. *Proc. Natl. Acad. Sci. USA* **84**, 2145-2149 (1987).

171 Eckert, V. *et al.* Cloning and functional expression of the human GlcNAc-1-P transferase, the enzyme for the committed step of the dolichol cycle, by heterologous complementation in Saccharomyces cerevisiae. *Glycobiology* **8**, 77-85 (1998).

172 Lehrman, M. A. Biosynthesis of N-acetylglucosamine-P-P-dolichol, the committed step of asparagine-linked oligosaccharide assembly. *Glycobiology* **1**, 553-562 (1991).

173 Yamashita, Y. *et al.* A Novel Gene Required for Rhamnose-Glucose Polysaccharide Synthesis in Streptococcus mutans. *J. Bacteriol.* **181**, 6556-6559 (1999).

174 DiGiandomenico, A. *et al.* Glycosylation of Pseudomonas aeruginosa 1244 Pilin: Glycan Substrate Specificity. *Mol. Microbiol.* **2**, 519-530 (2002).

175 Lehrer, J., Vigeant, K. A., Tatar, L. D. & Valvano, M. A. Functional Characterization and Membrane Topology of Escherichia coli WecA, a Sugar-Phosphate Transferase Initiating the Biosynthesis of Enterobacterial Common Antigen and O-Antigen Lipopolysaccharide. *J. Bacteriol.* **189**, 7618-2628 (2007).

176 Brown, S., Meredith, T., Swoboda, J. & Walker, S. Staphylococcus aureus and Bacillus subtilis W23 Make Polyribitol Wall Teichoic Acids Using Different Enzymatic Pathways. *Chemistry & Biology* **17**, 1101-1110 (2010).

177 Sewell, E. W. C. & Brown, E. D. Taking aim at wall teichoic acid synthesis: new biology and new leads for antibiotics. *J. Antibiot.* **67**, 43-51 (2014).

178 Mondego, J. M. c. C., Simões-Araújo, J. L., Oliveira, D. E. d. & Alves-Ferreira, M. A gene similar to bacterial translocase I (mra Y) identified by cDNA-AFLP is expressed during flower bud development of Arabidopsis thaliana. *Plant Science* **164**, 323-331 (2003).

179 Machida, M. *et al.* Genes for the peptidoglycan synthesis pathway are essential for chloroplast division in moss. *Proc. Natl. Acad. Sci. USA* **103**, 6753-6758 (2006).

180 Homi, S. *et al.* The Peptidoglycan Biosynthesis Genes MurA and MraY are Related to Chloroplast Division in the Moss Physcomitrella patens. *Plant Cell Physiol.* **50**, 2047-2056 (2009).

181 Boyle, D. S. & Donachie, W. D. mraY is an essential gene for cell growth in Escherichia coli. *J. Bacteriol.* **180**, 6429-6432 (1998).

182 Bouhss, A., Mengin-Lecreulx, D., Beller, D. L. & Heijenoort, J. v. Topological analysis of the MraY protein catalysing the ®rst membrane step of peptidoglycan synthesis. *Molecular microbiology* **34**, 576-585 (1999).

183 Omasits, U., Ahrens, C. H., Müller, S. & Wollscheid, B. Protter: interactive protein feature visualization and integration with experimental proteomic data. *Bioinformatics*, doi:10.1093/bioinformatics/btt607 (2013).

184 Anderson, J. S., Matsuhashi, M., Haskin, M. A. & Strominger, J. L. Lipid-phosphoacetylmuramyl-pentapeptide and lipid phosphodisaccharide-pentapeptide: Presumed membrane transport intermediates in cell wall synthesis. *Proc. Natl. Acad. Sci. USA* **53**, 881-889 (1965).

185 Struve, W. G. & Neuhaus, F. C. Evidence for an initial acceptor of UDP-NAc-muramyl-pentapeptide in the synthesis of bacterial mucopeptide. *Biochem. Biophys. Res. Commun.* **18**, 6-12 (1965).

186 Heijenoort, J. v. Lipid intermediates in the biosynthesis of bacterial peptidoglycan. *Microbiology and Molecular Biology Reviews* **71**, 620-635 (2007).

187 Ma, Y. *et al.* Preparative Scale Cell-free Production and Quality Optimization of MraY Homologues in Different Expression Modes. *J. Biol. Chem.* **286**, 38844-38853 (2011).

188 Branstrom, A. A. *et al.* Assay for Identification of Inhibitors for Bacterial MraY Translocase or MurG Transferase. *Analytical Biochemistry* **280**, 315-319 (2000).

189 Hyland, S. A. & Anderson, M. S. A high-throughput solid-phase extraction assay capable of measuring diverse polyprenyl phosphate: sugar-1-phosphate transferases as exemplified by the WecA, MraY, and MurG proteins. *Analytical Biochemistry* **317**, 156-164 (2003).

190 Stachyra, T. *et al.* Fluorescence Detection-Based Functional Assay for High-Throughput Screening for MraY. *Antimicrob. Agents Chemother.* **48**, 897-902 (2004).

191 Schouten, J. A. *et al.* Fluorescent reagents for in vitro studies of lipid-linked steps of bacterial peptidoglycan biosynthesis: derivatives of UDPMurNAc-pentapeptide containing D-cysteine at position 4 or 5. *Mol. BioSyst.* **2**, 484-491 (2006).

192 Mendel, S., Holbourn, J. M., Schouten, J. A. & Bugg, T. D. H. Interaction of the transmembrane domain of lysis protein E from bacteriophage ϕX174 with bacterial translocase MraY and peptidyl-prolyl isomerase SlyD. *Microbiology* **152**, 2959-2967 (2006).

193 White, C. L., Kitich, A. & Gober, J. W. Positioning cell wall synthetic complexes by the bacterial morphogenetic proteins MreB and MreD. *Mol. Microbiol.* **76**, 616-633 (2010).

194 Bettinger, G. E. & Young, F. E. Tunicamycin, An Inhibitor of Bacillus Peptidoglycan Synthesis: A New Site of Inhibition. *Biochem. Biophys. Res. Commun.* **67**, 16-21 (1975).

195 Ward, J. B. Tunicamycin inhibition of bacterial wall polymer synthesis. *FEBS Lett.* **78**, 151-154 (1977).

196 Takatsuki, A. & Tamura, G. Preferential incorporation of tunicamycin, an antiviral antibiotic containing glucosamine into the cell membrane. *J. Antibiot.* **25**, 362-264 (1972).

197 Brandish, P. E. *et al.* Slow Binding Inhibition of Phospho-N-acetylmuramyl-pentapeptide- translocase (Escherichia coli) by Mureidomycin A. *J. Biol. Chem.* **271**, 7609-7614 (1996).

198 Murakami, R. *et al.* A-102395, a New Inhibitor of Bacterial Translocase I, Produced by Amycolatopsis sp. SANK 60206. *J. Antibiot.* **60**, 690-695 (2007).

199 Murakami, R. *et al.* A-94964, a Novel Inhibitor of Bacterial Translocase I, Produced by Streptomyces sp. SANK 60404. *J. Antibiot.* **61**, 537-544 (2008).

200 Bernhardt, T. G., Roof, W. D. & Young, R. Genetic evidence that the bacteriophage φX174 lysis protein inhibits cell wall synthesis. *Proc. Natl. Acad. Sci. USA* **97**, 4297-4302 (2000).

201 Bernhardt, T. G., Struck, D. K. & Young, R. The Lysis Protein E of φX174 Is a Specific Inhibitor of the MraY-catalyzed Step in Peptidoglycan Synthesis. *J. Biol. Chem.* **276**, 6093-6097 (2001).

202 Ghachi, M. E. *et al.* Colicin M Exerts Its Bacteriolytic Effect via Enzymatic Degradation of Undecaprenyl Phosphate-linked Peptidoglycan Precursors. *J. Biol. Chem.* **281**, 22761-22772 (2006).

203 Kaushal, G. P. & Elbein, A. D. Purification and properties of UDP-GlcNAc:Dolichyl-phosphate GlcNAc-1-phosphate transferase. *J. Biol. Chem.* **260**, 16303-16309 (1985).

204 Bretthauer, R. K. Structure, expression, and regulation of UDP-GlcNAc: dolichol phosphate GlcNAc-1-phosphate transferase (DPAGT1). *Curr. Drug Targets* **10**, 477-482 (2009).

205 Datta, A. K. & Lehrman, M. A. Both potential dolichol recognition sequences of hamster GlcNAc-1-phosphate transferase are necessary for normal enzyme function. *J. Biol. Chem.* **268**, 12663-12668 (1993).

206 Dan, N. & Lehrman, M. A. Oligomerization of Hamster UDP-GlcNAc:Dolichol-P GlcNAc-1-P Transferase, an Enzyme with Multiple Transmembrane Spans. *J. Biol. Chem.* **272**, 14214-14219 (1997).

207 Spiro, R. G. Protein glycosylation: nature, distribution, enzymatic formation, and disease implications of glycopeptide bonds. *Glycobiology* **12**, 43R-56R (2002).

208 Lowe, J. B. & Marth, J. D. A genetic approach to mammalian glycan function. *Annual Review of Biochemistry* **72**, 643-691 (2003).

209 Eklund, E. A. & Freeze, H. H. Essentials of Glycosylation. *Seminars in Pediatric Neurology* **12**, 134-143 (2005).

210 Raman, R., Raguram, S., Venkataraman, G., Paulson, J. C. & Sasisekharan, R. Glycomics: an integrated systems approach to structure-function relationships of glycans. *Nature Methods* **2**, 817-824 (2005).

211 Varki, A. *et al. Essentials of Glycobiology*. 2nd edn, (Cold Spring Harbor Laboratory Press, 2009).

212 Kelley W. Moremen, M. T. a. A. V. N. Vertebrate protein glycosylation: diversity, synthesis and function. *Nature Reviews Molecular Cell Biology* **14**, 448-462 (2012).

213 Roth, Z., Yehezkel, G. & Khalaila, I. Identification and Quantification of Protein Glycosylation. *International Journal of Carbohydrate Chemistry* **2012**, doi: 10.1155/2012/640923 (2012).

214 Cummings, R. D. The repertoire of glycan determinants in the human glycome. *Mol. BioSyst.* **5**, 1087-1104 (2009).

215 Helenius, A. & Aebi, M. Roles of N-linked glycans in the endoplasmic reticulum. *Annual Review of Biochemistry* **73**, 1019-1049 (2004).

216 Molinari, M. N-glycan structure dictates extension of protein folding or onset of disposal. *Nature Chemical Biology* **3**, 313-320 (2007).

217 Olden, K., Pratt, R. M. & Yamada, K. M. Role of carbohydrates in protein secretion and turnover: effects of tunicamycins on the major cell surface glycoprotein of chick embryo fibroblasts. *Cell* **13**, 461-473 (1978).

218 Helenius, A. & Aebi, M. Intracellular Functions of N-Linked Glycans. *Science* **291**, 2364-2369 (2001).

219 Apweiler, R., Hermjakob, H. & Sharon, N. On the frequency of protein glycosylation, as deduced from analysis of the SWISS-PROT database. *Biochim. Biophys. Acta* **1473**, 4-8 (1999).

220 Pfeffer, S. *et al.* Structure of the mammalian oligosaccharyl-transferase complex in the native ER protein translocon. *Nature Communications* **5**, doi:10.1038/ncomms4072 (2014).

221 Lizak, C., Gerber, S., Numao, S., Aebi, M. & Locher, K. P. X-ray structure of a bacterial oligosaccharyltransferase. *Nature* **474**, 350-355 (2011).

222 Jarrell, K. F. *et al.* N-Linked Glycosylation in Archaea: a Structural, Functional, and Genetic Analysis. *Microbiol. Mol. Biol. Rev.* **78**, 304-341 (2014).

223 Furlong, S. E. & Valvano, M. A. Characterization of the highly conserved VFMGD motif in a bacterial polyisoprenyl-phosphate N-acetylaminosugar-1-phosphate transferase. *Protein Science* **21**, 1366-1375 (2012).

224 Kaushal, G. P. & Elbein, A. D. Properties of Solubilized UDP-GlcNAc: Dolichyl Phosphate-GlcNAc-1-P-Transferase from Soybean Cultured Cells. *Plant Physiol.* **82**, 748-752 (1986).

225 Sharma, C. B., Lehle, L. & Tanner, W. Solubilization and Characterization of the Initial Enzymes of the Dolichol Pathway from Yeast. *Eur. J. Biochem.* **126**, 319-325 (1982).

226 Chandra, N. C., Doody, M. B. & Bretthauer, R. K. Specific Lipids Enhance the Activity of UDP-GlcNAc: Dolichol Phosphate GlcNAc-1-Phosphate Transferase in Rat Liver Endoplasmic Reticulum Membrane Vesicles. *Archives of Biochemistry and Biophysics* **290**, 345-354 (1991).

227 Singh, Y., Shirhatti, V., Liu, C. T., Feller, D. R. & Krishna, G. Inhibition of protein synthesis: A basis for tunicamycin-induced decrease in rat liver cytochrome P-450. *Life Sciences* **37**, 1411-1417 (1985).

228 Chang, J. Y. & Korolev, V. V. Specific toxicity of tunicamycins in induction of programmed cell death of sympathetic neurons. *Experimental Neurology* **137**, 201-211 (1996).

229 Carlberg, M. *et al.* Short exposures to tunicamycins induce apoptosis in SV40-transformed but not in normal human fibroblasts. *Carcinogenesis* **17**, 2589-2596 (1996).

230 Schröder, M. & Kaufman, R. J. The mammalian unfolded protein response. *Annual Review of Biochemistry* **74**, 739-789 (2005).

231 Ron, D. & Walter, P. Signal integration in the endoplasmic reticulum unfolded protein response. *Nature Reviews Molecular Cell Biology* **8**, 519-529 (2007).

232 Wang, X. *et al.* ER stress modulates cellular metabolism. *BIochemical Journal* **435**, 285-296 (2011).

233 Bull, V. H. & Thiede, B. Proteome analysis of tunicamycin-induced ER stress. *Electrophoresis* **33**, 1814-1823 (2012).

234 Hetz, C., Chevet, E. & Harding, H. P. Targeting the unfolded protein response in disease. *Nature Reviews Drug Discovery* **12**, 703-719 (2013).

235 Elbein, A. D. Inhibitors of the biosynthesis and processing of N-linked oligosaccharide chains. *Annual Review of Biochemistry* **56**, 497-534 (1987).

236 Hancock, I. C., Wiseman, G. & Baddiley, J. Biosynthesis of the unit that links teichoic acid to the bacterial cell wall: inhibition by tunicamycin. *FEBS Lett.* **69**, 75-80 (1976).

237 Bracha, R. & Glaser, L. An intermediate in teichoic acid biosynthesis. *Biochem. Biophys. Res. Commun.* **72**, 1091-1098 (1976).

238 Swoboda, J. G., Campbell, J., Meredith, T. C. & Walker, S. Wall Teichoic Acid Function, Biosynthesis, and Inhibition. *ChemBioChem.* **11**, 35-45 (2010).

239 Brown, S., Jr, J. P. S. M. & Walker, S. Wall Teichoic Acids of Gram-Positive Bacteria. *Annu. Rev. Microbiol.* **67**, 313-336 (2013).

240 Soldo, B., Lazarevic, V. & Karamata, D. tagO is involved in the synthesis of all anionic cell-wall polymers in Bacillus subtilis 168. *Microbiology* **148**, 2079-2087 (2002).

241 Formstone, A., Carballido-López, R., Noirot, P., Errington, J. & Scheffers, D.-J. Localization and Interactions of Teichoic Acid Synthetic Enzymes in Bacillus subtilis. *J. Bacteriol.* **190**, 1812-1821 (2008).

242 Swoboda, J. G. *et al.* Discovery of a Small Molecule that Blocks Wall Teichoic Acid Biosynthesis in Staphylococcus aureus. *ACS Chem. Biol.* **4**, 875-883 (2009).

243 Campbell, J. *et al.* Synthetic Lethal Compound Combinations Reveal a Fundamental Connection between Wall Teichoic Acid and Peptidoglycan Biosyntheses in Staphylococcus aureus. *ACS Chem. Biol.* **6**, 106-116 (2011).

244 Holland, L. M., Conlon, B. & O'Gara, J. P. Mutation of tagO reveals an essential role for wall teichoic acids in Staphylococcus epidermidis biofilm development. *Microbiology* **157**, 408-418 (2011).

245 Pasquina, L. W., Maria, J. P. S. & Walker, S. Teichoic acid biosynthesis as an antibiotic target. *Current Opinion in Microbiology* **16**, 531-537 (2013).

246 Weidenmaier, C. *et al.* Role of teichoic acids in Staphylococcus aureus nasal colonization, a major risk factor in nosocomial infections. *Nature Medicine* **10**, 243-245 (2004).

247 Al-Dabbagh, B., Mengin-Lecreulx, D. & Bouhss, A. Purification and Characterization of the Bacterial UDP-GlcNAc:Undecaprenyl-Phosphate GlcNAc-1-Phosphate Transferase WecA. *J. Bacteriol.* **190**, 7141-7146 (2008).

248 Ishizaki, Y. *et al.* Inhibition of the First Step in Synthesis of the Mycobacterial Cell Wall Core, Catalyzed by the GlcNAc-1-phosphate Transferase WecA, by the Novel Caprazamycin Derivative CPZEN-45. *J. Biol. Chem.* **288**, 30309-30319 (2013).

249 Valvano, M. A. in *Comprehensive Natural Products II: Chemistry and Biology* (eds Lewis Mander & Hung-Wen Liu) Ch. 6.10, 297-300 (Elsevier Science, 2010).

250 Meier-Dieter, U., Starman, R., Barr, K., Mayern, H. & Rick, P. D. Biosynthesis of Enterobacterial Common Antigen in Escherichia coli. *J. Biol. Chem.* **265**, 13490-13497 (1990).

251 Linder, M. E. & Deschenes, R. J. Palmitoylation: policing protein stability and traffic. *Nature Reviews Molecular Cell Biology* **8**, 74-84 (2007).

252 Draper, J. M. & Smith, C. D. Palmitoyl acyltransferase assays and inhibitors (Review). *Mol. Membr. Biol.* **26**, 5-13 (2006).

253 Greaves, J. & Chamberlain, L. H. DHHC palmitoyl transferases: substrate interactions and (patho)physiology. *Trends in Biochemical Sciences* **36**, 245-253 (2011).

254 Resh, M. D. Covalent lipid modifications of proteins. *Current Biology* **23**, R431-435 (2013).

255 Baumann, N. A. & Menon, A. K. in *Biochemistry of Lipids, Lipoproteins and Membranes* (eds D. E. Vance & J. E. Vance) Ch. 2, 37-54 (Elsevier Science B.V., 2002).

256 Patterson, S. I. & Skene, J. H. P. Inihibtion of Dynamic Protein Palmitoylation in Intact Cells with Tunicamycin. *Methods in Enzymology* **250**, 284-300 (1995).

257 Politis, E. G., Roth, A. F. & Davis, N. G. Transmembrane Topology of the Protein Palmitoyl Transferase Akr1. *J. Biol. Chem.* **280**, 10156-10163 (2005).

258 Nomura, S. *et al.* Tunicamycin-resistant mutants and chromosomal locations of mutational sites in Bacillus subtilis. *J. Bacteriol.* **136**, 818-821 (1978).

259 Noda, Y., Yoda, K., Takatsuki, A. & Yamasaki, M. TmrB protein, responsible for tunicamycin resistance of Bacillus subtilis, is a novel ATP-binding membrane protein. *J. Bacteriol.* **174**, 4302-4307 (1992).

260 Noda, Y., Takatsuki, A., Yoda, K. & Yamasaki, M. TmrB Protein, Which Confers Resistance to Tunicamycin on Bacillus subtilis, Binds Tunicamycin. *Biosci. Biotech. Biochem.* **59**, 321-322 (1995).

261 Makarova, K. S. *et al.* Genome of the Extremely Radiation-Resistant Bacterium Deinococcus radiodurans Viewed from the Perspective of Comparative Genomics. *Microbiol. Mol. Biol. Rev.* **65**, 44-79 (2001).

262 Kapp, U. *et al.* Structure of Deinococcus radiodurans tunicamycin- resistance protein (TmrD), a phosphotransferase. *Acta Cryst.* **F64**, 479-486 (2008).

263 E.Walker, J., Saraste, M., J.Runswick, M. & NicholasJ.Gay. Distantly related sequences in the alpha- and beta-subunits of ATP synthase, myosin, kinases and other ATP-requiring enzymes and a common nucleotide binding fold. *EMBO J.* **1**, 945-951 (1982).

264 Zeng, Y. & Elbein, A. D. UDP-N-acetylglucosamine:dolichyl-phosphate N-acetylglucosamine-1-phosphate transferase is amplified in tunicamycin-resistant soybean cells. *Eur. J. Biochem.* **233**, 458-466 (1995).

265 Katakura, K., Peng, Y., Pithawalla, R., Detke, S. & Chang, K.-P. Tunicamycin-resistant variants from five species of Leishmania contain amplified DNA in extrachromosomal circles of different sizes with a transcriptionally active homologous region. *Molecular and Biochemica Parasitology* **44**, 233-244 (1991).

266 Koizumi, N., Ujino, T., Sano, H. & Chrispeels, M. J. Overexpression of a Gene That Encodes the First Enzyme in the Biosynthesis of Asparagine-Linked Glycans Makes Plants Resistant to Tunicamycin and Obviates the Tunicamycin-Induced Unfolded Protein Response. *Plant Physiol.* **121**, 351-361 (1999).

267 Rosenwald, A. G., Stoll, J. & Krag, S. S. Regulation of Glycosylation, Three Enzymes Compete for a Common Pool of Dolichyl Phosphate In Vivo. *J. Biol. Chem.* **265**, 14544-14553 (1990).

268 Zhu, X., Zeng, Y. & Lehrman, M. A. Evidence That the Hamster Tunicamycin Resistance Gene Encodes UDP-G1cNAc:Dolichol Phosphate N-Acetylglucosamine-1-phosphate Transferase. *J. Biol. Chem.* **267**, 8895-8902 (1992).

269 Chen, G., Bradford, W. D., Seidel, C. W. & Li, R. Hsp90 stress potentiates rapid cellular adaptation through induction of aneuploidy. *Nature* **482**, 246-250 (2012).

270 Reiling, J. H. *et al.* A haploid genetic screen identifies the major facilitator domain containing 2A (MFSD2A) transporter as a key mediator in the response to tunicamycin. *Proc. Natl. Acad. Sci. USA* **108**, 11756-11765 (2011).

271 Newman, D. J. & Cragg, G. M. Natural Products As Sources of New Drugs over the 30 Years from 1981 to 2010. *J. Nat. Prod.* **75**, 311-335 (2012).

272 Tsvetanova, B. C., Kiemle, D. J. & Price, N. P. J. Biosynthesis of Tunicamycin and Metabolic Origin of the 11-Carbon Dialdose Sugar, Tunicamine. *J. Biol. Chem.* **277**, 35289-35296 (2002).

273 Price, N. P. J. & Tsvetanova, B. Biosynthesis of the Tunicamycins: A Review. *J. Antibiot.* **60**, 485-491 (2007).

274 Wyszynski, F. J., Hesketh, A. R., Bibb, M. J. & Davis, B. G. Dissecting tunicamycin biosynthesis by genome mining: cloning and heterologous expression of a minimal gene cluster. *Chem. Sci.* **1**, 581-589 (2010).

275 Muto, A. & Osawa, S. The guanine and cytosine content of genomic DNA and bacterial evolution. *Proc. Natl. Acad. Sci. USA* **84**, 166-169 (1987).

276 Chen, W. *et al.* Characterization of the tunicamycin gene cluster unveiling unique steps involved in its biosynthesis. *Protein Cell* **1**, 1093-1105 (2010).

277 Karki, S., Kwon, S.-Y. & Kwon, H.-J. Cloning of Tunicamycin Biosynthetic Gene Cluster from Streptomyces chartreusis NRRL 3882. *J. Korean Soc. Appl. Biol. Chem.* **54**, 136-140 (2011).

278 Wöhler, F. Ueber künstliche Bildung des Harnstoffs. *Ann. Phys. Chem.* **12**, 253-256 (1828).

279 Fukuda, Y., Sasi, H. & Suami, T. Synthetic Approach toward Antibiotic Tunicamycins. *Bull. Chem. Soc. Jpn.* **54**, 1830-1833 (1981).

280 Suami, T. *et al.* Synthetic Approach Toward Antibiotic Tunicamycins, 4. X-Ray Crystal Structure Analysis of a Higher-Carbon Nitro Sugar. *J. Carbohydrate Chemistry* **1** (1982).

281 Fukuda, Y., Kitasato, H., Sasi, H. & Suami, T. Synthetic Approach toward Antibiotic Tunicamycins. II. *Bull. Chem. Soc. Jpn.* **55**, 880-886 (1982).

282 Suami, T., Sasi, H. & Matsuno, K. Synthesis of Methyl Hexaacetyl-tunicamyl Uracil. *Chemistry Letters*, 819-822 (1983).

283 Sasai, H., Matsuno, K. & Suami, T. Synthetic Approach Toward Antibiotic Tunicamycins - VII. Synthesis of Tunicamine and Tunicaminyl Uracil Derivative. *J. Carbohydrate Chemistry* **4**, 99-112 (1985).

284 Danishefsky, S. & Barbachyn, M. A Fully Synthetic Route to Tunicaminyluracil. *J. Am. Chem. Soc.* **107**, 7761-7762 (1985).

285 Myers, A. G., Gin, D. Y. & Widdowson, K. L. Silicon-Mediated Reductive Coupling of Aldehydes and Allylic Alcohols. A Stereoselective Synthesis of Tunicaminyluracil. *J. Am. Chem. Soc.* **113**, 9661-9663 (1991).

286 Ramza, J. & Zamojski, A. New Convenient Synthesis of Tunicamine. *Tetrahedron* **48**, 6123-6134 (1992).

287 Ramza, J. & Zamojski, A. The synthesis of S-C-(bdeoxy-1,2:3,4-di-O-isopropylidene-α-D-galactopyranos-6-yl)-2,3-O-isopropylidene-D-aIlo-pentofuranose [deaminotri-O-isopropylidene tunicamine]. *Carbohyd. Res.* **228**, 205-216 (1992).

288 Karpiesiuk, W. & Banaszek, A. Simple Synthesis of O,N-protected Tunicamine - The Undecose Part of Tunicamycins. *Bioorganic & Medicinal Chemistry Letters* **4**, 879-882 (1994).

289 Karpiwiuk, W. & Banazek, A. Simple Approach to O-Protected Deaminotunicaminyluracil. *Tetrahedron* **50**, 2965-2974 (1994).

290 Sarabia-García, F. & López-Herrera, F. J. Studies on the Synthesis of Tunicamycin. The Preparation of 7-deoxy-2-deamino-6-Hydroxy Tunicamine and Related Products. *Tetrahedron* **52**, 4757-4768 (1996).

291 Karpiesiuk, W. & Banaszek, A. Stereoselective syntheses of the O,N-protected subunits of the tunicamycins. *Carbohyd. Res.* **299**, 245-252 (1997).

292 Silva, D. J. & Sofia, M. J. Novel carbohydrate scaffolds. Assembly of a uridine–mannose scaffold based on tunicamycin. *Tetrahedron Letters* **41**, 855-858 (2000).

293 Sarabia, F., Martín-Ortiz, L. & López-Herrera, F. J. Synthetic studies towards the tunicamycins and analogues based on diazo chemistry. Total synthesis of tunicaminyl uracil. *Org. Biomol. Chem.* **1**, 3716-3725 (2003).

294 Ichikawa, S. & Matsuda, A. Synthesis of Tunicaminyluracil Derivatives. *Nucleosides, Nucleotides and Nucleic Acids* **23**, 239-253 (2004).

295 Fukuda, Y., Sasai, H. & Suami, T. Synthetic Approach toward Antibiotic Tunicamycins. 3. Methyl 3,4,7,8-Tetra-O-acetyl-10-O-benzyl-2-benzyloxycarbonylamino-2,6-dideoxy-11,12-O-isopropylidene-β-L-dodecadialdo-(12R)-furanose-(12,9)-pyranosides-(1,5). *Bull. Chem. Soc. Jpn.* **55**, 1574-1578 (1982).

296 Suami, T. *et al.* Synthetic approach toward antibiotic tunicamycins - VI. Total synthesis of tunicamycins. *Tetrahedron Letters* **25**, 4533-4536 (1984).

297 Suami, T., Sasai, H., Matsuno, K. & Suzuki, N. Total synthesis of tunicamcyin. *Carbohyd. Res.* **143**, 85-89 (1985).

298 Myers, A. G., Gin, D. Y. & Rogers, D. H. A Convergent Synthetic Route to the Tunicamycin Antibiotics. Synthesis of (+)-Tunicamycin V. *J. Am. Chem. Soc.* **5**, 2036-2038 (1993).

299 Myers, A. G., Gin, D. Y. & Rogers, D. H. Synthetic Studies of the Tunicamycin Antibiotics. Preparation of (+)-Tunicaminyluracil, (+)-Tunicamycin-V, and 5'-epi-Tunicamycin-V. *J. Am. Chem. Soc.* **116**, 4697-4718 (1994).

300 Hashim, O. H. & Cushley, W. Minor modifications to the structure of tunicamycin lead to loss of the biological activity of the antibiotic. *Biochimica et Biophysica Acta* **923**, 362-370 (1987).

301 Kominato, K., Ogawa, S. & Suami, T. Synthesis of a 2-acetamido-2-deoxy-α-D-galactopyranosyl analogue of tunicamycin. *Carbohyd. Res.* **174**, 360-368 (1988).

302 Suami, T., Sasai, H. & Matsuno, K. Synthesis of Methyl Hexaacetyl-tunicamyl Uracil. *Chemistry Letters*, 819-822 (1983).

303 Alderwick, L. J., Birch, H. L., Mishra, A. K., Eggeling, L. & Besra, G. S. Structure, function and biosynthesis of the Mycobacterium tuberculosis cell wall: arabinogalactan and lipoarabinomannan assembly with a view to discovering new drug targets. *Biochemical Society Transactions* **35**, 1325-1328 (2007).

304 Mengin-Lecreulx, D. & Heijenoort, J. v. Copurification of Glucosamine-1-phosphate Acetyltransferase and N-acetylglucosamine-1-phosphate Uridyltransferase Activities of Escherichia coli: Characterization of the glmU gene Product as a Bifunctional Enzyme Catalyzing Two Subsequent Steps in the Pathway for UDP-N-acetylglucosamine Synthesis.. *J. Bacteriol.* **176**, 5788-5795 (1994).

305 Huang, C.-Y. *et al.* Crystal Structure of Staphylococcus aureus Transglycosylase in Complex with a Lipid II Analog and Elucidation of Peptidoglycan Synthesis Mechanism. *PNAS* **109**, 6496-6501 (2012).

# *Chapter Two*

## *Semi-synthesis of Tunicamycin Core Scaffolds and Lipid Analogues*

## 2.1 Introduction

In the current era of antimicrobial resistant bacteria, the search for new clinical antibiotics remains elusive and challenging. As discussed in **Chapter 1**, tunicamycins are potent antimicrobial agents. However, they are also toxic to mammalian cells, which render them clinically impractical to use to treat infectious diseases. Instead, they have been used extensively as biochemical tools to study the *N*-linked glycosylation of proteins. However, despite such a routine application, their inhibitory mechanisms are still not clear. As part of our on-going work to understand the tunicamycin biosynthetic pathway,[1] we are also interested in the synthesis of non-toxic tunicamycin analogues as potential new antibiotic drug candidates. In order to achieve this goal, we first need to understand their mode of inhibition by understanding the biological activities of the tunicamycin core scaffolds. Then, we can use the scaffolds as chemical templates for creating analogues. In this chapter, the chemical degradation of tunicamycins and the semi-synthetic strategy that allow for the selective addition of lipid chains at the 10'-*N* and 2"-*N* positions of tunicamycin to yield a library of the novel tunicamycin lipid analogues are discussed.

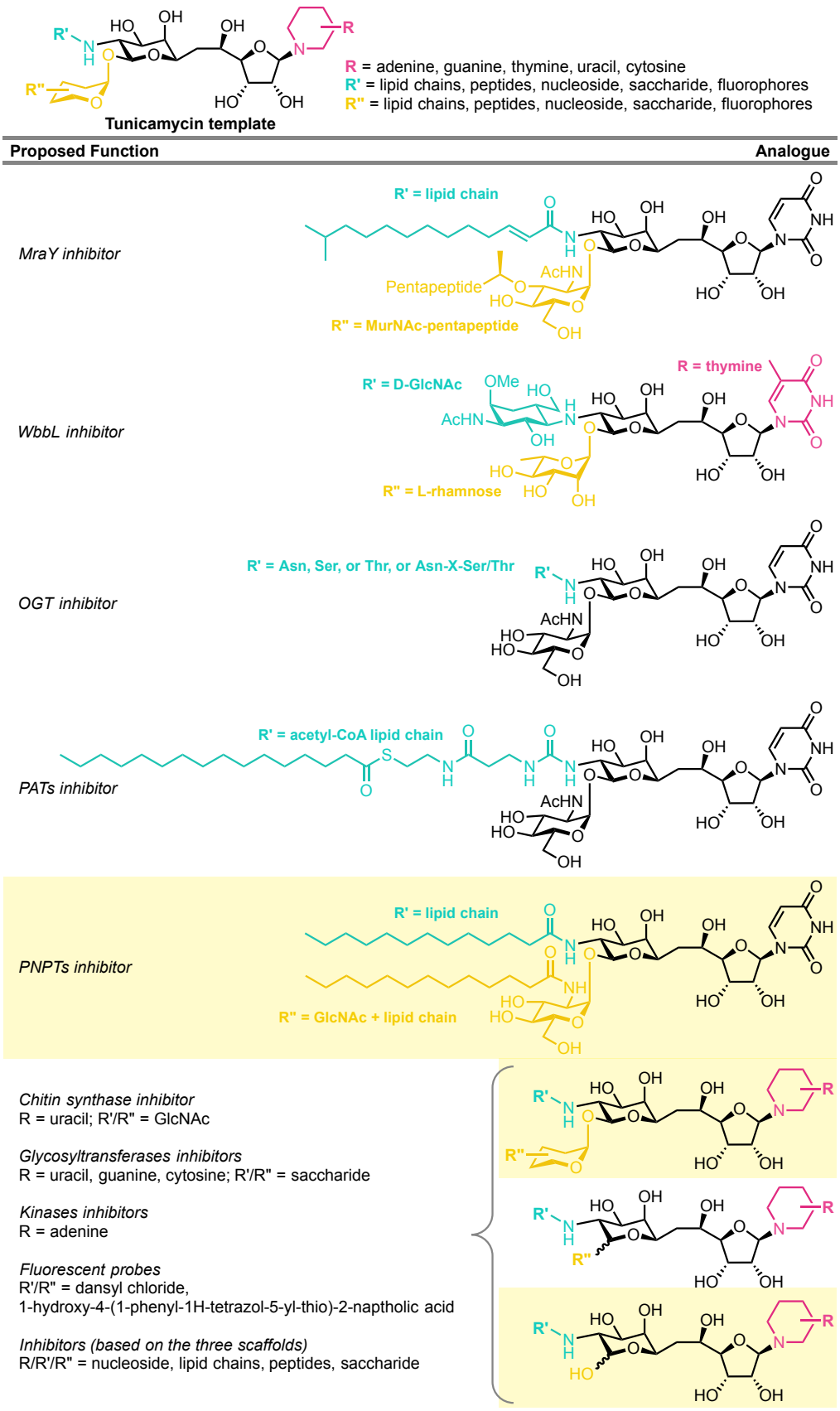


**Figure 2.1 | The proposed tunicamycin analogues.** As described in Chapter 1 **Fig. 1.39**, there are a wide range of analogues that can be created from tunicamycins. The core scaffolds and the analogues described in this chapter are highlighted in yellow boxes.

## 2.2 Results and Discussion

### 2.2.1 Isolation of Tunicamycins from *Streptomyces chartreusis* NRRL3882

Tunicamycins can be chemically synthesised. However, the synthesis involves multi-step procedures that are time consuming and offer poor yields, providing insufficient quantities for use in chemical and biological studies.[2-17,18-22] Although tunicamycins are commercially available, they are very expensive.[i] Fortunately, they can be isolated from various *Streptomyces* species, and even *Bacillus cereus* and *Clavibacter toxicus.*[23-28] Thus, we decided to isolate tunicamycins from *Streptomyces chartreusis* NRRL3882. *S. chartreusis* NRRL3882 accumulates more tunicamycins compared to the other tunicamycin-producing bacteria.[29,30] Several reports have been published on the fermentation, extraction, and isolation methods.[23,25,29] We compiled those reported protocols and devised a protocol that provided approximately 41 mg of pure tunicamycins per litre of culture, where both the broth and the mycelium were used to isolate the tunicamycins (**Fig. 2.2**). The isolated crude tunicamycins were characterised by TLC, LC/MS, HPLC, and $^{1}$H NMR. The crude tunicamycins were also compared with a commercial standard from Enzo Life Sciences and the purity of tunicamycins was determined by HPLC (**Fig. 2.3**).

[i] Sigma Aldrich, £206.50 per 10 mg; Enzo Life Sciences, £116.00 per 10 mg.

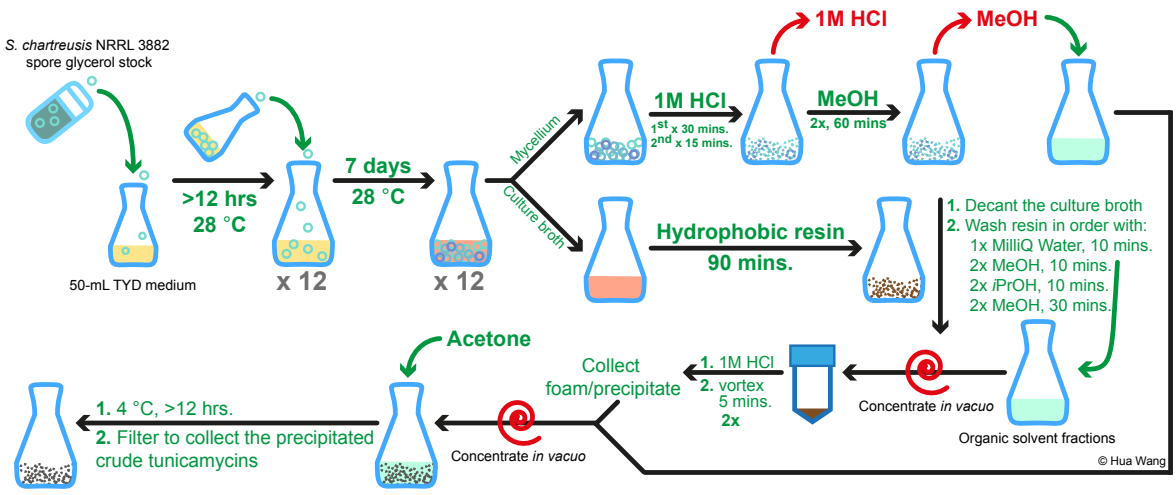


**Figure 2.2 | The extraction process of tunicamycins from *Streptomyces chartreusis* NRRL3882 fermentation culture**.

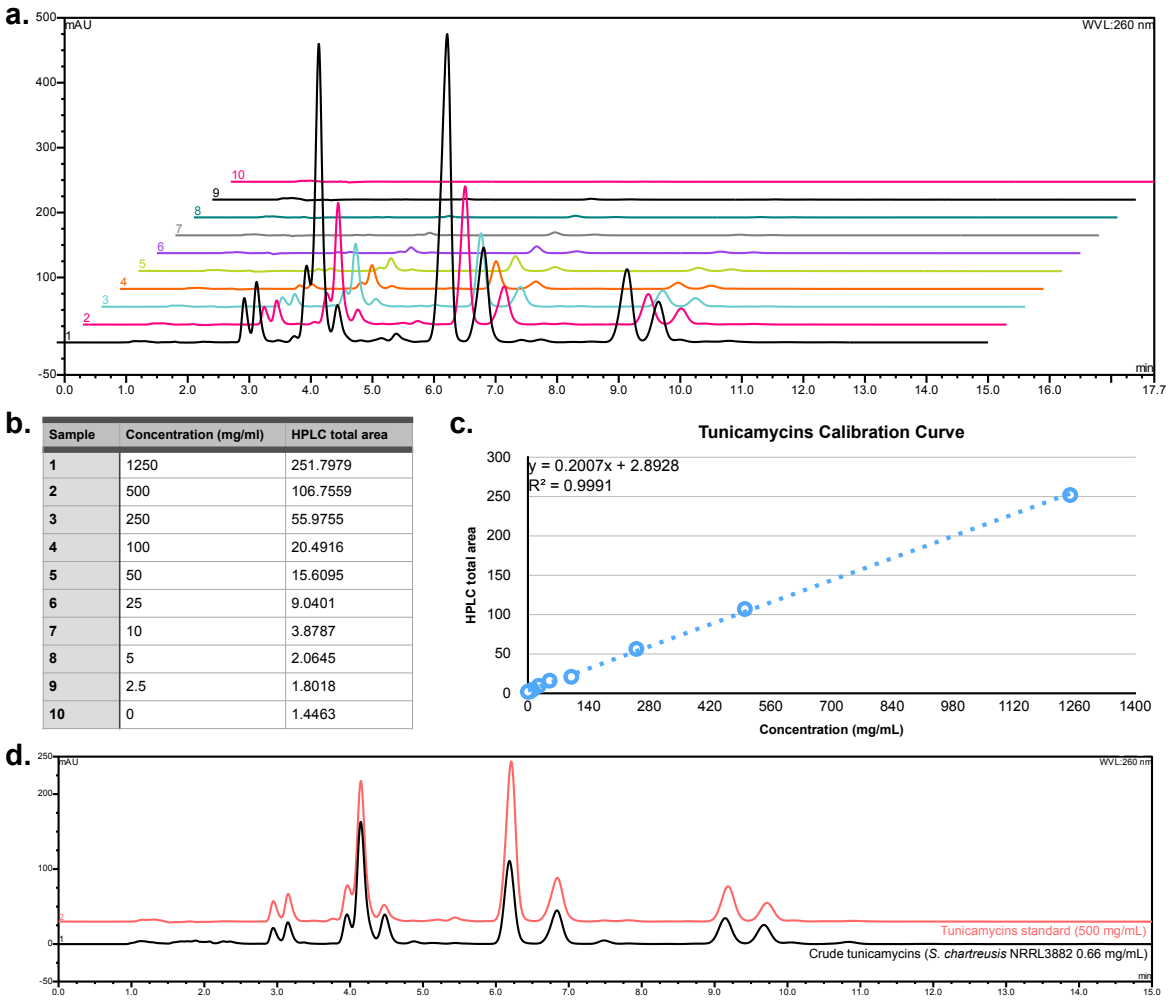


| Sample | Concentration (mg/ml) | HPLC total area |
|---|---|---|
| 1 | 1250 | 251.7979 |
| 2 | 500 | 106.7559 |
| 3 | 250 | 55.9755 |
| 4 | 100 | 20.4916 |
| 5 | 50 | 15.6095 |
| 6 | 25 | 9.0401 |
| 7 | 10 | 3.8787 |
| 8 | 5 | 2.0645 |
| 9 | 2.5 | 1.8018 |
| 10 | 0 | 1.4463 |

**Figure 2.3 | HPLC analysis of tunicamycins.** The analysis was carried out using a WATERS Symmetry reversed-phase C18 column **(a)** Chromatograms of tunicamycins samples at 260 nm. **(b)** Table of diluted tunicamycins sample concentrations. **(c)** Tunicamycins calibration curve plotted from the HPLC chromatogram total area with respect to tunicamycins concentration. **(d)** HPLC

chromatograms of the commercial tunicamycins standard (black) and the isolated crude tunicamycins (red).

### 2.2.2 Chemical Degradation of Tunicamycins: Isolation of *N*-acetyl-tunicaminyl uracil

It has been previously reported by Myers *et al*. that by heating tunicamycins (**1**) under reflux in 3 M HCl(aq.) for 3 h and then acetylating the crude reaction mixture, the heptaacetyl-tunicaminyl uracil (**2**) can be isolated in 30% yield.[22] The same degradation procedure was followed using the crude tunicamycins extracted and both the α and β anomers of heptaacetyl-tunicamyl-uracil were isolated in 64% yield (α/β ratio 53:47), (**Fig. 2.4**).

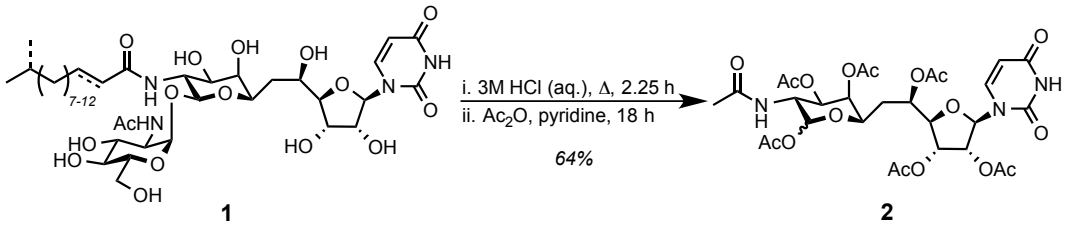


**Figure 2.4 | Hydrolysis of tunicamycins (1).**

In a subsequent step, the heptaacetyl-tunicaminyl uracil (**2**) was subjected to de-acetylation using 0.01M sodium methoxide in methanol to afford the *N*-acetyl-tunicaminyl uracil (**3**) in 98% yield (α/β ratio 37:63) (**Fig. 2.5**).[31] The *N*-acetyl-tunicaminyl uracil (**3**) is a useful core scaffold for biological studies. It allows for the evaluation of the tunicamycin core for antimicrobial activities without the GlcNAc and the lipid chain, can be used as an intermediate substrate in the tunicamycin biosynthetic pathway, and can also be used as a tunicamycin template for further diversification at the 10' and 11' position to create tunicamycin analogues (**Fig. 2.1**).

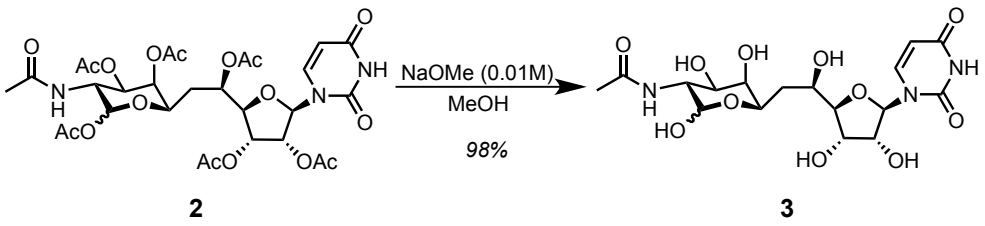


**Figure 2.5 | Synthesis of the *N*-acetyl-tunicaminyl uracil (3).**

### 2.2.3 Lipid cleavage of Tunicamycins: Isolation of the α-D-*N*-acetylglucosamine-(1”-11’)-*N*-acetyl-tunicaminyl uracil

Previously, F. J. Wyszyński devised a method for the cleavage of the lipid chain on tunicamycins, which enabled the isolation of the non-lipidated form of tunicamycin, α-D-*N*-acetylglucosamine-(1”-11’)-*N*-acetyl-tunicaminyl uracil (**4**), from crude tunicamycins (**1**) (**Fig. 2.6**).[31] This non-lipidated tunicamycin is particularly special because it eliminates the heterogeneity arising from the lipid chains and allows us to evaluate the biological activities of tunicamycin without the lipid chain and to understand the biological relevance of the lipid chain.

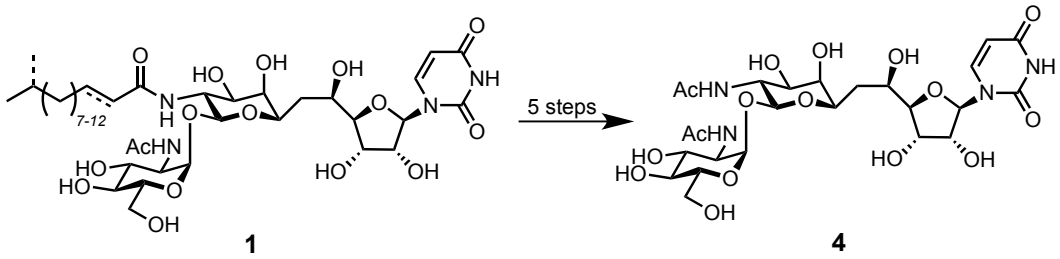


**Figure 2.6 | Chemical degradation of tunicamycins toward the isolation of the α-D-*N*-acetylglucosamine-(1”-11’)-*N*-acetyl-tunicaminyl uracil (4).** The five steps include: acetylation, bocylation, deacetylation, debocylation, and finally acetylation.

Using the same procedure reported by F. J. Wyszyński, crude tunicamycins (**1**) isolated from *S. chartreusis* NRRL3882 fermentation culture were dissolved in pyridine and then treated with acetic anhydride (**Fig. 2.7**). After two rounds of flash column

purification, pure octa-*O*-acetylated tunicamycins (**5**) were isolated in 23-82% yield (dependent on the purity of the crude tunicamycins used as starting material).

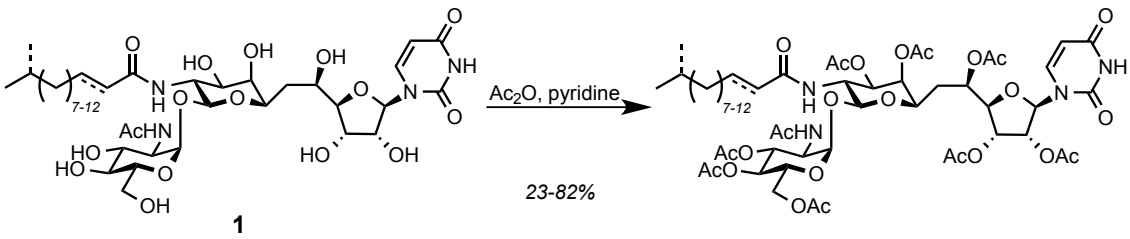


**Figure 2.7 | Acetylation of crude tunicamycins (1).**

Next, in order to cleave the lipid chain, the *tert*-butoxylcarbonyl (Boc) protecting group was added to the secondary amides at positions 3, 10', and 2" to afford the tri-*N*-Boc-octa-*O*-acetylated tunicamycins (**6a**) (**Fig. 28**). Amide cleavage usually involves the use of a strong acid or base and high temperatures, but these harsh conditions would be unsuitable to use in the presence of the uridine moiety as they would degrade the tunicamycins. Several methodologies have been published on how to remove the highly stable and unreactive acetyl group.[32-34] One of them is Kunieda's mild *N*-Bocylation methodology.[32] In this, the presence of the Boc group on the secondary amide acts as an electron withdrawing group to remove the electron density from the amide carbonyl, which weakens the carbonyl bond and allows the acetyl group to be readily cleaved in the presence of a base.

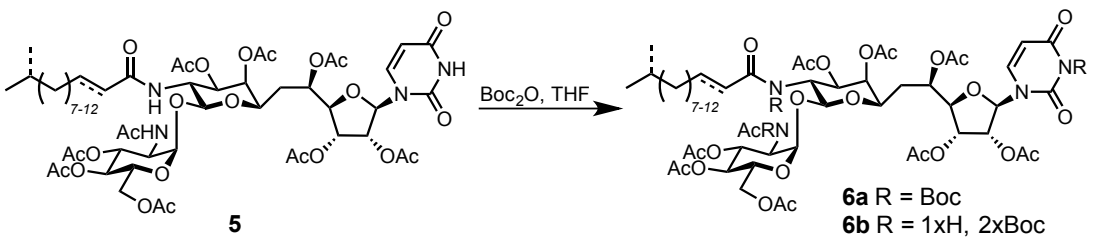


**Figure 2.8 | Bocylation of the octa-*O*-acetylated tunicamycins (5).**

The desired product (**6a**) was isolated in 34% yield and the incomplete di-*N*-Boc protected product (**6b**) was isolated in 24% yield. The **6b** product can be saved and used in the same reaction condition to isolate the **6a** product. The **6b** product would have been sufficient for the subsequent step if the Boc protecting groups were at positions 10' and 2". Unfortunately, $^{1}$H NMR analysis of **6b** shows a mixture of the Boc protecting groups at positions 3, 10', and 2" of tunicamycins, thus it would have been difficult to separate and purify the desired 10' and 2" Boc protected **6b**.

We investigated different reaction conditions to drive the *N*-Boc protection of **5** to completion, or at least to a higher yield (**Table 2.1**). However, this proved to be difficult. First we prolonged the reaction time but that did not appear to make a huge difference to the yield. Next, we increased the equivalents of the di-tert-butyl dicarbonate ($Boc_2O$) and 4-dimethylaminopyridine (DMAP). The yields increased slightly, but the conditions were not able to drive the reaction to completion. It may be due to the bulkiness of the Boc protecting group and the sterically hindered secondary amides on **5**, which do not seem to be in our favour. Thus, less bulky amide protecting groups, such as trichloroacetyl, trifluoroacetyl, vinyloxycarbonyl, allyloxycarbonyl, and propargyloxycarbonyl would be worth considering for future endeavours.[35,36]

**Table 2.1 | Reaction conditions for the *N*-Boc protection.**

| Compound | Solvent | $Boc_2O$ (eq.) | Base (eq.) | Temperature (°C) | Time (h) | Yield |
|---|---|---|---|---|---|---|
| **5** | THF | 20 | DMAP (0.2) | 60 | 24 | 34% |
| **5** | THF | 40* | DMAP (0.2) | 60 | 36 | 53% |
| **5** | THF | 20* | DMAP (0.5) | 60 | 36 | 23% |
| **5** | THF | 20* | DMAP (0.5) | 60 | 80 | 38% |
| **5** | THF | 20* | DMAP (1) | 60 | 24 | 47% |
| **5** | THF | 20* | DMAP (1) | 60 | 48 | 24% |
| **5** | THF | 20* | DMAP (2.2) | 60 | 144 | 27% |
| **5** | THF | 20* | DMAP (3.3) | 60 | 19 | 14% |
| **5** | THF | 20* | DMAP (4) | 60 | 24 | 36% |
| **5** | THF | 20* | DMAP (4) | 60 | 28 | 20% |
| **5** | THF | 20* | DMAP (4) | 60 | 50 | 27% |
| **5** | THF | 10 | DMAP (0.5), 2,6-lutidine (1) | 60 | 28 | NP |
| **6a** | ACN | 2 | DMAP (3) | 60-90 | 40 | 3% |

*Final equivalent. 10 eq. was added overtime.
NP = No product. No product was isolated.

Finally, in a multi-step procedure carried out at room temperature, **6a** was treated with NaOMe to deacetylate the hydroxyl groups and liberate the lipid chain (**Fig. 2.9**). Unfortunately, methoxide cleavage of the uracil ring on tunicamycins was observed when the reaction was left for longer than 4 h. To avoid the excessive methoxide cleavage of the uracil ring in the reaction mixture, the reaction was stopped after 4 h even though there were still partially deacetylated intermediates. The crude reaction mixture was neutralised with Dowex $H^+$ resin, treated with TFA followed by acetic anhydride, and then neutralised with Dowex $^-OH$ resin. The final product (**4**) was obtained in 23% yield.

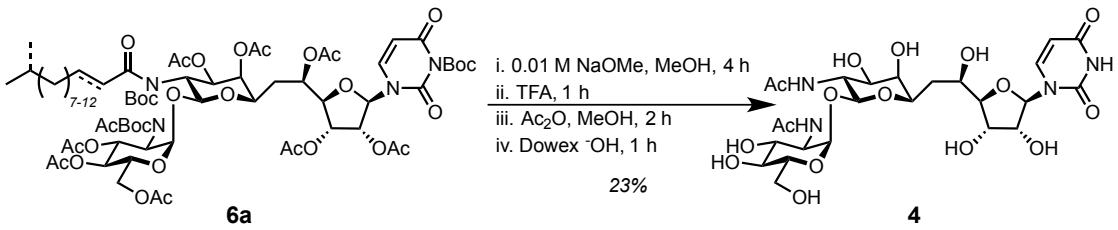


**Figure 2.9 | Isolation of α-D-*N*-acetylglucosamine-(1”-11’)-*N*-acetyl-tunicaminyl uracil (4).**

### 2.2.4 Isolation of the α-D-Glucosamine-(1”-11’)-Tunicaminyl Uracil Dihydrochloride, the Dihydrochloride Salt of Tunicamycins

Next, we were interested in utilising the two tunicamycin core scaffolds (**3**) and (**4**) to create tunicamycin analogues. The free amine salt of tunicamycins, tunicaminyl uracil hydrochloride salt (**7**) (**Fig. 2.10**), is a highly attractive scaffold for us as a template that would allow the synthesis of a library of analogues, as shown in **Fig. 2.1**.

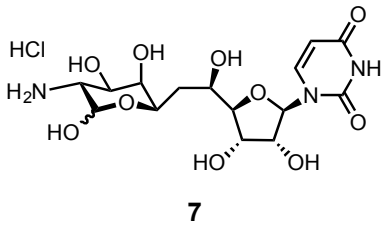


**Figure 2.10 | Tunicaminyl uracil hydrochloride salt**

We attempted to isolate the tunicaminyl uracil hydrochloride salt (**7**) scaffold following the original reported procedure using tunicamycins.[37] Unfortunately, no product was isolated. The unsuccessful attempts to isolate the hydrochloride chloride salt derivative may be due to the use of crude tunicamycins, which contained a high amount of contaminants. Therefore, the contaminants may have reacted with the free amine. However, since the chemical degradation step involving the acidic hydrolysis of tunicamycins that resulted in low yields, we considered an alternative approach and target for creating the tunicamycin analogue due the scarce quantity of tunicamycins that are

available. Thus, instead of the chemical degradation approach to use scaffold **3**, a scaffold that does not contain the GlcNAc moiety, we decided to use scaffold **4** as a template to create analogues.

The isolation of scaffold **4** does not involve the harsh acidic hydrolysis of the crude tunicamycins. For our purpose of investigating the tunicamycins core scaffolds, we did not find it useful to modify the uracil and the tunicamine moieties of tunicamycin as both are speculated to interact with MraY, and whilst the importance of the tunicaminyl uracil scaffold in antibacterial activity and the GlcNAc moiety in mammalian cytotoxicity are reported, the GlcNAc and/or lipid chain have never been directly shown to contribute to either (as discussed in **Chapter 1** and shown in **Fig. 2.1**). Thus, biological evaluations of scaffold **3** and scaffold **4** may help to fill in the gap in the literature regarding the biological relevance of the GlcNAc moiety and the lipid chain. A tunicamycin analogue resembling the substate-product transition-state could be more selective to MraY than GPT, or disrupting the substrate-product transition-state mimicry may help to abolish tunicamycins cytotoxicity (**Fig. 2.11**). This may also imply that the tunicamycin core scaffold without the lipid chain would be the ideal template to use for designing analogues due to the substrate-product transition state mimicry that involves nucleoside sugar substrate. Additionally, further speculations from other natural inhibitors of MraY also appeared to suggest these implications where they are non-toxic to mammalian cells by having the complex spatial architecture resembling the substrate-product transition-state mimicry but without the GlcNAc moiety. Thus, scaffold **4** seems to be a better starting point to create tunicamycin analogues in addition to avoid wasting of tunicamycins with the chemical degradation process. Essentially, we were interested in modifying the

GlcNAc moiety to reduce the structural similarity of tunicamycins to UDP-GlcNAc while retaining the carbon chain and its lipid character. Although the elimination of the GlcNAc moiety would be the suggested approach to prevent inhibition towards GPT, the absence of the GlcNAc moiety on the analogue may even reduce the overall feature of tunicamycins as an UDP-HexNAc mimic and lose its antimicrobial activity. As discussed in **Chapter 1**, minor modifications on tunicamycins have been reported to result in great consequences to tunicamycins bioactivity but further investigation would be needed to understand the molecular basis of tunicamycins mode of inhibition. The free amine scaffold (**7**), however, is definitely worth considering in the future after the initial bioactivity test of the tunicamycin core scaffolds and even as inhibitors for other enzymes as discussed in **Chapter 1** and shown in **Fig. 2.1**.

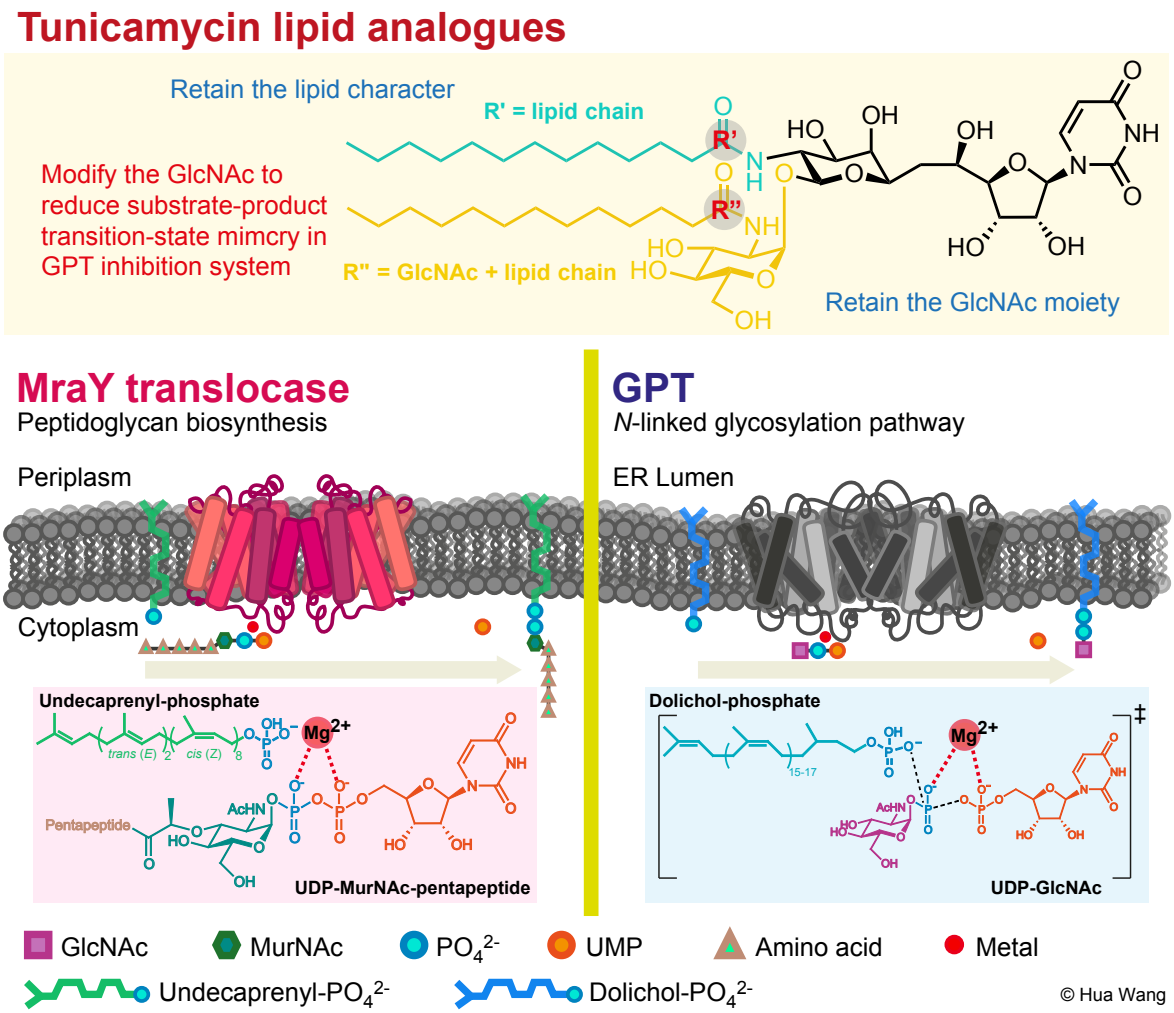


**Figure 2.11 | Designing the tunicamycin lipid analogues.** The designing of the tunicamycin lipid analogues took into consideration the substrate, product, and substrate-product transition-state mimicries in the MraY and GPT systems. The lipid chain on the analogue can be any desired lipid chain. The tunicamycin lipid analogue may resemble the substate-product transition-state of MraY system and may disrupt the substrate-product transition-state mimicry in the GPT system that may help to abolish tunicamycins cytotoxicity.

As discussed above, the acetylation of crude tunicamycins was considered for two reasons; firstly, it would be the most efficient use of the crude tunicamycins isolated from *S. chartreusis* culture and, secondly, it would allow for the liberation of the lipid chain upon addition of the Boc protecting group. In the process of isolating scaffold **4**, the *in situ* tri-*N*-Boc-tunicamycin intermediate (**8**) resulting from the lipid cleavage reaction appeared

to be a promising and accessible scaffold in making the dihydrochloride salt (**9**) as the free amine salt equivalent of the tunicaminyl uracil hydrochloride salt scaffold (**7**) (**Fig. 2.12**).

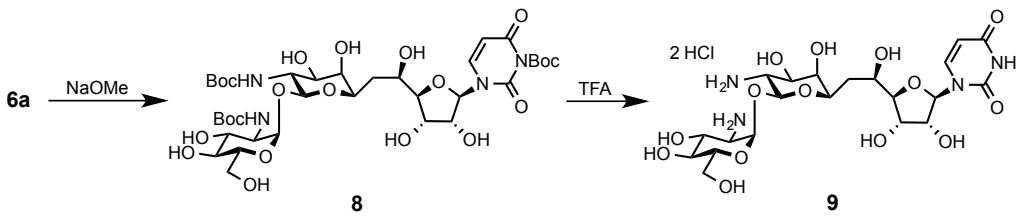


**Figure 2.12 | Synthetic approach towards the isolation of the α-D-glucosamine-(1”-11’)-tunicaminyl uracil dihydrochloride (9), the dihydrochloride salt of tunicamycins**

The dihydrochloride salt (**9**) is an invaluable scaffold that allows for dual modifications on two locations on tunicamycins. This method is uniquely capable of synthesising tunicamycin analogues and tunicamycin lipid analogues by retaining the overall feature of tunicamycins as an UDP-GlcNAc/Glc mimic (**Fig. 2.11**). As discussed in **Chapter 1**, the GlcNAc moiety on tunicamycin appears to be important to their inhibitory action as substrate mimic or substrate-product transition-state mimic. The dual modification method fulfills our aim of retaining the lipid characteristics of tunicamycin by allowing us to attach a lipid chain on the 10” position as well as the 2” position. In doing so, the dual modification method modifies the glucosamine moiety that would reduce the transition-state analogue resemblance while also allowing us to selectively add a lipid chain of our choice (**Fig. 2.11**). As we have hypothesised, the lipid character of tunicamycin is important to its overall bioactivity; modification of the GlcNAc moiety abolishes its inhibitory action towards GPT, thus eliminating tunicamycins cytotoxicity towards mammalian cells while simultaneously retaining its antimicrobial properties.

The tri-*N*-Boc-octa-*O*-acetylated tunicamycins (**6a**) — which, as described previously, were derived from crude tunicamycins — were treated with NaOMe to

deacetylate the hydroxyl groups and liberate the lipid chain (**Fig. 2.13**). This reaction was carried out at room temperature for 6 h. Again, the methoxide cleavage of the uracil ring was observed as previously mentioned. The reaction was discontinued after 6 h and the product was isolated after flash column chromatography to afford 45% yield of the di-*N*-Boc product (**8a**). The Boc protecting group on the nitrogen of the uracil was lost during flash column chromatography. This was indicated by a change in product $R_f$ value of the product in the collected fractions. The di-*N*-Boc product (**8a**) was confirmed by MS and NMR. Gratifyingly, the loss of the *N*-Boc on the uracil had no impact on the synthesis of the tunicamycin dihydrochloride salt (**9**).

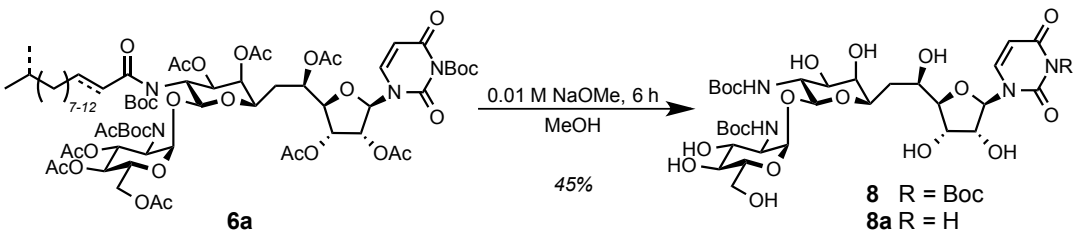


**Figure 2.13 | Isolation of tri-*N*-Boc-tunicamycins (8) and di-*N*-Boc-tunicamycins (8a)**.

We investigated milder deacetylation conditions to liberate the acetyl and the lipid groups, as the use of NaOMe was found to result in the degradation of the uracil ring. Meier *et al*. reported using triethylamine (TEA) in methanol/water to remove the acetyl protecting groups.[38] The cleavage of the acetyl protecting group is proposed to be TEA-catalysed, forming a complex with the water, acetate, and methanol (**Fig. 2.14**).

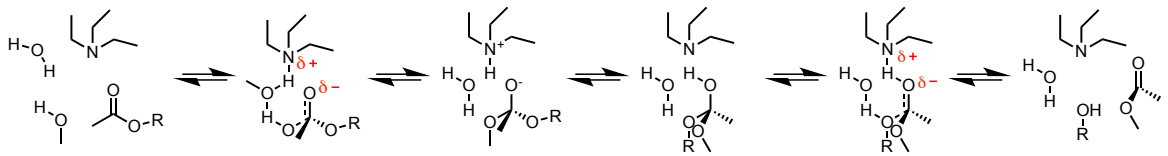

**Figure 2.14 |** The triethylamine-catalysed cleavage of the acetyl protecting group in the presence of methanol and water.

The TEA-catalysed cleavage of the acetyl protecting groups was first attempted on **6a** at room temperature. The reaction time was longer compared to the use of NaOMe, but this milder reaction condition successfully removed the acetyl protecting groups and the lipid chain with no degradation of the uracil (**Fig. 2.15**). Next, we attempted to improve the reaction condition to decrease the reaction time (**Table 2.2**). We found that a reaction temperature of 71 °C and by increasing the equivalents of TEA used showed good yields of the desired di-*N*-Boc-tunicamycins (**8a**). The product **8a** was purified by using preparative-scale RP-HPLC (**Fig 2.16**) for the purpose of the lyophilisation process in the subsequent step.

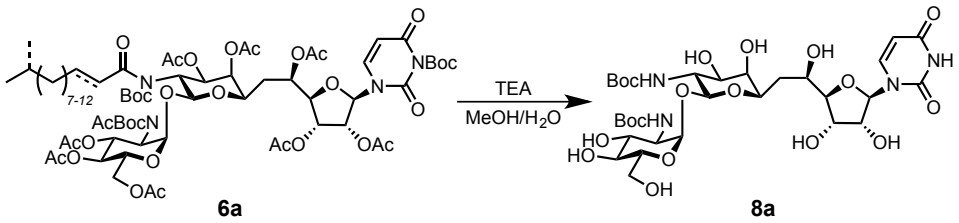


**Figure 2.15 | Isolation of di-*N*-Boc-tunicamycins (8a) *via* triethylamine-catalysed cleavage of 6a.**

**Table 2.2 | Reaction conditions for the TEA-catalysed cleavage.**

| Starting material | TEA (eq.) | MeOH:$H_2O$ | Temperature (°C) | Time (h) | Yield |
|---|---|---|---|---|---|
| 6a | 10 | 3:1 | RT | 141 | 77.00% |
| 6a | 10 | 3:1 | 71 | 50 | 60%* |
| 6a | 25 | 3:1 | 71 | 9 | 52%* |

*Yield after HPLC purification

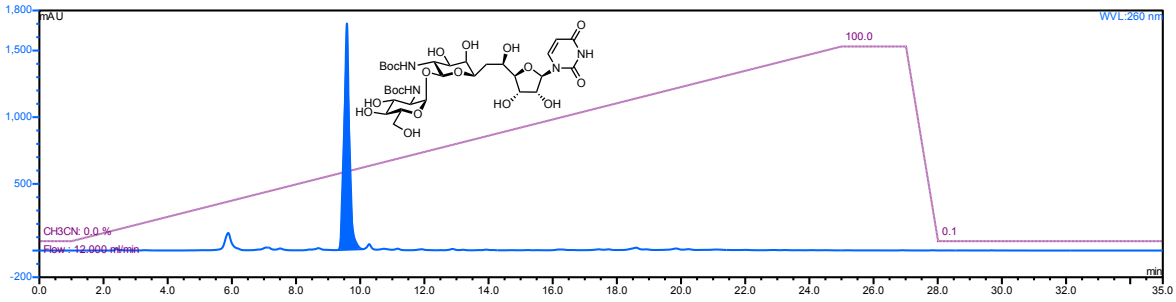


**Figure 2.16 | HPLC chromatogram of di-*N*-Boc-tunicamycins (8a).** The chromatogram at 260 nm from preparative scale purification using Phenomenex Synergi 4µ Hydro-RP 80Å 100 x 21.20 mm column.

Finally, the treatment of **8a** with TFA and then HCl afforded the desired α-D-glucosamine-(1”-11’)-tunicaminyl uracil dihydrochloride (**9**) in 85% yield after lyophilisation (**Fig. 2.17**). Due to the high purity of the starting material from HPLC purification, no purification step was required. In the deprotecting step using TFA, the Boc protecting group was degraded into volatile by-products, $CO_2$ and isobutylene.[33,39] TFA was removed *via* lyophilisation.

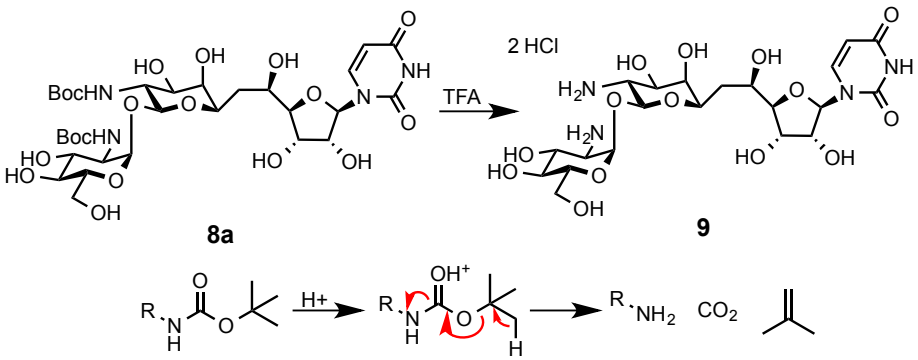


**Figure 2.17 | The isolation of the α-D-glucosamine-(1”-11’)-tunicaminyl uracil dihydrochloride (9) from 8a.**

### 2.2.5 Synthesis of the Novel Tunicamycin Lipid Analogues

The success in obtaining the dihydrochloride salt (**9**) then enabled us to proceed to create a library of tunicamycin lipid analogues as noted in **Fig. 2.1** and **2.11**. Of all the possible analogues that can be synthesised from **9**, we decided to synthesise the lipid

analogues **10 - 16** (**Fig. 2.14**) to test our hypothesis and to understand the effect of the lipid chain. The role of the lipid chain on tunicamycin homologues is still unclear in the literature and we thought that the lipid analogues could help fill this gap. We also decided to use simple saturated lipid chains ranging from seven to twelve carbon atoms. A citronellic variation of eight carbon chain length was also synthesised in order to investigate the effect of the unsaturation and the branching on the lipid chain. The citronellic acid is a short chain mimic of the polyprenyl phosphates that has been used in the membrane stages of the peptidoglycan assays as a lipid analogue.[40-42] The similarity of the lipid chain between the citronellyl analogue (**16**) and undecaprenyl lipid compare to octanoyl analogue (**11**) could favour the **16** as a better inhibitor for MraY.

The wide range of fatty acids, including the ones used in the syntheses, are commercially available, thus a larger library of various lipid carrier analogues can be made to study the biological effect of the lipid in the tunicamycin mode of action. Moreover, lipid analogues tailored with a specific lipid chain could be used as target specific inhibitors due to substrate mimicry or lipid-protein interaction. Last, but not least, scaffold **9** could also be immobilised on resins for pull down studies to identify and characterise tunicamycin-binding proteins and interactions.

| Structure | Name |
|---|---|
| 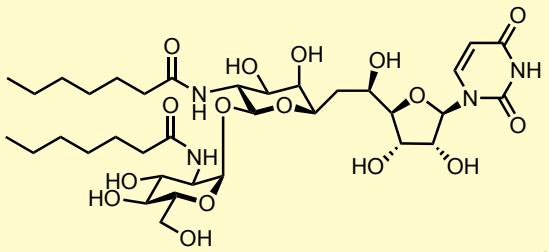 | **Di-*N′,N″*-heptanoyl tunicamycin (10)** |
| 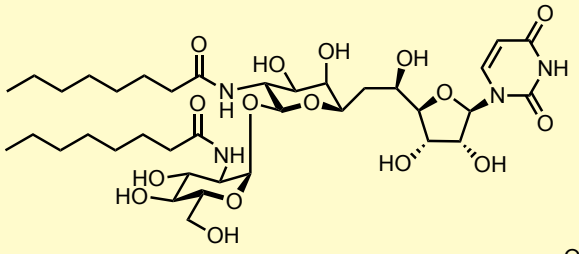 | **Di-*N′,N″*-octanoyl tunicamycin (11)** |
| 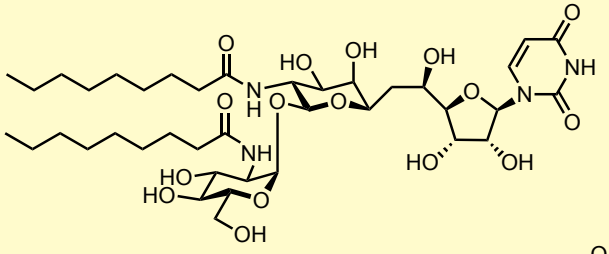 | **Di-*N′,N″*-nonanoyl tunicamycin (12)** |
| 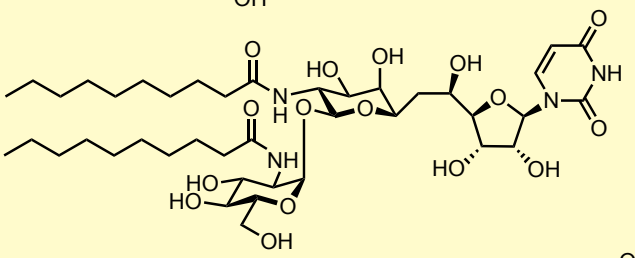 | **Di-*N′,N″*-decanoyl tunicamycin (13)** |
| 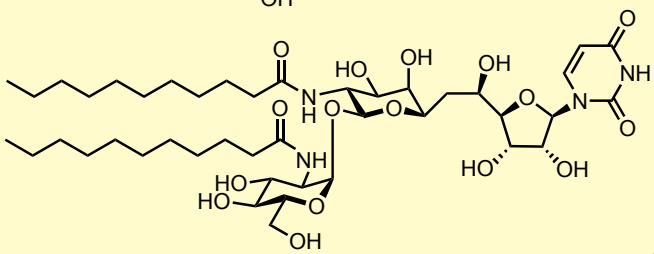 | **Di-*N′,N″*-undecanoyl tunicamycin (14)** |
| 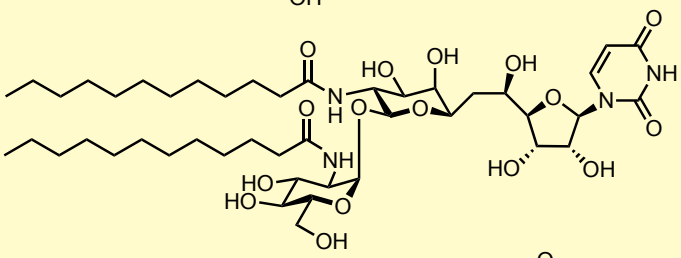 | **Di-*N′,N″*-dodecanoyl tunicamycin (15)** |
| 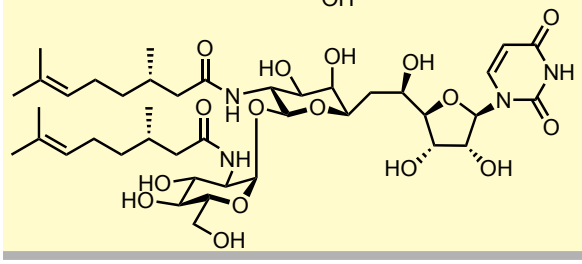 | **Di-*N′,N″*-citronellyl tunicamycin (16)** |

**Figure 2.18 | Tunicamycin lipid analogues (10-16).**

Since the synthesis of the lipid analogues can be achieved directly from **8a** as the starting material instead of **9**, we tried this in our first attempt to synthesise the di-*N',N''*-octanoyl-tunicamycin (**11**) (**Fig. 2.19**). However, the reaction condition involved multi-steps that were not easily reproduced from the small scale reaction. The direct amide coupling to the dihydrochloride (**9**) is a starting point that would allow better monitoring of the reaction. The lipid chains were coupled on to tunicamycin *via* conventional coupling chemistry (**Fig. 2.19**). An extensive review of these methods are reported.[43,44]

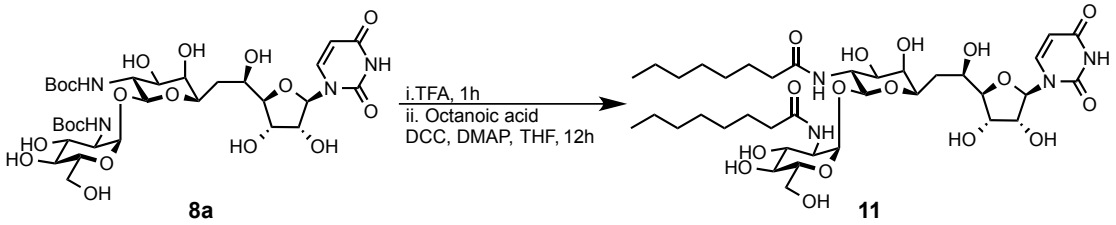


**Figure 2.19 | The first synthesis of the di-*N',N''*-octanoyl tunicamycin (11) from (8a).** The di-*N*-Boc-tunicamycin (8a) was first treated with TFA for an hour followed by neutralization of reaction mixture by TEA. Steglich esterification proceeded by using octanoic acid, *N*,*N*′-dicyclo-hexylcarbodiimide (DCC), DMAP in THF. The reaction was left overnight followed by aqueous workup and then reversed-phase flash chromatography to afford 65% of the product.

Before we used the dihydrochloride salt (**9**) as the starting material, we first carried out using **9** in two test reactions to couple with nonanoic acid using *N*,*N*′-dicyclo-hexylcarbodiimide (DCC) to form di-*N',N''*-nonanoyl tunicamycin (**12**). In the first test reaction, we avoided using TEA due to the difficulties associated with removing it by flash column chromatography, and instead used an excess amount of DMAP. The reaction was stopped after 30 h and the product was purified by flash column chromatography. However, $^{1}$H NMR and RP-HPLC analyses showed no presence of our desired product **12**. In the second test reaction, both the DMAP and TEA were used. The reaction was monitored by analytical scale RP-HPLC using the same condition as tunicamycins analysis

(**Fig. 2.20**). The RP-HPLC chromatogram from the reaction showed two distinctive peaks, the eluted peak at 8-8.5 min representing the mono-nonanoyl product of **12** and the later eluted peak at 14.5-15 min representing the desired lipid analogue product **12**. The reaction was stopped after ten days in order to isolate and characterise the product and to not compensate the yield due to the formation of by products observed at 18 min.

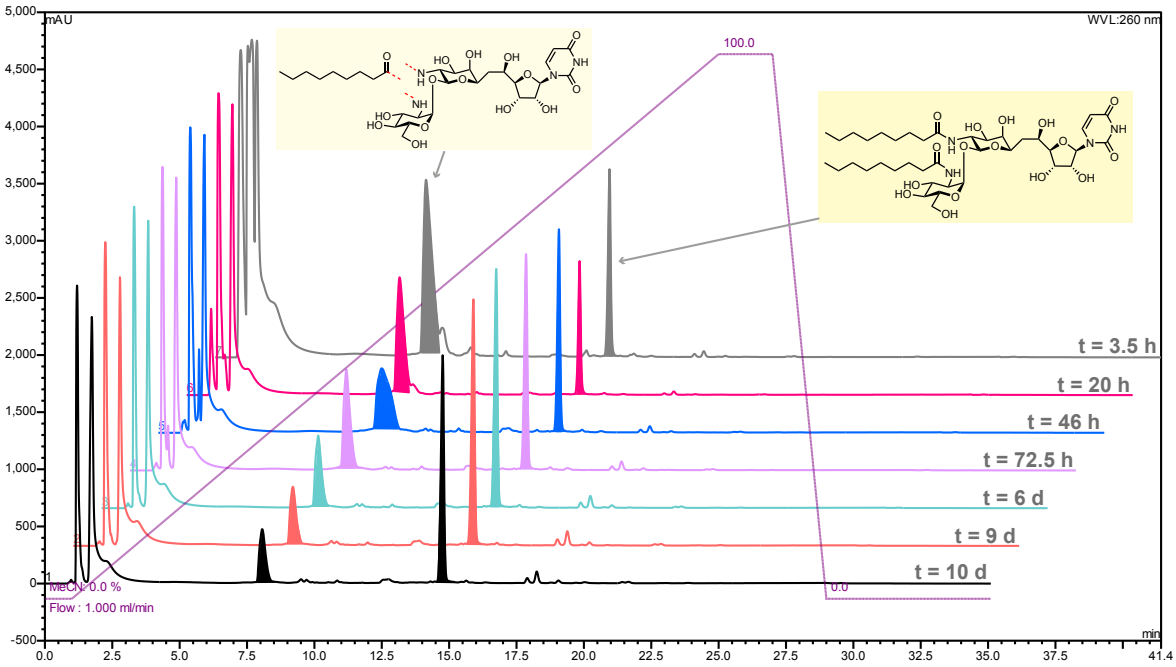


**Figure 2.20 | HPLC chromatogram of the formation of the di-*N'*,*N"*-nonanoyl tunicamycin (12) from 9.** The chromatogram at 260 nm from the analytical scale analysis using Phenomenex Synergi 4µ Hydro-RP 80Å 100 x 4.60 mm column. The amide coupling reaction for **12** was monitored over 10 days.

Although we managed to synthesise the desired nonanoyl lipid product (**12**), the purification of the reaction product proved to be a challenge due to the contamination of *N*,*N'*-dicyclohexylurea (DCU) by-product from the use of DCC in the coupling reaction. $^{1}$H NMR analysis of the contaminated lipid product showed a one-to-one ratio with the DCU by-product, even after further purification by reversed-phase HPLC (RP HPLC) and

normal phase flash column chromatography. A MS analysis of the same sample showed two masses that corresponded to the lipid product (**12**) and DCU (**Fig. 2.21**).

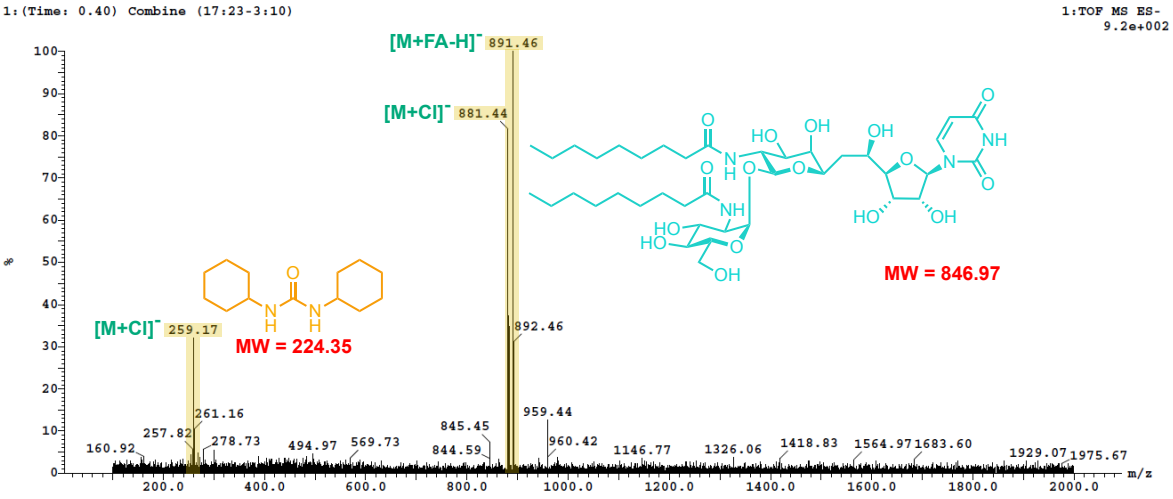


**Figure 2.21 | TOF MS ES⁻ spectrum of DCU-contaminated product (12).**

The difficulty in separating the DCU and lipid product (**12**) was suspected to be due to the hydrogen bonding and hydrophobic interactions between the lipid chain and the DCU. Fortunately, we were able to isolate a 69% yield of the pure product after acetylation and deacetylation followed by purification using RP-HPLC, with an overall yield of 26% (**Fig. 2.22, 2.23**).

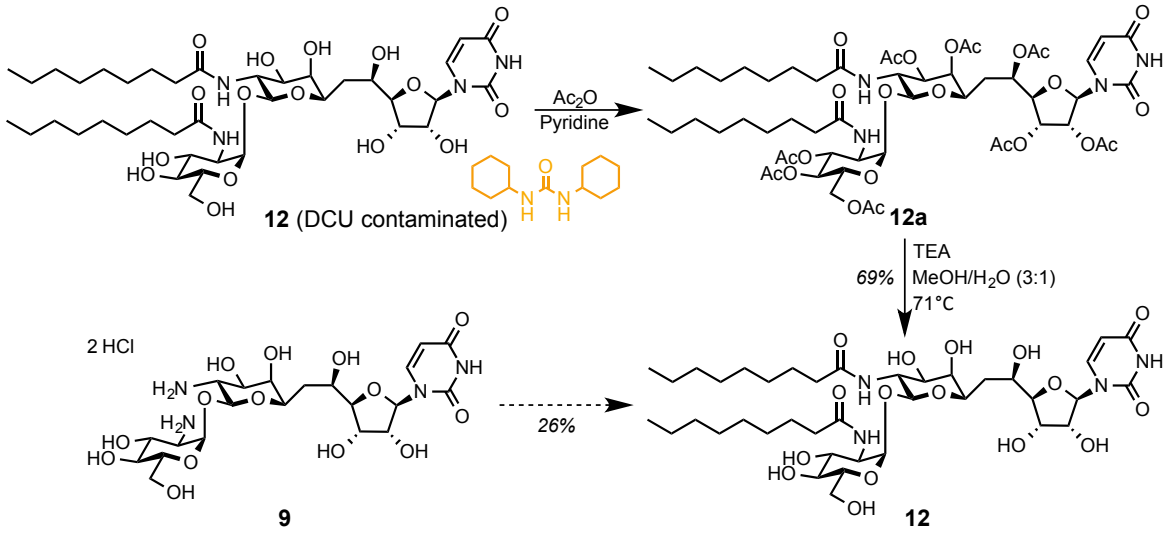


**Figure 2.22 | Acetylation of DCU-contaminated 12 and isolation of 12.**

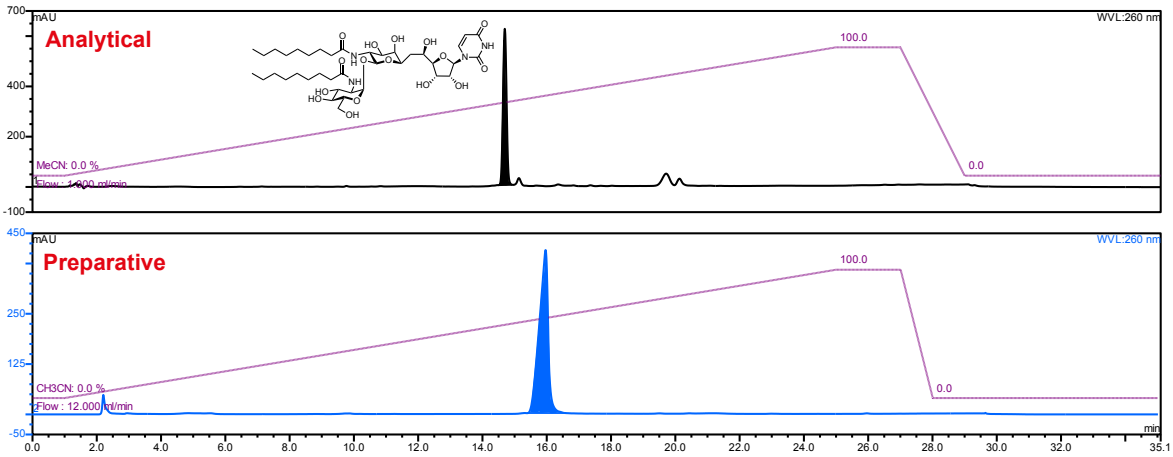


**Figure 2.23 | Analytical and preparative scale HPLC chromatogram of 12.** The chromatogram at 260 nm from the analytical scale analysis using Phenomenex Synergi 4µ Hydro-RP 80Å 100 x 4.60 mm column and the preparative scale purification using Phenomenex Synergi 4µ Hydro-RP 80Å 100 x 21.20 mm column. The sample collected from the preparative scale purification of **12** showed no contamination of DCU.

The coupling reaction with DCC was a slow process; as indicated by RP-HPLC (**Fig. 2.20**), the mono-nonanoyl tunicamycin intermediate was still present in the reaction mixture after the 10 d. The reaction was stopped at the end of this period in order to isolate and fully characterise the novel tunicamycin lipid analogue (**12**). The incomplete reaction partially contributed to the low overall yield of 26% of **12** from **9**. The slow reaction time

may be due to the steric hinderance resulting from the first addition of the lipid chain to either of the free amines at positions 10' or 2", thus the second amine to be coupled to the lipid chain would not be as accessible.

We investigated other coupling agents in order to avoid the problematic DCU by-product that resulted from using DCC. We conducted test reactions using the starting materials glucosamine and nonanoic acid, then evaluated the success of the amide bond formation and, more importantly, the ease of removing the coupling by-product of the chosen coupling reagent. The coupling reagents we investigated were *N*,*N*'-diisopropyl-carbodiimide (DIC), and 1-ethyl-3-(3-dimethylaminopropyl)carbodiimide (EDC) (**Fig. 2.24**).[43,44] We found that DIC was a better choice than DCC or EDC for mediating the formation of the amide bond. The coupling reaction using DIC was higher yielding than the one using EDC after 20 hours. Additionally, the urea by-product from DIC was easily removed by washing the product with DCM. The low yield of 1% from using EDC may have been due to the poor quality of the EDC used, however the DCM-soluble urea DIC by-product was more suitable than water for the purification process in handling milligram samples. Moreover, in the initial attempt to remove DCU from **12**, the lipid product was found to be soluble in MeOH or DMF and not in water, DCM, chloroform, or EtOAc. This determined that the DCM-soluble DIC urea by-product would be the ideal coupling reagent.

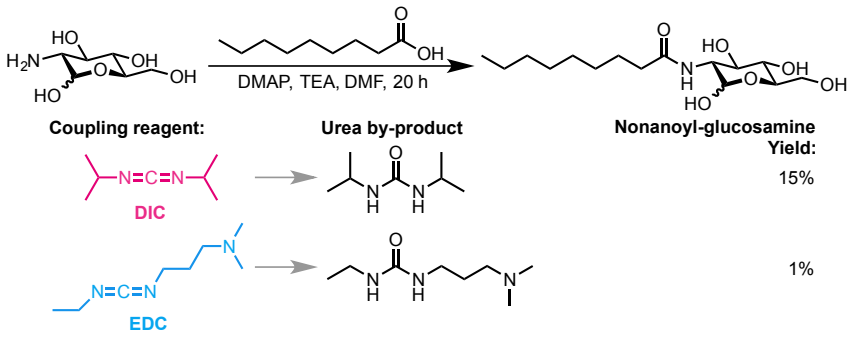


**Figure 2.24 | DIC and EDC test reactions.**

The test was performed by adding different lipid chain lengths to the dihydro-chloride salt (**12**). The syntheses used a number of fatty acids including heptanoic acid, octanoic acid, nonanoic acid, decanoic acid, undecanoic acid, dodecanoic acid, and citronellic acid to complete the library of the lipid analogues shown in **Fig. 2.18**. Similarly, analytical scale RP-HPLC was used to monitor the reaction progress as shown in **Fig. 2.20**. The HPLC chromatograms of all the tunicamycin lipid analogues (**10-16**) are shown in **Fig. 2.25**. The reaction conditions and associated yields are summarised in **Table 2.3**. It was observed that the amide bond formation with the lipid chains consistently failed to reach to completion even after adding additional equivalents of the DMAP, TEA, fatty acid or DIC. We experimented with adding additional equivalents of the fatty acid, adding DIC exceeding the total 2.5 equivalent in the reaction mixture, and increasing the reaction time. All of these appeared to favour the formation of minor by-products as indicated by HPLC and LC/MS (**Fig. 2.26**). The by-products appeared to be the addition of one or two lipid(s) to the product. One possible by-product may be the result of the esterification of the primary 5" hydroxyl group. TEA and the DIC urea by-product were common contaminants after RP-HPLC preparative scale purification process and flash column chromatography. As discussed before (**Fig. 2.24**), DIC was used not only because it promoted the amide bond formation but also because the urea by-product can be easily removed by DCM. Any

TEA contaminant was removed by washing the lipid product with MilliQ water. A back-to-back DCM-MilliQ water washing routine was established for all the lipid analogue products prior to characterisation or biological evaluations.

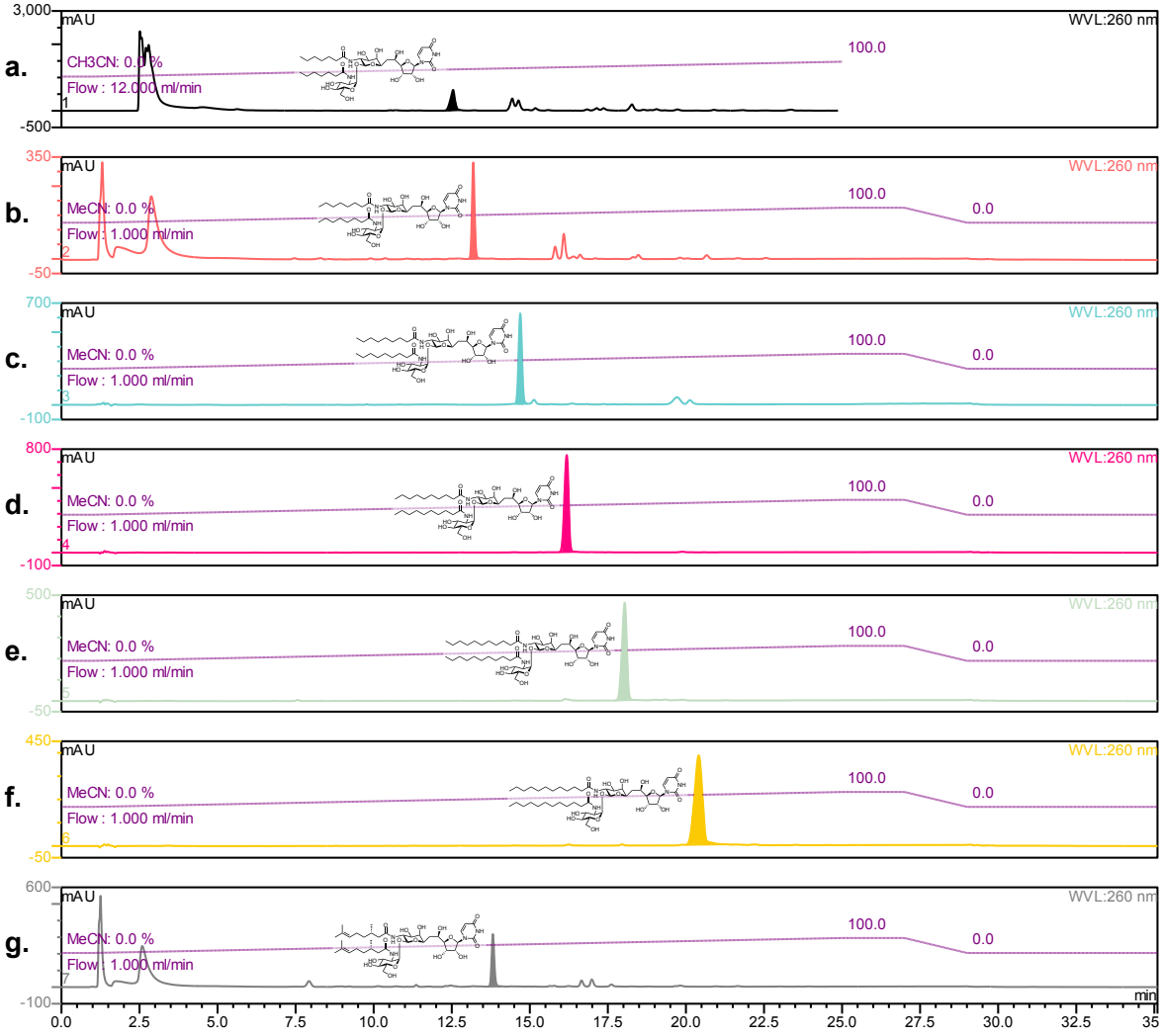


**Figure 2.25 | HPLC chromatogram of the tunicamycin lipid analogues (10-16).** The chromatogram at 260 nm from the analytical scale analysis using Phenomenex Synergi 4µ Hydro-RP 80Å 100 x 4.60 mm column, except for **(a)** where the chromatogram is from the preparative scale purification using Phenomenex Synergi 4µ Hydro-RP 80Å 100 x 21.20 mm column. **(a)** di-*N',N''*-heptanoyl-tunicamycin (**10**). **(b)** di-*N',N''*-octanoyl-tunicamycin (**11**). **(c)** di-*N',N''*-nonanoyl-tunicamycin (**12**). **(d)** di-*N',N''*-decanoyl-tunicamycin (**13**). **(e)** di-*N',N''*-undecanoyl-tunicamycin (**14**). **(f)** di-*N',N''*-dodecanoyl-tunicamycin (**15**). **(g)** di-*N',N''*-citronellyl-tunicamycin (**16**).

**Table 2.3 | Reaction summary of the tunicamycin lipid analogues (10-16).**

| Starting material | Fatty acid (eq.) | Reagents (eq.) | Time (h) | Yield |
|---|---|---|---|---|
| **8a** | Octanoic acid | TFA, TEA, DCC (2.8), DMAP (1), THF | 12 | 65% (**11**) |
| **9** | Nonanoic acid | DCC (2.5), DMAP (2), TEA (4), DMF | 240 | 26% (**12**)* |
| **9** | Heptanoic acid (2.5) | DIC (2.5), DMAP (2), TEA (4), DMF | 24 | 39% (**10**)* |
| **9** | Octanoic acid (2.5) | DIC (2.5), DMAP (2), TEA (4), DMF | 78 | 33% (**11**)* |
| **9** | Nonanoic acid (2.5) | DIC (2.5), DMAP (2), TEA (4), DMF | 78 | 39% (**12**)* |
| **9** | Decanoic acid (2.5) | DIC (2.5), DMAP (2), TEA (4), DMF | 78 | 39% (**13**)* |
| **9** | Undecanoic acid (2.5) | DIC (2.5), DMAP (2), TEA (4), DMF | 78 | 36% (**14**)* |
| **9** | Dodecanoic acid | DIC (2.5), DMAP (2), TEA (4), DMF | 68 | 31% (**15**)* |
| **9** | Citronellic acid (2.5) | DIC (2.5), DMAP (2), TEA (4), DMF | 168 | 54% (**16**)* |

*Yield determined after HPLC purification.

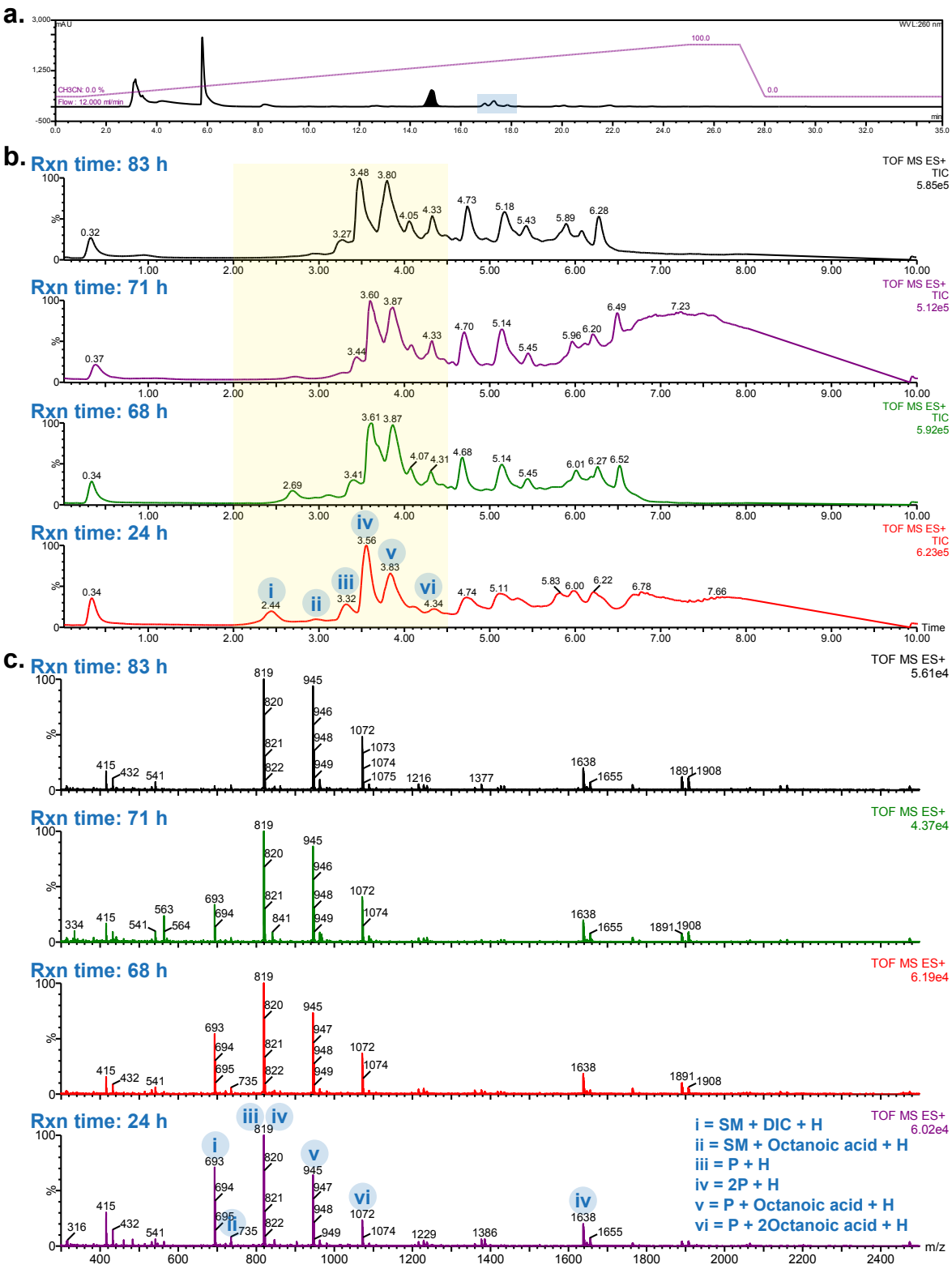


**Figure 2.26 | HPLC and LC/MS analysis of the reaction formation of lipid analogue (12). (a)** Preparative scale HPLC chromatogram at 260 nm. The product (**11**) is highlighted in black. The by-product is highlighted in blue. **(b)** TIC chromatogram of the same reaction at different time. **(c)** TOF MS ES$^+$ of the reaction progress. The corresponding masses are noted by roman numerals i-vi (TIC chromatogram time 2 - 4.5 min.). Starting material (**9**), SM: m/z 566.52. Product (**11**), P: m/z 818.92.

## 2.3 Conclusion and outlook

In this chapter, two tunicamycin core scaffolds (**3, 4**) have been isolated in addition to the dihydrochloride salt (**9**) of tunicamycin. The semi-synthetic strategy presented here would enables further fine-tuning of the tunicamycin core scaffold for the development of novel antimicrobial drug candidates. More importantly, the dihydrochloride salt (**9**) template has enabled selective lipid chain addition to both the 10'-*N* and 2"-*N* positions of tunicamycin, thereby creating the first library of novel tunicamycin lipid analogues. The outlook for this template **9** is extremely promising for applications in therapeutics and as chemical probes, as discussed in **Chapter 1.5**. With a library of tunicamycin core scaffolds and lipid analogues, the biological properties of tunicamycins can now be assessed to understand the importance of the GlcNAc moiety, the presence of the lipid chain, and the effect of the lipid chain length. In summary (**Fig. 2.27**), we have developed a semi-synthetic strategy to synthesise tunicamycin analogues with a defined lipid chain, a modified GlcNAc moiety, and a final product that is not a mixture of homologues. This semi-synthetic strategy has allowed the development of the first tunicamycin lipid analogues known to date.

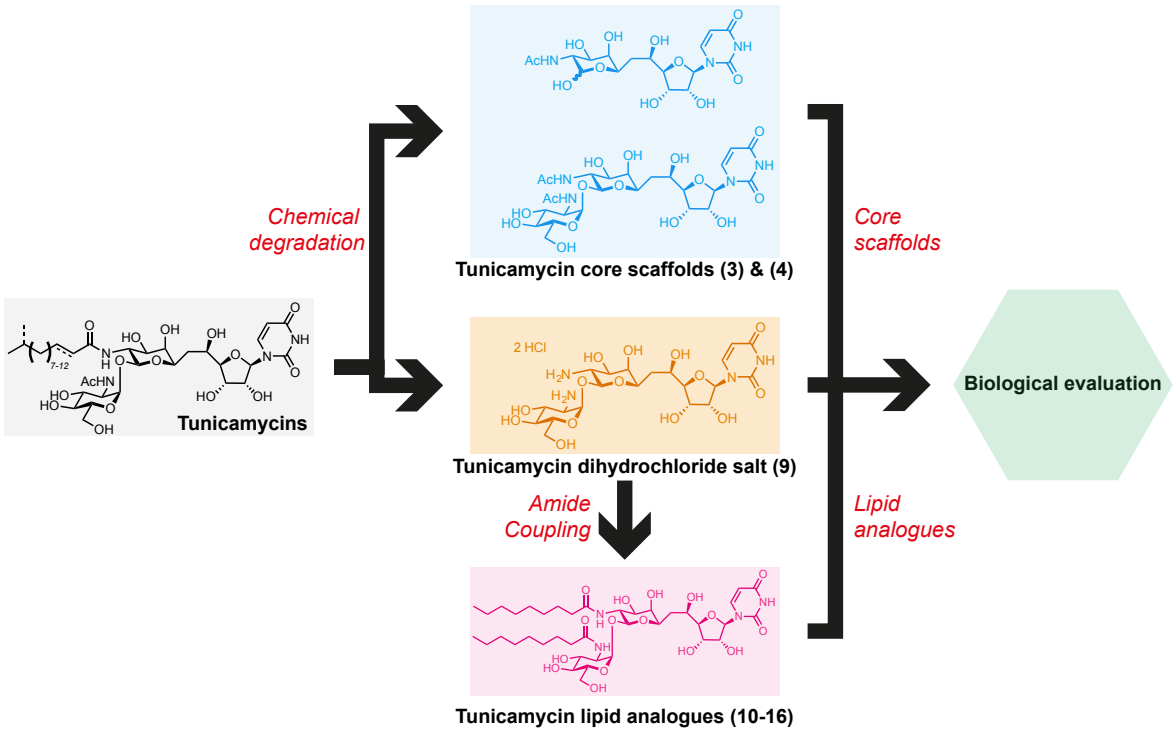


**Figure 2.27 | A summary of Chapter 2.**

## 2.4 References


1 Wyszynski, F. J., Hesketh, A. R., Bibb, M. J. & Davis, B. G. Dissecting tunicamycin biosynthesis by genome mining: cloning and heterologous expression of a minimal gene cluster. *Chem. Sci.* **1**, 581-589 (2010).

2 Fukuda, Y., Sasi, H. & Suami, T. Synthetic Approach toward Antibiotic Tunicamycins. *Bull. Chem. Soc. Jpn.* **54**, 1830-1833 (1981).

3 Suami, T. *et al.* Synthetic Approach Toward Antibiotic Tunicamycins, 4. X-Ray Crystal Structure Analysis of a Higher-Carbon Nitro Sugar. *J. Carbohydrate Chemistry* **1** (1982).

4 Fukuda, Y., Kitasato, H., Sasi, H. & Suami, T. Synthetic Approach toward Antibiotic Tunicamycins. II. *Bull. Chem. Soc. Jpn.* **55**, 880-886 (1982).

5 Suami, T., Sasi, H. & Matsuno, K. Synthesis of Methyl Hexaacetyl-tunicamyl Uracil. *Chemistry Letters*, 819-822 (1983).

6 Sasai, H., Matsuno, K. & Suami, T. Synthetic Approach Toward Antibiotic Tunicamycins - VII. Synthesis of Tunicamine and Tunicaminyl Uracil Derivative. *J. Carbohydrate Chemistry* **4**, 99-112 (1985).

7 Danishefsky, S. & Barbachyn, M. A Fully Synthetic Route to Tunicaminyluracil. *J. Am. Chem. Soc.* **107**, 7761-7762 (1985).

8 Myers, A. G., Gin, D. Y. & Widdowson, K. L. Silicon-Mediated Reductive Coupling of Aldehydes and Allylic Alcohols. A Stereoselective Synthesis of Tunicaminyluracil. *J. Am. Chem. Soc.* **113**, 9661-9663 (1991).

9 Ramza, J. & Zamojski, A. New Convenient Synthesis of Tunicamine. *Tetrahedron* **48**, 6123-6134 (1992).

10 Ramza, J. & Zamojski, A. The synthesis of S-C-(bdeoxy-1,2:3,4-di-O-isopropylidene-α-D-galactopyranos-6-yl)-2,3-O-isopropylidene-D-aIlo-pentofuranose [deaminotri-O-isopropylidene tunicamine]. *Carbohyd. Res.* **228**, 205-216 (1992).

11 Karpiesiuk, W. & Banaszek, A. Simple Synthesis of O,N-protected Tunicamine - The Undecose Part of Tunicamycins. *Bioorganic & Medicinal Chemistry Letters* **4**, 879-882 (1994).

12 Karpiwiuk, W. & Banazek, A. Simple Approach to O-Protected Deaminotunicaminyluracil. *Tetrahedron* **50**, 2965-2974 (1994).

13 Sarabia-García, F. & López-Herrera, F. J. Studies on the Synthesis of Tunicamycin. The Preparation of 7-deoxy-2-deamino-6-Hydroxy Tunicamine and Related Products. *Tetrahedron* **52**, 4757-4768 (1996).

14 Karpiesiuk, W. & Banaszek, A. Stereoselective syntheses of the O,N-protected subunits of the tunicamycins. *Carbohyd. Res.* **299**, 245-252 (1997).

15 Silva, D. J. & Sofia, M. J. Novel carbohydrate scaffolds. Assembly of a uridine–mannose scaffold based on tunicamycin. *Tetrahedron Letters* **41**, 855-858 (2000).

16 Sarabia, F., Martín-Ortiz, L. & López-Herrera, F. J. Synthetic studies towards the tunicamycins and analogues based on diazo chemistry. Total synthesis of tunicaminyl uracil. *Org. Biomol. Chem.* **1**, 3716-3725 (2003).

17 Ichikawa, S. & Matsuda, A. Synthesis of Tunicaminyluracil Derivatives. *Nucleosides, Nucleotides and Nucleic Acids* **23**, 239-253 (2004).

18 Fukuda, Y., Sasai, H. & Suami, T. Synthetic Approach toward Antibiotic Tunicamycins. 3. Methyl 3,4,7,8-Tetra-O-acetyl-10-O-benzyl-2-benzyloxycarbonylamino-2,6-dideoxy-11,12-O-isopropylidene-β-L-dodecadialdo-(12R)-furanose-(12,9)-pyranosides-(1,5). *Bull. Chem. Soc. Jpn.* **55**, 1574-1578 (1982).

19 Suami, T. *et al.* Synthetic approach toward antibiotic tunicamycins - VI. Total synthesis of tunicamycins. *Tetrahedron Letters* **25**, 4533-4536 (1984).

20 Suami, T., Sasai, H., Matsuno, K. & Suzuki, N. Total synthesis of tunicamcyin. *Carbohyd. Res.* **143**, 85-89 (1985).

21 Myers, A. G., Gin, D. Y. & Rogers, D. H. A Convergent Synthetic Route to the Tunicamycin Antibiotics. Synthesis of (+)-Tunicamycin V. *J. Am. Chem. Soc.* **5**, 2036-2038 (1993).

22 Myers, A. G., Gin, D. Y. & Rogers, D. H. Synthetic Studies of the Tunicamycin Antibiotics. Preparation of (+)-Tunicaminyluracil, (+)-Tunicamycin-V, and 5'-epi-Tunicamycin-V. *J. Am. Chem. Soc.* **116**, 4697-4718 (1994).

23 Takatsuki, A., Arima, K. & Tamura, G. Tunicamycin, A New Antibiotic. I: Isolation and Characterization of Tunicamycin. *The Journal of Antibiotics* **24**, 215-223 (1971).

24 Kenig, M. & Reading, C. Holomycin and an Antibiotic (MM 19290) Related to Tunicamycin, Metabolites of Streptomyces clavuligerus. *The Journal of Antibiotics* **32**, 549-554 (1979).

25 Hamill, R. L. Process for preparing tunicamycin. United States patent 4237225 (1980).

26 Tejera, E., Currie, S. A., Flor, J. E. & Monaghan, R. L. Process for producing tunicamycin. United States patent 4330624 (1982).

27 Kamogashira, T., Takegata, S. & Sugiura, K. Isolation of Tunicamycin Produced by Bacillus cereus K-279. *Agric. Biol. Chem.* **52**, 859-861 (1988).

28 Doroghazi, J. R. *et al.* Genome Sequences of Three Tunicamycin-Producing Streptomyces Strains, S. chartreusis NRRL 12338, S. chartreusis NRRL 3882, and S. lysosuperificus ATCC 31396. *J. Bacteriol.* **193**, 7021-7022 (2011).

29 Tsvetanova, B. C., Kiemle, D. J. & Price, N. P. J. Biosynthesis of Tunicamycin and Metabolic Origin of the 11-Carbon Dialdose Sugar, Tunicamine. *J. Biol. Chem.* **277**, 35289-35296 (2002).

30 Karki, S., Kwon, S.-Y. & Kwon, H.-J. Cloning of Tunicamycin Biosynthetic Gene Cluster from Streptomyces chartreusis NRRL 3882. *J. Korean Soc. Appl. Biol. Chem.* **54**, 136-140 (2011).

31 Wyszyński, F. J. *Dissecting tunicamycin biosynthesis: A potent carbohydrate processing enzyme inhibitor* D.Phil. thesis, University of Oxford, (2010).

32 Ishizuka, T. & Kunieda, T. Mild and selective ring-cleavage of cyclic carbamates to amino alcohols. *Tetrahedron Letters* **28**, 4185-4188 (1987).

33 Greene, T. W. & Wuts, P. G. M. *Protective Groups in Organic Synthesis*. 3rd edn, (John Wiley & Sons, Inc., 1999).

34 Kocienski, P. J. *Protecting Groups*. 3rd edn, (Thieme Publishing Group, 2005).

35 Wolfrom, M. L. & Bhat, H. B. Trichloroacetyl and Trifluoroacetyl as N-blocking Groups in Nucleoside Synthesis with 2-Amino Sugars. *J. Org. Chem.* **32**, 1821-1823 (1967).

36 Isidro-Llobet, A., Álvarez, M. & Albericio, F. Amino Acid-Protecting Groups. *Chem. Rev.* **109**, 2455-2504 (2009).

37 *Tunicamycin*. (Japan Scientific Societies Press, 1982).

38 Meier, L., Monteiro, G. C., Baldissera, R. A. M. & Sá, M. M. Simple Method for Fast Deprotection of Nucleosides by Triethylamine-Catalyzed Methanolysis of Acetates in Aqueous Medium. *J. Braz. Chem. Soc.* **21**, 859-866 (2010).

39 Beilin, E., Baker, L. J., Aikins, J. & Baryla, N. E. Effect of incomplete removal of the tert-butoxycarbonyl protecting group during synthesis of a pharmaceutical drug substance on

the residual solvent analysis. *Journal of Pharmaceutical and Biomedical Analysis* **52**, 316-319 (2010).

40 Auger, G., Heijenoort, J. v., Mengin-Lecreulx, D. & Blanot, D. A MurG assay which utilises a synthetic analogue of lipid I. *FEBS Microbiology Letters* **219**, 115-119 (2003).

41 Kahne, S. W., Men, H., Park, P. & Ge, M. Substrate analogs for MurG, methods of making same and assays using same. US6703213B2 (2004).

42 Stachyra, T. *et al.* Fluorescence Detection-Based Functional Assay for High-Throughput Screening for MraY. *Antimicrob. Agents Chemother.* **48**, 897-902 (2004).

43 Montalbetti, C. A. G. N. & Falque, V. Amide bond formation and peptide coupling. *Tetrahedron* **61**, 10827-10852 (2005).

44 Valeur, E. & Bradley, M. Amide bond formation: beyond the myth of coupling reagents. *Chem. Soc. Rev.* **38**, 606-631 (2009).

# *Chapter Three*

## *Biological Evaluations of the Tunicamycin Core Scaffolds and Lipid Analogues*

## 3.1 Introduction

Tunicamycin homologues are reported to exhibit different levels of *N*-linked glycosylation inhibition in eukaryotic cells, but little is described about their individual antimicrobial activities.[1-7] Whilst it is proposed that the tunicaminyl uracil scaffold acts as an UDP mimic[8] and the GlcNAc moiety contributes to the mammalian cytotoxicity (see **Chapter 1**), this GlcNAc has never been directly shown to be the cause of the cytotoxicity.[9-11] Moreover, it has been speculated that the lipid chain of tunicamycin homologues influences their biological activity, but again, this has never been directly shown to be associated with the antimicrobial or the mammalian cytotoxic activities.[1-7,12] Thus, we wanted to investigate the biological effects of the tunicamycin core scaffolds and the novel lipid analogues, as described in **Chapter 2**, to understand their mode of action. In this chapter, the biological properties of the tunicamycin core scaffolds and the lipid analogues (**Fig. 3.1**) are described.

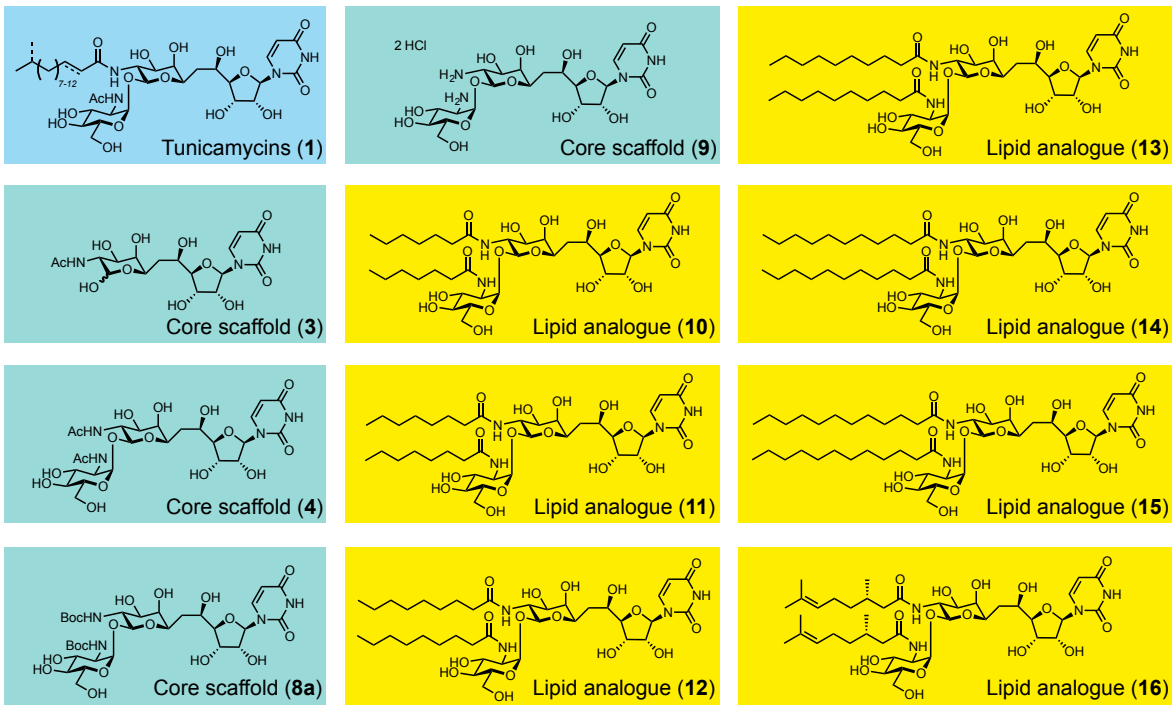


**Figure 3.1 | Tunicamycins (1), the tunicamycin core scaffolds (3, 4, 8a, and 9), and the tunicamycin lipid analogues (10-16).**

## 3.2 Results and Discussion

### 3.2.1 Kirby-Bauer Disc Diffusion Test of the Tunicamycin Core Scaffolds and Lipid Analogues

We first evaluated the core scaffolds (**3**, **4**, **8a**, **9**) and the lipid analogues (**10**-**16**), shown in **Fig. 3.1**, for antibacterial activities. This was carried out by the Kirby-Bauer disc diffusion susceptibility test.[13] We used the tunicamycins sensitive and resistant bacteria strains, *Bacillus subtilis* EC1524 and *Micrococcus luteus*, respectively, in the antibacterial susceptibility test.[14,15] Additionally, we also performed the antibacterial susceptibility test using a few common standard test strains such as the opportunistic pathogens *Bacillus cereus* ATCC11778, *Staphylococcus aureus* ATCC29219 and *Pseudomonas aeruginosa* ATCC27853, and lastly the non-pathogenic strain *Escherichia coli* ATCC25922.[16] These common strains were chosen because they cause some of the most dangerous bacterial infections. Generally, *B. cereus* is associated with causing serious and potentially fatal non-gastrointestinal-tract infections,[17,18] *S. aureus* is a major concern due to the high incidence of skin infections in hospitals and the wide-spread emergence of antibiotic-resistant strains,[19-21] while *P. aeruginosa* is a highly adaptive Gram-negative bacterium that is a concern typically in hospitals. *P. aeruginosa* causes respiratory infections and also affects patients after antibiotic treatment due to the disruption of the patient bacterial flora, compromising the natural defences.[22-24] Although *E. coli* is an important member of the human intestinal bacterial flora, certain strains can cause serious intestinal complications.[25-27] Thus finding new antibacterial drugs to combat these threats are vital to improving human health, especially considering the emerging problems with antimicrobial resistant bacteria.[28-30]

The Kirby-Bauer disc diffusion test is a routine qualitative approach for determining the antibacterial activity and could be considered as an quantitative approach to determine the minimal inhibition concentration (MIC) values of an antibiotic.[31,32] The test provides the zone of inhibition of bacterial growth for a specific antibiotic of specific dose. In order to carry out the test, a blank disc is impregnated with a known concentration of the antibiotic, and then carefully placed on an agar plate that has been inoculated with bacteria and then incubated for 16-24 h at 35±2 °C.[33,34] The diameter of the inhibition zone is the reported value. In theory, the antibiotic on the disc quickly diffuses into the agar where the concentration of the antibiotic is highest closest to the disc and decreases as the distance from the disc increases. This rate of diffusion is dependent on various factors, such as the properties of the antibiotic being tested, the solubility, the molecular weight, and others including temperature, time, and as well as the agar medium with regards to the salt concentration and nutrient composition.[35] The diameter of the zone where there is no bacterial growth is related to the susceptibility of the tested bacterium to the tested antibiotic. The antibiotic concentration around the diameter of the zone would be the critical concentration that is approximately equal to the MIC obtained from a broth dilution susceptibility test, and would require a series of tested concentrations in order to obtain a linear plot to determine the MIC value unless an Epsilometer is used.[13,36]

We first evaluated the compounds shown in **Fig. 3.1** for antimicrobial activity by Kirby-Bauer disc diffusion test. The purpose of using the Kirby-Bauer disc diffusion test first is that it provides a quick and simple preliminary qualitative antibacterial evaluation of the tunicamycin core scaffolds and the lipid analogues prior to the broth dilution susceptibility test to quantitatively determine the MIC, half-maximal inhibition con-

centration ($IC_{50}$) and also minimum bactericidal concentration (MBC) without much optimisation work to find the inhibitory concentration zone.[36,37] We decided to use the broth dilution test to determine the susceptibility values because it allowed us to carry out the experiment in a micro broth dilution scale using a 96-well plate. This would not use a large quantity of the precious tunicamycin compounds. The experiment was conducted in the liquid culture where diffusion is neglected compared to the Kirby-Bauer disc diffusion test, and it allowed for serial dilutions to obtain a set of data points to plot for a dose-response curve to determine the $IC_{50}$. Furthermore, the same experimental culture can be used to determine the MBC values.[36,37] The process for the susceptibility tests that we performed is summarised in **Fig. 3.2**.

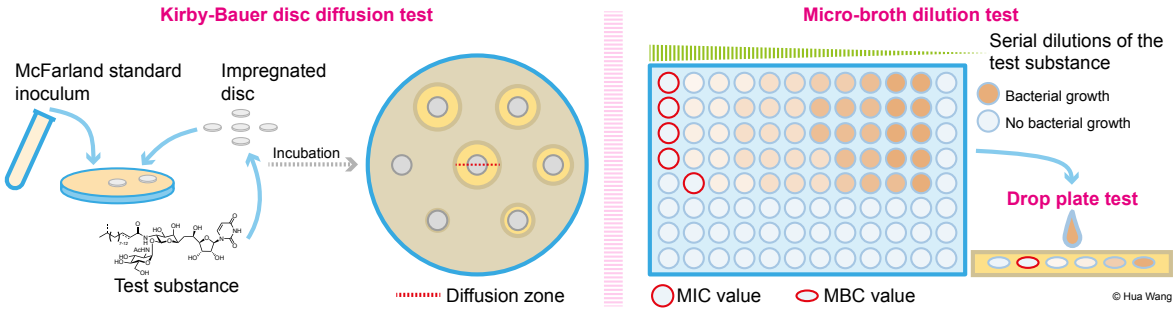


**Figure 3.2 | A schematic diagram showing the process to determine antibacterial susceptibility values.** Kirby-Bauer disc diffusion, micro-broth dilution, and drop plate tests are shown. The Kirby-Bauer disc diffusion test followed the Clinical and Laboratory Standards Institute standards to ensure uniformity and reproducibility of the results.

A stock of each compounds (**Fig. 3.1**) was prepared by dissolving the compound in either MilliQ water or methanol depending on the test compound's solubility and then impregnating a specific dose on to a 6mm Oxoid blank disc. The Kirby-Bauer diffusion tests were done on Mueller-Hinton agar plate according to the Clinical and Laboratory Standards Institute (CLSI) standards for reproducibility as previously mentioned. **Fig 3.3**

shows the results from the Kirby-Bauer disc test and **Table 3.1** summarises the zone of inhibition values.

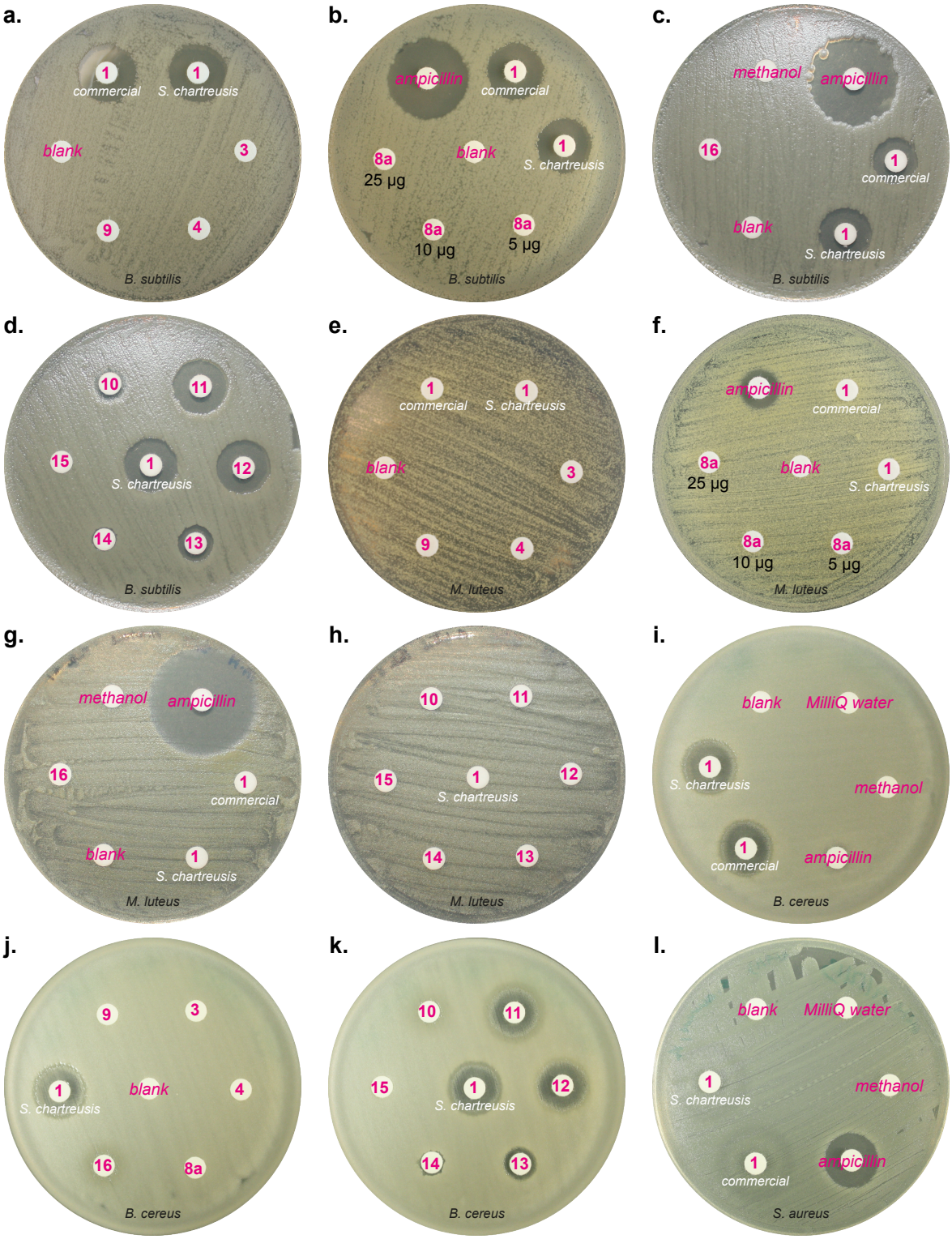


**Figure 3.3 (continued) | The Kirby-Bauer disc diffusion test.** Each disc was impregnated with 5 µg of each antibiotic, unless indicated otherwise (**Fig. 3.1**), and evaluated for antimicrobial activity against *B. subtilis* (**a-d**), *M. luteus* (**e-h**), *B. cereus* (**i-k**), *S. aureus* (**l-n**, **r**, **s**), and *P. aeruginosa* (**o-q**, **t**, **u**). Due to the the pigments produced by *P. aeruginosa,* the light zone of inhibition diameter is indicated by a dotted line from the lipid analogues (**12**), (**13**), and (**14**) on the plate (**q** and **u**). The

disc with methanol was left to evaporate off before placing on the agar, as with the others, to ensure no false-positives.

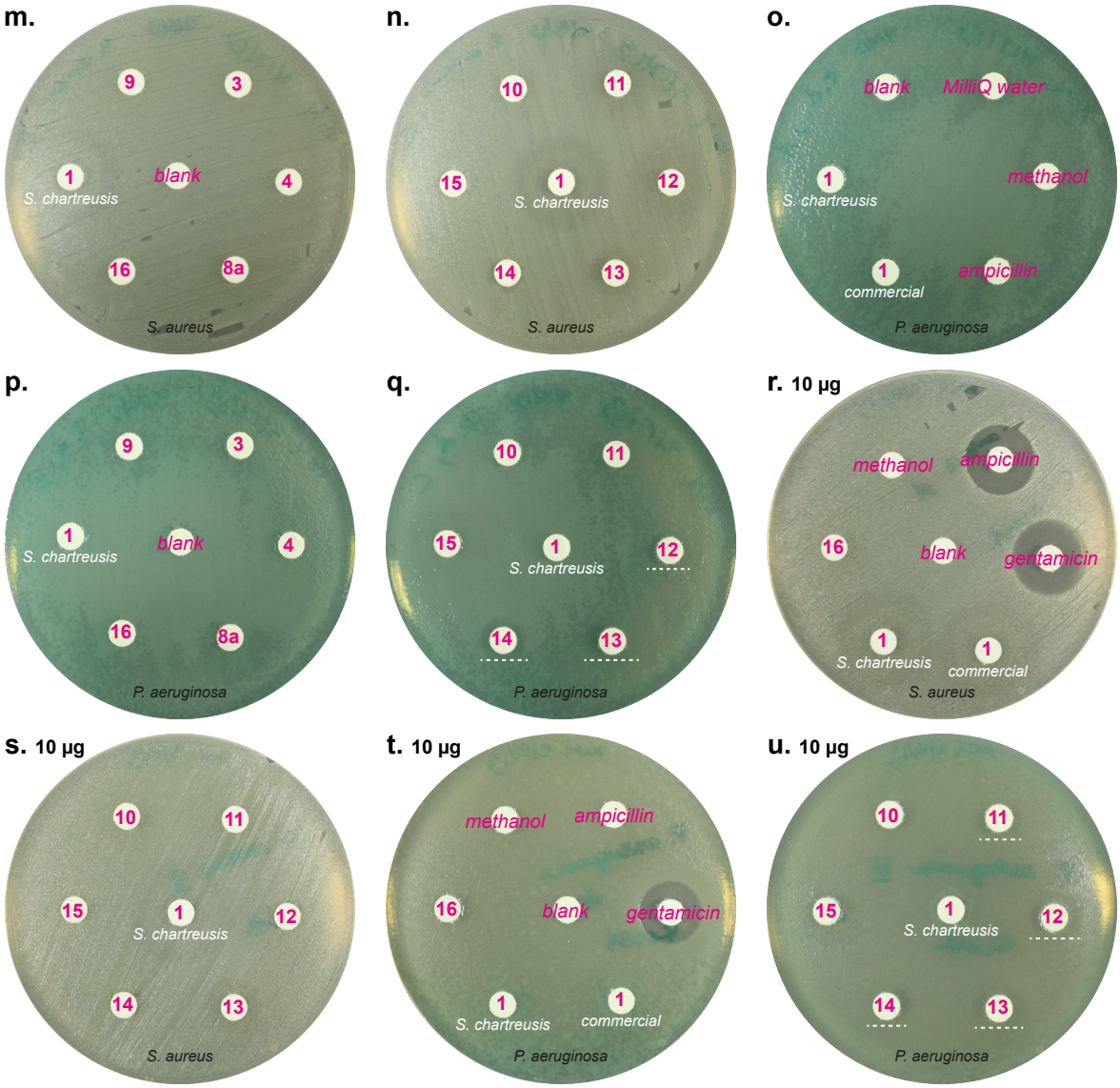


**Figure 3.3 (continued) | The Kirby-Bauer disc diffusion test.** Each disc was impregnated with 5 µg of each antibiotic, unless indicated otherwise (**Fig. 3.1**), and evaluated for antimicrobial activity against *B. subtilis* (**a-d**), *M. luteus* (**e-h**), *B. cereus* (**i-k**), *S. aureus* (**l-n**, **r**, **s**), and *P. aeruginosa* (**o-q**, **t**, **u**). Due to the the pigments produced by *P. aeruginosa,* the light zone of inhibition diameter is indicated by a dotted line from the lipid analogues (**12**), (**13**), and (**14**) on the plate (**q** and **u**). The disc with methanol was left to evaporate off before placing on the agar, as with the others, to ensure no false-positives.

**Table 3.1 | Zone of inhibition for the standards and test compounds (Fig. 3.1).**

| Compound | Zone of inhibition (mm):dose (µg) | | | | | |
|---|---|---|---|---|---|---|
| | ***B. subtilis*** **EC1524** | ***M. luteus*** | ***B. cereus*** **ATCC11778** | ***S. aureus*** **ATCC29219** | ***P. aeruginosa*** **ATCC27853** | ***E. coli*** **ATCC25922** |
| Ampicillin | 24:5 | 31:5 | NI:5 | 16:10 | NI:10 | 17:10 |
| Gentamicin | N/A | N/A | N/A | 18:10 | 15:10 | N/A |
| **(1)** Comm. | 15:5 | NI:5 | 13:5 | 25*:10 | NI:10 | NI:10 |
| **(1)** *S. chart.* | 16:5 | NI:5 | 13:5 | 25*:10 | NI:10 | NI:10 |
| **(3)** | NI:5 | NI:5 | NI:5 | NI:10 | NI:10 | NI:10 |
| **(4)** | NI:5 | NI:5 | NI:5 | NI:10 | NI:10 | NI:10 |
| **(8a)** | NI:5, 10, 25 | NI:5, 10, 25 | NI:5 | NI:10 | NI:10 | NI:10 |
| **(9)** | NI:5 | NI:5 | NI:5 | NI:10 | NI:10 | NI:10 |
| **(10)** | NI:5 | NI:5 | NI:5 | NI:10 | 7*:10 | NI:10 |
| **(11)** | 10:5 | NI:5 | 12:5 | 20*:10 | 9*:10 | NI:10 |
| **(12)** | 16:5 | NI:5 | 13:5 | 23*:10 | 13*:10 | NI:10 |
| **(13)** | 16:5 | NI:5 | 9:5 | 14*:10 | 12*:10 | NI:10 |
| **(14)** | 10:5 | NI:5 | 7:5 | NI:10 | 12*:10 | NI:10 |
| **(15)** | 6:5 | NI:5 | NI:5 | NI:10 | 8*:10 | NI:10 |
| **(16)** | NI:5 | NI:5 | NI:5 | NI:10 | NI:10 | NI:10 |

N/A = no evaluation was carried out.
NI = no inhibition observed.
*Not the inhibition zone but the diameter of the halo ring, indicative of mild inhibition and resistance.

It has been hypothesised in the literature that the lipid chain of tunicamycins could facilitate the transfer of tunicamycins through the phospholipid bilayer of the bacterial outer membrane.[7,12,38] Excitingly, for the first time, using the Kirby-Bauer disc test, we have shown that tunicamycins without their lipid chain lose their inhibitory activity against the tunicamycin sensitive *B. subtilis* EC1524 strain and other bacterial standards including *B. cereus* and *P. aeurginosa*. Whether or not the GlcNAc moiety is present, the tunicamycin's core scaffolds did not exhibit any observable antibacterial activity towards *Bacillus* strains as long as the lipid chain is not present, as shown for scaffolds (**3**, **4**, **8a**, and **9**) in the Kirby-Bauer disc test (**Fig. 3.3**, **Table 3.1**). This implies that if tunicamycins lose the GlcNAc moiety but retain their lipid chain, then selective toxicity towards

bacterial cells and not mammalian cells might be possible, specifically targeting MraY transferase instead of GPT. However, as discussed in **Chapter 1**, the GlcNAc moiety or, the hexosamine structure, may be necessary in order to preserve or increase inhibition as a substrate mimic or substrate-product transition state mimic. This speculation is supported by the results obtained from the tunicamycin lipid analogues (**10-16**). The tunicamycin lipid analogues with carbon chain length between seven to ten were shown to have similar inhibitory activity towards *B. subtilis* as commercial tunicamycins. Interestingly, as chain length increases, the inhibitory activity appeared to decrease as shown in **Fig. 3.3**, from eleven to twelve carbon chain length as observed for lipid analogues (**14**) and (**15**). The lipid analogue (**11**), with eight carbon chain, appeared to be more toxic than mixtures of tunica-mycins. In contrast, when the eight carbon chain was not fully saturated and includes methyl branches such as the citronellic acid derivative lipid analogue (**16**), the antibacterial activity was lost drastically. This is interesting because citronellic acid derivatives has been used as short chain analogues of the bacterial undecaprenyl phosphate lipid chain in inhibition studies.[39-41] Only a light halo was observed around lipid analogue (**16**) impregnated disc compared to a large zone of inhibition from the lipid analogue (**11**). This may suggest that the lipid analogue (**16**) is not as effective as **11** in facilitating the transfer through the bacterial membrane to reach to the MraY transferase cytosolic active site, or other similar enzyme targets, or that the unsaturation and the methyl branches affected the inhibition binding at the active site and the putative hydrophobic groove on MraY as discussed in **Chapter 1**. Moreover, it has been demonstrated that lipid chain length or presence of the methyl groups can dramatically affect the inhibitory activity of tunica-mycins based on homologue activity studies.[1,3-5]

A stark resemblance in antibacterial activity to either the tunicamycins from the commercial source or isolated from *S. chartreusis* was observed for lipid analogues (**11**), (**12**), and (**13**), suggesting that eight-, nine-, and ten-carbon chain lengths and/or degree of saturations may play important roles in the antibacterial properties of tunicamycins (**Fig. 3.3**, **Table 3.1**).

The tunicamycins and the lipid analogues appeared to exhibit similar potent inhibitory activity against both *B. subtilis* and *B. cereus* (**Fig. 3.3d,k**, **Table 3.1**). The other bacterial strains that were used in the Kirby-Bauer disc diffusion test, such as *M. luteus*, *S. aureus*, *E. coli*, and *P. aeruginosa,* were found to be less sensitive. Unsurprisingly, the lipid analogues were found to be similar as tunicamycins inhibitory activity towards those strains that have been reported to be less sensitive.[7] Surprisingly, the lipid analogues appeared to have very mild inhibitory activity against *P. aeruginosa* that was not observed for tunicamycins (**Fig. 3.3q,u**, **Table 3.1**). Thus, this could imply that further tailoring of scaffold (**9**) to create a wider range of lipid analogues with different lipid chain characteristics may uncover tunicamycin lipid analogues that can increase their potency towards *P. aeruginosa*, *E. coli*, and other Gram-negative bacteria. This is particularly attractive for further investigation of potential new antibiotics to target Gram-negative bacteria and emerging antimicrobial resistant bacteria.[28-30]

### 3.2.2 MIC, $IC_{50}$, and MBC Determination of the Tunicamycin Core Scaffolds and Lipid Analogues

MIC and $IC_{50}$ values can be determined from a micro-broth dilution test, and MBC values by a drop plate test as previously discussed (**Fig. 3.2**).[13,36,37] These are routine procedures used to quantitatively determine antimicrobial susceptibility values.

First, the micro-broth dilution test was carried out using a 96-well plate to determine MIC values (**Fig. 3.4**). The highest concentration that was tested was 400 or 50 μg $mL^{-1}$, depending on the sensitivity of the bacteria being used to the test compounds, and ten to twenty serial dilutions were made to find the dilution range that would show no bacterial growth in the mid-range. The plate was incubated for 18-24 h at 35±2 °C. The well with the lowest concentration of the test compound that did not show any visible bacterial growth would give the MIC value based on the dilutions (**Fig. 3.2**, **Fig. 3.4**, **Table 3.2**). Tunicamycins and the lipid analogues were prepared in methanol. Thus, in order to avoid methanol contamination and false-positive results, all test compounds (**Fig. 3.1**) were first added to a small volume of MH growth medium and the methanol was left to evaporate before adding the bacterial inoculum. The 96-well plate also contained positive and negative control growth wells to ensure that any antibacterial activity was not due to methanol contamination.

The tests that were undertaken on *B. subtilis* and *M. luteus* at up to 50 μg $mL^{-1}$ of the test compounds (**Fig. 3.4**). From this set of results, it became apparent that the core scaffolds were not as effective as the lipid analogues in inhibiting bacterial growth. Thus,

at this stage, we focused our efforts on determining the susceptibility values of the lipid analogues (**Table 3.2**).

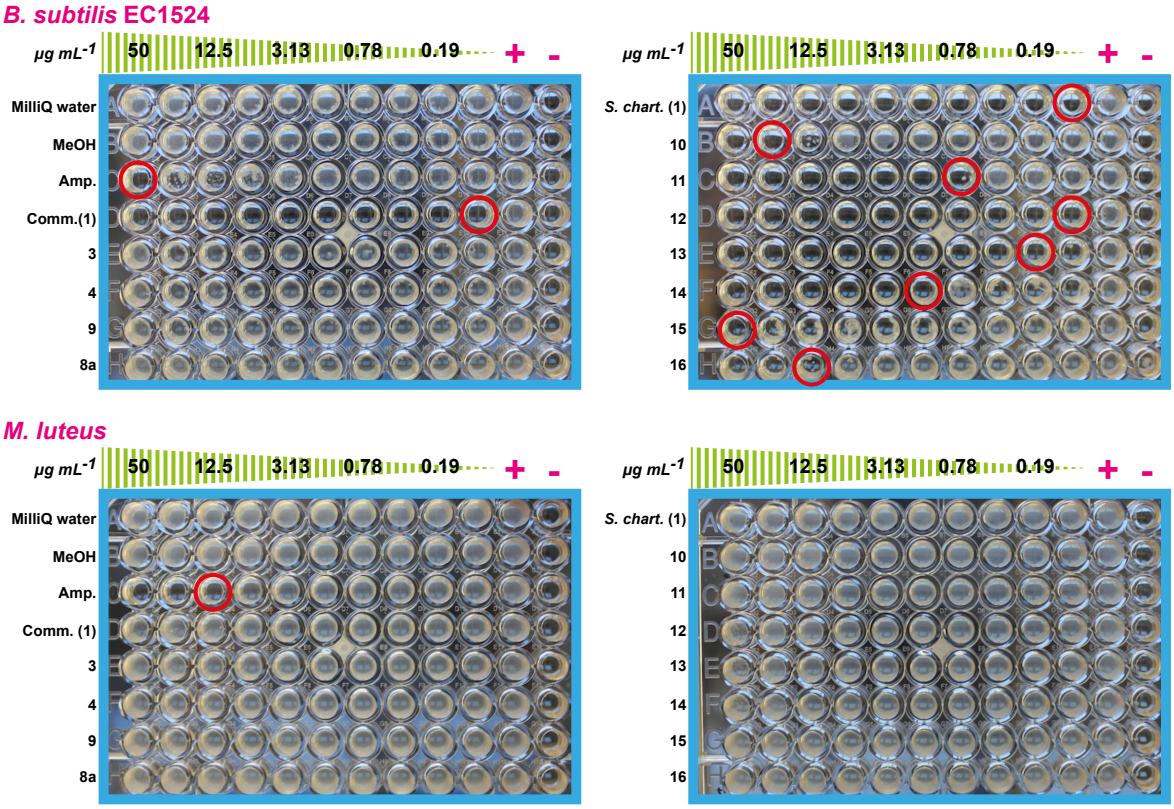


**Figure 3.4 | The micro-broth dilution 96-well antimicrobial susceptibility test.** A set of *B. subtilis* EC1524 and *M. luteus* micro-broth dilution tests is shown, with serial dilutions from 50 - 0.098 μg $mL^{-1}$. The MIC values are deduced from the clear culture wells with the lowest concentration of the test compound, as depicted by the red circled wells with respect to their concentration. The (+) and (-) columns were the positive growth and the negative controls. The MIC values are summarised in **Table 3.2**.

**Table 3.2 | MIC values for the tunicamycin core scaffolds and lipid analogues.**

| Compound | MIC values* (μg mL$^{-1}$) | | | | | |
|---|---|---|---|---|---|---|
| | ***B. subtilis*** **EC1524** | ***M. luteus***[a] | ***B. cereus*** **ATCC11778** | ***S. aureus*** **ATCC29219** | ***P. aeruginosa*** **ATCC27853** | ***E. coli*** **ATCC25922** |
| Ampicillin | 1.56 ±0.90 | 12.50 ±3.61 | >200 | 50.00 ±14.43 | ND | ND |
| Gentamicin | ND | ND | 1.56 ±0.45 | ND | 0.78 ±0.23 | 1.56 ±0.45 |
| **(1)** Comm. | 0.0015 ±0.0011 | >50 | 0.02 ±0.06 | 50.00 ±14.43 | >400 | >400 |
| **(1)** *S. chart.* | 0.0015 ±0.0011 | >50 | 0.02 ±0.06 | 50.00 ±14.43 | >400 | >400 |
| **(3)** | >50[a] | >50 | ND | ND | ND | ND |
| **(4)** | >50[a] | >50 | ND | ND | ND | ND |
| **(8a)** | >50[a] | >50 | ND | ND | ND | ND |
| **(9)** | >50[a] | >50 | ND | ND | ND | ND |
| **(10)** | 6.25 ±1.80 | >50 | 100.00 ±28.87 | 200.00 ±57.74 | 100.00 ±28.87 | >400 |
| **(11)** | 0.78 ±0.23 | >50 | 6.26 ±1.81 | 200.00 ±57.74 | 100.00 ±28.87 | >400 |
| **(12)** | 0.024 ±0.001 | >50 | 0.78 ±0.23 | 100.00 ±28.87 | 100.00 ±28.87 | >400 |
| **(13)** | 0.39 ±0.11 | >50 | 0.39 ±0.11 | 100.00 ±28.87 | 100.00 ±28.87 | >400 |
| **(14)** | 1.56 ±0.45 | >50 | 0.78 ±0.23 | 200.00 ±57.74 | 100.00 ±28.87 | >400 |
| **(15)** | 100.00 ±28.87 | >50 | 50.00 ±14.43 | 200.00 ±57.74 | 200.00 ±57.74 | >400 |
| **(16)** | 6.25 ±1.80 | >50 | 100.00 ±28.87 | >400 | 200.00 ±57.74 | >400 |

The MIC values were obtained from a triplicate experiment.
*We tested up to 400 μg mL$^{-1}$ and made serial dilutions by half concentration of each compounds to determine the MIC values. If the bacteria growth was observed up to the concentration tested, or if we observed very little growth at a specific concentration, then we noted as > than the concentration.
ND = not determined. The compound was not tested against the bacteria.
[a]50 μg mL$^{-1}$ = highest concentration tested.

Then, we generated the dose-response curves from the turbidity value (optical density, $OD_{600}$) of each well with respect to each dilution concentration (**Fig. 3.5**) from the micro-dilution plates. The $IC_{50}$ values were determined from the dose-response curve using Prism 6.0 software. A summary of the $IC_{50}$ values are summarised in **Table 3.3**.

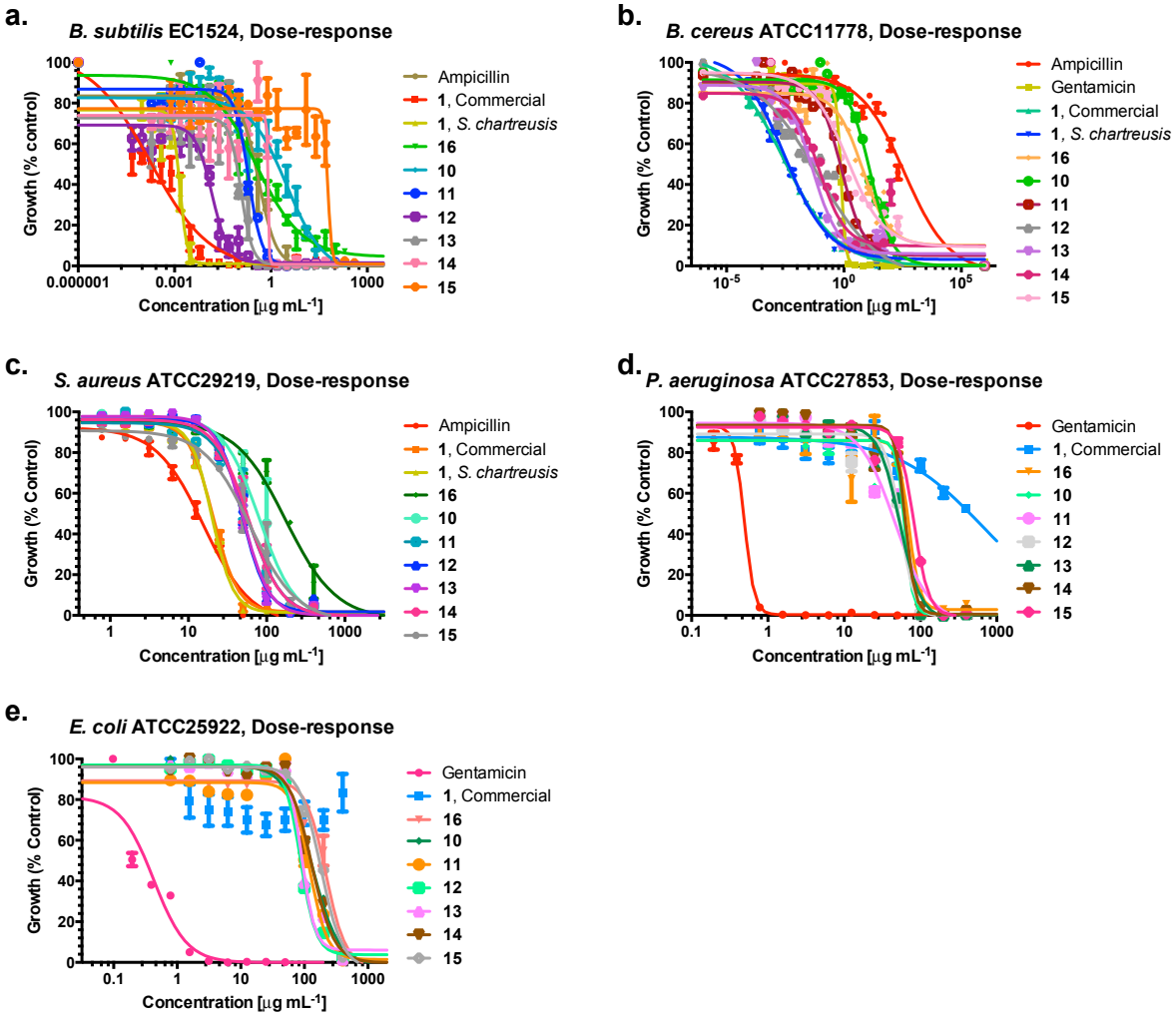


**Figure 3.5 | The dose-response curves from the MIC determination of the tunicamycin core scaffolds and the lipid analogues.** The dose-response curves were generated by Prism 6.0 software by plotting percent growth (normalised $OD_{600}$ values) vs. logarithmic scale of the concentrations. The data shown are mean ±SEM errors of three independent experiments. **(a)** *B. subtilis* EC1524. **(b)** *B. cereus* ATCC11778. **(c)** *S. aureus* ATCC29219. **(d)** *P. aeruginosa* ATCC27853. **(e)** *E. coli* ATCC25922. The $IC_{50}$ values are summarised in **Table 3.3**.

**Table 3.3 | $IC_{50}$ values for the tunicamycin core scaffolds and lipid analogues.**

| Compound | $IC_{50}$ values* (μg $mL^{-1}$) | | | | | |
|---|---|---|---|---|---|---|
| | ***B. subtilis*** **EC1524** | ***M. luteus*** | ***B. cereus*** **ATCC11778** | ***S. aureus*** **ATCC29219** | ***P. aeruginosa*** **ATCC27853** | ***E. coli*** **ATCC25922** |
| Ampicillin | 0.42 ±0.14 | ND | 386.00 ±128.67 | 15.58 ±5.23 | ND | ND |
| Gentamicin | ND | ND | 0.74 ±0.25 | ND | 0.49 ±0.16 | 0.43 ±0.14 |
| **(1)** Comm. | 0.00018 ±0.00006 | ND | 0.0029 ±0.0010 | 20.78 ±6.93 | 655.30 ±218.43 | ND |
| **(1)** *S. chart.* | 0.00015 ±0.0005 | ND | 0.0031 ±0.0011 | 20.12 ±6.71 | ND | ND |
| **(3)** | ND | ND | ND | ND | ND | ND |
| **(4)** | ND | ND | ND | ND | ND | ND |
| **(8a)** | ND | ND | ND | ND | ND | ND |
| **(9)** | ND | ND | ND | ND | ND | ND |
| **(10)** | 3.12 ±1.04 | ND | 13.33 ±4.45 | 80.49 ±26.83 | 62.44 ±20.81 | 131.20 ±43.73 |
| **(11)** | 0.20 ± 0.07 | ND | 0.78 ±0.26 | 58.36 ±19.45 | 46.57 ±15.52 | 122.70 ±40.90 |
| **(12)** | 0.015 ±0.005 | ND | 0.072 ±0.024 | 48.92 ±16.31 | 54.98 ±18.32 | 87.06 ±29.02 |
| **(13)** | 0.12 ±0.04 | ND | 0.046 ±0.015 | 49.29 ±16.43 | 53.46 ±17.82 | 91.63 ±30.54 |
| **(14)** | 0.85 ±0.28 | ND | 0.088 ±0.029 | 58.03 ±19.34 | 63.17 ±21.06 | 131.10 ±43.70 |
| **(15)** | 58.92 ±19.64 | ND | 1.40 ±0.47 | 61.88 ±20.63 | 81.74 ±27.31 | 181.60 ±60.53 |
| **(16)** | 0.36 ±0.12 | ND | 6.29 ±2.10 | 176.70 ±58.90 | 70.29 ±23.43 | 217.90 ±72.63 |

*$IC_{50}$ values were derived from the MIC data from **Table 3.2**. We tested up to 400 μg $mL^{-1}$ of each compounds to determine the MIC values. If bacteria growth was observed up to the concentration tested, or if we observed very little growth at a concentration, then we noted as > than the concentration.
ND = not determined. The compound was not tested against the bacteria.

Lastly, with the drop-plate test, 2-3 μL of the culture from each 96 wells was plated on a freshly prepared MH agar plate. The plate was then further incubated for additional 18-24 h at 35±2 °C. The lowest concentration culture inoculated on the MH agar plate that did not have any visible bacterial growth was noted as the MBC value (**Fig. 3.2**, **Fig. 3.6**). The MBC values are summarised in **Table 3.4**.

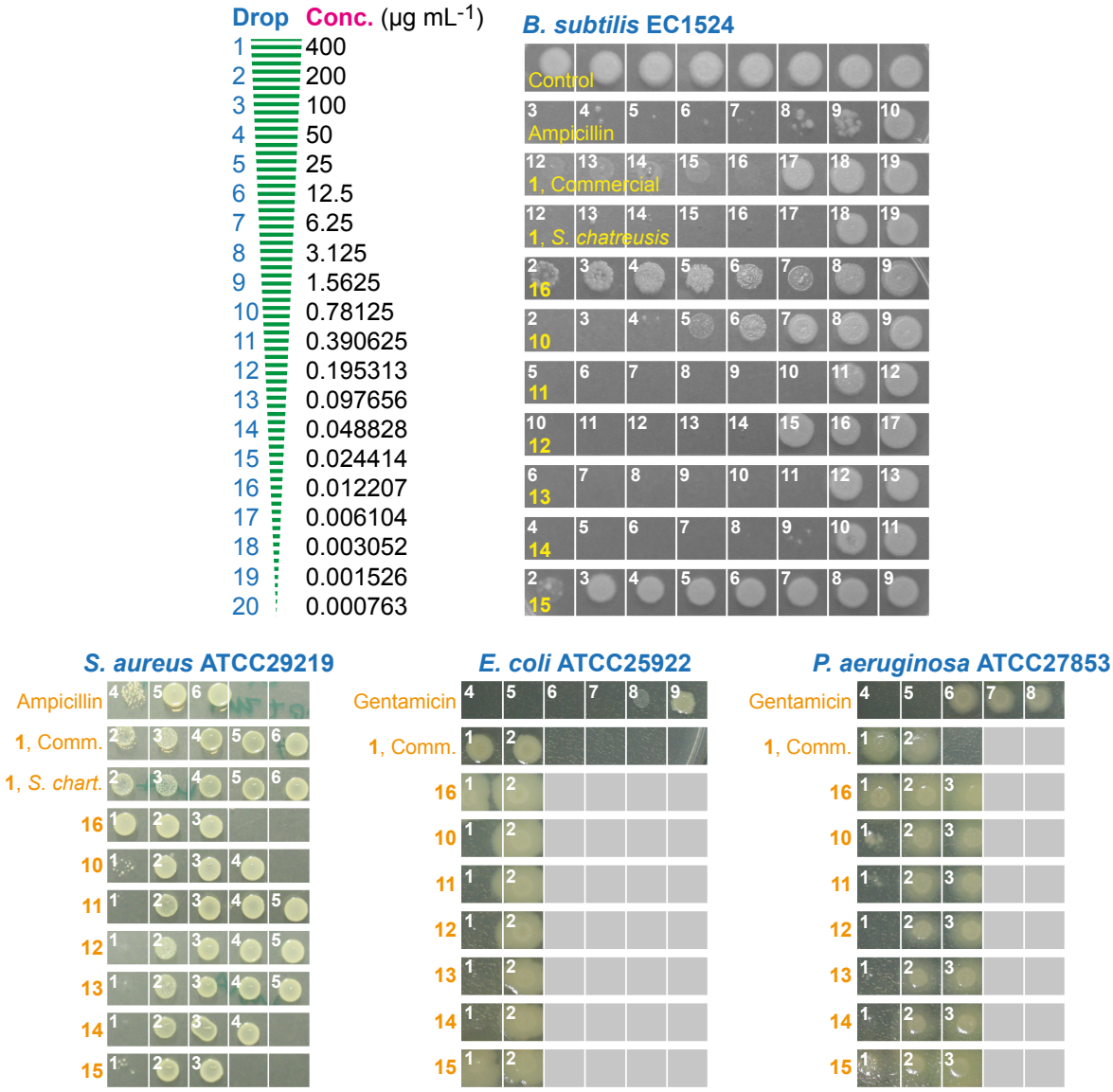


**Figure 3.6 | The drop-plate test from *B. subtilis*, *B. cereus*, *S. aureus*, and *P. aeruginosa* MBC evaluation of the tunicamycin core scaffolds and the lipid analogues.** The MBC value was determined by inoculating 2-3 μL of the culture from the MIC experiment on an MH agar plate. The MBC values are summarised in **Table 3.4**.

**Table 3.4 | MBC value for the tunicamycin core scaffolds and the lipid analogues.**

| Compound | MBC values* (μg mL$^{-1}$) | | | | | |
|---|---|---|---|---|---|---|
| | ***B. subtilis*** **EC1524** | ***M. luteus***[a] | ***B. cereus*** **ATCC11778** | ***S. aureus*** **ATCC29219** | ***P. aeruginosa*** **ATCC27853** | ***E. coli*** **ATCC25922** |
| Ampicillin | >50 | 25.00 | >200 | >50 | ND | ND |
| Gentamicin | ND | ND | 12.50 | ND | 25.00 | >3.13 |
| **(1)** Comm. | >0.012 | >50 | 25.00 | >200 | >400 | >400 |
| **(1)** *S. chart.* | >0.006 | >50 | 25.00 | >200 | >400 | >400 |
| **(3)** | >50[a] | >50 | ND | ND | ND | ND |
| **(4)** | >50[a] | >50 | ND | ND | ND | ND |
| **(8a)** | >50[a] | >50 | ND | ND | ND | ND |
| **(9)** | >50[a] | >50 | ND | ND | ND | ND |
| **(10)** | >50 | >50 | >200 | >400 | >400 | >400 |
| **(11)** | >0.78 | >50 | >50 | 400 | >400 | 400 |
| **(12)** | >0.048 | >50 | >25 | 400 | 400 | 400 |
| **(13)** | >0.39 | >50 | 12.50 | 400 | 400 | 400 |
| **(14)** | >1.56 | >50 | >25 | 400 | 400 | 400 |
| **(15)** | >200 | >50 | >200 | 400 | >400 | >400 |
| **(16)** | >200 | >50 | >200 | >400 | >400 | >400 |

*MBC values were derived from the MIC experiment culture. The standard deviation values are not shown because the MBC values were consistent in triplicate. We tested up to 400 μg mL$^{-1}$ of each compounds to determine the MBC values. If bacteria growth was observed up to the concentration tested, or if we observed very little growth at a concentration, then we noted as > than the concentration.
ND = not determined. The compound was not tested against the bacteria.
[a]50 μg mL$^{-1}$ = highest concentration tested.

Satisfyingly, all the lipid analogues were shown to be potent antibacterial drug candidates, particularly lipid analogues (**11**) and (**12**) which were most active. The micro-broth dilution tests showed similar results to Kirby-Bauer disc diffusion test. The highest concentration tested was 400 μg mL$^{-1}$. The lipid analogues (**11**) and (**12**) exhibited nanomolar potency, with the susceptibility values similar to that of tunicamycins in inhibiting *B. subtilis* and *cereus* growth (**Table 3.2**, **Table 3.3**, **Table 3.4**). Although there seemed to be a ten-fold decrease in potency compared to tunicamycins, the bioactivity arising from each tunicamycin homologues must be considered as noted in **Chapter 1**. Nonetheless, the lipid analogues with nanomolar potency are worthy of further pursuit.

Interestingly, the lipid analogues were not as effective at inhibiting the growth of *S. aureus* as tunicamycins. Conversely, tunicamycins were not as effective at inhibiting the growth of *P. aeruginosa* and *E. coli*, but the lipid analogues appeared to have some effect on *P. aeruginosa*. This inhibitory activity was similarly observed before from the Kirby-Bauer disc diffusion test (**Fig. 3.3**). Based on our results, it appeared that the lipid analogues may be more effective at targeting Gram-negative bacteria compared to tunicamycins. It may be that the fully saturated dual lipid characteristic of the lipid analogues plays a role in membrane interaction or protein interaction that enhances the antibacterial activity against *P. aeruginosa*. However, this would need further investigation to understand the localisation of the tunicamycins. As suggested in **Chapter 1**, creating a fluorescently-labelled tunicamycin as a chemical probe could provide some insights into the localisation of tunicamycins in bacterial and mammalian cells.

It may be possible that the tunicamycins and lipid analogues target MraY and TagO/TarO in Gram-positive bacteria such as the *Bacillus* species. This may explain the sensitivity of *B. subtilis* and *cereus* towards tunicamycins and the lipid analogues. The differences in *S. aureus* and *M. luteus* cell wall may explain their resistance to tunicamycins and the lipid analogues, but other resistance mechanisms are as equally plausible. In Gram-negative bacteria, such as the ones were tested, *P. aeruginosa* and *E. coli*, tunicamycins and the lipid analogues may have not only targeted MraY but also WecA. However, these speculations would require further investigation and *in vitro* studies.

Our findings have opened up the possibility that a wider range of tunicamycin lipid analogues may enhance the antibacterial properties of tunicamycins to target Gram-negative bacteria by facilitating the interaction with the bacterial cell wall, MraY translocase, or MraY-related enzymes present in Gram-negative bacteria such as WecA (**Chapter 1**). Moreover, there is also the potential to design the lipid analogues to target specific microbes where phospholipids and lipopolysaccharides play a particular role in the ineffectiveness or efficacy of antibiotics, such as in most Gram-negative bacteria.[42]

### 3.2.3 Tunicamycin Lipid Analogues are Active Against *M. tuberculosis*

In order to find out if the lipid analogues (**10-16**) were potential WecA inhibitors, we tested the tunicamycin core scaffolds and lipid analogues against *Mycobacterium tuberculosis*. *M. tuberculosis* is the causative agent of tuberculosis (TB), a pandemic infectious disease causing 1.3 million deaths per annum worldwide.[43] As discussed in **Chapter 1**, WecA is responsible for the sugar transfer from UDP-GlcNAc to the lipid carrier $C_{50}$-P in the mycolylarabinogalactan biosynthesis pathway present in *M. tuberculosis*. Tunicamycins are reported to inhibit WecA in *M. tuberculosis* but cytotoxicity has hindered their clinical potential.[44] Currently no clinical drug targets WecA, thus designing non-cytotoxic tunicamycin analogues that can target WecA as anti-*M. tuberculosis* drugs would be extremely valuable.

The core scaffolds and the lipid analogues were tested against pathogenic *M. tuberculosis* strain *M. tuberculosis* H37Rv.[i] Pleasingly, all the lipid analogues were active against *M. tuberculosis*. In particular, the nine carbon chain length lipid analogue (**12**) has

[i] The MIC determination for the tunicamycin core scaffolds and the lipid analogues against *M. tuberculosis* H37Rv was carried out by Helena Boshoff from National Institute of Health, Maryland, USA.

similar potency as current first line drugs such as Isoniazid and are five-fold more potent than the tunicamycins with MIC values of 0.04 μg $mL^{-1}$ in GAST/Fe growth medium and 0.35 μg $mL^{-1}$ in 7H9 growth medium (**Table 3.5**). The most potent clinically used TB drugs are Isoniazid (MIC 0.02-0.25 μg $mL^{-1}$) and Rifampicin (MIC 0.015-0.4 μg $mL^{-1}$). [45-47]

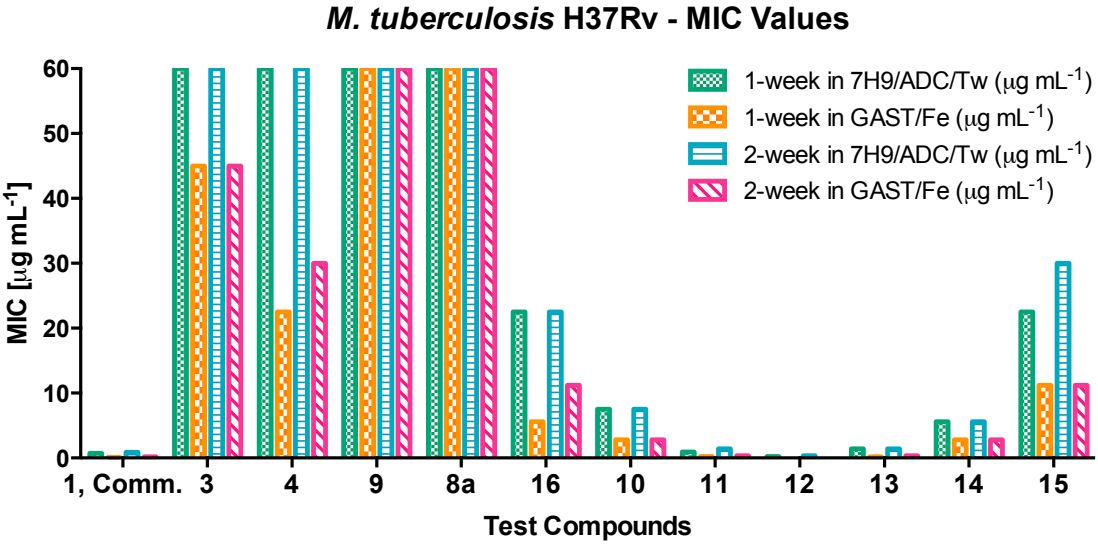


**Figure 3.7 | MIC values for *M. tuberculosis* H37Rv from one- and two-week treatment with tunicamycin core scaffolds and lipid analogues.** The graph shows the titration of the antibacterial activity due to the difference by one carbon in the lipid analogues.

**Table 3.5 | MIC values for *M. tuberculosis* H37Rv from one- and two-week treatment with tunicamycin core scaffolds and lipid analogues.**

| Compound | MIC values (μg mL$^{-1}$) | | | |
|---|---|---|---|---|
| | One-week | | Two-week | |
| | 7H9/ADC/Tw | GAST/Fe | 7H9/ADC/Tw | GAST/Fe |
| MilliQ Water | No inhibition | No inhibition | No inhibition | No inhibition |
| Methanol | No inhibition | No inhibition | No inhibition | No inhibition |
| **1, Comm.** | 0.70 | 0.12 | 0.90 | 0.18 |
| **3** | >60 | 45.00 | >60 | 45.00 |
| **4** | ≥60 | 22.50 | >60 | 30.00 |
| **8a** | >60 | >60 | >60 | >60 |
| **9** | >60 | >60 | >60 | >60 |
| **10** | 7.50 | 2.80 | 7.50 | 2.80 |
| **11** | 0.94 | 0.23 | 1.40 | 0.35 |
| **12** | 0.23 | 0.029 | 0.35 | 0.040 |
| **13** | 1.40 | 0.18 | 1.40 | 0.35 |
| **14** | 5.60 | 2.80 | 5.60 | 2.80 |
| **15** | 22.50 | 11.20 | 30.00 | 11.20 |
| **16** | 22.50 | 5.60 | 22.50 | 11.20 |

The potent anti-*M. tuberculosis* activity of the lipid analogues prompted us to investigate the stability of the lipid analogues and their efficacy in killing *M. tuberculosis* in infected macrophage. We chose the four most potent lipid analogues for investigation, based on the MIC values (**Table 3.5**). Satisfyingly, our results showed high stability and effective killing of *M. tuberculosis* in infected macrophages (**Fig. 3.8**).[ii]

[ii] The microsomal stability test and the macrophage studies were carried out by Andaleeb Sajid from National Institute of Health, Maryland, USA.

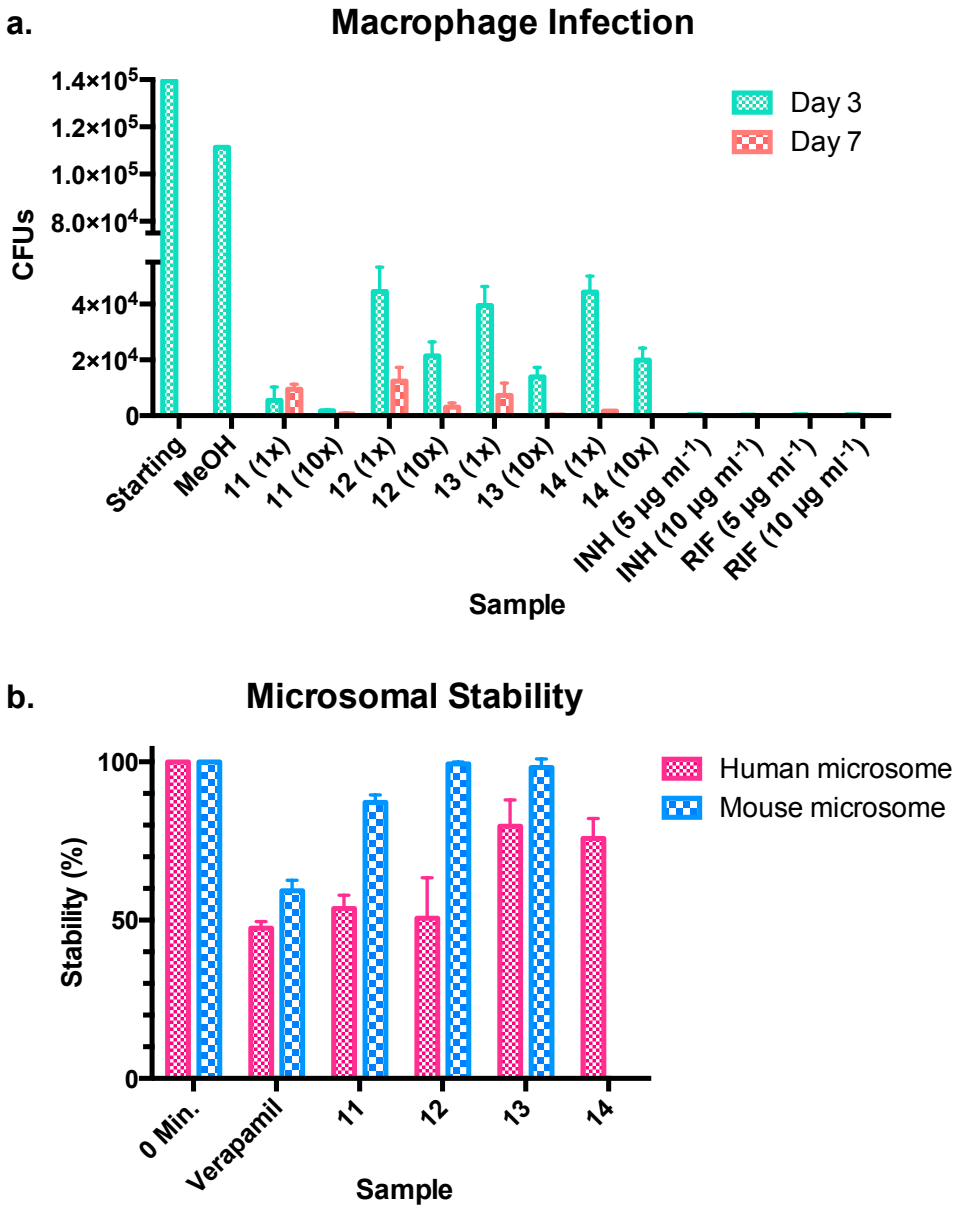


**Figure 3.8 | Macrophage infection assay and microsomal stability test. (a)** Macrophage infection assay. The 1x is the MIC values of the lipid analogues, and 10x is the 10x of the MIC values. INH and RIF are Isoniazid (MIC 0.02-0.25 μg $mL^{-1}$) and Rifampicin (MIC 0.015-0.4 μg $mL^{-1}$), respectively.[45-47] The day in the macrophage graph represent the number of days the macrophage was infected and treated with the antibiotics. The CFUs were counted after 25 days from culture grown from lysed cells.

### 3.2.4 Cytotoxicity Test of the Tunicamycin Core Scaffolds and Lipid Analogues

The cytotoxicity of tunicamycins to eukaryotic cells has been the primary reason for its unsuitability for clinical use as an antibiotic (**Chapter 1**). This and the following

subsections describe the evaluations of the tunicamycins core scaffolds and the lipid analogues on eukaryotic cell proliferation, cell cycle, and *N*-linked glycosylation.

In order to probe the effect of the aliphatic chain on cytotoxicity, we evaluated the effect of the core scaffolds and our lipid analogues (**Fig. 3.1**) on HepG2, HEK293 and Raji cells in MTS proliferation assays (**Fig. 3.9**) to obtain the dose-response curve, and we used microscopy to observe any morphological changes, a typical effect of tunicamycins treatment.[48-51]

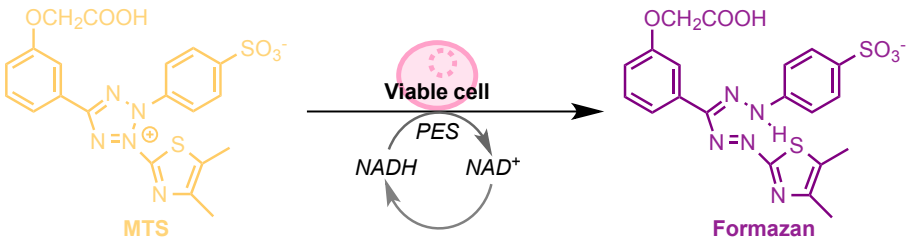


**Figure 3.9 | The MTS cell proliferation assay.** CellTiter 96® AQueous One Solution Cell Proliferation Assay. A colorimetric method by the live cells ability to reduce MTS (tetrazolium compound, 3-(4,5-dimethylthiazol-2-yl)-5-(3-carboxymethoxyphenyl)-2-(4-sulfophenyl)-2H-tetrazolium) with PES (phenazine ethosulfate) to formazan (absorbance maximum at 490 nm). The solution changes from yellow to dark purple depending on the cell viability. This bioreduction conversion is presumably done by NADPH or NADH in metabolically active cells.

An initial tunicamycin cytotoxicity test using HepG2 cells was carried out to determine the optimum conditions for use with the analogues. We found that 24 h incubation with tunicamycins provided a good indication of both cytotoxicity and morphological changes on the cells, compared with longer time frames, where cell stress responses may distorted the dose-response curve for the proliferation assay (**Fig. 3.10**). The proliferation assay was carefully done to avoid any methanol contamination. It is reported in the literature that HepG2 cells are sensitive to methanol.[52] As previously

mentioned, the lipid analogues were prepared as a stock in methanol solvent. The methanol solvent was evaporated off from the growth medium before any cells were added. Methanol positive and negative control were prepared to avoid false-negatives.

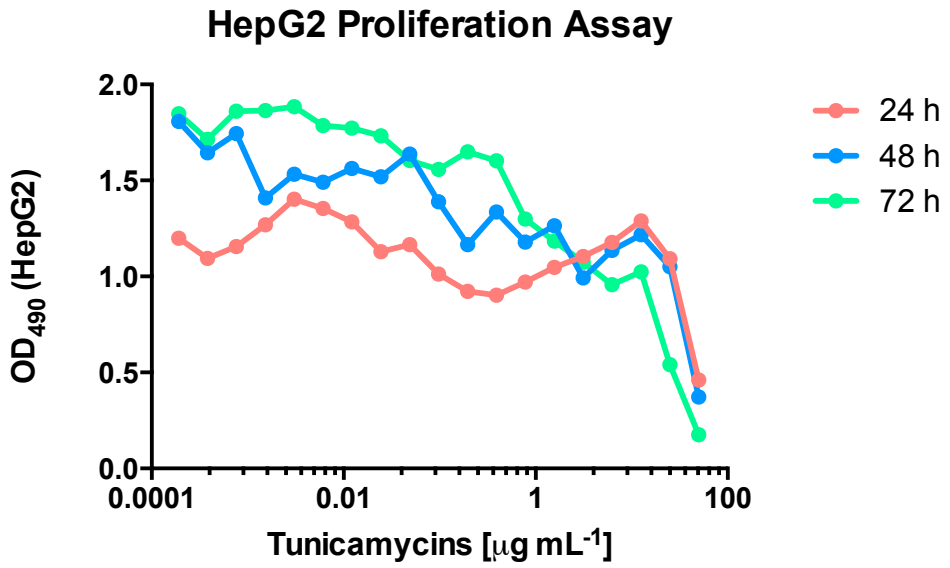


**Figure 3.10 | The tunicamycins treated HepG2 proliferation assay over 72 h.** HepG2 cells were treated up to 50 μg $mL^{-1}$ of tunicamycins over 18 dilutions. The culture was seeded with about 1e5 cells per well and then treated with tunicamycins. The cells viability was determined by MTS proliferation assay.

Based on our results (**Fig. 3.11**, **Table 3.6**), we found that tunicamycins have an $LD_{50}$ around 45 ±5 μg $mL^{-1}$, 50 ±31 μg $mL^{-1}$, and 27 ±11 μg $mL^{-1}$ for HepG2, HEK293 and Raji cells, respectively. Interestingly, the core scaffolds did not appear to have any cytotoxic effect on HepG2 and HEK293 cells, but mild toxicity was observed for Raji cells. The aliphatic analogues at 400 μg $mL^{-1}$ also induced mild cytotoxicity in Raji cells, but appeared to be chain length dependent.

Furthermore, we were delighted to find that there were at least 75% viable cells with no morphological changes after 24 hours for HEK293 cells that were treated with a

high dosage (400 μg $mL^{-1}$) of the lipid analogues (**11**) and (**12**). The results from **11** and **12** could presume to reflect similar outcome to the other lipid analogues if there is a small difference in activity, but further investigation would be needed to determine the values for other lipid analogues. This was not the case for the tunicamycins treated HEK293 cells. These cells appeared swollen and apoptotic above 50 μg $mL^{-1}$ of tunicamycins. This further suggested that the lipid analogues do not have the same effect on mammalian cell as tunicamycins, and may not have any affect on the cell cycle. Thus, this is a good indication that the lipid analogues *in vivo* may not have serious consequences in the mammalian system over a short period of time until the drugs are excreted.

The modification of the GlcNAc moiety to reduce structural similarity with the substrate-product transition state analogue of GPT can also reduce tunicamycins cytotoxic effect as observed from the aliphatic analogues. Together, our results show for the first time that tunicamycins without a aliphatic chain dramatically lose their cytotoxic effect in HepG2 and HEK293 cells, and the lipid addition to the GlcNAc moiety can separate mammalian cytotoxicity from antibacterial activity, leading to a greater range in dose efficacy and offering promising antimicrobial drug candidates.

Moreover, the aliphatic chain may play more important roles than just facilitating the transfer through the membrane, as speculated in the bacterial system. It may also be involved in the interaction with GPT. This is plausible since recent structural insight into the MraY catalytic site was recently revealed by Chung *et al.* from the crystal structure of MraY from *Aquifex aeolicus*, showing the catalytic site with $Mg^{2+}$ and possibly the hydrophobic groove for undecaprenol phosphate.[53]

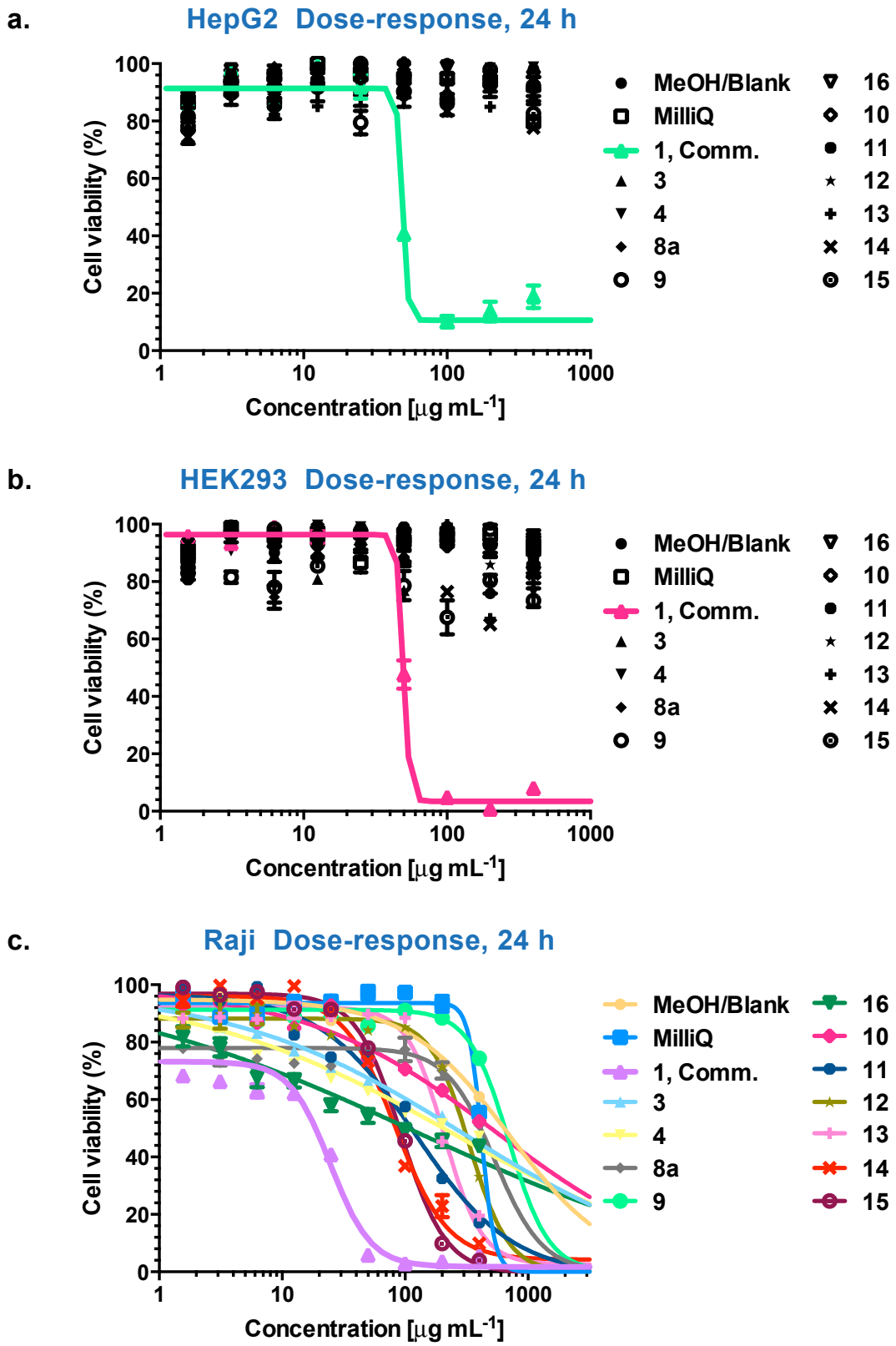


**Figure 3.11 | The dose-response from the MTS proliferation assay of HepG2, HEK293, and Raji cells treated with the tunicamycin core scaffolds and lipid analogues.** The dose-response curves were generated by Prism 6.0 software by plotting percent growth (normalised $OD_{490}$ values) vs. logarithmic scale of the concentrations. The data shown are mean ±SEM errors of three

independent experiments. **(a)** HepG2. **(b)** HEK293. **(c)** Raji. The $LD_{50}$ values are summarised in **Table 3.6**.

**Table 3.6 | $LD_{50}$ values for the tunicamycin core scaffolds and the lipid analogues.**

| Compound | $LD_{50}$ values (μg $mL^{-1}$), Avg. ± Std. Dev. | | |
|---|---|---|---|
| | HEK293 | HepG2 | Raji |
| MilliQ Water | N/A | N/A | N/A |
| Methanol | N/A | N/A | N/A |
| **1** | 51.25 ±31.27 | 44.74 ±4.73 | 26.82 ±11.46 |
| **2** | N/A | N/A | 303.80 ±9.83 |
| **3** | N/A | N/A | 212.30 ±51.48 |
| **8a** | N/A | N/A | 608.9 ±394.9 |
| **9** | N/A | N/A | 698.3 |
| **10** | N/A | N/A | 431.10 ±241.81 |
| **11** | N/A | N/A | 211.05 ±125.94 |
| **12** | N/A | N/A | 355.57 ±194.57 |
| **13** | N/A | N/A | 196.17 ±47.61 |
| **14** | N/A | N/A | 103.65 ±34.34 |
| **15** | N/A | N/A | 81.29 ±30.20 |
| **16** | N/A | N/A | 177.75 ±75.17 |

N/A = not available. No or low cytotoxicity observed at highest concentration tested (400 μg $mL^{-1}$), thus a reliable dose-response curve could not be generated from the experimental data.

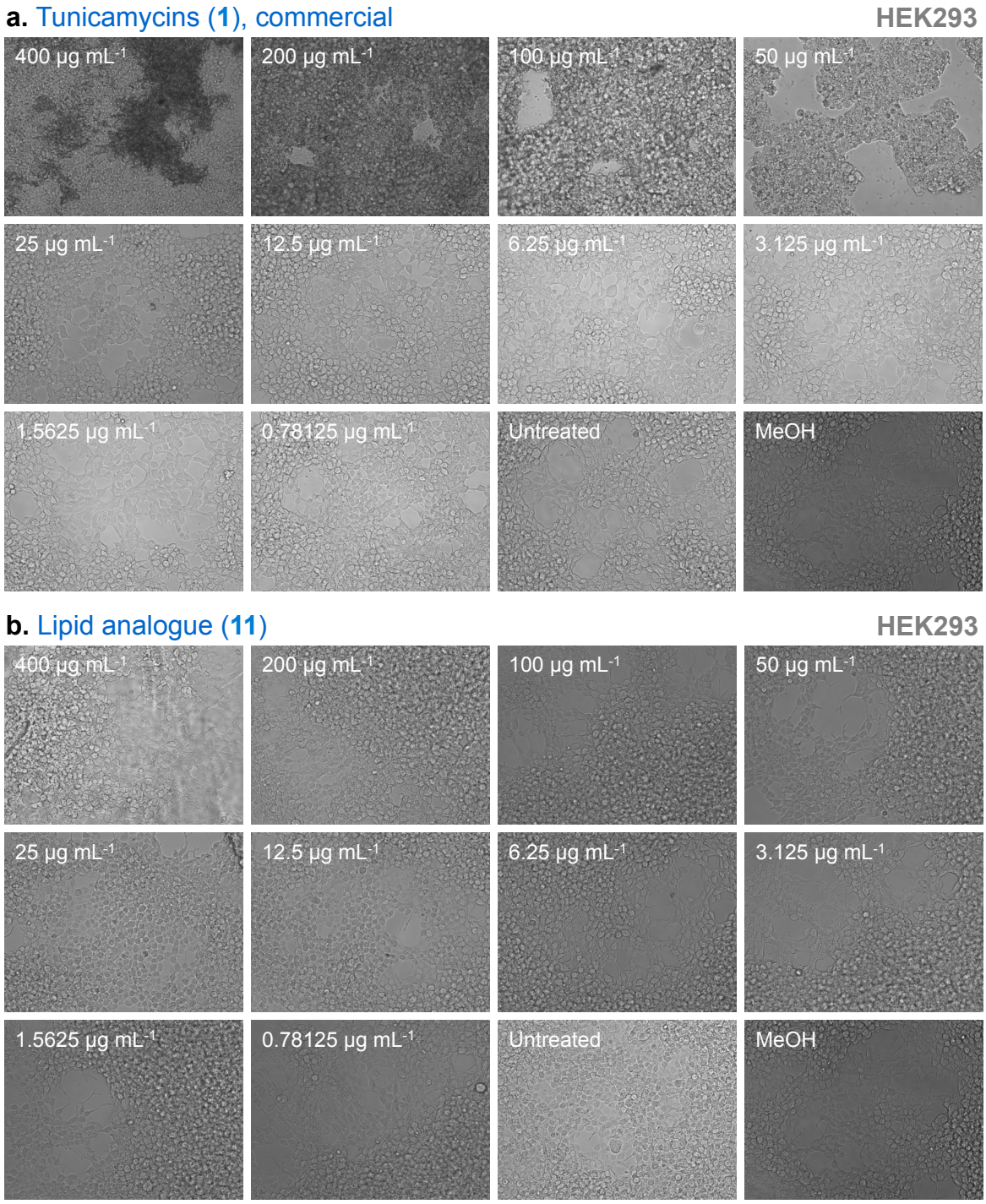


**Figure 3.12 | Tunicamycins (1) and the lipid analogues (11 and 12) treated HEK293 cell microscope images after 24 h.** The images were obtained using FLoid® Cell Imaging Station (Life Technologies). The MeOH control culture was prepared to exclude any false-negatives. This was prepared by adding the same volume of methanol as volume of test compounds used to the culture medium and left to evaporate before adding the cells. **(a)** tunicamycins (**1**) treated HEK293 cells. Apoptotic cells were observed at 400 µg $mL^{-1}$. The change in cell morphology was apparent with tunicamycins (**1**) above 25 µg $mL^{-1}$. **(b)** No apparent changes to the cell morphology of HEK293 cells treated with **11**. **(c)** No apparent changes to the cell morphology of HEK293 cells treated with **12**.

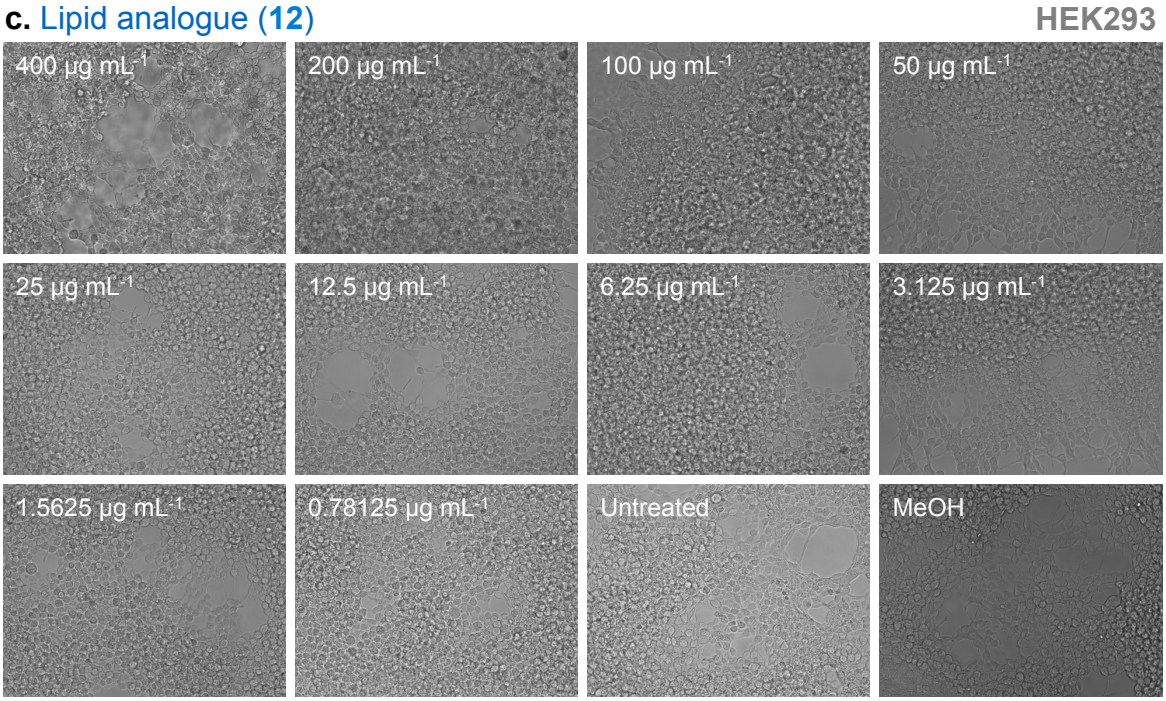


**Figure 3.12 (continued) | Tunicamycins (1) and the lipid analogues (11 and 12) treated HEK293 cell microscope images after 24 h.** The images were obtained using FLoid® Cell Imaging Station (Life Technologies). The MeOH control culture was prepared to exclude any false-negatives. This was prepared by adding the same volume of methanol as volume of test compounds used to the culture medium and left to evaporate before adding the cells. **(a)** tunicamycins (**1**) treated HEK293 cells. Apoptotic cells were observed at 400 µg $mL^{-1}$. The change in cell morphology was apparent with tunicamycins (**1**) above 25 µg $mL^{-1}$. **(b)** No apparent changes to the cell morphology of HEK293 cells treated with **11**. **(c)** No apparent changes to the cell morphology of HEK293 cells treated with **12**.

### 3.2.5 Cell Cycle Arrest Test

The results from our antibacterial susceptibility test, cytotoxicity test, and the anti-*M. tuberculosis* studies all suggested that the lipid analogues are promising antibacterial drug candidates. However, thus far, our mammalian cell studies have been limited to a short period time frame of 24 h. Additionally, although the lipid analogues showed no cytotoxicity after 24 h of antibiotic treatment, we also needed to consider the effect of the unfolded protein response induced by tunicamycins (see **Chapter 1**) that consequently affects the eukaryotic cell cycle and viability.[51,54-62] Thus, we investigated the effect of the

lipid analogues on the cell cycle by quantifying the cell phases through cell cycle arrest test. We chose to test only lipid analogues (**11**) and (**12**) because they have the most potent antimicrobial activity of the lipid analogues and displayed no cytotoxicity up to 400 μg $mL^{-1}$. The results from **11** and **12** were presumed to reflect similar outcome to the other lipid analogues unless a particular trend was observed. The cell cycle arrest test was carried out using propidium iodide (PI) staining and FACS analysis. The PI stain allows the differentiation of fixed cells in the $G_0/G_1$, S, and $G_2/M$ cell phases due to the differences in DNA content in each, thus allowing FACS to measure the quantity of the DNA in the cell, which reflects the cell cycle (**Fig. 3.13**). FACS is also a very useful method to quantitatively evaluate cell death and changes in cell morphology.

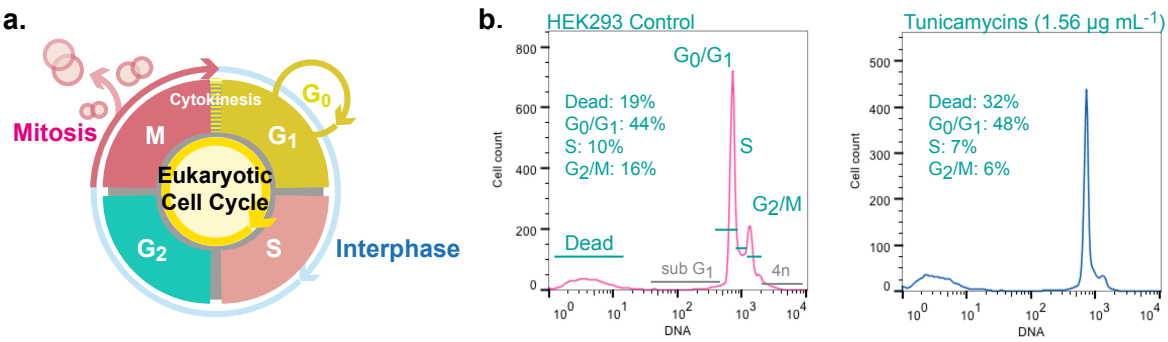


**Figure 3.13 | The eukaryotic cell cycle[63-65] and FACS histogram. (a)** The eukaryotic cell cycle. **(b)** Propidium iodide FACS histogram of DNA content of HEK293 cell phases of untreated and tunicamycins-treated after 24 h.

First, we carried out an initial cell cycle analysis of a 24 h incubation period with HEK293 cells in the presence of tunicamycins, and the two most potent lipid analogues (**11**) and (**12**), based on the MIC values (**Table 3.5**). We tested up to a concentration of 400 μg $mL^{-1}$ (**Fig. 3.14**). As expected from our proliferation studies, the appearance of dead and apoptotic cells dramatically increased in the presence of tunicamycins concentration greater than 20 μg $mL^{-1}$. The number of cells in the presence of the lipid analogues did not

appear to be drastically different in the cell phases compared to the control growth (points on the Y-axis). The cells in $G_0$/ $G_1$ phase in the presence of tunicamycins appeared to be higher than the control. This has also been observed in the literature.[54,55,59,61] Since tunicamycins inhibit and disrupt the *N*-linked glycosylation pathway in the ER, it would be reasonable to observe a higher percentage of the cells arrested in the $G_0/G_1$ phase in their checkpoint undergoing UPR, which would prevent the cells from proceeding into the synthesis phase, S phase, until homeostasis was restored.[55]

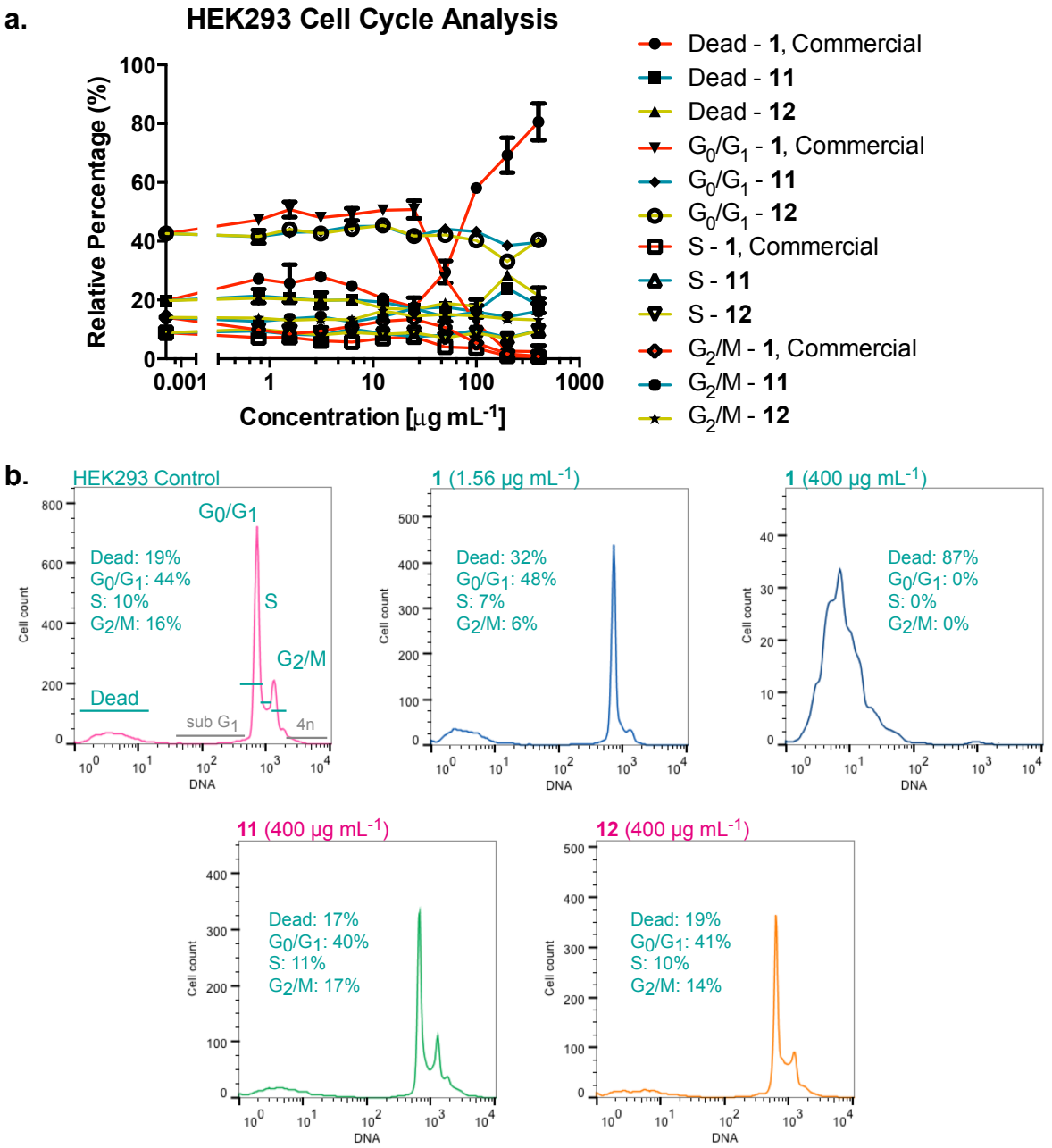


**Figure 3.14 | 24 h cell cycle analysis of HEK293 cell treated with tunicamycins (1) and lipid analogues (11) and (12). (a)** The percentage from propidium iodide FACS histogram of DNA content of HEK293 cell cell cycles are shown. **1**, **11**, and **12** were evaluated up to a concentration of 400 µg mL$^{-1}$ The 1e$^{-6}$ x-value on the Y-axis represents the control growth. An increase of cells in the $G_0/G_1$ phases was observed for tunicamycin treated cells, but not for **11** and **12** treated cells. Consequently, a decrease of cells in S phases was observed for tunicamycin treated cells. The **11** and **12** treated cells appeared normal compared to the control (Y-axis values). A sudden increase in dead cells occurs at about 50 µg mL$^{-1}$ of tunicamycins, which corresponded to about the reported $LD_{50}$ of tunicamycins for HEK293 cells (**Table 3.6**). **(b)** Propidium iodide FACS histogram of DNA content of HEK293 cell phases of control, **1**-, **11**-, and **12**-treated after 24 h.

Finally, when we carried out time-course cell cycle arrest studies, we quantified the cell cycles at 0, 24, 48, and 72 h in the presence of tunicamycins, the lipid analogues, and in other antibiotics standards such as actinomycin, vancomycin, and 5-fluorouracil (**Fig. 3.15**).[66] Our results showed that the cells treated with the lipid analogues (**11**) and (**12**) appeared to be similar to the control HEK293 cells. The concentrations used in the experiment were based on literature values where differences in cell phases can be observed that would not result in cell death over several days. Our results suggested that the lipid analogues may not affect the cell cycle compared to tunicamycins. This further supported our cytotoxicity studies suggesting that the lipid analogues do not have the same effect on mammalian cell as tunicamycins and may not have any affect on the cell cycle over 72 h. This is, again, a good indication that the lipid analogues *in vivo* may not have a detrimental effect on a mammalian system over a short period of time. Moreover, this could indicate that the lipid analogues do not inhibit GPT or the *N*-linked glycosylation pathway.

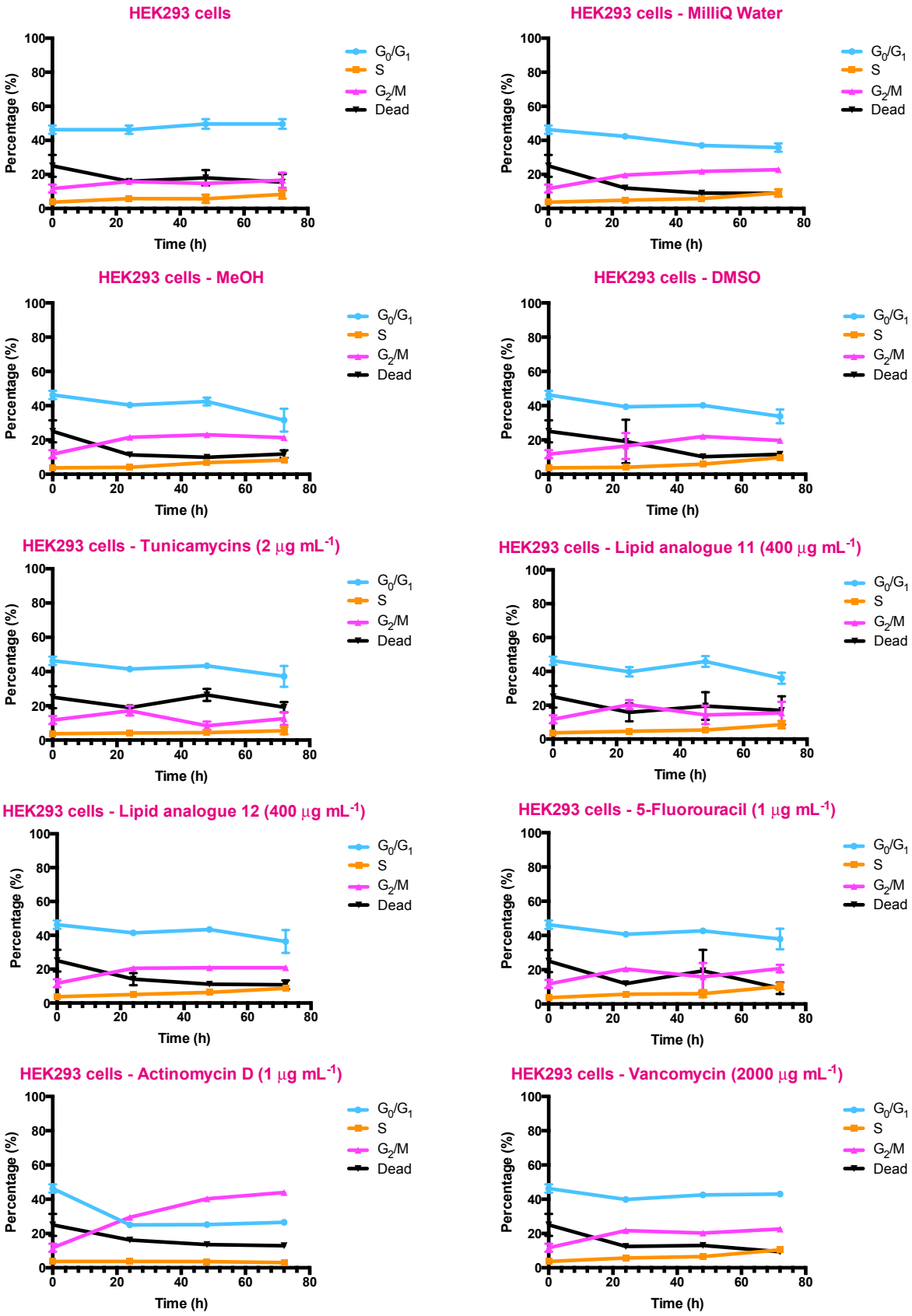


**Figure 3.15 | 24, 48, and 72 h cell cycle analyses of HEK293 cells.** HEK293 cells treated with tunicamycins, lipid analogues **11** and **12**, 5-fluoruracil, actinomycin D, and vancomycins. The

graphs show the cell cycle results based on the percentage of DNA content of HEK293 cells over time from propidium iodide FACS histogram.

### 3.2.6 *N*-linked Glycosylation test: IgG1Fc expression

We showed previously that the lipid analogues (**11**) and (**12**) did not appear to affect the cell cycle compared to tunicamycins. Thus, we also wanted to investigate if the lipid analogues had any effect on the *N*-linked glycosylation pathway. As discussed in **Chapter 1**, tunicamycins inhibit the *N*-linked glycosylation pathway by inhibiting GPT. We followed a reported protocol that used a HEK293T:pHLsec/IgG1Fc-$His_6$ expression system to study the *N*-glycan on IgG1Fc-$His_6$ (~37 kDa).[67] IgG1Fc has only one *N*-linked glycosylation site, thus it can be easily observed by SDS-PAGE and Western blot analyses if the expressed IgG1Fc-$His_6$ is not glycosylated. The maximum non-toxic concentration of tunicamycins at 10 μg $mL^{-1}$ was used, based on the literature reported range between 0.5-10 μg $mL^{-1}$ to show *N*-glycosylation inhibition, where higher concentration of tunicamycins would simply result in cell apoptosis.[68] Notably, based on our findings (**Fig. 3.16**), the lipid analogues did not appear to inhibit *N*-linked glycosylation of IgG1Fc in HEK293T cells in comparison to tunicamycins. Interestingly, serial dilution of tunicamycins showed a gradual transition from normal glycosylated IgG1Fc to non-glycosylated IgG1Fc, and then to no expression of IgG1Fc. This shows that tunicamycins not only inhibited the *N*-linked glycosylation process but also protein synthesis, or that the non-glycosylation of protein led to the halt in protein synthesis.

In our SDS-PAGE and Western blot analyses (**Fig. 3.16**), the IgG1Fc-$His_6$ appeared glycosylated. We wanted to investigate if the glycosylated IgG1Fc-$His_6$ expressed by the HEK293T cells that were treated with the lipid analogues (**11**) or (**12**) had the same glycan

attached as the non-treated HEK293T cells that expressed IgG1Fc-$His_6$. In order to characterise the glycan, we performed in-gel PNGase F digest.[67] In the digest, the PNGase F cleaves the *N*-linked glycan, deposits the glycan in the aqueous solution, from which the glycan can be extracted. Unfortunately, the glycan solution was not able to crystallise on the matrix plate for MALDI analysis despite several attempts to clean the sample *via* Vivaspin (3K MWCO and 5K MWCO) and C-18 RP-column to remove any impurities. Glycerol or SDS gel contaminants may be the cause of the problem. Nonetheless, the lipid analogues did not appear to inhibit the *N*-linked glycosylation pathway.

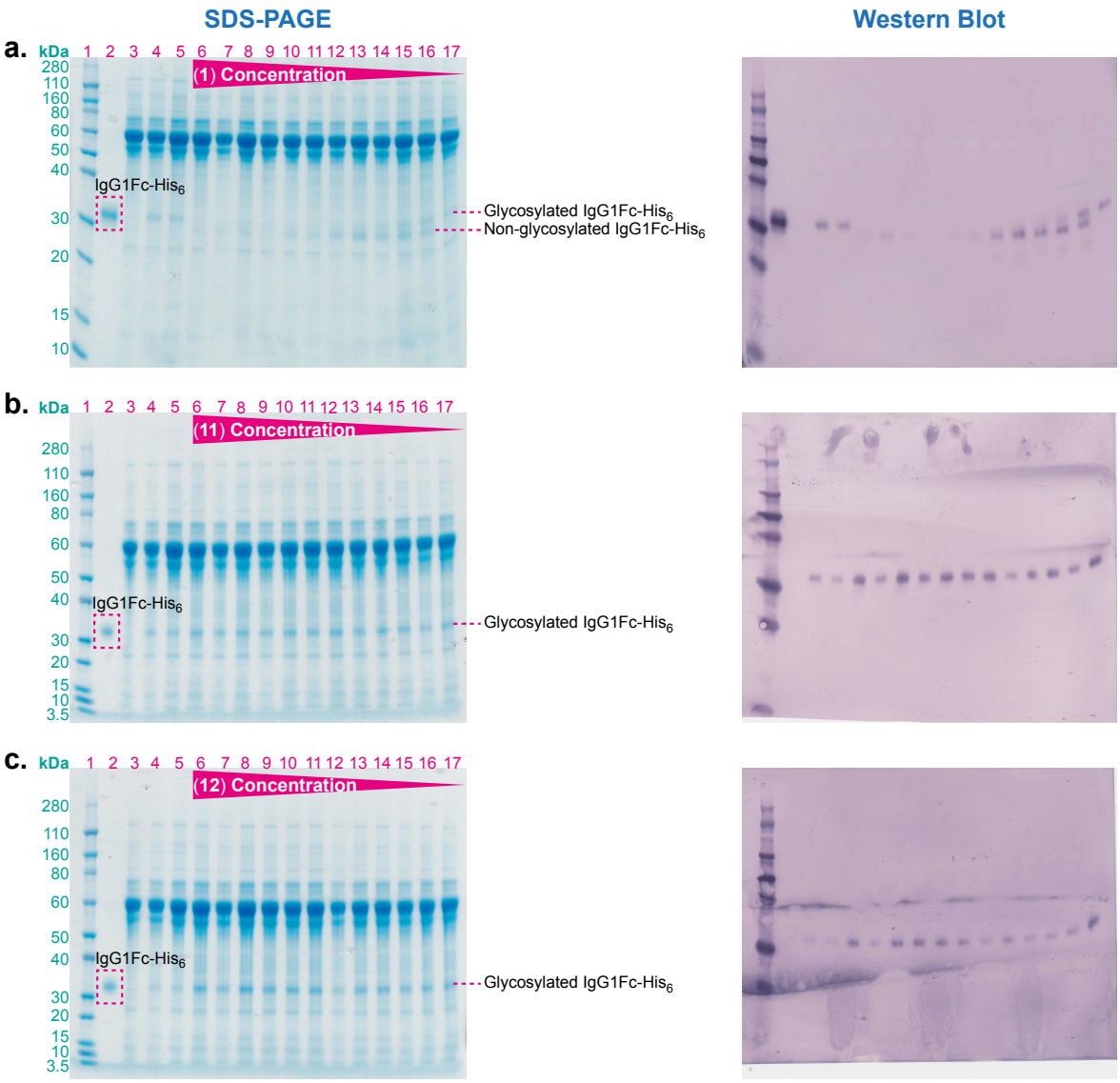


**Figure 3.16 | SDS-PAGE and Western blot analyses of IgG1Fc-His$_6$ expression.** Left: SDS-PAGE analysis. Right: Western blot analysis confirming the IgG1Fc-His$_6$. Lane 1: molecular ruler. Lane 2: IgG1Fc-His$_6$ standard[iii]. Lane 3: negative control. Lane 4: positive control. Lane 5: MeOH control. Lane 6-17: test compound concentration in two-fold dilutions from 10 μg mL$^{-1}$ down to 0.0049 μg mL$^{-1}$. **(a)** IgG1Fc-His$_6$ expression in presence of tunicamycins (**1**). **(b)** IgG1Fc-His$_6$ expression in presence of lipid analogue (**11**). **(c)** IgG1Fc-His$_6$ expression in presence of lipid analogue (**12**).

## 3.3 Conclusion and Outlook

Firstly, our results have shown the importance of the lipid chains for cytotoxicity activity in both eukaryotic and prokaryotic systems. For the first time, we have shown that

[iii] IgG1Fc-His$_6$ sample provided by Keisuke Yamamoto, University of Oxford.

in prokaryotic and eukaryotic systems, the inhibitory property for tunicamycins are abolished in absence of their lipid chain. Early studies succeeded in only showing longer chain homologues are generally more biologically active in prokaryotes, whereas shorter chain homologues are generally more active in eukaryotes.[1-7] Additionally, the tunicamycin lipid analogues were found to be potent antibacterial agents, revealing a titrated inhibitory effect that is dependent on their lipid chain length. This suggests that the use of tunicamycins as a mixture of their homologues should be carefully evaluated to minimise ambiguity. Furthermore, our results showed that from our library of lipid analogues, the cytotoxicity can be drastically reduced while maintaining nanomolar antibacterial potency by modifying the GlcNAc moiety of tunicamycin with the addition of a lipid chain that is between seven to twelve carbons in length. These revealed the importance and effect of the chain length and lipid modification on GlcNAc moiety of tunicamycin on the antibacterial activity and mammalian cytotoxicity. In essence, these results supported our hypothesis that by retaining the lipid character of the tunicamycin structure and modifying the GlcNAc moiety then the antimicrobial activity would be retained but the inhibitory action towards GPT would be abolished, thus eliminating tunicamycins toxicity towards mammalian cells (**Chapter 1**).

Moreover, our biological evaluations have highlighted the essential role for a lipid chain on tunicamycin. These add further evidence to the suggested hydrophobic interaction mechanisms of tunicamycins with either lipid membranes or target enzymes, as demonstrated in yeast protoplast through the interaction between tunicamycins and the cell membrane phospholipids.[3-5,12,38] This further shows the importance of retaining hydrophobic character in designing tunicamycin analogues. However, it remains to be seen

whether our lipid analogues will be effective against tunicamycin resistant strains.[4,12] While we have revealed the importance of the lipid chain on tunicamycin on antibacterial activity and modification of GlcNAc moiety on mammalian cytotoxicity, it is not known whether the analogues exhibited any interaction with MraY translocase or GPT, or induced any ER stress response. Future work could include real-time PCR, kinetic, inhibition, and crystallisation studies. Regardless, our scaffolds could assist with the design of the next generation of tunicamycin analogues for inhibition studies and resistance mechanism in prokaryotes and eukaryotes (**Chapter 1**).

Secondly, structure-based tunicamycin analogues can be now designed using MraY structural data that may result in more potent inhibitors and be used to study other enzymes in the PNPT superfamily.[53] In a broader sense, our scaffolds and lipid analogues may be tailored for crystallisation studies, binding studies, chemotherapeutic cancer drugs, or molecular probes to study the unfolded protein response, eukaryotic cell development, or bacterial membrane cellular growth during the division process, considering the known bioactivities tunicamycins exhibit.

Lastly, and most importantly, we have developed a set of tunicamycin lipid analogues that are as effective as tunicamycins as antibacterial agents but without the mammalian cytotoxicity effect. In comparison to tunicamycins, our lipid analogues have relative therapeutic index values up to several thousand folds more than tunicamycins (**Table 3.7**). Additionally, we have not only developed a set of promising antibacterial drug candidates but also a set of promising anti-*M. tb* drug candidates.

**Table 3.7 | The relative therapeutic index of the tunicamycins and the lipid analogues.**

| Minimal lethal dose (**MLD**), minimal inhibitory concentration (**MIC**), relative therapeutic index (**RTI***) | | | | | | | | | | |
|---|---|---|---|---|---|---|---|---|---|---|
| **Compound** | **MLD** | | 2 wk in 7H9/ ADC/Tw | | 2 wk in GAST/Fe | | **MIC** | | **MIC** | |
| | Hep G2 | HEK 293 | M. tuberculosis H37RV | **RTI** | M. tuberculosis H37RV | **RTI** | B. subtilis EC1524 | **RTI** | B. cereus NRRL11778 | **RTI** |
| (1) | 100 | 100 | 0.90 | 111 | 0.18 | 556 | 0.00 | 66667 | 0.20 | 513 |
| (10) | >400 | >400 | 7.50 | 107 | 2.80 | 286 | 6.25 | 128 | 100.00 | 8 |
| (11) | >400 | >400 | 1.40 | 571 | 0.35 | 2286 | 0.78 | 1026 | 6.25 | 128 |
| (12) | >400 | >400 | 0.35 | 2286 | 0.040 | 20000 | 0.024 | 33333 | 0.78 | 1026 |
| (13) | >400 | >400 | 1.40 | 571 | 0.35 | 2286 | 0.39 | 2051 | 0.39 | 2051 |
| (14) | >400 | >400 | 5.60 | 143 | 2.80 | 286 | 1.56 | 513 | 0.78 | 1026 |
| (15) | >400 | >400 | 30.00 | 27 | 11.20 | 71 | 100.00 | 8 | 50.00 | 16 |
| (16) | >400 | >400 | 22.50 | 36.0 | 11.20 | 71.0 | 6.25 | 128.0 | 100.00 | 8.0 |

*Relative therapeutic index (RTI). RTI is the ratio between the minimal lethal dose and the minimal inhibition concentration. The micro-broth dilution and the cytotoxicity tests were carried out by serial 2-fold dilutions. For no detectable cytotoxicity at 400 μg $mL^{-1}$ (>400), a minimal lethal dose of 800 μg $mL^{-1}$ was used to calculate the RTI.

## 3.4 References


1 Mahoney, W. C. & Duskin, D. Biological activities of the two major components of tunicamycin. *J. Biol. Chem.* **254**, 6572-6576 (1979).

2 Keenan, R. W., Hamill, R. L., Occolowitz, J. L. & Elbein, A. D. Biological Activities of Isolated Tunicamycin and Streptovirudin Fractions. *Biochemistry* **20**, 2968-2973 (1981).

3 Duksin, D. & Mahoney, W. C. Relationship of the Structure and Biological Activitoyf the Natural Homologues of Tunicamycin. *J. Biol. Chem.* **257**, 3105-3109 (1982).

4 Duskin, D., Seiberg, M. & Mahoney, W. C. Inhibition of Protein Glycosylation and Selective Cytotoxicity toward Virally Transformed Fibroblasts Caused by B3-Tunicamycin. *Eur. J. Biochem.* **129**, 77-80 (1982).

5 Seiberg, M. & Duksin, D. Selective Cytotoxicity of Purified Homologues of Tunicamycin on Transformed BALB/3T3 Fibroblasts. *Cancer Res.* **43**, 845-850 (1983).

6 Eren, R. & Duskin, D. Inhibition of the formation of lipid-linked intermediates in normal and transformed cells by a purified tunicamycin homologue. *Molecular and Cellular Biochemistry* **67**, 39-46 (1985).

7 Kamogashira, T., Takegata, S. & Sugiura, K. Isolation of Tunicamycin Produced by Bacillus cereus K-279. *Agric. Biol. Chem.* **52**, 859-861 (1988).

8 Xu, L., Appell, M., Kennedy, S., Momany, F. A. & Price, N. P. J. Conformational Analysis of Chirally Deuterated Tunicamycin as an Active Site Probe of UDP-N-Acetylhexosamine:Polyprenol-P N-Acetylhexosamne-1-P Translocases. *Biochemistry* **43**, 13248-13255 (2004).

9 Heifetz, A., Keenan, R. W. & Elbein, A. D. Mechanism of Action of Tunicamycin on UDP-GlcNAc:Dolichyl-Phosphate GlcNAc-1-Phosphate Transferase. *Biochemistry* **18**, 2186-2192 (1979).

10 Lehrman, M. A. Biosynthesis of N-acetylglucosamine-P-P-dolichol, the committed step of asparagine-linked oligosaccharide assembly. *Glycobiology* **1**, 553-562 (1991).

11 Price, N. P. & Momany, F. A. Modeling bacterial UDP-HexNAc: polyprenol-P HexNAc-1-P transferases. *Glycobiology* **15**, 29R-42R, doi:10.1093/glycob/cwi065 (2005).

12 Kuo, S. C. & Lampen, O. Tunicamycin Inhibition of [3H] Glucosamine Incorporation into Yeast Glycoprotein: Binding of Tunicamycin and Interaction with Phospholipids. *Archives of Biochemistry and Biophysics* **172**, 574-581 (1976).

13 Wiegand, I., Hilpert, K. & Hancock, R. E. W. Agar and broth dilution methods to determine the minimal inhibitory concentration (MIC) of antimicrobial substances. *Nature Protocols* **3**, 163-175 (2008).

14 Wyszynski, F. J., Hesketh, A. R., Bibb, M. J. & Davis, B. G. Dissecting tunicamycin biosynthesis by genome mining: cloning and heterologous expression of a minimal gene cluster. *Chem. Sci.* **1**, 581-589 (2010).

15 Wyszyński, F. J. *Dissecting tunicamycin biosynthesis: A potent carbohydrate processing enzyme inhibitor* D.Phil. thesis, University of Oxford, (2010).

16 Cavalieri, S. J. *et al. Manual of Antimicrobial Susceptibility Testing*. (American Society for Microbiology, 2005).

17 Kotiranta, A., Lounatmaa, K. & Haapasalo, M. Epidemiology and pathogenesis of Bacillus cereus infections. *Microbes and Infection* **2**, 189-198 (2000).

18 Bottone, E. J. Bacillus cereus, a Volatile Human Pathogen. *Clin. Microbiol. Rev.* **23**, 382-398 (2010).

19 Liu, G. Y. Molecular Pathogenesis of Staphylococcus aureus Infection. *Pediatr. Res.* **65**, 71R-77R (2009).

20 Plata, K., Rosato, A. E. & Węgrzyn, G. Staphylococcus aureus as an infectious agent: overview of biochemistry and molecular genetics of its pathogenicity. *Acta Biochimica Polonica* **56**, 597-612 (2009).

21 Miller, L. S. & Cho, J. S. Immunity against Staphylococcus aureus cutaneous infections. *Nature Reviews Immunology* **11**, 505-518 (2011).

22 Lister, P. D., Wolter, D. J. & Hanson, N. D. Antibacterial-Resistant Pseudomonas aeruginosa: Clinical Impact and Complex Regulation of Chromosomally Encoded Resistance Mechanisms. *Clin. Microbiol. Rev.* **22**, 582-610 (2009).

23 Hauser, A. R. & Ozer, E. A. Pseudomonas aeruginosa. *Nature Reviews Microbiology* (2011).

24 Gellatly, S. L. & Hancock, R. E. W. Pseudomonas aeruginosa: new insights into pathogenesis and host defenses. *Pathogens and Disease* **67**, 159-173 (2013).

25 Nataro, J. P. & Kaper, J. B. Diarrheagenic Escherichia coli. *Clin. Microbiol. Rev.* **11**, 142-201 (1998).

26 Kaper, J. B., Nataro, J. P. & Mobley, H. L. T. Pathogenic Escherichia Coli. *Nature Reviews Microbiology* **2**, 123-140 (2004).

27 Harrington, S. M., Dudley, E. G. & Nataro, J. P. Pathogenesis of enteroaggregative Escherichia coli infection. *FEMS Microbiol. Lett.* **254**, 12-18 (2006).

28 Walsh, C. Where Will New Antibiotics Come From? *Nature Reviews Microbiology* **1**, 65-70 (2003).

29 Antibiotics Resistance Threats in the United States. (Centers for Disease Control and Prevention, 2013).

30 Reardon, S. Antibiotic Resistance Sweeping Developing World. *Nature* **509**, 141-142 (2014).

31 Bauer, A. W., Perry, D. M. & Kirby, W. M. M. Single disc antibiotic sensitivity testing of Staphylococci. *A.M.A. Arch. Intern. Med.* **104**, 208-216 (1959).

32 Bauer, A. W., Kirby, W. M. M., Sherris, J. C. & Turck., M. Antibiotic susceptibility testing by a standardized single disk method. *Am. J. Clin. Pathol.* **36**, 493-496 (1966).

33 Institute, C. a. L. S. *Methods for Dilution Antimicrobial Susceptibility Tests for Bacteria That Grow Aerobically; Approved Standard—Ninth Edition*. Vol. 32 (Clinical and Laboratory Standards Institute, 2012).

34 Institute, C. a. L. S. *Performance Standards for Antimicrobial Disk Susceptibility Tests; Approved Standard—Eleventh Edition*. Vol. 32 (Clinical and Laboratory Standards Institute, 2012).

35 Finn, R. K. Theory of Agar Diffusion Methods for Bioassay. *Analytical Chemistry* **31**, 975-977 (1959).

36 Jorgensen, J. H. & Ferraro, M. J. Antimicrobial Susceptibility Testing: A Review of General Principles and Contemporary Practices. *Medical Microbiology* **49**, 1749-1755 (2009).

37 Andrews, J. M. Determination of minimum inhibitory concentrations. *J. Antimicrob. Chemother.* **48**, S5-16 (2001).

38 Tkacz, J. S. & Lampen, J. O. Tunicamycin Inhibition of Polyisoprenyl N-Acetylglucosaminyl Pyrophosphate Formation in Calf-Liver Microsomes. *Biochem. Biophys. Res. Commun.* **65**, 248-257 (1975).

39 Auger, G., Heijenoort, J. v., Mengin-Lecreulx, D. & Blanot, D. A MurG assay which utilises a synthetic analogue of lipid I. *FEBS Microbiology Letters* **219**, 115-119 (2003).

40 Kahne, S. W., Men, H., Park, P. & Ge, M. Substrate analogs for MurG, methods of making same and assays using same. US6703213B2 (2004).

41 Stachyra, T. *et al.* Fluorescence Detection-Based Functional Assay for High-Throughput Screening for MraY. *Antimicrob. Agents Chemother.* **48**, 897-902 (2004).

42 Delcour, A. H. Outer membrane permeability and antibiotic resistance. *Biochimica et Biophysica Acta* **1794**, 808-816 (2009).

43 Global Tuberculosis Report. (World Health Organization, 2013).

44 Ishizaki, Y. *et al.* Inhibition of the First Step in Synthesis of the Mycobacterial Cell Wall Core, Catalyzed by the GlcNAc-1-phosphate Transferase WecA, by the Novel Caprazamycin Derivative CPZEN-45. *J. Biol. Chem.* **288**, 30309-30319 (2013).

45 Richard J. Wallace, J., Nash, D. R., Steele, L. C. & Steingrube, V. Susceptibility Testing of Slowly Growing Mycobacteria by a Microdilution MIC method with 7H9 Broth. *Journal of Clinical Microbiology* **24**, 976-981 (1986).

46 Rastogi, N., Labrousse, V. & Goh, K. S. In Vitro Activities of Fourteen Antimicrobial Agents Against Drug Susceptible and Resistant Clinical Isolates of Mycobacterium tuberculosis and Comparative Intracellular Activities Against the Virulent H37Rv stain in Human Macrophages. *Current Microbiology* **33**, 167-175 (1996).

47 Banfi, E., Scialino, G. & Monti-Bragadin, C. Development of a microdilution method to evaluate Mycobacterium tuberculosis drug susceptibility. *J. Antimicrob. Chemother.* **52**, 796-800 (2003).

48 Takatsuki, A., Shimizu, K.-I. & Tamura, G. Effect of Tunicamycin on Microorganisms: Morphological Changes and Degradation of RNA and DNA Induced by Tunicamycin. *The Journal of Antibiotics* **25**, 75-85 (1972).

49 Kohno, K., Hiragun, A., Mitsui, H., Takatsuki, A. & Tamura, G. Effect of Tunicamycin on Cell Growth and Morphology of Nontransformed and Transformed Cell Lines. *Agric. Biol. Chem.* **43**, 1553-1561 (1979).

50 Nedvidek, J., Antalikova, L. & Romanovsky, A. Cell surface morphology of the mophorgenetically active system of the embryo after treatment with Tunicamycin, a glycosylation blocking drug. *Histochemical Journal* **17**, 529-531 (1985).

51 Engstrom, W. & Larsson, O. The effects of glycosylation inhibitors on the proliferation of spontaneously transformed cell line (3T6) in vitro. *Journal of cell science* **90**, 447-455 (1988).

52 Gu, Y., Tokiwa, T., Kino, K., Ohno, T. & Namba, M. Cytotoxicity Test of Methanol using Various Human Hepatoma Cell Lines. *AATEX* **2**, 105-108 (1993).

53 Chung, B. C. *et al.* Crystal Structure of MraY, an Essential Membrane Enzyme for Bacterial Cell Wall Synthesis. *Science* **341**, 1012-1016 (2013).

54 Savage, K. E. & Baur, P. S. Effect of Tunicamycin, An Inhibitor of Protein Glycosylation, on Division of Tumour Cells In Vitro. *J. Cell. Sci.* **64**, 295-306 (1983).

55 Brewer, J. W., Hendershot, L. M., Sherr, C. J. & Diehl, J. A. Mammalian unfolded protein response inhibits cyclin D1 translation and cell-cycle progression. *PNAS* **96**, 8505-8510 (1999).

56 Brewer, J. W. & Diehl, J. A. PERK mediates cell-cycle exit during the mammalian unfolded protein response. *PNAS* **97**, 12625-12630 (2000).

57 Schröder, M. & Kaufman, R. J. The mammalian unfolded protein response. *Annual Review of Biochemistry* **74**, 739-789 (2005).

58 Ron, D. & Walter, P. Signal integration in the endoplasmic reticulum unfolded protein response. *Nature Reviews Molecular Cell Biology* **8**, 519-529 (2007).

59 Leleu, X. *et al.* Endoplasmic reticulum stress is a target for therapy in Waldenstrom macroglobulinemia. *Blood* **113** (2009).

60 Torres-Quiroz, F., García-Marqués, S., Coria, R., Randez-Gil, F. & Prieto, J. A. The Activity of Yeast Hog1 MAPK Is Required during Endoplasmic Reticulum Stress Induced by Tunicamycin Exposure. *The Journal of biological chemistry* **285**, 20088-20096 (2010).

61 Wang, X. *et al.* ER stress modulates cellular metabolism. *BIochemical Journal* **435**, 285-296 (2011).

62 Bull, V. H. & Thiede, B. Proteome analysis of tunicamycin-induced ER stress. *Electrophoresis* **33**, 1814-1823 (2012).

63 Schafer, K. A. The Cell Cycle: A Review. *Vet. Pathol.* **35**, 461-478 (1998).

64 Vermeulen, K., Bockstaele, D. R. V. & Berneman, Z. N. The cell cycle: a review of regulation, deregulation and therapeutic targets in cancer. *Cell Prolif.* **36**, 131-149 (2003).

65 *Apoptosis, Cytotoxicity and Cell Proliferation*. 4th edn, (Roche Diagnostics GmbH, 2008).

66 Chan, G. K. Y., Kleinheinz, T. L., Peterson, D. & Moffat, J. G. A Simple High-Content Cell Cycle Assay Reveals Frequent Discrepancies between Cell Number and ATP and MTS Proliferation Assays. *PloS one* **8**, e63583 (2013).

67 Bowden, T. A. *et al.* Chemical and Structural Analysis of an Antibody Folding Intermediate Trapped during Glycan Biosynthesis. *J. Am. Chem. Soc.* **134**, 17554–17563 (2012).

68 Powell, L. D. Inhibition of N-Linked Glycosylation. *Current Protocols in Immunology* **9**, 8.14.11–18.14.19 (2001).

# *Chapter Four*

## *Investigation of the tunB and tunF Knockout in the tun Gene Cluster*

## 4.1 Introduction

In recent work published by our group, the pathway start point catalysed by the gene products TunA and TunF were investigated.[1] Amino acid sequence homology analyses revealed structural similarity of TunA to NAD-dependent epimerase/dehydratases and TunF to 4-OH-sugar epimerases.[2] After recapitulation of TunA activity *in vitro* and in addition to the TunA crystal structure, TunA was observed to be the first natural enzyme to exhibit NDP-sugar 5,6-dehydrogenase activity converting the 4, 5, and 6 positions of GlcNAc into an allylic alcohol moiety. This may also be considered to be the first vinyl ether (*exo*-glycal) in sugar biology.[1] A 1,2-reduction was observed rather than a 1,4-reduction of a 4-keto-5,6-ene-hexose intermediate – to the best of our knowledge, this is the first of its kind. In a time-course $^{1}$H NMR assay of TunF with UDP-GlcNAc showed the establishment of a 30 % equilibrium of UDP-GalNAc. Similarly, 30% equilibrium of GalNAc-*exo*-glycal from GlcNAc-*exo*-glycal.[1] Furthermore, the recapitulation of TunF activity *in vitro* showed a kinetic preference (~8-fold) for the TunA 5,6-ene product over UDP-GlcNAc. This suggests that TunA precedes TunF in the tunicamycin biosynthetic pathway.[1]

The investigation of TunA and TunF activities led to the revision of the tunicamycins biosynthetic pathway. The results suggested that TunA acts on UDP-GlcNAc to produce an exo-glycal intermediate product, which appeared to be a substrate for TunF (**Fig. 4.1**). The formation of the GalNAc-*exo*-glycal intermediate suggests, in turn, that the tunicamine backbone may be the product of a radical addition mechanism.[1] To test these hypotheses, relevant mutations in the tunicamycins biosynthetic pathway needed to be made. In this chapter, the investigations of single knockout strains of *Streptomyces* to test

the possibilities of TunA's unique control of reductive regioselective enzymatic reaction and the formation of intriguing *exo*-glycal intermediate are discussed.

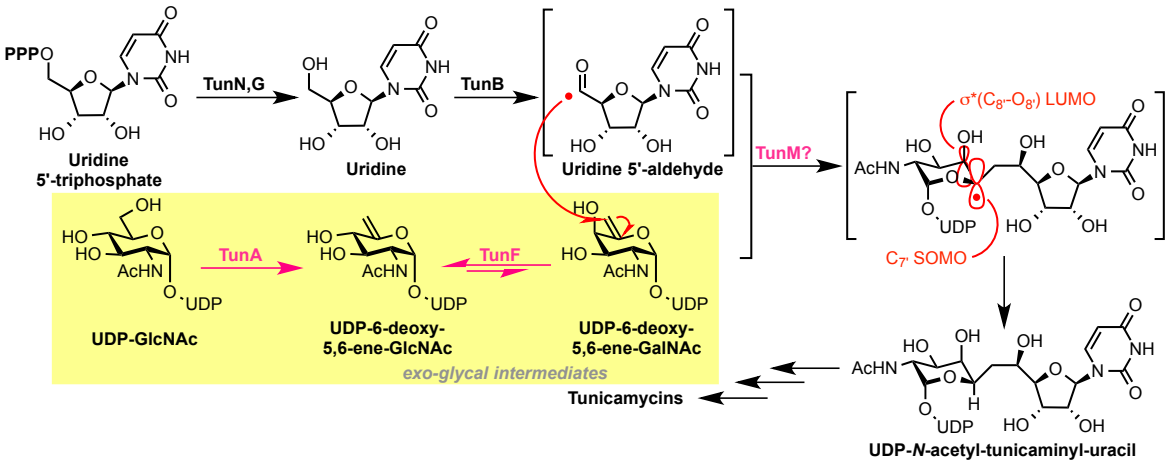


**Figure 4.1 | The revised tunicamycins biosynthetic pathway.[1]**

## 4.2 Results and Discussion

### 4.2.1 Construction of *tunB* and *tunF* Knockout in the *tun* Gene Cluster in Heterologous host *S. coelicolor* by PCR-targeting

We carried out the mutational studies on the tunicamycins biosynthetic (*tun*) gene cluster for heterologous expression in *Streptomyces coelicolor* to detect the *tunA exo*-glycal product, UDP-6-deoxy-GlcNAc-5,6-ene, or UDP-6-deoxy-GalNAc-5,6-ene product. Recently *S. coelicolor* was genetically manipulated to produce tunicamycins in a heterologous manner.[2] Using the same method, we made constructed individual knockouts of *tunB* and *tunF* in the *tun* gene cluster, in pIJ12003a, for heterologous expression. The knockout was accomplished by the PCR-targeting method reported by Gust *et al*. (**Fig. 4.2**).[3,4] Based on our revised proposed tunicamycins biosynthetic pathway from *tunA* and *tunF* studies, we proposed that the knockout of *tunB* or *tunF* would halt tunicamycins production while *exo*-glycal intermediate metabolite production continues (**Fig. 4.1**).

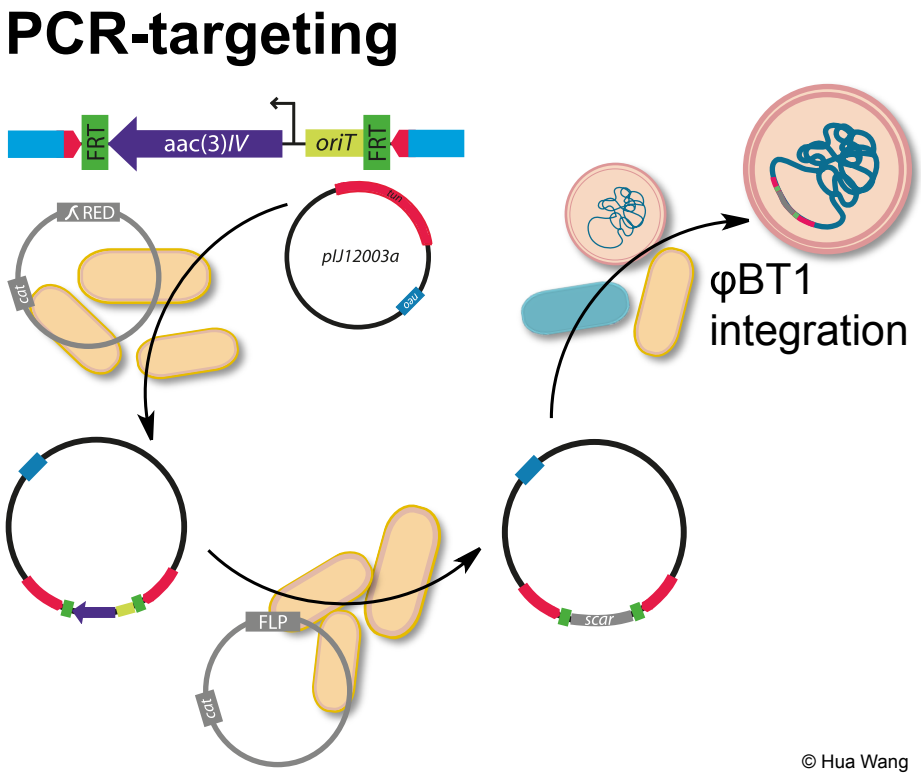


**Figure 4.2 | The PCR targeting process**.

The mutant construct, made by PCR-targeting, was transferred into *S. coelicolor* M1152 by conjugation *via* tri-parental mating, as shown in the last stage in **Fig. 4.2**. Successful integration of the mutant construct into the chromosomal φBT1 attachment site was determined by single-colony PCR and kanamycin resistant selection.[5] The kanamycin resistance gene is derived from the pIJ12003a construct. We denoted the mutant recombinant strains of *Streptomyces* as *S. coelicolor* M1152:*tunB*(-) and *S. coelicolor* M1152:*tunF*(-). Heterologous expression was carried out in TYD liquid culture. The cultures, along with relevant controls, were grown for five days before the mycelium pellets were collected and extracted *via* acid treatment (for cell lysis, nucleotide sugars extraction, and tunicamycins precipitation) or methanol (for tunicamycins extraction). In order to detect the *exo*-glycal product from *tunA*, extractions from acid treatment were neutralised and purified *via* solid-phase extraction (SPE) to isolate the sugar nucleotides

from the cell lysate.[6] We used LC-MS analysis to detect the *exo*-glycal product with mass of 589 Da.

### 4.2.2. Detection of TunA Intermediate Metabolite, LC-MS Analysis of Sugar Nucleotides from Heterologous Expression.

After SPE, cell lysate was subjected to LC-MS analysis.[6] Our results confirmed the presence of several known nucleotide sugars, including UDP-HexNAc and UDP-Gal, associated with cellular metabolism (**Fig. 4.3**). More importantly, a mass of 588 $[M-H]^-$ corresponded to our proposed TunA *exo*-glycal product was observed (**Fig. 4.3e)**. Tunicamycins (Enzo Life Sciences) were used as the standard in LC-MS. TYD cultures from our positive control *S. coelicolor* M1131 harbouring the minimal *tun* gene cluster showed tunicamycins production, whilst the negative control *S. coelicolor* M1135 without *tun* gene cluster showed no tunicamycins production (**Fig. 4.4**). We also isolated authentic tunicamycins from *Streptomyces chartreusis* that matched with commercial standard and heterologous expressed tunicamycins in *S. coelicolor* (**Fig. 4.4c**). For the mutant strains, cell lysate of *S. coelicolor* M1152 *tunB*(-) after SPE showed detectable amounts of *exo*-glycal product (588 $[M-H]^-$) along with UDP-Gal (565, $[M-H]^-$) and UDP-HexNAc (606, $[M-H]^-$) (**Fig. 4.3e**). No tunicamycins were detected in *S. coelicolor tunB*(-). The cell lysate from *S. coelicolor* M1152:*tunF*(-) after SPE also contained UDP-Gal and UDP-HexNAc but showed only trace amount of *exo*-glycal product (**Fig. 4.5**). We also spiked the cell lysate with *tunA* product to show the same elution and mass with just the cell lysate alone. Based on these results, we offered further evidence to support the TunA *in vitro* studies showing this novel enzyme as an UDP-GlcNAc 5,6-dehydratase.

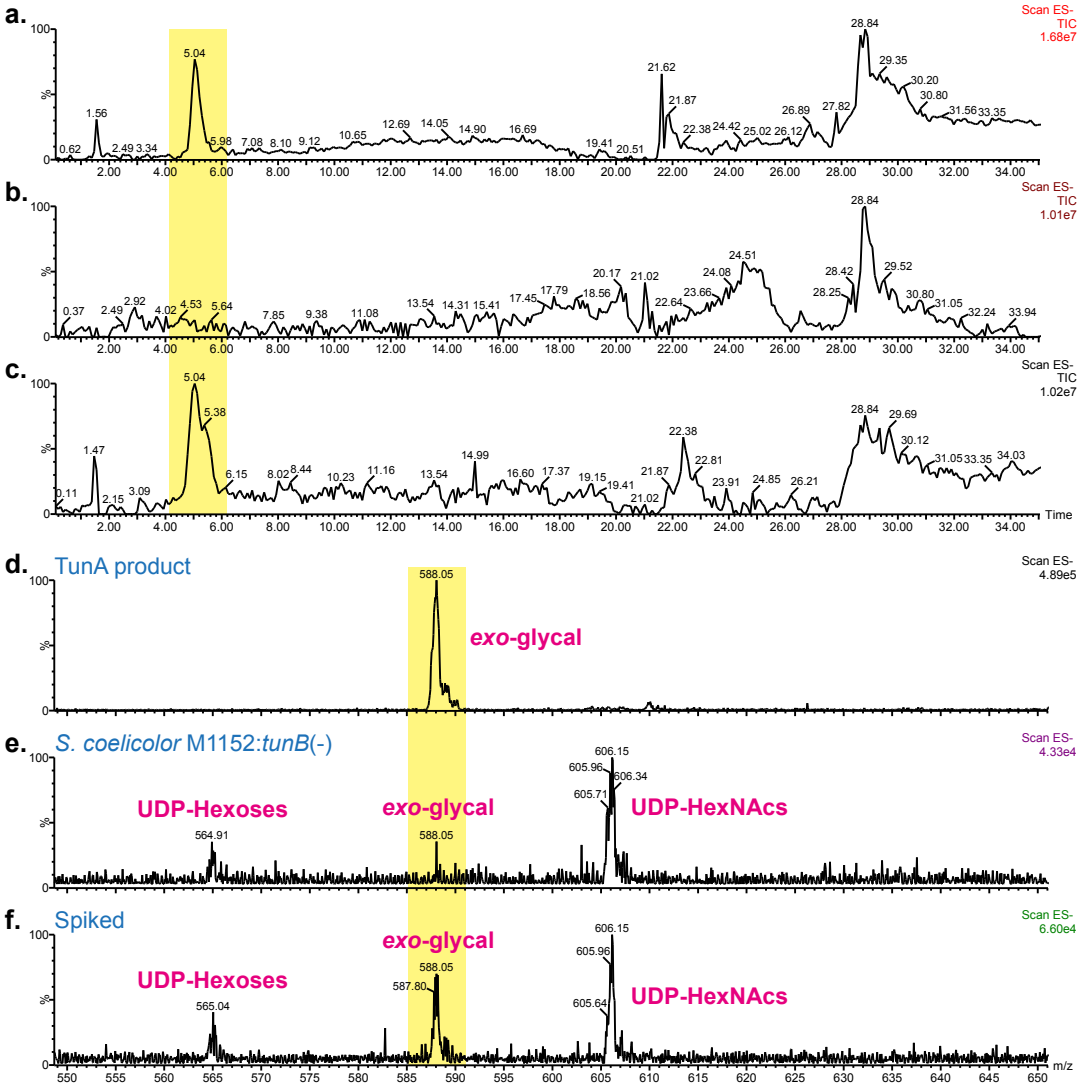


**Figure 4.3 | LC-MS analysis of the nucleotide-rich extract of *S. coelicolor* M1152:*tunB*(-) culture. (a)** TIC chromatogram of TunA *exo*-glycal product. **(b)** TIC chromatogram of the acid extract from *S. coelicolor* M1152:*tunB*(-) culture. **(c)** TIC chromatogram of *S. coelicolor* M1152:*tunB*(-) extract spiked with TunA *exo*-glycal product. **(d)** TOF-ESMS$^-$ of the TunA *exo*-glycal product. **(e)** TOF-ESMS$^-$ of the acid extract from *S. coelicolor* M1152:*tunB*(-) culture, showing the presence of the *exo*-glycal along with other nucleotide sugars (retention time, 4-6 min.). **(f)** TOF-ESMS$^-$ of the acid extract from *S. coelicolor* M1152:*tunB*(-) culture spiked with TunA *exo*-glycal product, showing the intensified peaked from the addition of TunA *exo*-glycal product.

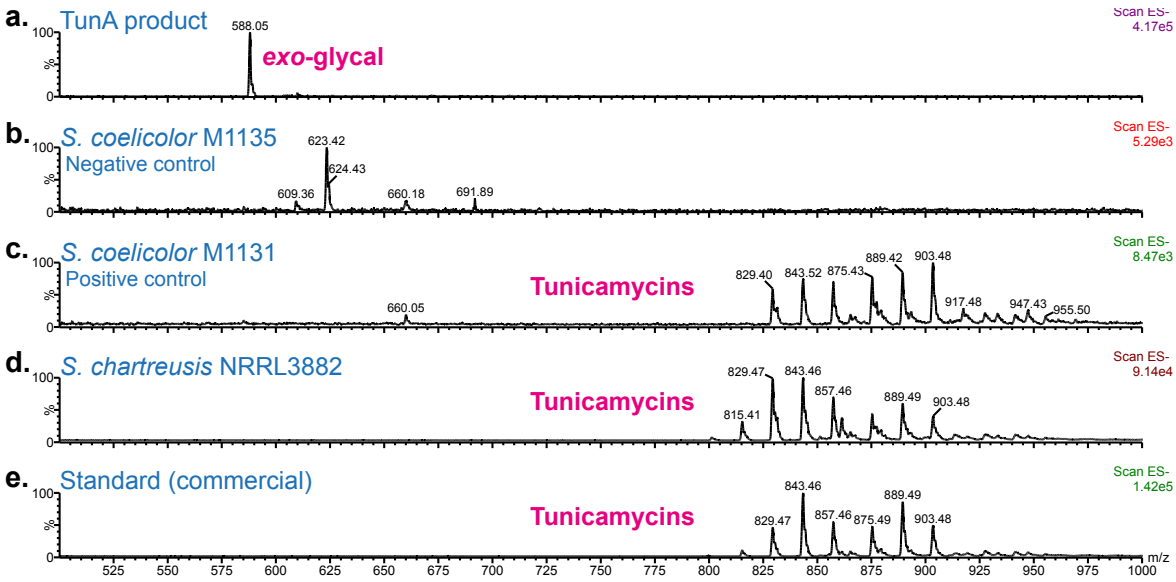


**Figure 4.4 | LC-MS chromatogram analysis of the methanol extract of *S. coelicolor* M1135 and *S. coelicolor* M1131 cultures.** No tunicamycins were detected in *S. coelicolor tunB*(-). **(a)** TOF-ESMS$^-$ of the TunA *exo*-glycal product. **(b)** TOF-ESMS$^-$ of the methanol extract from the negative control, *S. coelicolor* M1135:*tun*(-) without the *tun* gene cluster (only the pRT802 vector), showing no production of tunicamycins. **(c)** TOF-ESMS$^-$ of the methanol extract from the positive control, *S. coelicolor* M1131:*tun*(+) harbouring the *tun* gene cluster for heterologous expression, showing the production of tunicamycins. **(d)** TOF-ESMS$^-$ of the methanol extract from *S. chartreusis* showing the production of tunicamycins. **(e)** TOF-ESMS$^-$ of the commercial tunicamycins standard.

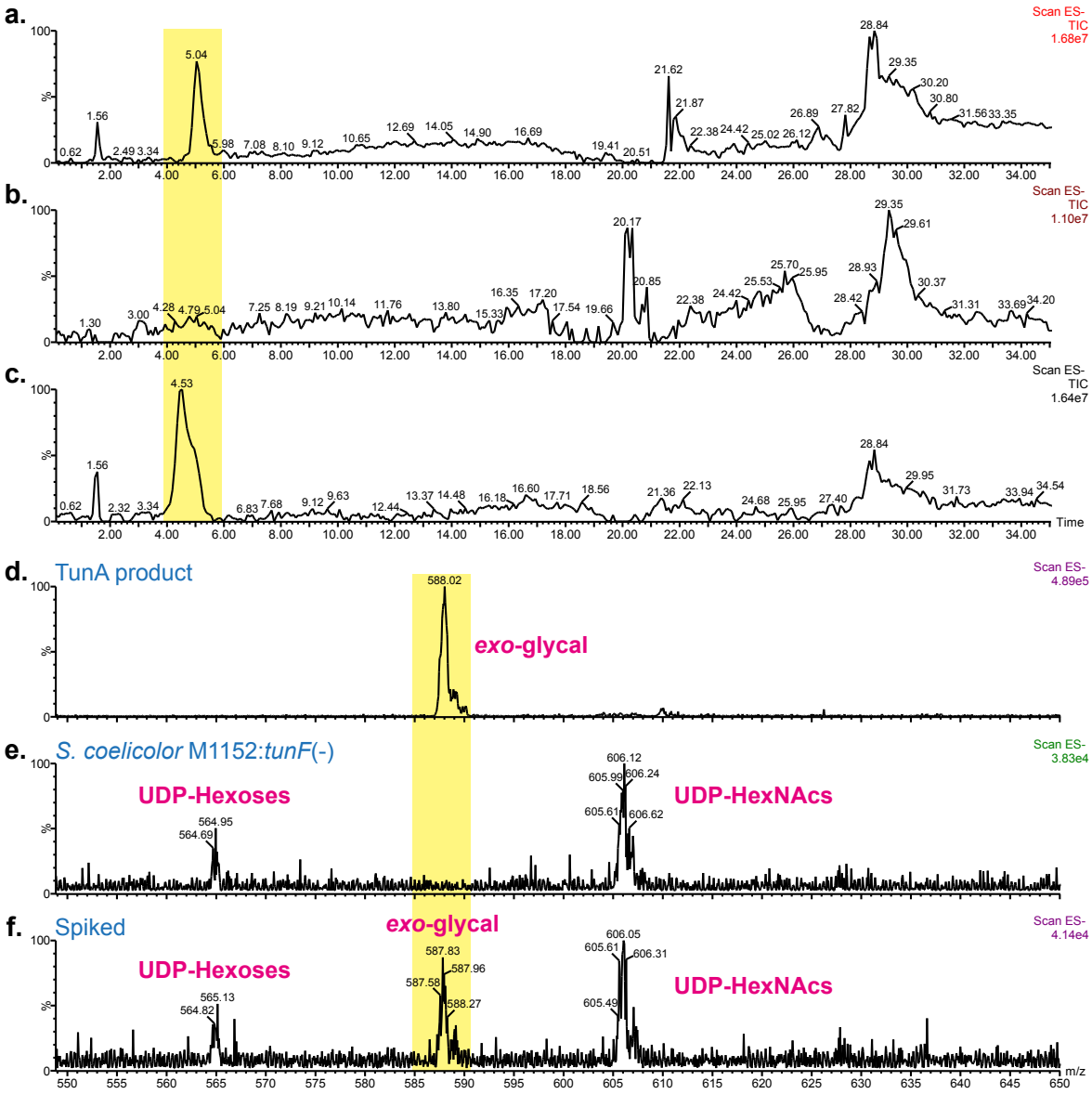


**Figure 4.5 | LC-MS analysis of the nucleotide-rich extract of *S. coelicolor* M1152:*tunF*(-) culture.** LC-MS **(a)** TIC chromatogram of TunA *exo*-glycal product. **(b)** TIC chromatogram of the acid extract from *S. coelicolor* M1152:*tunF*(-) culture. **(c)** TIC chromatogram of *S. coelicolor* M1152:*tunF*(-) extract spiked with TunA *exo*-glycal product. **(d)** TOF-ESMS$^-$ of the TunA *exo*-glycal product. **(e)** TOF-ESMS$^-$ of the acid extract from *S. coelicolor* M1152:*tunF*(-) culture, showing the presence nucleotide sugars. The cell lysate from *S. coelicolor* M1152:*tunF*(-) after SPE also contained UDP-Gal and UDP-HexNAc but showed only trace amount of *exo*-glycal product that can be observed at specific time in the LC-MS analysis. The average of the retention time 4-6 min. is shown. **(f)** TOF-ESMS$^-$ of the acid extract from *S. coelicolor* M1152:*tunF*(-) culture spiked with TunA *exo*-glycal product, showing the peak from the addition of TunA *exo*-glycal product.

### 4.2.3 *tunB* and *tunF* Complementation Studies

In addition to the mutant constructs, *S. coelicolor* M1152:*tunB*(-) and *S. coelicolor* M1152:*tunF*(-), the complement constructs, noted as *S. coelicolor* M1489:*tunB*(+) and *S. coelicolor* M1490:*tunF*(+) were also investigated.[i] Essentially, the *tunB* or *tunF* gene was inserted back in the knockout strain's chromosome of the respected *S. coelicolor* M1152 mutant (**Fig. 4.6**). This was to confirm that the results from our analysis were not due to the disruption of the gene knockout in the *tun* cluster. The same procedures for the knockout studies were followed to isolate and to analyse the metabolites from the complementation strains. Satisfyingly, our LC-MS analysis of the metabolites from the methanol extracts of *S. coelicolor* M1489:*tunB*(+) and *S. coelicolor* M1490:*tunF*(+) cultures indicated the revival of the tunicamycins production (**Fig. 4.7**). This further confirms our *S. coelicolor* M1152:*tunB*(+) results.

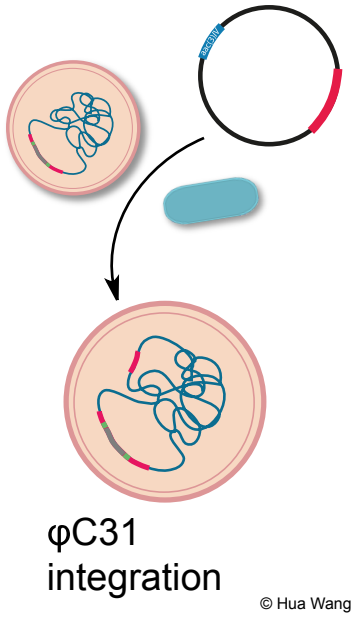


**Figure 4.6 | The construction process of the complementation strain.** The gene was inserted at another chromosomal integration site, ϕC31 (see **Appendix**).

[i] The complementation constructs, *S. coelicolor* M1152 *tunB*(+) and *S. coelicolor* M1152 *tunF*(+), were made by Juan Pablo Gomez-Escribano, John Innes Centre, Norwich, UK.

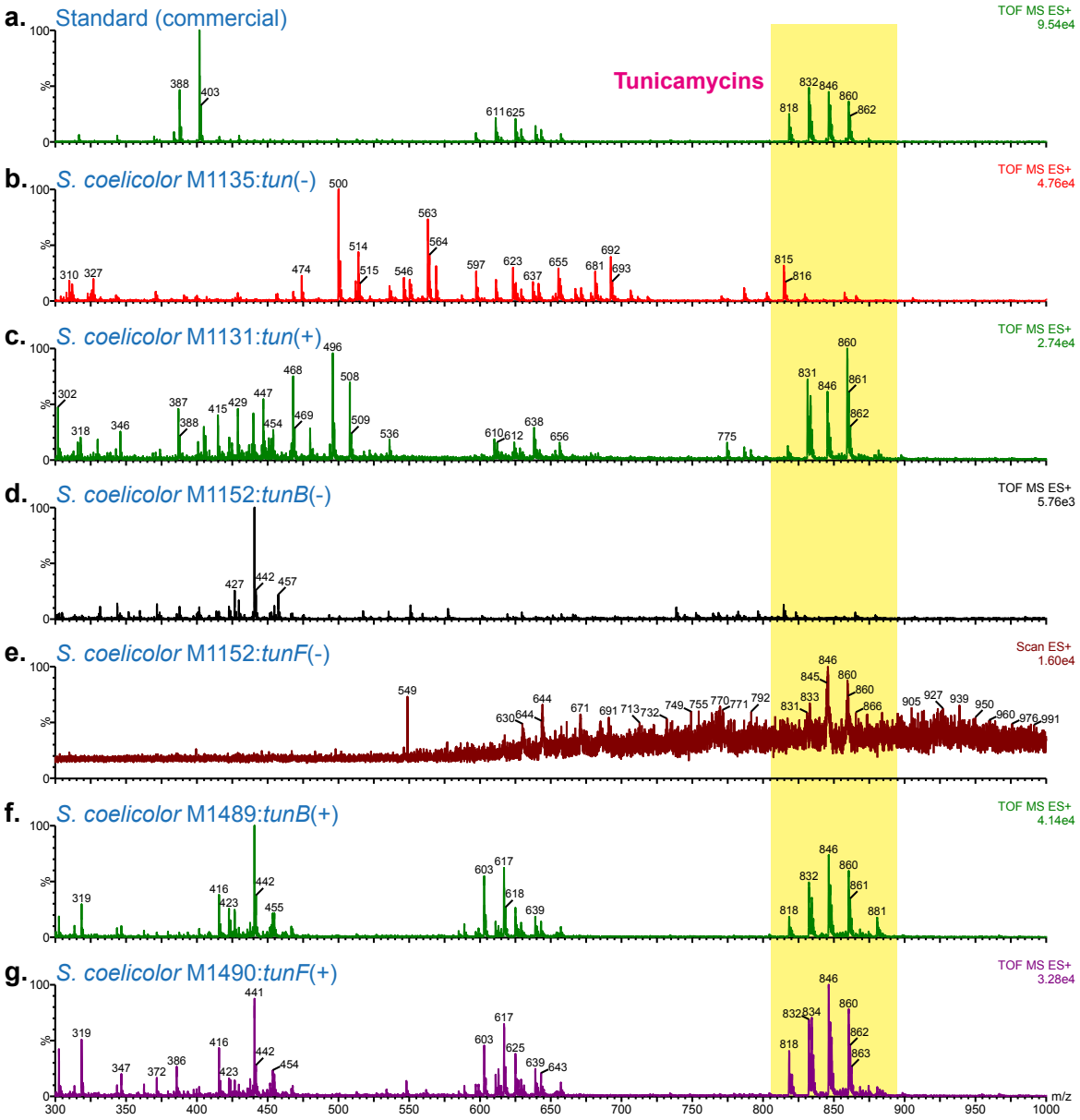


**Figure 4.7 | LC-MS analysis of the methanol extract of *tunB* and *tunF* complement *S. coelicolor* M1489:*tunB*(+) and *S. coelicolor* M1490:*tunF*(+) cultures.** No tunicamycins were observed from the negative control M1037. The complementation strains showed the revival of the tunicamycins production. Based on the *S. coelicolor* M1040:*tun*(+) control strain, the production of tunicamycins was observed after one day of incubation in L scale culture. In a 100 mL scale, the tunicamycins production was observed after three days of incubation, which may indicate that small-scale culture did not produce detectable quantity of tunicamycins for the sample preparation until the third day. The *S. chartreusis* culture produced sufficient quantity of tunicamycins that were detectable by LC-MS from 100 mL culture from one day of incubation (see subsection **4.2.4**, **Table 4.1**, **Appendix**).

### 4.2.4 Investigation of Mutant *S. coelicolor* M1152:*tunF*(-) Metabolite

Gene sequence alignment predicted TunF as a putative UDP-GlcNAc-4-epimerase, based on the closest protein homologue UDP-glucose-4-epimerase.[2] The knockout of *tunF* in the *tun* gene cluster experiment provided some insight in its role in the tunicamycin biosynthetic pathway. We proposed that by knocking out *tunF* in the pathway, it would either impede the production of tunicamycins or result the C7'-OH of tunicamycins in glucose configuration instead of the galactose configuration. Interestingly, we observed a minuscule quantity of tunicamycin mass-like products from the methanol extract by MS analysis (**Fig. 4.8**).

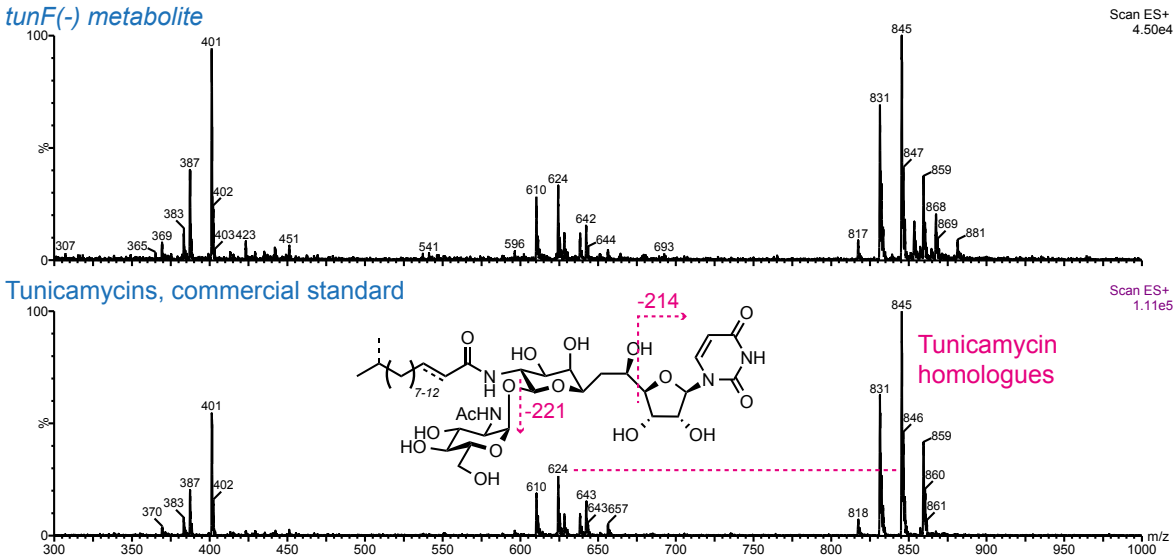


**Figure 4.8 | MS/MS analysis of the crude *S. coelicolor* M1152:*tunF*(-) metabolite.**[7] The -221 mass lost corresponding to a HexNAc moiety.

This suggested that the biosynthesis of tunicamycins may have continued, even without the epimerase TunF as proposed, and if the tunicamycin mass-like products observed could be the glucose configuration of tunicamycins. Thus, we investigated the *S. coelicolor* M1152:*tunF*(-) tunicamycin mass-like products.

First, we monitored the tunicamycins production to observe any differences between the native strain *S. chartreusis* NRRL 3882, and heterologous expression strains *S. coelicolor* M1037 (negative control), M1040 (positive control, containing *tun* gene cluster), M1152:*tunB*(-), and M1152:*tunF*(-). The same growth conditions were followed as previously described in TYD medium.[2] A 50 mL seedling culture was first grown overnight from spore stock. Samples were collected after 24 h on consecutive days following the initial inoculation from the seedling culture. Extract sample preparation involved 5-10 mL methanol extraction from mycelium pellet, with 10 mL of culture, using a pestle and mortar. The methanol extracts were concentrated *in vacuo* and filtered *via* 0.2 μm membrane before LC-MS analysis.

The monitoring of *S. coelicolor* M1152:*tunF*(-) growth over seven days is summarised in **Fig. 4.9**. The tunicamycin mass-like products from the methanol extract appeared after three days of growth at 30 °C. The LC-MS analysis showed production of tunicamycins from the natural producer *S. chartreusis* just after 24 h from the initial inoculation in 100 mL TYD medium from the seedling culture. The heterologous *S. coelicolor* strains harbouring the *tun* gene cluster, as a positive control, and *tun* gene cluster with *tunF* knockout started to produce an observable quantity of tunicamycin mass-like products at day three, by LC-MS. This, in comparison to the natural tunicamycins producing strain and the heterologous expression strains, showed a large difference in tunicamycins production time. This may be the result of the differences in the metabolic process. As expected, no observable quantity of tunicamycins was produced by *S. coelicolor* without *tun* gene cluster, as a negative control, and *S. coelicolor* harbouring the

*tun* gene cluster with *tunB* knockout. A summary of the observation from each *Streptomyces* strains is noted in **Table 4.1**.

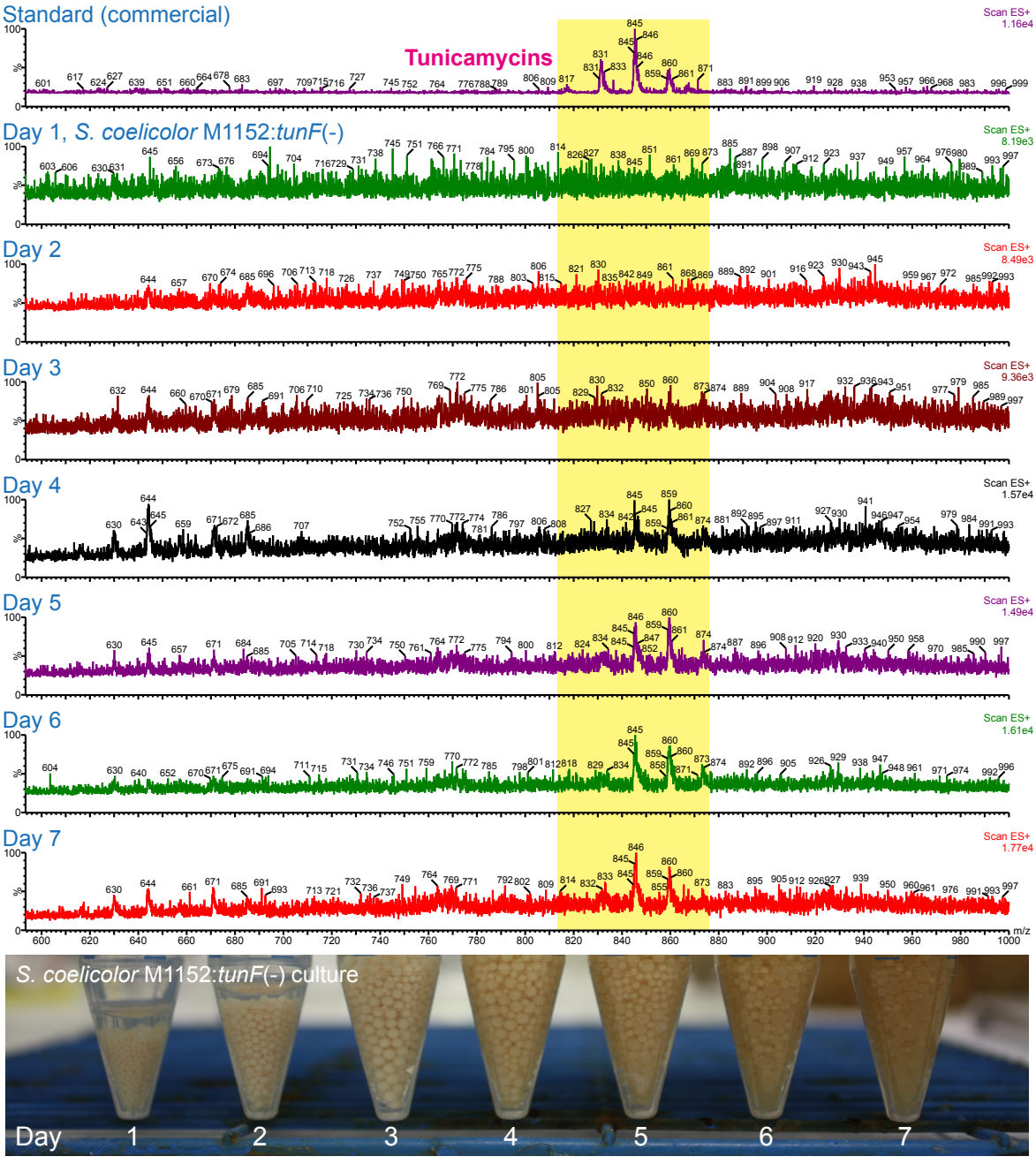


**Figure 4.9 | LC-MS analysis of the methanol extract of *S. coelicolor* M1152:*tunF*(-) culture over seven days.**

**Table 4.1 | Tunicamycins production by *Streptomyces* over seven days.**

| ***Streptomyces*** | **Growth Period (day) & Tunicamycins* Detected by LC-MS[a]** | | | | | | |
|---|---|---|---|---|---|---|---|
| | One | Two | Three | Four | Five | Six | Seven |
| *S. chartreusis* | TM | TM | TM | TM | TM | TM | TM |
| *S. coelicolor* M1137:*tun*(-) | No TM | No TM | No TM | No TM | No TM | No TM | No TM |
| *S. coelicolor* M1140:*tun*(+) | No TM | No TM | No TM | TM | TM | TM | TM |
| *S. coelicolor* M1152:*tunB*(-) | No TM | No TM | No TM | No TM | No TM | No TM | No TM |
| *S. coelicolor* M1152:*tunF*(-) | No TM | No TM | No TM | TM | TM | TM | TM |
| *S. coelicolor* M1140:*tun*(+)[a] | TM | TM | TM | TM | TM | TM | TM |
| S. coelicolor M1489:tunB(+)[a] | TM | TM | TM | TM | TM | TM | TM |
| S. coelicolor M1490:tunF(+)[a] | TM | TM | TM | TM | TM | TM | TM |

*Methanol extracts from the *Streptomyces* culture were used for the LC-MS analysis.
[a]Based on the *S. coelicolor* M1040:*tun*(+) control strain, the production of tunicamycins was observed after one day of incubation with a 1 L scale culture. On a 100 mL scale, the tunicamycins production was observed after three days of incubation, which may indicate that the small-scale culture did not produce detectable quantities of tunicamycins for the sample preparation until the third day. The *S. chartreusis* culture produced a sufficient quantity of tunicamycins that were detectable by LC-MS from 100 mL culture from one day of incubation.

Next, we carried out $^{1}$H NMR analysis of the *S. coelicolor* M1152 *tunF*(-) crude tunicamycin mass-like products from methanol extraction. Despite *tunF* being knocked-out from the *tun* gene cluster, tunicamycin mass-like products continued to be produced, albeit in extremely low quantities (crude, <1.7 mg per L culture, see **Appendix**). Oddly, repeated attempts to extract the tunicamycin mass-like products, using the same methodology for tunicamycins extraction from *S. chartreusis*, from 1 L scale cultures were less successful, but detectable amounts were observed by LC-MS from the methanol extracts. This may be due to the fact that the production of tunicamycin mass-like products in *S. coelicolor* was extremely low, the metabolic processes in the engineered *S. coelicolor* greatly differ from that of *S. chartreusis* and the *S. coelicolor* M1152 *tunF*(-) growth condition may need optimisation to improve the yield, or the extraction protocol need to be optimised for *S. coelicolor* cultures. With the crude tunicamycin mass-like products sample, we analysed the sample by LC-MS, MS/MS, $^{1}$H NMR, and COSY. Our analyses

showed that the tunicamycin mass-like products strongly resemble the structure of tunicamycins. The similarities included the presence of lipid chain, tunicaminyl uracil, and GlcNAc adduct (**Fig. 4.10,** see **Appendix**). More importantly, based on the existence of the anomeric H-11' coupling with H-10' and H-9', the galactose configuration was observed, thus it showed that the tunicamycin mass-like products did not have a glucose configuration (**Fig. 4.10**c). The H-9' and H-8' eq-ax coupling was not observed and appeared to be overlapped as it is also reported in the literature, which is similarly observed with the commercial standard.[8] Even though *tunF* had been eliminated from the tunicamycin biosynthetic pathway, it appeared that other epimerases present in the *S. coelicolor* metabolic pathway may have also acted on the tunicamycins intermediate resulting in the galactose configuration. An example of such epimerase could be the UDP-glucose-4-epimerase in *S. coelicolor* A3(2).[9]

The result from the *tunF* knockout experiment showed that TunF does play an important role in the tunicamycin biosynthetic pathway. The *exo*-glycal intermediate appeared capable of being transformed by other epimerases in *S. coelicolor*. Moreover, *S. coelicolor* and *S. chartreusis* belong to the largest genus of *Actinobacteria* known for their production of secondary metabolites for medicinal purposes, thus it is also possible that orthologues of TunF epimerase exist in *S. coelicolor*. This is a plausible explanation as *Streptomyces* are known to produce a wide range of antibiotics.[10]

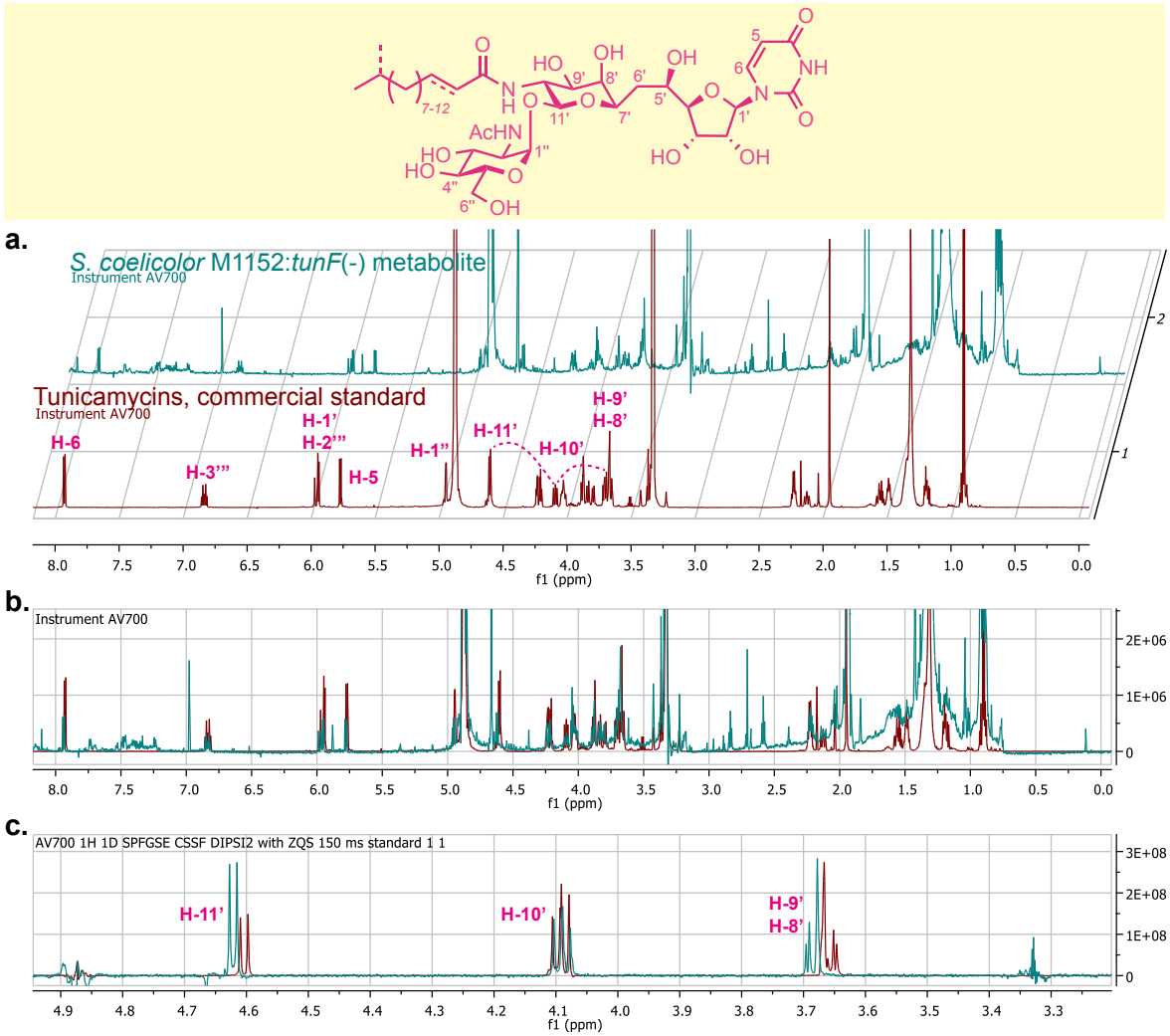


**Figure 4.10 | $^{1}$H NMR and 1-D TOCSY of the *S. coelicolor* M1152:*tunF*(-) metabolite.[8](a)** $^{1}$H NMR spectra of tunicamycins and the crude *S. coelicolor* M1152:*tunF*(-) metabolite. The chemical shifts corresponding to the tunicaminyl uracil, lipid chain, and GlcNAc can be observed in the metabolite spectrum. **(b)** Overlap of $^{1}$H NMR spectra of the two samples. **(c)** Overlap of 1D TOCSY spectra of tunicamycins and *S. coelicolor* M1152:*tunF*(-) metabolite, irradiation of the H-11'. The slight distortion of the metabolite spectrum from the tunicamycins spectrum may be caused by impurities and the homologues.

## 4.3 Conclusion and Outlook

In summary (**Fig. 4.11**), the *tunB* knockout studies were successful in showing the *exo*-glycal product of TunA and indicated the importance of TunB in the tunicamycin biosynthetic pathway. These results suggested that the tunicamine backbone may, in fact, be the product of an exciting radical addition mechanism.[1] Although we did not fully

characterised *tunF*(-) tunicamycin mass-like products, the possibility of other epimerases in the *S. coelicolor* may be the cause of the minuscule production of tunicamycins from the *tunF* knockout studies, and the tunicamycin mass-like products appeared to retain the galactose and not the glucose configuration for the tunicamine scaffold. In the complement studies, *S. coelicolor* M1489:*tunB*(+) and M1490:*tunF*(+), tunicamycins production was successfully revived as expected in returning the necessary genes in the tunicamycin gene cluster for tunicamycins production. Tunicamycins production was observed in M1131 and not in M1135, as expected. *S. coelicolor* M1489 and M1490 fully regained their production of tunicamycins. Moreover, the PCR-targeting method appeared to be a useful method for studying other genes and stop points in the tunicamycin biosynthetic pathway, and possibly isolating intermediates that can be used as templates for synthesising analogue. Lastly, it would be interesting to engineer the tunicamycin biosynthetic pathway to produce tunicamycin analogues. This is not far fetched as our complementation studies were able to restore the tunicamycins production, and engineering the pathway with enzymes to perform similar or different enzymatic processes may be a worthwhile pursuit to create tunicamycin analogues.

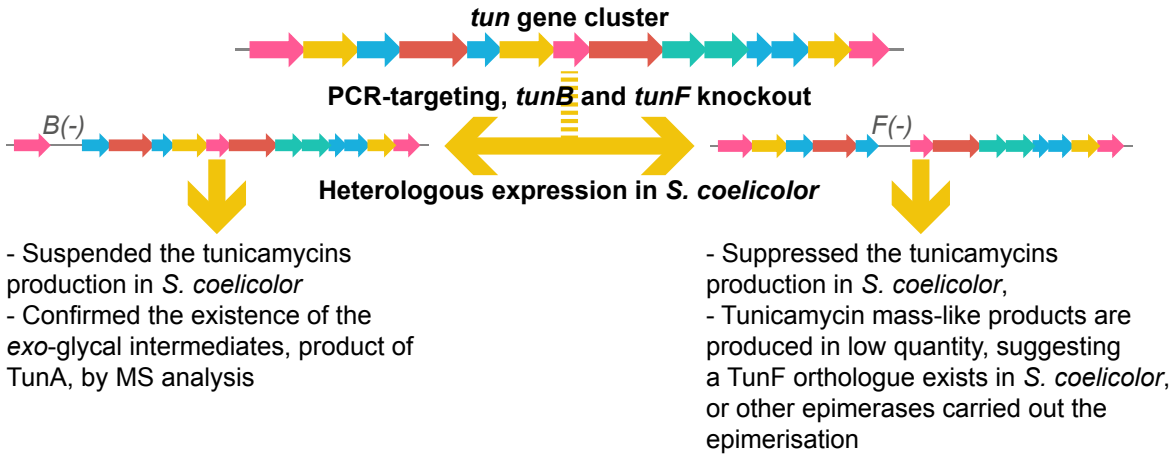


**Figure 4.11 | A summary of the *tunB* and *tunF* knockout studies.**

## 4.4 References


1 Wyszynski, F. J. *et al.* Biosynthesis of the tunicamycin antibiotics proceeds via unique exo-glycal intermediates. *Nature Chemistry* **4**, 539-546 (2012).

2 Wyszynski, F. J., Hesketh, A. R., Bibb, M. J. & Davis, B. G. Dissecting tunicamycin biosynthesis by genome mining: cloning and heterologous expression of a minimal gene cluster. *Chem. Sci.* **1**, 581-589 (2010).

3 Gust, B., Kieser, T. & Chater, K. *PCR targeting system in Streptomyces coelicolor A3(2)* (John Innes Centre, Norwich, UK).

4 Gust, B. *et al.* Lambda red-mediated genetic manipulation of antibiotic-producing Streptomyces. *Advances in Applied Microbiology* **54**, 107-128 (2004).

5 Gregory, M. A., Till, R. & Smith, M. C. M. Integration Site for Streptomyces Phage φBT1 and Development of Site-Specific Integrating Vectors. *Journal of bacteriology* **185**, 5320–5323 (2003).

6 Räbinä, J. *et al.* Analysis of nucleotide sugars from cell lysates by ion- pair solid-phase extraction and reversed-phase high-performance liquid chromatography. *Glycoconjugate* **18**, 799-805 (2001).

7 Tsvetanova, B. C., Kiemle, D. J. & Price, N. P. J. Biosynthesis of Tunicamycin and Metabolic Origin of the 11-Carbon Dialdose Sugar, Tunicamine. *J. Biol. Chem.* **277**, 35289-35296 (2002).

8 Xu, L., Appell, M., Kennedy, S., Momany, F. A. & Price, N. P. J. Conformational Analysis of Chirally Deuterated Tunicamycin as an Active Site Probe of UDP-N-Acetylhexosamine:Polyprenol-P N-Acetylhexosamne-1-P Translocases. *Biochemistry* **43**, 13248-13255 (2004).

9 Bentley, S. D. *et al.* Complete genome sequence of the model actinomycete Streptomyces coelicolor A3(2). *Nature* **417**, 141-147 (2002).

10 Chater, K. F. Streptomyces inside-out: a new perspective on the bacteria that provide us with antibiotics. *Phil. Trans. R. Soc. B* **362**, 761-768 (2006).

# *Chapter Five*

## *Investigation of the TunD and TunE Enzymatic Activities in the Tunicamycin Biosynthetic Pathway*

## 5.1 Introduction

TunD and TunE are the putative glycosyltransferase and *N*-deacetylase, respectively, in the tunicamycin biosynthetic pathway.[1,2] Wyszyński *et al*. proposed that TunD catalyses the α,β-1,1-glycosidic linkage between the GlcNAc and tunicaminyl uracil, and the TunE is proposed to deacetylate the *N*-acetyl moiety of either *N*-acetyl-tunicaminyl uracil (**3**), tunicaminyl uracil (**7**), or α-D-*N*-acetylglucosamine-(1”-11’)-*N*-acetyl-tunicamyl uracil (**4**). Since the order of TunD and TunE is uncertain, where **3** can either first be deacetylated or glycosylated, three possible pathways for TunD and TunE have been proposed (**Fig. 5.1**).[2] The two proposed substrates, **3** and **4**, for either TunD or TunE were prepared from chemical degradation of crude tunicamycins isolated from *S. chartreusis* NRRL3882 discussed in **Chapter 2**. As discussed in **Chapter 1** and concluded in **Chapter 4**, functional characterisation of TunD and TunE would provide insights to the unique biological chemistry that could enable us to construct tunicamycin analogues *in vitro* and engineer the pathway to create tunicamycin analogues. In this chapter, the investigation of TunD and TunE are discussed.

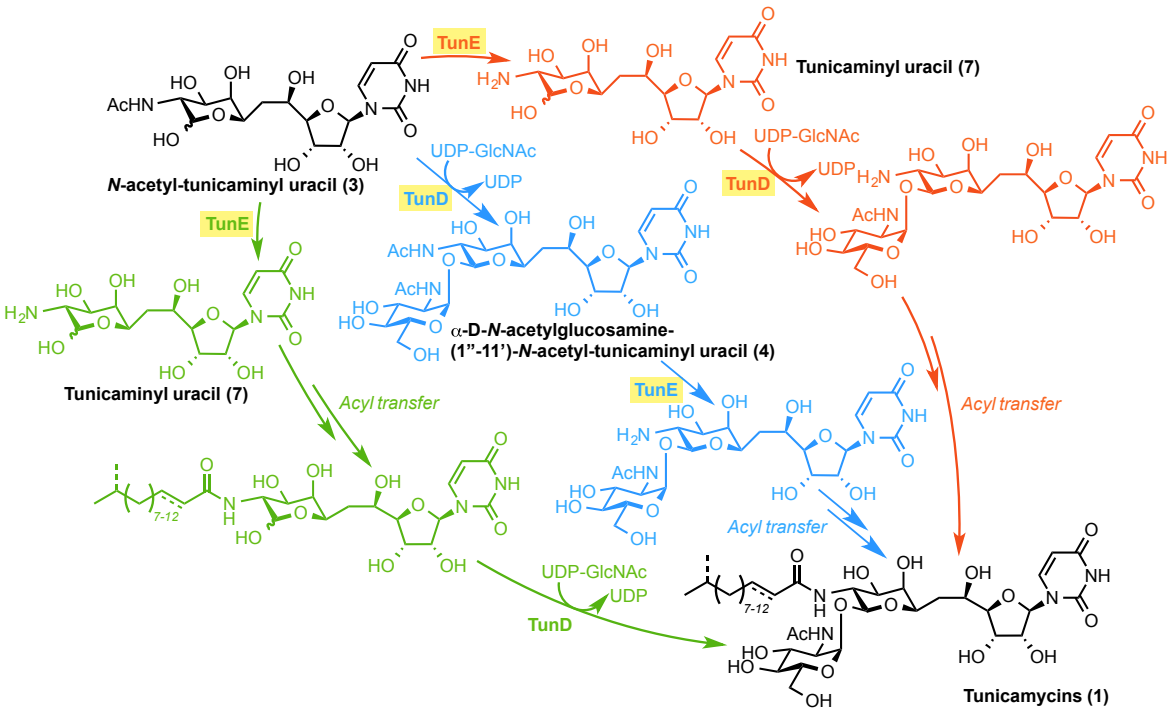


**Figure 5.1 | The three proposed enzymatic pathways for TunD and TunE in the tunicamycin biosynthetic pathway.**[2] The order of the enzymatic reaction of TunD and TunE in the tunicamycin biosynthesis is unknown. It is proposed that substrates **3**, **4**, and **7** can be the starting substrate of either TunD or TunE. The pathway steps investigated in this chapter is highlighted in yellow.

## 5.2 Results and Discussion

### 5.2.1 Gene analysis of *tunD*

The TunD is predicted to be a putative glycosyltransferase in the tunicamycin biosynthetic pathway.[1] A BLAST[i] sequence alignment analysis of TunD showed amino acid sequence character of a GT1 family and a GT-B type fold glycosyltransferase.[2] GT-A type is considered to be metal-dependent glycosyltransferase, whereas GT-B type is considered to be metal-independent glycosyltransferase.[3]

[i] Basic Local Alignment Search Tool. http://blast.ncbi.nlm.nih.gov

**Table 5.1 | TunD amino acid sequence.**[2]

| Protein | Amino acids | Amino acid sequence | MW (avg.) / pI |
|---|---|---|---|
| Native TunD | 472 | MEIIFTVSDQVWGGKHRYMHDMALGLAQAGHTVTVLAEEGG AMLQQCRAAGVTTVSVPAFASDDAAEAVRKALRHRRPHIVCV SGRADAAAVHHAQSQGVTDAAVCLFRHSAFPLGTTDEVRDLF TGVNLVFTTSLEQRQRQFEPLINAGVLKDEQVEILTSGVGEPL LAALDAADRGAARKELRAESDQFVFLVLARLAWEKGIDQVIDA FADLELPPDAAPPLLVVAGEGPLEAELRGQTIERGVAERVQFL GHQDHVAPVIKASDAVVLTSTVPETGPLALKEAMAAGRPVIAS VQGGIPEFVEDERHGLLVIDDEDLRQAMQRLLSDREAAETMG AAGSESVRGGHRAVRRVEYLAHRLDLLALEQLAPDTVLHEVV WDDVRLREETQGGFVFVPRTSHIMELDSATYAVVRTAVEAGD PLQLIKLPEETLGVIAHRLYAMGALVRQDGQATPAARTADGER PVTEPA | Mw = 50832 Da<br>pI = 5.01 |

### 5.2.2 Recombinant Expression of TunD in *E. coli*

Previously, in the work that was carried in our the group by F. J. Wyszyński, TunD was heterologously expressed in *E. coli* as a recombinant protein.[2] However, despite several attempts in different cloning expression vectors and optimising the expressions, TunD was mainly expressed in the inclusion bodies, except the *E. coli* BL21(DE3)/ pET-21a:*tunD* system resulted in partially soluble TunD-$His_6$ protein. The TunD-$His_6$ protein was isolated as impure fractions from $Ni^{2+}$ affinity purification. It was showed that by using the spectrophotometric coupled assay for glycosyltransferases of TunD the hydrolysis of UDP-GlcNAc was observed. However, no isolation of the product was noted.[2] This may have resulted from using the wrong acceptor for the glycosyltransferase, or due to unspecific hydrolysis of UDP-GlcNAc by unknown contaminants in the TunD-$His_6$ sample.

We repeated *E. coli* BL21(DE3)/pET-21a:*tunD* expression system in order to investigate the possible substrate acceptor and possible enzymatic activity observed from the TunD-$His_6$. Unfortunately, no soluble protein was detected in the soluble fraction after using BugBuster system to lyse cells (TunD-$His_6$ ~52 kDa) based on SDS-PAGE and

Western blot analyses (**Fig. 5.2**) after several attempts were made to reproduce and isolate the partially soluble TunD-$His_6$, although TunD appeared to be highly expressed. Due to the high level of protein expression, we slowed the protein expression by lowering the incubation temperatures (37 to 30, 23, 18, and 15 ℃) in the hope that we could induce proper folding of the proteins. Additionally, we also attempted using *E. coli* Lemo21(DE3) expression system[4] (*E. coli* Lemo21(DE3):pET-21a:*tunD*) (**Fig. 5.2**). Again, unfortunately TunD was consistently expressed in the inclusion bodies. This could suggest that the *E. coli* recombinant expression system may not be most suitable to express the *Streptomyces* proteins[5] or that the TunD would need to be co-expressed[6] with another protein in the tunicamycin biosynthetic pathway in equivalence for complex formation based on the closely overlap of the genes in the *tun* gene cluster.

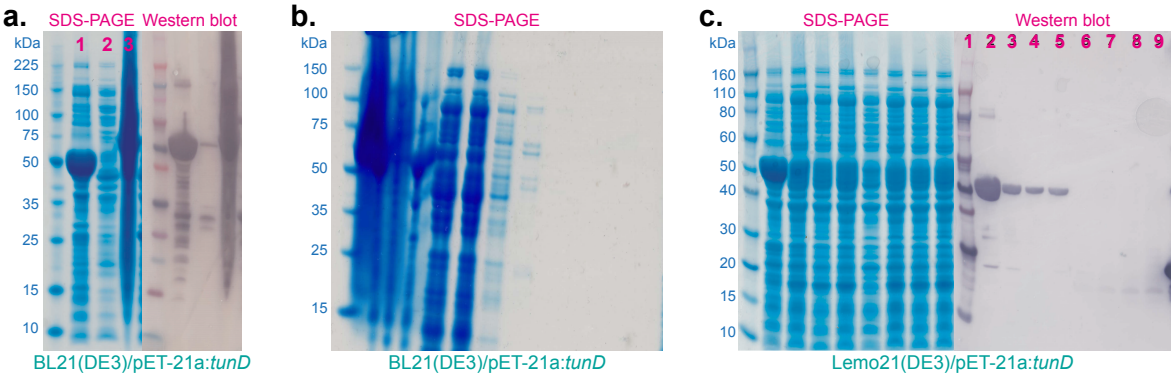


**Figure 5.2 | TunD expression. (a)** Lanes 1-3 correspond to cell lysate, soluble fraction, inclusion bodies. TunD-$His_6$ was in the inclusion body. **(b)** Manual Ni-NTA purification by discontinuous imidazole gradient. No soluble TunD-$His_6$ was isolated. **(c)** Lemo21(DE3) expressions were induced by L-rhamnose (Western blot lanes 2 to 6 correspond to 0, 250, 750, 2000 μM). Lanes 6-9 correspond to the soluble fractions. As shown, no soluble TunD-$His_6$ was isolated.

Next, considering the high expression level of TunD, we attempted protein refolding using the iFOLD Protein Refolding System 1 Kit to determine the optimum protein refolding condition. The iFOLD screened 92 conditions with different buffer, pH,

salts, detergents, reducing agents, and metals (**Fig. 5.3**). First we maximised the TunD inclusion bodies using *E. coli* BL21(DE3)/pET-21a:*tunD* system in TB+glycerol medium, 15 °C overnight expression. The insoluble protein was washed, denatured and then screened for the optimum refolding condition in the iFOLD plate by measuring the turbidity of each condition in the plate (**Fig. 5.4)**. The absorbance was measured at A340. The low absorbance may indicate folded protein. However, the absorbance values need to be interpreted with caution as low absorbance does not necessary correlate with properly folded or active protein. From the conditions screened, we chose the condition in well E7 (50 mM Tris, pH 8.0, 250 mM NaCl, 1 mM TCEP, 12.5 mM β-cyclodextrin) with A340 absorbance value of 0.1340 to proceed forward. E7 was chosen because of its low absorbance and the refolding condition that was absent of EDTA and GuHCl compared with the other conditions, which may indicate properly folded protein.


**Figure 5.3 | iFOLD protein refolding system 1 96-well plate refolding conditions.** In Tris buffer. The 'cyclodextrin' refers to methyl-β-cyclodextrin.

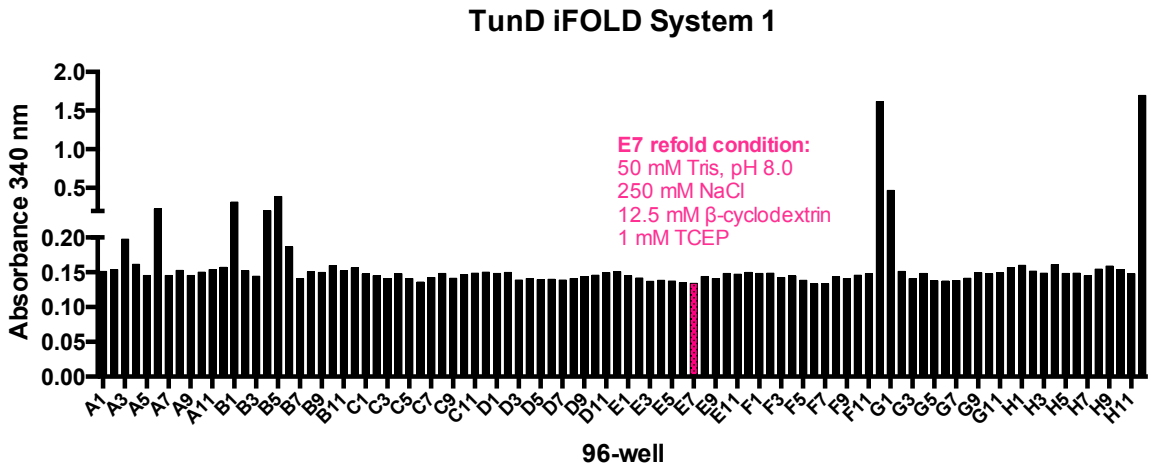


**Figure 5.4 | Bar graph showing the absorbance values from the TunD refolding in the 96-well iFOLD plate.** The E7 well has an absorbance value of 0.1340.

We repeated the refolding process and then purified the refolded TunD *via* manual Ni-NTA. The protein was eluted using discontinuous imidazole gradient (25 mM, 50 mM, 100 mM, 250 mM, 500 mM). The eluted samples were analysed by SDS-PAGE (**Fig. 5.5**). Fractions containing pure TunD were collected, concentrated, and dialysed in the E7 refolding buffer to remove the imidazole. The concentration of the dialysed TunD sample was measurement by BCA assay, ~3 mL sample volume at 1.4 mg $mL^{-1}$ (**Fig. 5.5**). The purified TunD sample was further analysed by CD (**Fig. 5.5**), which showed TunD with α-helical structure. A convoluted CDNN analysis using 0.5 mg $mL^{-1}$ sample showed mostly helical protein structure. The purified refolded TunD-$His_6$ mass was confirmed by LCMS (**Fig. 5.6**).

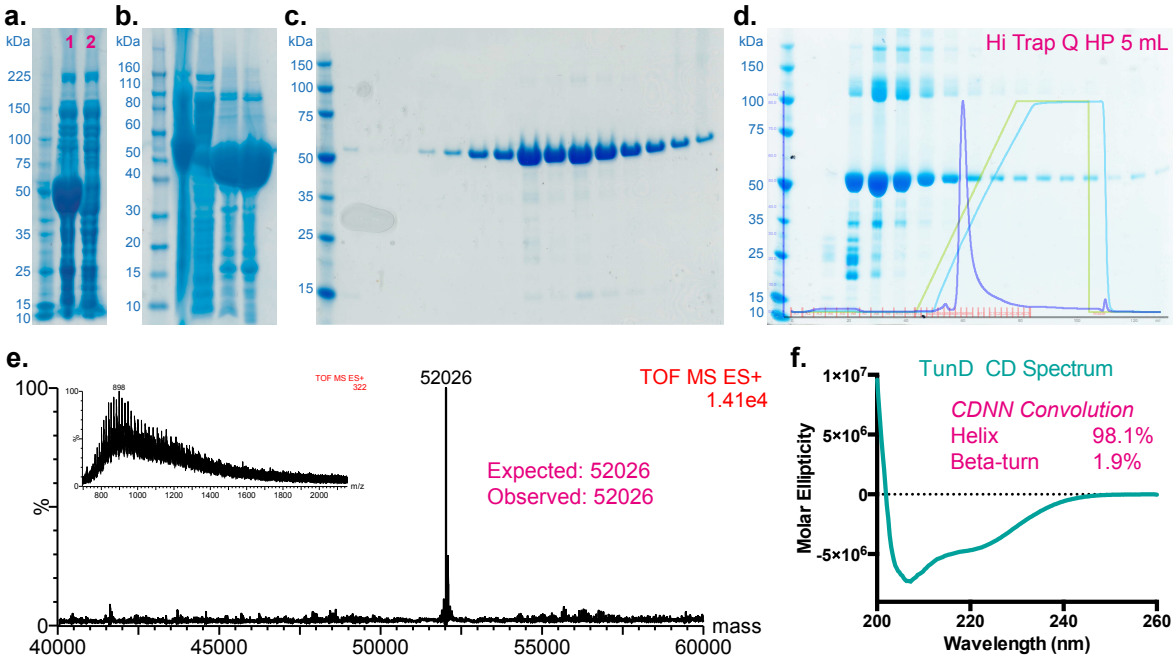


**Figure 5.5 | Refolding of TunD. (a)** Lanes 1 and 2 correspond to cell lysate and soluble fraction, respectively. **(b)** The washed samples of the inclusion bodies from iFOLD process. **(c)** Manual Ni-NTA purification by discontinuous imidazole gradient. Soluble TunD-$His_6$ was isolated. **(d)** A FPLC chromatogram of TunD purification *via* anion exchange purification on Hi Trap Q HP 5 mL, 1 M NaCl gradient in 20 mM Tris pH 7.5. SDS-PAGE showing the eluted protein fractions. **(e)** MS analysis of the purified, refolded TunD-His6. Expected mass: 52026, observed mass: 52026. **(f)** CD spectrum of 0.5 mg $mL^{-1}$ of refolded TunD sample in 50 mM Tris, pH 8.0, 250 mM NaCl.

We also dialysed the refolded TunD in HEPES buffer with and without $MgCl_2$ to see if salt affected the protein solubility. TunD is predicted to resemble a GT-B fold glycosyltransferase, which is metal-independent, thus the addition of metal ion should not have much affect on the protein. However, we did not want to rule out the possibility that divalent metal plays a role in the protein folding process. Based on the CD analysis, the protein sample after dialysis appeared to show no difference if $MgCl_2$ was added. The protein concentration was determined using BCA assay and the most concentrated protein obtained was about 2 mg $mL^{-1}$ before any precipitation occurred. Additionally, refolded TunD was also dialysed in presence of KCl, metals, and other buffer conditions and protein stabilising agents (see **Table 5.2**). We used the continuous spectrophotometric

glycosyltransferase activity assay to measure TunD activity (**Fig. 5.6**).[7] We ensured that the assay was functional by spiking the assay mixture with UDP as a positive control compared with a negative control without the presence of UDP-GlcNAc. Sadly, despite our efforts to observe any activity from the refolded TunD and by using the proposed substrates, *N*-acetyl-tunicamyl uracil (**3**) as the proposed acceptor and UDP-GlcNAc as the proposed donor, and other possible acceptors and donors, no activity was observed. The conditions and substrates used in the activity assay are summarised in **Table 5.2**.

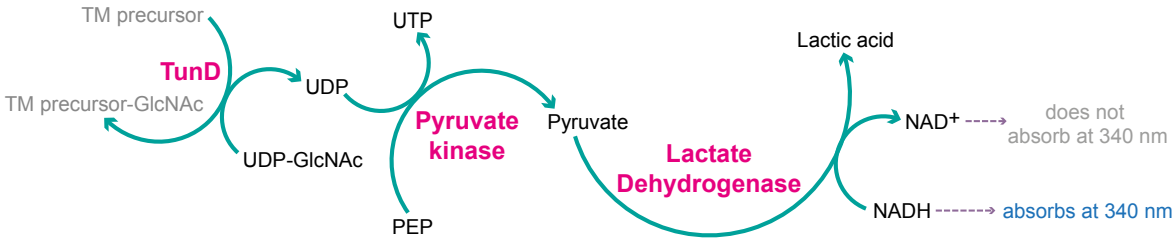


**Figure 5.6 | The continuous spectrophotometric glycosyltransferase activity assay.**[7] The activity assay continuously measures the absorbance of NADH at 340 nm. The consumption of NADH is represented by the decreased in absorbance.

**Table 5.2 | A summary of the combination of TunD reaction condition and substrates.**

| Assay* | TunD (μg mL$^{-1}$) | Buffer[a]* | Acceptor[b] | Donor[c] | Activity |
|---|---|---|---|---|---|
| 1 | 100 | B1, B2, B3, B4, or B5 | A1, A2, or A3 | D1 | No |
| 2 | 100 | B1, B2, or B3 | A2 | D1 | No |
| 3 | 100 | B1, B2, or B5 | A4 | D3 | No |
| 4 | 600 | B5 | A1, A5, A6, or A7 | D1, or D2 | No |
| 5 | 500 | B5, or B6 | A1, A5, A6, or A7 | D1, or D2 | No |
| 6 | 500 | B7 + 10 mM $MgCl_2$ | A1, A5, A6, or A7 | D1, or D2 | No |
| 7 | 500 | B7 + 10 mM $MnCl_2$ | A1, A5, A6, or A7 | D1, or D2 | No |

*Assay condition: standard assay mixture contains 10 mM $MgCl_2$.
temp. = 30 °C, volume = 100-200 μL
[a]Buffer:
B1 = 50 mM HEPES, pH 7.5, 5 mM $MgCl_2$, 10% glycerol
B2 = 50 mM HEPES, pH 7.5, 10% glycerol
B3 = 50 mM Tris, pH 8.0, 250 mM NaCl, 1mM TCEP, β-cyclodextrin
B4 = 50 mM Tris, pH 8.0, 250 mM NaCl, 1mM TCEP
B5 = 50 mM HEPES, pH 7.5, 5 mM $MgCl_2$, 250 mM KCl, 10% glycerol
B6 = 50 mM MOPS, pH 7.5, 5 mM $MgCl_2$, 250 mM KCl, 10% glycerol
B7 = 50 mM Tris, pH 8.0, 250 mM NaCl
B8 = 20 mM Tris, pH 8.0
[b]Acceptor:
A1 = *N*-acetyl-tunicaminyl uracil (**3**)
A2 = Glucosamine (Glu)

A3 = Galactosamine (Gal)
A4 = Glu, Gal, Fucose (Fuc), Fructose (Fru), Rhamnose (Rha), Mannose (Man), N-acetylglucosamine (GlcNAc), N-acetylgalactosamine (GalNAc), Glucose-6-phosphate (Glu6P), Fructose-6-phosphate (Fru6P), Ribose-6-phosphate (Rib6P), Galactosamine-1-phosphate (Gal6P), (**3**)
A5 = Glu, Gal, Fuc, Fru, Rha, Man, GlcNAc, GalNAc
A6 = Glu, Gal
A7 =Glc6P, Fru6P, Rib6P, Man6P, Gal1P
[c]Donor:
D1 = UDP-GlcNAc
D2 = UDP-Glc
D3 = UDP-Glc, UDP-Gal, UDP-GlcNAc, UDP-GalNAc, GDP-Man, GDP-Fuc, GDP-Glc

Due to the many unsuccessful attempts to observe any enzymatic activity from the refolded TunD sample, we screened the other 91 refolded TunD samples in iFOLD system. In the activity assay, we used GlcNAc as the acceptor and UDP-GlcNAc as the donor substrate. Since GlcNAc and UDP-GlcNAc were used as acceptor and donor, respectively, then the expected product would be GlcNAc-GlcNAc (m/z 424) if the refolded TunD sample acted as a glycosyltransferase upon the release of UDP (m/z 404). Unfortunately, no product was found by LCMS that correlated with the predicted mass.

We also set up crystallisation plates (**Table 5.3**). The refolded TunD sample was purified by cation exchange chromatography (**Fig. 5.7**). Ion exchange purification on refolded protein could separate forms of misfolded protein due to their differences in surface charge. Ion exchange purification of refolded TunD eluted as one peak and mass was confirmed by LCMS. The protein sample was co-crystallised with UDP-GlcNAc. We obtained several crystals, but unfortunately the X-ray diffraction from those crystals revealed as salt crystals.

**Table 5.3 | Crystallisation conditions**

| Plate | Condition | Observation | Result |
|---|---|---|---|
| 1 | JCSG | crystals | salt |
| 2 | PEG/ION | crystals | salt |
| 3 | STRUCTURE | - | - |
| 4 | PACT | - | - |

We were puzzled with the refolded TunD sample not showing any activity on proposed substrates and from other acceptors and donors screened, thus we investigated if there is any biomolecular interaction between the refolded TunD and the selected donors and acceptors. This led us to carry out substrate-protein binding studies. For the binding studies, to determine if the proposed substrates have any kind of interaction with the refolded TunD sample, isothermal titration calorimetry (ITC) was used. ITC is a powerful instrument to study biomolecular interactions. It measures the heat released/absorbed during binding events. From a single experiment several binding parameters can be determined simultaneously (n, reaction stoichiometry; Kb, binding constant; ΔH, enthalpy; Δ S, entropy). ITC experiments were carried out using the proposed donor UDP-GlcNAc and acceptor *N*-acetyl-tunicaminyluracil. Due to the nature of glycosyltransferase, it can be metal-dependent or –independent and the presence of donor and divalent metals have been reported in the literature to induce conformational changes in the enzyme that would open another active site for the binding of the acceptor.[3] However, as previously mentioned, since TunD is predicted to have the GT-B fold as metal-independent glycosyltransferase, we did not want to rule out the possibility of metal-dependency or in protein stability. Presumably, the induced conformational change would appear to have biomolecular interaction of the enzyme and the proposed acceptor *N*-acetyl-tunicaminyl uracil and that would allow us to detect any biomolecular interactions. Unfortunately, the ITC

experiments showed no biomolecular interactions between the refolded TunD with UDP-GlcNAc or *N*-acetyl-tunicaminyl uracil. Moreover, no interaction was observed in the presence of divalent metal ($Mg^{+2}$, $Mn^{+2}$, $Ca^{+2}$), nor in the presence of divalent metal with sugar nucleotide present (UDP-GlcNAc).

From our efforts to recapitulate the TunD activity *in vitro,* the enzymatic activity of TunD remained a mystery. There are several potential reasons that might explain why we were not able to observe any activity from TunD. It could be that the refolded TunD may not have folded properly, the substrates we used were not the correct ones, the TunD substrate may be the lipid intermediate shown in **Fig. 5.1**, or TunD forms a complex with other enzymes in the tunicamycin biosynthetic pathway in order to carry out the activity. With regards to TunD solubility, TunD could attempt expression in a *Streptomyces* host. Alternatively, as mentioned before, on the overlap of the genes in the *tun* gene cluster, TunD can be co-expressed with other proteins in the pathway that may assist in protein folding, stability, complex formation, and activity.

### 5.3 Gene analysis of *tunE*

The TunE is predicted to be a putative *N*-deacetylase in the tunicamycin bio-synthetic pathway.[1] Based on homology comparison, TunE belongs to the PIG-L super-family of enzymes.[1,2] TunE has an HPDD zinc-binding motif. Thus, it is proposed that TunE catalyses a $Zn^{2+}$-mediated cleavage of either **3**, **4**, or the lipid substrate intermediate to reveal the free amine in preparation for the addition of the lipid chain or the GlcNAc in the tunicamycin biosynthetic pathway, as previously discussed in **Fig. 5.1**. *In vitro* functional characterisation of TunE would allow selective deacetylation at position 10’ of **3**

or **4**. This would not only allow selective addition of lipid chains to create specific tunicamycin homologues but also a selection of tunicamycin analogues *via* amine alkylation or acylation.

**Table 5.4 | TunE amino acid sequence.** The HPDD zinc-binding motif is highlighted.

| Protein | Amino acids | Amino acid sequence | MW (avg.) / pI |
|---|---|---|---|
| Native TunE | 234 | VKVLVIAAHPDDEVLGAGATVSALSQQGAVVQIHILAEGISLRH SGVKIEEARERCQVAAKDLGAAEVSFGGLAADGRLLADLPQR QVVDAVSHALREAEPEVVFTHHPGDIHADHRSVAHAVGYGTR ILGSGSVRQVLHFEVLSSTEQQTGLVAPFTPNLFYDVTGHVEA KCRALAAYPYELYDPPHPRSLAAVRTLASYRGTQVGVEAAEA FMIGRELRGPMAAVPSGVDVR | Mw = 24799 Da<br>pI = 5.93 |

### 5.3.1 Recombinant Protein Expression of TunE in *E. coli*

Previously, in the work that was carried in our the group by F. J. Wyszyński, TunE was heterologously expressed in *E. coli* as a recombinant protein.[2] An extensive array of expression hosts and conditions were screened and the *E. coli* BL21(DE3)/pET-28a:*tunE* expression system resulted in the low quantity of soluble $His_6$-TunE protein. HPLC was used to carry out the TunE activity assay to detect the deacetylation of **3**, but no activity or product was found.

We repeated the $His_6$-TunE (26,994 Da) expression in *E. coli* BL21(DE3)/ pET-28a:*tunE* expression system and managed to isolate partially soluble $His_6$-TunE protein (**Fig. 5.7**).

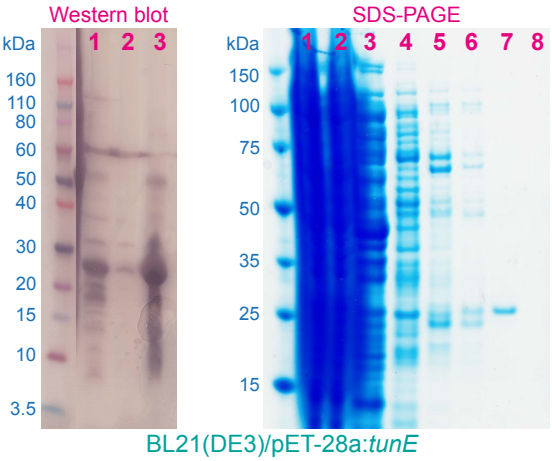


**Figure 5.7 | TunE expression.** Western blot, lanes 1-3 correspond to cell lysate, soluble fraction, inclusion bodies. SDS-PAGE shows the $His_6$-TunE (~ 27 kDa) fractions collected from manual Ni-NTA purification. Lane 7 shows the solubilised TunE.

### 5.3.2 HPLC activity assay of TunE

We also reassessed the enzyme activity using substrates **3** and **4**. Furthermore, since we were intrigued with the fact that there may be harmonious protein interaction in the tunicamycin biosynthetic pathway due to the overlap of the genes in the *tun* gene cluster, we tested TunE with TunD in a complementation reaction.

In the TunD and TunE complementation HPLC assay (**Fig. 5.8** and **5.9**), the proposed substrate and product clearly showed distinct differences in the chromatogram. The activity assay for TunD used *N*-acetyl-tunicamyl uracil (**3**) and UDP- GlcNAc. Reaction was initiated after adding TunD and incubated at 30 °C for one hour. A sample of the reaction mixture was used for HPLC analysis. In the complementation assay, using the same TunD reaction mixture, TunE was added. This was to investigate if the proposed pathway from TunD to TunE was able to yield the proposed product (**Fig. 5.9**). The same process was carried out for TunE and then TunD. Unfortunately, based the HPLC complementation assay, no activity or product was observed from either TunD or TunE.

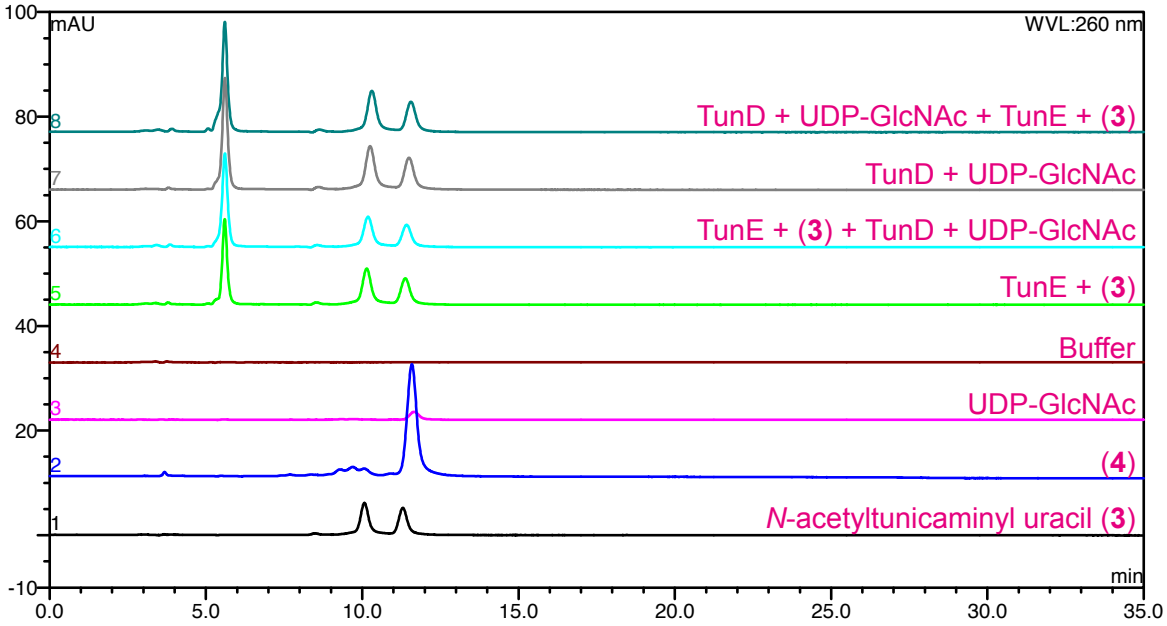


**Figure 5.8 | TunD and TunE HPLC assay.** Overlap of HPLC chromatograms, 260 nm. No product (**4**) was detected from the reactions.

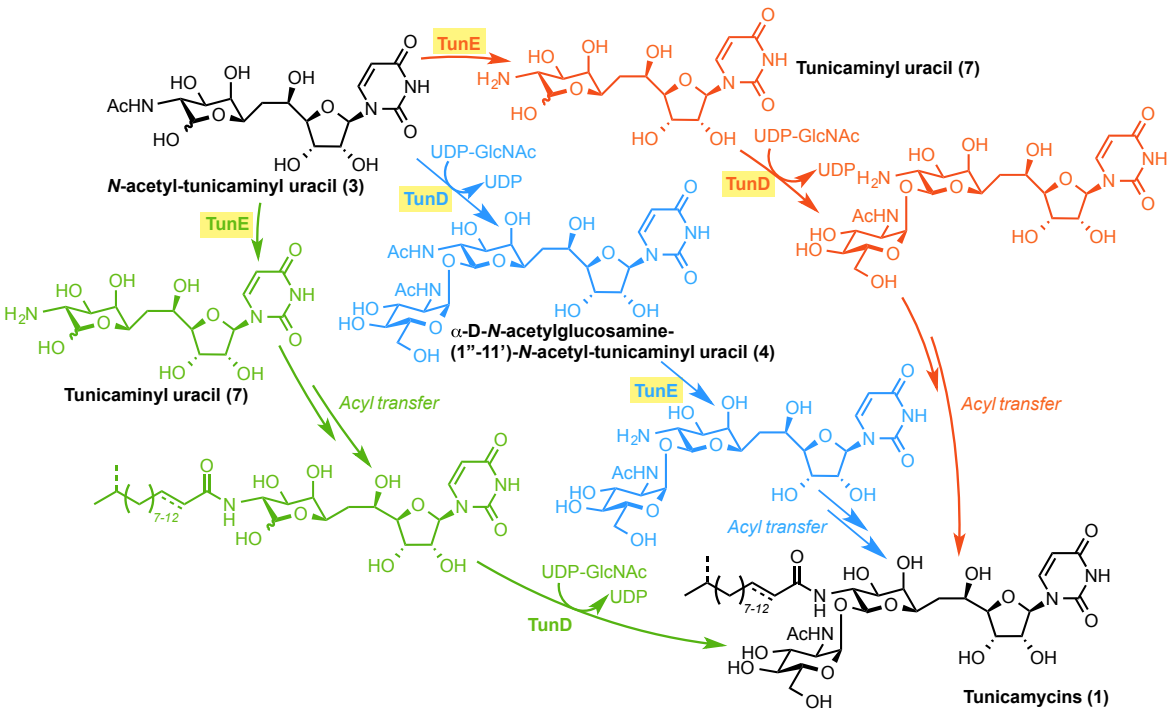


**Figure 5.9 | The three proposed enzymatic pathways for TunD and TunE in the tunicamycin biosynthetic pathway.**[2] This is the same figure as **Fig. 5.1**.

## 5.4 Conclusion and Outlook

The activity for TunD and TunE was not determined. The challenge in TunD and TunE was mainly in protein expression and the isolation of soluble proteins. Despite our efforts to improve protein expression, to refold TunD, and carrying out binding and activity assays, none of these methods showed any activity with our proposed substrates. The protein refolding attempts were promising, but we were unable to confirm properly folded TunD without the crystal structure or recapitulation of its activity. Although we were able to obtain the soluble TunD from refolding, it did not confirm properly folded protein. The CD analysis was limited to mainly secondary structure analysis. The tertiary structure analysis could be done at 320-260 nm where aromatic amino acids and disulfide bonds can provide some form of indication for three dimensional structure (incorrect fold or molten-globule), but this would still be a challenge without a clear indication of a similar protein or able to show the protein activity. The complementation activity assay with TunD and TunE would be an interesting approach for future work when working with soluble proteins. Nonetheless, this led us to consider other heterologous host expression systems and alternatively to reevaluate the tunicamycin biosynthetic pathway. Based on the complementation studies of *tunB* and *tunF* knockout heterologous expression of tunicamycins in *S. coelicolor* (see **Chapter 4**), *S. coelicolor* or other *Streptomyces* strains could be used as a potential host for protein expression. In the complementation strains, the *tunB* or *tunF* gene was reintroduced back in respected *S. coelicolor* knockout strain. This was similarly done by Park *et al.*[8] and is a promising approach for TunD expression. Moreover, we reconsidered the interpretation of the *tun* gene cluster, instead of viewing the each gene product individually as one, the overlap of the genes in the pathway may suggest co-expression, equivalences in expression, or complex formation that is needed for

*tun* proteins solubility, stability or activity. Thus, alternative host expression system or co-expression system would be an ideal approach to solve the TunD and TunE expression problem.

## 5.5 References

1 Wyszynski, F. J., Hesketh, A. R., Bibb, M. J. & Davis, B. G. Dissecting tunicamycin biosynthesis by genome mining: cloning and heterologous expression of a minimal gene cluster. *Chem. Sci.* **1**, 581-589 (2010).

2 Wyszyński, F. J. Dissecting tunicamycin biosynthesis: A potent carbohydrate processing enzyme inhibitor *D.Phil. thesis, University of Oxford*, (2010).

3 Lairson, L. L., Henrissat, Davies, G. J. & Withers, S. G. Glycosyltransferases: Structures, Functions, and Mechanisms. *Annu. Rev. Biochem.* **77**, 521-555 (2008).

4 Wagner, S. et al. Tuning Escherichia coli for membrane protein overexpression. *PNAS* **105**, 14371-14376 (2008).

5 Vallin, C. et al. Streptomyces as a host for the secretion of heterologous proteins for the production of biopharmaceuticals. *Journal of Business Chemistry* **2**, 107-111 (2005).

6 Romier, C. et al. Co-expression of protein complexes in prokaryotic and eukaryotic hosts: experimental procedures, database tracking and case studies. *Acta. Cryst.* **D62**, 1232-1242 (2006).

7 Gosselin, S., Alhussaini, M., Streiff, M. B., Takabayashi, K. & Palcic, M. M. A Continuous Spectrophotometric Assay for Glycosyltransferases. *Analytical Biochemistry* **220**, 92-97 (1994).

8 Park, J. W. et al. Discovery of parallel pathways of kanamycin biosynthesis allows antibiotic manipulation. *Nature Chemical Biology* **7**, 843-852 (2011).

# *Chapter Six*

## *Summary*

### 6.1 Chapter One: *An Introduction to Tunicamycins and the Bacterial Cell Wall*

The central objective of this thesis was to develop novel tunicamycin analogues that are non-toxic to eukaryotic cells as potential antimicrobial drug candidates. We hypothesised that by retaining the lipid character of tunicamycin structure and modifying the GlcNAc moiety then the antimicrobial activity would be retained but the tunicamycins inhibitory action towards GPT would be abolished, thus diminishing tunicamycins cytotoxicity towards mammalian cells. When we envisioned the tunicamycin analogue design, taking into consideration of what has been reported in the literature, we chose not to modify the uracil or the tunicamine moieties of tunicamycin as both are speculated to interact with MraY. Whilst the importance of the tunicaminyl uracil scaffold in anti-bacterial activity and the GlcNAc moiety in mammalian cell cytotoxicity are reported, the GlcNAc and/or aliphatic chain have never been directly shown to contribute to either. More so, we were particularly interested in modifying the GlcNAc moiety to reduce the structural similarity of tunicamycin to UDP-GlcNAc but to retain the carbon chain and its lipid character.

We devised a semi-synthetic approach to isolate the tunicamycins from *S. chartreusis* and then chemically degrade the tunicamycins to isolate the core scaffolds and additionally use those scaffolds to synthesise the novel tunicamycin lipid analogues. Moreover, the scaffolds may be used as intermediate substrates for the *tun* enzymes and

also in the investigation of the biological properties of the tunicamycin core scaffolds and the lipid analogues to fill the gap in the literature regarding the influence of the lipid chain.

**6.2 Chapter Two:** *Semi-synthesis of Tunicamycin Core Scaffolds and Lipid Analogues*

In this chapter, two tunicamycin core scaffolds (**3, 4**) have been isolated in addition to the dihydrochloride salt (**9**) of tunicamycins. The semi-synthetic strategy presented here enables further fine-tuning of the tunicamycin core scaffold for the development of novel antimicrobial drug candidates. More importantly, the dihydrochloride salt (**9**) template has enabled selective lipid chain addition to both the 10'-*N* and 2"-*N* positions of tunicamycin. This has allowed the selective addition of lipid chains to be added, thereby creating the first library of novel tunicamycin lipid analogues. The outlook for this template **9** is extremely promising for applications as therapeutics and chemical probes. With a library of tunicamycin core scaffolds and lipid analogues, the biological properties of tunicamycins can now be assessed to understand the importance of the GlcNAc, the presence of the lipid chain, and the effect of the lipid chain length. In summary, we have developed a semi-synthetic strategy to synthesise tunicamycin analogues with a defined lipid chain, a modified GlcNAc moiety, and a final product that is not a mixture of homologues. This semi-synthetic strategy has allowed the development of the first tunicamycin lipid analogues known to date.

**6.3 Chapter Three:** *Biological Evaluations of the Tunicamycin Core Scaffolds and Lipid Analogues*

The tunicamycin homologues are reported to exhibit different levels of *N*-linked glycosylation inhibition in eukaryotic cells, but little is described about their individual

antimicrobial activity.[1-7] Whilst it is proposed that the tunicaminyl uracil scaffold acts as a UDP mimic[8] and the GlcNAc moiety contributes to the mammalian cytotoxicity, the GlcNAc has ever been directly shown to cause the cytotoxicity.[9-11] Moreover, it has been speculated that the lipid chain on tunicamycin homologues influences their biological activity, but again, this has never been directly shown to be associated with the antibacterial or the mammalian cytotoxic activities.[1-7,12]. Thus, we investigated the biological activities of the tunicamycin core scaffolds and the novel lipid analogues to understand their mode of action.

Firstly, our results have shown the importance of the lipid chains for the toxic activity in both eukaryotic and prokaryotic systems. For the first time, we have shown that in prokaryotic and eukaryotic systems, tunicamcyins inhibitory properties are abolished in absence of their lipid chain. Early studies succeeded in only showing longer chain homologues are generally more biologically active in prokaryotes, whereas shorter chain homologues are generally more active in eukaryotes.[1-7] In addition, the tunicamycin lipid analogues were found to be potent antibacterial agents, revealing a titrated inhibitory effect that is dependent upon their lipid chain length. This suggests that the use of tunicamycins as a mixture of their homologues should be carefully evaluated to minimise ambiguity. Our results further showed that from our library of lipid analogues, the cytotoxicity can be drastically reduced while maintaining nanomolar antibacterial potency by modifying the GlcNAc moiety of tunicamycin with the addition of an lipid chain that is between seven to twelve carbons in length. These revealed the importance and effect of the chain length and GlcNAc modification on tunicamycin on the antibacterial activity and mammalian cytotoxicity. In essence, these results supported our hypothesis that by retaining the lipid

character of the tunicamycin structure and modifying the GlcNAc moiety then the antimicrobial activity would be retained but the inhibitory action towards GPT would be abolished, thus eliminating tunicamycins cytotoxicity towards mammalian cells (**Chapter 1**).

Moreover, our biological evaluations highlighted the essential role for the lipid chain in tunicamycins function and importance of retaining hydrophobic character in designing tunicamycin analogues. This may further suggest the hydrophobic interaction mechanisms of tunicamycins with either lipid membranes or target enzymes, as reported in yeast protoplast through the interaction between tunicamycins and the cell membrane phospholipids.[3-5,12,13] However, it remains to be seen whether our lipid analogues will be effective against tunicamycin resistant strains.[4,12] While we have revealed the importance of the tunicamycins lipid chain on antibacterial activity and modification of GlcNAc moiety on mammalian cell cytotoxicity, it is not known whether the analogues exhibited any interaction with MraY translocase or GPT, or induced any ER stress response. Future work could include real-time PCR, kinetic, inhibition, and crystallisation studies. Regardless, our scaffolds could assist with the design of the next generation of tunicamycin analogues to study the molecular basis for the inhibition and resistance mechanism in prokaryotes and eukaryotes (**Chapter 1**).

More importantly, we have developed a set of tunicamycin lipid analogues that are as effective as tunicamycins as antibacterial agents but without the mammalian cytotoxicity effect. In comparison to tunicamycins, our lipid analogues have relative therapeutic index values up to several thousand folds more than tunicamycins.

Additionally, we have not only developed a set of promising antimicrobial drug candidates but also a set of promising anti-*M. tb* drug candidates.

**6.4 Chapter Four:** *Investigation of the tunB and tunF Knockout in the tun Gene Cluster*

The products of TunA and TunF were investigated.[14] Amino acid sequence homology analyses revealed structural similarity of TunA to NAD-dependent epimerase/ dehydratases and TunF to 4-OH-sugar epimerases.[15] Previously, the recapitulation of TunA activity *in vitro* and in addition with the TunA crystal structure, TunA was observed to be the first natural enzyme to exhibit NDP-sugar 5,6-dehydrogenase activity. The formation of the GalNAc-*exo*-glycal intermediate suggests, in turn, that the tunicamine backbone may, in fact, be the product of an exciting radical addition mechanism. To test these hypotheses, *tunB* and *tunF* mutated strains of *Streptomyces* heterologous host were made to test these possibilities of TunA's unique control of reductive regioselective enzymatic reaction and the formation of intriguing *exo*-glycal intermediates.

We made individual *tunB* and *tunF* knockout by PCR-targeting. The *tunB* knockout studies were successful in showing the *exo*-glycal product of TunA, and indicated the importance of TunB enzyme in the tunicamycins biosynthetic pathway. The possibility of other epimerase in the *S. coelicolor* may resulted in the minuscule production of tunicamycins found in the *tunF* knockout studies, but the tunicamycins in the methanol extract from *tunF*(-) strain appeared to retain the galactose and not the glucose configuration for the tunicamine scaffold. Lastly, it would be interesting to engineer the tunicamycin biosynthetic pathway to produce tunicamycin analogues. This is not far fetched as our complementation studies were able to restore the tunicamycins production and engineering

the pathway with enzymes that perform similar or different enzymatic process may be worth of future pursuit to create tunicamycin analogues.

**6.5 Chapter Five:** *Investigation of the TunD and TunE Enzymatic Activities in the Tunicamycin Biosynthetic Pathway*

TunD and TunE are the putative glycosyltransferase and *N*-deacetylase, respectively, in the tunicamycin biosynthetic pathway.[15,16] Since the order of TunD and TunE is uncertain, three possible pathways for TunD and TunE have been proposed.[16] The two proposed substrates, **3** and **4**, for either TunD or TunE were prepared from chemical degradation of crude tunicamycins isolated from *S. chartreusis* NRRL3882 discussed in **Chapter 2**. The functional characterisation of TunD and TunE would provide insights to the unique biological chemistry that could enable us to construct tunicamycin analogues *in vitro* and engineer the pathway to create tunicamycin analogues.

The activity for TunD and TunE was not determined. The challenge in TunD and TunE was mainly in protein expression and the isolation of soluble proteins. Despite our efforts to improve protein expression, to refold TunD from inclusion bodies, and carrying out binding and activity assays, none of these methods showed any activity with our proposed substrates. The protein refolding attempts were promising, but we were unable to confirm properly folded TunD without the crystal structure or recapitulation of its activity. This led us to consider other heterologous host expression systems and alternatively to reevaluate the tunicamycin biosynthetic pathway. In the complementation strains, the *tunB* or *tunF* gene was introduced back in respected *S. coelicolor* knockout strain. This was similarly done by Park *et al.*[17] and is a promising approach for TunD expression.

Moreover, we reconsidered the interpretation of the *tun* gene cluster, instead of viewing the each gene product individually as one, the overlap of the genes in the pathway may suggest co-translation, equivalences in expression, or multi-complex formation that is needed for *tun* proteins solubility, stability or activity. Thus, alternative host expression system or co-expression system would be an ideal approach to solve the TunD and TunE expression problem.

## 6.6 References


1 Mahoney, W. C. & Duskin, D. Biological activities of the two major components of tunicamycin. *J. Biol. Chem.* **254**, 6572-6576 (1979).

2 Keenan, R. W., Hamill, R. L., Occolowitz, J. L. & Elbein, A. D. Biological Activities of Isolated Tunicamycin and Streptovirudin Fractions. *Biochemistry* **20**, 2968-2973 (1981).

3 Duksin, D. & Mahoney, W. C. Relationship of the Structure and Biological Activitoyf the Natural Homologues of Tunicamycin. *J. Biol. Chem.* **257**, 3105-3109 (1982).

4 Duskin, D., Seiberg, M. & Mahoney, W. C. Inhibition of Protein Glycosylation and Selective Cytotoxicity toward Virally Transformed Fibroblasts Caused by B3-Tunicamycin. *Eur. J. Biochem.* **129**, 77-80 (1982).

5 Seiberg, M. & Duksin, D. Selective Cytotoxicity of Purified Homologues of Tunicamycin on Transformed BALB/3T3 Fibroblasts. *Cancer Res.* **43**, 845-850 (1983).

6 Eren, R. & Duskin, D. Inhibition of the formation of lipid-linked intermediates in normal and transformed cells by a purified tunicamycin homologue. *Molecular and Cellular Biochemistry* **67**, 39-46 (1985).

7 Kamogashira, T., Takegata, S. & Sugiura, K. Isolation of Tunicamycin Produced by Bacillus cereus K-279. *Agric. Biol. Chem.* **52**, 859-861 (1988).

8 Xu, L., Appell, M., Kennedy, S., Momany, F. A. & Price, N. P. J. Conformational Analysis of Chirally Deuterated Tunicamycin as an Active Site Probe of UDP-N-Acetylhexosamine:Polyprenol-P N-Acetylhexosamne-1-P Translocases. *Biochemistry* **43**, 13248-13255 (2004).

9 Heifetz, A., Keenan, R. W. & Elbein, A. D. Mechanism of Action of Tunicamycin on UDP-GlcNAc:Dolichyl-Phosphate GlcNAc-1-Phosphate Transferase. *Biochemistry* **18**, 2186-2192 (1979).

10 Lehrman, M. A. Biosynthesis of N-acetylglucosamine-P-P-dolichol, the committed step of asparagine-linked oligosaccharide assembly. *Glycobiology* **1**, 553-562 (1991).

11 Price, N. P. & Momany, F. A. Modeling bacterial UDP-HexNAc: polyprenol-P HexNAc-1-P transferases. *Glycobiology* **15**, 29R-42R, doi:10.1093/glycob/cwi065 (2005).

12 Kuo, S. C. & Lampen, O. Tunicamycin Inhibition of [3H] Glucosamine Incorporation into Yeast Glycoprotein: Binding of Tunicamycin and Interaction with Phospholipids. *Archives of Biochemistry and Biophysics* **172**, 574-581 (1976).

13 Tkacz, J. S. & Lampen, J. O. Tunicamycin Inhibition of Polyisoprenyl N-Acetylglucosaminyl Pyrophosphate Formation in Calf-Liver Microsomes. *Biochem. Biophys. Res. Commun.* **65**, 248-257 (1975).

14 Wyszynski, F. J. *et al.* Biosynthesis of the tunicamycin antibiotics proceeds via unique exo-glycal intermediates. *Nature Chemistry* **4**, 539-546 (2012).

15 Wyszynski, F. J., Hesketh, A. R., Bibb, M. J. & Davis, B. G. Dissecting tunicamycin biosynthesis by genome mining: cloning and heterologous expression of a minimal gene cluster. *Chem. Sci.* **1**, 581-589 (2010).

16 Wyszyński, F. J. *Dissecting tunicamycin biosynthesis: A potent carbohydrate processing enzyme inhibitor* D.Phil. thesis, University of Oxford, (2010).

17 Park, J. W. *et al.* Discovery of parallel pathways of kanamycin biosynthesis allows antibiotic manipulation. *Nature Chemical Biology* **7**, 843-852 (2011).

# *Chapter Seven*

## *Outlook*

The following subsections are discussion of preliminary results and future directions that may be useful in creating tunicamycins analogues, studying the molecular basis of the MraY enzyme mechanism, understanding the tunicamycins biosynthetic pathway, and expanding the use of tunicamycins core scaffolds as chemical tools or other therapeutic applications discussed in **Chapter 1**. Methods and preliminary results can be found in the **Experimental** and the **Appendix**.

### 7.1 Semi-synthesis of *N*-acetyl-tunicaminyl uracil analogues

The methodology used to isolate the dihydrochloride salt of tunicamycins (**9**), discussed on **Chapter 2**, may also be employed to isolate the tunicaminyl uracil hydrochloride salt (**7**). The interesting feature of this core scaffold is the absence of the GlcNAc. Although we have discussed the implications of the presence of the GlcNAc moiety that contributes to the overall mimicry of UDP-GlcNAc substrate and also the sensitivity of tunicamycin structure losing its bioactivity from minor modifications, it would be interesting to use this core scaffold for lipid analogues and other biological applications as discussed in **Chapter 1**.

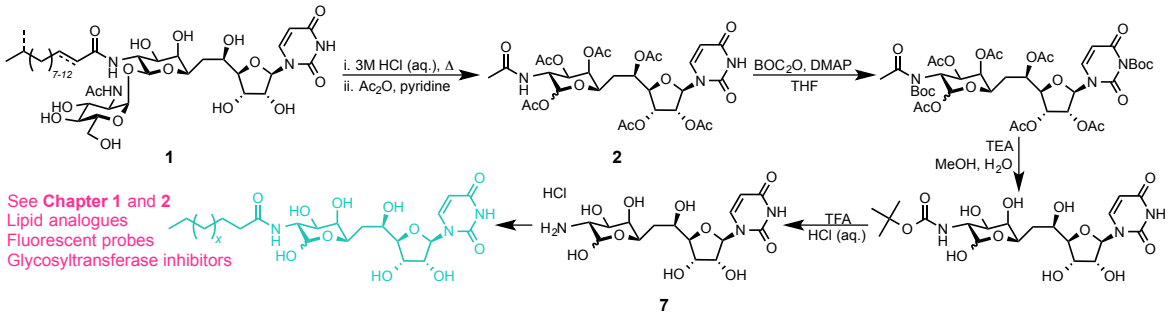


**Figure 7.1 | Semi-synthetic route towards tunicaminyl uracil dihydrochloride salt (7) and analogues.**

## 7.2 Towards a continuous UMP-coupled assay (PAP-PK-LDH-coupled assay)

The study of MraY and the PNPTs family of enzymes are not only limited due to their nature as integral membrane proteins but also because there are limited methods available to evaluate their activity. Current methods have mainly relied on radio-labelling or placing fluorescent tags on the substrate.[1-4] Furthermore, the PK-LDH coupled assay for glycosyltransferases has been limited to NDP-released enzymatic reactions.[5] A high throughput assay is proposed for MraY, PNPTs family of enzymes, and NMP-release enzymes. The idea is to modify the conventional continuous spectrophotometric assay for NDP dependent glycosyltransferase for NMP-release enzymes. If UMP is to convert to UDP, UMP kinase could be used. However, ATP is required for UMP kinase and this reaction would release ADP as a by-product. With UDP and ADP in the reaction mixture for continuous spectrophotometric assay, pyruvate kinase will take both ADP and UDP as substrate to phosphorylate phosphoenolpyruvate (PEP). Thus, UMP from MraY enzymatic reaction needs to be phosphorylated in a manner that does not depend on ATP. Poly-phosphate has been known for some time to be a source of energy storage in organism, and polyphosphate-phosphotransferase is known to use polyphosphate to phosphorylate NDP sugars. More importantly, there is a polyphosphate:AMP-phosphotransferase (PAP), which

is a polyphosphate-dependent nucleoside monophosphate kinase.[6-10] PAP has been shown to also phosphorylate other nucleoside sugars with different specificities dependent on the reaction condition. Here we begin to explore possibly a novel continuous spectrophotometric assay for MraY transferase and other enzymatic reactions that release NMP as a by-product.

The introduction of PAP to the PK-LDH coupled assay system would allow for the continuous assessment of NMP-release enzymes (**Fig. 7.2**). This would be a valuable tool for studying enzyme kinetics. PAP was recombinantly expressed in *E. coli*. Preliminary tests of the PAP-PK-LDH-coupled assay have shown promising results. Further optimisation would be required.

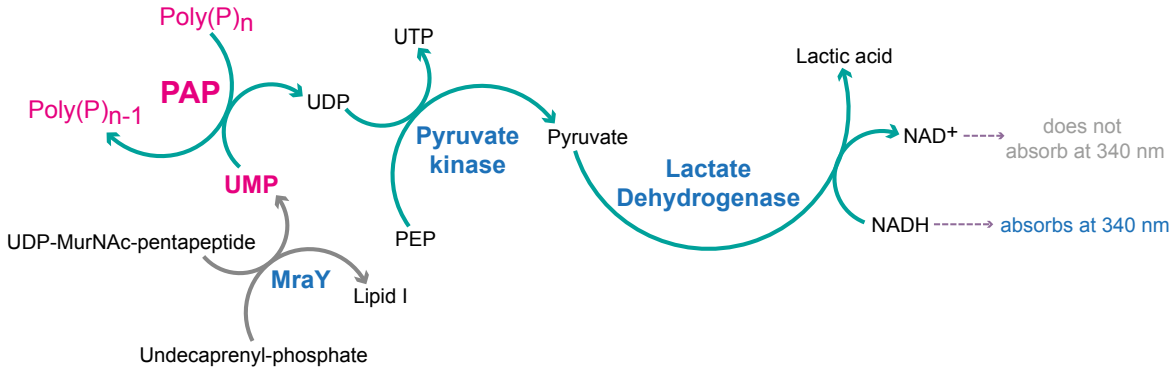


**Figure 7.2 | PAP-PK-LDH coupled assay system.**

### 7.3 Isolation of the UDP-MurNAc-pentapeptide

One of many limitations to study the bacterial cell wall is the difficulty in obtaining the peptidoglycan precursors. UDP-MurNAc-pentapeptide is a substrate used by MraY translocase in the synthesis of the Lipid I, a building block to the peptidoglycan. In our development of tunicamycin lipid analogues and evaluations of the antibacterial activities,

we did not carry out MraY inhibition studies to evaluate the kinetic properties of the lipid analogues. Thus, MraY inhibition studies would help to understand the inhibitory mechanisms of the lipid analogues and can also help in designing the next generation of tunicamycin analogues. The protocols from the literature were followed and UDP-MurNAc-pentapeptide was extracted from *Bactillus subtilis* W23 culture.

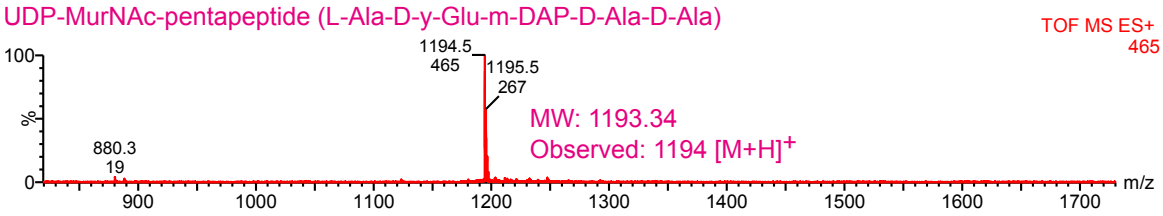


**Figure 7.3 | MS analysis of UDP-MurNAc-pentapeptide extract from *B. subtilis* W23.**

## 7.4 *N*-acetyl-tunicaminyl uracil as putative inhibitors of glycosyltransferase and kinases

Tunicamycins are proposed to inhibit the PNPTs family of enzymes by mimicking the UDP and chelating with a magnesium ion at the active site, as discussed in **Chapter 1**. We investigated if the tunicamine core mimics UDP, as this could be very helpful to know in developing better inhibitors for MraY and for biochemical tools to study glycosyltransferases. We carried out OtsA inhibition assay, using the PK-LDH coupled assay system, with *N*-acetyltunicaminyl uracil.[5] Our preliminary results showed mild inhibition, but further investigation is needed to confirm the inhibitory action. A mild inhibition was also observed in the PK-LDH system alone, thus it may be possible that the pyruvate kinase is also inhibited by *N*-acetyltunicaminyl uracil.

The crystal structure for OtsA has been reported,[11] which makes OtsA a good co-crystallisation candidate with *N*-acetyltunicaminyl uracil. We isolated OtsA and carried out differential scanning fluorometry analysis to investigate the *N*-acetyltunicamyl uracil interaction with OtsA. It appeared to have a similar interaction as the natural substrates that may indicate enzyme-substrate interaction (**Fig. 7.4**), but further analysis is needed.[12] Then, we prepared crystallisation plates by the hanging-drop method with OtsA protein soaked in *N*-acetyltunicaminyl uracil (**Fig. 7.4**). We were able to obtain protein crystals, but they were poorly scattered. These were promising preliminary results. The future work to attempt co-crystallisation using other crystallisation conditions may able to obtain crystals that can be scattered and to determine if the *N*-acetyltunicaminyl uracil is present in the OtsA active site.

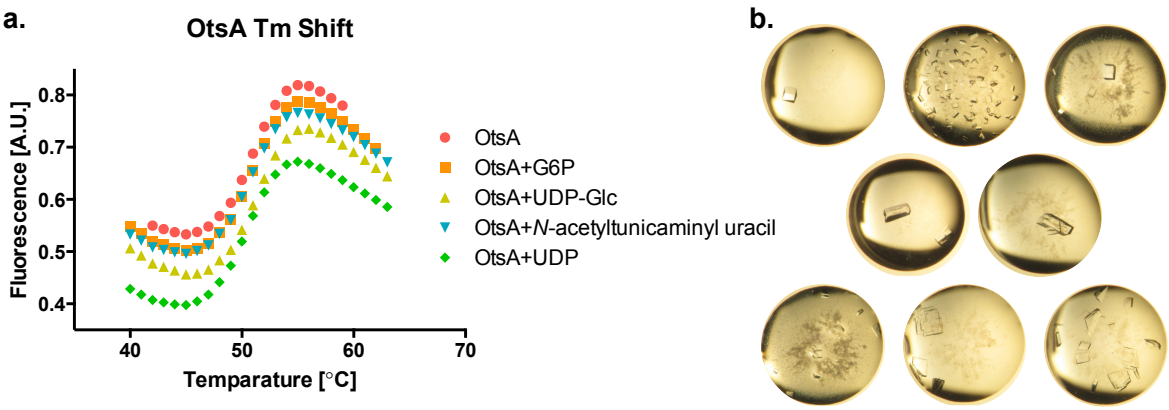


**Figure 7.4 | OtsA Tm shift and and crystals. (a)** The Tm shift of OtsA with natural substrates and *N*-acetyltunicaminyl uracil. **(b)** OtsA crystals in *N*-acetyltunicaminyl uracil solutions.

## 7.5 References


1 Branstrom, A. A. et al. Assay for Identification of Inhibitors for Bacterial MraY Translocase or MurG Transferase. *Analytical Biochemistry* **280**, 315-319 (2000).

2 Hyland, S. A. & Anderson, M. S. A high-throughput solid-phase extraction assay capable of measuring diverse polyprenyl phosphate: sugar-1-phosphate transferases as exemplified by the WecA, MraY, and MurG proteins. *Analytical Biochemistry* **317**, 156-164 (2003).

3 Stachyra, T. et al. Fluorescence Detection-Based Functional Assay for High-Throughput Screening for MraY. *Antimicrob*. *Agents Chemother*. **48**, 897-902 (2004).

4 Schouten, J. A. et al. Fluorescent reagents for in vitro studies of lipid-linked steps of bacterial peptidoglycan biosynthesis: derivatives of UDPMurNAc-pentapeptide containing D-cysteine at position 4 or 5. *Mol*. *BioSyst*. **2**, 484-491 (2006).

5 Gosselin, S., Alhussaini, M., Streiff, M. B., Takabayashi, K. & Palcic, M. M. A Continuous Spectrophotometric Assay for Glycosyltransferases. *Analytical Biochemistry* **220**, 92-97 (1994).

6 Pick, U., Bental, M., Chitlarua, E. & Weiss, M. Polyphosphate-hydrolysis- a protective mechanism against alkaline stress? *FEBS* **274**, 15-18 (1990).

7 Bonting, C. F. C., Korstee, G. J. J. & Sehnder, A. J. B. Properties of Polyphosphate:AMP Phosphotransferase of Acinetobacter Strain 210A. *Journal* of *Bacteriology* **173**, 6484-6488 (1991).

8 Ishige, K. & Noguchi, T. Polyphosphate:AMP Phosphotransferase and Polyphosphate:ADP Phosphotransferase Activities of Pseudomonas aeruginosa. *Biochemical and Biophysical Research communications* **281**, 821-826 (2001).

9 Shiba, T. et al. Polyphosphate:AMP Phosphotransferase as a Polyphosphate-Dependent Nucleoside Monophosphate Kinase in Acinetobacter johnsonii 210A. *Journal of Bacteriology* **187**, 1859-1865 (2005).

10 Nocek, B. et al. Polyphosphate-dependent synthesis of ATP and ADP by the family-2 polyphosphate kinases in bacteria. *PNAS* **105**, 17730-17735 (2008).

11 Gibson, R. P., Lloyd, R. M., Charnock, S. J. & Davies, G. J. Characterization of Escherichia coli OtsA, a trehalose-6-phosphate synthase from glycosyltransferase family 20. *Acta Crystallographica Section D* **D58**, 349-351 (2002).

12 Niesen, F. H., Berglund, H. & Vedadi, M. The use of differential scanning fluorimetry to detect ligand interactions that promote protein stability. *Nature Protocols* **2**, 2212-2221 (2007).

# *Experimental*

## *Chemical Syntheses and Characterisations*

***General considerations***

Proton nuclear magnetic resonance ($\delta_H$) spectra were recorded on Bruker DPX 200 (200 MHz), Bruker DPX 400 (400 MHz), Bruker DQX 400 (400 MHz), Bruker AVC 500 (500 MHz), or Bruker AV 700 (700 MHz) spectrometer. Carbon nuclear magnetic resonance spectra were recorded on DPX 200 (50 MHz), Bruker DQX 400 (100 MHz), Bruker AVC 500 (125 MHz) with a $^{13}C$ cryoprobe (125 MHz), or Bruker AV 700 (176 MHz) with a $^{13}C$ cryoprobe (176 MHz). Spectra were fully assigned using a combination of $^{1}H$, $^{13}C$, HSQC, HMBC, COSY, and TOCSY. All chemical shifts were quoted on δ-scale in ppm, with residual solvent as internal standard. Coupling constants (*J*) are reported in hertz (Hz). Infrared spectra were recorded on a Bruker Tensor 27 Fourier Transform spectrophotometer recorded in wave numbers ($cm^{-1}$). Low-resolution mass spectra were recorded on a LCT Premier XE using electrospray ionisation (ES). High-resolution mass spectra were recorded on a Bruker microTOF. Specific rotations were measured on Perkin Elmer 241 polarimeter, or Perkin Elmer 341 polarimeter, with pathlength of 1.0 dm and concentration (*c*) in g/100 mL. Thin layer chromatography (TLC) was performed on Merck EMD Kieselgel $60F_{254}$ precoated aluminum backed plates. Reverse-phase thin layer chromatography (RF-TLC) was performed on Merck EMD Silica Gel RP-18 W F254s precoated glass backed plates. TLC and RF-TLC were visualised in combination of: 254/365 nm UV lamp; sulfuric acid (2 M in EtOH/W 1:1); ninhydrin (2% ninhydrin in EtOH); aqueous $KMnO_4$ (5% KMnO4 in 1 M NaOH); aqueous phosphomolybdic acid/

Ce(IV) (2.5% phosphomolybdic acid hydrate, 1% cerium(IV) sulfate hydrate, and 6% $H_2SO_4$); or ammonium molybdate (5% in 2M $H_2SO_4$). Flash chromatography was carried out with Fluka Kiegselgel 60 220-440 mesh silica gel. All solvents (analytical or HPLC) used were purchased from Sigma Aldrich, Fisher Scientific, or Rathburn. Anhydrous solvents were purchased from Sigma Aldrich and stored over molecular sieves (<0.005% $H_2O$). Petrol refers to the fraction of petroleum ether boiling point in the range of 40 – 60 °C. Brine refers to saturated solution of NaCl.

**Analytical and Preparative HPLC Method for tunicamyins-like compound:**

Analytical-scale HPLC analysis and preparative-scale HPLC purification were done on UltiMate 3000, and data was analysed on Chromeleon software.

*Analytical Scale Analysis.* Column: Phenomenex, Synergi 4u Hydro-RP 80Å 100 x 4.60 mm 4micron**;** Flow rate: 1 mL/min.**;** Solvent A: 5% ACN and 0.1% FA in H20**;** Solvent B: 0.1% FA in ACN**;** UV 260 nm.

Eluent gradient

| Min. | %B |
|---|---|
| 1.000 | 0.0 [%] |
| 25.000 | 100.0 [%] |
| 27.010 | 100.0 [%] |
| 29.010 | 0.0 [%] |
| 35.010 | 0.0 [%] |

*Preparative Scale Purification.* Column: Phenomenex, Synergi 4u Hydro-RP 80Å 100 x 21.20 mm 4micron**;** Flow rate: 12 mL/min.**;** Solvent A: 5% ACN and 0.1% FA in H20**;** Solvent B: 0.1% FA in ACN**;** UV 260 nm.

Eluent gradient

| Min. | %B |
|---|---|
| 1.000 | 0.0 [%] |
| 25.000 | 100.0 [%] |
| 27.010 | 100.0 [%] |
| 28.010 | 0.0 [%] |
| 35.010 | 0.0 [%] |

## Chemical Syntheses and Characterisations

### Tunicamycins (1)[1]

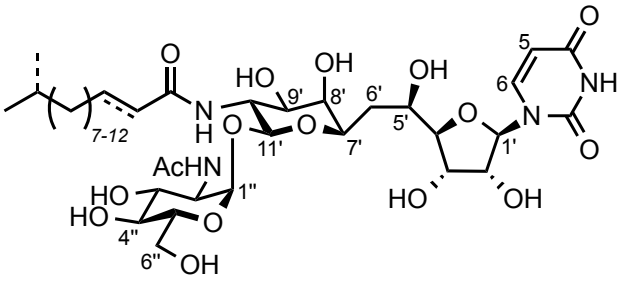


Crude tunicamycins (**1**) were isolated from *S. chartreusis* NRRL3882 fermentation culture by methanol extraction (**Experimental: Biological Materials and Methods**). **TLC**: $R_f$ 0.3 in water/isopropanol/ethyl acetate (W/*i*POH/EtOAc, 1:3:6); **$^1$H NMR** (400 MHz, $CD_3OD$) δ ppm 0.89, 0.91 (2 x s, 2 x 3 H, -CH($CH_3$)$_2$), 1.14 – 1.66 (m, n x $CH_2^{fatty\ acid}$), 1.95 (s, 3 H, -$CH_3^{NHAc}$), 3.36 – 4.05 (m, -$CH_2^{sugar}$, -$CH^{sugar}$), 4.10 (t, $J$ = 9.30 Hz, 1 H, H-10'), 4.20 (t, $J_{2',1'}$ = 5.80 Hz, 1 H, H-2'), 4.59 (d, $J_{11',10'}$ = 8.9 Hz, 1 H, H-11'), 4.94 (d, $J$ = 3.6 Hz, 1 H, H-1''), 5.77 (d, $J_{5,6}$ = 8.2 Hz, 1 H, H-$5^{uracil}$), 5.95 (d, $J_{1',2'}$ = 5.5 Hz, 1 H, H-1'), 5.96 (d, $J_{HC=CH\ trans}$ = 15.4 Hz, 1 H, =C*H*C(O)-), 6.84 (dt, $J_{HC=CH\ trans}$ = 14.5 Hz, $J$ = 7.85 Hz, 1 H, -$CH_2$*H*C=), 7.94 (d, $J_{6,5}$ = 8.2 Hz, 1 H, H-$6^{uracil}$); **LRMS** *m/z* ($ESI^+$): [(M + $Na)^+$] = 839 (18%), 853 (100%), 867 (92%), 881 (30%); ($ESI^-$): [$(M + Cl)^-$] = 851 (20%), 865 (100%), 879 (94%), 893 (34%). Flanking peaks with mass ± 14 corresponded to 8 x $CH_2$, 9 x $CH_2$, 10 x $CH_2$, and 11 x $CH_2$. **IR**: 3325, 2925, 2360, 2342, 1665, 1376, 1234, 1093, 1025; **LC/MS** *m/z* (TOF MS ES+): 761, 775, 789, 803, 817, 831, 845, 859, 873, 887, 901. Full assignment was not possible due to the presence of possibly at least 11 homologues with mass ± 14.

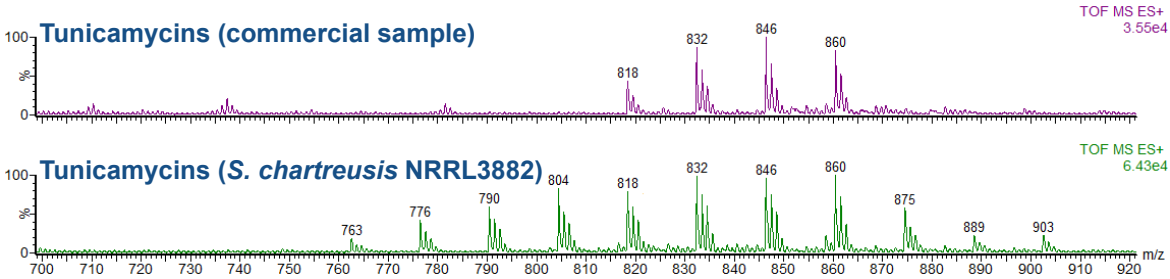


**LC-MS Analysis of Tunicamycin Production by *S. chartreusis* NRRL 3882 by TOF-MS**: Crude tunicamycins extracted from *S. chartreusis* culture, and commercial tunicamycins standard (retention time, 14-19 min.).

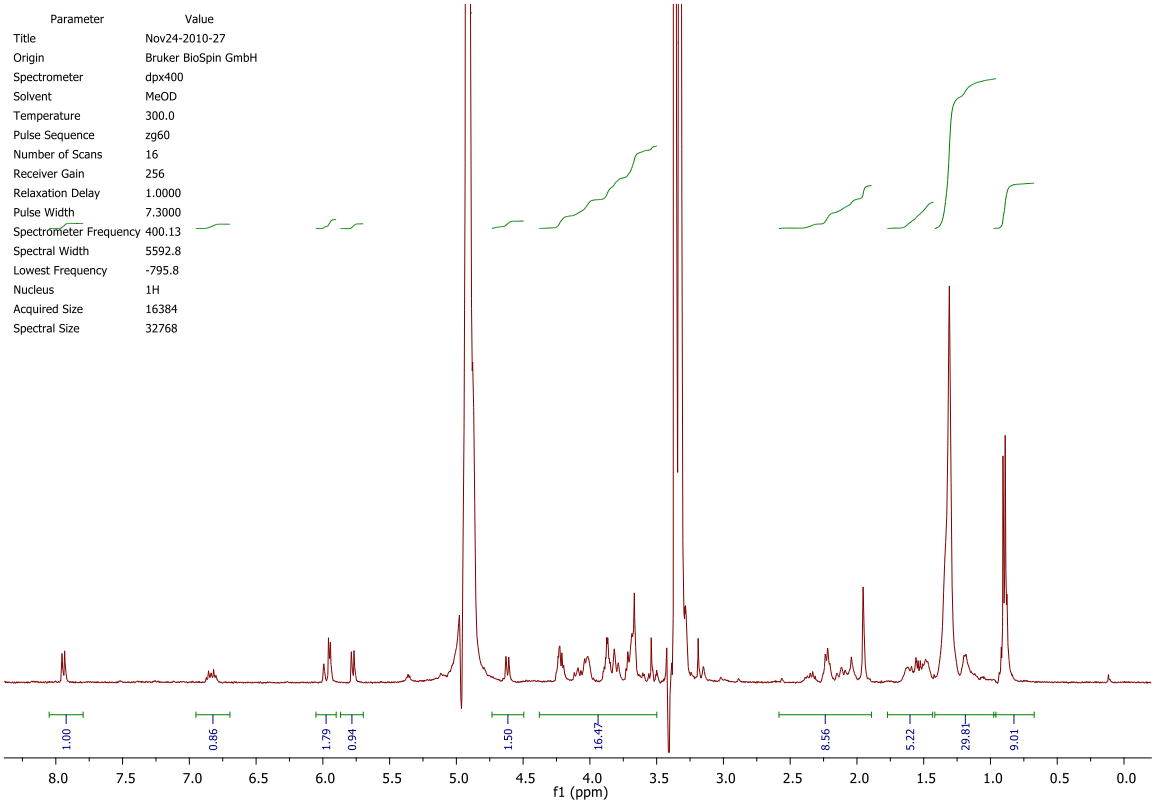


**Tunicamycins (1) $^{1}$H NMR spectrum**

**Heptaacetyl-tunicaminyl uracil (2)**[2]

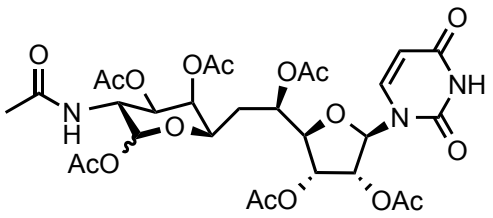


Crude (**1**) (183 mg, 0.218 mmol) was suspended in 3 M aq. HCl (5 mL) and stirred under reflux at 105 °C for 2 h and 15 min. After 2 h and 15 min the solvent was co-evaporated with toluene *in vacuo*. The residue was re-dissolved in dry pyridine (3 mL) and $Ac_2O$ (2 mL). After 18 h of stirring at RT, TLC showed a product spot with $R_f$ 0.3. After solvent was evaporated *in vacuo*, flash column chromatography (MeOH/EtOAc, 1:19) afforded **3** (98.4 mg, 0.141 mmol, 64%, α/β ratio 53:47); **TLC:** $R_f$ 0.3 in methanol/ethyl acetate (MeOH/EtOAc, 1:19); **$^1$H NMR** (500 MHz, $CDCl_3$) δ ppm 8.53 (d, $J$ = 1.00 Hz, 1 H, N-H$^{uracil,\beta}$), 8.43 (d, $J$ = 0.95 Hz, 1 H, N-H$^{uracil,\alpha}$), 7.22 (d, $J_{6,5}$ = 8.2 Hz, 1 H, H-6$^{uracil,\alpha}$), 7.19 (d, $J_{6,5}$ = 8.2 Hz, 1 H, H-6$^{uracil,\beta}$), 6.13 (d, $J_{11',10'}$ = 3.5 Hz, 1 H, H-11'$^{\alpha}$), 5.90 (d, $J_{1',2'}$ = 5.4 Hz, 1 H, H-1'$^{\alpha}$), 5.83 (d, $J_{1',2'}$ = 3.8 Hz, 1 H, H-1'$^{\beta}$), 5.80 (d, $J$ = 2.2 Hz, 1 H, H-5$^{uracil,\alpha}$), 5.78 (dd, $J$ = 2.1 Hz, $J_{5,6}$ = 8.0, 1 H, H-5$^{uracil,\beta}$), 5.64 (d, $J_{11',10'}$ = 8.8 Hz, 1 H, H-11'$^{\beta}$), 5.55 (d, $J_{N\text{-}H,10'}$ = 9.5 Hz, 1 H, N-H$^{Ac,\beta}$), 5.44 (d, $J_{N\text{-}H,10'}$ = 9.1 Hz, 1 H, N-H$^{Ac,\alpha}$), 5.42 (dd, $J_{3',4'}$ = 5.4 Hz, $J_{3',2'}$ = 10.4 Hz, 1 H, H-3'$^{\beta}$), 5.36 (dd, $J_{3',4'}$ = 5.0 Hz, $J_{3',2'}$ = 5.9 Hz, 1 H, H-3'$^{\alpha}$), 5.33 (app t, $J_{2',1'}$ = $J_{2',3'}$ = 5.7 Hz, 1 H, H-2'$^{\alpha}$), 5.30 (app t, $J_{2',1'}$ = $J_{2',3'}$ = 6.0 Hz, 1 H, H-2'$^{\beta}$), 5.25 (d, $J_{9',8'}$ = $J_{9',10'}$ = 2.8 Hz, 1 H, H-9'$^{\alpha}$), 5.22 (dd, $J_{8',7'}$ = 3.2 Hz, $J_{8',9'}$ = 6.6 Hz, 1 H, H-8'$^{\beta}$), 5.19 (dd, $J_{5',4'}$ = 1.9 Hz, $J_{5',6'}$ = 3.5 Hz, 1 H, H-5'$^{\beta}$), 5.19 (dd, $J_{8',7'}$ = 1.5 Hz, $J_{8',9}$ = 3.5 Hz, 1 H, H-8'$^{\alpha}$), 5.12 (ddd, $J$ = 2.8 Hz, $J_{5',4'}$ = 5.0 Hz, $J_{5',6'}$ = 7.9 Hz, 1 H, H-5'$^{\alpha}$), 5.08 (dd, $J_{9',8'}$ = 3.50 Hz, $J_{9',10'}$ = 11.3 Hz, 1 H, H-9'$^{\beta}$), 4.72 (ddd, $J_{10',11'}$ = 4.1 Hz, $J_{10',N\text{-}H}$ = 9.5 Hz, $J_{10',9'}$ = 11.4 Hz, 1 H, H-10'$^{\alpha}$), 4.42 (ddd, $J_{10'9'}$ = 7.6 Hz, $J_{10',N\text{-}H'}$ = 9.5 Hz, $J_{10',9'}$ = 11.3 Hz, 1 H, H-10'$_{\beta}$), 4.13 (app t, $J_{4',5'}$ = $J_{4',3'}$ = 4.7 Hz, 1 H, H-4'$^{\beta}$), 4.09

(app t, $J_{4',5'} = J_{4',3'} = 4.7$ Hz, 1 H, H-4'$^{\alpha}$), 4.05 - 4.07 (m, 1 H, H-7'$^{\alpha}$), 3.90 (dd, $J_{7',8'} = 2.5$ Hz, $J_{7',6'} = 9.7$ Hz, 1 H, H-7'$^{\beta}$), 2.20 (s, 3 H, -$CH_3^{Ac,\alpha}$), 2.20 (s, 3 H, -$CH_3^{Ac,\beta}$), 2.18, 2.13 (2 x s, 2 x 3 H, 2 x -$CH_3^{Ac,\alpha}$), 2.13, 2.12, 2.11, 2.11 (4 x s, 4 x 3 H, 4 x -$CH_3^{Ac,\beta}$), 2.09 (2 x s, 2 x 3 H, 2 x -$CH_3^{Ac,\alpha}$), 2.04 (s, 3 H, -$CH_3^{Ac,\alpha}$), 2.02 (s, 3 H, -$CH_3^{Ac,\beta}$), 1.99 - 2.01 (m, 1 H, H-6'$^{\beta}$), 1.97 - 1.99 (m, 1 H, H-6'$^{\alpha}$), 1.96 (s, 3 H, -$CH_3^{NHAc,\alpha}$), 1.94 (s, 3 H, -$CH_3^{NHAc,\beta}$), 1.74 (ddd, $J_{6',7'} = 3.5$ Hz, $J_{6',5'} = 6.9$ Hz, $J_{6'a,6b'} = 14.9$ Hz, 1 H, H-6'$^{\beta}$), 1.57 (ddd, $J_{6',7'} = 1.9$ Hz, $J_{6',5'} = 8.2$ Hz, $J_{6'a,6'b} = 16.7$Hz, 1 H, H-6'$^{\alpha}$); **$^{13}$C NMR** (126 MHz, $CDCl_3$) δ ppm 173.6, 171.2, 170.7, 170.6, 170.6, 170.3, 170.1, 170.0, 169.7, 169.6, 169.4, 169.3, 169.3, 169.1 (14 x s, 14 x C, C=$O^{NHAc,\alpha}$, 14 x C=$O^{NHAc,\beta}$, 6 x C=$O^{Ac,\alpha}$, 6 x C=$O^{Ac,\beta}$), 162.5 (C-4 C=$O^{\beta}$), 162.5 (C-4 C=$O^{\alpha}$), 149.8 (C-2 C=$O^{\alpha}$), 149.8 (C-2 C=$O^{\beta}$), 140.1 (C-$6^{uracil,\beta}$), 139.8 (C-$6^{uracil,\alpha}$), 103.4 (C-$5^{uracil,\alpha}$), 103.3 (C-$5^{uracil,\beta}$), 93.0 (C-11'$^{\beta}$), 91.1 (C-11'$^{\alpha}$), 88.7 (C-1'$^{\beta}$), 88.1 (C-1'$^{\alpha}$), 82.5 (C-4'$^{\beta}$), 82.5 (C-4'$^{\alpha}$), 72.4 (C-2'$^{\alpha}$), 72.4 (C-2'$^{\beta}$), 71.0 (C-7'$^{\beta}$), 70.5 (C-9'$^{\beta}$), 69.6, 69.6, 69.3, 68.7, 68.1 (5 x s, 7 x C, C-3'$^{\alpha}$, C-3'$^{\beta}$, C-5'$^{\alpha}$, C-5'$^{\beta}$, C-8'$^{\alpha}$, C-8'$^{\beta}$, C-9'$^{\alpha}$), 49.6 (C-10'$^{\beta}$), 46.7 (C-10'$^{\alpha}$), 32.5 (C-6'$^{\alpha}$), 31.5 (C-6'$^{\beta}$), 23.3 (-$CH_3^{NHAc,\beta}$), 23.2 (-$CH_3^{NHAc,\alpha}$), 20.3 – 21.0 (12 x C, 6 x -$CH_3^{Ac,\alpha}$, 6 x -$CH_3^{Ac,\beta}$); **IR**: 3370, 1736, 1710, 1697, 1651, 1635, 1540, 1520, 1370; **LRMS** *m/z* ($ESI^+$): 722 [$(M+Na)^+$, 100%]; ($ESI^-$): 734 [$(M+Cl)^-$, 100%]. **HRMS** *m/z* ($ESI^+$): calc. for $C_{29}H_{37}N_3NaO_{17}$ $(M+Na)^+$ = 722.2015, found 722.2023.

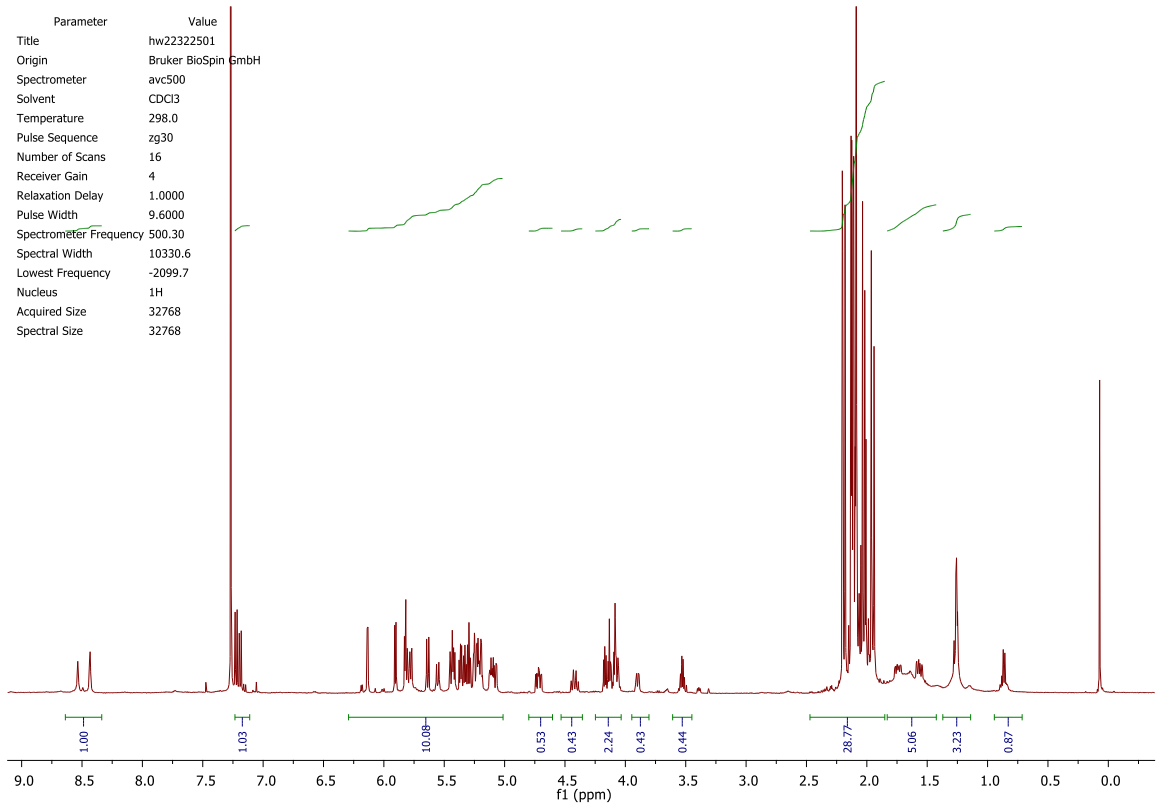


**Heptaacetyl-tunicaminyl uracil (2) $^{1}$H NMR spectrum**

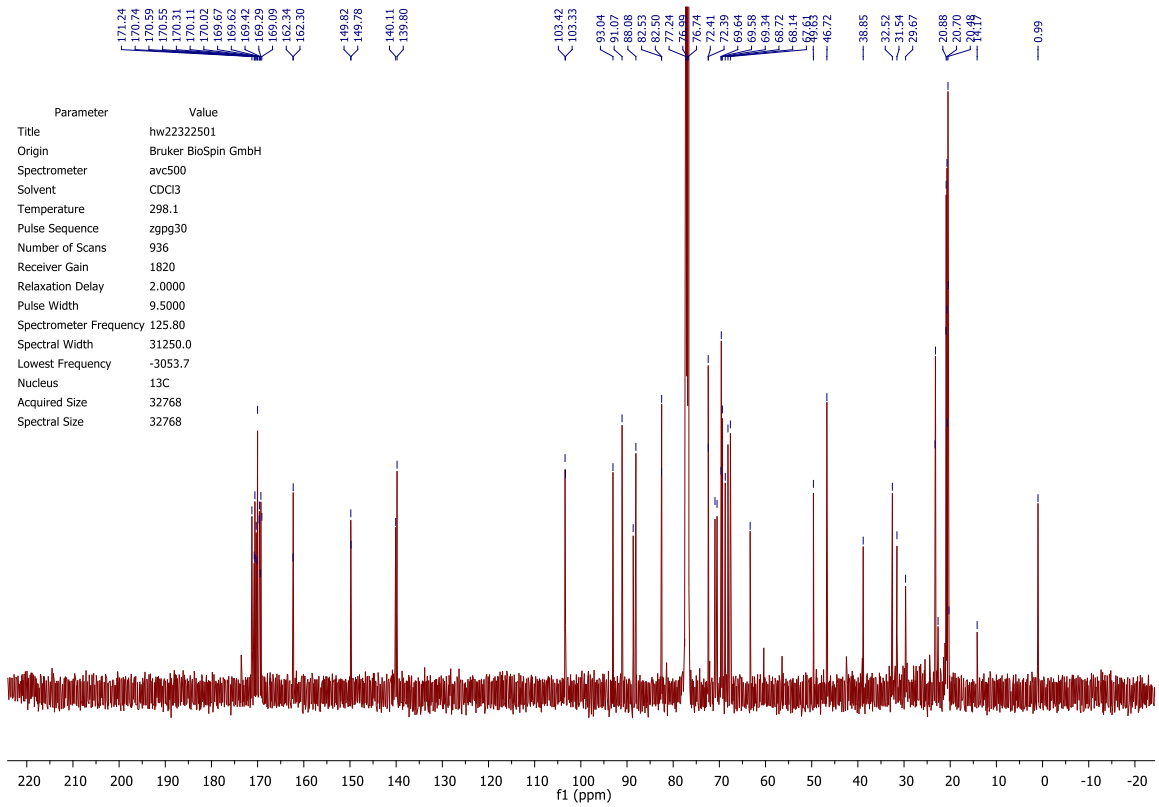


**Heptaacetyl-tunicaminyl uracil (2) $^{13}$C NMR spectrum**

***N*-acetyl-tunicaminyl uracil (3)**

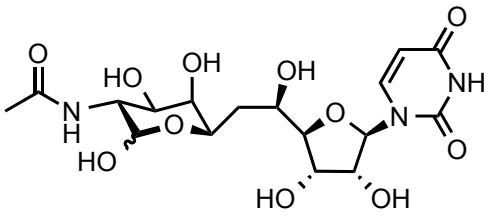

**2** (41.4 mg, 0.059 mmol) was dissolved in dry MeOH (5 mL), stirred and cooled to 0° C. NaOMe was then added to make a final concentration of 0.01 M. Reaction was monitored by TLC (1:2:2, W/*i*POH/EtOAc). Then, the reaction was neutralised after 3 h with Dowex 50W X8 $H^+$ resin. Finally, the reaction solution was filtered and concentrated *in vacuo*. Flash column chromatography (W/*i*POH/EtOAc, 1:2:2) afforded **3** (25.9 mg, 0.058 mmol, 98 %, α/β ratio 37:63); **TLC**: $R_f$ 0.5, 0.6 in water/isopropanol/ethyl acetate (W/*i*POH/EtOAc, 1:2:2); **$[\alpha]_D^{23}$** = +12, c = 1, $H_2O$; **$^1$H NMR** (500 MHz, $D_2O$) δ ppm 7.78 (d, $J_{6,5}$ = 8.2 Hz, 1 $H^{\alpha}$, H-$6^{uracil,\alpha}$), 7.76 (d, $J_{6,5}$ = 8.2 Hz, 1 $H^{\beta}$, H-$6^{uracil,\beta}$), 5.87 (m, 1 $H^{\alpha}$ + 1 $H^{\beta}$, H-1'$^{\alpha}$, H-1'$^{\beta}$), 5.84 (d, $J_{5,6}$ = 8.2 Hz, 1 $H^{\alpha}$, H-$5^{uracil,\alpha}$), 5.82 (d, $J_{5,6}$ = 8.2 Hz, 1 $H^{\beta}$, H-$5^{uracil,\beta}$), 5.13 (d, $J_{11',10'}$ = 3.8 Hz, 1 $H^{\alpha}$, H-11'$^{\alpha}$), 4.58 (d, $J_{11',10'}$ = 8.5 Hz, 1 $H^{\beta}$, H-11'$^{\beta}$), 4.23 - 4.27 (m, 2 $H^{\alpha}$ + 2$H^{\beta}$, H-2'$^{\alpha}$, H-2'$^{\beta}$, H-3'$^{\alpha}$, H-3'$^{\beta}$), 4.19 (d, $J$ = 9.1 Hz, 1 $H^{\alpha}$, H-7'$^{\alpha}$), 4.04 (dd, $J_{10',9'}$ = 11.0 Hz, $J_{10',11}$ = 3.8 Hz, 1 $H^{\alpha}$, H-10'$^{\alpha}$), 4.00 (dt, $J$ = 10.7 Hz, $J$ = 3.2 Hz, 1 $H^{\beta}$, H-5'$^{\beta}$), 3.92 - 3.97 (m, 2 $H^{\alpha}$ + 1 $H^{\beta}$, H-4'$^{\alpha}$, H-4'$^{\beta}$, H-5'$^{\alpha}$), 3.88 (dd, $J_{9',10'}$ = 11.4 Hz, $J_{9',8'}$ = 3.2 Hz, 1 $H^{\alpha}$, H-9'$^{\alpha}$), 3.79 (d, $J_{8',9'}$ = 3.5 Hz, 1 $H^{\alpha}$, H-8'$^{\alpha}$), 3.78 (dd, $J_{10',9'}$ = 10.7 Hz, $J_{10',9'}$ = 8.2 Hz, 1 $H^{\beta}$, H-10'$^{\beta}$), 3.75 (dd, $J_{7',6'}$ = 8.5 Hz, $J_{7',8}$ = 1.0 Hz, 1 $H^{\beta}$, H-7'$^{\beta}$), 3.73 (d, $J_{8',9'}$ = 3.5 Hz, 1 $H^{\beta}$, H-8'$^{\beta}$), 3.69 (dd, $J_{9',10'}$ =10.7 Hz, $J_{9'.8'}$ = 3.2 Hz, 1 $H^{\beta}$, H-9'$^{\beta}$), 1.98 (s, 3 $H^{\alpha}$ + 3 $H^{\beta}$, -$CH_3^{NHAc,\beta}$, -$CH_3^{NHAc,\alpha}$), 1.86 - 1.96 (m, 1 $H^{\alpha}$ + 1$H^{\beta}$, H-6a'$^{\alpha}$, H-6a'$^{\beta}$), 1.54 - 1.63 (m, 1 $H^{\alpha}$ + 1$H^{\beta}$, H-6b'$^{\alpha}$, H-6b'$^{\beta}$); **$^{13}$C NMR** (126 MHz, $D_2O$) δ ppm 175.0, 174.7 (C=$O^{NHAc,\beta}$, C=$O^{NHAc,\alpha}$), 166.22 (C-4 C=$O^{\alpha+\beta}$), 151.9 (C-2 C=$O^{\alpha+\beta}$), 141.8 (C-$6^{uracil,\alpha+\beta}$), 102.5 (C-$5^{uracil,\alpha+\beta}$), 95.3 (C-11'$^{\beta}$), 90.9 (C-11'$^{\alpha}$), 88.1 (C-1'$^{\alpha+\beta}$), 87.1, 87.1 (C-4'$^{\alpha}$, C-4'$^{\beta}$),

73.4, 73.4 (C-2'$^{\alpha}$, C-2'$^{\beta}$), 71.2, 71.1, 70.8, 70.4 (C-7'$^{\beta}$, C-8'$^{\beta}$, C-9'$^{\beta}$, C-8'$^{\alpha}$), 68.9, 68.9 (C-3'$^{\alpha}$, C-3'$^{\beta}$), 67.5 (C-9'$^{\alpha}$), 67.1, 67.0 (C-5'$^{\alpha}$, C-5'$^{\beta}$), 66.3 (C-7'$^{\beta}$), 53.6 (C-10'$^{\beta}$), 50.2 (C-10'$^{\alpha}$), 33.7, 33.6 (C-6'$^{\alpha}$, C-6'$^{\beta}$), 23.3, 22.2 (-$CH_3^{NHAc,\alpha}$, -$CH_3^{NHAc,\beta}$)**; IR** ν: 3362, 1638, 1410, 1264, 1072; **LRMS** *m/z* ($ESI^+$): 470 [$(M+Na)^+$, 100%]; ($ESI^-$): 482 [$(M+Cl)^-$, 100%]; **HRMS** *m/z* ($ESI^+$): calc. for $C_{17}H_{25}N_3NaO_{11}$ $(M+Na)^+$ = 470.1381, found 470.1367.

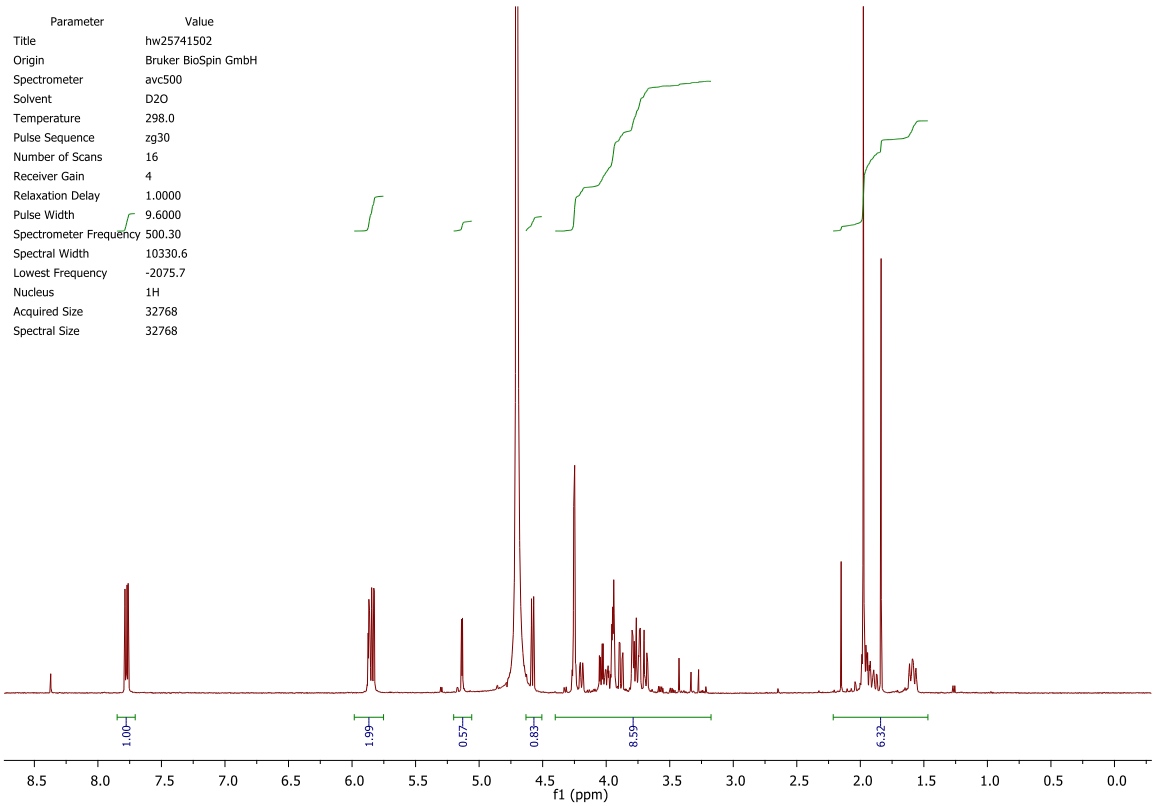


***N*-acetyl-tunicaminyl uracil (3) $^{1}$H NMR spectrum**

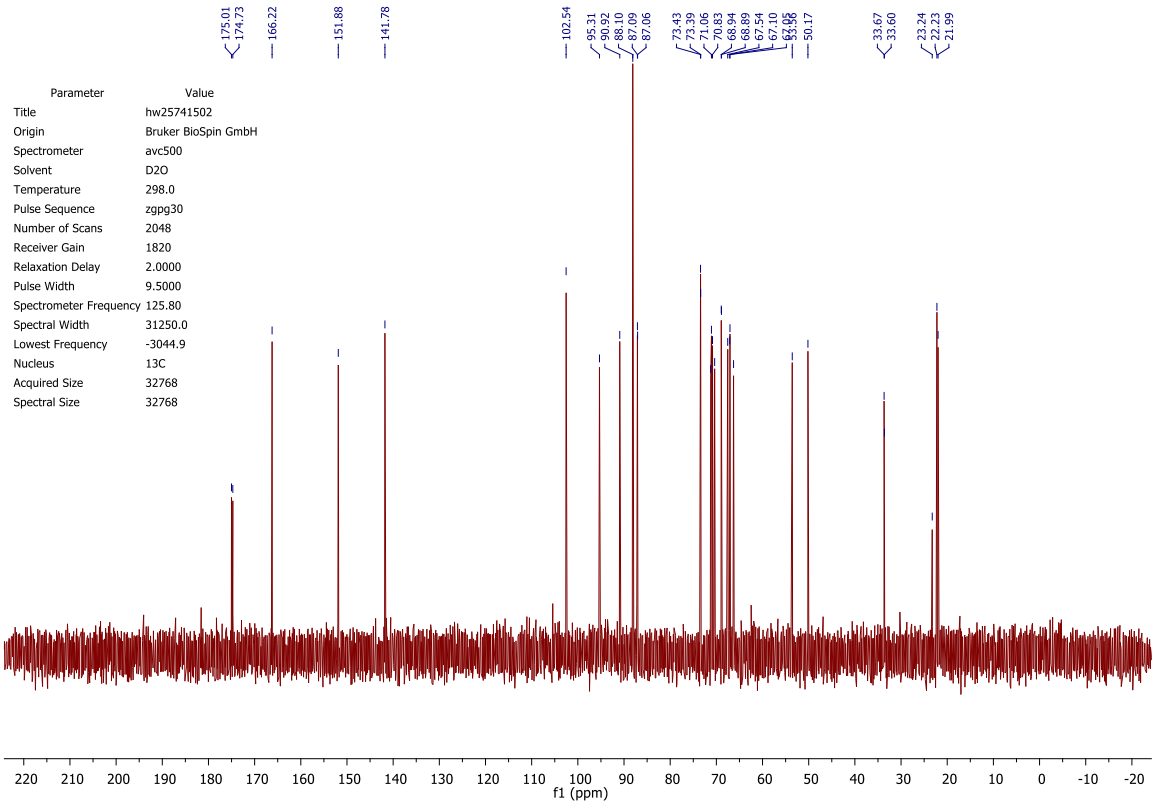


***N*-acetyl-tunicaminyl uracil (3) $^{13}$C NMR spectrum**

**α-D-*N*-acetylglucosamine-(1”-11’)-*N*-acetyl-tunicaminyl uracil (4)**

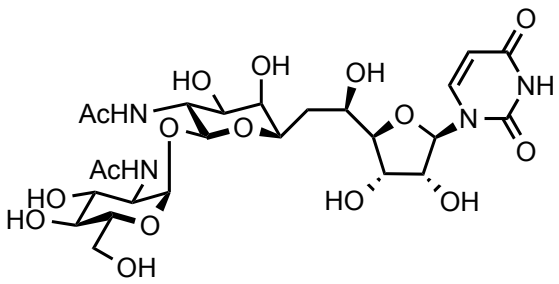

**6a** (127 mg, 0.086 mmol) was dissolved in dry MeOH (5 mL), stirred and cooled to 0° C. NaOMe was added to make a final concentration of 0.01 M, and monitored by TLC (1:3:6, W/*i*POH/EtOAc). The reaction was neutralised after 4 h with Dowex 50W X8 $H^+$ resin. Then, it was filtered and concentrated *in vacuo*, and redissolved in TFA (1 mL) and stirred at RT for 1 h. TFA was co-evaporated with toluene and then redissolved in MeOH (5 mL) with the addition of $Ac_2O$ (1 mL). The reaction was stirred at RT for 12 h and then neutralised to pH 6-7 with Dowex Marathon A $^-$OH resin, and stirred for additional 1 h. The reaction solution was filtered and purified *via* flash column chromatography (W/*i*POH/EtOAc, 1:2:2) to afford **4** (13.1 mg, 0.020 mmol, 23%) as yellow glass; **TLC:** $R_f$ 0.3, in water/isopropanol/ethyl acetate (W/*i*POH/EtOAc, 1:2:2); **$[\alpha]_D^{23}$** = +50.7, c = 0.7, $H_2O$; **$^1$H NMR** (500 MHz, $CD_3OD$) δ ppm 7.76 (d, $J_{6,5}$ = 7.9 Hz, 1 H, H-6$^{uracil}$), 5.84 (d, $J_{1',2'}$ = 7.9 Hz, 1 H, H-1’), 5.83 (d, $J_{5,6}$ = 5.4 Hz, 1 H, H-5$^{uracil}$), 4.98 (d, $J_{1'',2''}$ = 3.5 Hz, 1 H, H-1”), 4.58 (d, $J_{11',10'}$ = 8.5 Hz, 1 H, H-6$^{uracil}$), 4.25 (dd, $J_{2',1'}$ = 5.4 Hz, $J_{2',3'}$ = 9.1 Hz, 1 H, H-2’), 4.22 (dd, $J_{3',4'}$ = 3.5 Hz, $J_{3',2'}$ = 5.7 Hz, 1 H, H-3’), 4.08 – 4.03 (m, 2 H, H-4’, H-5’), 3.87 (dd, $J_{10',9'}$ = 10.7 Hz, $J_{10',11'}$ = 8.5 Hz, 1 H, H-10’), 3.82 – 3.82 (m, 1 H, H-4”), 3.80 (dd, $J_{2'',1''}$ = 3.8 Hz, $J_{2'',3''}$ = 10.7, 1 H, H-2”), 3.77 (d, $J$ = 10.1 Hz, 1 H, H-7’), 3.73 – 3.67 (m, 2 x 1 H, H-8’, H-6b”), 3.70 (dd, $J_{3'',2''}$ = 10.7 Hz, $J_{3'',4''}$ = 3.2 Hz, 1 H, H-3”), 3.68 – 3.41 (m, 2 H, H-6”a, H-9’), 3.44 (app t, $J_{5'',6a''}$ = 9.8 Hz, 1 H, H-5”), 1.98, 1.94 (2 x s, 2 x 3 H, 2 x -C$H_3^{NHAc}$), 1.94 (dd, $J_{6b',6a'}$ = 6.6 Hz, $J_{6b',5'}$ = 3.2 Hz,

1 H, H-6b'), 1.57 (app t, $J_{6a',6b'} = J_{6a',5'}$ = 13.2 Hz, 1 H, H-6a'); **$^{13}$C NMR** (126 MHz, $CD_3OD$) δ ppm 174.5, 174.1 (2 x C=O$^{NHAc}$), 166.2 (C-4, C=O)**,** 151.8 (C-2, C=O)**,** 141.9 (C-6$^{uracil}$)**,** 102.5 (C-5$^{uracil}$)**,** 99.8 (C-11')**,** 98.3 (C-1")**,** 88.5 (C-1')**,** 87.2 (C-4')**,** 73.4 (C-2')**,** 72.6 (C-4")**,** 71.3 (C-7')**,** 71.1, 70.4, 69.8 (C-3", C-8', C-9')**,** 69.6 (C-5")**,** 68.9 (C-3')**,** 67.0 (C-5')**,** 60.4 (C-6")**,** 53.4 (C-2")**,** 52.8 (C-10')**,** 33.5 (C-6')**,** 22.2, 22.1 (2 x -C$H_3^{NHAc}$); **IR** (neat) ν: 3344, 2362, 2341, 2110, 1636, 1371, 1216; **LRMS** *m/z* (ESI$^+$): 673.26 [(M+Na)$^+$, 23%]; (ESI$^-$): 649.23 [(M-H)$^-$, 100%]; **HRMS** *m/z* (ESI$^+$): calc. for $C_{25}H_{38}N_4NaO_{16}$ (M +Na)$^+$ = 673.2175, found 673.2195.

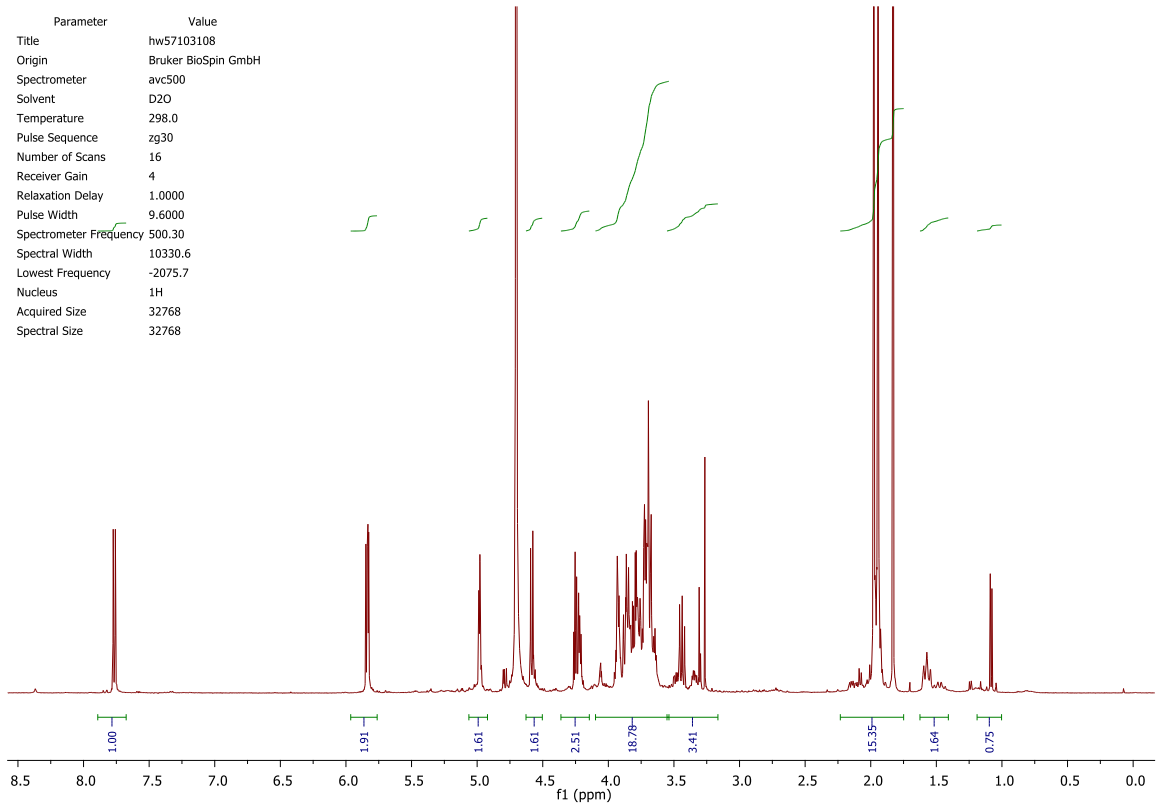


**α-D-*N*-acetylglucosamine-(1”-11’)-*N*-acetyl-tunicaminyl uracil (4) $^{1}$H NMR spectrum**

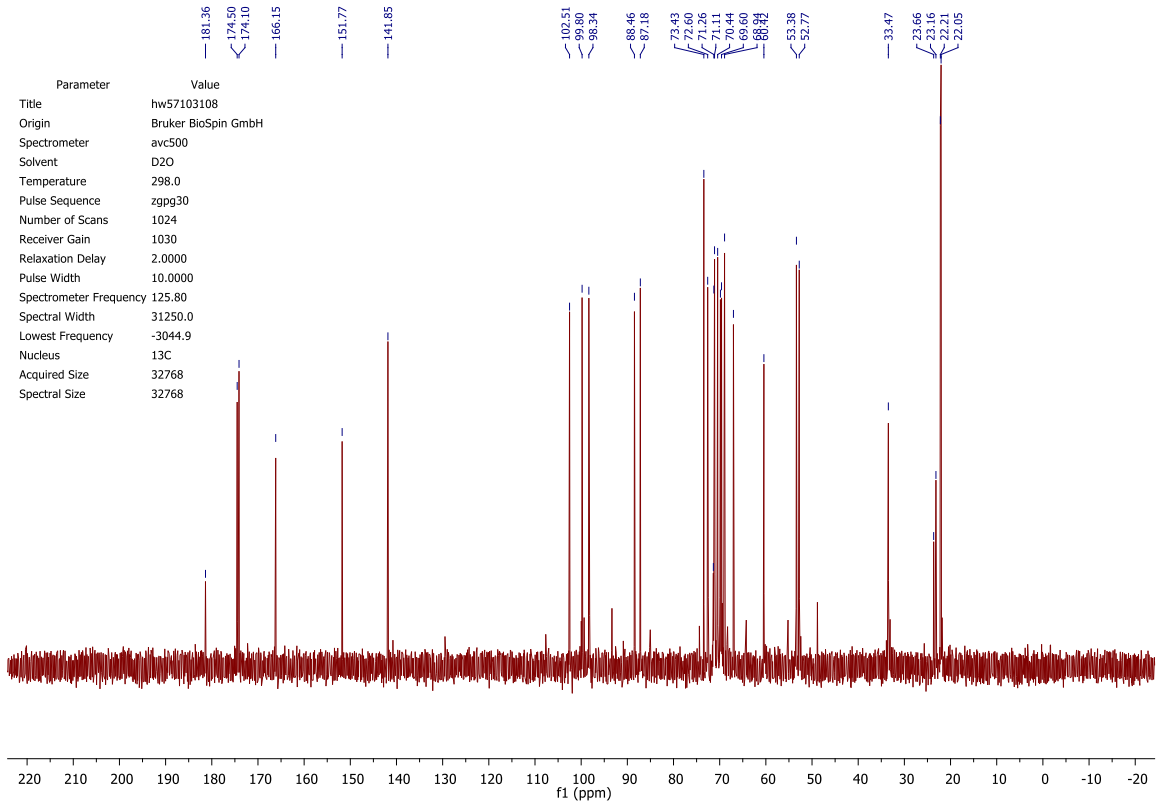


**α-D-*N*-acetylglucosamine-(1”-11’)-*N*-acetyl-tunicaminyl uracil (4) $^{13}$C NMR spectrum**

**Octa-*O*-acetyl-tunicamycins (5)**

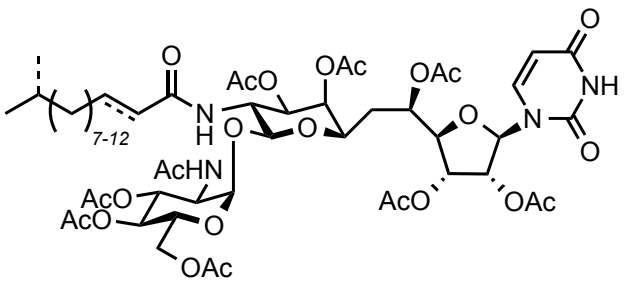


Crude (**1)** (682 mg, 0.814 mmol) was dissolved in dry pyridine (5 mL) with an addition of $Ac_2O$ (3 mL). After stirring at RT for 18 h TLC (EtOAc) show a major product at $R_f$ 0.4 (**2**). The solvent was evaporated *in vacuo* and purified *via* flash chromatography (MeOH/DCM, 3:97) to afford **5** (782 mg, 0.667 mmol, 82 %) as clear glass. The percentage yield various between 23-82%, which was dependent on the purity of the crude tunicamycins (**1**); **TLC:** $R_f$ 0.4 in methanol/dichloromethane (MeOH/DCM, 3:97)**; $^1$H NMR** (500 MHz, $CD_3OD$) δ ppm 7.48 (d, $J_{6,5}$ = 8.0 Hz, 1 H, H-6$^{uracil}$), 6.83 (dt, $J_{HC=CH\ trans}$ = 14.2 Hz, $J$ = 7.3 Hz, 1 H, C=C*H*-$CH_2$), 5.87 (d, $J_{HC=CH\ trans}$ = 15.5 Hz, 1 H, C=C*H*-CO), 5.81 (d, $J_{1',2'}$ = 5.1 Hz, 1 H, H-1'), 5.75 (d, $J_{5,6}$ = 8.0 Hz, 1 H, H-5$^{uracil}$), 5.56 (dd, $J_{3',2'}$ = 6.1 Hz, $J_{3',4'}$ = 5.5 Hz, 1 H, H-3'), 5.51 (dd, $J_{2',1'} = J_{2',3'}$ = 5.3 Hz, 1 H, H-2'), 5.26 (dd, $J_{3'',2''}$ = 10.6 Hz, $J_{3'',4''}$ = 9.9 Hz, 1 H, H-3''), 5.27 (ddd, $J_{5',6'}$ = 9.7 Hz, $J_{5',4'}$ = 6.8 Hz, $J$ = 3.6 Hz, 1 H, H-5'), 5.11 (dd, $J_{8',9'}$ = 9.7 Hz, $J_{8',7'}$ = 7.3 Hz, 1 H, H-8'), 5.07 (app t, $J_{4'',5''}$ = 11.3 Hz, $J_{4'',3''}$ = 3.2 Hz, 1 H, H-4''), 5.03 (dd, $J_{9',10'}$ = 3.6 Hz, $J_{9',8'}$ = 3.2 Hz, 1 H, H-9'), 4.98 (d, $J_{1'',2''}$ = 4.9 Hz, 1 H, H-1''), 4.75 (d, $J_{11',10'}$ = 8.4 Hz, 1 H, H-11'), 4.33 (dd, $J_{6a'',6b''}$ =11.1 Hz, $J_{6'',5''}$ = 3.9 Hz, 1 H, H-6''), 4.34 (dd, $J_{10',9'}$ = 4.6 Hz, $J_{10',11'}$ = 3.6 Hz, 1 H, H-10'), 4.32 (ddd, $J_{5'',4''}$ = 10.4, $J_{5'',6''}$ = 2.9 Hz, $J_{5'',6''}$ = 2.2 Hz, 1 H, H-5''), 4.20 (dd, $J_{4',3'}$ = 7.7 Hz, $J_{4',5'}$ = 3.6 Hz, 1 H, H-4'), 4.19 (dd, $J_{2'',3''}$ = 7.2 Hz, $J_{2'',1''}$ = 3.1 Hz, 1 H, H-2''), 4.19 (dd, $J_{6a'',6b''}$ = 14.2 Hz, $J_{6'',5''}$ = 2.6 Hz, 1 H, H-6''), 3.92 (ddd, $J$ = 9.4 Hz, $J_{7',6'}$ = 3.8 Hz, $J_{7',8'}$ = 3.1 Hz, 1 H, H-7'), 2.22 (s, 3 H, C$H_3^{Ac}$), 2.17 (m, 2 H, -C$H_2$CH=C), 2.14 (s, 6 H, 2 x C$H_3^{Ac}$), 2.10

(s, 3 H, C$H_3^{Ac}$), 2.06 (m, 2 H, H-6'), 2.04, 2.03, 1.98, 1.95, 1.89 (5 x s, 5 x 3 H, 5 x C$H_3^{Ac}$), 1.78 (ddd, $J_{6b',a'}$ = 14.8 Hz, $J_{6',5'}$ = 8 Hz, $J_{6',7'}$ = 3.3 Hz, 1 H), 1.55 (spt, $J$ = 6.7 Hz, 1 H, -C$H$($CH_3$)$_2$), 1.46 (quin, $J$ = 6.8 Hz, 2 H, -C$H_2$$CH_2$CH=C), 1.23 - 1.37 (m, 14 H, -C$H_2^{acyl}$), 1.18 (dt, $J$ = 13.1, 7.0 Hz, 2 H, C$H_2$CH($CH_3$)$_2$), 0.91, 0.89 (2 x s, 2 x 3 H, -CH(C$H_3$)$_2$); **$^{13}$C NMR** (126 MHz, $CD_3OD$) δ ppm 173.2, 172.4, 172.3, 172.3, 172.0, 171.7, 171.5, 171.3, 171.2 (9 x s, 9 x C, 8 x C=O$^{Ac}$, C=O$^{NHAc}$), 169.5 (C=O$^{acyl}$), 165.9 (C-4 C=O), 151.8 (C-2 C=O), 147.7 (C=*C*H-$CH_2$), 143.4 (C-6$^{uracil}$), 124.2 (C=*C*H-CO), 103.5 (C-5$^{uracil}$), 101.6 (C-11'), 100.0 (C-1''), 91.1 (C-1'), 84.1 (C-4'), 73.5 (C-2'), 72.2 (C-3''), 72.2 (C-9'), 71.7 (C-7'), 70.9 (C-3'), 70.8, 70.3 (C-5', C-8'), 69.8 (C-5''), 69.7 (C-4''), 63.0 (C-6''), 52.6 (C-2''), 51.8 (C-10'), 40.3 (-*C*$H_2$CH($CH_3$)$_2$), 33.2 (-*C*$H_2$CH=C), 33.1 (C-6'), 30.3 - 31.1 (5 x C, 5 x -*C*$H_2^{acyl}$), 29.4 (-*C*$H_2$$CH_2$CH=C), 29.2 (-*C*H($CH_3$)$_2$), 28.6 (-*C*$H_2^{acyl}$), 23.0, 23.1 (2 x C, -CH(*C*$H_3$)$_2$), 22.9 (-*C*$H_3^{NHAc}$), 21.1 (-*C*$H_3^{Ac}$), 20.7 (2 x C, 2 x -*C*$H_3^{Ac}$), 20.6, 20.6, 20.6, 20.6, 20.3 (5 x C, 5 x -*C*$H_3^{Ac}$); **IR** ν: 2927, 2361, 2341, 1745, 1696, 1540, 1369, 1219, 1031; **MS** *m/z* (ESI$^+$): 1203 [(M+Na)$^+$, 100%]; (ESI$^-$): 1179 [(M +Cl)$^-$, 100%]. Flanking peaks with mass ± 14 corresponded to 8 x $CH_2$, 9 x $CH_2$, 10 x $CH_2$, and 11 x $CH_2$. Full assignment was not possible due to the presence homologues with mass ± 14.

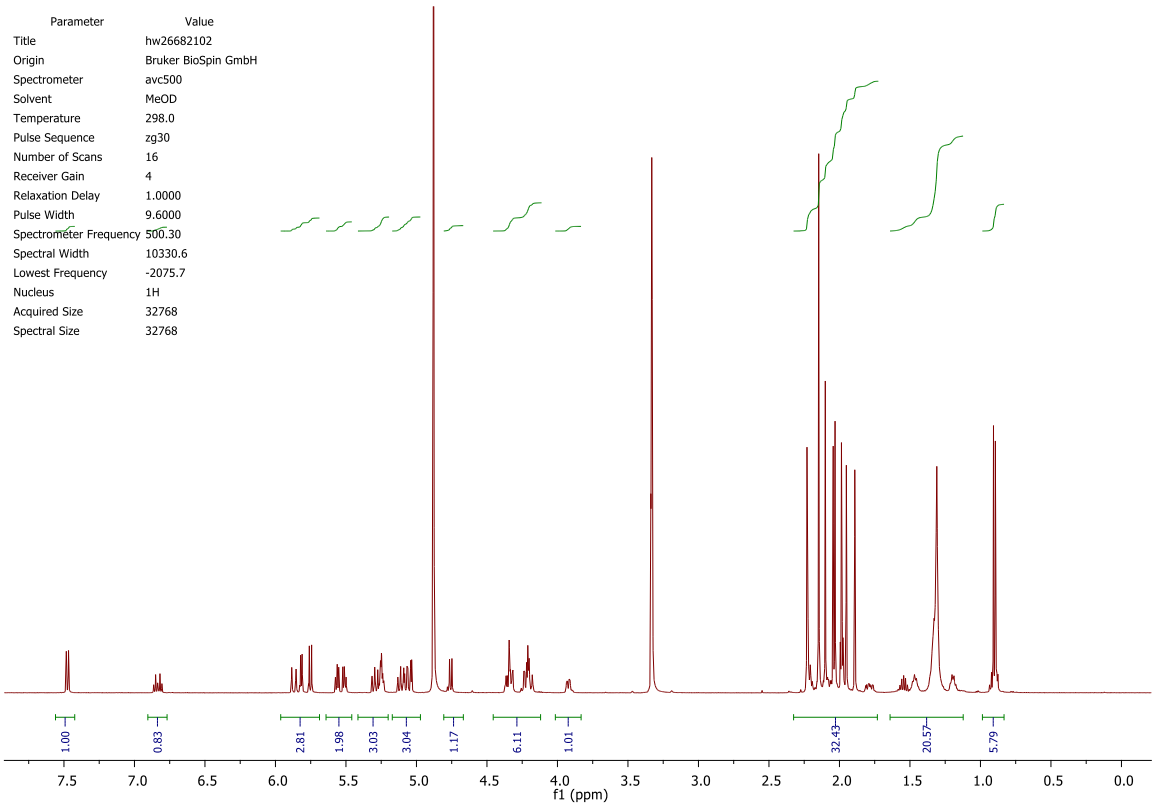


**Octa-*O*-acetyl-tunicamycins (5) $^{1}$H NMR spectrum**

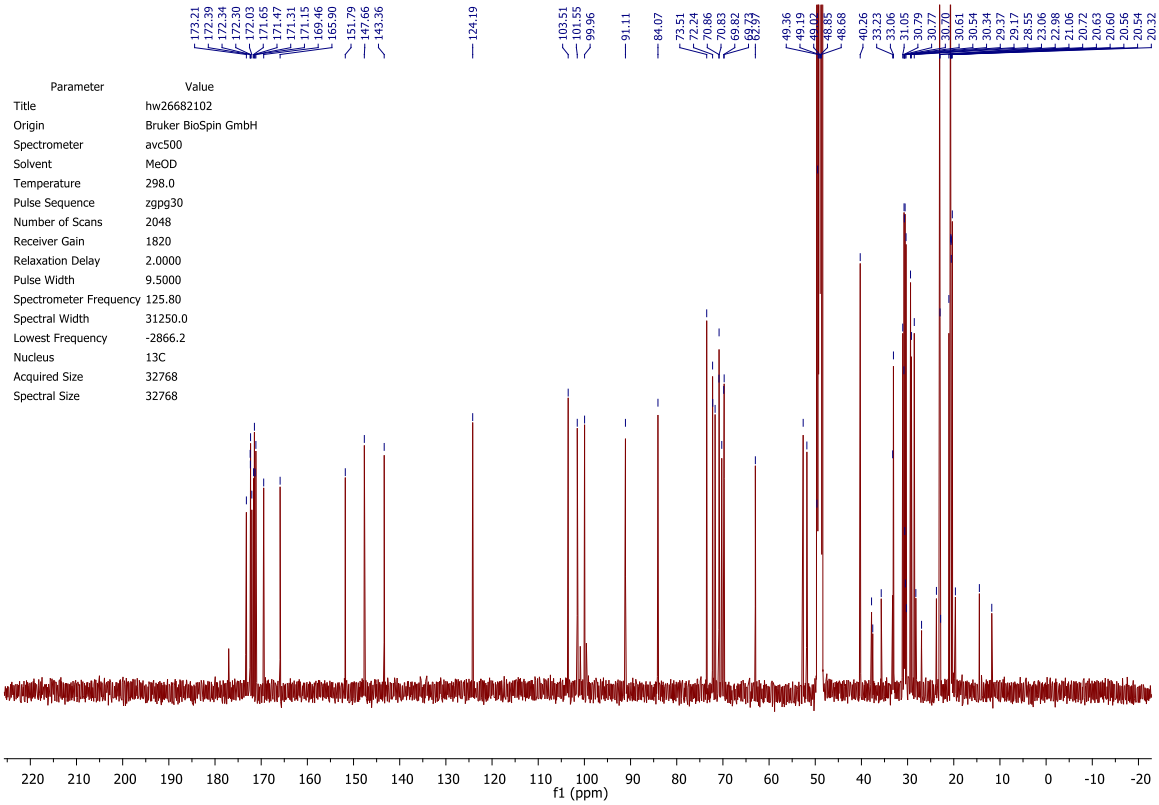


**Octa-*O*-acetyl-tunicamycins (5) $^{13}$C NMR spectrum**

**Tri-*N*-(tert-butoxylcarbonyl)-octa-*O*-acetyl-tunicamycins (6a)**

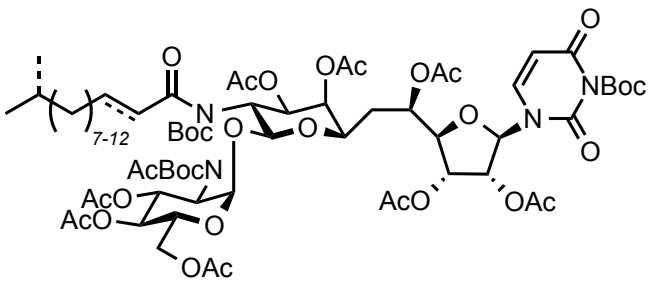


**5** (101 mg, 0.086 mmol) was dissolved in dry THF (1.5 mL) with the addition of 4-(dimethylamino)pyridine (2.10 mg, 0.017 mmol) and di-*tert*-butyl dicarbonate (750 mg, 3.44 mmol) with 10 eq. added over time to a final of 40 eq. The reaction flask was fitted over an oven dried condenser and heated to 60 °C with stirring. After 36 h TLC (EtOAc/ Petrol, 6:4) showed $R_f$ 0.3 (**6a**) and 0.1 (**6**). The reaction was cooled and solvent was evaporated *in vacuo*. Flash column chromatography (EtOAc/Petrol, 6:4) afforded the desired **6a** (67.1 mg, 0.045 mmol, 53 %) as yellow glass. The partially Boc-protected (**6**) was saved for repeated reactions in the same condition; **TLC**: $R_f$ 0.5 in ethyl acetate/petrol (EtOAc/Petrol, 6:4); **$^1$H NMR** (500 MHz, $CDCl_3$) δ ppm 7.48 (d, $J_{6,5}$ = 8.0 Hz, 1 H, H-6$^{uracil}$), 6.89 (dt, $J_{HC=CH\ trans}$ = 15.1 Hz, $J$ = 6.9 Hz, 1 H, C=C*H*-$CH_2$), 6.82 (dt, $J_{HC=CH\ trans}$ = 14.5 Hz, $J$ = 7.6 Hz, 1 H, C=C*H*-$CH_2$), 6.39 (d, $J_{HC=CH\ trans}$ = 15.1 Hz, 1 H, C=C*H*-CO), 6.27 (d, $J_{HC=CH\ trans}$ = 15.4 Hz, 1 H, C=C*H*-CO), 6.11 (m, 1 H, C-H$^{anomeric}$), 5.85 (m, 1 H, C-H$^{anomeric}$, H-5$^{uracil}$), 5.83 (d, $J$ = 8.2 Hz, 1 H, H-5$^{uracil}$), 5.61 (dd, $J$ = 11.5 Hz, $J$ = 3.3 Hz, 1 H), 5.53 (dd, $J$ = 11.3 Hz, $J$ = 3.5 Hz, 1 H), 5.49 (d, $J$ = 8.2 Hz, 1 H), 5.43 (m, 1 H), 5.29 – 5.35 (m, 1 H), 5.09 – 5.25 (m, 4 H), 5.01 – 4.10 (m, 1 H), 4.99 (d, $J$ = 9.1 Hz), 4.94 (dd, $J$ = 11.5 Hz, $J$ = 3.3 Hz, 1 H), 4.91 (s, 1 H), 4.52 – 4.60 (m, 1 H), 4.30 – 4.39 (m, 1 H), 4.17 (d, $J$ = 10.4 Hz, $J$ = 2.2 Hz, 1 H), 4.05 – 4.10 (m, 1 H), 3.76 (dd, $J$ = 8.8 Hz, J = 3.5 Hz, 1 H), 3.68 (dd, $J$ = 9.9 Hz, $J$ = 2.0 Hz, 1 H), 2.34 (s, 1 H), 2.29 (s, 2 H, C$H_3^{NHAc}$), 2.27 (s, 1 H, C$H_3^{NHAc}$), 1.87 – 2.22 (m, 24 H, 8 x $CH_3^{Ac}$), 1.59, 1.56, 1.55, 1.53, 1.52 (5 x s, 27

H, 9 x $CH_3^{Boc}$), 1.40 (m, 13 H), 1.08 – 1.18 (m, 2 H, $CH_2^{acyl}$), 0.86, 0.85 (2 x s, 2 x 3 H, $CH_3^{acyl}$); **IR** ν: 2928, 2361, 2341, 1743, 1686, 1369, 1218, 1143, 1029; **MS** *m/z* ($ESI^+$): 1503 [$(M+Na)^+$, 100%]; ($ESI^-$): 1515 [$(M+Cl)^-$, 100%]. Flanking peaks with mass ± 14 corresponded to 8 x $CH_2$, 9 x $CH_2$, 10 x $CH_2$, and 11 x $CH_2$. Full assignment was not possible due to the presence homologues with mass ± 14.

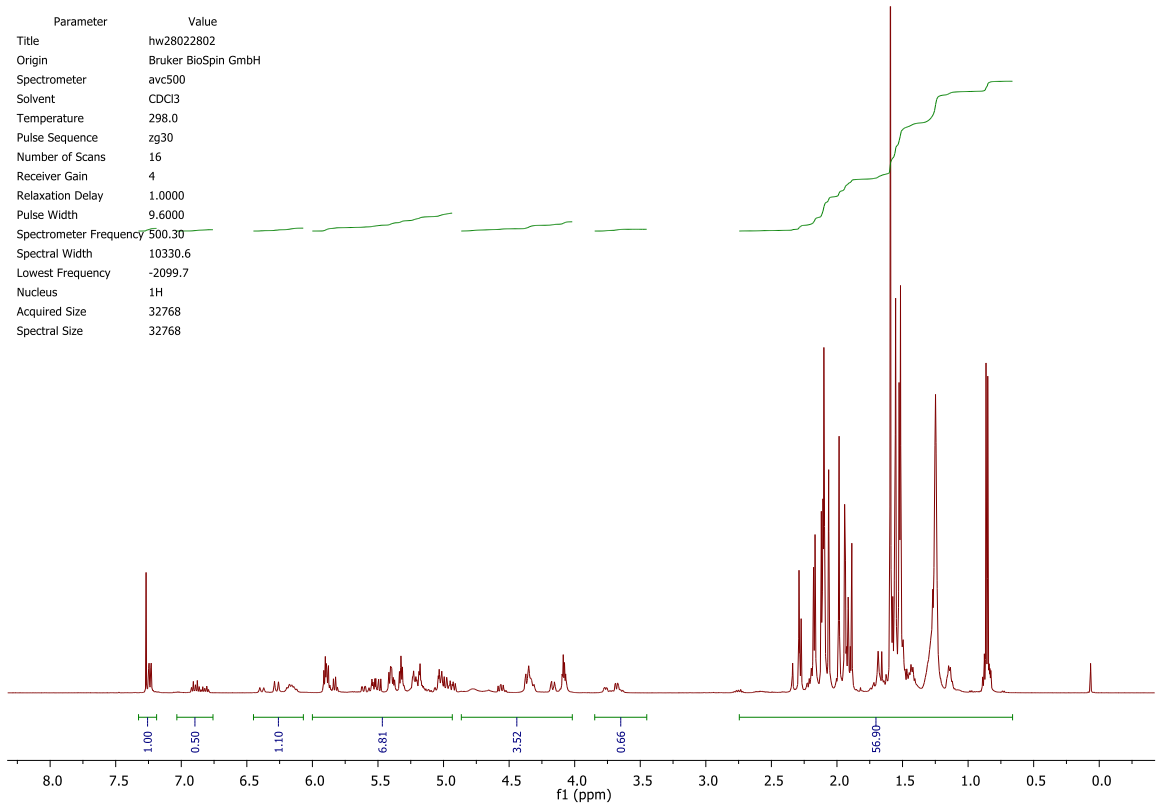


**Tri-*N*-(tert-butoxylcarbonyl)-octa-*O*-acetyl-tunicamycins (6a) $^{1}$H NMR spectrum**

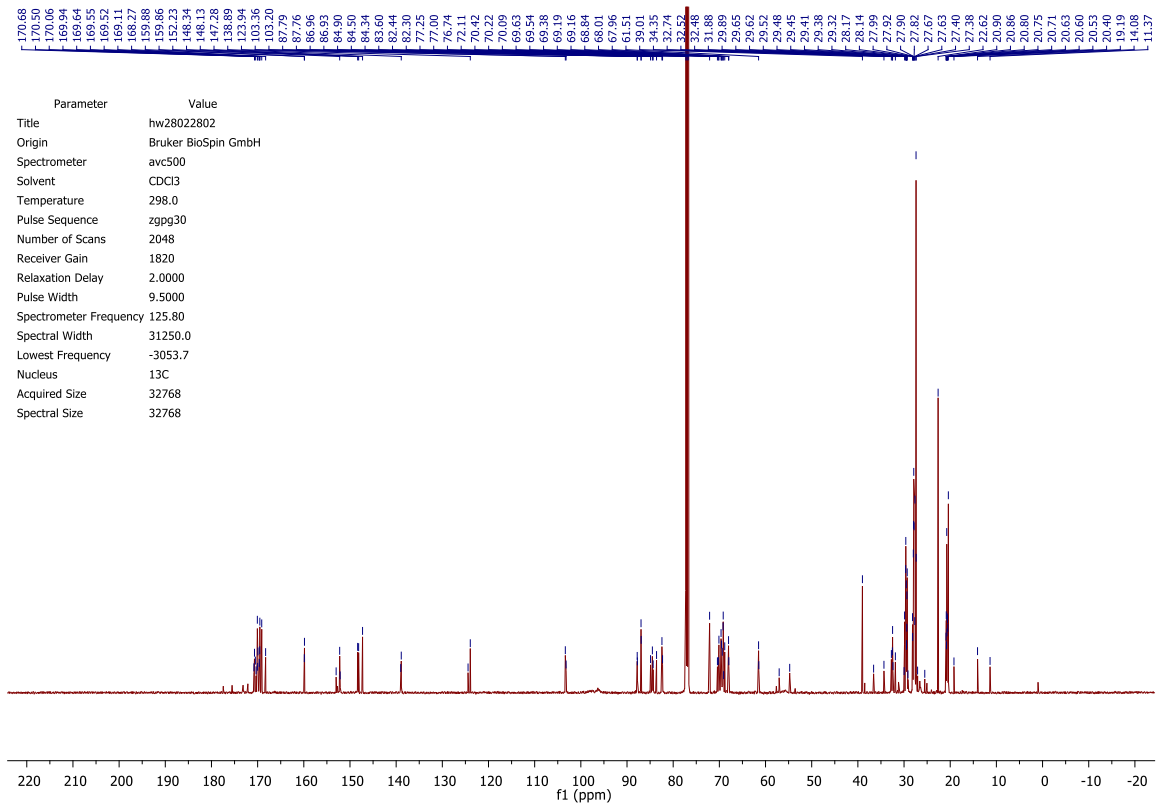


**Tri-*N*-(tert-butoxylcarbonyl)-octa-*O*-acetyl-tunicamycins (6a) $^{13}$C NMR spectrum**

**10',2"-Di-*N*-(tert-butoxycarbonyl)-deacyl-tunicamycin (8a)**

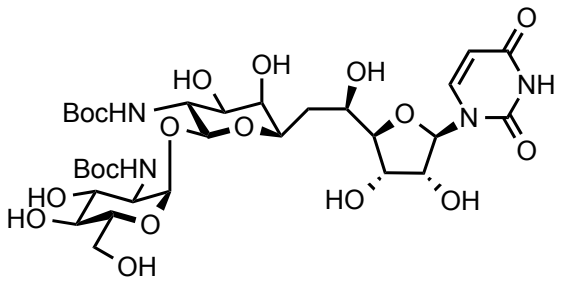


*Reaction condition 1*: **6a** (55.7 mg, 0.038 mmol) was dissolved in dry MeOH (5 mL) and then cooled over ice. NaOMe was added to make a final concentration of 0.01 M. The reaction progress was monitored by TLC (1:3:6, W/*i*POH/EtOAc). After 7 h, the reaction was neutralised with Dowex 50W X8 $H^+$ resin. Then, it was filtered and concentrated *in vacuo*. The product was purified *via* flash column chromatography (W/*i*POH/EtOAc, 1:3:6) to afford **8a** (13.1 mg, 0.017 mmol, 45%) as white amorphous powder.

*Reaction condition 2*: **6a** (13.3 mg, 0.090 mmol) was dissolved in MeOH:$H_2O$ (v/v, 3:1) with the addition of TEA (10 equiv. 0.900 mmol, 6.6 μL), and stirred at RT. The reaction progress was monitored by TLC (1:3:6, W/*i*POH/EtOAc). Reaction was completed after 141 h. The product was purified *via* flash column chromatography (W/*i*POH/EtOAc, 1:3:6) to afford **8a** (5.30 mg, 0.007 mmol, 77%) as white amorphous powder.

*Reaction condition 3*: **6a** (134 mg, 0.091 mmol) was dissolved in MeOH:H2O (v/v, 3:1) with the addition of TEA (25 equiv. 2.27 mmol, 317 μL). The reaction was heated to 71 ˚C. The reaction progress was monitored by TLC (1:2:6, W/*i*POH/EtOAc). Reaction was stpped after 43 h. The crude product was purified by preparative scale HPLC (product

eluted at 9.5 min.) and afforded the **8a** (36.4 mg, 0.047 mmol, 52 %) as white amorphous powder; **TLC:** $R_f$ 0.3 in water/isopropanol/ethyl acetate (W/*i*POH/EtOAc, 1:2:6); **$[\alpha]_D^{20}$** = +54.9 ±0.3 (c 1, MeOH); **Mp** (amorphous) 177.4-181.2 ˚C; **$^1$H NMR** (500 MHz, MeOD) δ ppm 7.91 (d, *J* = 8.1 Hz, 1H, H-6), 5.93 (d, *J* = 5.9 Hz, 1H, H-1'), 5.75 (d, *J* = 8.1 Hz, 1H, H-5), 4.99 (s, 1H, H-1"), 4.70 (d, *J* = 7.9 Hz, 1H, H-11'), 4.24 – 4.16 (m, 2H, H-2', H-3'), 4.05 – 3.97 (m, 2H, H-5', H-5"), 3.86 (t, *J* = 3.3 Hz, 1H, H-4'), 3.81 (dd, *J* = 11.7, 1.8 Hz, 1H, H-6"), 3.77 – 3.65 (m, 3H, H-7', H-9', H-6"), 3.64 (d, *J* = 3.1 Hz, 1H, H-8'), 3.62 (d, *J* = 4.9 Hz, 2H, H-2", H-3"), 3.49 (t, *J* = 9.6 Hz, 1H, H-10'), 3.37 – 3.33 (m, 1H, H-4"), 2.12 – 2.05 (m, 1H, H-6'), 1.57 – 1.49 (m, 1H, H-6'), 1.47 (s, 9H, C$H_3$), 1.45 (s, 9H, C$H_3$); **$^{13}$C NMR** (126 MHz, MeOD) δ ppm 166.17 (C-4), 158.72 (C=O$^{Boc}$), 158.52 (C=O$^{Boc}$), 152.65 (C-2), 142.81 (C-6), 103.09 (C-5), 101.41 (C-11'), 100.62 (C-1"), 89.71 (C-1'), 89.54 (C-4'), 80.74 (*C*-(CH$_3$)$_3$), 80.30 (*C*-(CH$_3$)$_3$), 75.47 (C-2'), 74.51 (C-5"), 73.65 (C-3"), 72.72, 72.57, 72.43 (C-7', C-9', C-4"), 72.36 (C-8'), 70.87 (C-3'), 68.42 (C-5'), 63.17 (C-6"), 56.63 (C-4"), 55.77 (C-10'), 35.94 (C-6'), 29.07((*C*H$_3$)$_3$), 28.85 ((*C*H$_3$)$_3$); **IR** (neat) ν: 3367 (N-H, O-H), 2979 (=C-H), 2930 (-C-H), 1684 (C=O); **LRMS** m/z (ESI$^+$): 789 [(M +Na)$^+$, 100%]; **HRMS** m/z (ESI$^+$): calc. $C_{31}H_{50}N_4O_{18}Na$ (M+Na)$^+$ = 789.3012, found 789.3017.

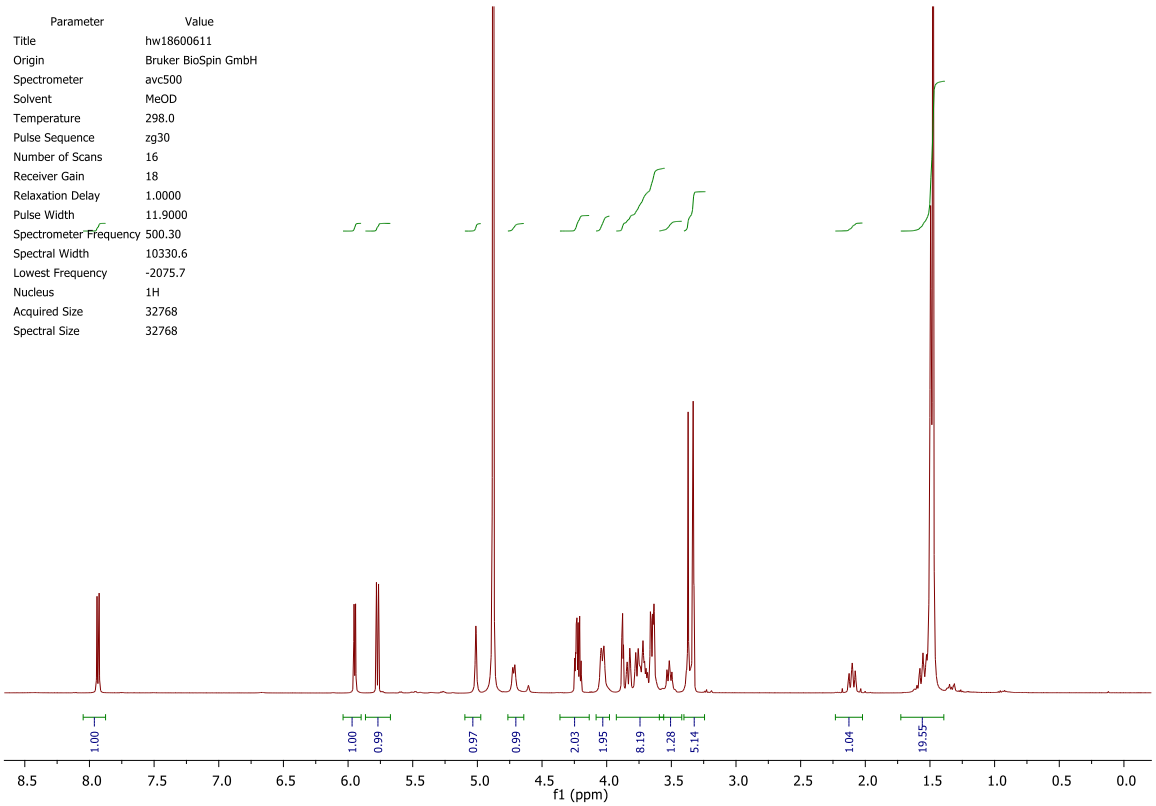


**10',2"-Di-N-(tert-butoxycarbonyl)-deacyl-tunicamycin (8a) $^{1}$H NMR spectrum**

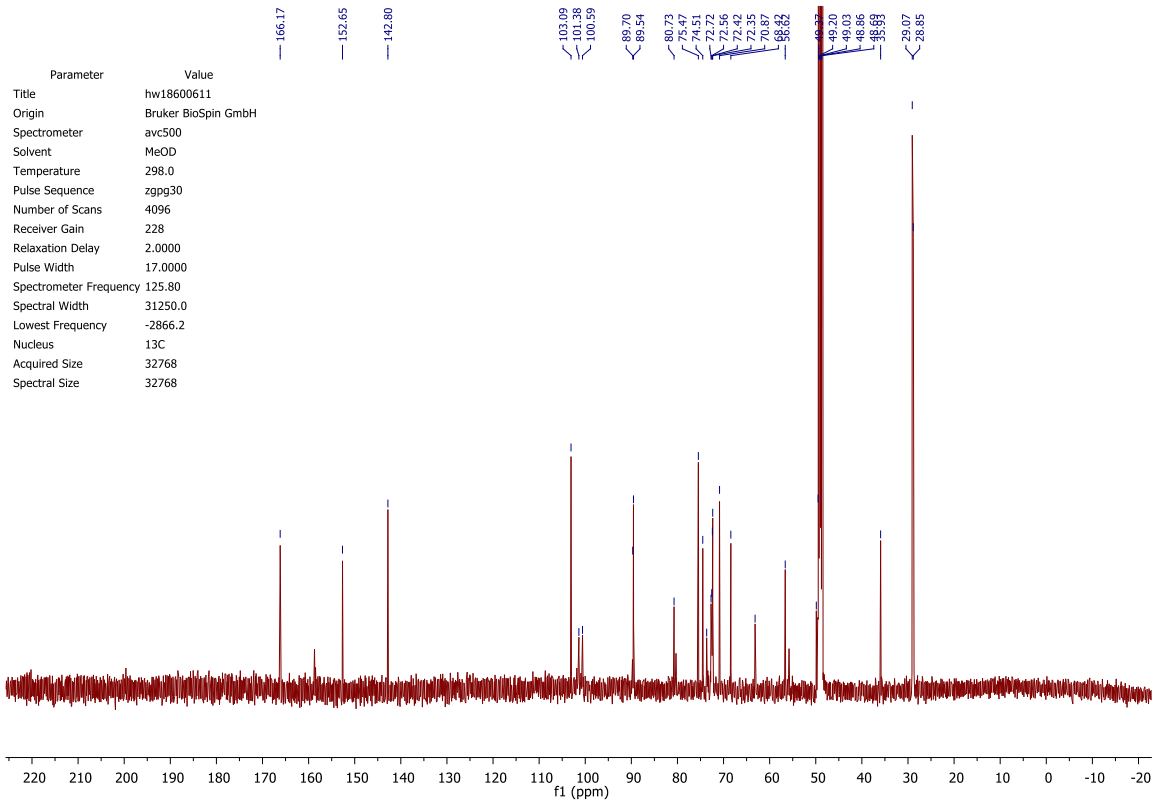


**10',2"-Di-*N*-(tert-butoxycarbonyl)-deacyl-tunicamycin (8a) $^{13}$C NMR spectrum**

**α-D-glucosamine-(1”-11’)-tunicaminyl uracil dihydrochloride (9)**

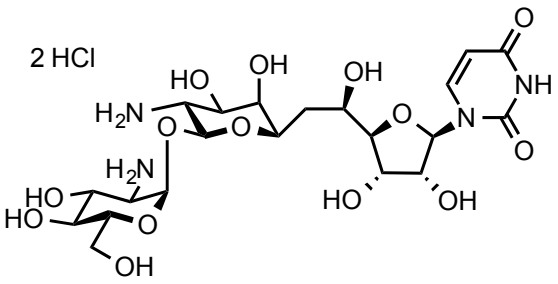


**8a** (1.50 mg, 0.002 mmol) was dissolved in DCM (120 µL) and TFA (0.393 mmol, 30 µL). The reaction was stirred at room temperature for 1 h. The reaction progress was monitored by TLC (1:2:2, W/*i*POH/EtOAc). When the reaction was complete, the reaction mixture was concentrated *in vacuo* and dried. The dried crude product was washed twice with $H_2O$ and DCM. The aqueous fraction was collected, concentrated *in vacuo* and dried. The dried crude product was redissoved in 1 M HCl (1 mL) and stirred for 1 h at room temperature. The product was obtained after lyophilisation, in 99% yield of **9** (1.20 mg, 0.002 mmol). **$[\alpha]_D^{20}$ =** +60.1 ±0.2 (c 1, $H_2O$); **$^1$H NMR** (700 MHz, $D_2O$) δ ppm 7.82 (d, *J* = 8.2 Hz, 1 H, H-6), 5.87 (d, *J* = 8.2 Hz, 1 H, H-5) 5.86 (d, *J* = 5.3 Hz, 1 H, H-1’), 5.53 (d, *J* = 3.4 Hz, 1 H, H-1”), 5.00 (d, *J* = 8.3 Hz, 1 H, H-11’), 4.31 - 4.26 (m, 2 H, H-2’, H-3’), 4.06 (td, *J* = 2.6, 11.1 Hz, 1 H, H-5’), 3.94 (dd, *J* = 3.3, 11.0 Hz, 1 H, H-9’), 3.92 - 3.87 (m, 3 H, H-7’, H-3”, H-5”), 3.84 (d, *J* = 3.2 Hz, 1 H, H-8’), 3.79 (dd, *J* = 3.8, 12.5 Hz, 1 H, H-6”), 3.70 (dd, *J* = 2.2, 12.4 Hz, 1 H, H6”), 3.57 (t, *J* = 9.6 Hz, 1 H, H-4”), 3.39 (dd, *J* = 3.5, 10.8 Hz, 1 H, H-2”), 3.31 (dd, *J* = 8.4, 11.0 Hz, 1 H, H-10’), 1.97 (ddd, *J* = 2.0, 10.4, 14.6 Hz, 1 H, H-6’), 1.70 - 1.64 (dtd, *J* = 2.8, 11.2 Hz, 1 H, H-6’); **$^{13}$C NMR** (176 MHz, MeOD) δ ppm 166.17 (C-4), 151.77 (C-2), 141.98 (C-6), 102.45 (C-5), 99.42 (C-11’), 97.04 (C-1”), 88.68 (C-1’), 86.90 (C-4’), 73.43 (C-2’), 73.22 (C-5”), 71.81 (C-7”), 69.54 (C-8’), 69.31 (C-3”), 69.18 (C-9’), 68.94 (C-4’), 68.72 (C-3’), 66.89 (C-5’), 59.85 (C-6”), 53.82 (C-2”), 52.98 (C-10’), 33.28 (C-6’); **IR** (neat) ν: 3295 (N-H, O-H), 3057 (=C-H),

2922 (-C-H), 1673 (C=O), 1263 (C-N), 1109 (C-O), 1064 (C-O); **LRMS** m/z ($ESI^+$): 567 [$(M+H)^+$, 100%]; **HRMS** m/z ($ESI^+$): calc. $C_{21}H_{35}N_4O_{14}$ $(M+H)^+$ = 567.2144, found 567.2136.

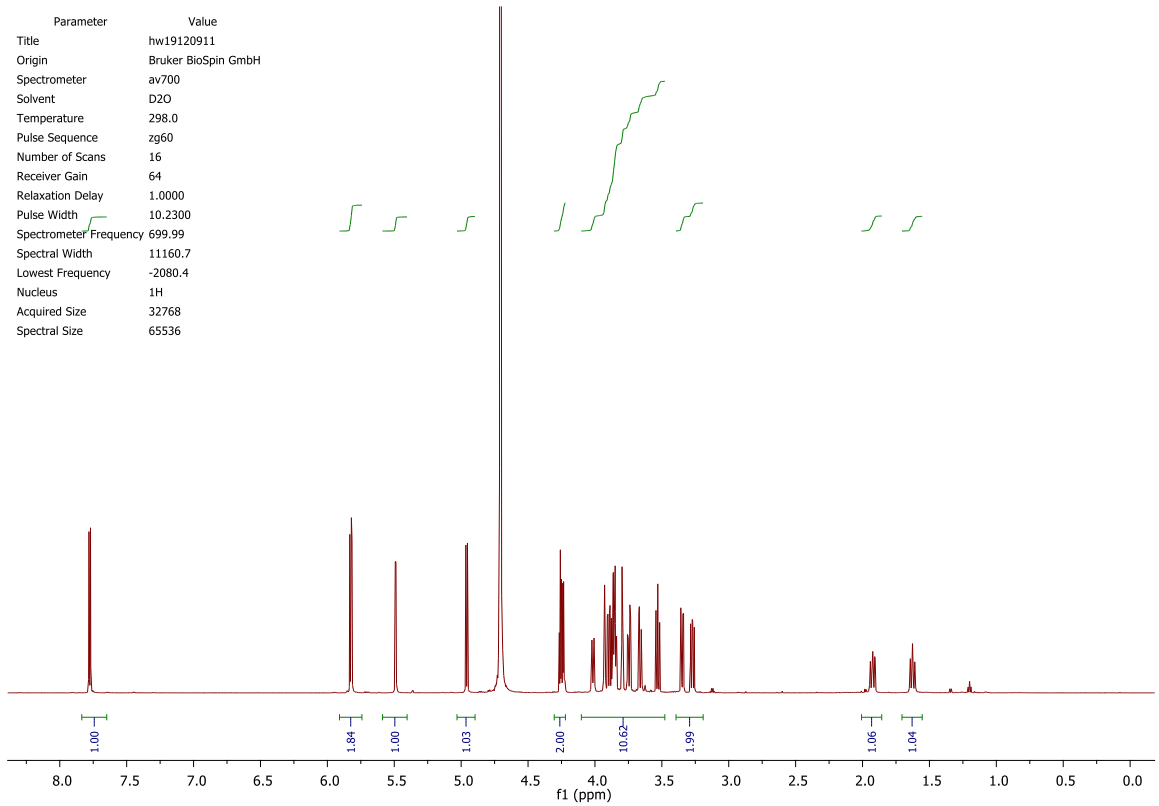


**α-D-glucosamine-(1”-11’)-tunicaminyl uracil dihydrochloride (9) $^{1}$H NMR spectrum**

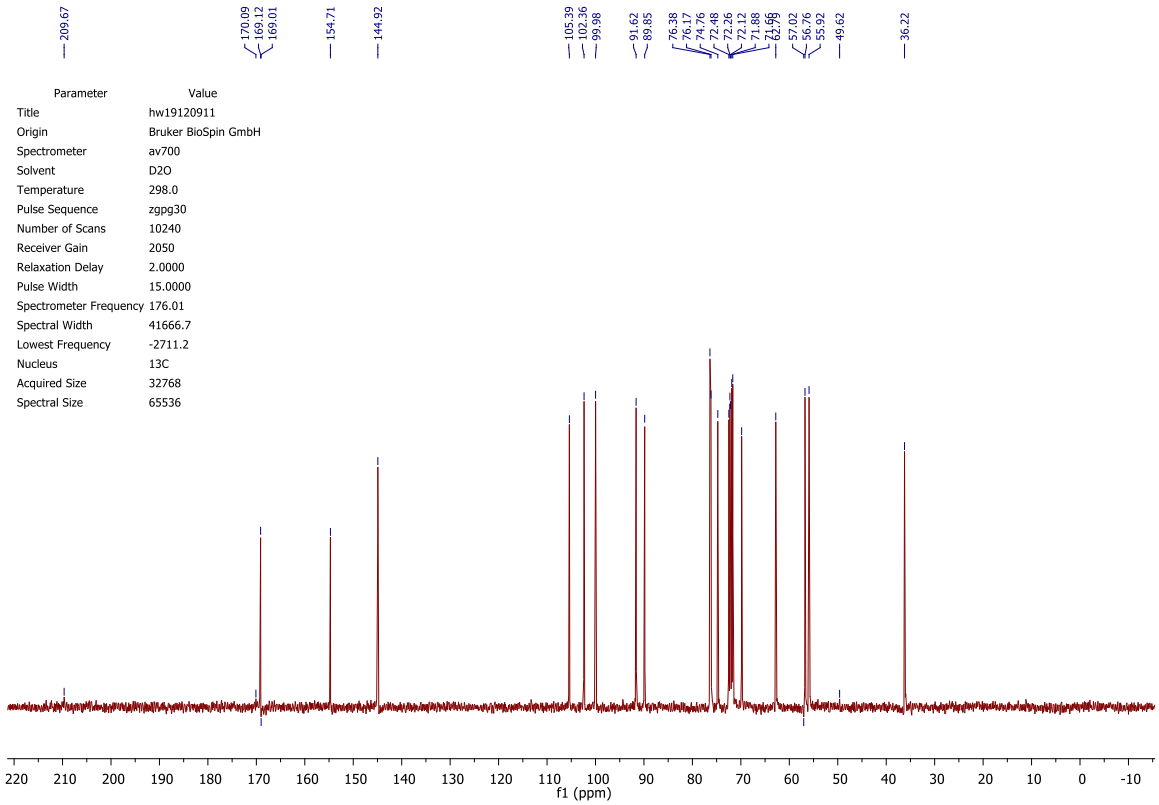


**α-D-glucosamine-(1”-11’)-tunicaminyl uracil dihydrochloride (9) $^{13}$C NMR spectrum**

**Di-*N'*,*N"*-heptanoyl tunicamycin (10)**

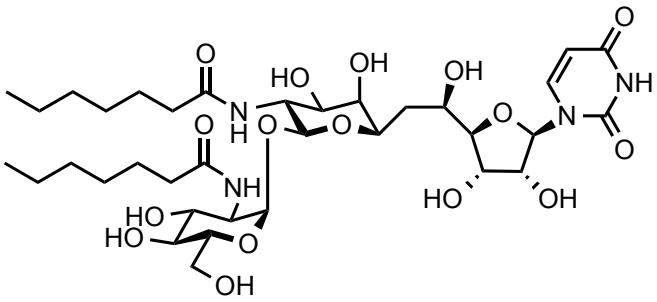

Heptanoic acid (5.5 µL, 0.039 mmol, 2.5 eq.) was added to DMF (0.25 mL) with the addition of TEA (2 µL) and DMAP (3.80 mg, 0.031 mmol, 2 eq.) and stirred at room temperature for 1 h. Then, **9** (10 mg, 0.016 mmol) was dissolved in DMF (0.25 mL) with the addition of TEA (4.1 µL), and added to the heptanoic acid reaction mixture. TEA was added to final of 4 equivalents (8.7 µL total). The reaction mixture was stirred at room temperature. The reaction progress was checked by TLC (1/3/6, $H_2O$/*i*PrOH/EtOAc) and HPLC. The reaction was stopped after 24 h. The product was purified by HPLC, eluted at 12 min. The lyophilised product was washed with DCM and MilliQ water and resulted in 4.80 mg (0.006 mmol) of the final product (**10**) in 39% yield. $\mathbf{R_f}$ = 0.4 (1/3/6, $H_2O$/*i*PrOH/ EtOAc); $\mathbf{[\alpha]_D^{20}}$ = +26.8 ±0.7 (c 0.2, MeOH); **Mp** N/A; **$^1$H NMR** (500 MHz, MeOD) δ ppm 7.92 (d, *J* = 8.1 Hz, 1H, H-6), 5.93 (d, *J* = 6.0 Hz, 1H, H-1'), 5.75 (d, *J* = 8.1 Hz, 1H, H-5), 4.94 (d, *J* = 3.4 Hz, 1H, H-1"), 4.61 (d, *J* = 8.5 Hz, 1H, H-11'), 4.24 – 4.16 (m, 2H, H-2', H-3'), 4.06 – 3.99 (m, 2H, H-5', H-5"), 3.95 (dd, *J* = 10.2, 8.6 Hz, 1H, H-10'), 3.90 (dd, *J* = 10.6, 3.5 Hz, 1H, H-2"), 3.87 – 3.81 (m, 2H, H-4', H-6"), 3.77 (appt br d, *J* = 9.1 Hz, 1H, H-7'), 3.71 – 3.62 (m, 4H, H-8', H-9', H-3", H-6"), 3.34 (appt s, 1H, H-4"), 2.38 – 2.02 (m, 5H, 2x$CH_2^{\text{fatty acyl}}$, H-6'), 1.69 – 1.49 (m, 5H, 2x$CH_2^{\text{fatty acyl}}$, H-6'), 1.41 – 1.28 (m, 15H, $CH_2^{\text{fatty acyl}}$), 0.92 (t, *J* = 6.8 Hz, 6H, $CH_3^{\text{fatty acyl}}$); **$^{13}$C NMR** (126 MHz, MeOD) δ ppm 177.18, 176.59, (2C, -N-C=O$^{\text{fatty acyl}}$), 166.17, (C-4), 152.64, (C-2), 142.77, (C-6), 103.06, (C-5), 101.28, (C-11'), 99.92, (C-1"), 89.77, (C-1'), 89.63, (C-4'), 75.53, (C-2'),

74.37, (C-5”), 73.04, (2C, C-8’, C-9’), 72.61, (C-4”), 72.49, (C-7’), 72.11, (C-3”), 70.89, (C-3’), 68.34, (C-5’), 63.27, (C-6”), 54.76, (C-2”), 54.47, (C-10’), 37.81, 37.22, (2C, -CO*C*$H_2$-$^{\text{fatty acyl}}$), 35.94, (C-6’), 32.87, 32.81, 30.26, 27.01, 26.82, 23.68, (6C, -*C*$H_2$-$^{\text{fatty acyl}}$), 14.44. (1C, -*C*$H_3^{\text{fatty acyl}}$); **IR** (neat) ν: 3305 (O-H), 2927 (C-H), 2856 (C-H), 1682 (C=O), 1645 (C=O),1552 (C=C), 1467 ($CH_2$), 1376 ($CH_3$), 1259 (C-O), 1094 (C-N); **LRMS** m/z ($ESI^+$): 813 [$(M+Na)^+$, 100%]; **HRMS** m/z ($ESI^+$): calc. $C_{35}H_{58}N_4O_{16}$ $(M+Na)^+$ = 813.3740, found 813.3708.

*H-4” signal in the $^1H$ NMR spectrum observed to be partially overlapped by the solvent peak. Not all aliphatic signals in carbon spectrum were resolved. Characterisation was assisted by COSY and HSQC.*

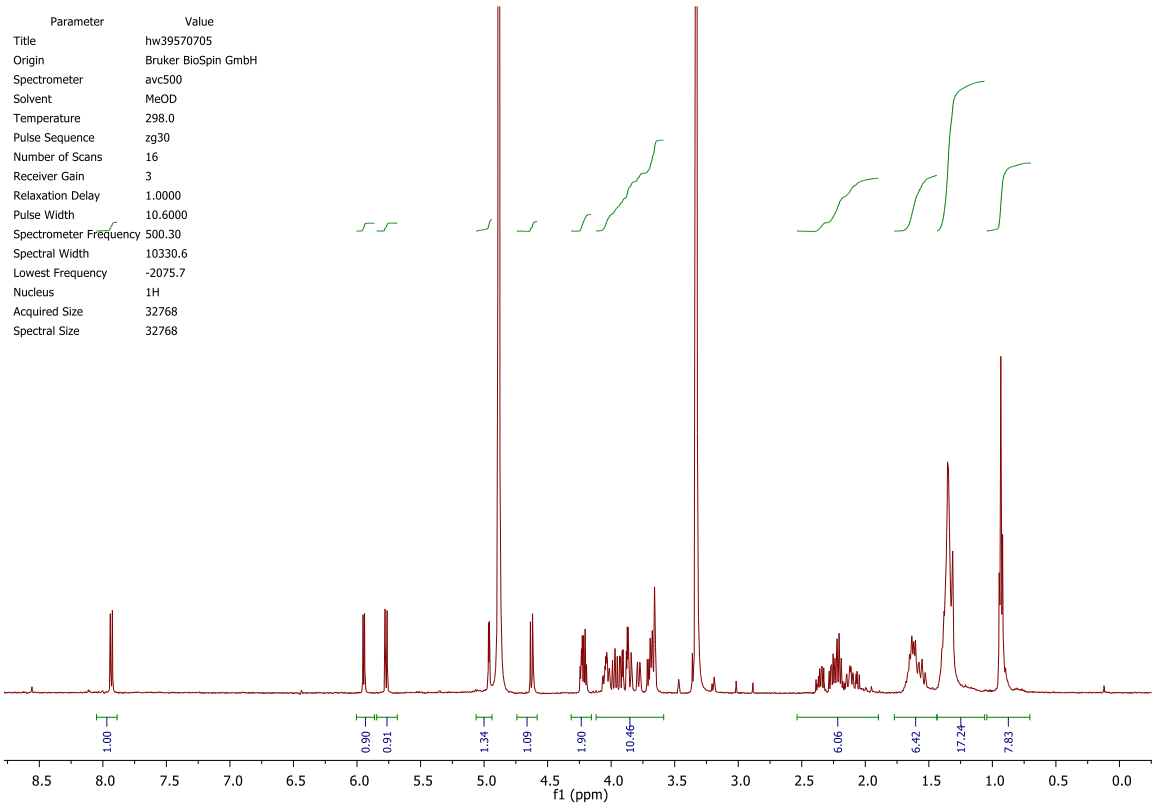


**Di-*N'*,*N"*-heptanoyl tunicamycin (10) $^{1}$H NMR spectrum**

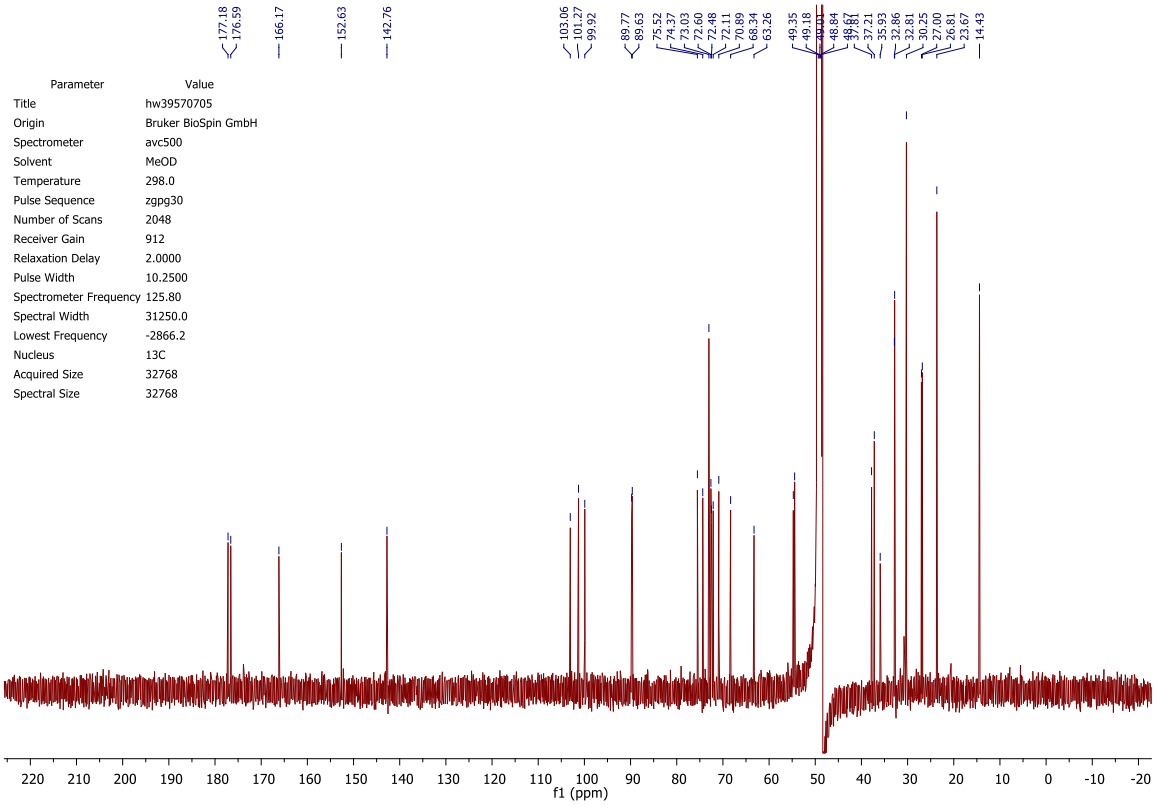


**Di-*N'*,*N"*-heptanoyl tunicamycin (10) $^{13}$C NMR spectrum**

**Di-*N'*,*N"*-octanoyl tunicamycin (11)**

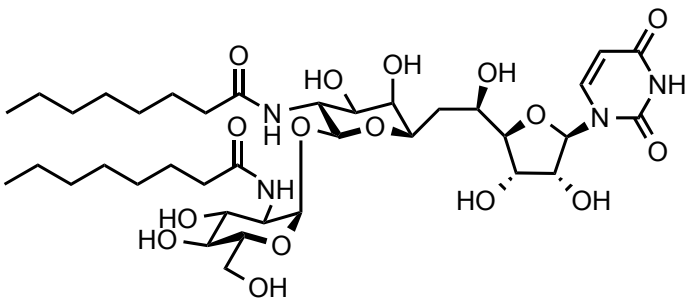

*Reaction condition 1*: **8a** (13.0 mg, 0.017 mmol) was dissolved in TFA (1 mL) and stirred 1 h. TLC (1:2:2, W/*i*POH/EtOAc) showed baseline spot. The reaction mixture was cooled to 0 °C and neutralised by TEA by dropwise addition. The neutralised mixture was then concentrated *in vacuo,* redissolved in THF with the addition of 4-(dimethylamino)pyridine (2.07 mg, 0.017 mmol), *N,N'*-dicyclohexylcarbodiimide (10.0 mg, 0.048 mmol), and octanoic acid (10 eq., 0.170 mmol, 26.8 µL). After 12 h TLC (W/*i*PrOH/EtOAc, 1:2:2) showed mixture of products. Work up with water and hexane, water fraction collected, filtered and co-evaporated with toluene. Purification *via* reverse-phase flash column chromatography (1:9 to 5:5, ACN/W) afforded **11** (9.00 mg, 0.011 mmol, 65%) as off-white powder; **TLC:** $R_f$ 0.4 in isopropanol/ethyl acetate (*i*POH/EtOAc, 3:7); **RP-TLC:** $R_f$ 0.3 in water/acetonitrile (W/ACN, 1:1)

*Reaction condition 2*: Octanoic acid (19 µL, 0.117 mmol, 2.5 eq.) was added to DMF (0.25 mL) with the addition of TEA (8.70 µL), *N,N'*-diisopropylcarbodiimide (2.5 eq., 18 µL, 15.0 mg, 0.117 mmol), and DMAP (11.5 mg, 0.094 mmol, 2 eq.), and stirred at room temperature for one hour. Then, **9** (30.0 mg, 0.047 mmol) was dissolved in DMF (0.25 mL) with the addition of TEA (17.5 µL), and added to the octanoic acid reaction mixture. TEA was added to final of 4 equivalents. The reaction mixture was stirred at room temperature. The reaction progress was checked by TLC (1/3/6, $H_2O$/*i*PrOH/EtOAc) and

HPLC. The reaction was stopped after 78 h. The product was purified by HPLC, eluted at 13.5 min. The lyophilised product was washed with DCM and MilliQ water and resulted in 2.5mg of the final product, 33% yield. **$R_f$** = 0.3 (1/3/6, $H_2O$/*i*PrOH/EtOAc); **$[\alpha]_D^{20}$** = +57.4 ±0.4 (c 0.2, MeOH); **Mp** N/A; **$^1$H NMR** (500 MHz, MeOD) δ ppm 7.91 (d, *J* = 8.1 Hz, 1H, H-6), 5.92 (d, *J* = 6.0 Hz, 1H, H-1'), 5.75 (d, *J* = 8.1 Hz, 1H, H-5), 4.94 (d, *J* = 3.4 Hz, 1H, H-1"), 4.60 (d, *J* = 8.5 Hz, 1H, H-11'), 4.24 – 4.15 (m, 2H, H-2', H-3'), 4.06 – 3.98 (m, 2H, H-5', H-5"), 3.95 (dd, *J* = 10.0, 8.6 Hz, 1H, H-10'), 3.90 (dd, *J* = 10.6, 3.4 Hz, 1H, H-2"), 3.87 – 3.80 (m, 2H, H-4', H-6"), 3.76 (dd, *J* = 10.6, 1.6 Hz, 1H, H-7'), 3.70 – 3.61 (m, 4H, H-8', H-9', H-3", H-6"), 3.34 (appt d, *J* = 4.0 Hz, 1H, H-4"), 2.38 – 2.14 (m, 4H, 2x$CH_2^{\text{fatty acyl}}$), 2.10 (m, 1H, H-6'), 1.70 – 1.57 (m, 4H, 2x$CH_2^{\text{fatty acyl}}$), 1.53 (ddd, *J* = 13.9, 11.4, 2.2 Hz, 1H, H-6'), 1.41 – 1.24 (appt br m, 16H, C*H*$_2^{\text{fatty acyl}}$), 0.91 (t, *J* = 6.9 Hz, 6H, C*H*$_3^{\text{fatty acyl}}$); **$^{13}$C NMR** (126 MHz, MeOD) δ ppm 177.17, 176.58, (2C, -N-C=O$^{\text{fatty acyl}}$), 166.16 (C-4), 152.63 (C-2), 142.76 (C-6), 103.07 (C-5), 101.31 (C-11'), 99.95 (C-1"), 89.78 (C-1'), 89.63 (C-4'), 75.53 (C-2'), 74.37 (C-5"), 73.05 (2C, C-8', C-9'), 72.61 (C-4"), 72.49 (C-7'), 72.11 (C-3"), 70.90 (C-3'), 68.34 (C-5'),63.27 (C-6"), 54.76 (C-2"), 54.47 (C-10'), 37.81, 37.21 (2C, -CO*C*H$_2$-$^{\text{fatty acyl}}$), 35.94 (C-6'), 33.00, 32.97, 30.56, 30.33, 30.27, 27.05, 26.85, 23.75 (8C, -*C*H$_2$-$^{\text{fatty acyl}}$), 14.45 (2C, -*C*H$_3^{\text{fatty acyl}}$); **IR** (neat) ν: 3297 (O-H), 2957 (C-H), 2925 (C-H), 2853 (C-H), 1684 (C=O), 1644 (C=O), 1556 (C=C), 1469 ($CH_2$), 1258 (C-O), 1091 (C-N), 1016 (=C-H); **LRMS** m/z (ESI$^-$): 931 [(M+TFA-H)$^-$, 100%]; **HRMS** m/z (ESI$^+$): calc. $C_{37}H_{62}N_4O_{16}Na$ (M+Na)$^+$ = 841.4053, found 841.4045.

*H-4" signal in the $^1$H NMR spectrum observed to be partially overlapped by the solvent peak. Not all aliphatic signals in carbon spectrum were resolved. Characterisation was assisted by COSY and HSQC.*

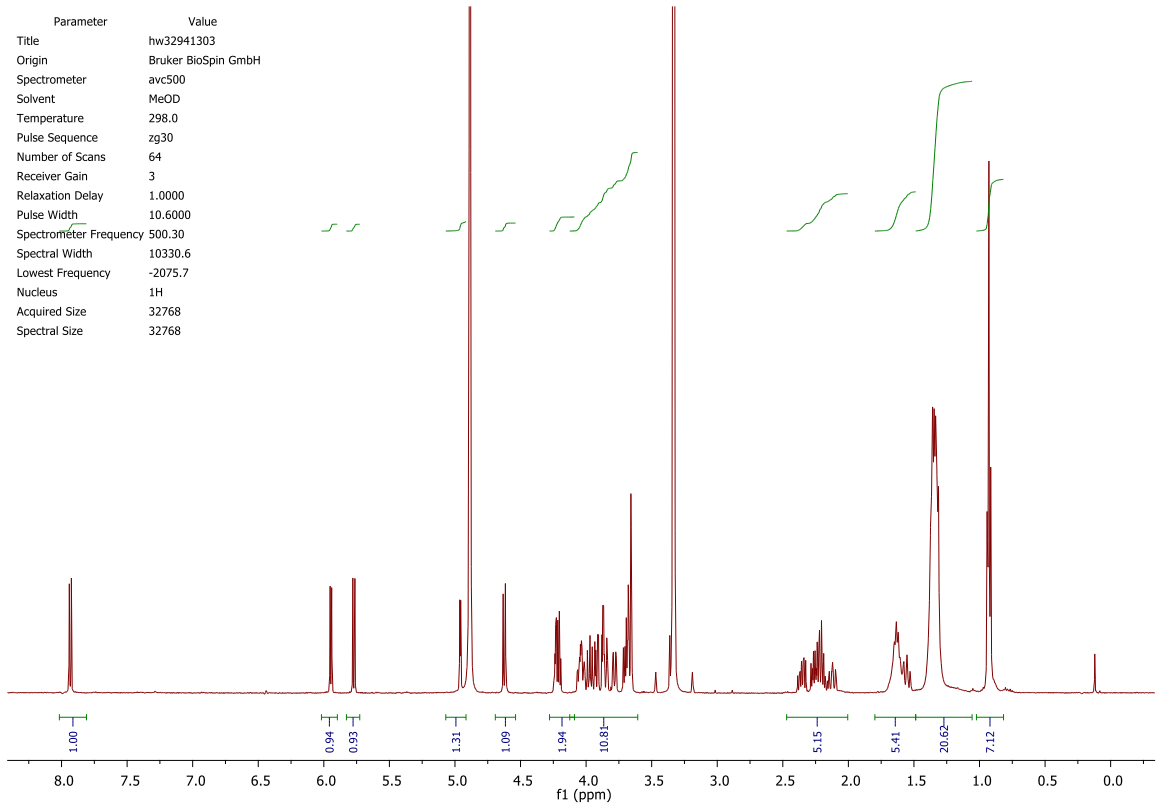


**Di-*N'*,*N"*-octanoyl tunicamycin (11) $^{1}$H NMR spectrum**

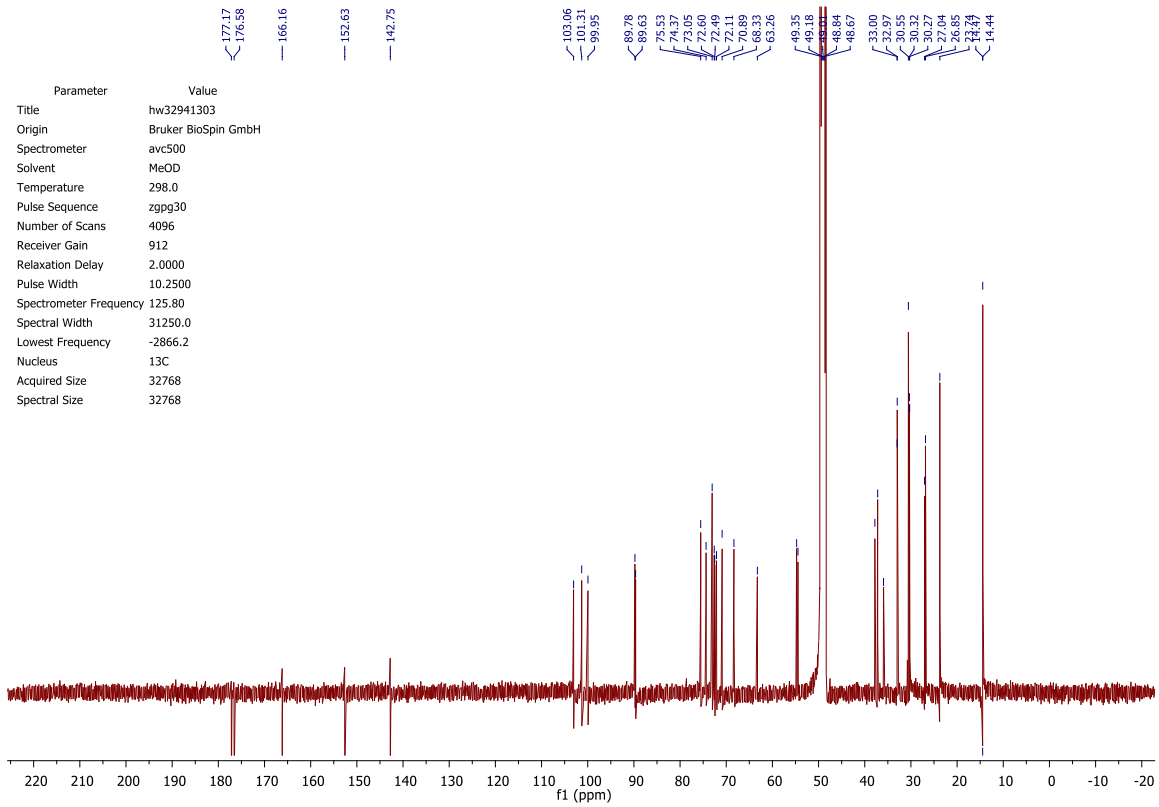


**Di-*N'*,*N"*-octanoyl tunicamycin (11) $^{13}$C NMR spectrum**

**Di-*N'*,*N"*-nonanoyl tunicamycin (12)**

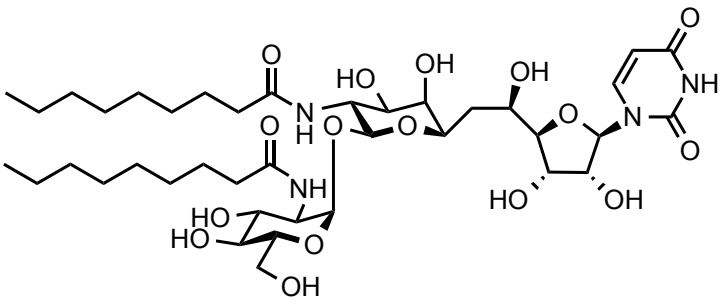

Nonanoic acid (20.0 µL, 0.117 mmol, 2.5 eq.) was added to DMF (0.25 mL) with the addition of TEA (8.70 µL), *N,N'*-diisopropylcarbodiimide (2.5 eq., 18 µL, 15.0 mg, 0.117 mmol), and DMAP (11.5 mg, 0.094 mmol, 2 eq.), and stirred at room temperature for one hour. Then, **9** (30.0 mg, 0.047 mmol) was dissolved in DMF (0.25 mL) with the addition of TEA (17.5 µL), and added to the nonanoic acid reaction mixture. TEA was added to final of 4 equivalents (26.2 µL total). The reaction mixture was stirred at room temperature. The reaction progress was checked by TLC (1/3/6, $H_2O$/*i*PrOH/EtOAc) and HPLC. The reaction was stopped after 78 h. The product was purified by HPLC, eluted at 15 min. The lyophilised product was washed with DCM and MilliQ water and resulted in 3.4 mg of the final product, 39% yield. $\mathbf{R_f}$ = 0.4 (1/3/6, $H_2O$/*i*PrOH/EtOAc); $\mathbf{[\alpha]_D^{20}}$ = +53.8 ±1.2 (c 0.3, MeOH); **Mp** N/A; **$^1$H NMR** (500 MHz, MeOD) δ ppm 7.93 (d, *J* = 8.1 Hz, 1H, H-6), 5.95 (d, *J* = 5.9 Hz, 1H, H-1'), 5.77 (d, *J* = 8.1 Hz, 1H, H-5), 4.96 (d, *J* = 3.0 Hz, 1H, H-1"), 4.62 (d, *J* = 8.6 Hz, 1H, H-11'), 4.26 – 4.18 (m, 2H, H-2', H-3'), 4.08 – 4.00 (m, 2H, H-5', H-5"), 3.97 (t, *J* = 9.1 Hz, 1H, H-10'), 3.92 (dd, *J* = 10.7, 3.2 Hz, 1H, H-2"),3.89 – 3.81 (m, 2H, H-4', H-6"), 3.78 (appt br d, *J* = 9.8 Hz, 1H, H-7'), 3.73 – 3.63 (m, 4H, H-8', H-9', H-3", H-6"), 3.36 (appt d, *J* = 4.2 Hz, 1H, H-4"), 2.41 – 2.16 (m, 4H, 2x$CH_2^{\text{fatty acyl}}$), 2.12 (appt br t, *J* = 12.1 Hz, 1H, H-6'), 1.71 – 1.59 (m, *J* = 6.7 Hz, 4H, 2x$CH_2^{\text{fatty acyl}}$), 1.55 (appt br t, *J* = 12.6 Hz, 1H, H-6'), 1.34 (s, 20H, C$H_2^{\text{fatty acyl}}$), 0.93 (t, *J* = 6.5 Hz, 6H, C$H_3^{\text{fatty acyl}}$); **$^{13}$C NMR** (126 MHz, MeOD) δ ppm 177.17, 176.58 (2C, -N-

C=O$^{\text{fatty acyl}}$), 166.16 (C-4), 152.63 (C-2), 142.76 (C-6), 103.06 (C-5), 101.32 (C-11'), 99.97 (C-1"), 89.78 (C-1'), 89.62 (C-4'), 75.53 (C-2'), 74.37 (C-5"), 73.06, 73.04 (2C, C-8', C-9'), 72.60 (C-4"), 72.49 (C-7'), 72.11 (C-3"), 70.89 (C-3'), 68.33 (C-5'), 63.27 (C-6"), 54.76 (C-2"), 54.46 (C-10'), 37.82, 37.21 (2C, -CO*C*H$_2$-$^{\text{fatty acyl}}$), 35.94 (C-6'), 33.10, 33.09, 30.62, 30.58, 30.45, 30.43, 27.05, 26.85, 23.77 (9C, -*C*H$_2$-$^{\text{fatty acyl}}$), 14.47 (1C, -*C*H$_3$$^{\text{fatty acyl}}$); **IR** (neat) ν: 3301 (O-H), 2923 (C-H), 2852 (C-H), 1738 (C=O), 1646 (C=O), 1544 (C=C), 1420 ($CH_2$), 1366 ($CH_3$), 1229 (C-O), 1092 (C-N), 1015 (=C-H); **LRMS** m/z (ESI$^-$): 891 [(M+FA-H)$^-$, 100%]; **HRMS** m/z (ESI$^-$): calc. $C_{39}H_{65}N_4O_{16}$ $(M-H)^-$ = 845.4401, found 845.4412.

*H-4" signal in the $^1$H NMR spectrum observed to be partially overlapped by the solvent peak. Not all aliphatic signals in carbon spectrum were resolved. Characterisation was assisted by COSY and HSQC.*

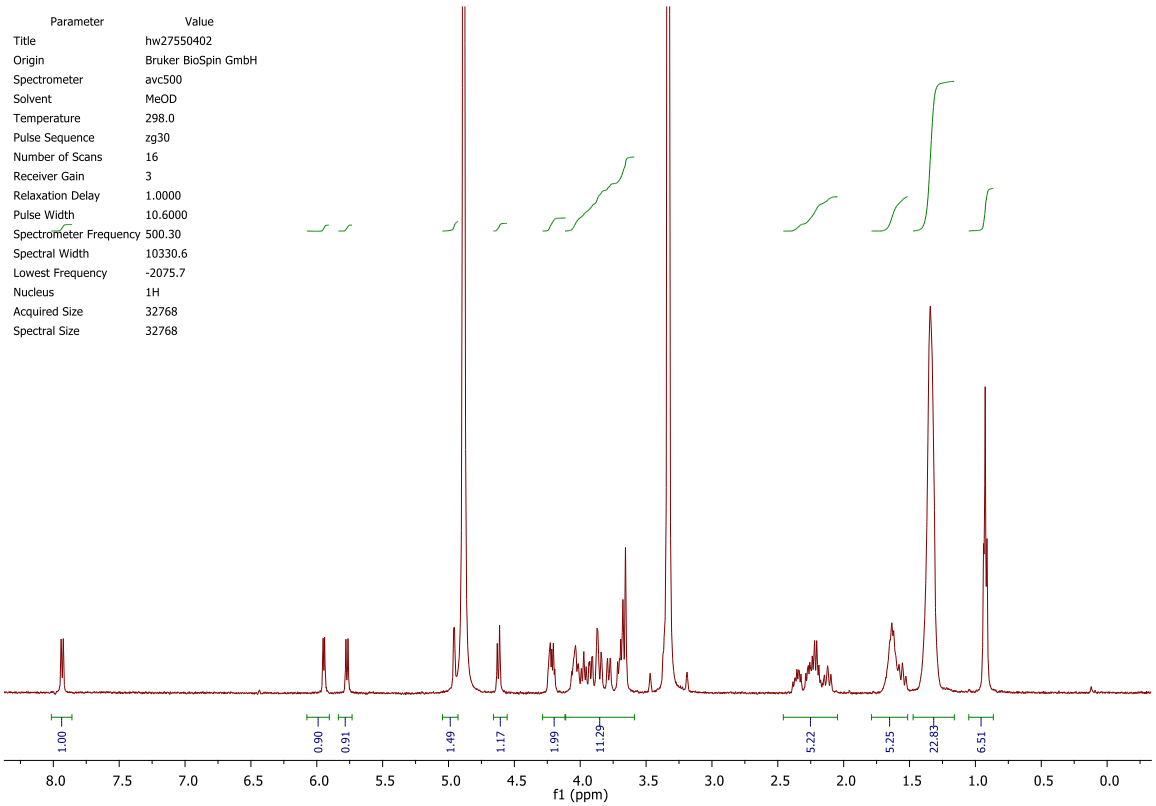


**Di-*N'*,*N"*-nonanoyl tunicamycin (12) $^{1}$H NMR spectrum**

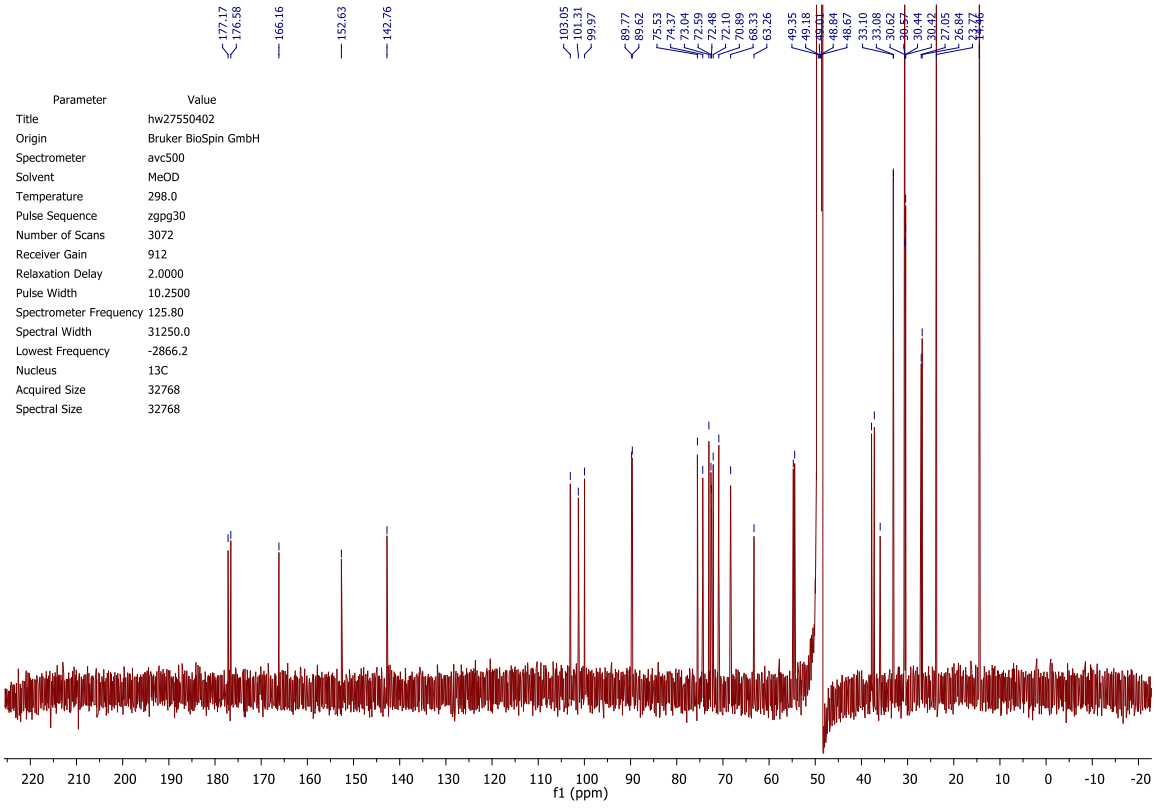


**Di-*N'*,*N"*-nonanoyl tunicamycin (12) $^{13}$C NMR spectrum**

**Di-*N'*,*N"*-decanoyl tunicamycin (13)**

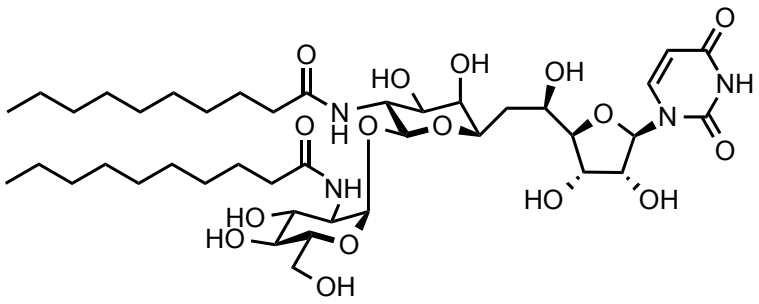

Decanoic acid (21.0 µL, 0.117 mmol, 2.5 eq.) was added to DMF (0.25 mL) with the addition of TEA (8.70 µL), *N,N'*-diisopropylcarbodiimide (2.5 eq., 18 µL, 15.0 mg, 0.117 mmol), and DMAP (11.5 mg, 0.094 mmol, 2 eq.), and stirred at room temperature for one hour. Then, **9** (30.0 mg, 0.047 mmol) was dissolved in DMF (0.25 mL) with the addition of TEA (17.5 µL), and added to the decanoic acid reaction mixture. TEA was added to final of 4 equivalents (26.2 µL total). The reaction mixture was stirred at room temperature and reaction progress was checked by TLC (1/3/6, $H_2O$/*i*PrOH/EtOAc) and HPLC. The reaction was stopped after 78 hours. The product was purified by HPLC, eluted at 16.5 min. The lyophilised product was washed with DCM and MilliQ water and resulted in 3mg of the final product, 39% yield. **$R_f$** = 0.4 (1/3/6, $H_2O$/*i*PrOH/EtOAc); **$[\alpha]_D^{20}$** = +38.0 ±0.6 (c 0.3, MeOH); **Mp** N/A; **$^1$H NMR** (500 MHz, MeOD) δ ppm 7.91 (d, *J* = 8.1 Hz, 1H, H-6), 5.92 (d, *J* = 6.0 Hz, 1H, H-1'), 5.75 (d, *J* = 8.1 Hz, 1H, H-5), 4.93 (d, *J* = 3.4 Hz, 1H, H-1"), 4.59 (d, *J* = 8.5 Hz, 1H, H-11'), 4.23 – 4.16 (m, 2H, H-2', H-3'), 3.97 – 3.92 (m, 2H, H-5', H-5"), 3.90 (appt t, *J* = 8.5 Hz, 1H, H-10'), 3.84 (dd, *J* = 10.6, 3.4 Hz, 1H, H-2"), 3.87 – 3.80 (m, 2H, H-4', H-6"), 3.76 (appt br dd, *J* = 10.7, 1.7 Hz, 1H, H-7'), 3.71 – 3.61 (m, 4H, H-8', H-9', H-3", H-6"), 3.33 (appt d, *J* = 5.8 Hz, 1H, H-4"), 2.38 – 2.02 (m, 4H, 2x$CH_2^{\text{fatty acyl}}$), 2.10 (m, 1H, H-6'), 1.69 – 1.49 (m, 4H, 2x$CH_2^{\text{fatty acyl}}$), 1.55 (m, 1H, H-6'), 1.30 (s, 24H, $CH_2^{\text{fatty acyl}}$), 0.90 (t, *J* = 6.9 Hz, 6H, $CH_3^{\text{fatty acyl}}$); **$^{13}$C NMR** (126 MHz, MeOD) δ ppm 177.17, 176.58 (2C, -N-C=O$^{\text{fatty acyl}}$), 166.16 (C-4),

152.63 (C-2), 142.76 (C-6), 103.06 (C-5), 101.33 (C-11'), 100.00 (C-1"), 89.78 (C-1'), 89.62 (C-4'), 75.53 (C-2'), 74.37 (C-5"), 73.07, 73.04 (2C, C-8', C-9'), 72.60 (C-4"), 72.49 (C-7'), 72.11 (C-3"), 70.90 (C-3'), 68.33 (C-5'), 63.27 (C-6"), 54.76 (C-2"), 54.46 (C-10'), 37.82, 37.20 (2C, -CO*C*$H_2$-$^{\text{fatty acyl}}$), 35.94 (C-6'), 33.12, 30.74, 30.72, 30.68, 30.63, 30.53, 27.05, 26.84, 23.78 (9C, -*C*$H_2$-$^{\text{fatty acyl}}$), 14.48 (2C, -*C*$H_3$$^{\text{fatty acyl}}$); **IR** (neat) ν: 3305 (O-H), 2922 (C-H), 2851 (C-H), 1683 (C=O), 1645 (C=O),1551 (C=C), 1468 ($CH_2$), 1260 (C-O), 1094 (C-N), 1017 (=C-H); **LRMS** m/z ($ESI^-$): 919 [$(M+FA-H)^-$, 100%]; **HRMS** m/z ($ESI^+$): calc. $C_{41}H_{70}N_4O_{16}Na$ $(M+Na)^+$ = 897.4679, found 897.4666.

*H-4" signal in the $^1H$ NMR spectrum observed to be partially overlapped by the solvent peak. Not all aliphatic signals in carbon spectrum were resolved. Characterisation was assisted by COSY and HSQC.*

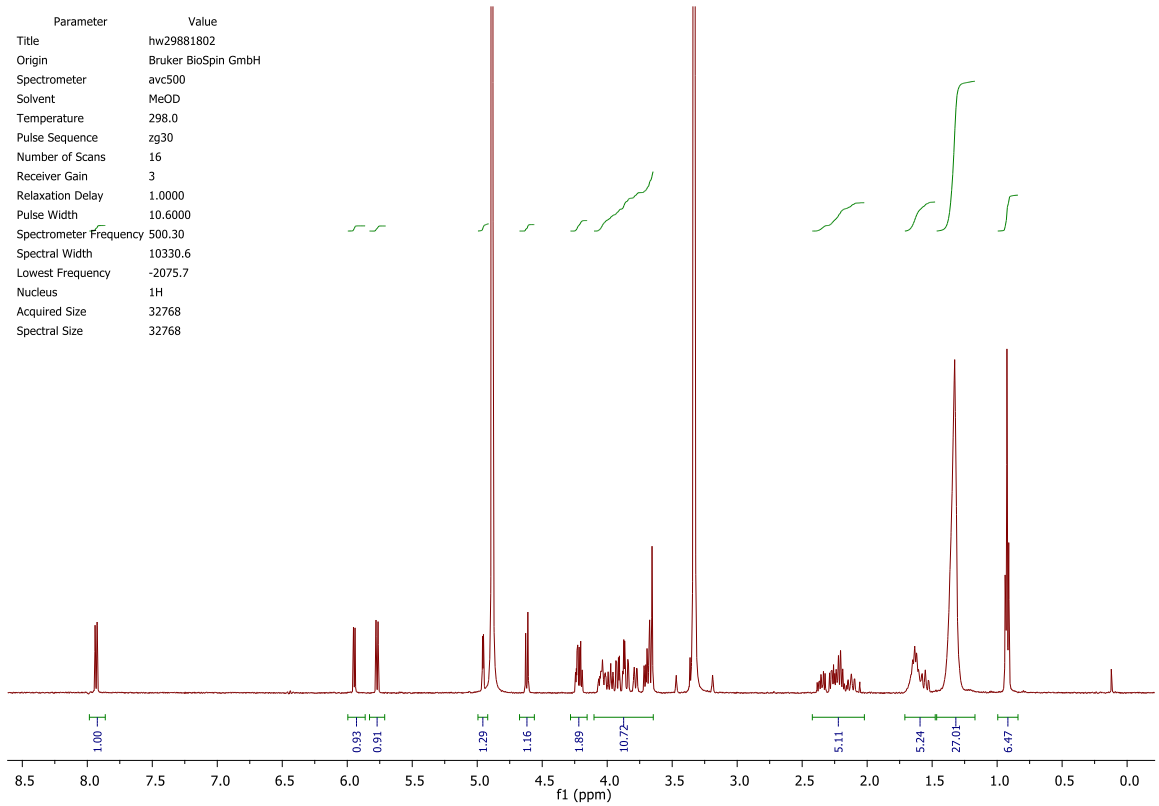


**Di-*N'*,*N"*-decanoyl tunicamycin (13) $^{1}$H NMR spectrum**

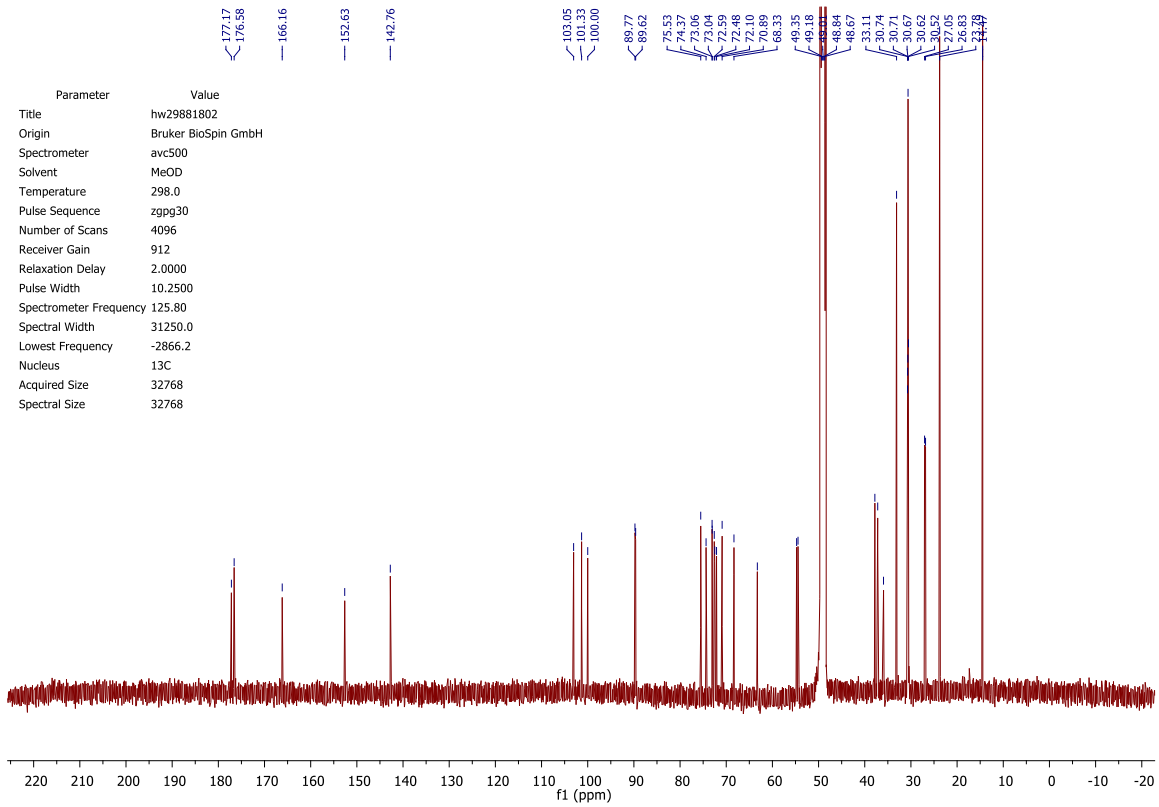


**Di-*N'*,*N"*-decanoyl tunicamycin (13) $^{13}$C NMR spectrum**

**Di-*N'*,*N"*-undecanoyl tunicamycin (14)**

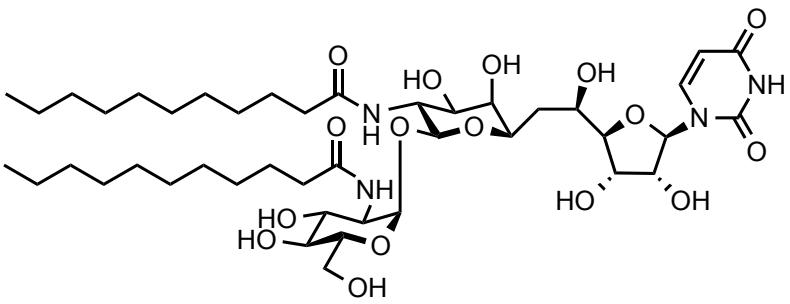

Undecanoic acid (23.0 μL, 0.117 mmol, 2.5 eq.) was added to DMF (0.25 mL) with the addition of TEA (8.70 μL), *N,N'*-diisopropylcarbodiimide (2.5 eq., 18 μL, 15.0 mg, 0.117 mmol), and DMAP (11.5 mg, 0.094 mmol, 2 eq.), and stirred at room temperature for one hour. Then, **9** (30.0 mg, 0.047 mmol) was dissolved in DMF (0.25 mL) with the addition of TEA (17.5 μL), and added to the undecanoic acid reaction mixture. TEA was added to final of 4 equivalents (26.2 μL total). The reaction mixture was stirred at room temperature and reaction progress was checked by TLC (1/3/6, $H_2O$/*i*PrOH/EtOAc) and HPLC. The reaction was stopped after 78 hours. The product was purified by HPLC, eluted at 18 min. The lyophilised product was washed with DCM and MilliQ water and resulted in 3mg of the final product, 36% yield. $\mathbf{R_f}$ = 0.4 (1/3/6, $H_2O$/*i*PrOH/EtOAc); $\mathbf{[\alpha]_D^{20}}$ = +30.9 ±0.4 (c 0.25, MeOH); **Mp** N/A; **$^1$H NMR** (500 MHz, MeOD) δ ppm 7.91 (d, *J* = 8.1 Hz, 1H, H-6), 5.92 (d, *J* = 6.0 Hz, 1H, H-1'), 5.75 (d, *J* = 8.1 Hz, 1H, H-5), 4.93 (d, *J* = 3.4 Hz, 1H, H-1"), 4.60 (d, *J* = 8.5 Hz, 1H, H-11'), 4.23 – 4.15 (m, 2H, H-2', H-3'), 4.05 – 3.98 (m, 2H, H-5', H-5"), 3.95 (m, 1H, H-10'), 3.90 (dd, *J* = 10.6, 3.4 Hz, 1H, H-2"), 3.86 – 3.80 (m, 2H, H-4', H-6"), 3.76 (appt br dd, *J* = 10.7, 1.8 Hz, 1H, H-7'), 3.71 – 3.61 (m, 4H, H-8', H-9', H-3", H-6"), 3.34 (m, 1H, H-4"), 2.37 – 2.14 (m, 4H, 2x$CH_2^{\text{fatty acyl}}$), 2.13 – 2.05 (m, 1H, H-6'), 1.68 – 1.56 (m, 4H, 2x$CH_2^{\text{fatty acyl}}$), 1.57 – 1.49 (m, 1H, H-6'), 1.30 (appt br s, 32H, $CH_2^{\text{fatty acyl}}$), 0.90 (t, *J* = 6.9 Hz, 6H, $CH_3^{\text{fatty acyl}}$); **$^{13}$C NMR** (126 MHz, MeOD) δ ppm 177.17, 176.57, (2C, -N-C=O$^{\text{fatty acyl}}$), 166.22 (C-4), 152.67

(C-2), 142.76 (C-6), 103.06 (C-5), 101.34 (C-11'), 100.02 (C-1"), 89.78 (C-1'), 89.62 (C-4'), 75.53(C-2'), 74.37(C-5"), 73.07, 73.05(2C, C-8', C-9'), 72.59 (C-4"), 72.49 (C-7'), 72.10 (C-3"), 70.90 (C-3'), 68.33 (C-5'), 63.27(C-6"), 54.76(C-2"), 54.46(C-10'), 37.82, 37.20(2C, -CO*C*$H_2$-$^{fatty\ acyl}$), 35.94(C-6'), 33.13, 30.82, 30.79, 30.77, 30.68, 30.64, 30.63, 30.54, 27.05, 26.83, 23.79 (11C, -*C*$H_2$-$^{fatty\ acyl}$), 14.48 (2C, -*C*$H_3$$^{fatty\ acyl}$); **IR** (neat) ν: 3297 (O-H), 2956 (C-H), 2921(C-H), 2852 (C-H), 1738 (C=O), 1719 (C=O), 1680 (C=C), 1645 (C=O), 1550 (N-H), 1468 ($CH_2$), 1366 ($CH_3$), 1229 (C-O-C), 1217 (C-OH), 1260 (C-O), 1092 (C-N), 1017 (=C-H); **LRMS** m/z ($ESI^-$): 947 [$(M+FA-H)^-$, 100%]; **HRMS** m/z ($ESI^+$): calc. $C_{43}H_{73}N_4O_{16}$ $(M-H)^-$ = 901.5027, found 901.5015.

*H-4" signal in the $^1H$ NMR spectrum observed to be partially overlapped by the MeOD solvent peak. Not all aliphatic signals in carbon spectrum were resolved. Characterisation was assisted by COSY and HSQC.*

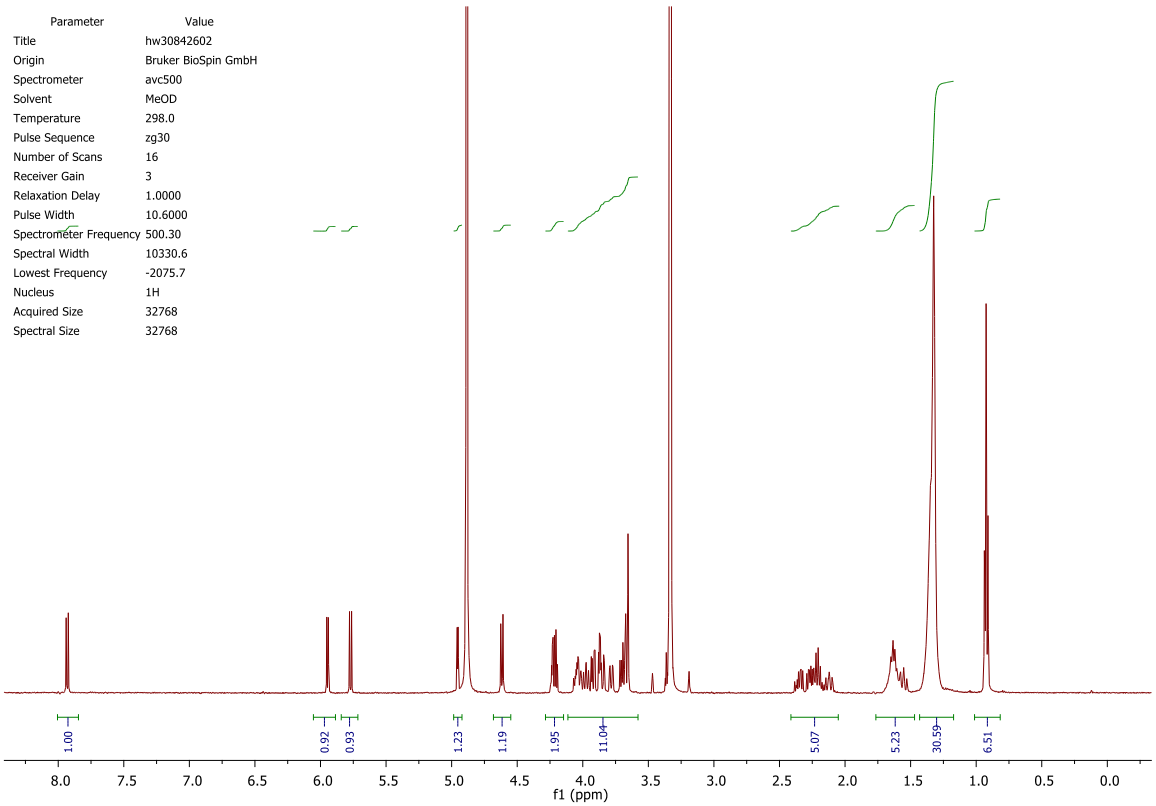


**Di-*N'*,*N"*-undecanoyl tunicamycin (14) $^{1}$H NMR spectrum**

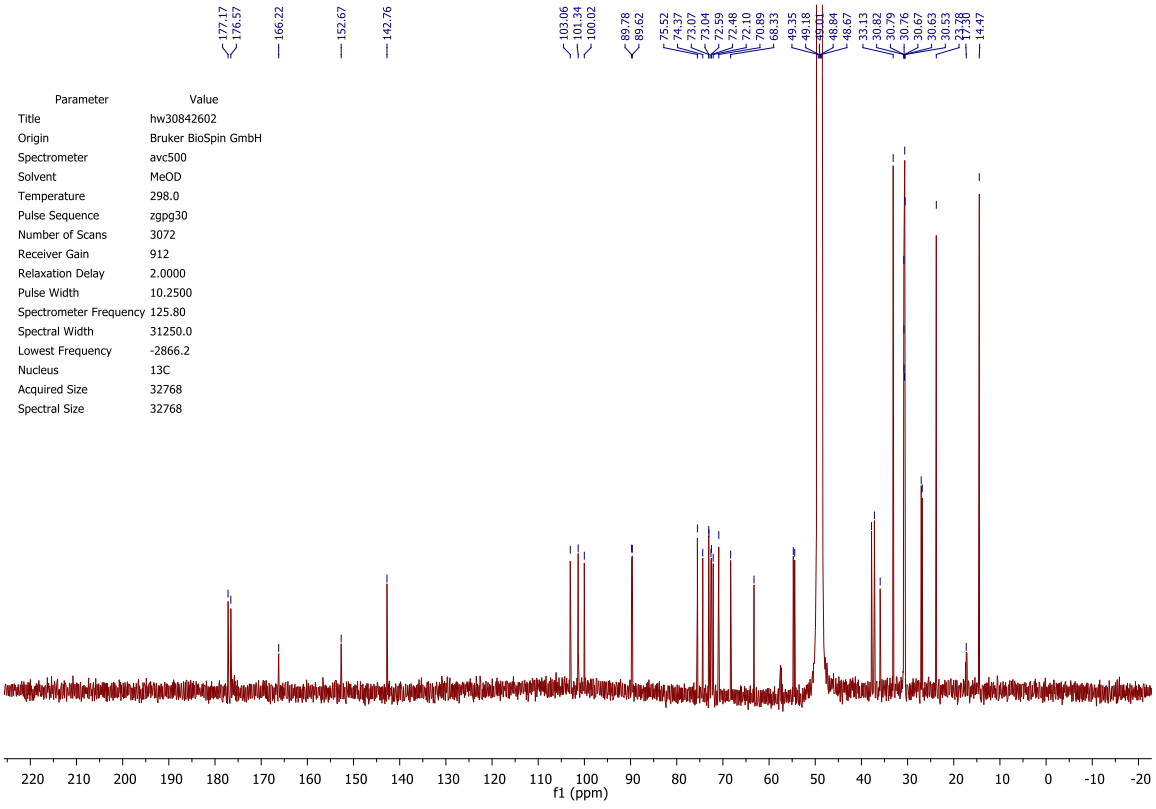


**Di-*N'*,*N"*-undecanoyl tunicamycin (14) $^{13}$C NMR spectrum**

**Di-*N'*,*N"*-dodecanoyl tunicamycin (15)**

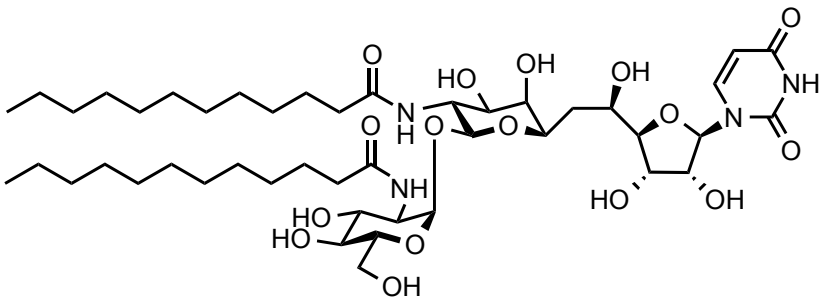

Dodecanoic acid (5.4 mg, 0.027 mmol, 2.5 equiv) was added to DMF (0.25 mL) with the addition of TEA (2.0 μL), *N,N'*-diisopropylcarbodiimide (2.5 eq., 4.3 μL, 0.028 mmol), and DMAP (2.60 mg, 0.022 mmol, 2 eq.), and stirred at room temperature for one hour. Then, **9** (6.90 mg, 0.011 mmol) was dissolved in DMF (0.25 mL) with the addition of TEA (4.0 μL), and added to the dodecanoic acid reaction mixture. TEA was added to final of 4 equivalents (6.0 μL total). The reaction mixture was stirred at room temperature and reaction progress was checked by TLC (1/3/6, $H_2O$/*i*PrOH/EtOAc) and HPLC. The reaction was stopped after 68 hours. The product was purified by HPLC, eluted at 20.5 min. The lyophilised product was washed with DCM and MilliQ water and resulted in 3mg of the final product, 31% yield. $\mathbf{R_f}$ = 0.4 (1/3/6, $H_2O$/*i*PrOH/EtOAc); $\mathbf{[\alpha]_D^{20}}$ = +15.9 ±0.4 (c 0.25, MeOH); **Mp** N/A; $^1$H NMR (500 MHz, MeOD) δ 7.92 (d, *J* = 8.1 Hz, 1H, H-6), 5.93 (d, *J* = 5.9 Hz, 1H, H-1'), 5.76 (d, *J* = 8.1 Hz, 1H, H-5), 4.94 (d, *J* = 3.5 Hz, 1H, H-1"), 4.60 (d, *J* = 8.5 Hz, 1H, H-11'), 4.24 – 4.17 (m, 2H, H-2', H-3'), 4.08 – 3.99 (m, 2H, H-5', H-5"), 3.96 (m, *J* = 8.6 Hz,1H, H-10'), 3.91 (dd, *J* = 10.6, 3.4 Hz, 1H, H-2"), 3.88 – 3.80 (m, 2H, H-4', H-6"), 3.77 (appt br dd, *J* = 11.1, 1.8 Hz, 1H, H-7'), 3.72 – 3.61 (m, 4H, H-8', H-9', H-3", H-6"), 2.39 – 2.15 (m, 4H, 2x$CH_2^{\text{fatty acyl}}$), 2.11 (m, 1H, H-6'), 1.70 – 1.57 (m, 4H, 2x$CH_2^{\text{fatty acyl}}$), 1.54 (m, 1H, H-6'), 1.40-1.28 (appt broad m, 32H, $CH_2^{\text{fatty acyl}}$), 0.91 (t, *J* = 6.9 Hz, 6H, $CH_3^{\text{fatty acyl}}$); **$^{13}$C NMR** (126 MHz, MeOD) δ ppm 177.17, 176.57 (2C, -N-C=O$^{\text{fatty acyl}}$), 166.16 (C-4), 152.63 (C-2), 142.76 (C-6), 103.06

(C-5), 101.35 (C-11'), 100.04 (C-1"), 89.77 (C-1'), 89.62 (C-4'), 75.52 (C-2'), 74.37 (C-5"), 73.08, 73.04 (2C, C-8', C-9'), 72.60 (C-4"), 72.49 (C-7'), 72.10 (C-3"), 70.90 (C-3'), 68.33 (C-5'), 63.27 (C-6"), 54.76 (C-2"), 54.45 (C-10'), 37.82, 37.19 (2C, -CO*C*$H_2$-$^{fatty\ acyl}$), 35.94 (C-6'), 30.87, 30.83, 30.79, 30.77, 30.68, 30.65, 30.63, 30.55, 27.05, 26.83, 23.79 (11C, -*C*$H_2$-$^{fatty\ acyl}$), 14.48 (2C, -*C*$H_3$$^{fatty\ acyl}$); **IR** (neat) ν: 3297 (O-H), 2956 (C-H), 2921 (C-H), 2851 (C-H), 1682 (C=O), 1646 (C=O), 1556 (C=C), 1468 ($CH_2$), 1260 (C-O), 1092 (C-N), 1016 (=C-H); **LRMS** m/z ($ESI^-$): 976 [$(M+FA-H)^-$, 100%]; **HRMS** m/z ($ESI^+$): calc. $C_{45}H_{78}N_4O_{16}Na$ $(M+Na)^+$ = 953.5305, found 953.5334.

*H-4" signal in the $^1H$ NMR spectrum observed to be partially overlapped by the solvent peak. Not all aliphatic signals in carbon spectrum were resolved. Characterisation was assisted by COSY and HSQC.*

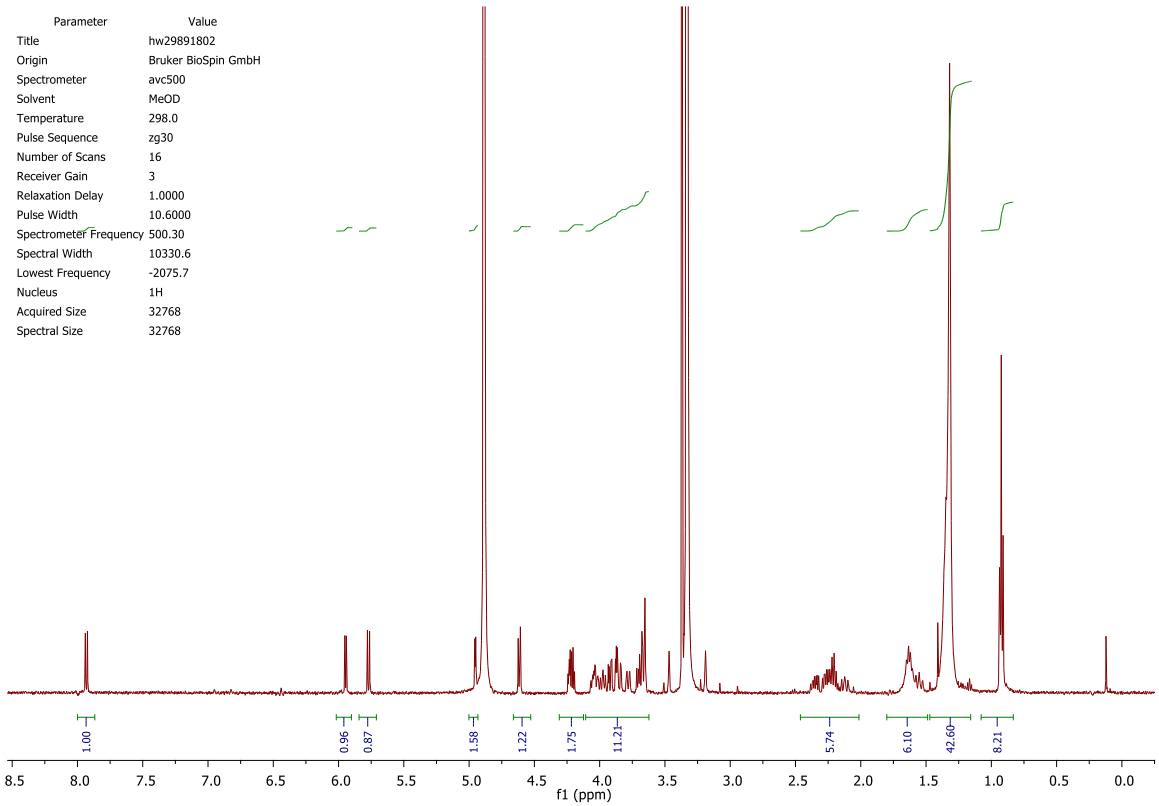


**Di-*N'*,*N"*-dodecanoyl tunicamycin (15) $^{1}$H NMR spectrum**

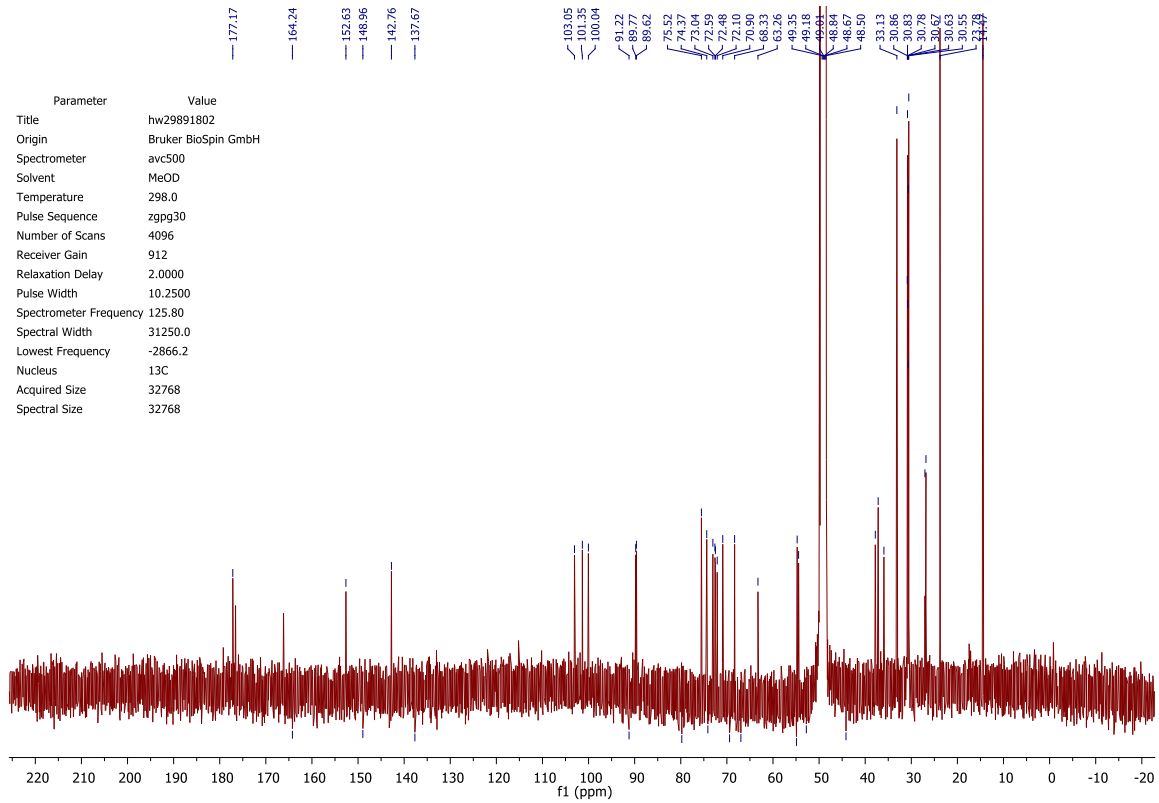


**Di-*N'*,*N"*-dodecanoyl tunicamycin (15) $^{13}$C NMR spectrum**

**Di-*N'*,*N"*-citronellyl tunicamycin (16)**

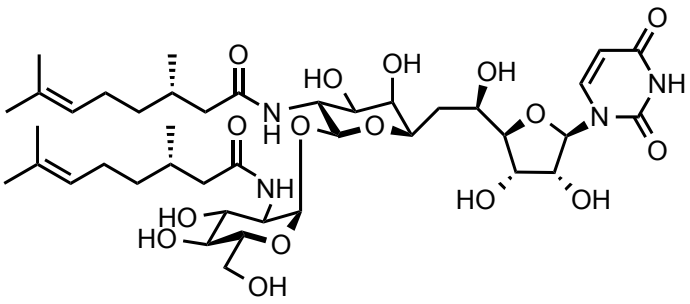

(S)-(-)-citronellic acid (5.0 µL, 0.027 mmol, 2.5 eq.) was added to DMF (0.25 mL) with the addition of TEA (2.0 µL), *N,N'*-diisopropylcarbodiimide (2.5 eq., 4.3 µL, 0.027 mmol), and DMAP (2.70 mg, 0.022 mmol, 2 eq.), and stirred at room temperature for one hour. Then, **9** (7.00 mg, 0.011 mmol) was dissolved in DMF (0.25 mL) with the addition of TEA (4.06 µL), and added to the citronellic acid reaction mixture. TEA was added to final of 4 equivalents (6.1 µL total). The reaction progress was checked by TLC (1/3/6, $H_2O$/*i*PrOH/EtOAc) and HPLC. The reaction was stopped after 168 h. The product was purified by HPLC, eluted at 14 min. The lyophilised product was washed with DCM and MilliQ water and resulted in 5.1mg of the final product, 54% yield. $\mathbf{R_f}$ = 0.4 (1/3/6, $H_2O$/ *i*PrOH/EtOAc); $\mathbf{[\alpha]_D^{20}}$ = +45.2 ±0.2 (c 0.4, MeOH); **Mp** N/A; **$^1$H NMR** (500 MHz, MeOD) δ ppm 7.91 (d, *J* = 8.1 Hz, 1H, H-6), 5.92 (d, *J* = 5.9 Hz, 1H), H-1'), 5.75 (d, *J* = 8.1 Hz, 1H, H-5), 5.11 (td, *J* = 7.0, 1.0 Hz, 2H, H-5"'), 4.96 (d, *J* = 3.4 Hz, 1H, H-1"), 4.58 (d, *J* = 8.5 Hz, 1H, H-11'), 4.24 – 4.15 (m, 2H, H-2', H-3'), 4.06 – 3.95 (m, 3H, H-5', H-10', H-5"), 3.91 (dd, *J* = 10.6, 3.5 Hz, 1H, H-2"), 3.87 – 3.80 (m, 2H, H-4', H-6"), 3.76 (appt dd, *J* = 9.5, 1.9 Hz, 1H, H-7'), 3.71 – 3.60 (m, 4H, H-8', H-9', H-3", H-6"), 3.33 (appt d, *J* = 9.4 Hz, 1H, H-4"), 2.24 (m, 2H, H-1"'), 2.17 – 1.88 (m, 9H, H-6', H-1"', H-2"', H-4"'), 1.67 (s, 6H, H-7"'), 1.61 (s, 6H, H-8"'), 1.52 (m, 1H, H-6'), 1.37 (m, 2H, H-3"'), 1.23 (m, 2H, H-3"'), 0.96 (d, *J* = 6.4 Hz, 6H, H-9"'); **$^{13}$C NMR** (126 MHz, MeOD) δ ppm 176.64, 176.02, (2C, -N-C=O$^{\text{aliphatic chain}}$),166.18 (C-4), 152.63 (C-2),

142.78 (C-6), 132.31, 132.26 (2C, C-6”’), 125.57, 125.50 (2C, C-5”’), 103.05 (C-5), 101.59 (C-11’), 99.99 (C-1”), 89.82 (C-1’), 89.62 (C-4’), 75.55 (C-2’), 74.37 (C-5”), 73.11, 73.00 (2C, C-8’, C-9’), 72.74 (C-4”), 72.48 (C-7’), 72.19 (C-3”), 70.86 (C-3’), 68.34 (C-5’), 63.23 (C-6”), 54.73 (C-2”), 54.36 (C-10’), 45.39, 44.91 (2C, C-1”’), 38.60, 38.50 (2C, C-3”’), 35.94 (C-6’), 31.78, 31.67 (2C, C-2”’), 26.66, 26.63 (2C, C-4”’), 25.94 (C-7”’), 19.65 (C-9”’), 17.83 (C-8”’); **IR** (neat) ν: 3291 (O-H), 2966 (C-H), 2928 (C-H), 1700 (C=O), 1638 (C=O),1541 (C=C), 1092 (C-N); **LRMS** m/z ($ESI^-$): 915 [$(M+FA-H)^-$, 100%]; **HRMS** m/z ($ESI^+$): calc. $C_{41}H_{65}N_4O_{16}$ $(M-H)^-$ = 869.4401, found 869.4407.

*H-4” signal in the $^1H$ NMR spectrum observed to be partially overlapped by the solvent peak. Not all aliphatic signals in carbon spectrum were resolved. Characterisation was assisted by COSY, HSQC, and HMBC.*

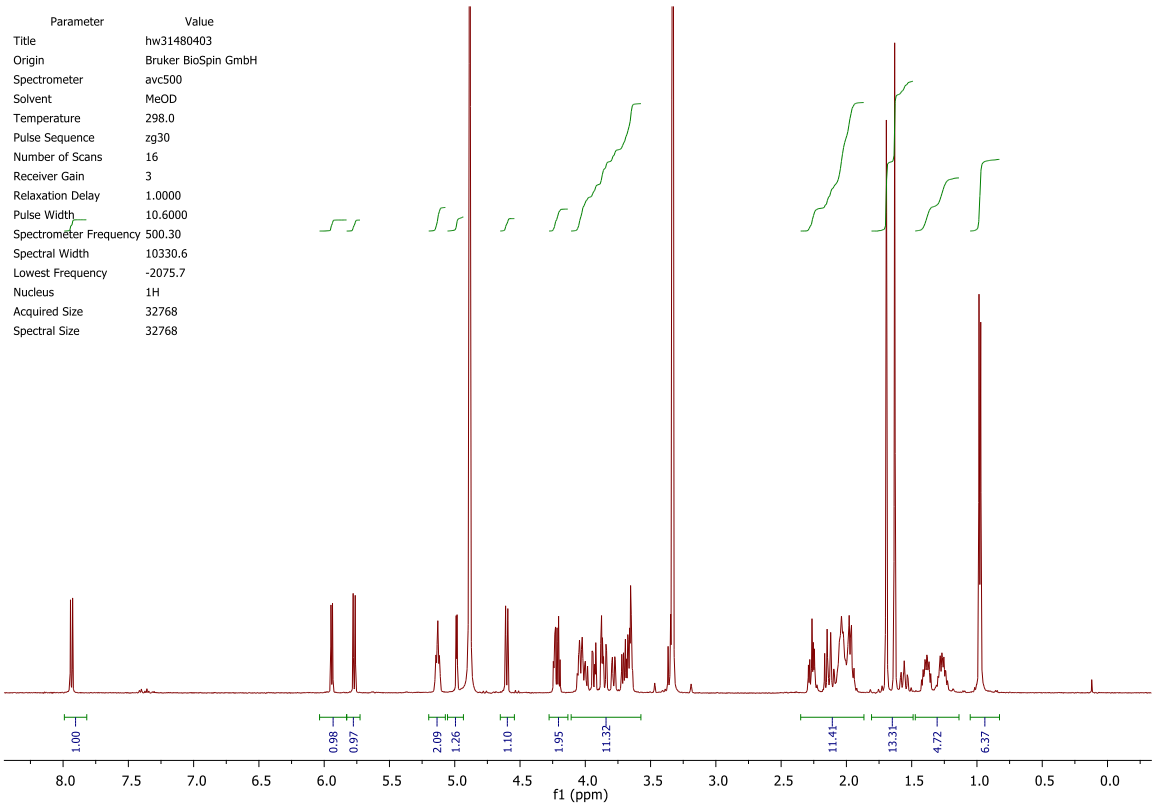


**Di-*N'*,*N"*-citronellyl tunicamycin (16) $^{1}$H NMR spectrum**

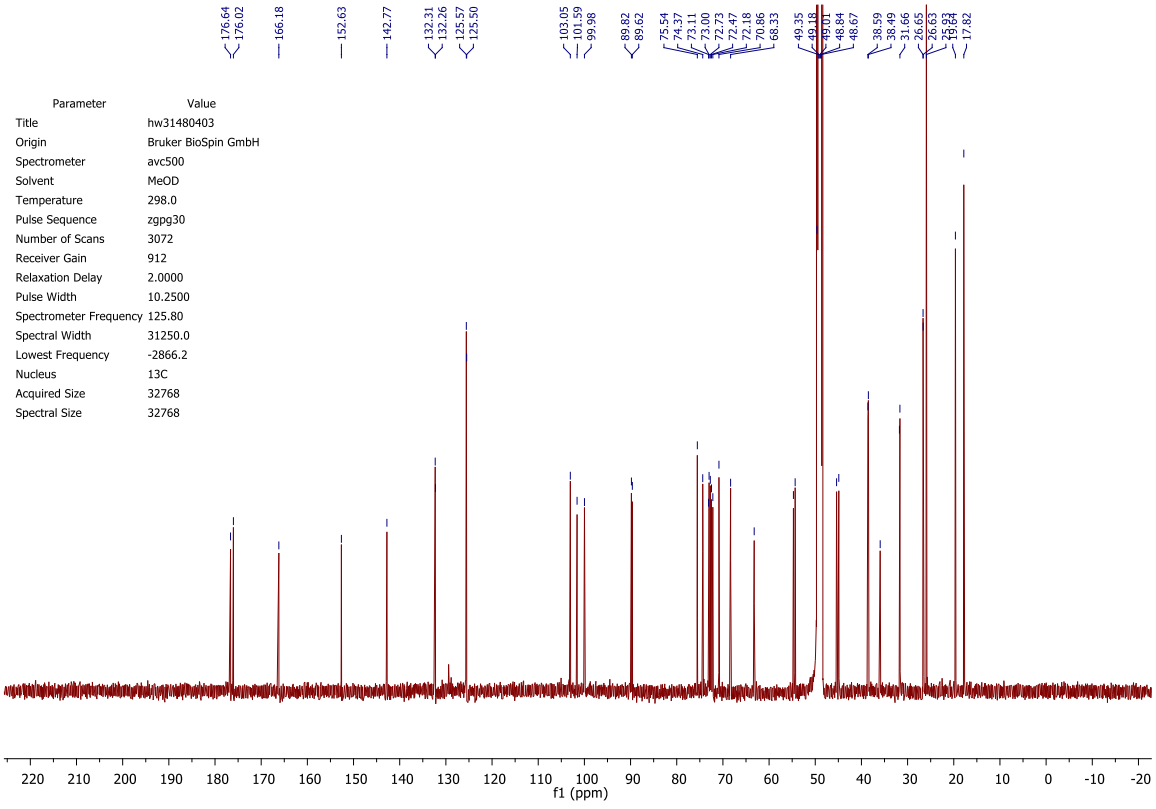


**Di-*N'*,*N"*-citronellyl tunicamycin (16) $^{13}$C NMR spectrum**

## References

1 Xu, L., Appell, M., Kennedy, S., Momany, F. A. & Price, N. P. J. Conformational Analysis of Chirally Deuterated Tunicamycin as an Active Site Probe of UDP-N-Acetylhexosamine:Polyprenol-P N-Acetylhexosamne-1-P Translocases. *Biochemistry* **43**, 13248-13255 (2004).

2 Myers, A. G., Gin, D. Y. & Rogers, D. H. Synthetic Studies of the Tunicamycin Antibiotics. Preparation of (+)-Tunicaminyluracil, (+)-Tunicamycin-V, and 5'-epi-Tunicamycin-V. *J. Am. Chem. Soc.* **116**, 4697-4718 (1994).

# *Experimental*

## *Biological Materials and Methods*

***General considerations***

All prepared biological solutions and equipment, such as media, plastic and glassware, used in handling of the microbial cultures were autoclaved/sterilised at 121 °C for 20 min. in LTE Scientific Ltd tabletop Touchclave-R autoclave. All biological work was performed in a Bassaire laminar flow cabinet. Bacterial cultures were incubated in New Brunswick Scientific, Innova 42 and 44 Incubator Shaker Series. Centrifugation was performed in Thermo Scientific Heraeus Megafuge 40R, Beckman Coulter Avanti J-25, Avanti J-26S XP, or Allegra X-12R centrifuge. Optical density was measured on BMG Labtech SPECTROstar Omega spectrophotometer or Amersham Bioscience Ultrospec 10. Water was deionised and passed through Millipore 0.22 μm filter prior to use. CD was measured on Applied Photophysics Chirascan circular dichroism spectrometer. Crystallisation plate was prepared by Art Robbins Instruments Phoenix/RE. FPLC was performed on Amersham Biosciences UPC-900 and ÄKTA GE Healthcare system by monitoring UV absorption at 254 nm. Protein samples that required denaturation were heated in a Techne Dri-Block DB-2A at 90 °C. PCR was performed on Applied Biosystems, GeneAmp PCR System 9700. Gel electrophoretic analyses were done using Apelex PS 304 Electrophoresis Power Supply, Bio-Rad Mini-sub Cell GT, Invitrogen XCell *Sure*Lock™, or BioRad Power Pac Basic. DNA concentration was determined using NanoDrop Spectrophotometer ND-1000. ITC analysis was carried out on MicroCal (GE Healthcare) ITC200 isothermal titration calorimeter.

All human tissue culture work was carried out in a designated tissue culture room, with equipments and biosafety cabinet. Mammalian culture was maintained in Binder $CO_2$ incubator. Fluorescence-activated cell sorting (FACS) analyses were done on BD FACSCalibur, and the raw data were processed on FlowJo software. Cell images were captured on FLoid® Cell Imaging Station by Life Technologies. Gloves and long-sleeve lab gown were worn at all times. Any bio-waste or consumable tissue culture materials were disposed in a designated auto-clave waste bin.

All antimicrobial and mammalian proliferation data were processed by GraphPad PRISM 5.01 software. These include dose-response curves plotted from independent data sets with SEM error bars.

All biological experimental work followed manufactured protocol, reported protocol, or protocol described in *Molecular Cloning: A Laboratory Manual* (CSHL Press, 3rd Edition, 2001) by Sambrook and Russell,[1] and *Practical Streptomyces Genetics* (John Innes Foundation) by Kieser *et al.*[2]

## Bacterial strains used in the thesis work[3,4]

| Name | Description | Source/Reference |
|---|---|---|
| *Streptomyces chartreusis* | NRRL3882, tunicamycins producing strain | DSMZ |
| *Bacillus subtilis* | EC1524, Tunicamycin sensitive strain | John Innes Centre (JIC) |
| *Micrococcus luteus* | Tunicamycin resistant strain | John Innes Centre (JIC) |
| *Bacillus cereus* | ATCC 11778 | DSMZ |
| *Escherichia coli* | ATCC 25922 | Thermo Scientific |
| *Staphylococcus aureus* | ATCC 29219 | Thermo Scientific |
| *Pseudomonas aeruginosa* | ATCC 27853 | Thermo Scientific |
| *Mycobacterium tuberculosis* | H37Rv | National Institutes of Health (NIH) |
| *S. coelicolor* M1131 | *S. coelicolor* M1146 carrying pIJ12003a | Wyszynski *et al*. 2010. |
| *S. coelicolor* M1135 | *S. coelicolor* M1146 carrying pRT802 (vector-only control) | Wyszynski *et al*. 2010. |
| *S. coelicolor* M1152 | *S. coelicolor* M1146 carrying a point mutation in *rpsL* for enhanced expression of antibiotic gene clusters | Gomez-Escribano J.P. personal communication (JIC) |
| *S. coelicolor* M1037 | Negative control, M1152+pRT801 | Wyszynski *et al*. 2014. |
| *S. coelicolor* M1040 | Positive control, M1152+pIJ12003a | Wyszynski *et al*. 2014. |
| *S. coelicolor* M1152 *tunB*(-) | Also named M1481. *S. coelicolor* M1152 carrying pIJ12003a_*tunB*(-). | Wyszynski *et al*. 2014. |
| *S. coelicolor* M1152 *tunF*(-) | Also named M1482. *S. coelicolor* M1152 carrying pIJ12003a_*tunF*(-) | Wyszynski *et al*. 2014. |
| *S. coelicolor* M1489 | *tunB* mutant complemented, M1152+pIJ12003aΔ*tunB* +pSET152_*ermE**p_*tunB* | J.P. Gomez-Escribano, personal communication (JIC) |
| *S. coelicolor* M1490 | *tunF* mutant complemented, M1152+pIJ12003aΔ*tunF* +pSET152_*ermE**p_*tunF* | J.P. Gomez-Escribano, personal communication (JIC) |
| *E. coli* DH5α/BT340 | Host strain for FLP recombination | J.P. Gomez-Escribano, personal communication (JIC) |
| *E. coli* BW25113 | Host strain for λ Red recombination | J.P. Gomez-Escribano, personal communication (JIC) |
| *E. coli* ET12567 | Methylation-deficient strain used for conjugation with *Streptomyces* | J.P. Gomez-Escribano, personal communication (JIC) |
| *E. coli* ET12567/pUB307 | Donor strain for conjugative transfer of mobilisable plasmids to *Streptomyces* | J.P. Gomez-Escribano, personal communication (JIC) |
| E. coli BL21(DE3) | General purpose expression host | Life Technologies |
| Lemo21(DE3) | Tunable expression controlled by varying the level of lysozyme (*lysY*), the natural inhibitor of T7 RNA polymerase. *E. coli* expression host used for difficult soluble protein expression. | New England BioLabs |

## Plasmids used in the thesis work

| Name | Description | Source/Reference |
|---|---|---|
| pIJ773 | Construct containing *aac(3)IV* resistance marker | J.P. Gomez-Escribano, personal communication (JIC) |
| pRT802 | Conjugative derivative of Supercos1 that integrates in a single copy at the ϕC31 attachment site in the *Streptomyces* host | J.P. Gomez-Escribano, personal communication (JIC) |
| pIJ790 | λ RED recombinase, chloramphenicol resistance | J.P. Gomez-Escribano, personal communication (JIC) |
| pUZ8002 | OriT-RP4 derivative, kanamycin resistance | J.P. Gomez-Escribano, personal communication (JIC) |
| BT340 | FLP recombinase, chloramphenicol and carbenicillin resistance | J.P. Gomez-Escribano, personal communication (JIC) |
| pIJ12003a | 12.9 Kbp minimal *tun* cluster cloned into the SacI site of pRT802 | Wyszynski *et al*. 2010. |
| pIJ12003a_*tunB*(-) | pIJ12003a with *tunB* sequence replaced by 81bp scar sequence | Wyszynski *et al*. 2014. |
| pIJ12003a_*tunF*(-) | pIJ12003a with *tunF* sequence replaced by 81bp scar sequence | Wyszynski *et al*. 2014. |
| pET21a:*tunD* | *tunD* from pET16b:*tunF* cloned into vector pET21a at *Nde*I-*Xho*I sites | F. J. Wyszynski, personal communication (Oxford) |
| pET28a:*tunE* | *tunE* from *S. chartreusis* cloned into vector pET28a(+) at *Nde*I-*Bam*HI sites. The *tunE* sequence was codon optimised for *E. coli* and synthesised by Genscript | F. J. Wyszynski, personal communication (Oxford) |
| pET22b:*otsA* | *tunA* from E. coli cloned into pET22b vector | Seung Seo Lee, personal communication (Oxford) |
| pET29a:PAP | *PAP* from *Acinetobacter johnsonii* cloned into vector pET29a at *Bam*HI-*Xho*I sites. The *PAP* sequence was codon optimised for *E. coli* and synthesised by Genscript | This thesis |

## Mammalian cell lines used in the thesis work

| Name | Description | Source/Reference |
|---|---|---|
| HepG2 | Human hepatocellular carcinoma cells | In-house |
| HEK293 | Human embryonic kidney cells | In-house |
| HEK293T | Human embryonic kidney cells | In-house |
| Raji | B-lymphocytes | In-house |

## Proteins

| Protein | Amino acids | Amino acid sequence[a] | MW (avg.) / pI |
|---|---|---|---|
| Native TunD | 472 | MEIIFTVSDQVWGGKHRYMHDMALGLAQAGHTVTVLAEEGG AMLQQCRAAGVTTVSVPAFASDDAAEAVRKALRHRRPHIVCV SGRADAAAVHHAQSQGVTDAAVCLFRHSAFPLGTTDEVRDLF TGVNLVFTTSLEQRQRQFEPLINAGVLKDEQVEILTSGVGEPL LAALDAADRGAARKELRAESDQFVFLVLARLAWEKGIDQVIDA FADLELPPDAAPPLLVVAGEGPLEAELRGQTIERGVAERVQFL GHQDHVAPVIKASDAVVLTSTVPETGPLALKEAMAAGRPVIAS VQGGIPEFVEDERHGLLVIDDEDLRQAMQRLLSDREAAETMG AAGSESVRGGHRAVRRVEYLAHRLDLLALEQLAPDTVLHEVV WDDVRLREETQGGFVFVPRTSHIMELDSATYAVVRTAVEAGD PLQLIKLPEETLGVIAHRLYAMGALVRQDGQATPAARTADGER PVTEPA | Mw = 50832 Da<br>pI = 5.01 |
| Native TunE | 234 | VKVLVIAAHPDDEVLGAGATVSALSQQGAVVQIHILAEGISLRH SGVKIEEARERCQVAAKDLGAAEVSFGGLAADGRLLADLPQR QVVDAVSHALREAEPEVVFTHHPGDIHADHRSVAHAVGYGTR ILGSGSVRQVLHFEVLSSTEQQTGLVAPFTPNLFYDVTGHVEA KCRALAAYPYELYDPPHPRSLAAVRTLASYRGTQVGVEAAEA FMIGRELRGPMAAVPSGVDVR | Mw = 24799 Da<br>pI = 5.93 |
| TunD-$His_6$ | 481 | MEIIFTVSDQVWGGKHRYMHDMALGLAQAGHTVTVLAEEGG AMLQQCRAAGVTTVSVPAFASDDAAEAVRKALRHRRPHIVCV SGRADAAAVHHAQSQGVTDAAVCLFRHSAFPLGTTDEVRDLF TGVNLVFTTSLEQRQRQFEPLINAGVLKDEQVEILTSGVGEPL LAALDAADRGAARKELRAESDQFVFLVLARLAWEKGIDQVIDA FADLELPPDAAPPLLVVAGEGPLEAELRGQTIERGVAERVQFL GHQDHVAPVIKASDAVVLTSTVPETGPLALKEAMAAGRPVIAS VQGGIPEFVEDERHGLLVIDDEDLRQAMQRLLSDREAAETMG AAGSESVRGGHRAVRRVEYLAHRLDLLALEQLAPDTVLHEVV WDDVRLREETQGGFVFVPRTSHIMELDSATYAVVRTAVEAGD PLQLIKLPEETLGVIAHRLYAMGALVRQDGQATPAARTADGER PVTEPAELEHHHHHH | Mw = 52026 Da<br>pI = 5.16 |
| $His_6$-TunE | 254 | MGSSHHHHHHSSGLVPRGSHM*KVLVIAAHPDDEVLGAGATV SALSQQGAVVQIHILAEGISLRHSGVKIEEARERCQVAAKDLG AAEVSFGGLAADGRLLADLPQRQVVDAVSHALREAEPEVVFT HHPGDIHADHRSVAHAVGYGTRILGSGSVRQVLHFEVLSSTE QQTGLVAPFTPNLFYDVTGHVEAKCRALAAYPYELYDPPHPR SLAAVRTLASYRGTQVGVEAAEAFMIGRELRGPMAAVPSGVD VR | Mw = 26994 Da<br>pI = 6.33 |
| PAP-$His_6$ | 517 | MKETAAAKFERQHMDSPDLGTLVPRGSMADIGSMDTETIASA VLNEEQLSLDLIEAQYALMNTRDQSNAKSLVILVSGIELAGKGE AVKQLREWVDPRFLYVKADPPHLFNLKQPFWQPYTRFVPAE GQIMVWFGNWYGDLLATAMHASKPLDDTLFDEYVSNMRAFE QDLKNNNVDVLKVWFDLSWKSLQKRLDDMDPSEVHWHKLH GLDWRNKKQYDTLQKLRTRFTDDWQIIDGEDEDLRNHNFAQ AILTALRHCPEHEKKAALKWQQAPIPDILTQFEVPQAEDANYK SELKKLTKQVADAMRCDDRKVVIAFEGMDAAGKGGAIKRIVKK LDPREYEIHTIAAPEKYELRRPYLWRFWSKLQSDDITIFDRTW YGRVLVERVEGFATEVEWQRAYAEINRFEKNLSSSQTVLIKFW LAIDKDEQAARFKARESTPHKRFKITEEDWRNRDKWDDYLKA AADMFAHTDTSYAPWYIISTNDKQQARIEVLRAILKQLKADRDT DALEHHHHHH | Mw = 60505 Da<br>pI = 6.02 |

The HPDD zinc-binding motif is highlighted.
[a]The vector-ended $His_6$ fusion is highlighted in red in the amino acid sequence.
*The initiating valine in native TunE has been mutated to a methionine in $His_6$-TunE.

## ***Materials and Media Recipes***

Restriction endonucleases, OneTaq Hot Start DNA Polymerase, 1kbp DNA Ladder, 6x Orange Loading Dye and other DNA modifying enzymes were purchased from New England Biolabs. MOPS and MES NuPAGE 20X running buffer, 10 % and 4 - 12 % NuPAGE Bis-Tris Gel, DH5α Subcloning Efficiency competent cells were purchased from Invitrogen. BL21(DE3) and Rosetta2(DE3) competent cells, Perfect Protein™ Marker 15 – 150 kDa and 10 – 225 kDa were purchased from Novagen. SOC media, BSA, BCIP/ NBT Liquid Substrate System, monoclonal anti-polyhistidine-phosphatase antibody produced in mouse were purchased from Sigma Aldrich. Undecaprenyl-MPDA (98 %) was purchased from Larodan Fine Chemicals. UDP-MurNAc-L-Ala-γ-D-Glu-*m*-DAP-D-Ala-D-Ala (96 %) was purchased from Warwick UK-BaCWAN. LB and TB media were purchased as dry granules from Melford and prepared according to manufacturer's instruction. Agar and glycerol were purchased from Fisher Scientific. Dialysis bag/case, Pierce BCA protein assay kit, 1-StepTM TMB-Blotting were purchased from Thermo Scientific. Vivaspin and syringe filter purchased from Sartorius Stedim Biotech. DPAGT1 (P-14) goat polyclonal IgG was purchased from Santa Cruz Biotechnology. Instant Blue coomassie blue stain was purchased from Expedeon Protein Solutions. All other biological media reagents, buffers, and antibiotics were purchased from common suppliers and used as purchased.

**Antibiotic stock solution (0.1 g $mL^{-1}$) preparation**

1 g of desired antibiotic dissolved in 10 mL of milliQ water, and the filtered via 0.20 μm filter. The stock can be used immediately, or stored at 4 °C.

**1 M IPTG stock solution preparation**

11.9 g (50 mmol) of IPTG dissolved in 50 mL of milliQ water, and the filtered via 0.20 μm filter. The stock can be used immediately, or stored at 4 °C or -20 °C.

**LB media preparation**

25 g of LB granules was dissolved in 1 L of deionized water in 2-L conical flask. The flask was covered with a foam stopper and aluminum foil, and autoclaved at 121 °C for 20 min. The media was allowed to cool down before use.

**TB + glycerol media preparation**

47.6 g of TB granules and 4 mL of glycerol were dissolved in 1 L of deionized water in 2-L conical flask. The flask was covered with a foam stopper and aluminum foil, and autoclaved at 121 °C for 20 min. The media was allowed to cool down before use.

**Agar plate preparation**

2.5 g of LB granules and 1.5 g of biological agar were dissolved in 100 mL of deionized water in 250-mL conical flask. The flask was covered with a foam stopper and aluminum foil, and autoclaved at 121 °C for 20 min. The agar medium was allowed to cool to ~50 °C before adding any antibiotics. Antibiotics: ampicillin = 100 mg/L; chloramphenicol = 100 mg/L; and/or kanamycin = 100 mg/L. After the addition of the antibiotic(s), the agar medium was poured into sterile Petri dishes (~10 mL per plate). The plates were set and cooled, and ready to be used or stored in 4 °C.

**DNA Agarose Gel Recipe**

| | |
|---|---|
| Agarose (Melford) | 0.4 g |
| TAE Buffer (Invitrogen) | 50 ml |
| Ethidium Bromide (Sigma-Aldrich) | 3 µl |

**DNA preparation and isolation**

QIAGEN QIAquick Gel Extraction Kit was used in gel extraction procedures. QIAGEN QIAprep Spin Miniprep Kit was used in isolation of plasmid from *E.coli* cultures. QIAGEN QIAquick PCR Purification Kit was used for PCR reaction and endonuclease digestion reactions. Protocols were followed as given by the manufacturer. All protocols can be accessed from the manufacturer without charge.

**Mueller-Hinton Broth**

Oxoid Mueller-Hinton broth was prepared according to manufacture procedure.

**Mueller-Hinton Agar**

Oxoid Mueller-Hinton Agar was prepared according to manufacture procedure.

**Mueller-Hinton Agar Plate**[5,6]

Muller-Hinton agar plate was prepared according to CLSI standards. Oxoid Mueller-Hinton Agar was prepared according to manufacture procedure. 25 mL of the warm agar solution was transferred to 100 mm petri plate *via* sterile pipette. The agar plate was cooled at room temperature for 15 minutes before use or storage at 4 ˚C up to two weeks.

**TYD** (Sterile dextrose solution is added after the medium has been autoclaved)

| | |
|---|---|
| Tryptone | 2 g |
| Yeast Extract | 2 g |
| $MgCl_2\,6H_2O$ | 0.3 g |
| Distilled water | 1000 ml |
| Dextrose | 6 g |

**MS** (autoclaved twice)

| | |
|---|---|
| Agar | 20 g |
| Mannitol | 20 g |
| Soya flour | 20 g |
| Tap water | 1000 ml |

**OA**

| | |
|---|---|
| Oats | 0.4 g |
| Agar | 0.2 g |
| Tap water | 100 ml |

**DNA**

4.6 g Difco Nutrient Agar

200 ml distilled water

**Stock preparation.** Stocks were prepared as 1.25 mg/mL or 1 mg/mL in MilliQ water or methanol, and stored at -20 ˚C.

**0.5 McFarland standard.** It is equivalent to bacterial suspension containing between 1e8 to 2e8 CFU $mL^{-1}$ of *E. coli*.

| | |
|---|---|
| $BaCl_2$ (0.048 mol $L^{-1}$, 1.175% wt/vol $BaCl_2 \cdot 2H_2O$) | 0.5 mL |
| $H_2SO_4$ (1% vol/vol) | 99.5 mL |

The standard can be verified by spectrophotometer for correct density. The measurement taken at 1-cm light path and absorbance at 625 nm should be 0.08 to 0.13 for the 0.5 McFarland standard. The suspension can be transferred as 4- to 6-mL aliquots in screw-cap glass vials of the same size used as those in standardising bacterial inoculums. The McFarland standard can be stored in the dark at room temperature.

**Tissue Culture**

Dulbecco's PBS (Sigma Aldrich, D8537)

Dulbecco's Modified Eagle's Medium (DMEM) (Sigma Aldrich, D8537)

RPMI-1640 Medium (Sigma Aldrich, R8758)

Fetal Bovine Serum, heat inactivated (Sigma Alrdich F9665)

Trypsin-EDTA(1X) 0.25%, (Gibco by Life Sciences)

**Propidium Iodide (PI)/RNase Staining Solution** (New England BioLabs)

The PI staining followed the manufacturer's instructions.

**CellTiter 96® AQueous One Solution Cell Proliferation Assay** (MTS) (Promega)

The assay followed the manufacturer's instructions.

## ***Protocols***

### *S. chartreusis* NRRL3882 culture and Tunicamycins extraction

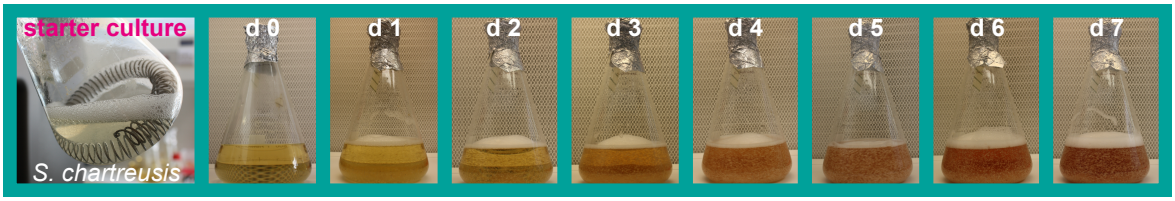


***S. chartreusis* culture.** *Streptomyces chartreusis* NRRL3882 purchased from DMSZ GmbH was used for tunicamycins production. *S. chartreusis* was initially grown on Oats Agar medium at 28 °C for 1-2 weeks period when sufficient single colonies of spores were present, but no more than two weeks to preserve spore viability. A single spore colony was then taken to propagate on a fresh Oats Agar plate and grown for another 1-2 weeks when sufficient spores were present to make a spores stock. The spores stock was prepared by saturating the spore colonies on the plate with glycerol (25% v/v) and gently scrapping the spore colonies. The spore solution was then filtered through cotton and into a sterile 1.8-ml TUNC Cryo vial. The spores stock can be stored at -20 °C. The spore stock was then use to produce seedlings in liquid medium culture flask, as described below.

Large-scale aerobic bacterial growth was employed for tunicamycins biosynthesis. Sterilised 50 mL TYD medium in a 100-mL Erlenmeyer flask with coiled-spring to prevent spores from clumping was inoculated with 5 µL of spores stock, and then incubated overnight at 28 °C, 200 rpm, to make a 50 mL of *S. chartreusis* seedling culture. With 12 L of TYD in 2-liter conical flasks, each was inoculated with 1 mL of the seedling culture of *S. chartreusis* spores and incubated with shaking at 28 °C, 200 rpm, for 7 days.

**Extraction of tunicamycins.** On the 7th day from the initial inoculation, the fermentation broth was sprung down *via* centrifugation at 8000 rpm, 4 °C, for 10 minutes. After centrifugation, the supernatant was filtered into a 5-liter conical flask via Fisherbrand filter paper to leave out any mycelial spore suspension and to separate from the mycelial cake. Alternatively, the culture can be left to settle and decant to separate the broth and the mycelium. Mycelial cake was then transferred into a 500-mL conical flask. The supernatant extraction and mycelial cake extraction were then carried out in two-part extraction before combining for purification. Both extraction processes are elucidated below.

**Tunicamycins extraction from culture broth.** Tunicamycins are secreted in the culture broth. For every liter of supernatant, 15 g of Amberlite XAD-16 (Sigma-Aldrich) was added; therefore, 180 g Amberlite XAD-16 for 12 liters of supernatant. The addition of the resin assisted in extraction of tunicamycins *via* hydrophobic interaction with the lipid chain of the homologues. The resin-supernatant mixture was stirred at room temperature for 90 minutes. After 90 minutes, the resin was left to settle, undisturbed, for at least 15 minutes before discarding the supernatant by decantation. The resin was transferred into a beaker and followed the washing sequence listed:

Amberlite XAD-16 wash sequence

| *Cycle* | *Solvent** | *Time* |
|---|---|---|
| 2X | MilliQ Water | 15 mins. |
| 2X | Methanol | 15 mins. |

2X *n*-isopropanol 15 mins.

1X Methanol 1 hour

*The amount of solvent added was to double the original volume of the resin.

The organic solvent fractions were collected and concentrated *in vacuo*. 15 mL of 1 M HCl (aq.) was added to every 1 mL of the concentrated extract. The acidic mixture was transferred into Falcon 50-mL tubes, vortexed for 5 minutes, and centrifuged at 3,750 rpm for 10 minutes at 4 °C. The white foam on the top of the solution and the precipitation on the bottom were collected and dissolved in 20 mL of methanol. The precipitation contains tunicamycins since tunicamycins are insoluble in acidic conditions.

**Tunicamycins extraction from mycelial cake.** 1 M HCl (aq.) was added to double the volume of the volume of mycelial cake obtained, or add MilliQ water to the mycelial cake of desired volume and make the mixture to final concentration of 1 M HCl (aq.); this process precipitated the tunicamycins, as they are insoluble in acidic environment while solubilising some cell residuals. The acidic mycelial mixture was stirred at room temperature for 30 min. It is important that the acid-cell mixture do not exceed longer than 30 minutes as the acidic condition may start to degrade the tunicamycins. After 30 min., the acidic cell mixture was centrifuged at 10,000 rpm for 10 min. at 4 °C. The acidic supernatant was discarded. Acidification process was repeated but the stir time was reduced to 15 minutes. Then methanol was added to triple the volume of the cell pellet. The methanol-cell pellet mixture was stirred for 90 min. at room temperature then centrifuged at 10,000 rpm for 10 min. at 4 °C. The methanol supernatant was collected.

The methanol extraction process was repeated second time. The methanol extracts were combined and continued with purification.

**Isolation and purification of crude tunicamycins.** The methanol fractions collected from supernatant and cell pellet extraction were combined, filtered *via* 0.2 μm membrane, and evaporated *in vacuo*. Crude tunicamycins extract was purified *via* flash chromatography (W/*i*PrOH/EtOAc, 1:3:6). A repeat of flash chromatography was necessary to obtained a cleaner sample.

Alternatively, the organic fractions after filtration can be evaporated in vacuo and then adding excessive amount of acetone and leave overnight at 4 °C. The precipitated tunicamycins can be collected through filtering (paper or glass) the acetone solution.

The crude tunicamycins fraction was collected, concentrated *in vacuo*, and freeze-dried. The crude tunicamycins can be stored at -20 °C. Isolated crude tunicamycins were characterised by TLC, $^{1}$H NMR, and LC/MS analysis and compared to an authentic sample purchased from Enzo Life Sciences. Commercial sample of tunicamycins contain four homologues, $n$ = 8, 9, 10, 11. The crude tunicamycins isolated from *S. chartreusis* appeared to contain 12 homologues (m/z 749, 763, 776, 790, 804, 818, 832, 846, 860, 875, 889, 904).

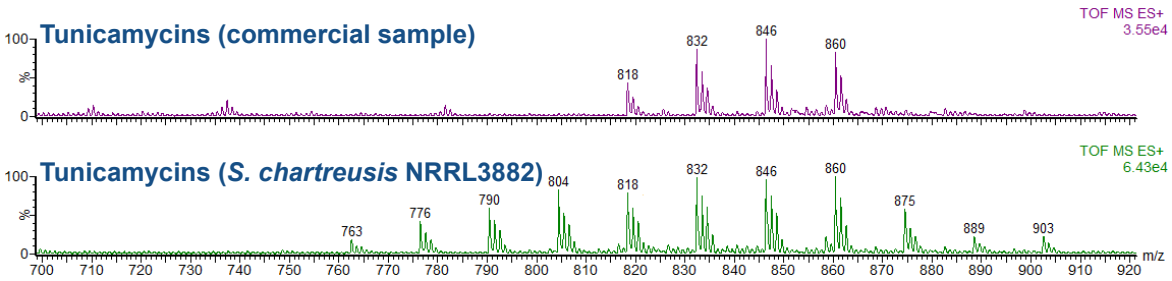

**Tunicamycins yield from extraction process.**

| *S. chartreusis* NRRL3882 Culture Date | Culture volume (Liter) | Crude tunicamycins (mg) | Sample[a] (mg $mL^{-1}$) | HPLC[b] (mg $mL^{-1}$) | Purity (%) | Final yield[c] (mg $Liter^{-1}$) |
|---|---|---|---|---|---|---|
| 09/06/2012 | 24 | 1066 | 1.30 | 1 | 79 | 35 |
| 14/082012 | 12 | 1483 | 1.40 | 0 | 34 | 42 |
| 13/11/2012 | 11 | 891 | 1.40 | 1 | 56 | 46 |
| | | | | Average | 56.00% | 40.8 mg $Liter^{-1}$ |

[a] Amberlite XAD-16 resin was used in the extraction process. The resin can be used once. However, the third time of reusing the resin can dramatically reduce the yield of tunicamycins by almost a half.
[a]HPLC injection sample concentration of crude tunicamycins
[b]Concentration determined by HPLC based on a standardised curve
[c]Tunicamycins yield from the culture, based on the % purity

**Kirby-Bauer Disc Diffusion Test.**[6,7] Oxoid Blank Disc was impregnated with the desired test substance. A 0.5 McFarland standard inoculum was prepared by adding 3-5 single colonies to 10 mL MH broth in 15 mL-falcon tube and standardised to 0.5-McFarland standard. The inoculum was used within 10 minutes. A sterile cotton swab was dipped in the inoculum, gently pressed against the side of the tube to remove excess liquid, and generously streaked on MH agar plate to fully cover the plate. The impregnated disc was carefully placed on the agar (important: once the disc has touched the agar, it should not be moved). The plate was incubated at 35 ˚C for 20 hrs overnight. A digital calliper was used to measure the zone diameter. The recorded zone diameter is an average of three zone diameters measured of one zone.

**Micro-broth dilution culture to determine minimal inhibition and minimal bactericidal concentrations (MIC and MBC).**[5,8] In a sterile 96-well plate, serial dilutions were made with the test substance to final volume of 50 µL. Inoculum was then prepared in Mueller-Hinton broth to 0.5 McFarland and diluted before adding 50 µL to the well to make ~1e5 CFU per mL. The culture plate was incubated at 35 ˚C for 20-24 h. A positive growth control and sterile wells were also prepared along with the culture wells.

Absorbance at $OD_{600}$ was taken using BMG Labtech SPECTROstar Omega spectrophotometer. MIC was determined by the lowest concentration without growth. $IC_{50}$ is determined from plotting a dose-response curve. To determine the MBC, using a multi-channel pipette, 1 μL of culture broth was taken from the same 96-well micro-dilution growth plate and carefully inoculated on surface of MH agar plate. The plate was then incubated for additional 20 h at 35 ˚C. The MBC value is the lowest concentration without observed growth on the agar.

**HepG2 and HEK293 cell culture.** Mammalian cells were cultured in DMEM medium supplemented with 10% heat inactivated fetal bovine serum (FBS, v/v). The cultures were maintained in a humidified incubator at 37 ˚C in 5% $CO_2$/95% air.

**Raji cell culture.** cells were cultured in RPMI-1640 medium supplemented with 10% heat inactivated fetal bovine serum (FBS, v/v). The cultures were maintained in a humidified incubator at 37 ˚C in 5% $CO_2$/95% air. FBS was reduced to 2% for the cell proliferation assay.

**Cell proliferation assay.** In sterile 96-well plate, each well is seeded with ~$1x10^5$ cells. The cells are then grown confluent overnight in 100 μL DMEM with 10% FBS. The medium is replenished with DMEM with 2% FBS and added vehicle control or test substance the next day. For test substance in methanol, stock was added to 25 μL of DMEM with 2% FBS or PBS and placed in the laminar flow hood to let the methanol evaporate (about 1-3 hrs). Once the methanol has evaporated, DMEM with 2% FBS was added to final volume of 100 μL of desired test concentration. A blank methanol control

should also be made to ensure any cytotoxicity is not resulted from methanol contamination. Cells are grown for additional 24 h. The cell viability was determined by using Promega CellTiter 96© $AQ_{ueous}$ One Solution Cell Proliferation Assay System following the manufacture protocol.

**Cell proliferation assay (Raji).** In sterile 96-well plate, each well was seeded with ~$1x10^5$ cells from $1x10^7$ cells/mL stock (10 µL of the stock to each well), in RPMI-1640 with 2% FBS. Test substance was prepared in RPMI-1640 with 2% FBS and added to the well to make final volume of 100uL with the desired dose. Raji cells were grown for additional 24 h after treated with the test substance. The cell viability was determined by using Promega CellTiter 96© $AQ_{ueous}$ One Solution Cell Proliferation Assay System and following the manufacturer's instructions.

**Cell Cycle Test.** The cell cycle tests were carried out in 96-well tissue culture plate. A stock of HEK293 cells was first grown in a T-75 tissue culture flask. Once the cells were about 90% confluent, the old medium was decanted and the cells were carefully washed with PBS and resuspended in DMEM with 10% FBS. HEK293 cells were then seeded into the 96-well plates (1e5 cells per well). Before placing the culture in the incubator (37 °C with 5% $CO_2$), the plate was set aside for 10 minutes for the cells to settle to the bottom of the plate. Once the cells were confluent the next day or when they are ready to be treated, DMEM with 2% FBS containing the test substance is prepared beforehand during the day of the cell treatment. For the 24 h cell cycle analysis, 2% FBS in growth medium was used. For the time-course cell cycle test (24, 48, 72), 10% FBS in growth medium was used (see below).

Once the cell culture was ready for harvesting, the cells are then fixed with cold 70% ethanol after two washes with PBS (w/ 0.1% BSA). The cells were fixed overnight at 4 °C. Propidium Iodide (PI)/RNase Staining Solution from NEB was used for DNA staining. The staining process followed the manufacturer's instructions.

For compounds in methanol, the methanol from stock solution was added to 50 uL of DMEM or PBS in a round-well plate (8-well plate) and placed in the laminar hood to have the methanol evaporated off (~1 h) and then adding the needed volume of DMEM with 2% FBS to the desired volume.

**Time-course Cell Cycle Test.** The time-course cell cycle test was carried out in 96-well tissue culture plate. Three sets of plates were prepared as described above with samples prepared in triplicate. A 0 h control cell culture was first collected before setting up the plates for treatment. Each plate was used for 24 h, 48 h or 72 h time-point data collection. Due to nature of the experiment, the DMEM used contained 10% Heat-inactivated FBS for the cells to have enough nutrients to the 72hr cell cycle. Once the cell culture is ready for harvesting, the cells are then fixed with cold 70% ethanol after two washes with PBS (w/ 0.1% BSA). The cells were fixed overnight at 4 °C. Propidium Iodide (PI)/RNase Staining Solution from NEB was used for DNA staining. The staining process followed the manufacturer's instructions**.**

**IgG1Fc *N*-Glycosylation test.** The test was carried out in a 6- or 8-well tissue culture plate. The transfected HEK293T/pHLsec:IgG1Fc cell culture harbouring pHLsec:IgG1Fc plasmid with a $His_6$-Tag IgG1Fc (Transfection protocol below) was grown for 2-3 days (37

°C with 5% $CO_2$) with or without the presence of the test compound. Then the growth medium is collected and analysed by SDS-PAGE and Western blot.

**Transfection Protocol** (DNA: 4 μg $mL^{-1}$, PEI (linear 25 kDa): 4.6 μg $mL^{-1}$). Transfection reagents and medium were prepared fresh every time. A PEI stock solution was first prepared (100 μg $mL^{-1}$). PEI was added in MilliQ water and HCl (aq.) was then added drop-wise with just enough to help solubilise the PEI. The PEI solution was filtered through 0.2 μm membrane in laminar sterile hood, and set aside. Then, the DNA stock solution was added to serum-free DMEM medium at room temperature to make a final DNA-DMEM concentration of 4 μg $mL^{-1}$. The PEI solution was then added to DMEM-DNA solution to make a final concentration of PEI at 4.6 μg $mL^{-1}$. The PEI-DNA transfection medium was then gently stirred at room temperature for 20 minutes before use. For the transfection step, the DNA-PEI transfection was first added and placed in the incubator (37 °C with 5% $CO_2$) for 10 minutes and then DMEM with 2% FBS was added. The DNA-PEI medium and DMEM with 2% FBS medium were added in 1:3 ratio.

**Summary of $LD_{50}$ values from dose-response curves of independent data sets.**

| Compound | $LD_{50}$ values (μg $mL^{-1}$) | | |
|---|---|---|---|
| | HEK293 | HepG2 | Raji |
| MilliQ Water | N/A | N/A | N/A |
| Methanol | N/A | N/A | N/A |
| **(1)** commercial | 49.76, 51.91, 98.94, 87.05, 27.79, 23.55, 19.75 | 49.39, 48.42, 37.61, 40.33, 45.51, 47.18 | 37.82, 32.89, 12.39, 10.16, 37.10, 24.70, 32.68 |
| **(3)** | N/A | N/A | 296.8, 310.7 |
| **(4)** | N/A | N/A | 248.7, 175.9 |
| **(8a)** | N/A | N/A | 1036, 533.8, 257 |
| **(9)** | N/A | N/A | 698.3* |
| **(10)** | N/A | N/A | 152.9, 549.60, 590.8 |
| **(11)** | N/A | N/A | 122, 300.1 |
| **(12)** | N/A | N/A | 172.8, 560.1, 333.8 |
| **(13)** | N/A | N/A | 143.6, 236.40, 208.5 |
| **(14)** | N/A | N/A | 83.65, 143.3, 83.99 |
| **(15)** | N/A | N/A | 104.5, 47.15, 92.23 |
| **(16)** | N/A | N/A | 230.9, 124.6 |

N/A = not available. No cytotoxicity was observed based from the experiments using up to a concentration of 400 μg $mL^{-1}$ of the test compounds. The methanol used was a control, the methanol was evaporated off to ensure no methanol contamination and no false-negatives.
*Other data was not able to provide a dose-response curve.

**PCR-targeting of *tun*B or *tun*F in *tun* gene cluster.** PCR-targeting followed protocols reported by Gust *et al.*[9,10] Apramycin disruption cassettes were amplified by PCR from pIJ773 using oligonucleotides designed with FRT sites and gene sequence matching the gene sequence before the gene of interest for disruption, as recommended, as well as containing the ribosomal GGAG binding site. GGAG and FRT sequences are indicted in bold shown in Table below. PCR targeting was done in *Escherichia coli* host using the recommended strains. *E. coli* BW25113 for λ RED recombination to replace *tunB* or *tunF* gene with apramycin resistance gene, and *E. coli* DH5α/BT340 for FLP recombination to replace the apramycin resistance gene with the 81bp scar sequence. Test oligonucleotides were designed for PCR test to confirm λ RED recombination from the disruption cassette

and gene replacement from FLP recombination (Table below). Predicted size of the PCR products, along with controls, after λ RED recombination and FLP recombination is provided below (Table below). DNA gel electrophorectic analysis of our PCR products after λ RED recombination and FLP recombination gene disruption for *tunB* or *tunF* in *tun* gene cluster is shown in Fig. below. The resultant mutant constructs of tunB(-) and tunF(-) were introduced into *S. coelicolor* M1152 via tri-parental mating using *E. coli* ET12567 and *E. coli* ET12567/pUC502. Successful integration of the mutant construct into the *S. coelicolor* M1152 chromosomal ϕC31 attachment site was determined by single-colony PCR using the same test primer in Table below and selected for kanamycin resistance. For kanamycin resistance selection, single colony from first-generation of tri-parental mated recombinant *S. coelicolor* was streaked on MS plates containing kanamycin, carbenicillin and nalixidic acid, for second-generation growth. Single colonies from the second-generation growth were streaked again on MS plates containing kanamycin, carbenicillin and nalixidic acid, for third generation growth and for collection of spores for liquid culturing. The single-colony PCR test used the same test oligonucleotides in Table below. Because PCR test can be highly sensitive, first generation of tri-parental mated recombinant *S. coelicolor* was streaked on DNA plates containing kanamycin and nalidixic acid and DNA plates contain kanamycin, carbencillin and nalidixic acid for fast non-sporulation growth. Kanamycin is used for selection derived from the kanamycin resistance gene integrated into the *S. coelicolor* chromosome, and carbencillin and nalidixic acid are used to selectively kill *E. coli* and prevent any DNA contamination (Fig. below). For single-colony PCR, recombinant *S. coelicolor* was selected from DNA plate containing kanamycin, carbenicillin and nalidixic acid. Our single-colony PCR test showed high efficiency integration from tri-parental mating, which is likely due to the

short 13kp pIJ12003a construct. The single recombinant colonies selected for single-colony PCR (Fig. below) all showed positive integration of modified pIJ12003a construct in *S. coelicolor* chromosome, matching out predicted PCR size (Table below).

Single-colony PCR used the same recommended PCR condition. The source of DNA is isolated from the non-sporulated growth of recombinant *S. coelicolor*. To do this, a sterile toothpick was used to scrap some *S. coelicolor* from the DNA plate containing kanamycin, carbenicillin and nalidixic acid and resuspended in 50 µL of sterile water in screw-cap vial. The suspension mixture was boiled for five minutes, and supernatant was collected after centrifugation. The source of DNA is in the supernatant. 5 µL of the supernatant was used for PCR reaction.

**Oligonucleotides used for PCR in apramycin cassette.***

| Oligonucleotide | Sequence |
|---|---|
| *tunB* | Forward:<br>5'-CTTCCAAGAGGAGGGGGCCGACTGATGACCGGCTACACCATTCCGGGGATCCGTCGACC-3'<br>Reverse:<br>5'-GGCCTCCCTGGACAAGGCCTACCTCACCTCCGCGCCTTCTGTAGGCTGGAGCTGCTTC-3' |
| *tunF* | Forward:<br>5'-GGTTCCCAGTGGAGTTGATGTGCGATGAGAGTGCTCGTGATTCCGGGGATCCGTCGACC-3'<br>Reverse:<br>5'-GCGTGGCGCAGTAGGTAGAGGTGCATGTCACTCCAGCGATGTAGGCTGGAGCTGCTTC-3' |

*GGAG and FRT sequences are indicted in red.

**PCR followed the recommended condition:**

PCR reaction component:

| | |
|---|---|
| Primers (100 pmoles/µl) | 0.5 µl each |
| Template DNA (100 ng/µl) | 0.5 µl |
| Buffer (10x) | 5 µl |
| dNTPs (10 mM) | 1 µl each |
| DMSO (100 %) | 2.5 µl |
| DNA polymerase (2.5 U/µl) | 1 µl |
| Water | 36 µl |
| Total volume | 50 µl |

PCR Cycle conditions*:

| | |
|---|---|
| 1. Denaturation: | 94°C, 2 min |
| *2. Denaturation:* | *94°C, 45 sec* |
| *3. Primer annealing:* | ***50°C**, 45 sec* |
| *4. Extension:* | *72°C, 90 sec* |
| *5. Denaturation:* | *94°C, 45 sec* |
| *6. Primer annealing:* | ***55°C**, 45 sec* |
| *7. Extension:* | *72°C, 90 sec* |
| 8. Final extension: | 72°C, 5 min |

*Note: step 2-4, repeat for 10 cycles; step 5-7, repeat for 15 cycles.

## Test oligonucleotides* for λ RED recombination and FLP recombination

| Oligonucleotide | Sequence |
|---|---|
| *tunBtst* | Forward: 5'-TCGCGACTTCACCTACATCA-3'<br>Reverse: 5'-TGAGGTCGTACAGGCGTATG-3' |
| *tunFtst* | Forward: 5'-TCACCCCCAACCTGTTCTAC-3'<br>Reverse: 5'-CGGAGACCAGACGATCTCAT-3' |

*annealing temperature for the test oligonucleotides used in PCR is 43 °C. The temperature is calculated based on the recommended $T_m$ - 5°C.

## Predict size of control PCR product

| PCR test | PCR product (bp) |
|---|---|
| *tunB control* | 1,402 |
| *tunF control* | 1,464 |

## Predict size of λ RED recombination and FLP recombination PCR product

| PCR test | λ RED recombination (bp) | FLP recombination (bp) |
|---|---|---|
| *tunB disruption* | 1,767 | 466 |
| *tunF disruption* | 1,862 | 561 |

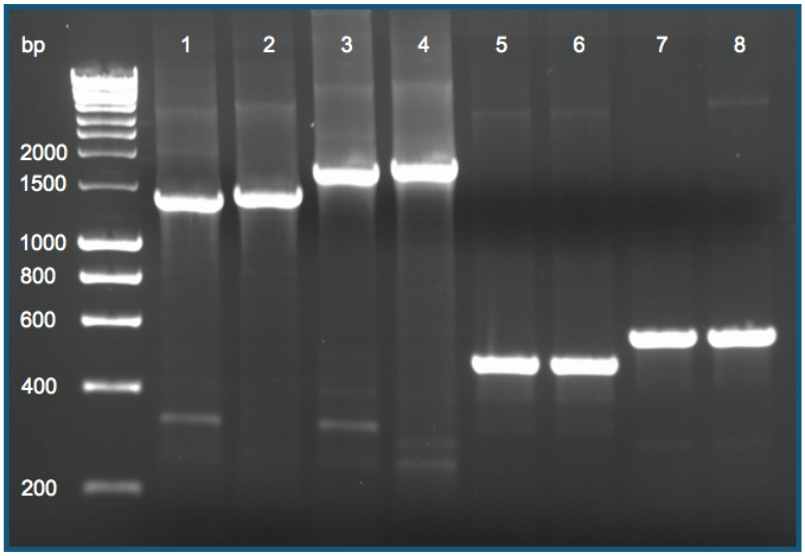


DNA gel electrophoretic analysis of PCR products from control (1,2), and after λ RED recombination (3,4) and FLP recombination (5,6,7,8)

**Lanes**

DNA ladder: BioLine Hyper Ladder 10000, 8000, 6000, 5000, 4000, 3000, 2500, 2000, 1500, 1000, 800, 600, 400, 200

1: control, *tunB* PCR product

2: control, *tunF* PCR product

3: *tunB* apramycin gene replacement after λ RED recombination PCR product

4: *tunF* apramycin gene replacement after λ RED recombination PCR product

5: *tunB* scar sequence gene replacement after FLP recombination PCR product, sample 1

6: *tunB* scar sequence gene replacement after FLP recombination PCR product, sample 2

7: *tunF* scar sequence gene replacement after FLP recombination PCR product, sample 1

8: *tunF* scar sequence gene replacement after FLP recombination PCR product, sample 2

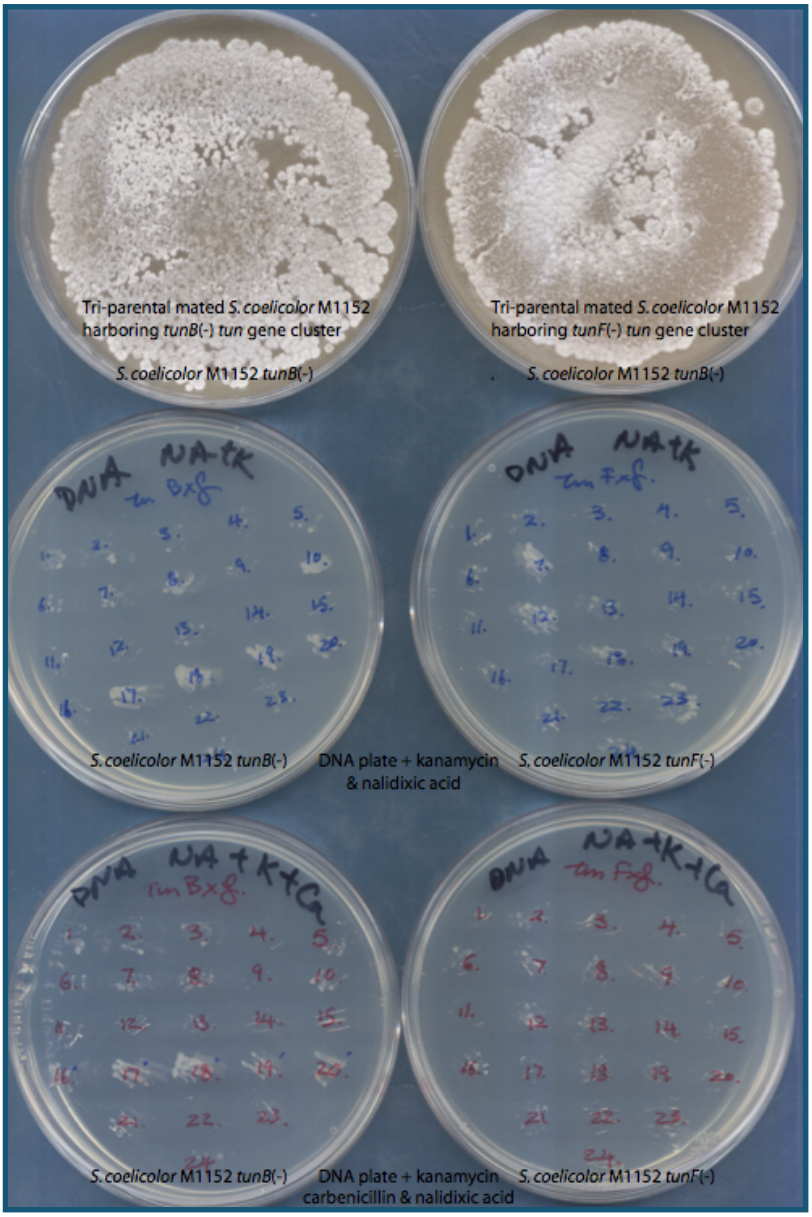


**Kanamycin selection.** Top: First generation of tri-parental mated recombinated *S. coelicolor* M1152 *tunB*(-) and *tunF*(-); middle: *S. coelicolor* M1152 *tunB*(-) and *tunF*(-) on DNA plate containing kanamycin and nalidixic acid; bottom: *S. coelicolor* M1152 *tunB*(-) and *tunF*(-) on DNA plate containing kanamycin, carbeniciilin and nalidixic acid.

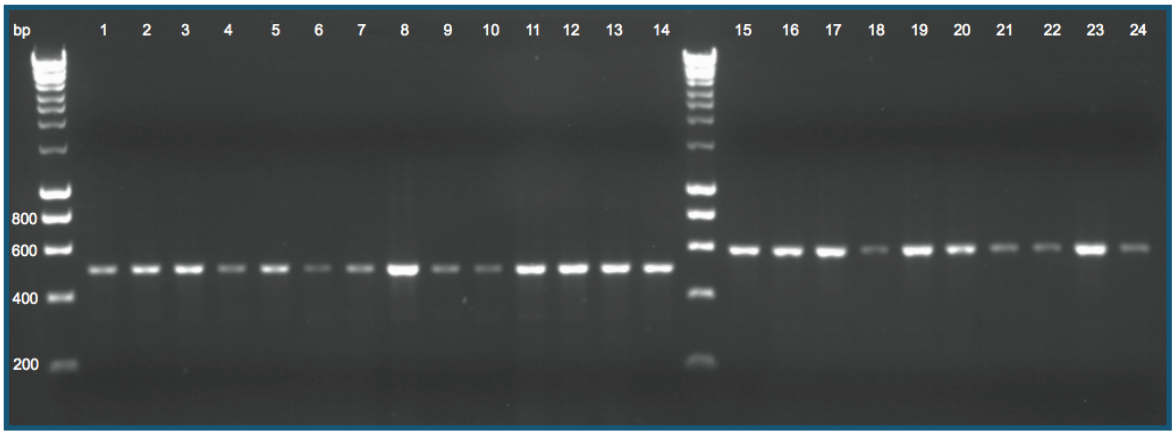


DNA gel electrophoretic analysis of single-colony PCR products from recombinant *S. coelicolor* M1152 *tunB*(-) and *tunF*(-) DNA.

**Lanes**

DNA ladder: BioLine Hyper Ladder 10000, 8000, 6000, 5000, 4000, 3000, 2500, 2000, 1500, 1000, 800, 600, 400, 200

1-14: Single-colony PCR products from recombinant single *S. coelicolor* M1152 tunB(-) colony.

14-24: Single-colony PCR products from recombinant single *S. coelicolor* M1152 tunF(-) colony.

**φBT1 Integration**

| Oligonucleotide | Sequence |
|---|---|
| BT1V1 | 5'-GGTGCGAATAAGGGACAGTG-3' |
| BT1C1 | 5'-CACGAGCGGAAACGTACC-3' |
| BT1C2 | 5'-GTACCAGTTGGCCGTCACC-3' |
| BT1V2 | 5'-ACGTCCACGAACTCACCTG-3' |

Notes:

1. Annealing temperature for the test oligonucleotides used in PCR was 43 °C based on recommended Tm - 5°C.

2. Test oligonucleotides were designed to anneal outside the gene disruption region.

3. Test oligonucleotides were designed to confirm correct integration of pIJ12003a *tunB(-)* at the chromosomal φBT1 *att* site.

4. Annealing temperature for the test oligonucleotides used in PCR was 60 °C based on recommended Tm - 5°C.

**pIJ12003a *tunB(-)* integration, predicted size of PCR products**

| PCR test | PCR product (bp) |
|---|---|
| BT1V1/BT1C1 | 444 |
| BT1V2/BT1C2 | 573 |

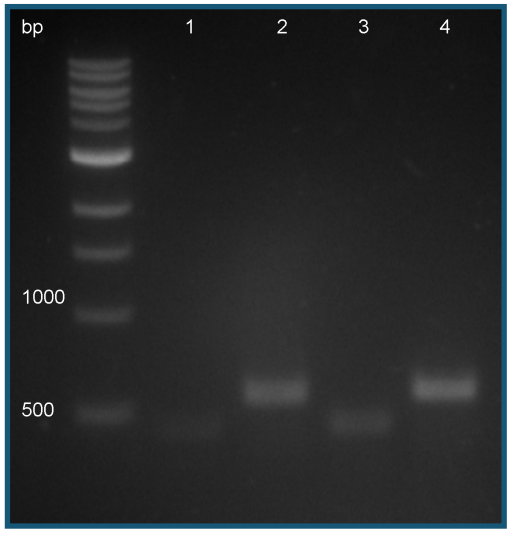


DNA gel electrophoretic analysis of PCR confirming correct integration of pIJ12003a *tunB(-)* at the chromosomal φBT1 *att* site in S. coelicolor chromosome. Lanes: DNA ladder: NEB 1kb ladder 10000, 8000, 6000, 5000, 4000, 3000, 2000, 1500, 1000, 500; pIJ12003a *tunB(-)* at the chromosomal φBT1 *att* site with BT1V1/BT1C1 primers, predicted product 444 bp; pIJ12003a *tunB(-)* at the chromosomal φBT1 *att* site with BT1V2/BT1C2 primers, predicted product 573 bp.

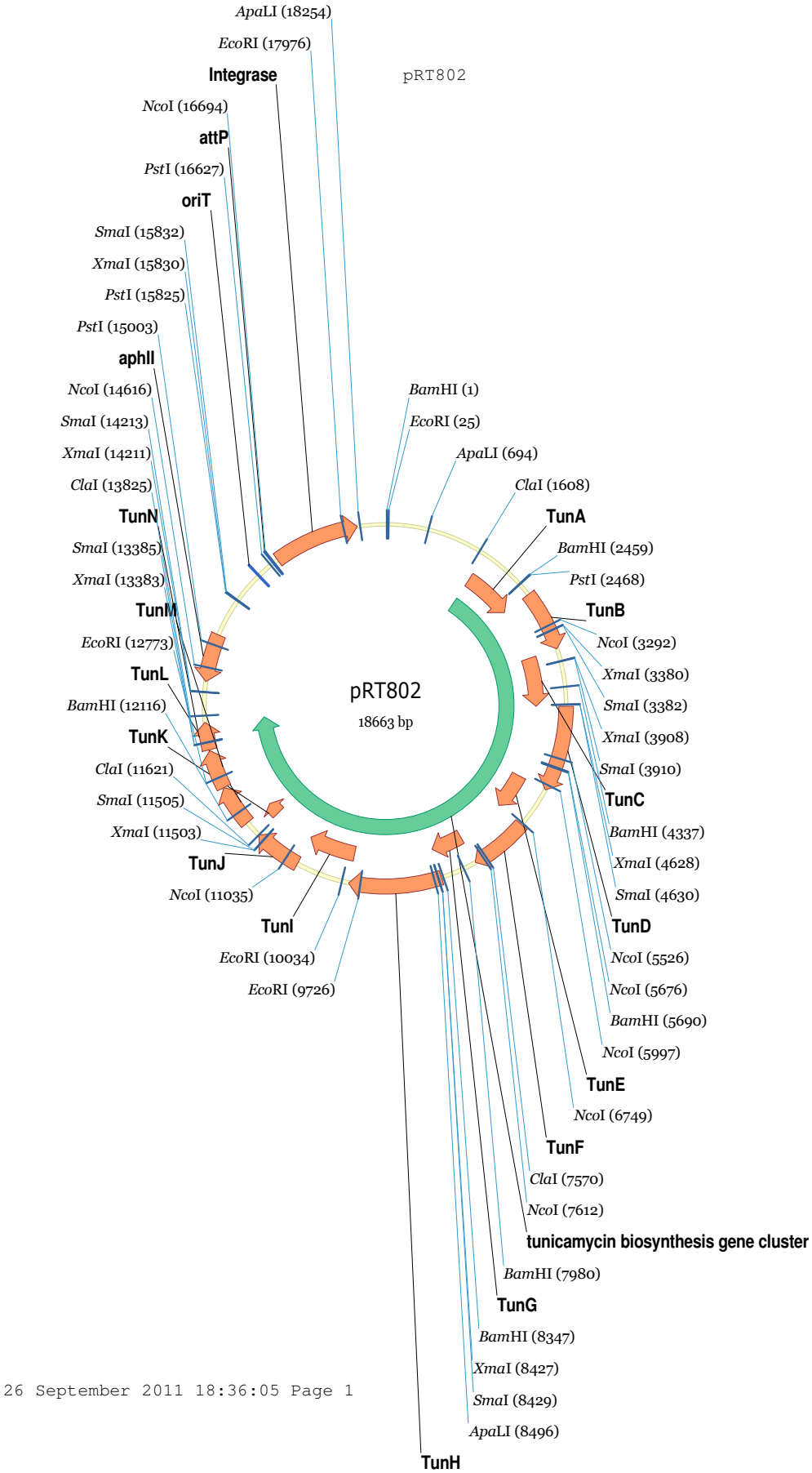
pRT802
pRT802
18663 bp
ApaLI (18254)
EcoRI (17976)
Integrase
NcoI (16694)
attP
PstI (16627)
oriT
SmaI (15832)
XmaI (15830)
PstI (15825)
PstI (15003)
aphII
NcoI (14616)
SmaI (14213)
XmaI (14211)
ClaI (13825)
TunN
SmaI (13385)
XmaI (13383)
TunM
EcoRI (12773)
TunL
BamHI (12116)
TunK
ClaI (11621)
SmaI (11505)
XmaI (11503)
TunJ
NcoI (11035)
TunI
EcoRI (10034)
EcoRI (9726)
BamHI (1)
EcoRI (25)
ApaLI (694)
ClaI (1608)
TunA
BamHI (2459)
PstI (2468)
TunB
NcoI (3292)
XmaI (3380)
SmaI (3382)
XmaI (3908)
SmaI (3910)
TunC
BamHI (4337)
XmaI (4628)
SmaI (4630)
TunD
NcoI (5526)
NcoI (5676)
BamHI (5690)
NcoI (5997)
TunE
NcoI (6749)
TunF
ClaI (7570)
NcoI (7612)
tunicamycin biosynthesis gene cluster
BamHI (7980)
TunG
BamHI (8347)
XmaI (8427)
SmaI (8429)
ApaLI (8496)
TunH
26 September 2011 18:36:05 Page 1

**pIJ12003a: construct containing tunicamycins biosynthesis gene cluster in pRT802.**

**Heterologous Expression and Culturing of *S. coelicolor* M1152 *tunB*(-) or *tunF*(-).** Heterologous expression of *S. coelicolor* M1152 *tunB*(-) and *tunF*(-) and relevant controls and extraction followed the same condition as previously reported.[3]

**Extraction of Nucleotide Sugars from Cell Lysate.**

Extraction procedure followed as reported by Räbina, J. *et al.*[11]

**LC-MS Analysis** (*Streptomyces* knockout metabolite analysis)**.** SPE sample was analysed by Micromass ZMD (ESI-TOF MS) coupled to Hewlett Packard Series 1050 with Waters Symmetry C18 column. Injection volume of 20 μL. Solvent A: 95% H2O, 4.9% ACN, 0.1% FA. Solvent B: 99.9% ACN, 0.1% FA]. The elution conditions were as follows: solvent A for 5 min. then solvent B in 20 min. gradient -- solvent B for 5 min. then back solvent A in 5 min. gradient – then solvent A for 5 min. Raw data were analysed on MassLyxn software.

**Expression and Purification of TunD and TunE.**[12] TunD and TunE genes from DNA sequence of *S. chartreusis* NRL 3882 were codon optimised for *E.coli* and synthesised and subcloned into pET16b and pET28a, respectively, by Genscript USA Inc. The TunD was further subcloned into pET21a, creating pET21a:TunD (TunD-$His_6$ ~ 52 kDa). The pET16b:TunD (TunD-$His_{10}$ ~ 53 kDa), pET21a:TunD (TunD-$His_6$ ~ 52 kDa), and pET28a:TunE (TunE-$His_6$ ~ 27 kDa) expression vectors were transformed into BL21(DE3) competent cells. Transformation followed the manufacturer's instructions. Analytical scale expression was done at 15 °C for 24 hr. growth period after 1 mM IPTG

induction, and 37 °C for 4 hr. period after 1 mM IPTG induction. Both expressions were analysed by SDS-PAGE and Western blot that showed the same positive expression with histidine-tag present with the predicted mass. Western blot and SDS-PAGE of 24 hr. expression at 15 °C is shown below. Other expression temperatures (37 to 30, 23, 18, and 15 ℃) attempted but no difference in expression was observed.

**Lemo21(DE3) expression system.** The transformation and expression followed the manufacturer's instructions.

**Western blot and SDS-PAGE from BL21(DE3) expression**

TunD-$His_6$ ~ 52 kDa

TunE-$His_6$ ~ 27 kDa

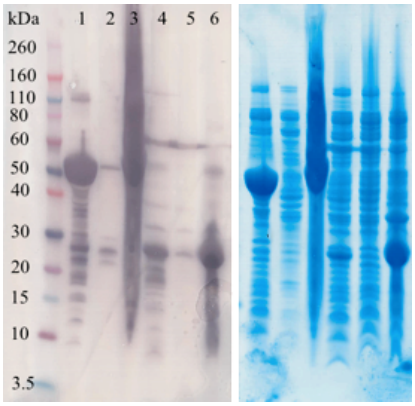


**Lanes**

**0 -** Marker

**1** - TunD cell lysate

**2** - TunD cell lysate supernatant

**3** - TunD inclusion body

**4** - TunE cell lysate

**5** - TunE cell lysate supernatant

**6** - TunE inclusion body

After cultures were grown at the temperature and time specified above, the cell pellets were collected by centrifugation (8,000 x g, 10 min. 4 °C) and then stored at -20 °C.

**Purification of TunD-His$_{10}$.** Protein purification was done at 4 °C. The cell pellet was resuspended in binding buffer D (5 mL per gram of wet cell pellet) with lysozyme (1 mg per 10 mL), DNAseI (0.1 mg per 10 mL), and ½ tablet of Complete EDTA-free protease cocktail (Roche) per 10 mL. The mixture was stirred for 30 min. at 4 °C, and then the cells were further broken by sonication (5 x 30 sec. 30 sec. cooling cycle on ice, 55 % amplitude). The resulting lysate was centrifuged at 65,000 x g for 45 min. at 4 °C, and filtered (0.2 μm). The supernatant was collected and incubated with $Ni^{+2}$ resin overnight at 4 °C. The slurry was added to Bio-Rad Eco column and eluted with binding buffer D with imidazole gradient of 10 mM to 500 mM to elute the protein. Fractions were collected and analysed by SDS-PAGE. The fractions containing the pure protein were pooled and dialysed in dialysis buffer D, concentrated via vivaspin (10,000 MWCO) and stored at 4 °C.

Binding Buffer D: 50 mM HEPES pH 7.5, 200 mM NaCl, 20 mM $MgCl_2$, 10 % glycerol, 10 mM imidazole

Dialysis Buffer D: 50 mM HEPES pH 7.5, 200 mM NaCl, 20 mM $MgCl_2$, 10 % glycerol

Unfortunately, TunD-$His_{10}$ protein was not soluble in the binding buffer as shown in the SDS-PAGE above that the protein is likely to still be in the inclusion body.

**Purification of TunD-$His_6$.** Same as above, except Buffer D1 was used (below).

Binding Buffer D1: 50 mM HEPES pH 7.5, 300 mM NaCl, 20 mM $MgCl_2$, 10 % glycerol, 20 mM imidazole + 0.5% Triton-X

Dialysis Buffer D1: 50 mM HEPES pH 7.5, 300 mM NaCl, 20 mM $MgCl_2$, 10 % glycerol

Unfortunately, TunD-$His_6$ protein was not soluble in the binding buffer D1.

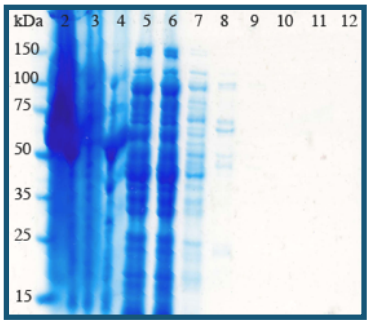


**Lanes**

**1 -** buffer D1 with 10 mM imidazole

**2 -** buffer D1 with 10 mM imidazole

**3 -** buffer D1 with 10 mM imidazole

**4 -** buffer D1 with 30 mM imidazole

**5 -** buffer D1 with 50 mM imidazole

**6 -** buffer D1 with 50 mM imidazole

**7 -** buffer D1 with 75 mM imidazole

**8 -** buffer D1 with 100 mM imidazole

**9 -** buffer D1 with 150 mM imidazole

**10 -** buffer D1 with 300 mM imidazole

**11 -** buffer D1 with 500 mM imidazole

**12 -** buffer D1 with 500 mM imidazole

**Purification of TunE-His$_6$**. Protein purification was done at 4 °C. The cell pellet was resuspended in binding buffer E (5 mL per gram of wet cell pellet) with lysozyme (1 mg per 10 mL), DNAseI (0.1 mg per 10 mL), and ½ tablet of Complete EDTA-free protease cocktail (Roche) per 10 mL. The mixture was stirred for 30 min. at 4 °C, and then the cells were further broken by sonication (5 x 30 sec. 30 sec. cooling cycle on ice, 55 % amplitude). The resulting lysate was centrifuged at 65,000 x g for 45 min. at 4 °C, and filtered (0.2 μm). The supernatant was collected and incubated with $Ni^{+2}$ resin overnight at 4 °C. The slurry was added to Bio-Rad Eco column and eluted with binding buffer E with imidazole gradient of 10 mM to 500 mM to elute the protein. The fractions containing the pure protein were pooled and dialyzed in dialysis buffer E, concentrated via vivaspin (10,000 MWCO) and stored at 4 °C.

Binding Buffer E: 50 mM HEPES pH 7.5, 300 mM NaCl, 10 % glycerol, 1 mM TCEP, 0.5 % Triton X-100, 10 mM imidazole

Dialysis Buffer E: 50 mM HEPES pH 7.5, 300 mM NaCl, 10 % glycerol, 1 mM TCEP, 0.05 % Triton X-100

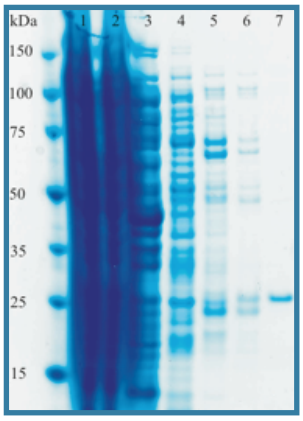


**Lanes**

**1 -** buffer E with 10 mM imidazole

**2 -** buffer E with 10 mM imidazole

**3 -** buffer E with 50 mM imidazole

**4 -** buffer E with 100 mM imidazole

**5 -** buffer E with 150 mM imidazole

**6 -** buffer E with 300 mM imidazole

**7 -** buffer E with 500 mM imidazole

**TunD sample form iFOLD**

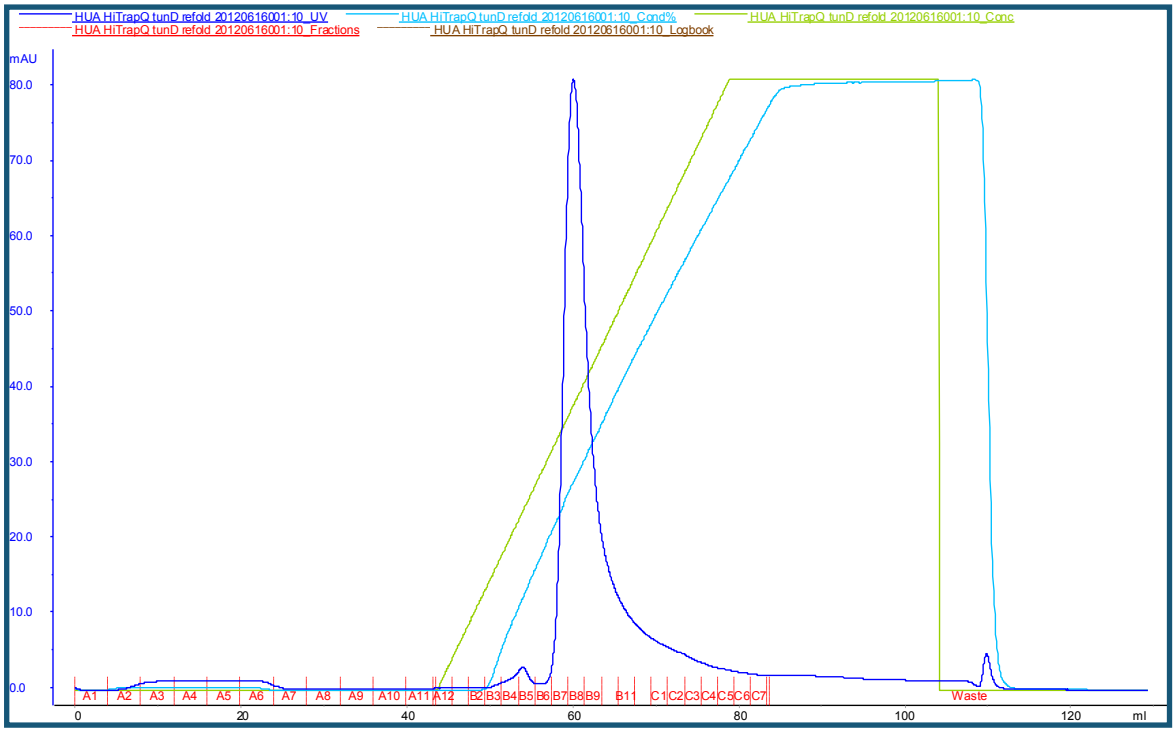


FPLC chromatogram of TunD refolded on ion-exchange Hi Trap Q HP 5mL. Buffer/Eluant condition: 20mM Tris, pH7.5, using 1M NaCl gradient from 0% to 100%

**Table 1.** Continuous spectrophotometric assay reaction condition

*Condition*

Measurement wavelength: 340 nm

Temperature: 30 ˚C

Total volume: 200 µL

Reaction time: 3hrs

Enzyme: 20 µg

Donor: UDP-GlcNAc, 1 mM

Acceptor: N-acetyl-tunicamyl uracil, 3 mM

Assay Mixture:

50 mM HEPES (pH 7.0)

10 mM $MgCl_2$

0.01% BSA

1 mM phosphoenol pyruvic acid

0.3 mM NADH

17 U pyruvate kinase

24 U lactate dehydrogenase

*The reaction is initiated by adding UDP-GlcNAc last, right before the measurement.

**Table 2.** Multiple donor-acceptor screening substrates

| *Acceptor* | *Donor* |
|---|---|
| Glucose | UDP-glucose |
| Galactose | UDP-galactose |
| Fucose | UDP-N-acetyl-glucosamine |
| Fructose | UDP-N-acetyl-galactosamine |
| Rhamnose | GDP-mannose |
| Mannose | GDP-fucose |
| Glucosamine HCl | GDP-glucose |
| Galactosamine HCl | |
| N-acetyl-glucosamine | |
| N-acetyl-galactosamine | |
| Glucose-6-phosphate | |
| Fructose-6-phosphate | |
| Ribose-5-phosphate | |

Mannose-6-phosphate

Galactose-1-phosphate

N-acetyl-tunicamycin uracil

**Table 3.** Continuous spectrophotometric assay reaction condition

*Condition*

Measurement wavelength: 340 nm

Temperature: 30 ˚C

Total volume: 200 μL

Reaction time: 7000 sec.

Enzyme: 100 μg

Acceptor: 1 mM each

Donor: 1 mM each

Assay Mixture:

50 mM HEPES or Tris (pH 7.0)

10 mM $MgCl_2$

1 mM phosphoenol pyruvic acid

0.3 mM NADH

17 U pyruvate kinase

24 U lactate dehydrogenase

*The reaction is initiated by adding NDP-sugar last, right before the measurement.

**Table 4.** Categorised acceptors and donors

*Acceptor* *Donor*

A1

- Glucose
- Galactose
- Fucose
- Fructose
- Rhamnose
- Mannose
- Glucosamine HCl
- Galactosamine HCl

A2

- N-acetyl-glucosamine
- N-acetyl-galactosamine

A3

- Glucose-6-phosphate
- Fructose-6-phosphate
- Ribose-5-phosphate
- Mannose-6-phosphate
- Galactose-1-phosphate

A4

- N-acetyl-tunicamycin uracil

D1

- UDP-glucose

D2

- UDP- N-acetyl-glucosamine

**Table 5.** Reaction condition.

*Condition*

Measurement wavelength: 340 nm

Temperature: 30 ˚C

Total volume: 100 µL

Reaction time: 3600 sec.

Enzyme: 50 µg

Acceptor: 1 mM each

Donor: 1 mM each

Assay Mixture:

50 mM HEPES or MOPS (pH 7.0)

10 mM $MgCl_2$

1 mM phosphoenol pyruvic acid

0.3 mM NADH

17 U pyruvate kinase

24 U lactate dehydrogenase

*The reaction is initiated by adding NDP-sugar last, right before the measurement.

**Table 6.** iFOLD protein sample activity assay condition

*Condition*

Measurement wavelength: 340 nm

Temperature: 30 ˚C

Total volume: 100 µL of iFOLD sample

Reaction time: 3600 sec.

Enzyme: 10 µg

GlcNAc: 1 mM each

UDP-GlcNAc: 1 mM each

Assay Mixture:

10 mM $MgCl_2$

1 mM phosphoenol pyruvic acid

0.3 mM NADH

17 U pyruvate kinase

24 U lactate dehydrogenase

*The reaction is initiated by added NDP-sugar last, right before the measurement.

**Table 7.** Refolding conditions showed indicative of UDP hydrolytic activity by the refolded protein in assay.

*Refold Condition*

A1: 1 mM TCEP, 20% Glycerol, pH 7.0

A5: 100 mM NaCl, 1 mM TCEP, 0.1% PEG 6000, pH 7.0

B3: 100 mM NaCl, 3.8/1.2 mM GSH/GSSG, 1 mM EDTA, pH 7.0

D12: $ddH_2O$, pH 7.5

*Note:* no product mass was observed.

**Crystallisation reagent set used for refolded TunD**

*Commercial Crystallisation Reagent Set*

- JCSG
- PEG/ION
- STRUCTURE
- PACT

**TunD & TunE HPLC activity assay.** Total reaction volume of 100 μL consisted of 10 mM HEPES pH 7.0, 5 mM $MgCl_2$, 2 μg of enzyme, and 500 μM of substrate(s). The reactions was incubated at 30 °C for 60 min. The reactions were ultrapurified via vivaspin (10,000 MWCO) before injecting into the HPLC and analyzing on $NH_2$ column (Phenomenex Luna $NH_2$ 5 μm, 4.6 x 250 mm) with ACN/W, 7:3, eluted isocratically at 0.50 mL $min^{-1}$ for 35 min.

**SDS-PAGE:** Analysis was done using MOPS and MES NuPAGE 20X running buffer, 10 % and 4 - 12 % NuPAGE Bis-Tris Gel, Invitrogen XCell *Sure*Lock™ purchased from Invitrogen following the manufacturer's instructions. The protein gel was stained using Coomassie based gel staining solution InstantBlue purchased from Expedeon following the manufacturer's instructions.

**Western Blot analysis.** The protein samples were separated by SDS-PAGE and then transferred to the membrane following iBlot Dry Blotting system by Invitrogen. The membranes were soaked in 5% (wt/v) BSA in PBS for 1 h at room temperature. After 1 h, the membrane was carefully washed with PBS and then soaked again in 5% (wt/v) BSA in PBS with the addition of recommended volume of monoclonal anti-polyhistidine-alkaline phosphatase antibody. The membrane was soaked under gentle rocking 2 h at room temperature. Finally, after 2 h, the membrane was gently washed with PBS and the stained with drop wise addition of the NBT-BCIP solution.

**Protein concentration determination.** Protein concentrations were calculated with bicinchoninic acid (BCA) protein assay (Pierce) according to manufacturer's instructions. Bovine serum albumin was used as a protein standard.

**Protein Refolding.** The TunD refolding followed the manufacture protocol for iFOLD Protein Refolding System 1.

**Glycosyltransferase coupled assay.**[13] The assay followed reported protocol by Gosselin *et al*. Modification of the assay would be noted.

**Heterologous expression of polyphosphate: AMP phosphotransferase (PAP).**[14-18] pET29:PAP plasmid vector was constructed with codon optimized for *E. coli* (PAP-$His_6$ ~ 57 kDa) by GenScript. The plasmid construct was transformed into BL21(DE3), expression condition were as followed: 1-L LB, 50 μg/mL kanamycin. When the cell culture reached $A_{600}$ 0.6, it was induced with 1 mM IPTG, continued with 30 °C overnight incubation with shaking (200 rpm) (28 and 16 °C overnight incubation were screened with no difference in expression level, Fig. 32). The cell pellet was collected and lysed with lysozyme, DNAse, and protease inhibitor, in 50 mM Tris buffer (pH 7.5) with 10 % glycerol. The cell lysis mixture was stirred for 1 hr and sonicated on ice at 30 sec. interval 3 times. Soluble fraction was collected via centrifugation at 60,000 x g, 40 min, 4 °C. The supernatant was filtered via 0.2 μm membrane before incubated with $Ni^{+2}$ resin with 10 mM imidazole, at 4 °C for 4 hours. Ni-NTA manual purification was carried out using the same Tris buffer with imidazole gradient (25 mM, 50 mM, 100 mM, 250 mM, 500 mM, each concentration eluted with 30 mL volume). The fractions were analyzed by SDS-

PAGE. The fractions containing the protein were pooled, concentrated, and dialyzed against the original Tris buffer. The protein was further analysed by CD showing helical structure for PAP.

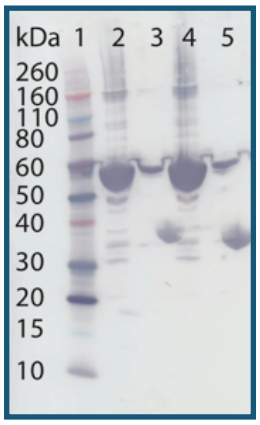


PAP expression western blot. Lane 1. marker; 2. cell lysate, expression at 28 °C; 3. soluble fraction, expression at 28 °C; 4. cell lysate, expression at 16 °C; 5. soluble fraction, expression at 16 °C.

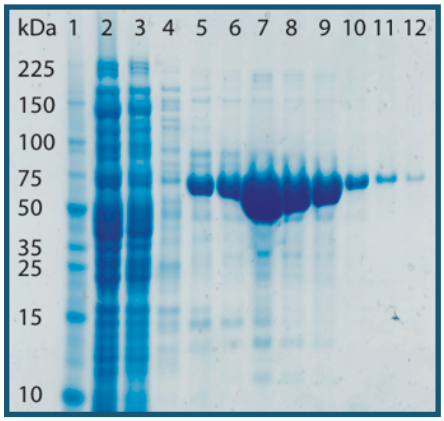


SDS-PAGE. Manual Ni-NTA purification of PAP.

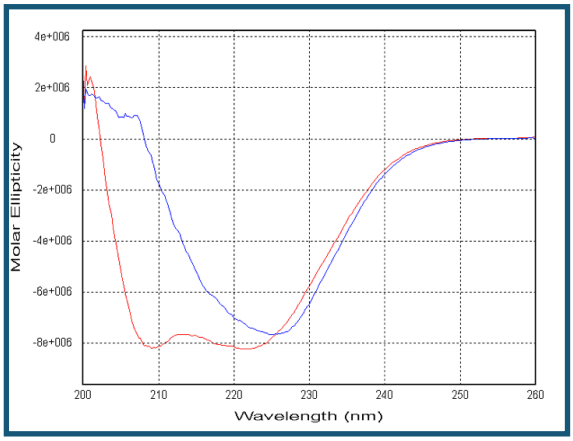


**CD spectra PAP.** Overlay, Blue: 1mg/ml; Red 0.5 mg/ml. Optimal at 0.5 mg/mL.

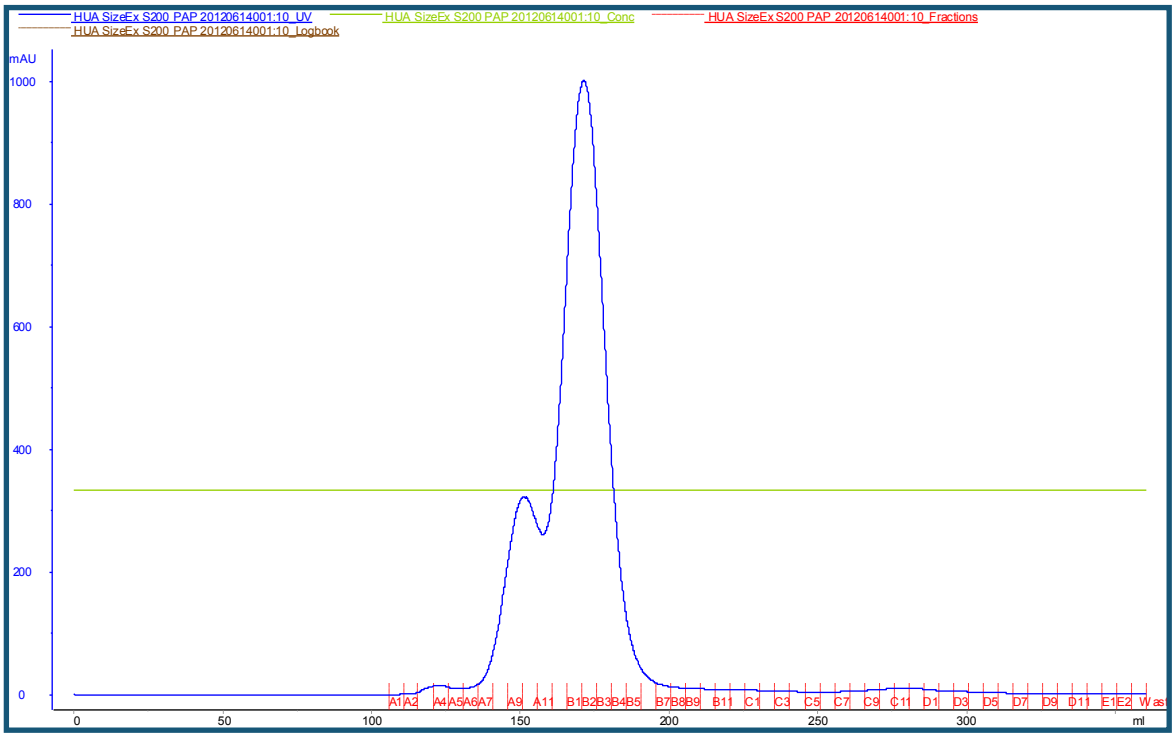


FPLC chromatogram, PAP size exclusion purification on Hi load 26/60 Superdex 200 prep grade. Buffer/eluent system: 50 mM Tris, pH 7.5, 10% Glycerol.

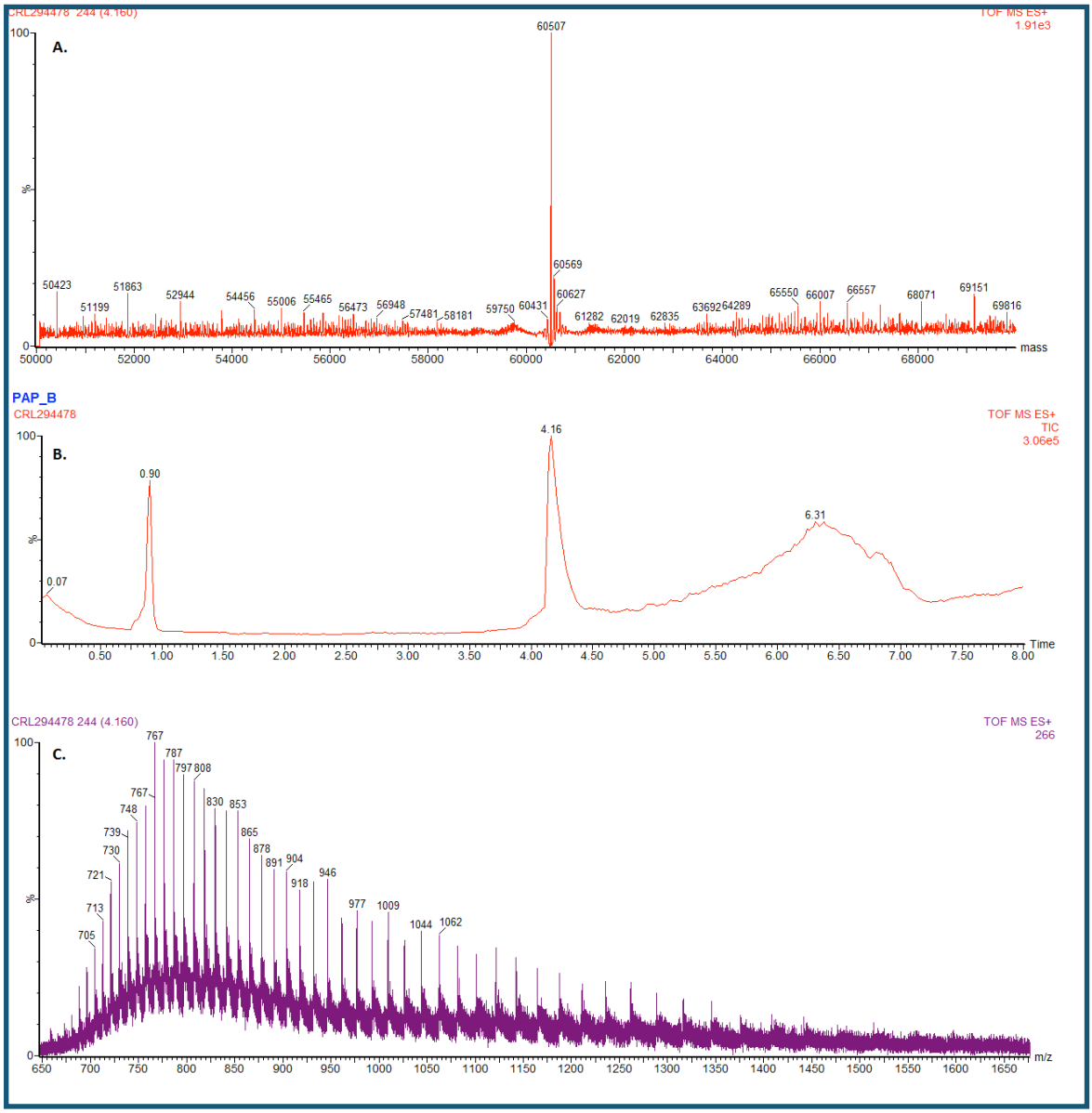


**LCMS of PAP sample.** A. Expected: 60405, Observed: 60407. B. TIC chromatogram. C. ES+ spectrum.

**PAP activity assay:** The reaction condition screens were carried out in 96-well plate, in 200µL volume: Tris buffer, pH 8.5, 37 °C. The addition of UDP was used as a positive control, and the blank as the negative control where no NADH is being consumed by LD. $MgCl_2$ was screened using 100mM, 75mM, 50mM, 25mM, or 10mM concentration in the Tris reaction mixture. Phosphorylation of UDP by PAP using polyphosphate was optimum

between 25-50mM of $MgCl_2$ (Fig. 7). However, using higher concentration of $MgCl_2$ does make the reaction mixture cloudy. pH was screened using Tris buffer pH of 5, 6, 7, 8, 9. Phosphorylation of UDP by PAP using polyphosphate in Tris buffer was optimum between the pH of 8 and 9 (Fig. 8). As for the effect of temperature on the phosphorylation of UDP by PAP using polyphosphate in Tris buffer pH 8.5, 37 °C was found to be optimum from screening 23, 37, and 50 °C (Fig. 9a-c). Lastly, different buffer system was screened at pH 8.5 and carried out the reaction at 37 °C. HEPES was found to be optimum to reduce reaction time by about 15 minutes compared to Tris (Fig. 10a-c). TAPS and Tricine buffer system could also be an option as no precipitation was observed compared to other buffer systems. HEPES and Tris buffer system do turn cloudy after some time.

**PAP Continuous spectrophotometric assay**

**Assay condition:** Absorbance reading at 340 nm

Temperature set at 37 C

Timed for 70 minutes

Reading every 18 sec.

**PAP-assay mixture**

| Components | Stock | Concentration in 200µL | vol. (µL) |
|---|---|---|---|
| Buffer Δ, pH Δ, 8.5 optimum | 1 M | 50 mM | 10 |
| $MgCl_2$ | 1 M | Δ, 25mM optimum | Δ, 5 |
| Phosphoenolpyruvic acid | 100 mM | 1mM | 2 |

| | | | |
|---|---|---|---|
| NADH | 100 mM | 300 µM | 0.6 |
| Lactate dehydrogenase | 6000U/mL | 24 U | 0.8 |
| Pyruvate kinase | 5000U/mL | 17 U | 0.68 |
| PAP | 1 mg/mL | 250 ng/mL | 50 |
| Polyphosphate45±5 | 43 mM | 1 mM | 4.65 |
| UDP* | 50 mM | 1 mM | 4 |
| UMP* | 50 mM | 1 mM | 4 |
| Distilled water | - | - | add to 200 total |

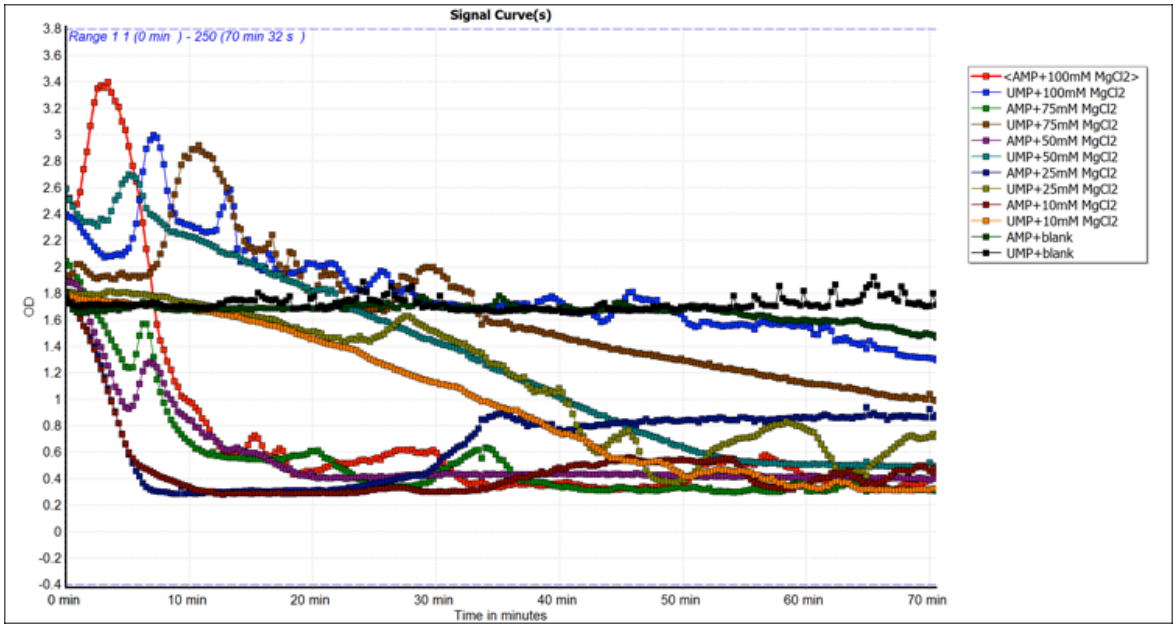


Effect of $MgCl_2$ on PAP activity with UMP.

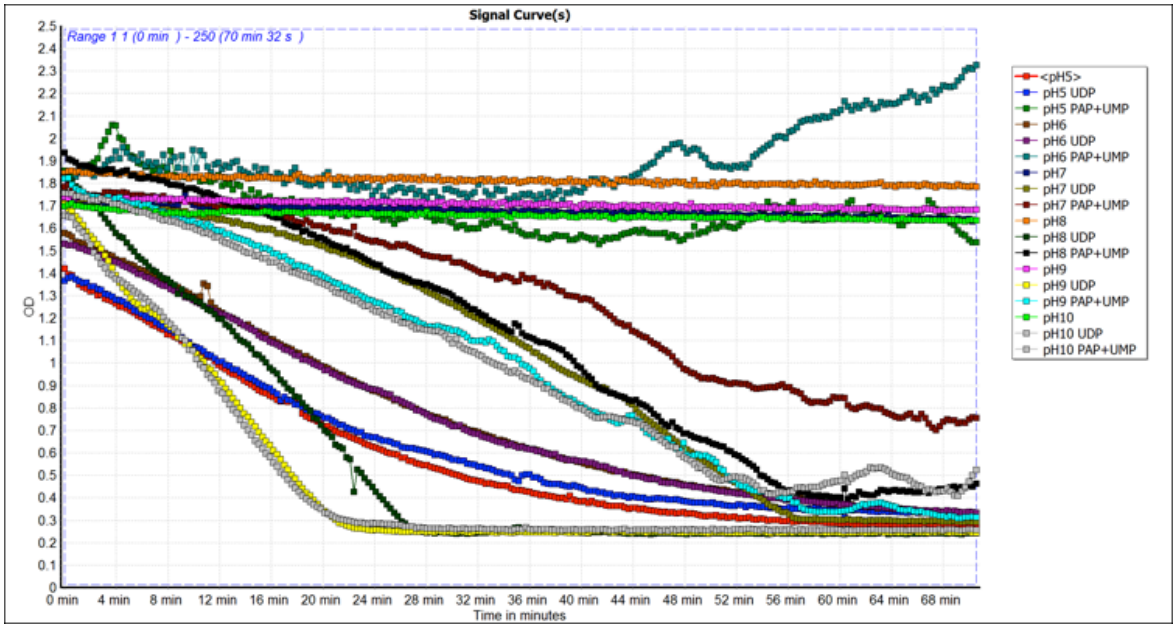


pH effect on PAP activity with UMP.

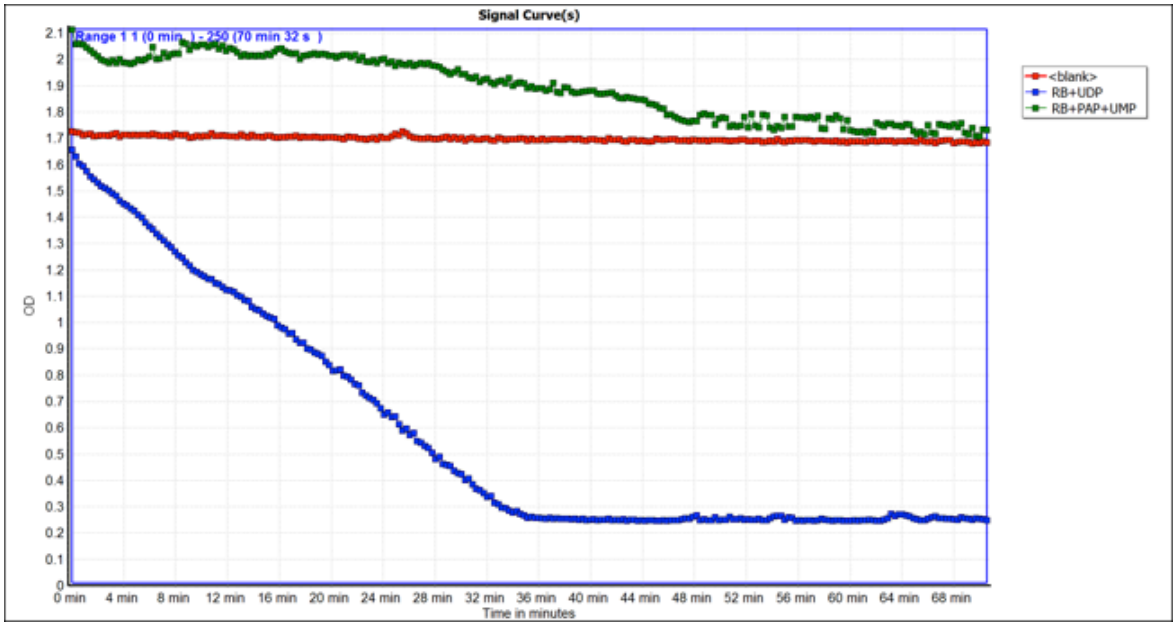


PAP activity with UMP at 23 °C.

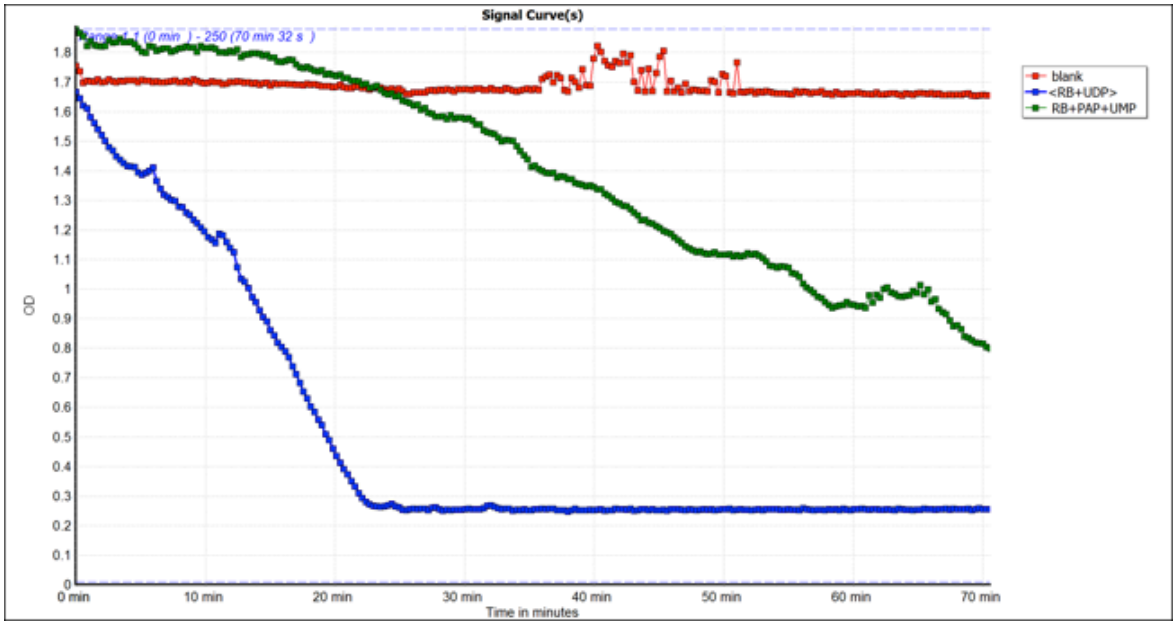


PAP activity with UMP at 37 °C.

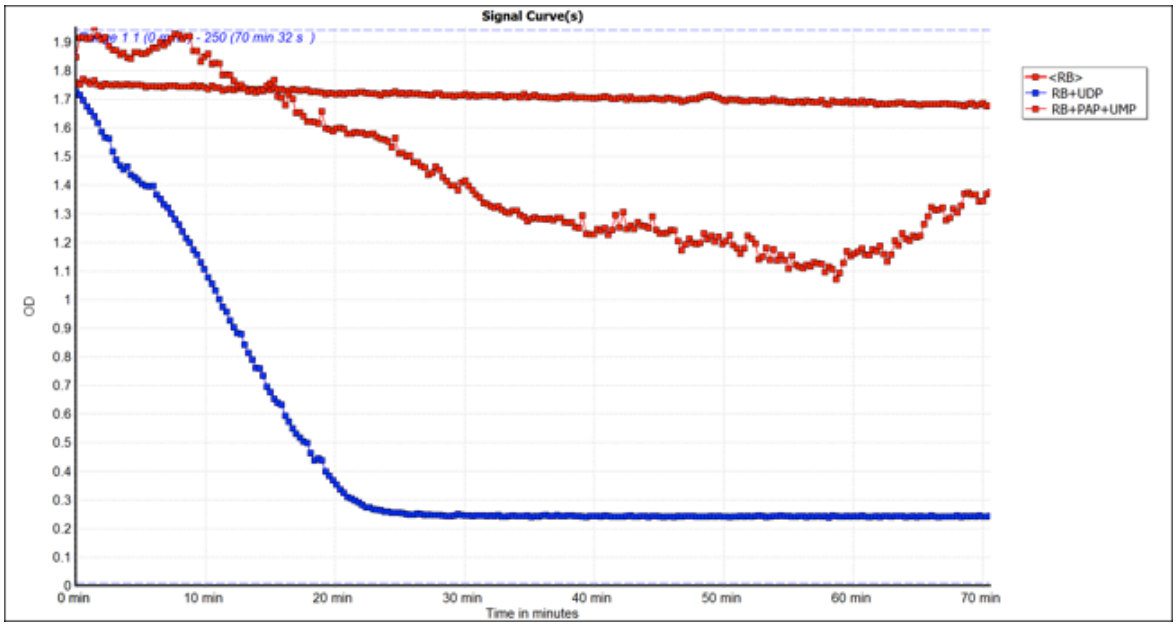


PAP activity with UMP at 50 °C.

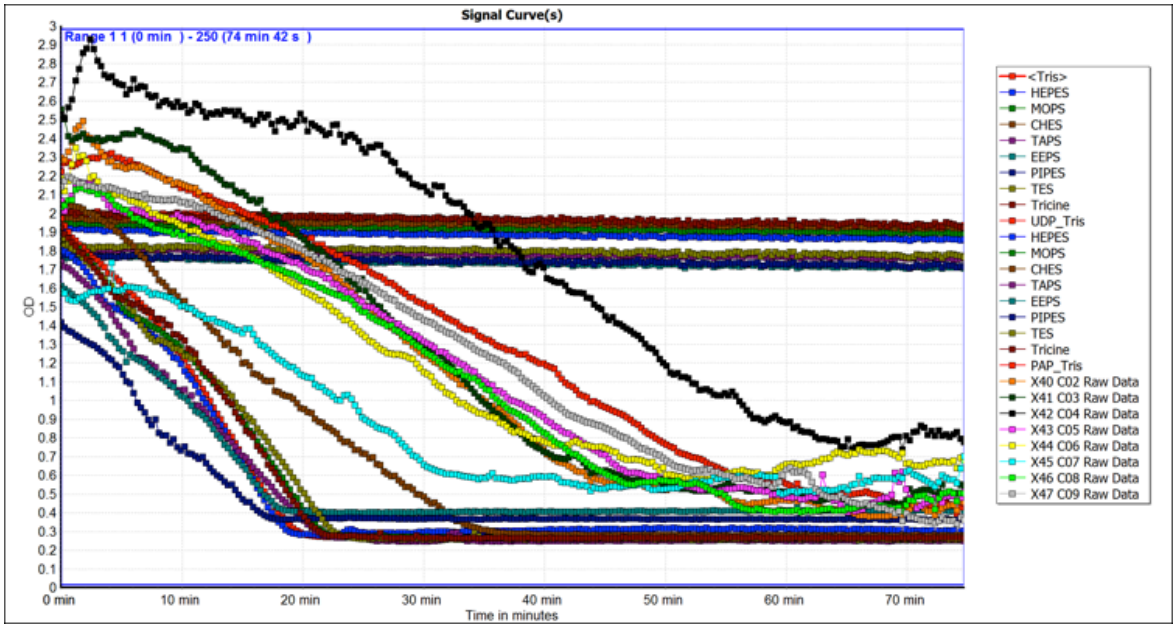


Buffer effect on PAP activity with UMP. Overlap of blank, UDP spike, and PAP with UMP.

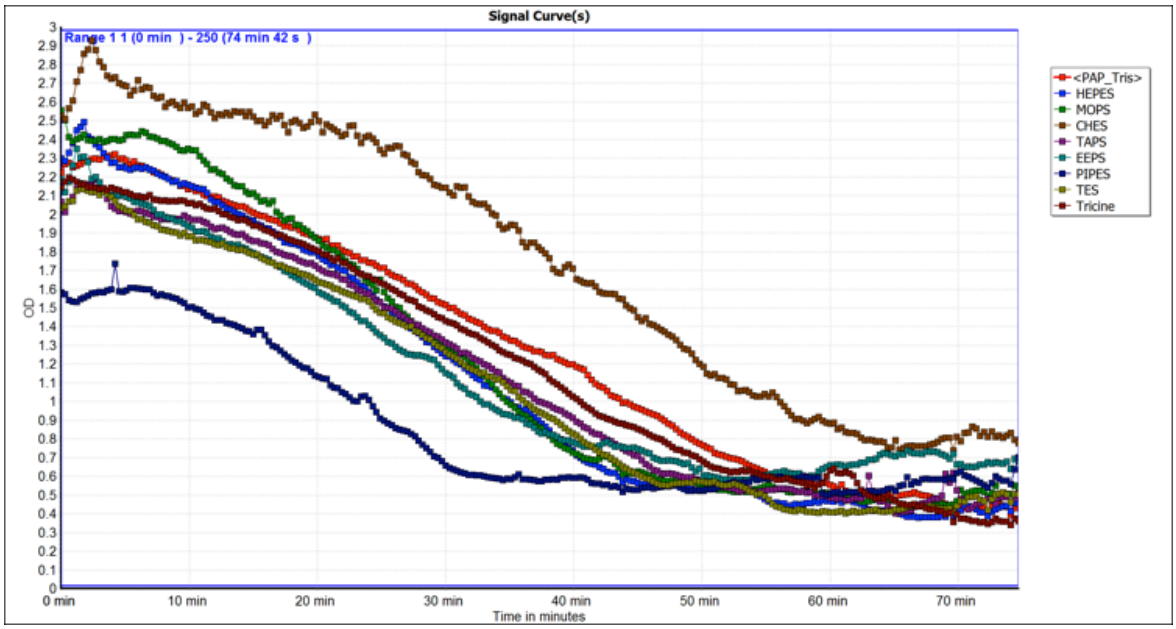


Buffer effect on PAP activity with UMP.

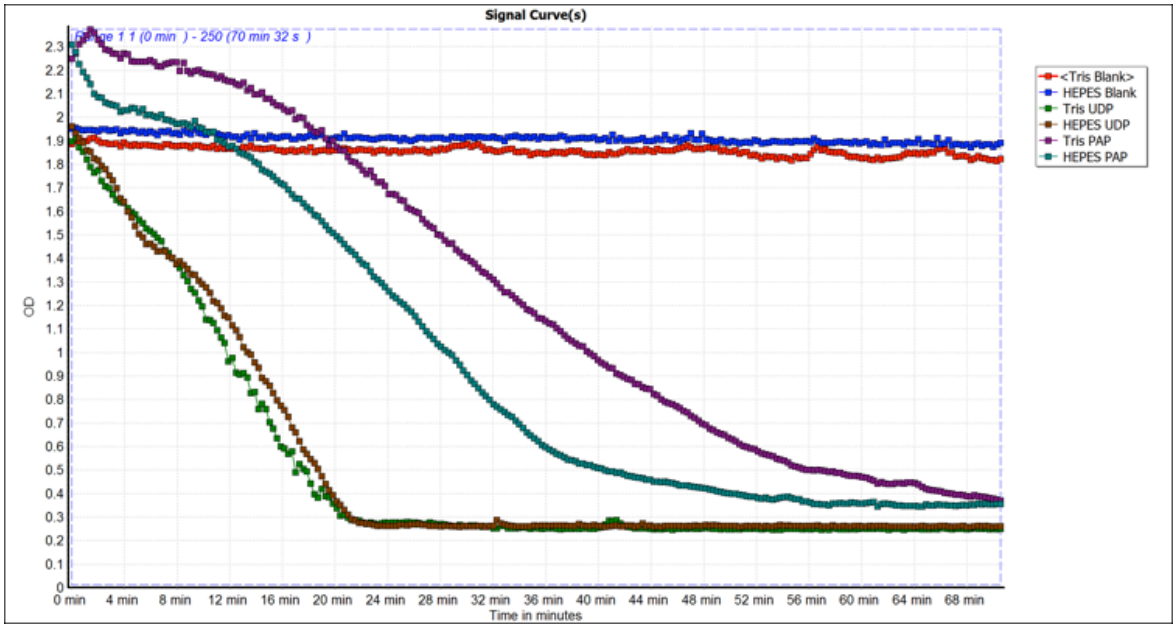


Effect of buffer on PAP activity with UMP. Comparison between Tris and HEPES.

**Expression and purification of OtsA.**[19] The expression and purification followed protocol reported by Davies, G. *et al* (2002). 10-mL test expression was done, followed by western blot to detect the His-tagged OtsA. The expression was scaled up to 1-L. OtsA was first purified by step-wise Ni-NTA purification (Fig. 19), followed by gel-filtration (Fig. 20).

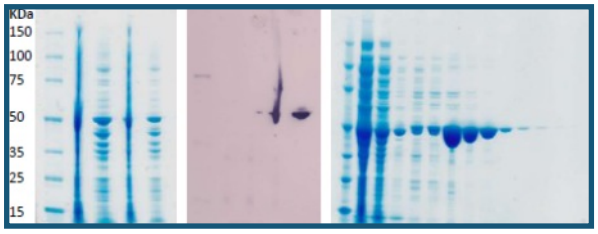


Left: SDS-PAGE, OtsA test expression; Middle: Western Blot of the OtsA test expression; Right: SDS-PAGE, step-wise Ni-NTA purification of OtsA.

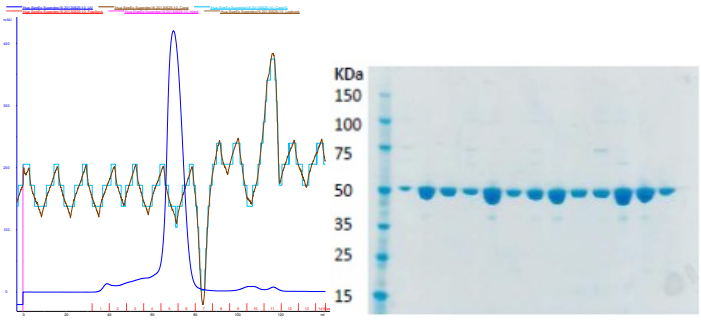


Left: FPLC size exclusion chromatography; Right: SDS-PAGE, FPLC fractions from multiple runs.

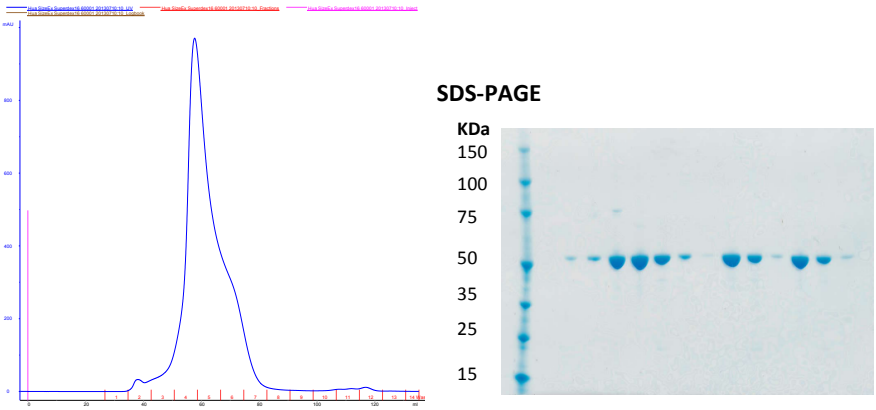


**OtsA FPLC Gel filtration and SDS-PAGE.**

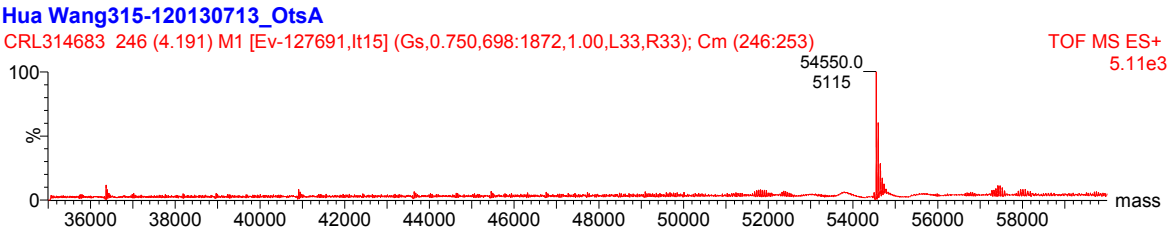


**OtsA MS analysis.** OtsA, Calc: 54545. Obs: 54550.

**OtsA activity assay.** The activity assay followed the continuous spectrophotometric assay using Pyruvate kinase + Lactate dehydrogenase and measuring the NADH absorption at 340nm.

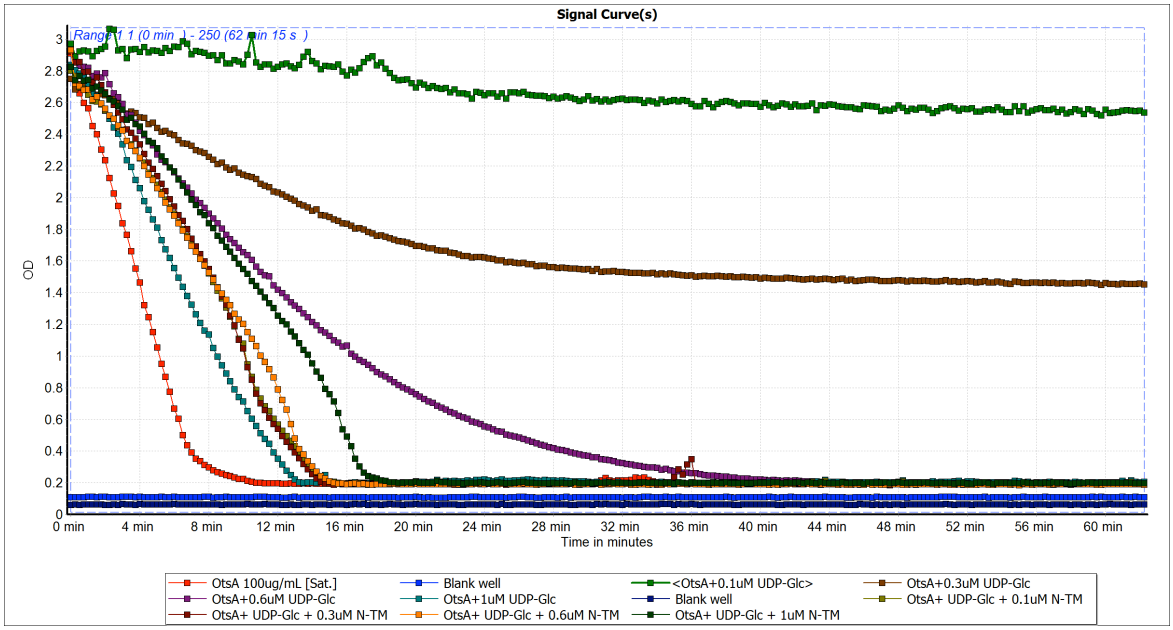


**OtsA rxn. condition:** 200 uL, RT, 100ug/mL OtsA, 1mM G6P, 1mM UDP-Glc, 50mM HEPES pH 7.0, 5mM MgCl2, 200mM NaCl

**Differential scanning fluorimetry.** OtsA Tm shift assay followed the reported protocol by Niesen *et al.*[20]

**UDP-MurNAc pentapeptide extraction, B. subtilise W23 culture growth.** Extracting UDP-MurNAc-pentapeptide from *Bacillus subtilis* W23 following published procedure has been a challenge in the past with no desired product detected by mass spectrometry (1194 m/z M+H corresponding to UDP-MurNAc-pentapeptide) after chloramphenicol and vancomycin treatment in cell-wall synthesis medium II (CWSM-II). Fortunately after investigating several growth conditions, the growth culture medium and extraction process, the optimised condition was found. The UDP-MurNAc-pentapeptide product was obtained after extraction and gel filtration. Isolated UDP-MurNAc-pentapeptide could now

be tagged with dansyl group, and then used in MraY fluorescent assay following a reported procedure.

Initial attempts to extract UDP-MurNAc-pentapeptide from *B. cereus* followed published protocol (+manufacturer protocol, Warwick BAcWAN) that did not yield any product. Then, growth medium was screened and extraction was also screened. Three growth medium was screened (Table 5). The growth medium that resulted UDP-MurNAc-pentapeptide after heat treated cell extraction was PYP. Additionally, CWSM-II medium was screened as given protocol from the manufacturer did not yield UDP-MurNAc-pentapeptide (Table 6). The CWSM-II without the addition of ampicillin resulted in the desired product. The extract was purified via gel filtration and detection wavelength was set at 254 nm. UV active fractions were pooled and analysed (see FPLC chromatogram, Fig. 14). The samples were analysed by LCMS, the initial fractions contained the desired product with mass correspond to UDP-MurNAc-pentapeptide (Fig. 15).

***B. subtilis* W23 growth medium**

| PYP (per liter) | PYP+Glucose (per liter) | CGPY+Glucose (per liter) |
|---|---|---|
| Bacteriological peptone, 20g | Bacteriological peptone, 20g | $Na_2HPO_4$, 6g |
| Yeast extract, 1.5g | Yeast extract, 1.5g | NaCl, 3g |
| $KH_2PO_4$, 5.5g | $KH_2PO_4$, 5.5g | $NH_4Cl$, 2g |
| | Glucose, 5g | $MgCl_2$ $6H_2O$, 0.1g |
| | | $Na_2SO_4$, 0.15g |
| | | $KH_2PO_4$, 3g |
| | | Bacto-peptone, 10g |
| | | Yeast extract, 0.1g |
| | | Glucose, 5g |

## CWSM-II recipes, pH 7.4

| CWSM-II (per liter) | CWSM-II (per liter) with ampicillin |
|---|---|
| $Na_2HPO_4$, 0.26g | $Na_2HPO_4$, 0.26g |
| $NH_4Cl$, 2g | $NH_4Cl$, 2g |
| KCl, 4g | KCl, 4g |
| $MgCl_2$ $6H_2O$, 4g | $MgCl_2$ $6H_2O$, 4g |
| $Na_2SO_4$, 0.15g | $Na_2SO_4$, 0.15g |
| $FeSO_4$, 0.1g | $FeSO_4$, 0.1g |
| Glucose, 2g | Glucose, 2g |
| Uracil, 40mg | Uracil, 40mg |
| l-glutamic acid, 120mg | l-glutamic acid, 120mg |
| L-lysine, 500mg | L-lysine, 500mg |
| 2,6-diaminopimelic acid, 120mg | 2,6-diaminopimelic acid, 120mg |
| L-alanine, 50mg | L-alanine, 50mg |
| Chloramphenicol, 50mg | Chloramphenicol, 50mg |
| Vancomycin, 12.5ug/mL | Vancomycin, 12.5ug/mL |
| | Ampicillin, 50mg |

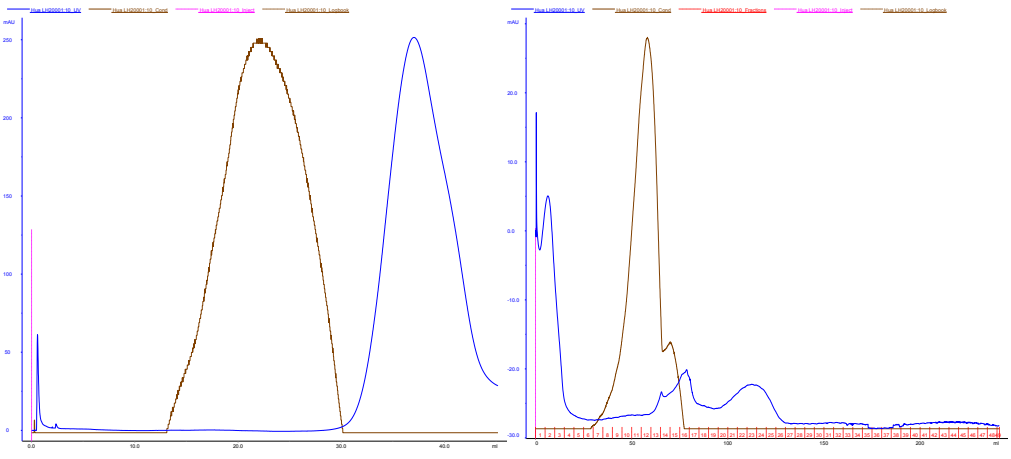

**FPLC gel filtration chromatogram of the *B. cereus* extract.**

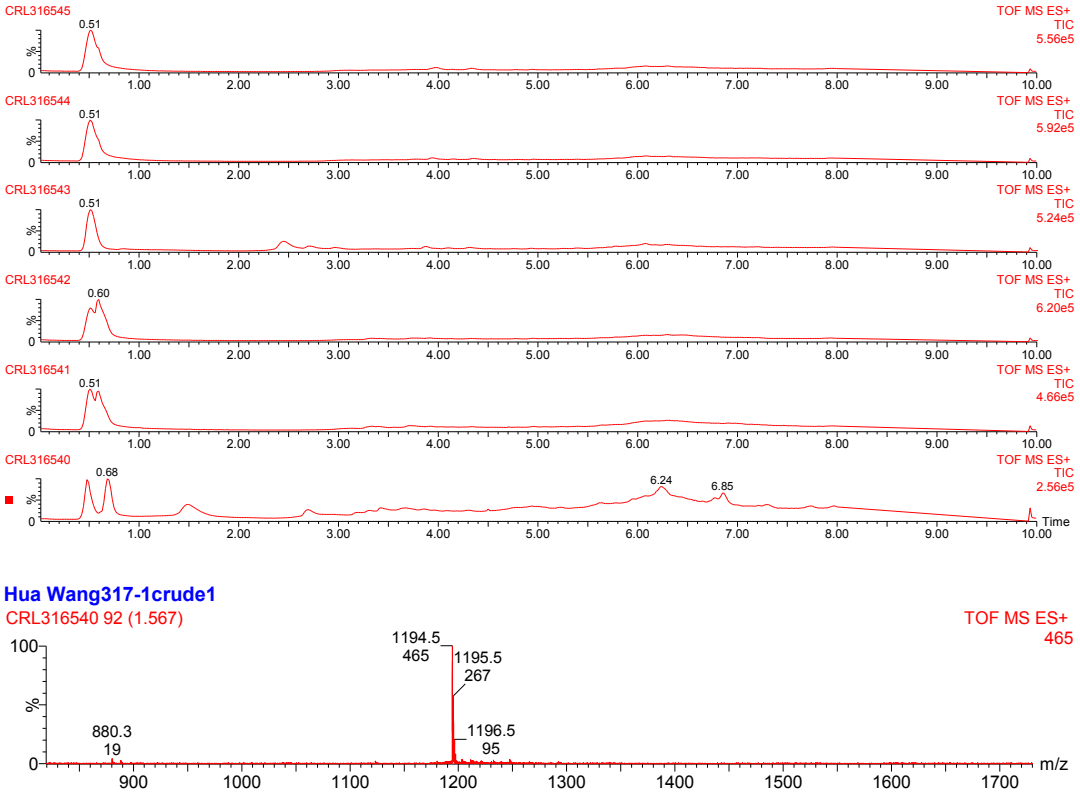





**LCMS analysis of the lyophilised fractions.** Top: TIC chromatogram. Bottom: MS of the desired product correspond to the 1.5 min. eluted peak of CRL316540 sample, the first UV active fraction from FPLC. UDP-MurNAc-pentapeptide (L-Ala-D-y-Glu-m-DAP-D-Ala-D-Ala). MW: 1193.34. Observed 1194 $[M+H]^+$.

## References


1 Sambrook, J. & Russell, D. W. *Molecular Cloning: A Laboratory Manual.* 3rd edn, (Cold Spring Harbor Laboratory Press, 2001).

2 Kieser, T., Bibb, M. J., Buttner, M. J., Chater, K. F. & Hopwood, D. A. *Practical Streptomyces Genetics.* (The John Innes Foundation, 2000).

3 Wyszynski, F. J., Hesketh, A. R., Bibb, M. J. & Davis, B. G. Dissecting tunicamycin biosynthesis by genome mining: cloning and heterologous expression of a minimal gene cluster. *Chem. Sci.* **1**, 581-589 (2010).

4 Wyszynski, F. J. et al. Biosynthesis of the tunicamycin antibiotics proceeds via unique exo-glycal intermediates. *Nature Chemistry* **4**, 539-546 (2012).

5 Institute, C. a. L. S. *Methods for Dilution Antimicrobial Susceptibility Tests for Bacteria That Grow Aerobically; Approved Standard—Ninth Edition.* Vol. **32** (Clinical and Laboratory Standards Institute, 2012).

6 Institute, C. a. L. S. *Performance Standards for Antimicrobial Disk Susceptibility Tests; Approved Standard—Eleventh Edition.* Vol. **32** (Clinical and Laboratory Standards Institute, 2012).

7 Andrews, J. M. & Howe, R. A. BSAC standardized disc susceptibility testing method (version 10). *J. Antimicrob. Chemother.* **66**, 2726-2757 (2011).

8 Wiegand, I., Hilpert, K. & Hancock, R. E. W. Agar and broth dilution methods to determine the minimal inhibitory concentration (MIC) of antimicrobial substances. *Nature Protocols* **3**, 163-175 (2008).

9 Gust, B., Kieser, T. & Chater, K. *PCR targeting system in Streptomyces coelicolor A3(2)* (John Innes Centre, Norwich, UK).

10 Gust, B. et al. Lambda red-mediated genetic manipulation of antibiotic-producing Streptomyces. *Advances in Applied Microbiology* **54**, 107-128 (2004).

11 Räbinä, J. et al. Analysis of nucleotide sugars from cell lysates by ion- pair solid-phase extraction and reversed-phase high-performance liquid chromatography. *Glycoconjugate* **18**, 799-805 (2001).

12 Wyszyński, F. J. Dissecting tunicamycin biosynthesis: A potent carbohydrate processing enzyme inhibitor *D.Phil. thesis, University of Oxford*, (2010).

13 Gosselin, S., Alhussaini, M., Streiff, M. B., Takabayashi, K. & Palcic, M. M. A Continuous Spectrophotometric Assay for Glycosyltransferases. *Analytical Biochemistry* **220**, 92-97 (1994).

14 Pick, U., Bental, M., Chitlarua, E. & Weiss, M. Polyphosphate-hydrolysis- a protective mechanism against alkaline stress? *FEBS* **274**, 15-18 (1990).

15 Bonting, C. F. C., Korstee, G. J. J. & Sehnder, A. J. B. Properties of Polyphosphate:AMP Phosphotransferase of Acinetobacter Strain 210A. *Journal of Bacteriology* **173**, 6484-6488 (1991).

16 Ishige, K. & Noguchi, T. Polyphosphate:AMP Phosphotransferase and Polyphosphate:ADP Phosphotransferase Activities of Pseudomonas aeruginosa. *Biochemical and Biophysical Research Communications* **281**, 821-826 (2001).

17 Shiba, T. et al. Polyphosphate:AMP Phosphotransferase as a Polyphosphate-Dependent Nucleoside Monophosphate Kinase in Acinetobacter johnsonii 210A. *Journal of Bacteriology* **187**, 1859-1865 (2005).

18 Nocek, B. et al. Polyphosphate-dependent synthesis of ATP and ADP by the family-2 polyphosphate kinases in bacteria. *PNAS* **105**, 17730-17735 (2008).

19 Gibson, R. P., Lloyd, R. M., Charnock, S. J. & Davies, G. J. Characterization of Escherichia coli OtsA, a trehalose-6-phosphate synthase from glycosyltransferase family 20. *Acta Crystallographica Section D* **D58**, 349-351 (2002).

20 Niesen, F. H., Berglund, H. & Vedadi, M. The use of differential scanning fluorimetry to detect ligand interactions that promote protein stability. *Nature Protocols* 2, 2212-2221 (2007).

**Abbreviations**

| | |
|---|---|
| **$^{1}$H NMR** | proton nuclear magnetic resonance |
| **$^{13}$C NMR** | carbon-13 nuclear magnetic resonance |
| **2,3-DMP** | 2,6-dimethyl pyridine |
| **°C** | degree Celsius |
| **[M]** | MS (see MS) molecular peak |
| **α** | alpha |
| **β** | beta |
| **δ** | delta, chemical shift |
| **λ** | lambda, wavelength |
| **µ** | mu, micro |
| **Amp.** | ampicillin |
| **aq.** | aqueous |
| **Ac** | acetyl |
| **ACN** | acetonitrile |
| **BCA** | bicinchoninic protein assay |
| **$Boc_2O$** | di-*tert*-butyl dicarbonate |
| **BSA** | bolvine serum albumin |
| **calc.** | calculated |
| **CD** | |
| **$CD_3OD$** | deuterated methanol |
| **$CDCl_3$** | deuterated chloroform |
| **conc.** | concentrated |
| **COSY** | correlated spectroscopy |
| **$D_2O$** | deuterated water |
| **Da** | Dalton |
| **DCC** | *N, N′*-dicyclohexylcarbodiimide |
| **DCM** | dichloromethane |
| **DDM** | *n*-dodecyl-β-D-maltopyranoside |
| **DMAP** | 4-dimethylamino pyridine |
| **DNA** | deoxyribose nucleic acid |
| ***e.g.*** | *exampli gratia* (Latin: for example) |
| **eq.** | equivalent |
| **ES** | electrospray |
| **Et** | ethyl |
| ***et al.*** | *et alia* (Latin: and others) |
| ***etc.*** | *et cetera* (Latin: and the rest) |
| **EtOAc** | ethylacetate |
| **FA** | formic acid |
| **g** | gram |
| **GalNAc** | *N*-acetylgalactosamine |
| **GlcNAc** | *N*-acetylglucosamine |
| **$H_2O$** | water |
| **HM** (singular) | Huamycin |
| **HMs** (plural) | Huamycins |
| **HM-#** | Huamycin-# |
| **HMBC** | hydrogen multiple bond correlation |
| **HMQC** | hydrogen multiple quantum correlated spectroscopy |
| **HPLC** | high-performance liquid chromatography |
| **HRMS** | high resolution mass spectrometry |
| **HSQC** | heteronuclear single quantum coherence |
| **Hz** | hertz |
| **h** | hour |
| ***i.e.*** | *id est* (Latin: that is) |
| **IMAC** | immobilized metal affinity chromatography |
| **IPTG** | isopropyl β-D-1-thiogalactopyranoside |
| **ITC** | |

| | |
|---|---|
| ***J*** | NMR coupling constant (Hz) |
| **k** | kilo |
| **Kana.** | kanamycin |
| **kbp** | kilo-base pair |
| **kDa** | kilodalton |
| **LB** | Luria Bertani |
| **LC-MS** | liquid chromatography-mass spectrometry |
| **LRMS** | low resolution mass spectrometry |
| **m** | milli or meter |
| **M** | Molarity |
| ***m/z*** | mass-to-charge ratio |
| **MALDI** | matrix-assisted laser desorption/ionization |
| **MeOH** | methanol |
| **MHz** | megahertz |
| **min.** | minute |
| **mL** | milliliter |
| **mol.** | mole |
| **molc.** | molecule |
| **m.p.** | melting point |
| **MS** | mass spectrometry |
| **MurNAc** | *N*-acetylmuramic acid |
| **NaOMe** | sodium methoxide |
| **NEB** | New England BioLabs® Inc. |
| ***neg.*** | negative |
| **nm** | nanometer |
| **NMR** | nuclear magnetic resonance |
| **NMR annotations:** | |
| | **app.** apparent |
| | **br.** broad |
| | **s** singlet |
| | **d** doublet |
| | **dd** doublet doublet |
| | **ddd** doublet doublet doublet |
| | **t** triplet |
| | **q** quartet |
| | **m** multiplet |
| **OD** | optical density |
| **PBS** | phosphate buffered saline |
| **PCR** | polymerase chain reaction |
| **pH** | $-\log_{10}[H^+]$ |
| ***pos.*** | positive |
| **ppm** | part per million |
| **pyr.** | pyridine |
| **quant.** | quantitative |
| **R** | unspecific chemical group |
| **$R_f$** | retention factor |
| **rpm** | revolution per minute |
| **RT** | room temperature |
| **Rxn** | reaction |
| **SDS-PAGE** | sodium dodecyl sulfate polyacrylamide gel electrophoresis |
| **soln.** | solution |
| **TB** | terrific broth |
| **TEA** | triethylamine |
| ***tert-*** | tertiary |
| **TFA** | trifluoroacetic acid |
| **THF** | tetrahydrofuran |
| **TLC** | thin layer chromatography |
| **TM** (singular) | tunicamycin |

| | |
|---|---|
| **TMs** (plural) | tunicamycins |
| **TOCSY** | total correlated spectroscopy |
| **W** | water |
| **WTA** | wall teichoic acid |

## Tunicamycins extraction record

| Tunicamycins (TM) Source | Cul. Vol. (L) | TM isolated[a] (mg) | Sample[b] (mg/mL) | HPLC[c] (mg/mL) | Purity (%) | TM/Liter (mg/L)[d] |
|---|---|---|---|---|---|---|
| M1040_1_(*tun*+)* | 1 | 31.60 | 31.60 | 0.1716 | 0.54% | 0.17 |
| M1040_2_(*tun*+)* | 1 | 11.80 | 11.80 | 0.0605 | 0.51% | 0.061 |
| M1040_3_(*tun*+)* | 1 | 29.20 | 29.20 | 0.5305 | 1.82% | 0.53 |
| M1489_1_(*tunB*-_*tunB*+)* | 1 | 42.90 | 42.90 | 1.1768 | 2.74% | 1.18 |
| M1489_2_(*tunB*-_*tunB*+)* | 1 | 40.30 | 40.30 | 1.7117 | 4.25% | 1.71 |
| M1489_3_(*tunB*-_*tunB*+)* | 1 | 128.60 | 128.60 | 1.0421 | 0.81% | 1.04 |
| M1490_1_(*tunF*-_*tunF*+)* | 1 | 44.00 | 44.00 | 0.9375 | 2.13% | 0.94 |
| M1490_2_(*tunF*-_*tunF*+)* | 1 | 52.50 | 52.50 | 1.7307 | 3.30% | 1.73 |
| M1490_3_(*tunF*-_*tunF*+)* | 1 | 96.00 | 96.00 | 1.3490 | 1.41% | 1.35 |
| TunF(-) Nov.29.2011_F1* | 3 | 22.00 | 22.00 | 0.0283 | 0.13% | 0.0095 |
| TunF(-) Nov.29.2011_F2* | 3 | 31.00 | 15.50 | 0.0005 | 0.003% | 0.00033 |
| TunF(-) Feb.9.2012* | 3 | 14.90 | 7.45 | 0.0200 | 0.27% | 0.013 |
| TunF(-) May.1.2012* | 12 | 55.60 | 46.30 | 0.0400 | 0.09% | 0.0040 |
| *S. chartreusis* May.5.2011* | 12 | 687.30 | 1.25 | 1.0296 | 82.40% | 47.20 |
| *S. chartreusis* Jun.9.2012** | 24 | 1066.40 | 1.30 | 1.0201 | 78.50% | 34.90 |
| *S. chartreusis* Aug.14.2012** | 12 | 1483.10 | 1.40 | 0.4718 | 33.70% | 41.70 |
| *S. chartreusis* Nov.13.2012** | 11 | 891.10 | 1.40 | 0.7899 | 56.40% | 45.70 |
| *S. chartreusis* Jan. 14.2013**# | 12 | 573.50 | 4.40 | 1.0616 | 24.10% | 11.50 |

[a]Crude sample
[b]Crude sample concentration injected into HPLC for analysis. TMs dissolved in methanol.
[c]Determined by HPLC, based on a standardised curve.
[d]Taken in consideration of % Purity and Cul. Vol. into the initial TM isolated.
*Purification by flash chromatography
**Purification by acetone precipitation
[#]old resin that have been reused more than three times were used in the extraction process.

## Macrophage and microsomal stability data

*The work was done by Helena Boshoff and Andaleeb Sajid National Institute of Health Tuberculosis Research Section, Maryland, USA.*

1. Macrophages were seeded in 24-well plates (2x10^5 cells/well).
2. Drugs were added in triplicates at their respective MIC multiples (1X and 10X)
3. M.tb culture was added to each well (MOI=1). same number of cells were plated (7H11 agar containing OADC) at day 0, to calculate the initial inoculum.
4. Isoniazid and rifampicin were taken positive controls for M.tb killing and DMSO/ Methanol were negative controls.
5. Infected Macrophages were incubated for 3 day and 7 day to assess the effect of drugs.
6. Macrophages were lyzed by 0.1% SDS and plated for cfu count after appropriate dilutions (each well in triplicates).
7. Colonies were counted after 25 days.

### Macrophage Infection Data

| | | concentration | cfu | stdev |
|---|---|---|---|---|
| day 3 | STARTING | | 139500 | 0 |
| | MeOH | | 111333 | 0 |
| | 11 | 1X | 5450 | 4879 |
| | 12 | 1X | 44467 | 8768 |
| | 13 | 1X | 39467 | 6883 |
| | 14 | 1X | 44317 | 5680 |
| | INH- 5 ug/ml | 5 ug/ml | 310 | 40 |
| | INH-10 ug/ml | 10 ug/ml | 237 | 5 |
| | RIF- 5 ug/ml | 5 ug/ml | 391 | 20 |
| | RIF-10 ug/ml | 10 ug/ml | 325 | 16 |

| | | cfu | stdev |
|---|---|---|---|
| STARTING | | 139500 | 0 |
| MeOH | | 111333 | 0 |
| OCTA-Tm | 10X | 1802 | 280 |
| NONA-Tm | 10X | 21467 | 4997 |
| DECA-Tm | 10X | 13917 | 3418 |
| UNDECA-Tm | 10X | 19917 | 4360 |

| | | | cfu | stdev |
|---|---|---|---|---|
| day 7 | STARTING | | 139500 | 0 |
| | MeOH | | 114000 | 0 |
| | 11 | 1X | 9533 | 1790 |
| | 12 | 1X | 12382 | 4927 |
| | 13 | 1X | 7278 | 4392 |
| | 14 | 1X | 1623 | 80 |
| | INH- 5 ug/ml | 5 ug/ml | 0 | 0 |
| | INH-10 ug/ml | 10 ug/ml | 0 | 0 |
| | RIF- 5 ug/ml | 5 ug/ml | 57 | 2 |
| | RIF-10 ug/ml | 10 ug/ml | 7 | 1 |

| | | cfu | stdev |
|---|---|---|---|
| STARTING | | 139500 | 0 |
| MeOH | | 114000 | 0 |
| 11 | 10X | 674 | 306 |
| 12 | 10X | 3031 | 1571 |
| 13 | 10X | 267 | 94 |
| 14 | 10X | 0 | 0 |

## Human microsomal stability test

| | | | | % remaining | stdev |
|---|---|---|---|---|---|
| Verapamil | 16.8614771 | 0.5615234 | 3.3302146 | 47.4986418 | 2.0583158 |
| | 8.0089726 | 0.0629839 | 0.7864170 | | |
| | | | | | |
| 11 | 2.3311094 | 0.0503788 | 2.1611525 | 53.6958403 | 4.2283978 |
| | 1.2517088 | 0.0788031 | 6.2956431 | | |
| | | | | | |
| 12 | 0.1962084 | 0.0047510 | 13.4213813 | 50.6107513 | 12.8018326 |
| | 0.0993026 | 0.0120973 | 12.1822840 | | |
| | | | | | |
| 13 | 0.0167923 | 0.0024640 | 14.6735616 | 79.6381759 | 8.3533039 |
| | 0.0133731 | 0.0002516 | 2.0330461 | | |

| | | | | | |
|---|---|---|---|---|---|
| 14 | 0.0033313 | 0.0001947 | 5.8446441 | 75.8472576 | 6.2717896 |
| | 0.0025267 | 0.0001693 | 6.6989352 | | |

**Mouse microsomal stability test data**

| | % | stdev |
|---|---|---|
| 0 MIN | 100 | 0 |
| Verapamil | 59 | 3 |
| 11 | 87 | 2 |
| 12 | 99 | 1 |
| 13 | 98 | 3 |
| 14 | NA* | NA* |

*Data not available. Non-specific pattern in LC-MS.
Verapamil taken as positive control.

**Other macrophage studies**

Brief protocol
Day -1: Macrophages infected with *M. tuberculosis* H37Rv (MOI=5)
Day 0: cells washed to remove remaining bacteria that did not infect, CFUs plated in triplicates
Day 0
drugs added in 3 concentration ranges (0.5X, 1X and 10X of their respective MIC values, in triplicates)
Rif and Inh taken as positive controls for experiment (two concentration range, in triplicates)
Day 4: cells lysed and plated for CFUs (each sample in triplicates)
Day 29: CFUs counted

| | **0.5X MIC** | | **1X MIC** | | **10X MIC** | |
|---|---|---|---|---|---|---|
| | CFU | STDEV | CFU | STDEV | CFU | STDEV |
| Day 0 | 436000 | 8720 | | | | |
| no drug | 95000 | 4880 | | | | |
| di-N-octanoyl-Tm | 31333.333 | 1527.5252 | 30333.333 | 1527.5252 | 14533 | 503 |
| di-N-nonanoyl-Tm | 3.88E+04 | 6009.9917 | 35666.667 | 2081.666 | 17467 | 1206 |
| di-N-decanoyl-Tm | 32666.667 | 1154.7005 | 31666.667 | 5686.2407 | 15500 | 866 |
| di-N-undecanoyl-Tm | 38333.333 | 2081.666 | 31666.667 | 2886.7513 | 18333 | 3215 |

| | | | | | | |
|---|---|---|---|---|---|---|
| | | | | | | |
| | | | | | | |
| | | | | | | |
| | 5ug/ml | | 10ug/ml | | | |
| | CFU | STDEV | CFU | STDEV | | |
| Day 0 (before drug treatment) | 436000 | 8720 | | | | |
| No drug | 95000 | 4880 | | | | |
| Isoniazid | 9333 | 577.35027 | 5333 | 577.35027 | | |
| Rifampicin | 9467 | 1006.6446 | 7200 | 1587.4508 | | |

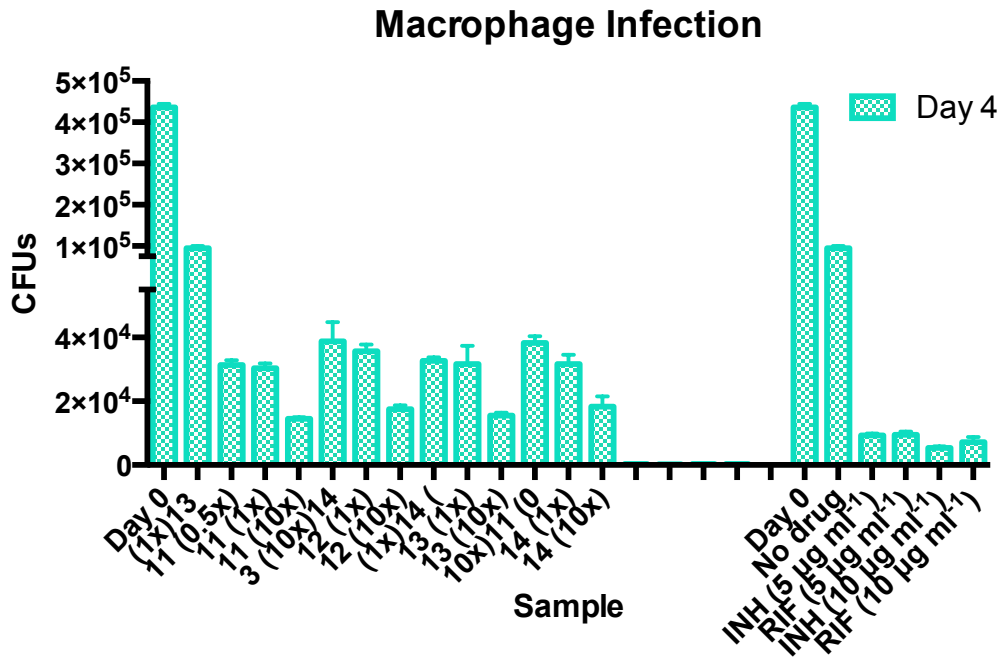

## FACS analysis

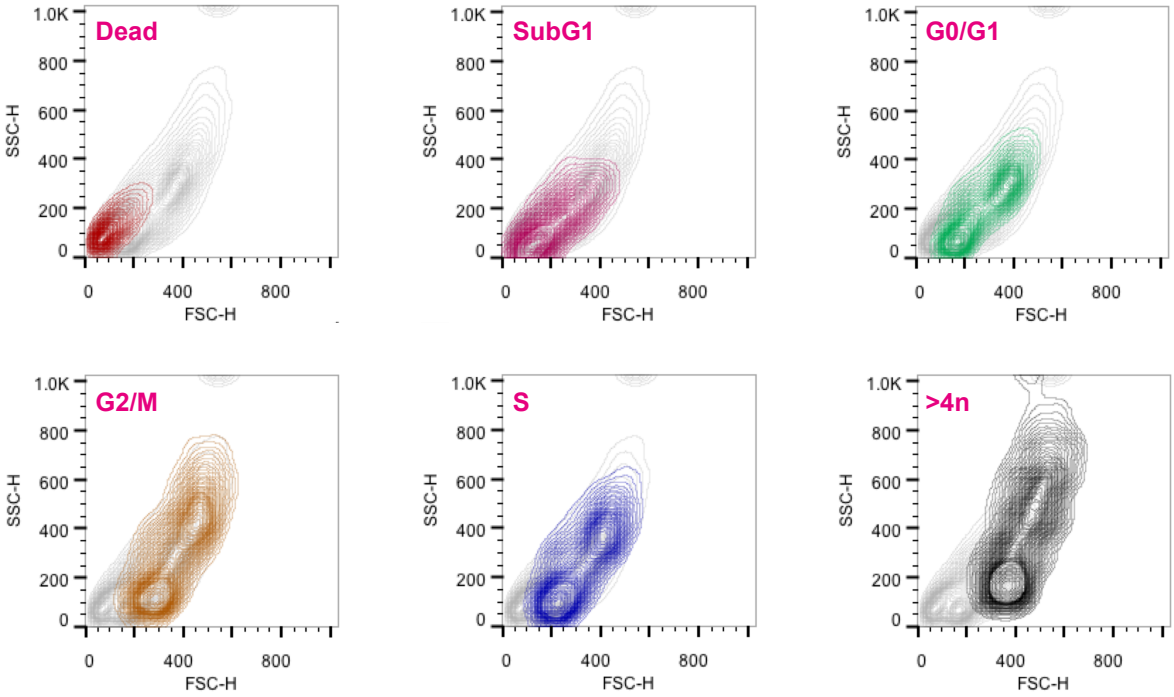


**Backgating analysis of propidium iodide stained HEK293 cells DNA content of the cell cycles.**

## ***tunB* and *tunF* complementation**

*The work was done by Juan Pablo Gomez-Escribano, John Innes Centre, Norwich, UK.*

The wild-type (pIJ12003a) and *tunB*-deleted (pIJ12541) or *tunF*-deleted (pIJ12542) gene clusters are in pRT801, vector with kanamycin resistance gene *neo* and that integrates in phiBT1 attachment site in the chromosome. Therefore the construct to complement must have another selection marker and must integrate in phiC31 attachment site. *tunB* or *tunF* have been cloned under the strong constitutive promoter *ermE**p in pSET152, that contains the apramycin resistance gene *aac(3)IV*, and introduced in M1152 strain that carries the gene cluster with *tunB* (M1481) or *tunF* (M1482) deleted, therefore testing from complementation of the gene function in *trans*. (Note: the pIJ and M numbers were taken from the first paper and the second manuscript)

1st) PCR amplification with construct pIJ12003a as template and primers (capitals indicate nucleotides changed to incorporate restriction site) [pages 202-203 lab-notebook 505329]:

>tunB1 (NdeI)
gacATatgaccggctacaccg

>tunB2 (HindIII)
ttAAGCTtggacaaggcctacctcac

>tunF1 (NdeI)
aaCATatgagagtgctcgtgactg

>tunF2 (HindIII)
ttAAGCTTgtagaggtgcatgtcactc

2nd) Blunt-end cloning of PCR products in EcoRV site of pBluescript II KS+ (pKS) [page 203 lab-notebook 505329]

3rd) Sequencing of several clones with M13R and M13F universal primers (that anneal with pKS). Analysis with Staden Package and selection of good clones (see folder "pKSEcoRV-tunBF(seqjob64883)" Note: a piece 111 nt piece of E.coli genome had been introduced between HindIII and EcoRV sites of vector in the *tunB* clone, unexplainable but not a problem; we have a full sequence of the construct and *tunB* is fully correct). [page 204 lab-notebook 505329]

4th) Extraction of *tunB* or *tunF* from pKS with NdeI/HindIII and ligation into pIJ10257 cut with the same enzymes. [pages 205-206 lab-notebook 505329]

5th) Digestion of pIJ10257tunB or pIJ10257tunF with BamHI/EcoRI to extract the gene together with the strong constitutive promoter *ermE**p; followed by ligation into pSET152 cut with the same enzymes. The final constructs were confirmed by sequencing with

universal M13R and M13F primers (see folder "pSETtunBF+176PstI(65256)") [pages 206-208 lab-notebook 505329]

*Note: pIJ10257 integrates in phiBT1, therefore is not suitable for complementation in this case (see first paragraph).*

6th) Conjugation of pSET152_*ermE**p_*tunB* in *S.coelicolor* M1481 (i.e. M1152+pIJ12003aΔ*tunB*) and of pSET152_*ermE**p_*tunF* in M1152+pIJ12003aΔ*tunF* (NOTE: I do not know if this strain has already an "M" number)

The resulting strains have been numbered as:

*S. coelicolor* M1489 (M1152+pIJ12003aΔ*tunB* +pSET152_*ermE**p_*tunB*) [*tunB* mutant complemented]

*S. coelicolor* M1490 (M1152+pIJ12003aΔ*tunF* +pSET152_*ermE**p_*tunF*) [*tunF* mutant complemented]

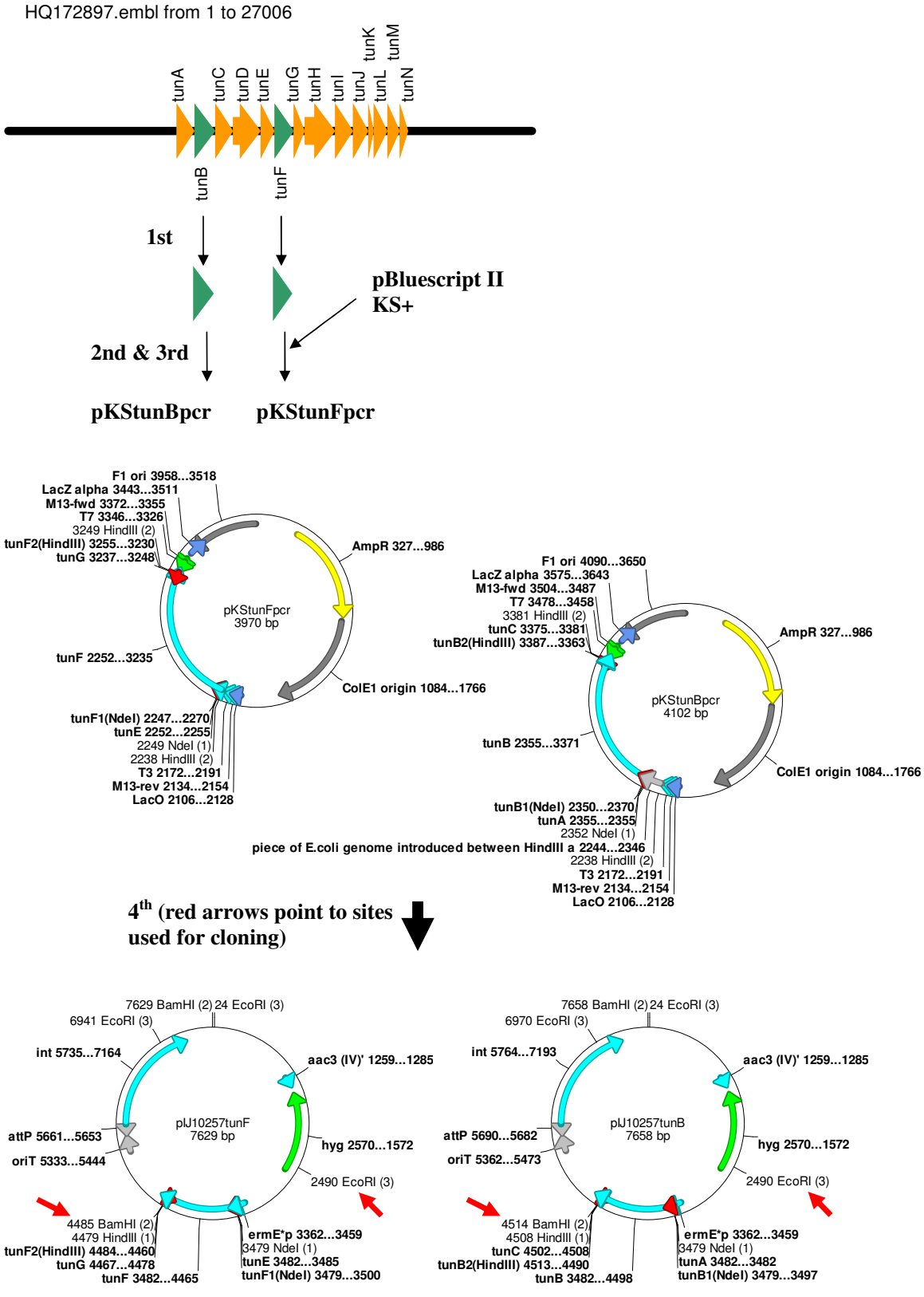
HQ172897.embl from 1 to 27006
tunA
tunC
tunD
tunE
tunG
tunH
tunI
tunJ
tunK
tunL
tunM
tunN
tunB
tunF
1st
pBluescript II KS+
2nd & 3rd
pKStunBpcr
pKStunFpcr
F1 ori 3958...3518
LacZ alpha 3443...3511
M13-fwd 3372...3355
T7 3346...3326
3249 HindIII (2)
tunF2(HindIII) 3255...3230
tunG 3237...3248
AmpR 327...986
pKStunFpcr
3970 bp
tunF 2252...3235
ColE1 origin 1084...1766
tunF1(NdeI) 2247...2270
tunE 2252...2255
2249 NdeI (1)
2238 HindIII (2)
T3 2172...2191
M13-rev 2134...2154
LacO 2106...2128
F1 ori 4090...3650
LacZ alpha 3575...3643
M13-fwd 3504...3487
T7 3478...3458
3381 HindIII (2)
tunC 3375...3381
tunB2(HindIII) 3387...3363
AmpR 327...986
pKStunBpcr
4102 bp
tunB 2355...3371
ColE1 origin 1084...1766
tunB1(NdeI) 2350...2370
tunA 2355...2355
2352 NdeI (1)
piece of E.coli genome introduced between HindIII a 2244...2346
2238 HindIII (2)
T3 2172...2191
M13-rev 2134...2154
LacO 2106...2128
4th (red arrows point to sites used for cloning)
7629 BamHI (2)
24 EcoRI (3)
6941 EcoRI (3)
int 5735...7164
aac3 (IV)' 1259...1285
pIJ10257tunF
7629 bp
attP 5661...5653
oriT 5333...5444
hyg 2570...1572
2490 EcoRI (3)
4485 BamHI (2)
4479 HindIII (1)
tunF2(HindIII) 4484...4460
tunG 4467...4478
tunF 3482...4465
ermE*p 3362...3459
3479 NdeI (1)
tunE 3482...3485
tunF1(NdeI) 3479...3500
7658 BamHI (2)
24 EcoRI (3)
6970 EcoRI (3)
int 5764...7193
aac3 (IV)' 1259...1285
pIJ10257tunB
7658 bp
attP 5690...5682
oriT 5362...5473
hyg 2570...1572
2490 EcoRI (3)
4514 BamHI (2)
4508 HindIII (1)
tunC 4502...4508
tunB2(HindIII) 4513...4490
tunB 3482...4498
ermE*p 3362...3459
3479 NdeI (1)
tunA 3482...3482
tunB1(NdeI) 3479...3497

**5th**

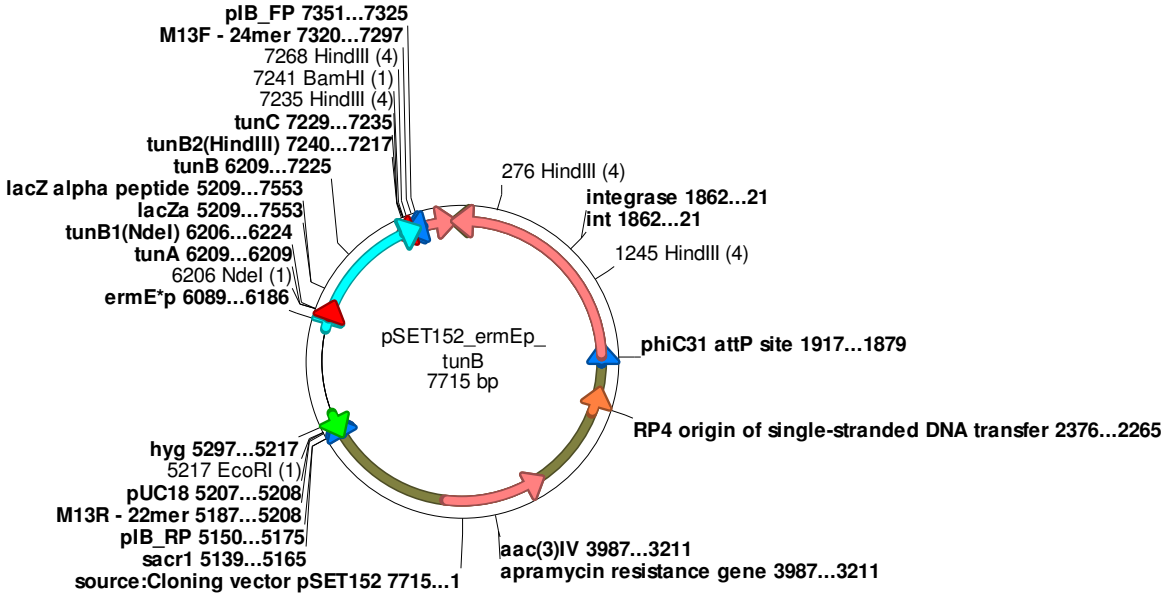
pIB_FP 7351...7325
M13F - 24mer 7320...7297
7268 HindIII (4)
7241 BamHI (1)
7235 HindIII (4)
tunC 7229...7235
tunB2(HindIII) 7240...7217
tunB 6209...7225
lacZ alpha peptide 5209...7553
lacZa 5209...7553
tunB1(NdeI) 6206...6224
tunA 6209...6209
6206 NdeI (1)
ermE*p 6089...6186
276 HindIII (4)
integrase 1862...21
int 1862...21
1245 HindIII (4)
pSET152_ermEp_
tunB
7715 bp
phiC31 attP site 1917...1879
RP4 origin of single-stranded DNA transfer 2376...2265
hyg 5297...5217
5217 EcoRI (1)
pUC18 5207...5208
M13R - 22mer 5187...5208
pIB_RP 5150...5175
sacr1 5139...5165
source:Cloning vector pSET152 7715...1
aac(3)IV 3987...3211
apramycin resistance gene 3987...3211

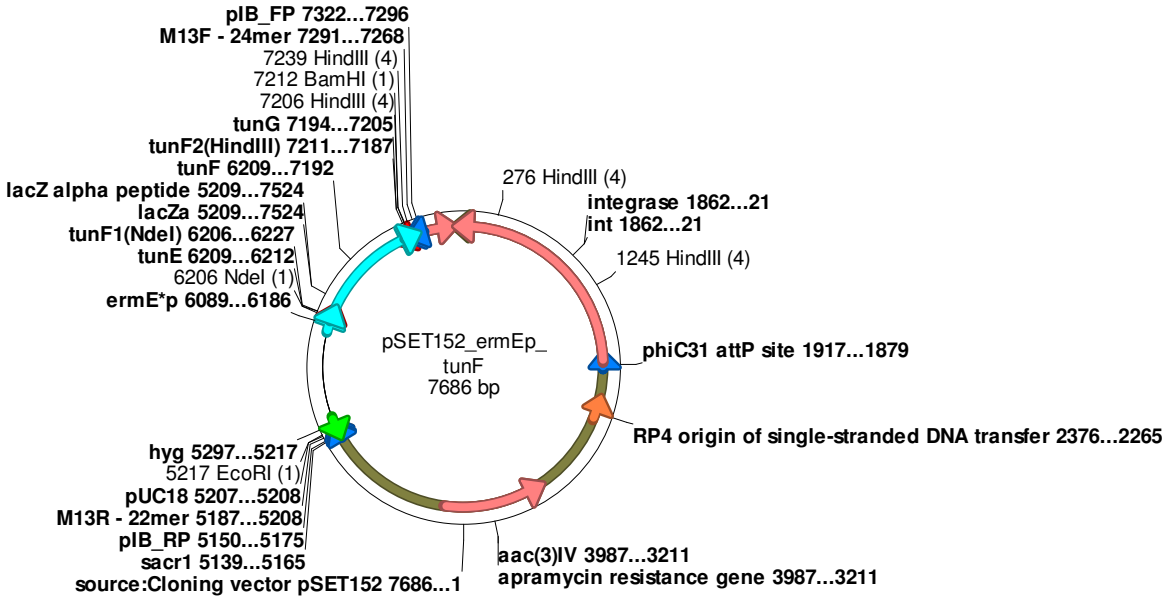
pIB_FP 7322...7296
M13F - 24mer 7291...7268
7239 HindIII (4)
7212 BamHI (1)
7206 HindIII (4)
tunG 7194...7205
tunF2(HindIII) 7211...7187
tunF 6209...7192
lacZ alpha peptide 5209...7524
lacZa 5209...7524
tunF1(NdeI) 6206...6227
tunE 6209...6212
6206 NdeI (1)
ermE*p 6089...6186
276 HindIII (4)
integrase 1862...21
int 1862...21
1245 HindIII (4)
pSET152_ermEp_
tunF
7686 bp
phiC31 attP site 1917...1879
RP4 origin of single-stranded DNA transfer 2376...2265
hyg 5297...5217
5217 EcoRI (1)
pUC18 5207...5208
M13R - 22mer 5187...5208
pIB_RP 5150...5175
sacr1 5139...5165
source:Cloning vector pSET152 7686...1
aac(3)IV 3987...3211
apramycin resistance gene 3987...3211

## TunF(-) metabolite studies

The *tunB* and *tunF* knockout strains were named as:
***S. coelicolor* M1481** (M1152+pIJ12003aΔ*tunB*)
***S. coelicolor* M1482** (M1152+pIJ12003aΔ*tunF*)

The *tunB* and *tunF* complementation strains were named as:
***S. coelicolor* M1489** (M1152+pIJ12003aΔ*tunB*+pSET152_*ermE**p_*tunB*)
***S. coelicolor* M1490** (M1152+pIJ12003aΔ*tunF*+pSET152_*ermE**p_*tunF*)

The negative and positive control strains were named as:
***S. coelicolor* M1037** (M1152+pRT801) - negative control
***S. coelicolor* M1040** (M1152+pIJ12003a) - positive control

This report elucidates the analysis from the complementation strains showing restored production of tunicamycins in respectable quantity. In addition, previous results will be used to supplement the overall analysis.

The aim of the work is to detect any production of tunicamycins from complementation strains. Additionally, we were also curious to determine when and how much of tunicamycins are produced compared to tunicamycins natural producer *S. chartreusis*.

**Observation of Tunicamycins Production (smale scale)**
Previous work using small scale growth cultures (100-mL) showed production of tunicamycins from positive control M1040 after 72 hours (day 3) versus native *S. chartreusis* 24 hours right after the innoculation from seedling culture. As expected, no detectable quanitity of tunicamycins was observed from the negative control M1037. The cultures were grown for 7 days. Growth condition was identical for both *S. coelicolor* and *S. chartreusis*. Detection of tunicamycins from the culture was done using LCMS. Commercial tunicamcyins were used as standard (Fig. 1, and Fig.2). See Table 1 for summary.

**Observation and Quantification of Tunicamycinss Production from Heterologous Expression and Complementation Strains (large scale)**
Three 1-Liter cultures of each complementation strains (M1489 and M1490) and positive control (M1040) were grown for 7 days. 10-mL from the culture after each 24 hours throughout the 7 days was extracted for LCMS analysis. Each liter of culture was later extracted separately to determine the yield of tunicamycins in triplicate. Surprisingly, production of tunicamycins was observed in positive control (M1040) in large scale after 24 hours compare to 72 hours in small scale culture (Fig. 3a and 3b). More importantly, both complementation strains (M1489 and M1490) regained their production of tunicamycins as we predicted (Fig. 4a, 4b, 5a, 5b). This further supports our previous work showing the role of TunB and TunF in the tunicamycins biosynthetic process.

Observation summary from tunicamycins production over 7 days is noted in Table 2. Quantification of tunicamycins isolated from each liter of culture is noted in Table 3.

Sample collection and extraction for LCMS analysis followed the sample protocol for small and large scale culture.

Mycelium was extracted by pestle and mortar processing using methanol to solubilize the tunicamycins present. Methanol extract was concentrated and analyzed by LCMS subjected to RP-C14 HPLC separation.

Comparison between the heterologous expression of tunicamycins by *S. coelicolor* and natural producer *S. chartreusis* cannot be conclusive at this time. It was observed that some contamination was present for the positive control cultures. The culture broth turned cloudy compare to clear of other strains. This was also observed in the past with small scale cultures. It is likely due to *E.coli* contamination. Despite the contamination, tunicamycins production was still able to be observed. This could explain the yield difference between the positive control and the complementation strains tunicamycins isolated, as shown in Table 3. The contaminant organism may have competed for the uptake of nutrients to result in low yield of tunicamycins.

Furthermore, previous work showed low quantity of tunicamycins in *tunF* knockout strain, M1482. Few attempts were made to isolate the compound. Not all were successful. However, for those ones that were able to isolate the tunicamycins, quantitative yield was extremely low and the product was not completely pure*. Tunicamycins isolated were easily analyzed by LCMS.

*It should be noted that tunicamycins extraction process for *S. chartreusis* when employed to *S. coelicolor* strains does not yield the same purity of tunicamycins. Tunicamycins isolated from *S. coelicolor* strain always seem to contain impurity, observed by NMR, that is not observed in tunicamycins isolated from *S. charturesis*. This may mean purification process for crude tunicamycins isolated from *S. chartreusis* is not optimized for crude tunicamycins extracted from heterologous expression host *S. coelicolor*.

**Observation from 100-mL culture (small scale). TM: tunicamycins.**

| Strain | Day 1 | Day 2 | Day 3 | Day 4 | Day 5 | Day 6 | Day 7 |
|---|---|---|---|---|---|---|---|
| **M1037** | No TM | No TM | No TM | No TM | No TM | No TM | No TM |
| **M1040** | No TM | No TM | No TM | TM | TM | TM | TM |
| **M1481** | No TM | No TM | No TM | No TM | No TM | No TM | No TM |
| **M1482** | No TM | No TM | No TM | TM | TM | TM | TM |

**Observation from 1-Liter culture (large scale).**

| Strain | Day 1 | Day 2 | Day 3 | Day 4 | Day 5 | Day 6 | Day 7 |
|---|---|---|---|---|---|---|---|
| **M1040** | TM | TM | TM | TM | TM | TM | TM |
| **M1489** | TM | TM | TM | TM | TM | TM | TM |
| **M1490** | TM | TM | TM | TM | TM | TM | TM |

Tunicamycins production from heterologous expression. Each batch is 1 liter. The yield determined from each batch is after one round of flash chromotagraphy, resulted as crude tunicamycins.

| Strain | Batch 1, mg/L | Batch 2, mg/L | Batch 3, mg/L | Average, mg/L |
|---|---|---|---|---|
| **M1040** | 31.6 | 11.8 | 29.2 | 24.2 |
| **M1489** | 42.9 | 40.3 | 128.6 | 70.6 |
| **M1490** | 44.0 | 52.5 | 96.0 | 64.2 |

**Isolation of *S. coelicolor* M1482 crude metabolite.**

| Batch | 3 Liters, mg/L | 12 Liters, mg/L | 7 Liters, mg/L | 3 Liters, mg/L |
|---|---|---|---|---|
| **M1482** | Total 5mg, 1.6 mg/L | N/A* | N/A* | Total 14.9mg, 5.0 mg/L |

*tunicamycins detected by LCMS but failed to isolate after extraction and purification

History of tunicamycins extraction. The average yield from 6- or 12-Liter batch after 2-3 flash column chromatography.

| Strain | Batch average, mg/L |
|---|---|
| ***S. chartreusis*** | 30.6, 10.8, 33.0, 62.5, 73.0, 104.0 |

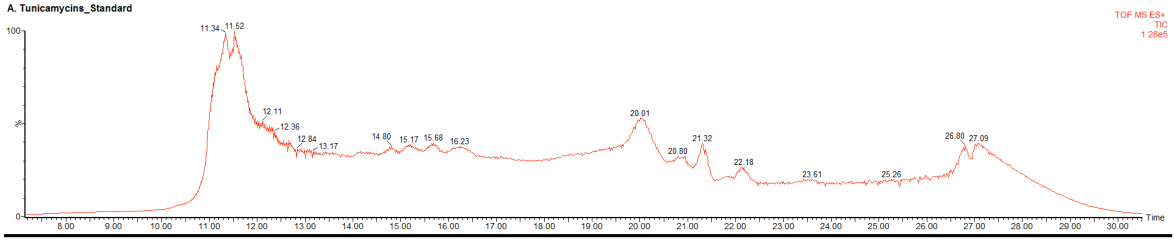


TIC: tunicamycins are eluted between 10.5 – 12 min.

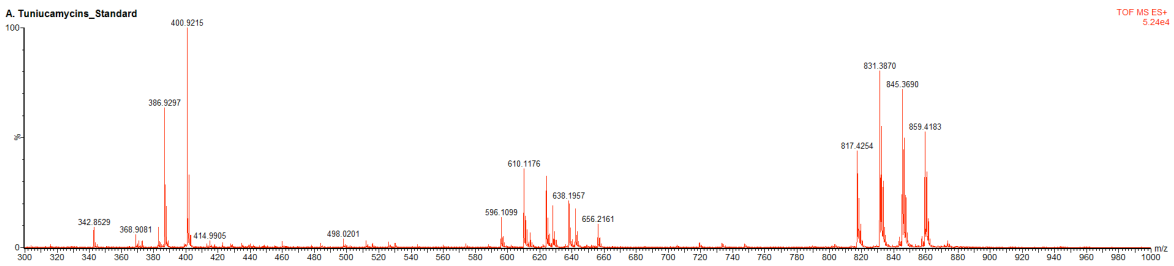


TOF-ES+: four homologues of tunicamycins along with mass observed from the loss of GlcNAc moiety from tunicamycins.

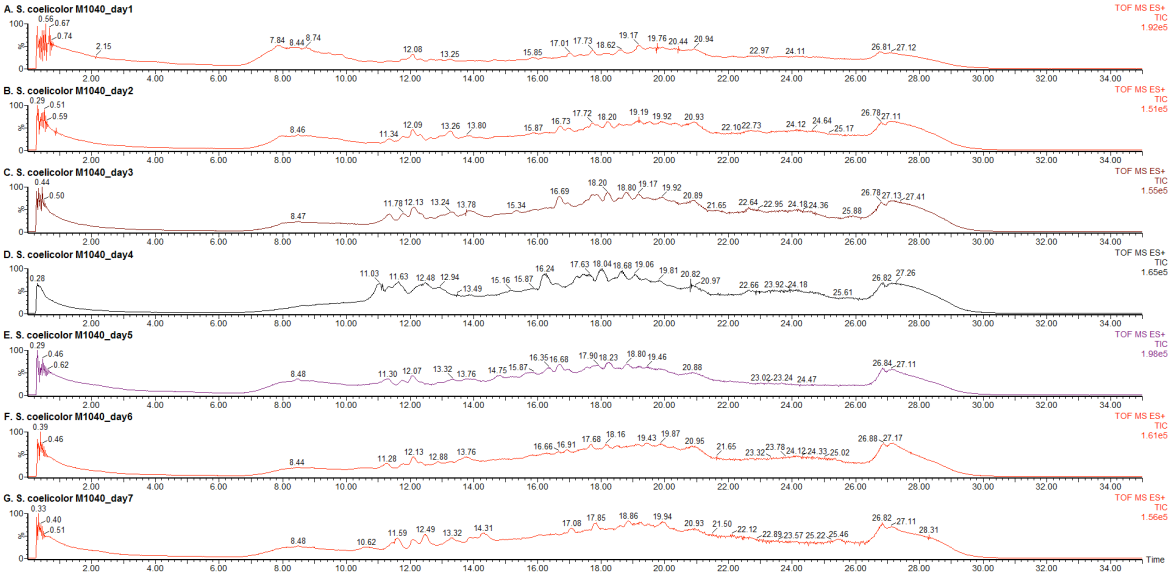


TIC: *S. coelicolor* M1040 day 1 to 7. Tunicamycins are eluted between 10.5 – 12 min.

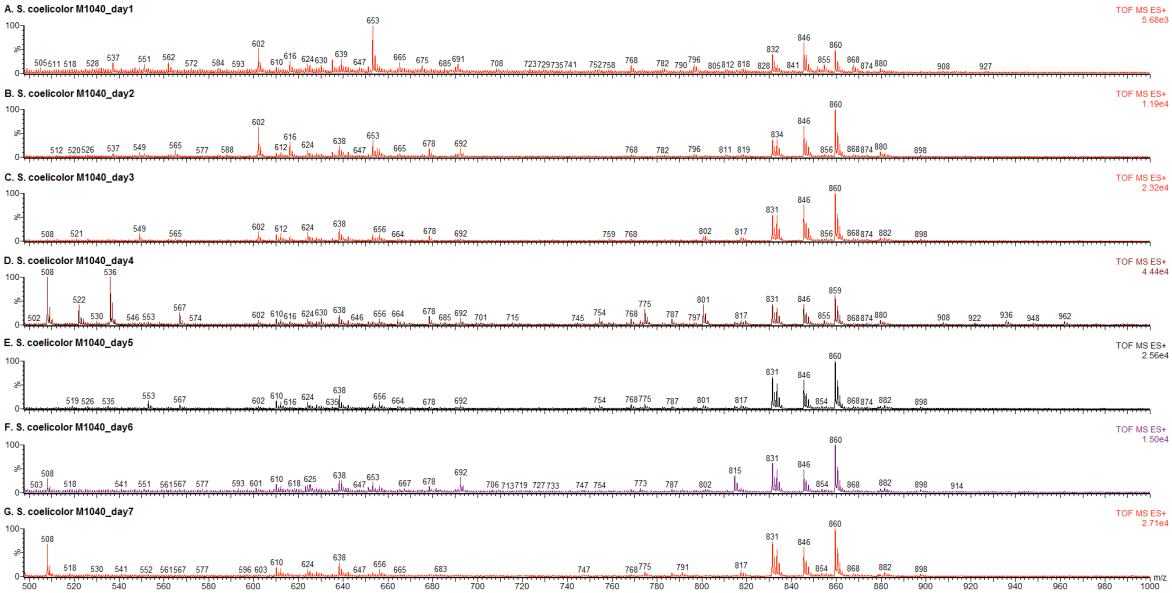


TOF-ES+: *S. coelicolor* M1040 day 1 – 7. Production of tunicamycins was observed each day.

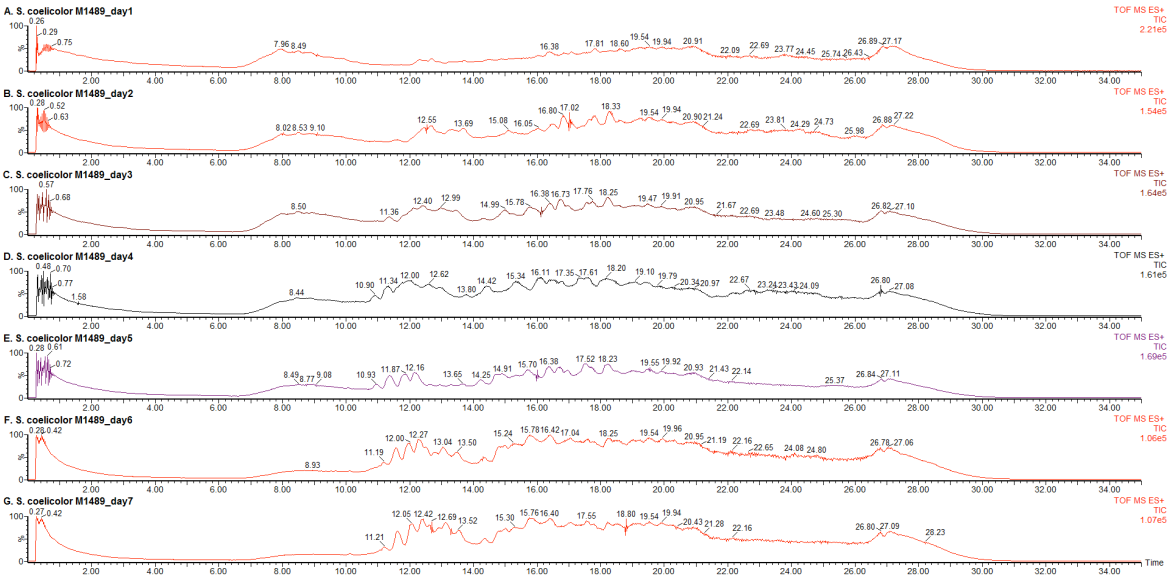


TIC: *S. coelicolor* M1489 day 1 to 7. Tunicamycins are eluted between 10.5 – 12 min.

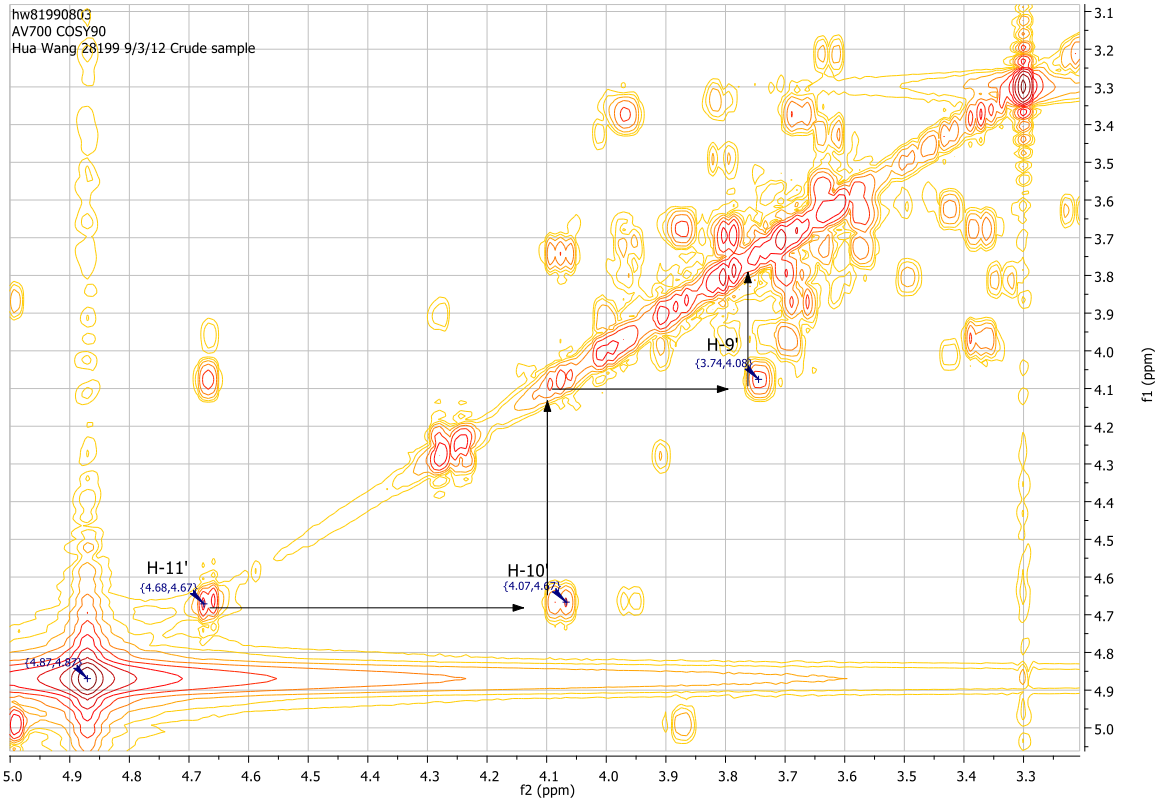

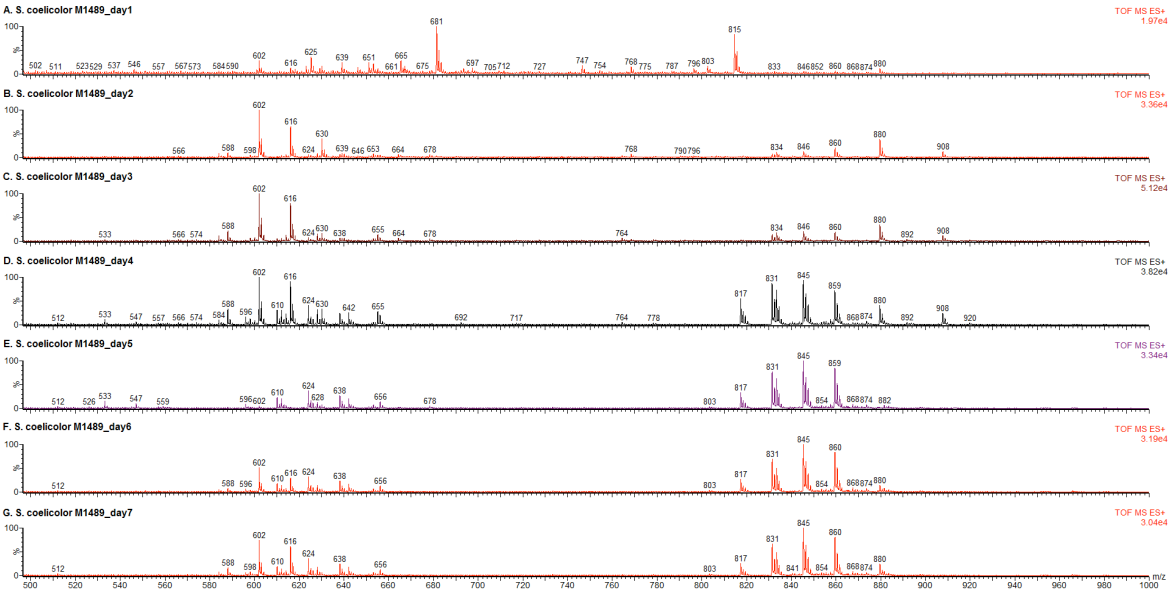


TOF-ES+: *S. coelicolor* M1489 day 1 – 7. Production of tunicamycins was observed each day.

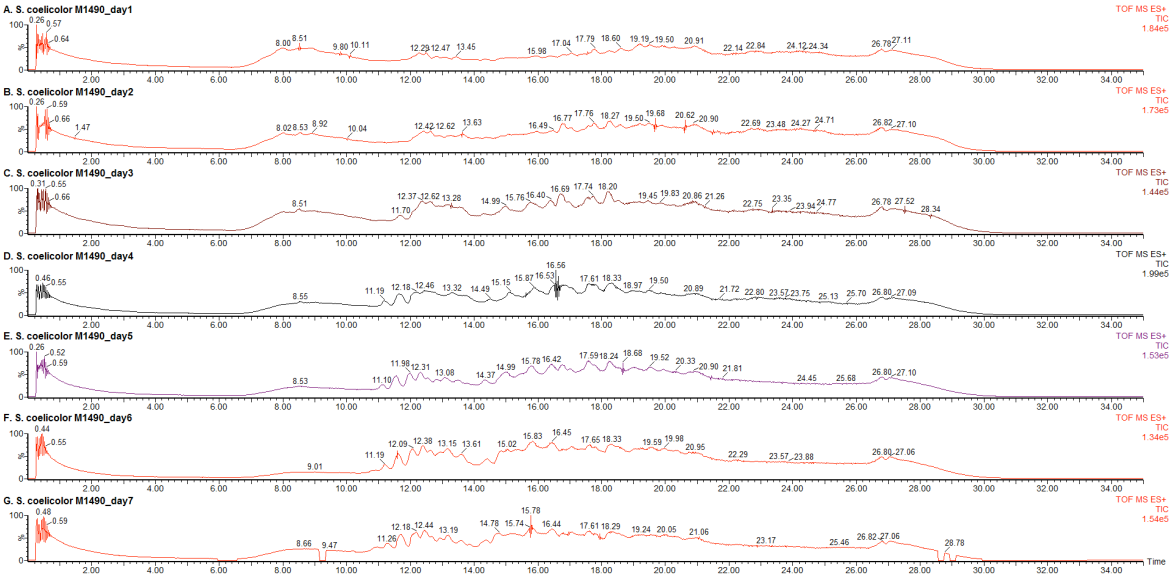


TIC: *S. coelicolor* M1490 day 1 to 7. Tunicamycins are eluted between 10.5 – 12 min.

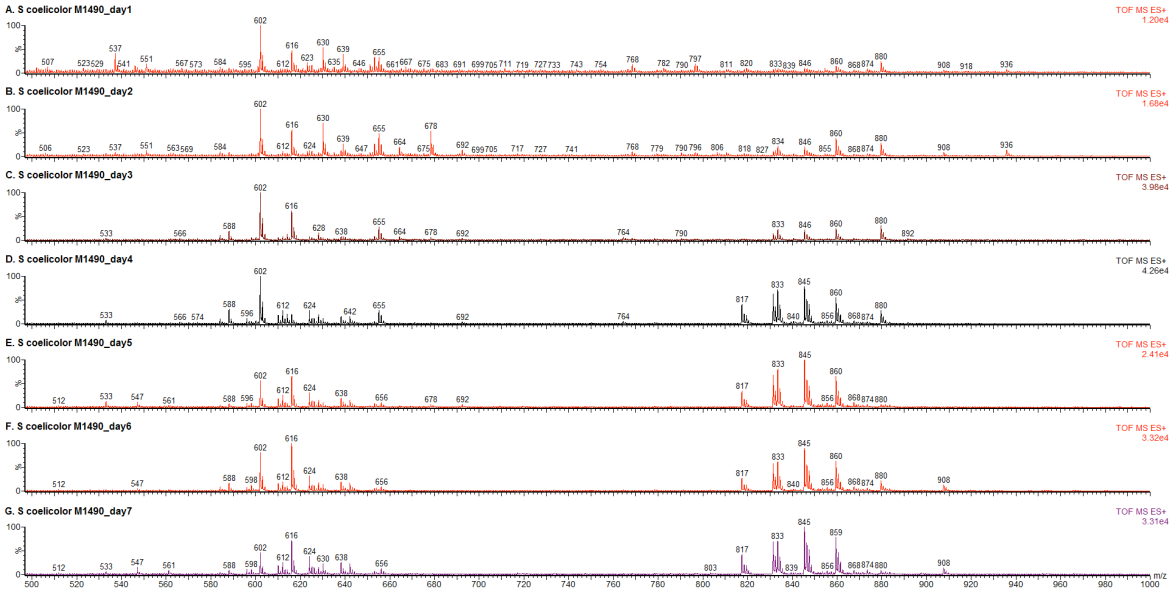


TOF-ES+: *S. coelicolor* M1490 day 1 – 7. Production of tunicamycins was observed each day.

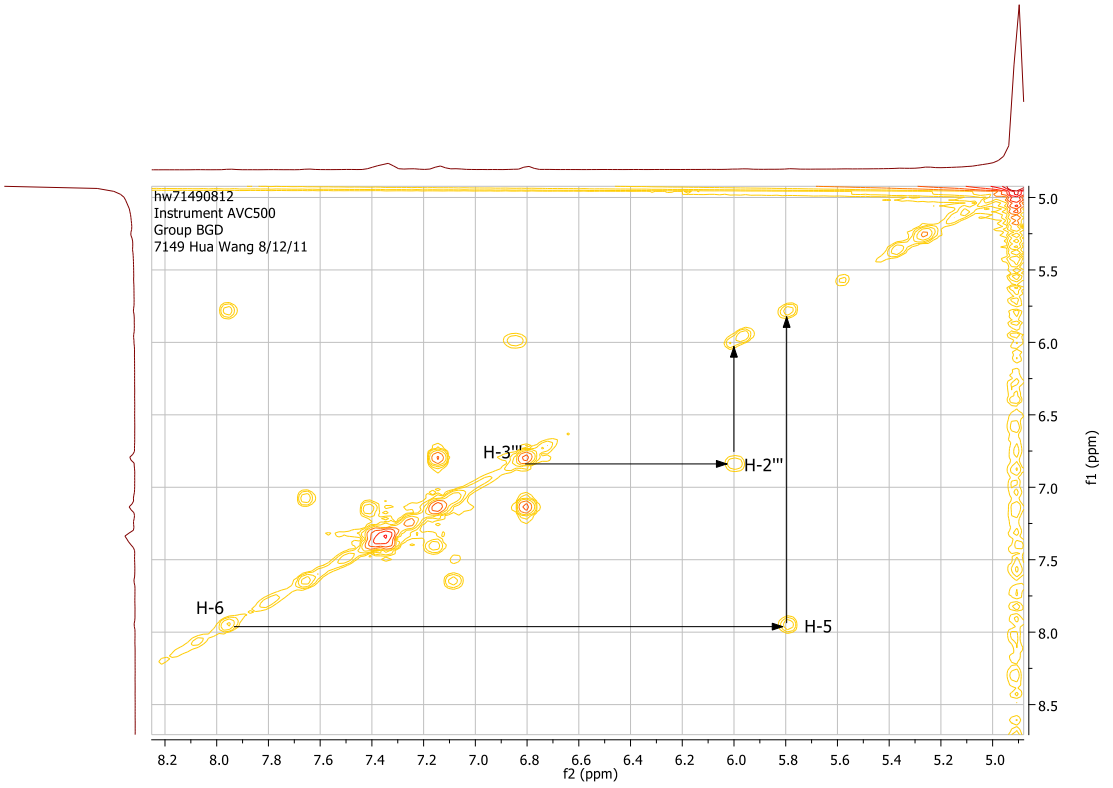


COSY 8 – 5 ppm.

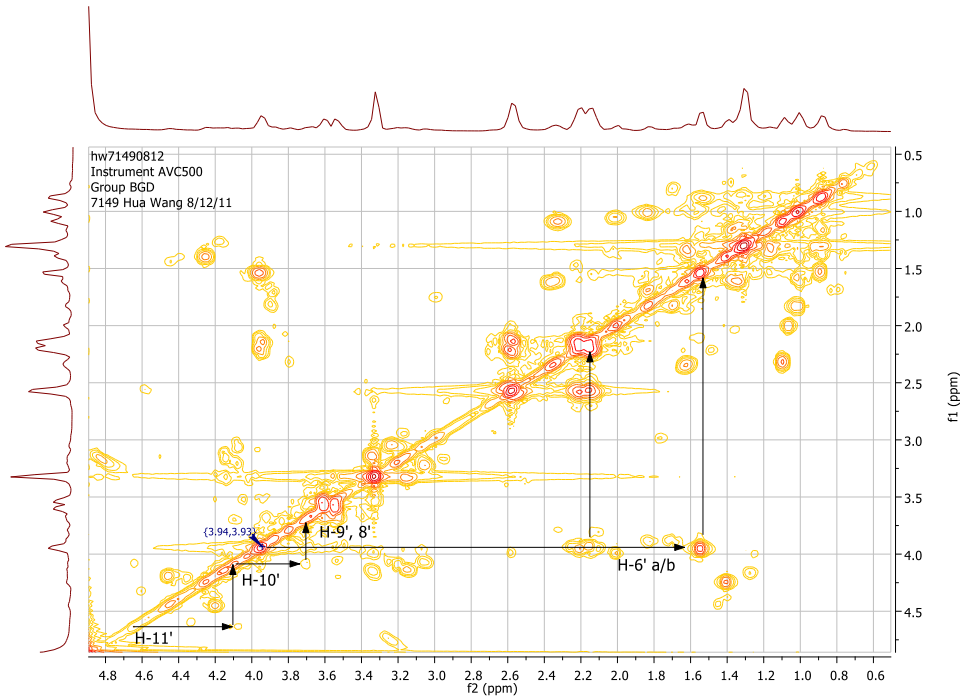


TunF metabolite COSY spectrum

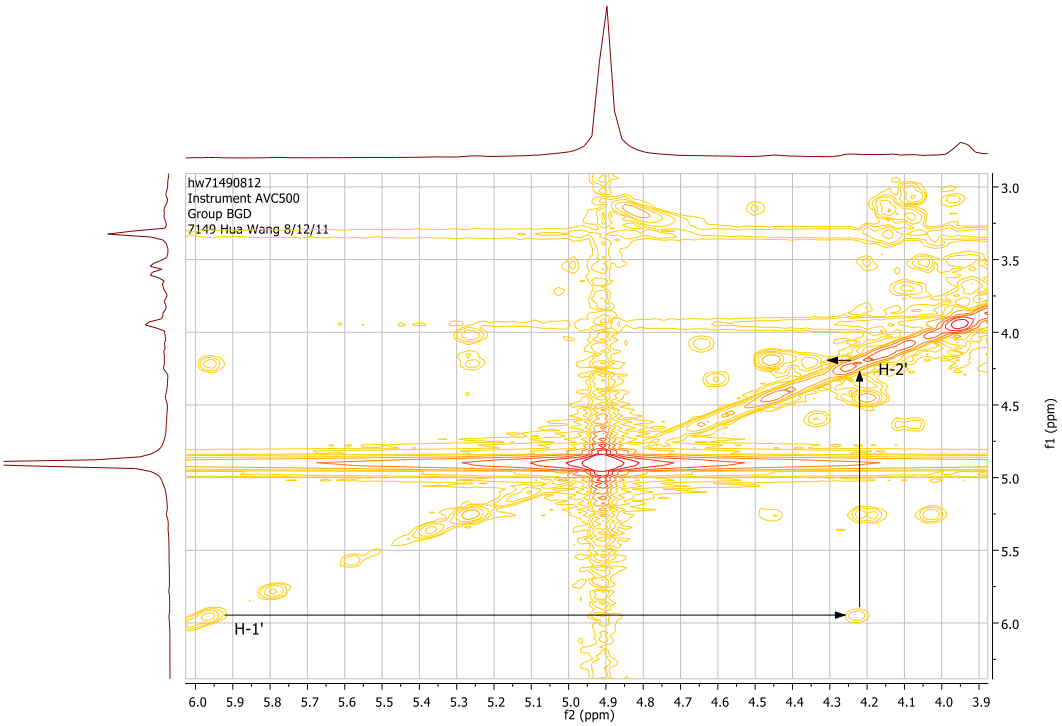


TunF metabolite COSY spectrum

tunicamycins, *S. chartreusis* sample, COSY

## TunD glycosyltransferase activity assay

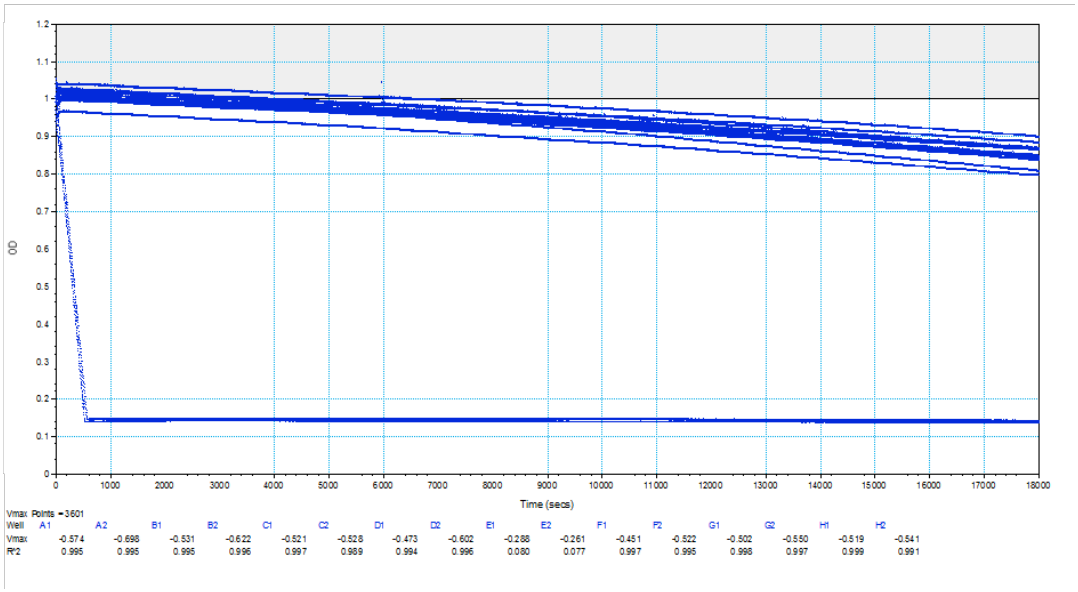


Overlay from the reaction screening. No activity was observed. The decreased in absorbance on the left is the UDP spike in reaction mixture.

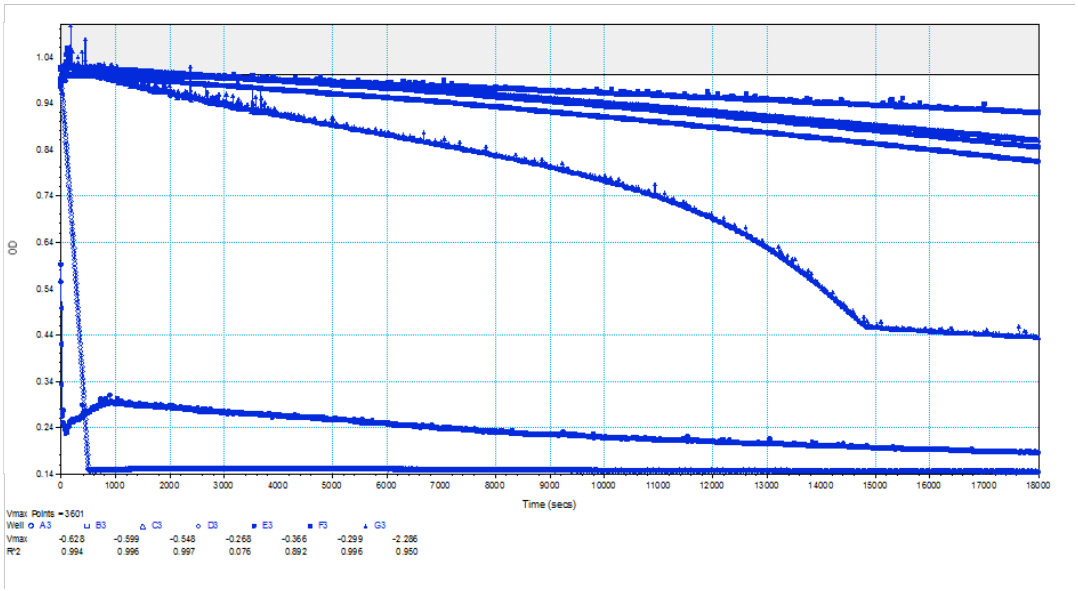


Overlay from TunD activity screening. Bottom line is positive control with UDP spiked the reaction mixture; second to bottom line is OtsA positive control. The curve line in the middle is F.J.W. TunD sample. Top lines are control and refolded TunD sample. No activity observed.

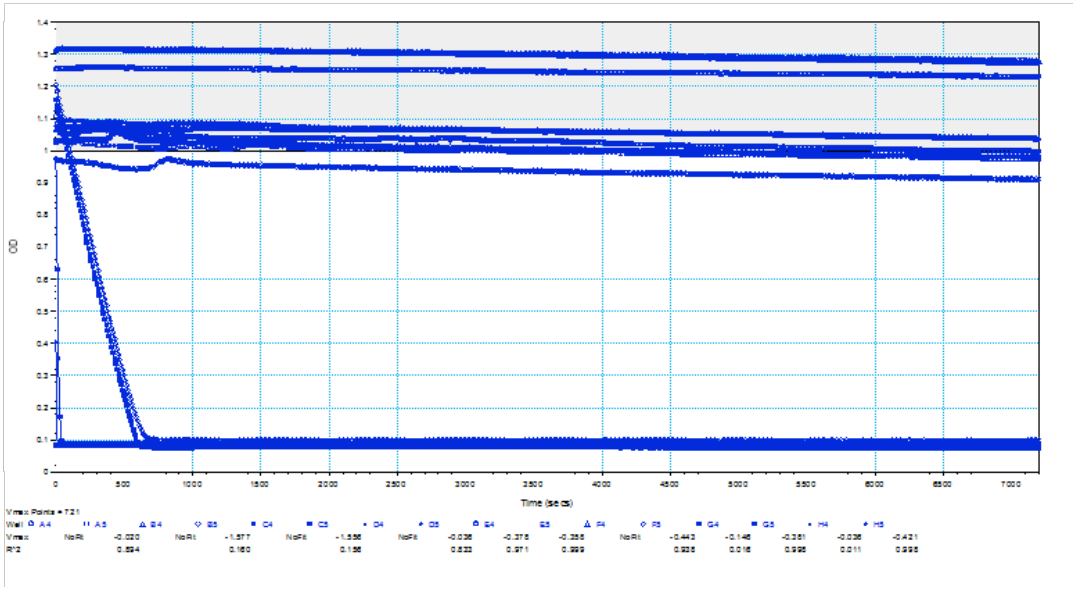


Overlay of TunD multiple acceptor-donor activity screening. Low absorbance lines on the bottom are result from UDP and ADP spike in reaction mixture. Negative control looks the same as reaction mixture containing TunD.

## TunD Isothermal titration calorimetry data

ITC analysis was carried out according to the manufacturer's instructions for the instrument. The sample volume was about 250 µL.

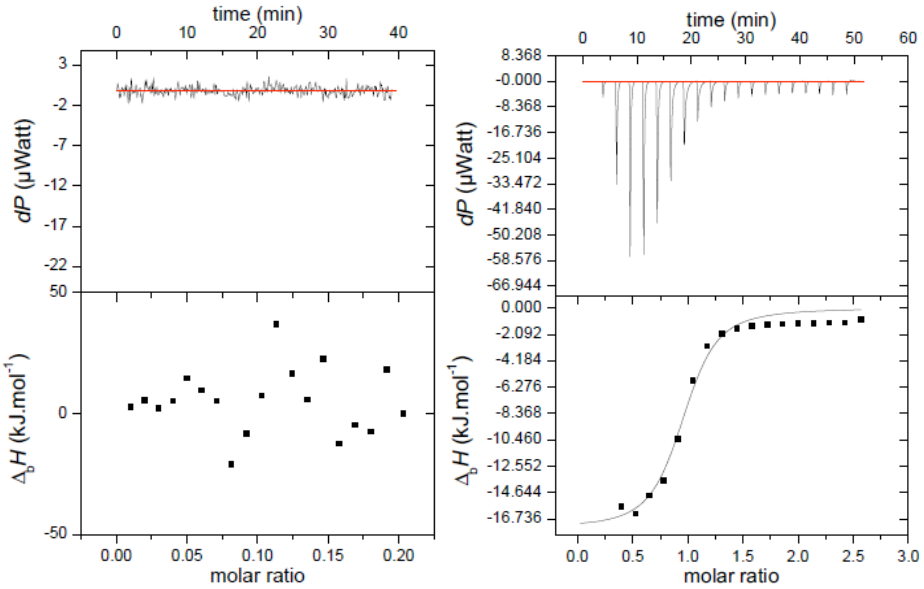


Top box: raw ITC data; bottom box: integrated isothermic curve. (L) water/water, (R) $CaCl_2$/EDTA

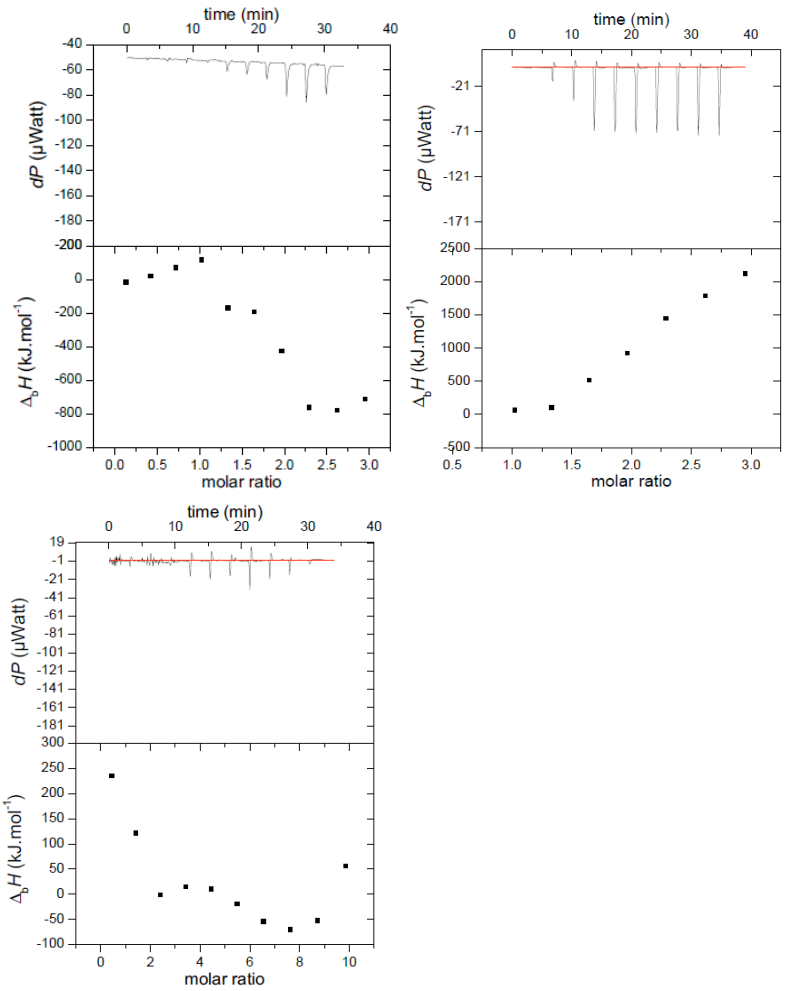


Top box: raw ITC data; bottom box: integrated isothermic curve.

*ITC experiment condition:*

**Buffer:** 20mM Tris, pH 7.5

**TunD:** 10uM

**UDP-GlcNAc:** 150 uM

**N-acetyl-tunicamyluracil:** 150uM

**(L).** Buffer/UDP-GlcNAc

**(M).** TunD/UDP-GlcNAc

**(R).** TunD/N-acetyl-tunicamyluracil

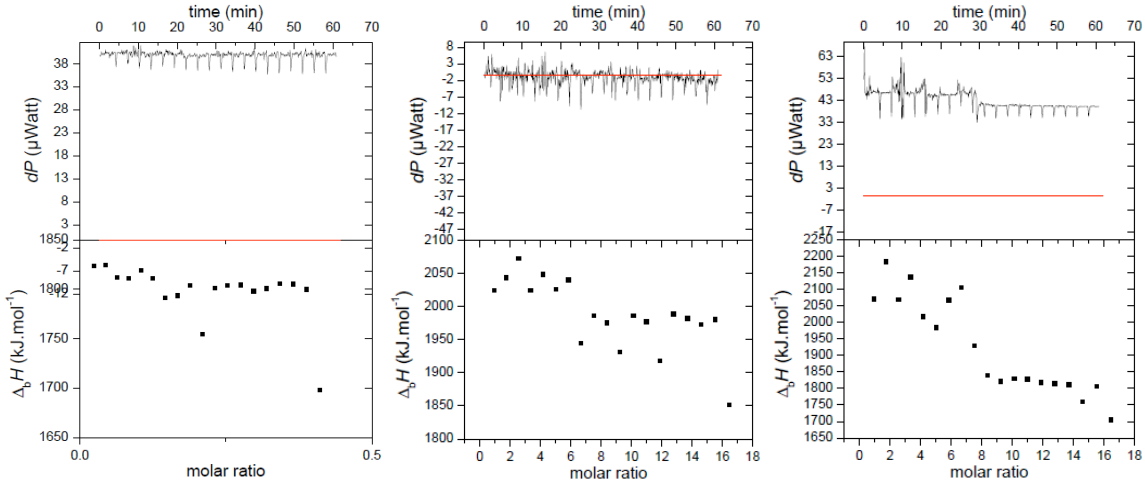


Top box: raw ITC data; bottom box: integrated isothermic curve.

*ITC experiment condition:*

**Buffer:** 50mM Tris, pH 8

**TunD:** 25uM

**UDP-GlcNAc:** 2 mM

**N-acetyltunicamyluracil**: 2mM

**$MgCl_2$:** 10 mM

**(L).** Buffer+$MgCl_2$/UDP-GlcNAc

**(M).** TunD+$MgCl_2$/UDP-GlcNAc

**(R).** TunD+$MgCl_2$+UDP-GlcNAc/N-acetyltunicamyluracil

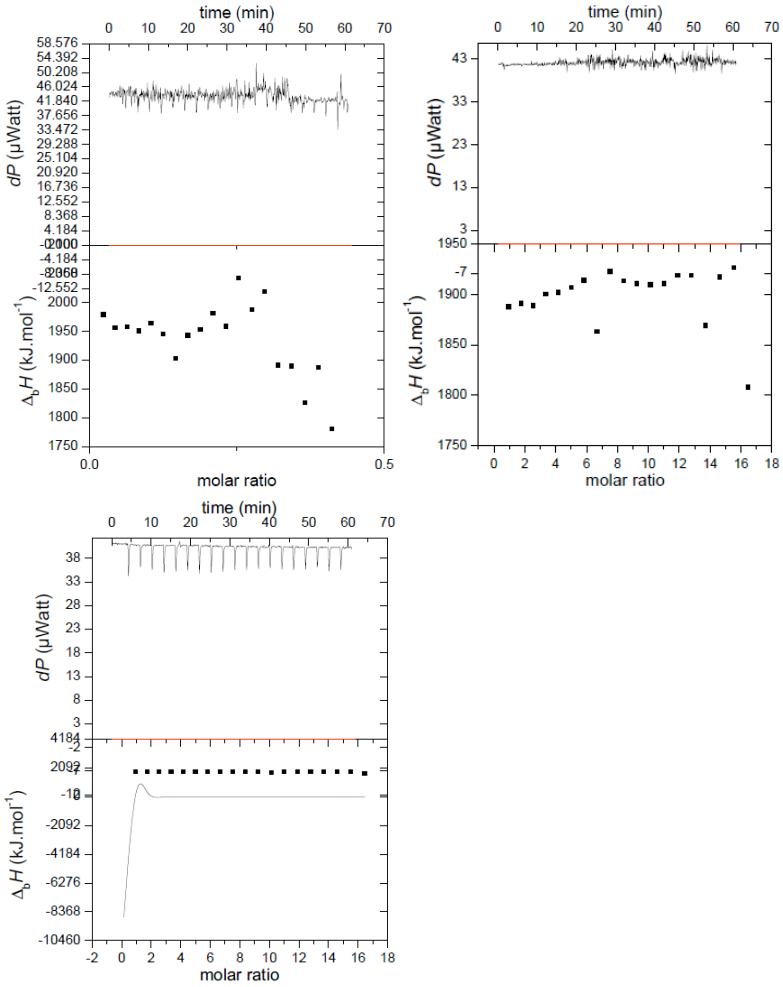


Top box: raw ITC data; bottom box: integrated isothermic curve.

ITC experiment condition:

**Buffer:** 50mM Tris, pH 8

**TunD:** 25uM

**UDP-GlcNAc:** 2 mM

**N-acetyltunicamyluracil**: 2mM

**$MnCl_2$:** 10 mM  1 mM

**(L).** Buffer+$MnCl_2$/UDP-GlcNAc

**(M).** TunD+$MnCl_2$/UDP-GlcNAc

**(R).** TunD+$MnCl_2$+UDP-GlcNAc/N-acetyl-tunicamyluracil

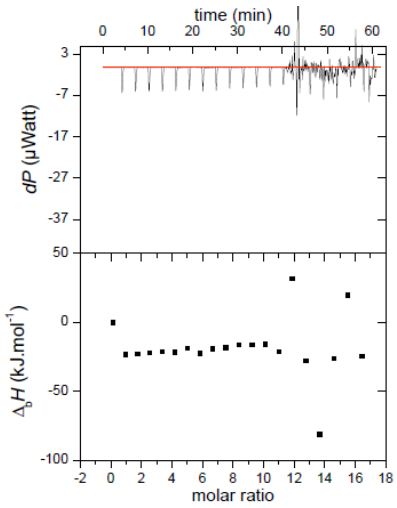


Top box: raw ITC data; bottom box: integrated isothermic curve. Repeat of experiment as shown in Fig. 10 (M). Concentration of $MnCl_2$ was reduced from 10 mM  1 mM to avoid precipitation.

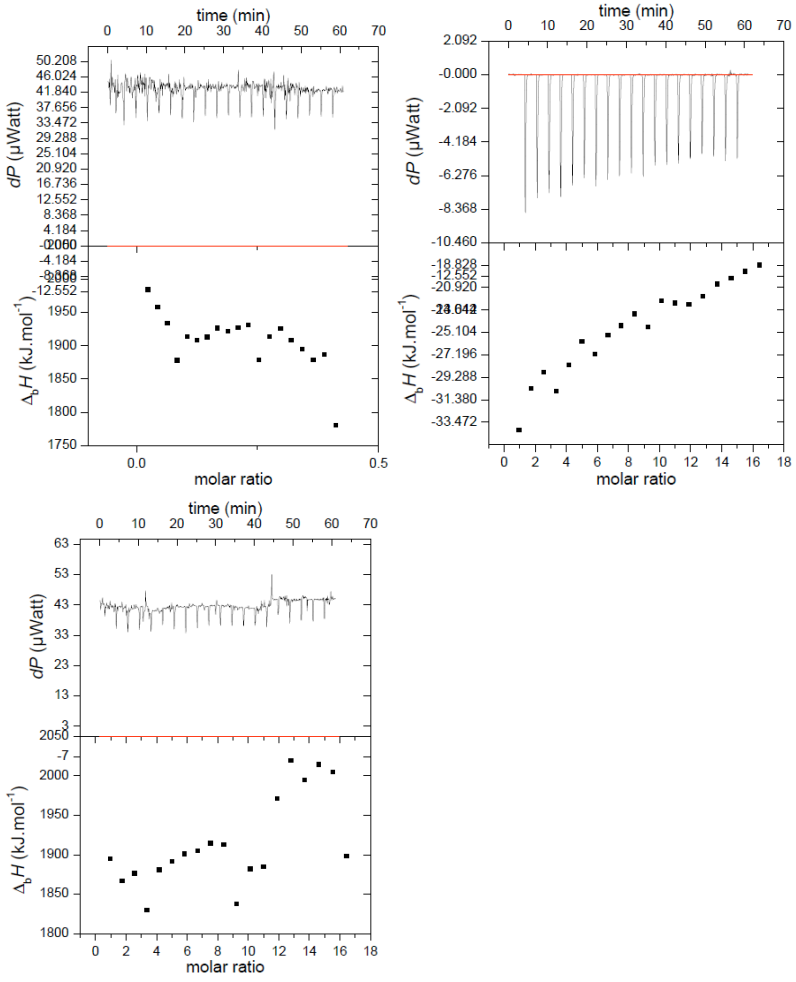


Top box: raw ITC data; bottom box: integrated isothermic curve.

*ITC experiment condition:*

**Buffer:** 50mM Tris, pH 8

**TunD:** 25uM

**UDP-GlcNAc:** 2 mM

**N-acetyltunicamyluracil**: 2mM
**$CaCl_2$:** 10 mM  1 mM
**(L).** Buffer+$CaCl_2$/UDP-GlcNAc
**(M).** TunD+$CaCl_2$/UDP-GlcNAc
**(R).** TunD+$CaCl_2$+UDP-GlcNAc/N-acetyl-tunicamyluracil

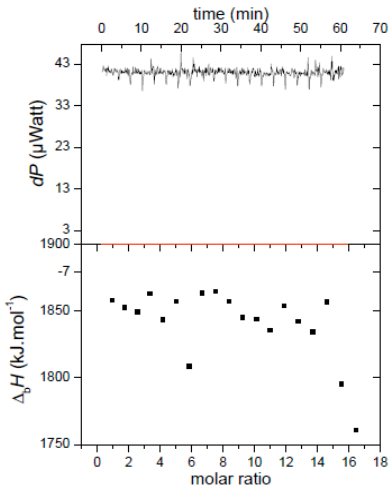


Top box: raw ITC data; bottom box: integrated isothermic curve. Repeat of experiment as shown in Fig. 11 (M). Concentration of $CaCl_2$ was reduced from 10 mM  1 mM to avoid precipitation.

## ***N*-acetyltunicaminyl uracil as putative inhibitor of glycosyltransferases and kinases**

**Note:** nTM or *N*-acetyl TM refers to *N*-acetyltunicaminyl uracil.

Activity assay used the pyruvate-kinase and lactate dehydrogenase coupling system by measuring the absorption of NADH at 340 nm.

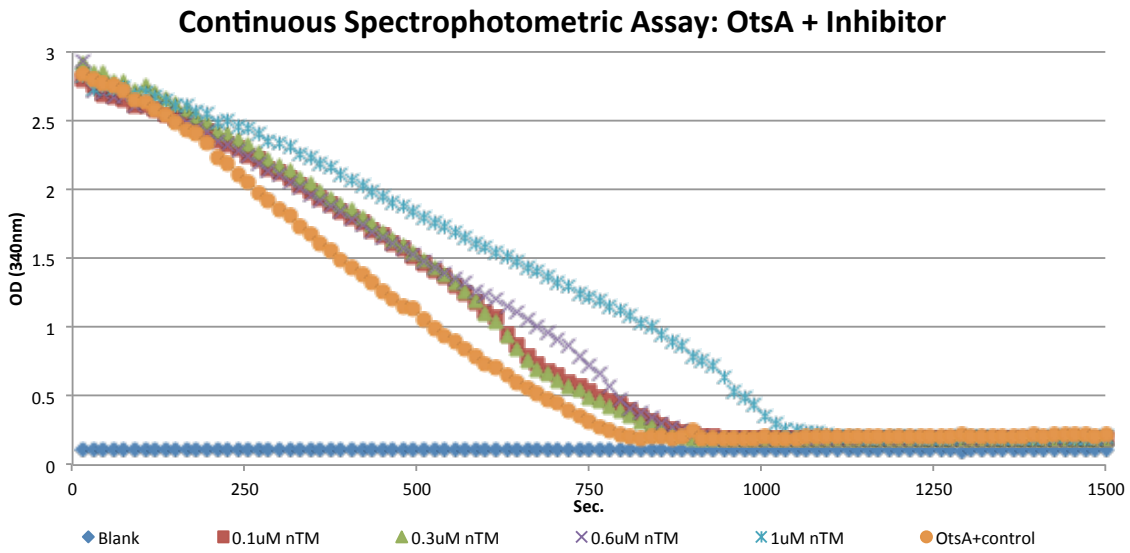


**OtsA inhibition studies #1.** Rxn. Condition: 200uL, RT, 100ug/mL OtsA, 1mM G6P, 1mM UDP-Glc, 50mM HEPES pH 7.0, 5mM MgCl2, 200mM NaCl

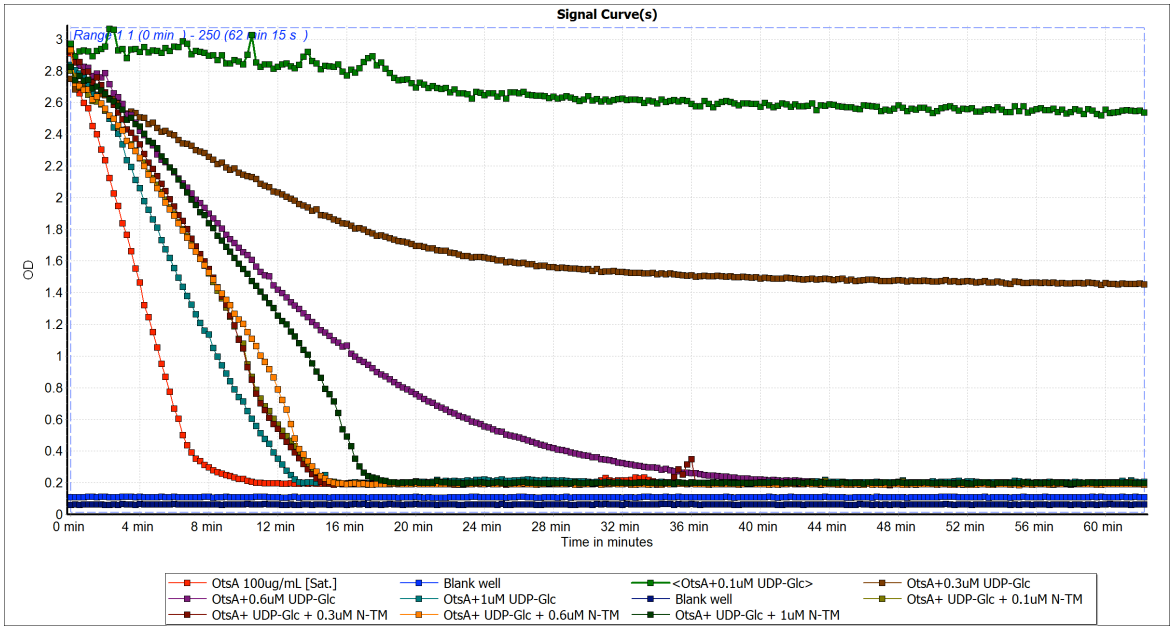


**OtsA inhibition studies #2.**

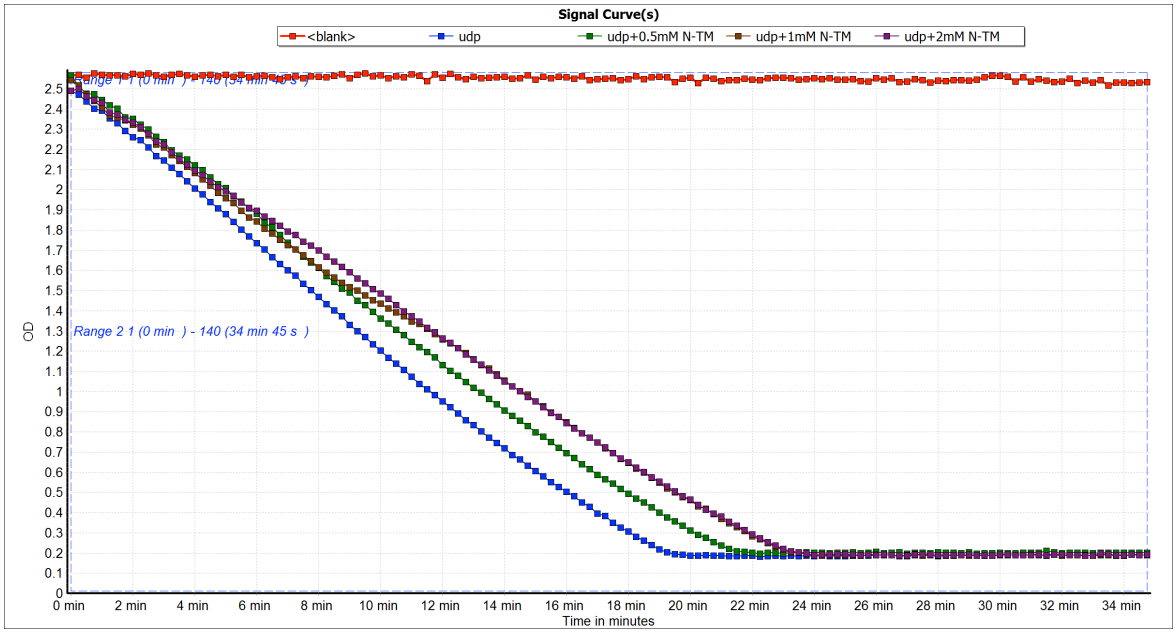


**Pyruvate kinase and lactate dehydrogenase coupled enzyme system in presence of N-acetyltunicaminyl uracil.**Rxn. Condition: 200uL, RT, ~~OtsA~~, 1mM G6P, 1mM UDP-Glc, 50mM HEPES pH 7.0, 5mM MgCl2, 200mM NaCl.

## OtsA Tm shift assay data

| Temp | | | |
|---|---|---|---|
| **42** | **0.55940** | **0.53750** | **0.55240** |
| **43** | **0.55080** | **0.53160** | **0.54680** |
| **44** | **0.54370** | **0.52590** | **0.54190** |
| **45** | **0.53780** | **0.52280** | **0.53860** |
| **46** | **0.54020** | **0.52810** | **0.54440** |
| **47** | **0.54820** | **0.53960** | **0.55600** |
| **48** | **0.56550** | **0.56060** | **0.57790** |
| **49** | **0.58790** | **0.58760** | **0.60520** |
| **50** | **0.62650** | **0.63390** | **0.65190** |
| **51** | **0.67110** | **0.68590** | **0.70630** |
| **52** | **0.71470** | **0.74090** | **0.76230** |
| **53** | **0.74990** | **0.78230** | **0.81090** |
| **54** | **0.77100** | **0.80870** | **0.84490** |
| **55** | **0.77710** | **0.81850** | **0.86130** |
| **56** | **0.77190** | **0.81600** | **0.86350** |
| **57** | **0.75960** | **0.80580** | **0.85530** |
| **58** | **0.74540** | **0.79310** | **0.84360** |
| **59** | **0.72910** | **0.78160** | **0.82910** |

# OtsA co-crystallisation screen

**Note:** nTM or *N*-acetyl TM refers to *N*-acetyltunicaminyl uracil.

## OtsA crystal screen conditions (hanging-drop)

0.1M trisodium citrate, pH 5.4 with:

| | | | | | |
|---|---|---|---|---|---|
| 1.60 M Li2SO4<br>1.0 M (NH4)2SO4 | 1.35 M Li2SO4<br>1.0 M (NH4)2SO4 | 1.10 M Li2SO4<br>1.0 M (NH4)2SO4 | 0.85 M Li2SO4<br>1.0 M (NH4)2SO4 | 0.60 M Li2SO4<br>1.0 M (NH4)2SO4 | 0.35 M Li2SO4<br>1.0 M (NH4)2SO4 |
| 1.60 M Li2SO4<br>0.7 M (NH4)2SO4 | 1.35 M Li2SO4<br>0.7 M (NH4)2SO4 | 1.10 M Li2SO4<br>0.7 M (NH4)2SO4 | 0.85 M Li2SO4<br>0.7 M (NH4)2SO4 | 0.60 M Li2SO4<br>0.7 M (NH4)2SO4 | 0.35 M Li2SO4<br>0.7 M (NH4)2SO4 |
| 1.60 M Li2SO4<br>0.4 M (NH4)2SO4 | 1.35 M Li2SO4<br>0.4 M (NH4)2SO4 | 1.10 M Li2SO4<br>0.4 M (NH4)2SO4 | 0.85 M Li2SO4<br>0.4 M (NH4)2SO4 | 0.60 M Li2SO4<br>0.4 M (NH4)2SO4 | 0.35 M Li2SO4<br>0.4 M (NH4)2SO4 |
| 1.60 M Li2SO4<br>0.1 M (NH4)2SO4 | 1.35 M Li2SO4<br>0.1 M (NH4)2SO4 | 1.10 M Li2SO4<br>0.1 M (NH4)2SO4 | 0.85 M Li2SO4<br>0.1 M (NH4)2SO4 | 0.60 M Li2SO4<br>0.1 M (NH4)2SO4 | 0.35 M Li2SO4<br>0.1 M (NH4)2SO4 |

Red: conditions with crystal hits.

**OtsA Crystal, 15-36hrs. OtsA + UDP + G6P**

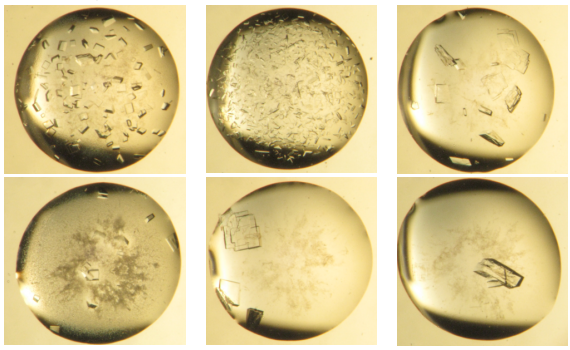

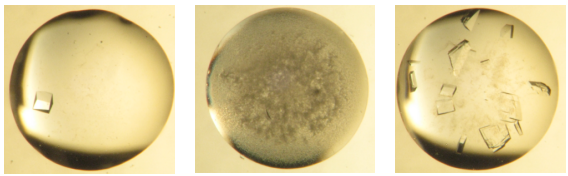

**OtsA Crystal, 2 weeks, OtsA + G6P + N-acetyl TM**

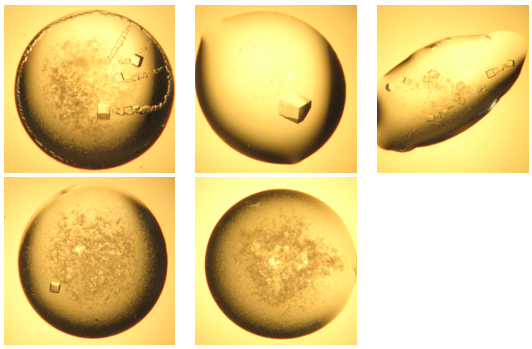

**OtsA Crystal, 15-36hrs. OtsA + G6P + N-acetyl TM**

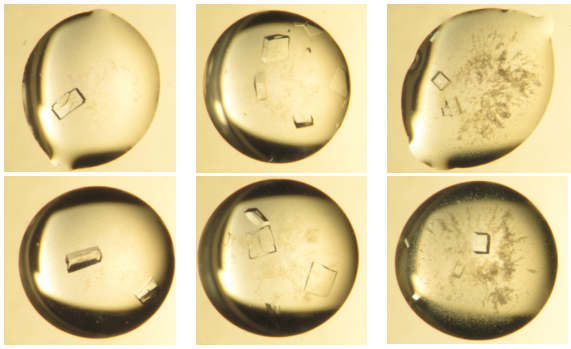

**- Data too mosaic**

## OtsA crystal screen conditions (hanging-drop)

1M NaOAc, pH 6.8, 8% v/v monomethylether PEG 550, 8% v/v PEG 20,000
1M NaHEPES, pH 6.8, 8% v/v monomethylether PEG 550, 8% v/v PEG 20,000

| | | | | | |
|---|---|---|---|---|---|
| 0.6 M NaOAc<br>0.20 M NaHEPES | 0.5 M NaOAc<br>0.20 M NaHEPES | 0.4 M NaOAc<br>0.20 M NaHEPES | 0.3 M NaOAc<br>0.20 M NaHEPES | 0.2 M NaOAc<br>0.20 M NaHEPES | 0.1 M NaOAc<br>0.20 M NaHEPES |
| 0.6 M NaOAc<br>0.15 M NaHEPES | 0.5 M NaOAc<br>0.15 M NaHEPES | 0.4 M NaOAc<br>0.15 M NaHEPES | 0.3 M NaOAc<br>0.15 M NaHEPES | 0.2 M NaOAc<br>0.15 M NaHEPES | 0.1 M NaOAc<br>0.15 M NaHEPES |
| 0.6 M NaOAc<br>0.10 M NaHEPES | 0.5 M NaOAc<br>0.10 M NaHEPES | 0.4 M NaOAc<br>0.10 M NaHEPES | 0.3 M NaOAc<br>0.10 M NaHEPES | 0.2 M NaOAc<br>0.10 M NaHEPES | 0.1 M NaOAc<br>0.10 M NaHEPES |
| 0.6 M NaOAc<br>0.05 M NaHEPES | 0.5 M NaOAc<br>0.05 M NaHEPES | 0.4 M NaOAc<br>0.05 M NaHEPES | 0.3 M NaOAc<br>0.05 M NaHEPES | 0.2 M NaOAc<br>0.05 M NaHEPES | 0.1 M NaOAc<br>0.05 M NaHEPES |

**- No crystals**